



**CHARACTERIZATION OF HETEROGENEITIES
CONTROLLING TRANSPORT AND FATE
OF POLLUTANTS IN UNCONSOLIDATED SAND AND
GRAVEL AQUIFERS:
FINAL REPORT**

**A research project of the
University Research Initiative
Research Initiation Program
U.S. Department of Defense**

**Carl D. McElwee and James J. Butler, Jr.
Kansas Geological Survey
The University of Kansas**

with

**Gwendolyn L. Macpherson
Department of Geology
The University of Kansas**

**Geoffrey C. Bohling, Richard D. Miller,
Christine M. Mennicke, Terrance Huettl,
Matthias Zenner, Zafar Hyder, Wenzhi Liu,
Michael Orcutt, Meredith L. Beilfuss, and Sashi Gonuguntla
Kansas Geological Survey
The University of Kansas**

**Kansas Geological Survey
Open File Report 95-16**

March, 1995

19950511 110

Approved for public release,
distribution unlimited

100-12
4524 and 45

REPORT DOCUMENTATION PAGE			Form Approved OMB No. 0704-0188	
<small>Public reporting burden for this collection of information is estimated to average 1 hour per response, including the time for reviewing instructions, searching existing data sources, gathering and maintaining the data needed, and completing and reviewing the collection of information. Send comments regarding this burden estimate or any other aspect of this collection of information, including suggestions for reducing this burden, to Washington Headquarters Services, Directorate for Information Operations and Reports, 1215 Jefferson Davis Highway, Suite 1204, Arlington, VA 22202-4302, and to the Office of Management and Budget, Paperwork Reduction Project (0704-0188), Washington, DC 20503.</small>				
1. AGENCY USE ONLY (Leave blank)	2. REPORT DATE 31 March 95	3. REPORT TYPE AND DATES COVERED Final, 1 June 91- 31 Dec. 94		
4. TITLE AND SUBTITLE Characterization of heterogeneities controlling transport and fate of pollutants in unconsolidated sand and gravel aquifers: Final report		5. FUNDING NUMBERS G AFOSR-91-0298 AFOSR-IR-95-0339		
6. AUTHOR(S) C. D. McElwee and J. J. Butler, Jr.				
7. PERFORMING ORGANIZATION NAME(S) AND ADDRESS(ES) Kansas Geological Survey The University of Kansas 1930 Constant Avenue Lawrence, KS		8. PERFORMING ORGANIZATION REPORT NUMBER KGS OFR 95-16		
9. SPONSORING/MONITORING AGENCY NAME(S) AND ADDRESS(ES) AFOSR/NE Building 410 Bolling AFB DC 20332-6448 NA		10. SPONSORING/MONITORING AGENCY REPORT NUMBER AFOSR- 91-0298		
11. SUPPLEMENTARY NOTES				
12a. DISTRIBUTION / AVAILABILITY STATEMENT Available from Publication Office of Kansas Geological Survey Approved for public release, distribution unlimited			12b. DISTRIBUTION CODE OFR 95-16	
13. ABSTRACT (Maximum 200 words) <p>The purpose of this project was to evaluate promising methods for characterization of heterogeneities in hydraulic conductivity and to assess which are best for the prediction of contaminant movement in shallow alluvium. Although work is still ongoing, this research has produced results of considerable practical significance. A major field and theoretical emphasis was on slug tests. A general model for slug tests in partially penetrating wells was developed, the viability of conventional slug-tests methods in homogeneous and heterogeneous formations was assessed, and a general model for slug tests in formations of high hydraulic conductivity was proposed. A major product was a series of practical guidelines for slug tests, which should considerably improve the quality of parameter estimates obtained using this technique. An important theoretical accomplishment of this project was the development of a new approach for the characterization of spatial variations in flow properties based on the principles of tomography. A major field accomplishment was the design and performance of a large-scale induced gradient tracer test. Although data analysis/interpretation is ongoing, this experiment has clearly yielded an extremely detailed data set describing tracer movement in heterogeneous alluvium. Additional field and laboratory work has produced an excellent data set characterizing parameter variations at the core scale. Five articles have been published on this work and additional articles are under preparation.</p> <p style="text-align: right;">DTIC QUALITY INSPECTED 5</p>				
14. SUBJECT TERMS Heterogeneities, alluvial aquifers, slug tests, site characterization, pollutant transport, pulse testing, tracer tests			15. NUMBER OF PAGES 594	
			16. PRICE CODE	
17. SECURITY CLASSIFICATION OF REPORT U	18. SECURITY CLASSIFICATION OF THIS PAGE U	19. SECURITY CLASSIFICATION OF ABSTRACT U	20. LIMITATION OF ABSTRACT	

CHARACTERIZATION OF HETEROGENEITIES CONTROLLING
TRANSPORT AND FATE OF POLLUTANTS
IN UNCONSOLIDATED SAND AND GRAVEL AQUIFERS:
FINAL REPORT

A research project of the
University Research Initiative
Research Initiation Program
U.S. Department of Defense

Carl D. McElwee and James J. Butler, Jr.
Kansas Geological Survey
The University of Kansas

with

Gwendolyn L. Macpherson
Department of Geology
The University of Kansas

Geoffrey C. Bohling, Richard D. Miller,
Christine M. Mennicke, Terrance Huettl,
Matthias Zenner, Zafar Hyder, Wenzhi Liu,
Michael Orcutt, Meredith L. Beilfuss, and Sashi Gonuguntla
Kansas Geological Survey
The University of Kansas

March, 1995

Accession For	
NTIS CRA&I	<input checked="checked" type="checkbox"/>
DTIC TAB	<input type="checkbox"/>
Unannounced	<input type="checkbox"/>
Justification _____	
By _____	
Distribution /	
Availability Codes	
Dist	Avail and/or Special
A-1	

ABSTRACT

A considerable body of research has shown that large-scale spatial variations (heterogeneities) in hydraulic conductivity play an important role in controlling the movement of a contaminant plume in the subsurface. Quantifying these heterogeneities, however, can be a very difficult task. If we are to improve our capabilities for predicting the fate and transport of pollutants in the subsurface, it is critical that we develop methodology that enables more accurate characterization of hydraulic conductivity variations. The purpose of this research project was to evaluate, both theoretically and experimentally, promising methodologies for the characterization of heterogeneities in hydraulic conductivity, and to attempt to assess which methods are best for the prediction of contaminant movement in shallow alluvium.

A major field and theoretical emphasis of the research was on slug tests, since this technique is probably the most commonly used field technique for the estimation of hydraulic conductivity at sites of suspected groundwater contamination. Several results of considerable practical significance were obtained through this work. Noteworthy accomplishments included the development and field verification of a general model for slug tests in partially penetrating wells in confined and unconfined anisotropic formations, a detailed assessment of the viability of conventional slug-test methods in homogeneous and heterogeneous formations, and the development and field verification of a general model for slug tests in formations of high hydraulic conductivity, which incorporates the effects of nonlinearities, inertia, viscosity, changing casing radii, and velocity distributions. A major product of this research was a series of practical guidelines for the design, performance, and analysis of slug tests, which should considerably improve the quality of parameter estimates obtained using this technique.

The slug test was not the only well testing methodology that was examined in this work. Theoretical investigations were also conducted to assess the potential of pulse testing (single pulses or a sinusoidally varying signal) and a steady-state inverse approach based on the principles of tomography. There were two major results of this work: 1) a sinusoidal signal generated at a central well can be transmitted significant distances, and 2) the sinusoidal signal can be analyzed for amplitude and phase to yield some useful information about heterogeneities (in particular the location of fairly discrete boundaries). Although the research is still in its early stages, the hydraulic tomography technique appears to hold considerable promise for the characterization of spatial variations in hydraulic conductivity.

A major focus of the latter portions of this research was the design, preparation, and performance of a large-scale induced gradient tracer test using a conservative

bromide tracer. This work involved a very large amount of field and laboratory effort. Noteworthy aspects of this work included the construction, installation, and development of 24 multilevel samplers (17 levels per sampler); laboratory analysis of approximately 6000 water samples collected during the 32 day tracer test, and preliminary assessment of the analyzed data using a semianalytical solution for tracer movement in a convergent flow field. Although the data assessment and interpretation is ongoing, this tracer test has clearly yielded one of the most detailed data sets describing tracer movement in heterogeneous alluvium. In addition, the network of multilevel sampling wells that has been created as part of this project will serve as an excellent resource for future studies of tracer movement in heterogeneous alluvium.

Throughout this research, a significant amount of work was directed at increasing our knowledge of the subsurface at the Geohydrologic Experimental and Monitoring Site (GEMS), the field site for this research. This included continued drilling and core sampling activities at GEMS; continued laboratory analysis of the cores obtained with the bladder sampler; a continuing study of the aqueous geochemistry of the alluvium and underlying bedrock at GEMS; wireline logging analysis; experimentation with a new single-well tracer test method that involves using a wireline logging system and an electrically conductive tracer to delineate vertical variations in hydraulic conductivity and porosity; and a high resolution seismic survey. These characterization efforts, which continued throughout this project, were directed towards the development of a detailed picture of the subsurface at GEMS, so that we could better assess the results of the hydraulic and tracer tests that were performed as part of this research. One noteworthy product of this characterization effort was the development of a large data set describing spatial variations in hydraulic conductivity, porosity, and various grain-size parameters at the scale of a small core. This data set should prove to be a very useful tool in further interpretation of the results of the induced gradient tracer test.

The research team for this project was composed of professional staff from the Kansas Geological Survey (KGS) and the Department of Geology of the University of Kansas. One indication of the level of activity of this research team is the five peer-reviewed publications concerning this research that were published or accepted during this grant period. Additional manuscripts are currently in review or under preparation. Three graduate students and one KGS staff member are using aspects of this project for their thesis research. Additional graduate students are benefitting from this project as a result of the establishment of a computer laboratory for graduate students in hydrogeology and the incorporation of material from this work into courses at the University of Kansas taught by members of the research team.

Acknowledgment

This research was sponsored in part by the Air Force Office of Scientific Research, Air Force Systems Command, USAF, under grant number AFOSR 91-0298. The views and conclusions contained in this document are those of the authors and should not be interpreted as necessarily representing the official policies, either expressed or implied, of the Air Force Office of Scientific Research or of the U.S. Government. The U.S. Government is authorized to reproduce and distribute reprints for Governmental purposes notwithstanding any copyright notation thereon.

TABLE OF CONTENTS*

I. INTRODUCTION

- A. Research Objectives
- B. Brief Outline of Report

II. THEORETICAL INVESTIGATIONS OF WELL TESTS

IN HETEROGENEOUS MEDIA

- A. A Continuous-in-Time Numerical Model for the Analysis of Well Tests in Three-Dimensional Nonuniform Aquifers
- B. Improvements to SUPRPUMP
- C. Sensitivity Analysis of Slug tests
- D. Slug tests in the Presence of a Well Skin
- E. Slug Tests in Partially Penetrating Wells
- F. The Use of Slug Tests to Describe Vertical Variations in Hydraulic Conductivity
- G. Hydraulic Tomography
- H. Pulse-Testing in Heterogeneous Formations
- I. Numerical Simulation of Induced Gradient Tracer Tests

III. FIELD INVESTIGATIONS OF MULTILEVEL SLUG TESTS

- A. KGS Multilevel Slug-Test System
- B. Multilevel Slug Tests at GEMS
- C. Slug Tests With Observation Wells
- D. A General Nonlinear Model for Analysis of Slug-Test Data
- E. Improving the Reliability of Parameter Estimates Obtained From Slug Tests

IV. SITE CHARACTERIZATION ACTIVITIES

- A. Drilling and Core Sampling Activities
- B. Laboratory Activities
- C. Aqueous Geochemistry at GEMS
- D. Analysis of GEMS Tracer Test Data
- E. GEMS Slug-Test Survey
- F. Pumping Test of Bedrock Well
- G. Wireline Logging Activities-Gems Natural Gamma and Induction Log Survey
- H. An Evaluation of a Borehole Induction Single-Well Tracer Test to Characterize the Distribution of Hydraulic Properties in an Alluvial Aquifer
- I. High-Resolution Seismic Reflection Study

V. CONSTRUCTION PROJECTS AND EQUIPMENT PURCHASES

VI. PERSONNEL AND PRODUCTIVITY ISSUES

- A. Published and Planned Papers
- B. List of Participating Personnel
- C. Interactions With Other Research Groups
- D. Teaching Activities

VII. SUMMARY OF PROJECT RESEARCH AND OUTLOOK FOR FUTURE RESEARCH

- A. Summary of Project Research
- B. Outlook for Future Research

VIII. REFERENCES

IX. APPENDICES

- A. Sensitivity Analysis of Slug tests: Part 1, the slugged well
- B. Sensitivity Analysis of Slug tests: Part 2, Observation wells
- C. Slug Tests in Partially Penetrating Wells
- D. The Use of Slug Tests to Describe Vertical Variations in Hydraulic Conductivity
- E. Improving the Reliability of Parameter Estimates Obtained From Slug Tests

* - Note that pages are numbered according to section and subsection.

I. INTRODUCTION

A. RESEARCH OBJECTIVES

The accurate prediction of the transport and fate of pollutants in aquifers is one of the most difficult and pressing problems in hydrogeology today. Physical, chemical, and microbial processes all play major roles in controlling contaminant movement in the subsurface. Before we can begin to understand the influence of the chemical and biological side of this problem, however, we must fully understand the role of physical processes and, specifically, the influence of the physical hydrogeological properties. Many researchers now recognize (e.g., Molz et al., 1989) that if we are to improve our predictive capabilities for subsurface transport, we must first improve our capabilities for measuring and describing conditions in the subsurface. That is the focus of the research described in this report. The specific objective of this research is to assess the potential of advanced well-testing technology for providing more accurate estimates of spatial variations in the physical properties that control contaminant plume movement in saturated porous media. Although effective porosity is clearly an important consideration, the major emphasis of this work is on characterizing spatial variations (heterogeneities) in hydraulic conductivity.

Ideally, heterogeneities in hydraulic conductivity must be studied and characterized at several different scales in order to understand their influence on the movement of a contaminant plume. Although theoretical modeling work is an important element of any study of the influence of spatial variations in hydraulic conductivity on contaminant movement, a rigorous study of this subject must have a major field component. A field site at which researchers at the University of Kansas can pursue work on the effects of heterogeneities in flow properties on subsurface transport has been set up as part of this research. The specific site of the field effort is the Geohydrologic Experimental and Monitoring Site (GEMS), which is located just north of Lawrence, Kansas on land owned by the University of Kansas Endowment Association. Figure 1 is a map showing the location of GEMS and some of the major features at the site. GEMS overlies approximately 70 feet (21.3 m) of Kansas River valley alluvium. These recent unconsolidated sediments overlie and are adjacent to materials of Pleistocene and Pennsylvanian age. A cross-sectional view of the subsurface at one of the well nests at GEMS is shown in Figure 2. The alluvial facies assemblage at this site consists of approximately 35 feet (10.7 m) of clay and silt overlying 35 feet (10.7 m) of sand and gravel. The stratigraphy is a complex system of stream-channel sand and overbank deposits. The general nature of the stratigraphy would lead one to expect that a

considerable degree of lateral and vertical heterogeneity in hydraulic conductivity would be found in the subsurface at GEMS. Although analyses of sampled cores do indicate considerable variability in hydraulic conductivity within the sand and gravel interval, it is not yet clear how the variability at the small scale of a core translates into variability at larger scales.

The major component of our activities during the final year of the research was directed toward the design, preparation, and performance of an induced-gradient tracer test using a conservative bromide tracer. The preparation and design activities included the construction (section V) of twenty four multilevel sampling wells (17 sampling ports per well), a theoretical investigation of the possible designs for the tracer-test monitoring well array (section II.I), and an intensive field effort to install the multilevel sampling wells (section IV.A). Preparation for and execution of the test occupied the majority of 1994. The tracer test began October 7, 1994 and continued until November 10, 1994, during which time almost 6000 water samples were collected and analyzed (section IV.B). Preliminary analysis of the data has been completed (section IV.D) and has given us the most detailed picture of subsurface hydraulic conductivity to date. This data set represents a valuable resource, containing a wealth of information that has yet to be fully explored. Further processing of the bromide concentration data and the performance of additional tracer tests (both in the single well and dipole formats, forward and reversed) to look at reproducibility of these results and to extend the work to nonconservative tracers are planned future activities.

Throughout the grant period a major focus of the work has been on the use of slug tests to describe spatial variations in hydraulic conductivity. A theoretical and field examination of the potential of multilevel slug tests for providing detailed information about conductivity variations in the vertical was the main emphasis during the early stages of the research. The analysis of response data from slug tests at GEMS turned out to be considerably more challenging than expected. It is clear from our work that conventional methodology for the analysis of slug-test data is not adequate when dealing with very high conductivity media, wells that are only partially screened across an anisotropic formation, wells with disturbed zones created by drilling or development activities, and layered media. Since the slug test has become the most common technique for estimation of hydraulic conductivity at sites of groundwater contamination, we expended much more effort on this phase of the project than was originally anticipated. However, this research has produced a number of very interesting results of practical significance, so we feel that it has been a profitable redirection of effort. Probably the result of most practical significance has been the definition of a series of guidelines for

the design, performance, and analysis of slug tests that should considerably improve the quality of parameter estimates obtained using this technique.

As a result of the redirection of our efforts (increased emphasis on slug-test research), the work on pulse tests has not progressed as far as originally expected. In the second year, we started work on pulse tests in three areas: 1) multiwell slug tests, where the excitation consists of a single pulse (slug); 2) hydraulic tomography in a steady-state flow field; and 3) an analytical solution for propagation of sinusoidal signals in heterogeneous formations. In the latter part of the grant period, we continued a theoretical investigation of the use of pulse tests in heterogeneous aquifers. Both analytical and numerical approaches were explored in an attempt to assess whether discrete zones in heterogeneous formations could be characterized with pulsing (sinusoidally varying) signals. We have performed preliminary field work using sinusoidally varying signals at GEMS and have found that the signal propagation amplitude does seem to be a good tool for looking at heterogeneity. The initial results seem promising and indicate further work is needed.

Throughout the grant period a considerable amount of work has been directed at increasing our knowledge of the subsurface at GEMS. This effort involved additional slug and pumping tests, analyses of the aqueous geochemistry, continued drilling and sampling of the alluvium, laboratory analyses of sampled cores, wireline logging surveys, two detailed seismic surveys, and experimentation with a new single-well tracer test method that involves using a wireline logging system and an electrically conductive tracer to delineate vertical variations in hydraulic conductivity and porosity. These characterization efforts were directed at providing the detailed information that would allow us to better assess the quality of the information provided by the various well-testing approaches evaluated in this work. In addition, this information was of value to help us design the bromide tracer test which was performed in the latter period of this project. The ultimate goal of these characterization efforts is to describe the site in so much detail that it effectively becomes an underground laboratory at which new technology can be evaluated.

B. BRIEF OUTLINE OF REPORT

The remainder of this report is divided into six major sections, each of which is essentially a self-contained unit. Pages, figures, and equations are labeled by section and, when warranted, by subsection for the convenience of the reader. Note that a number of the subsections of this report are very brief summaries of articles that have been or will

shortly be published in professional journals. The complete texts of these articles are given in Appendices A-E.

Section II describes theoretical work directed at developing a better understanding of the type of information that can be obtained from a variety of field techniques applied in heterogeneous media. A continuous-in-time numerical model, which has proven very useful for the analysis of well-test data, is introduced in the first subsection. Some improvements that were made to SUPRPUMP, a well-test analysis package developed at the Kansas Geological Survey and used throughout this work to perform analyses of hydraulic tests, are then described in subsection two. The third subsection performs a sensitivity analysis for slug tests. The fourth subsection presents some observations on the effective transmissivity determined from a slug test in the presence of a well skin. The next (fifth) subsection deals with slug tests in partially penetrating wells. The sixth subsection looks in detail at the use of slug tests to delineate horizontal layering in aquifers. A theoretical examination of hydraulic tomography is then considered in the seventh subsection. This is followed by an examination of the use of a sinusoidally varying signal to investigate simple aquifer heterogeneities in subsection eight. The final (ninth) subsection summarizes our activities directed at the design of a monitoring well array for the induced-gradient bromide tracer test.

Section III primarily describes further field investigations using slug tests. The first subsection describes field investigations with multilevel slug tests. A prototype multilevel slug test system, which has been developed at the KGS, is described and its use at GEMS is detailed. An extensive series of field experiments that were undertaken in order to understand the causes of anomalous behavior observed in slug-test data from wells in the sand and gravel section at GEMS are then described in the second subsection. The third subsection deals with the use of observation wells with slug tests (multiwell slug tests). The results of a program of field testing at GEMS and a subsequent theoretical analysis motivated by those results are described. In the fourth subsection, a general nonlinear model for slug tests that accounts for the major mechanisms thought to be affecting the GEMS slug-test data is presented. The application of this model to several sets of data from slug tests at GEMS demonstrates the potential of the approach. The last subsection summarizes many of the conclusions of our field and theoretical research on slug tests. The main goal of this subsection is to present a series of practical field guidelines that should help improve the reliability of parameter estimates obtained from slug tests.

Section IV primarily describes activities directed at increasing our knowledge of the subsurface at GEMS. The first subsection gives a description of the drilling and

sampling activities that have occurred over the grant period at GEMS. Work in the KGS core measurement laboratory is discussed in subsection two along with laboratory work associated with the bromide tracer test. A summary of the results of the aqueous geochemistry study at GEMS are presented in the third subsection. The preliminary analysis of the GEMS bromide tracer test data is given in the fourth subsection. A program of slug tests carried out in the wells screened in the sand and gravel section is described in the fifth subsection. A preliminary analysis of a pumping test performed in a well in the bedrock underlying the alluvial section at GEMS is then reported in subsection six. The seventh subsection gives a brief report on wireline logging activities at GEMS. The eighth subsection presents a report on experiments with a new single-well tracer test method using a wireline logging system and an electrically conductive tracer to delineate vertical variations in hydraulic conductivity and effective porosity. The last (ninth) subsection concludes with a detailed description of the shallow seismic surveys that were undertaken at GEMS.

Section V describes new equipment that was built or purchased during the grant period of this project and how it enhanced various aspects of the research.

Section VI describes the personnel of the research team that has been organized to pursue this work, and lists relevant publications of the team over the grant period. The section concludes with a discussion of the interactions with other research groups and teaching activities that have occurred during the last year.

Section VII summarizes the research of this project and briefly discusses the outlook for future research, building on the currently concluding project.

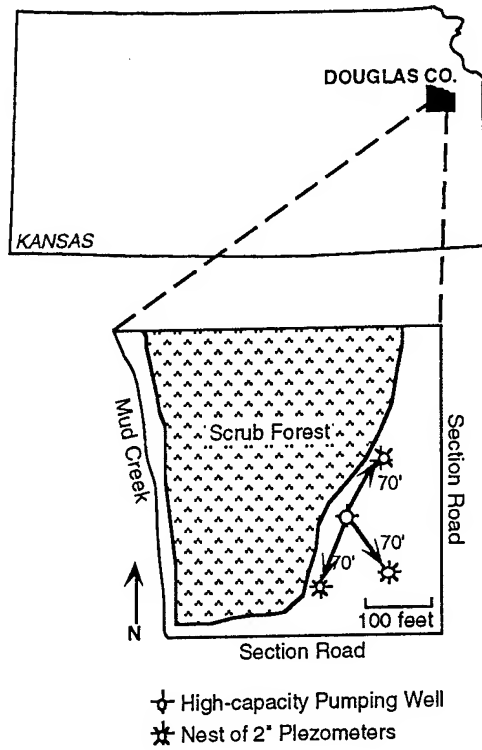


Figure 1 - Location map for the Geohydrologic Experimental and Monitoring Site (GEMS).

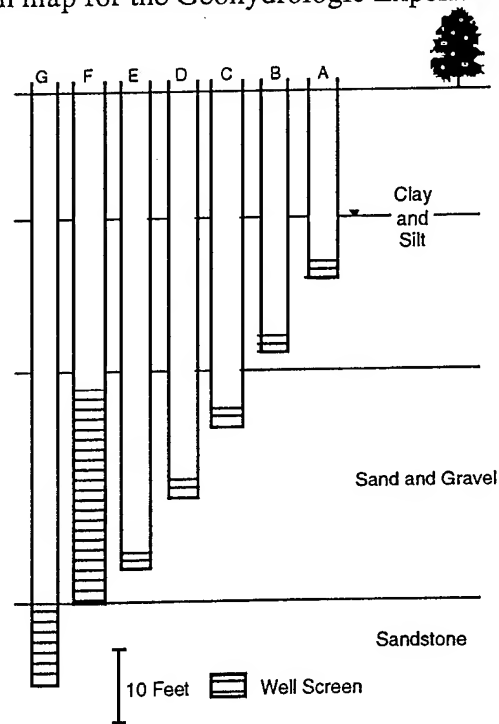


Figure 2. A typical well nest cross-section

II. THEORETICAL INVESTIGATIONS OF WELL TESTS IN HETEROGENEOUS MEDIA

A. A CONTINUOUS-IN-TIME NUMERICAL MODEL FOR THE ANALYSIS OF WELL TESTS IN THREE-DIMENSIONAL NONUNIFORM AQUIFERS

Introduction

Analytical solutions for drawdown in response to a pressure disturbance induced at a central well are the basis of conventional well-test analysis methodology. For the most part, these solutions consider hydraulic behavior in an idealized aquifer in which flow properties are invariant in space. Aquifers in nature, however, are characterized by a considerable degree of spatial variations (heterogeneities) in flow properties. Not surprisingly, analyses based on solutions to flow in idealized uniform systems may be of limited use in assessing heterogeneities in the vicinity of the stressed well. A better understanding of these near-well heterogeneities, however, is critical if we are to improve our ability to predict the fate and transport of pollutants in the subsurface. A component of the research in the first year of this project was therefore directed at further exploration of a numerical modeling approach that would allow the actual complexity of the geological system to be incorporated into the analysis of well-test data. This approach could then serve as a tool for both the development of insight into the role of heterogeneity in controlling well-test responses and the future analysis of well tests and tracer tests.

A general model for well-test analysis must allow the actual complexity of the geologic formation to be represented in the full three dimensions. Analytical solutions for well tests in simplified three-dimensional settings have been developed by a number of authors using traditional integral transform techniques (e.g., Russell and Prats, 1962; Papadopoulos, 1966; Prijambodo et al., 1985; Hayashi et al., 1987; Raghavan, 1989; McElwee et al., 1990). Because of the complexities introduced by the vertical component of flow at the stressed well and within the aquifer itself, however, an exact analytical solution has yet to be derived for the general case of well testing in a three-dimensional nonuniform system. Given the limitations of the traditional analytical solution methodology, a new approach for the analysis of well-test data is considered in this work. The approach considered here is based on the idea of combining the spatial discretization used in a conventional numerical model with the Laplace transform in time used in conventional analytical models. A solution to this hybrid numerical model is obtained in Laplace space using standard techniques of matrix algebra. A set of solutions in Laplace

space is then back transformed to real space, producing a solution in real space that can be formulated in a continuous manner over a range of times. In the following sections, the theoretical basis of this approach is explored and its implementation in this work is described.

A Time-continuous Numerical Method

Approximate numerical methods such as the finite difference (FD) or finite element (FE) approaches have been widely used in groundwater studies for applications where analytical solutions are not feasible. These numerical approaches involve both spatial and temporal discretization of the governing equations, with the quality of the approximation dependent on the discretization strategy. The size of the time increment is varied during the course of a simulation in order to improve computational efficiency. However, selection of the proper time increment may present difficulties when model output is required at particular points in time. In groundwater flow and transport applications, problems often arise with conventional numerical approaches when a comparison between model output and measured data is desired for the specific times at which the measurements were made. This is especially true when working with data from hydraulic or tracer tests, where the density of the data in time may be quite large.

In order to avoid some of the problems associated with temporal discretization, a hybrid method, which combines spatial discretization with a Laplace transform in time, is employed here. The spatial discretization scheme is the same as that in a conventional finite-difference model. The resultant spatially discretized system of algebraic equations in complex space is solved using complex arithmetic for the matrix inversion. The Laplace-space solution is then inverted back into real space using an appropriate numerical inversion scheme. This procedure yields a solution that is continuous over a range of times, with the only approximation in the temporal domain being that introduced by the numerical inversion scheme.

This time-continuous method has been employed by a number of workers during the past three decades (e.g., Gurtin, 1965; Javandel and Witherspoon, 1968; Chen and Chen, 1988; Sudicky, 1989; Moridis and Reddell, 1991; Sudicky and McLaren, 1992). The most difficult problem associated with this method has been the inversion of the Laplace-space solution back into real space. Various methods for approximate numerical inversion, all of which involve the evaluation and summation of the transform-space function, have been developed by a number of authors (e.g., Stehfest, 1970; Talbot, 1979; Crump, 1976). One focus of the research of this project is the development of a more efficient inversion algorithm. As noted by Sudicky (1989), De Hoog et al. (1982)

propose a quotient difference algorithm for increasing the rate of convergence of the summation-series approach of Crump (1976). This quotient-difference algorithm has been shown to have a significant computational advantage over other algorithms in decreasing the computations required for the analysis of well-test data (Liu and Butler, 1991). The computational savings are such that this method appears to hold considerable promise for use as a practical tool for analysis of well tests in fully three-dimensional systems. The following section describes a discrete-in-space, continuous-in-time model that has been developed for the analysis of well tests in systems where conventional analytical approaches are not viable.

The Three-Dimensional Finite Difference Time-continuous Model (3DFDTC)

The time-continuous approach can be used only if Laplace transforms exist for the governing equation together with all boundary and initial conditions. Thus, the approach described here only strictly applies to confined flow systems. The cylindrical-coordinate form of the governing equation for three-dimensional flow in a confined system is

$$\frac{1}{r} \frac{\partial}{\partial r} (r K_r \frac{\partial h}{\partial r}) + \frac{1}{r^2} \frac{\partial}{\partial \theta} (K_\theta \frac{\partial h}{\partial \theta}) + \frac{\partial}{\partial z} (K_z \frac{\partial h}{\partial z}) = S_s \frac{\partial h}{\partial t} \quad (1)$$

where

h = drawdown, [L];

S_s = specific yield, [1/L];

K_r , K_θ , K_z = hydraulic conductivity in the radial, angular, and vertical direction, respectively, [L/T];

t = time, [T];

r = radial distance, [L];

θ = angular position, in radians;

z = vertical depth from the top of the aquifer, [L].

For the case of a pumping test in a layered aquifer, the initial and boundary conditions are defined as

$$h(r, 0) = h_a, r < \infty \quad (2)$$

$$h(\infty, t) = h_a, t \geq 0 \quad (3)$$

$$2\pi \sum_{j=1}^J K_{rj} m_j \left(r \frac{\partial h}{\partial r} \right)_{r=r_w} = - \sum_{i=1}^{NP} q_i \square_i(t) \quad (4)$$

where

$$\square_i(t) = \text{box car function} = \begin{cases} 1, & \text{if } t_{1i} \leq t \leq t_{2i}, \quad i=1, 2, \dots, NP \\ 0, & \text{elsewhere} \end{cases}$$

h_a = initial head in the aquifer, [L];

NP = number of pumping periods;

t_{1i} = starting time for pumping period i, [T];

t_{2i} = ending time for pumping period i, [T];

r_w = radius of pumping well, [L];

q_i = pumpage for pumping period i, [L³/T];

J = total number of screened layers in the well bore;

K_{rj} = conductivity in radial direction for layer j;

m_j = thickness of layer j.

The application of the Laplace transformation to equations (1) and (4), in conjunction with (2), results in:

$$\frac{1}{r} \frac{\partial}{\partial r} \left(r K_r \frac{\partial h}{\partial r} \right) + \frac{1}{r^2} \frac{\partial}{\partial \theta} \left(K_\theta \frac{\partial h}{\partial \theta} \right) + \frac{\partial}{\partial z} \left(K_z \frac{\partial h}{\partial z} \right) = S_s (\bar{h}p - h_a) \quad (5)$$

$$2\pi \sum_{j=1}^J K_{rj} m_j \left(r \frac{\partial \bar{h}}{\partial r} \right)_{r=r_w} = - \sum_{i=1}^{NP} q_i \frac{e^{t_{1i}p} - e^{-t_{2i}p}}{p} \quad (6)$$

where

p = Laplace transform variable;

\bar{h} = head in Laplace space.

In order to improve the ease of radial discretization, the derivatives in the radial direction can be rewritten in a logarithmic form using the transformation $\bar{r} = \log_e \left(\frac{r}{r_w} \right)$.

This approach allows a discretization in the radial direction which increases exponentially when using $\Delta \bar{r}$. Thus, the form of equations (5) and (6) employed for the discretization is

$$\frac{1}{r^2} \frac{\partial}{\partial \bar{r}} \left(K_r \frac{\partial h}{\partial \bar{r}} \right) + \frac{1}{r^2} \frac{\partial}{\partial \theta} \left(K_\theta \frac{\partial h}{\partial \theta} \right) + \frac{\partial}{\partial z} \left(K_z \frac{\partial h}{\partial z} \right) = S_s (\bar{h}p - h_a) \quad (7)$$

$$2\pi \sum_{j=1}^J K_{rj} m_j \left(\frac{\partial h}{\partial r} \right)_{r=0} = - \sum_{i=1}^{NP} q_i \frac{e^{t_{1i}P} - e^{-t_{2i}P}}{P} \quad (8)$$

Unlike many analytical and numerical models, which assume the radius of the well to be infinitely small, the model developed here allows the influence of well bore storage to be taken into consideration. As noted by Papadopoulos and Cooper (1967), effects of well-bore storage on drawdown can be significant during early times when the majority of the water is being removed from storage inside the well bore. As time increases, the influence of well-bore storage will gradually diminish, eventually reaching a point at which the infinitely small well-bore assumption is viable.

The implementation of the well-bore storage option in the three-dimensional finite difference, time-continuous model (3DFDTC) is based on earlier work of Settari and Aziz (1974), Rushton and Chan (1977), and Butler (1986). As described by Butler (1986), the approach is based on rewriting the classical pipe flow equation (Vennard and Street, 1975) in a Darcy Law-like formulation and defining a term (involving the friction factor, the cross-sectional area of the well bore, and distance along the well bore) analogous to hydraulic conductivity. This approach allows flow inside the well bore to be governed by the porous media flow equation given by (7). Note that the initial implementation of this approach for this project produces an approximation of well-bore behavior that is equivalent to the hydrostatic head assumption employed in most analytical representations of the well bore (e.g., Papadopoulos and Cooper, 1967; Cooper et al., 1967).

In the three-dimensional representation employed here, the portion of the well bore passing through the modelled unit consists of several grid cells in the vertical. The storage coefficient is assumed to be one for the top cell of the well bore, while the storage coefficients for the remaining nodes in the well bore are set equal to the compressibility of water or zero (assuming water is incompressible). Since the radial-discretization scheme employed in the model uses logarithmic increments, the minimum radial location (r_{\min}) of the first radial node inside the well bore must be larger than zero (i.e. $0.0 < r_{\min} < r_w$). This produces a well bore in the shape of an annular ring rather than a circle. The storage coefficient of the well-bore cells must therefore be adjusted

(by a factor of $\frac{r_w^2}{r_w^2 - r_{\min}^2}$) to account for the decrease in well-bore cross-sectional area

produced by the annular ring representation of the well bore. In addition, the traditional

boundary condition at the well bore (8), which is based on the definition of radial flow along the well screen, is not used in this approach. Instead, a boundary condition at the top node of the well bore, based on the definition of the total flow out of the screened portion of the well, is employed. This flow boundary condition is written as

$$\pi K_{rJ} m_J \left(\frac{\partial h}{\partial r} \right)_{\bar{r} = \log_e \left(\frac{r_{min}}{r_w} \right)} = - \sum_{i=1}^{NP} q_i \frac{e^{-t_{1i}p} - e^{-t_{2i}p}}{p} \quad (9)$$

where m_J is the thickness of the top grid cell. Note that no-flow conditions in the radial direction are assumed at $r=r_{min}$ for the remaining nodes in the well bore. The use of (9) as a boundary condition makes this approach very useful for analyzing well tests in layered systems where the tested well may be screened in more than one layer (as in (4) with $J > 1$). Instead of having to define in advance the amount of water withdrawn from each layer, the model will implicitly calculate the flow out of each layer given the total flow out of the system defined by (9).

Since the representation of the well bore employed here is equivalent to the conventional hydrostatic head assumption, the hydraulic conductivity of the well bore must be defined such that the heads for all the nodes in the well bore are approximately equal. All three components of well-bore hydraulic conductivity must be at least five orders of magnitude larger than the aquifer conductivity in order to ensure negligible head loss along the well bore. In order to ensure that the majority of water will be drawn from the well bore at early times, the ratio of vertical well-bore hydraulic conductivity over its angular and radial counterparts must be large. An extensive set of experiments indicates that a ratio larger than 100 will ensure that all water will initially be drawn out of well-bore storage.

The 3DFDTC model is developed by applying a conventional central difference scheme to (7), which now represents conditions within both the aquifer and the well bore. After incorporating (9) and the Laplace transform of (3) into the finite difference scheme, the system of algebraic equations for 3DFDTC can be expressed in matrix form as

$$([A] + p[B]) [\bar{h}] = - [C] h_a + \sum_{i=1}^{NP} q_i \frac{e^{-t_{1i}p} - e^{-t_{2i}p}}{p} [D] \quad (10)$$

where A, B, C, and D are matrices of constant coefficients and \bar{h} is a vector of unknown heads. For the sake of conciseness, (10) is rewritten in the following form:

$$[G] [\bar{H}] = [W] \quad (11)$$

Both the left-hand side coefficient matrix G and the right-hand side matrix W of (11) involve the Laplace variable p , for which a value must be given before a solution in Laplace space can be obtained. The resultant solution in Laplace space can then be inverted back into real space using numerical inversion schemes such as those of Stehfest (1970) or Crump (1976). A detailed discussion of inversion algorithms with an emphasis on the method of Crump (1976) can be found in McElwee et al., 1992.

The Crump algorithm approximates the inversion of a Laplace space function by means of a Fourier series that involve both sine and cosine functions. This method has a smaller error than that of a similar method presented by Dubner and Abate (1968). If the value of h at node j is desired, h_j is found using the following equation developed by Crump [1976]:

$$h_j(t) \approx \frac{e^{p_0 t}}{T_{max}} \left\{ \frac{\bar{H}_j(p_0)}{2} + \sum_{k=1}^{2N+1} \left[\text{RE}(\bar{H}_j(p_k)) \cos\left(\frac{k\pi t}{T_{max}}\right) - \text{IM}(\bar{H}_j(p_k)) \sin\left(\frac{k\pi t}{T_{max}}\right) \right] \right\} \quad (12)$$

where

$\bar{H}_j(p_k)$ = solution from (11) at node j for $p = p_k$;

$2T_{max}$ = the period of the Fourier series approximating the inverse function on the interval $[0, 2T_{max}]$;

$\text{RE}(\bar{H})$ = real part of \bar{H} ;

$\text{IM}(\bar{H})$ = imaginary part of \bar{H} ;

Er = minimum relative error;

$p_k = p_0 + ik\pi/T_{max}$;

$p_0 = \mu - \ln(Er/2T_{max})$, the real part of p_k ;

μ = maximum real value of all the singularity points of the function in Laplace space;

$i = (-1)^{1/2}$.

Equation (12) shows that the time variable t appears only in the sine, cosine, and exponential functions. Since p_k is independent of time, we can perform the inversion

over a range of times based on one set of solutions of \bar{h} for one specific T_{\max} . The solution is thus continuous in time because once a set of \bar{h} values is calculated from (11), (12) will give the desired result at any time within the range of $[0, 2T_{\max}]$.

If the summation is performed as in (12), hundreds of terms (i.e. solutions of (11)) may be needed in order to obtain a solution that satisfies a given convergence criterion. Since the computational effort required for the calculation of each p-space solution of (11) is at least equal to that required for one time step in a conventional numerical model, considerable attention is paid to the convergence of the summation series given in (12). An algorithm developed by De Hoog et al. (1982) has been found to significantly accelerate the convergence of the summation series and has therefore been incorporated into the 3DFDTC model. The acceleration of the summation series is great enough that the continuous-in-time approach is often the most computationally efficient approach for the analysis of well tests in heterogeneous formations. A detailed explanation of the De Hoog algorithm is given in McElwee et al., 1992.

Discussion and Model Validation

The 3DFDTC model is considerably more flexible than its conventional analytical or numerical counterparts. Since no time-discretization scheme is employed, stability issues related to time-stepping scheme can be ignored and a solution can be obtained directly for any specific time. Boundary conditions can also be changed easily to adapt to different patterns of stress being placed on the test well. For example, by simply setting $q_i=0.0$ and changing h_i to H_0 in (10) for nodes located inside the well bore, 3DFDTC can be used to simulate a slug test with an initial head of H_0 . If necessary, partial penetration and well skin effects can be accounted for by specifying the vertical position of the well screen and the radius of the skin, respectively. Unequal spacing in both the angular and vertical direction is allowed in order to model spatial variations in flow properties. If there exists a symmetry in heads in either the angular or vertical direction, 3DFDTC will simulate only part of the aquifer system by assuming a no-flow condition along the plane of symmetry. Note also that 3DFDTC can be used in a one- or two-dimensional mode if heads can be assumed equal in the angular and/or vertical directions. In such cases, only one node should be used in the direction of equal heads.

In order to validate the implementation of the time-continuous approach and the well-bore approximation, 3DFDTC has been checked against many analytical solutions for both pumping and slug tests. In all cases, a comparison between the analytical results and those of 3DFDTC revealed very small differences. Three typical examples are chosen here to demonstrate the feasibility and viability of the 3DFDTC model.

The first example was designed to assess the viability of the well-bore approximation employed in the model. Drawdown produced by pumping at a constant rate from a well of finite radius in a uniform aquifer is simulated. In Figure II.A.1, the simulated results for drawdown within the pumping well are compared with the analytical results of Papadopoulos and Cooper (1967) for the same case. The results produced by the two approaches essentially fall on top of one another throughout the duration of the simulation. The small difference in the computed drawdown is attributed mainly to the error caused by the spatial discretization scheme employed in 3DFDTC. Further simulations have shown that by increasing the number of nodes in the radial direction, the difference between the analytical and 3DFDTC results will gradually disappear. Note that in addition to the two curves depicting well-bore storage effects, a third curve, depicting drawdown calculated by 3DFDTC when well-bore storage effects are not included, is plotted on Figure II.A.1 to illustrate the period when well-bore storage effects are important.

In the initial phases of this project, there was considerable concern about numerical problems that might accompany the well-bore approximation as a result of the dramatic change in hydraulic conductivities between the aquifer and the well bore that is required by the approach. The second example is thus chosen to illustrate the performance of 3DFDTC when adjacent hydraulic conductivities differ by many orders of magnitude. A slug test in a well surrounded by a low permeability well skin of finite radius was simulated in order to assess model performance when a permeability contrast of ten orders of magnitude is employed. The configuration consisted of three distinct zones of differing properties: a very high permeability well bore ($K=10^7$), a low permeability skin ($K=10^{-3}$), and an aquifer of moderate permeability ($K=1$). The well was assumed screened throughout the aquifer. Figure II.A.2 illustrates a comparison of the heads simulated by 3DFDTC with the results from the analytical solution of Moench and Hsieh (1985) for a slug test in a well with a skin of finite radius. The solid line in Figure II.A.2 depicts the head at the slugged well simulated by 3DFDTC, while the dashed line displays the results of the analytical solution. As with Figure II.A.1, the two lines essentially fall on top of one another. The differences between the two curves are again mainly due to the error introduced by spatial discretization, since only a total of six nodes are placed inside the well bore and the skin.

The last example is selected to illustrate model performance when there is a strong component of vertical flow, such as might occur in multilevel slug tests. A slug test is simulated in a well that is screened for only a portion of the aquifer thickness. The aquifer is assumed to be homogeneous and isotropic with respect to flow properties.

Figure II.A.3 displays a comparison of the normalized head (H/H_0) simulated by 3DFDTC with the results of the analytical solution of McElwee et al. (1990) for a slug test in a well partially penetrating the aquifer. The solid line in Figure II.A.3 depicts the head at the slugged well simulated by 3DFDTC, while the dashed line displays the results of the analytical solution. The inset provides details of the specific configuration employed for this example. As with the previous examples, 3DFDTC yields results that are essentially indistinguishable from those of the analytical solution.

Given the closeness of the match between the simulation results from 3DFDTC and those from the analytical solutions, it is clear that 3DFDTC can be a very useful tool for the design and analysis of well tests performed under conditions not readily represented by conventional analytical approaches. Therefore, in Section II.F of this report, 3DFDTC is used to examine the viability of multilevel slug tests in layered systems. The purpose of this numerical examination of multilevel slug tests in layered systems is to gain insight into how such tests might be designed in order to get more accurate information concerning vertical variations in the flow properties of a unit.

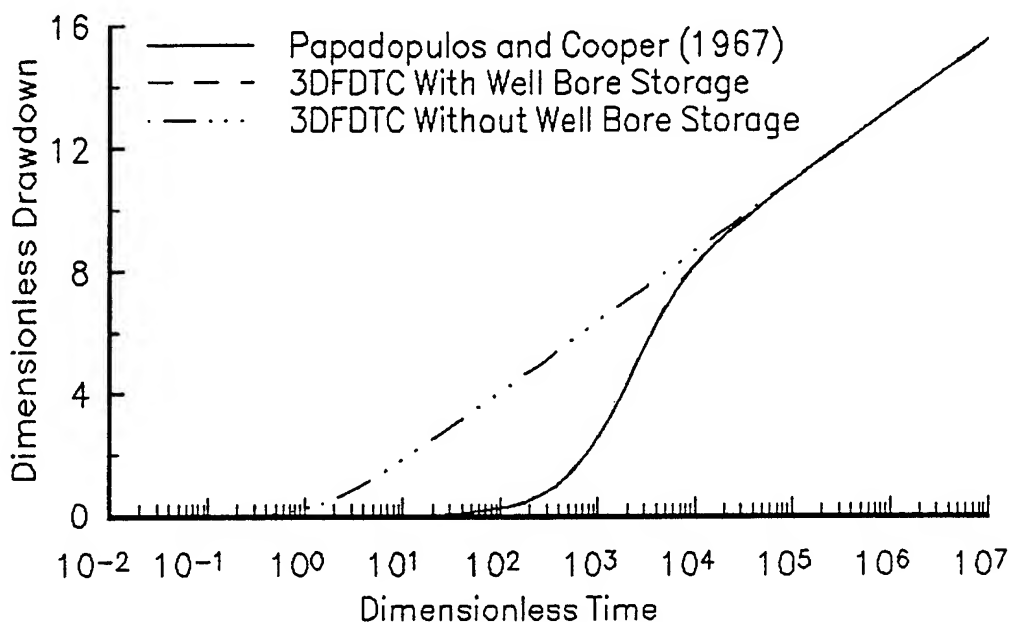


Figure II.A.1 Dimensionless drawdown ($4\pi T_s/Q$) versus time ($4Tt/Sr^2$) plot comparing the Papadopoulos and Cooper (1967) solution with 3DFDTC results. (Observation well is located at $r=4.6$; $r_w=0.167$, $T=1$ and $S=10^{-5}$; 3DFDTC discretization: 3 radial nodes inside well bore, 39 nodes in the radial from r_w to 37364.15 meters and 5 nodes in vertical).

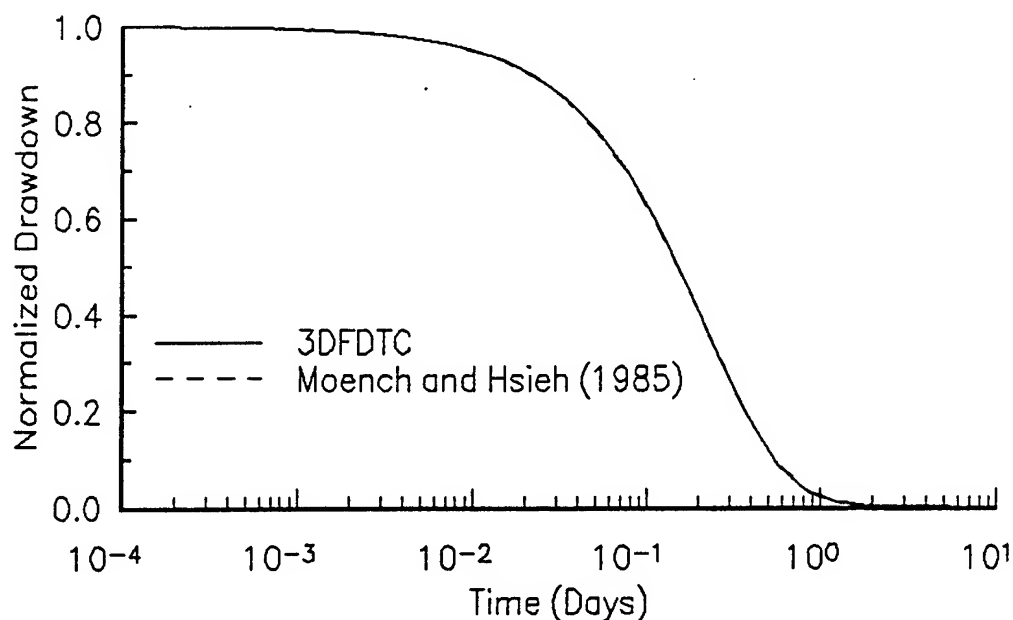


Figure II.A.2 Normalized drawdown (H/H_0) versus time plot comparing Moench and Hsieh (1985) solution with 3DFDTC results. ($r_w=0.167$, $r_{skin}=0.333$, $T_{skin}=10^{-3}$, $S_{skin}=10^{-3}$, $T_{aquifer}=1$, $S_{aquifer}=10^{-5}$; discretization as in Figure II.A.1 except that 3 of the 39 radial nodes are placed between r_w and r_{skin}).

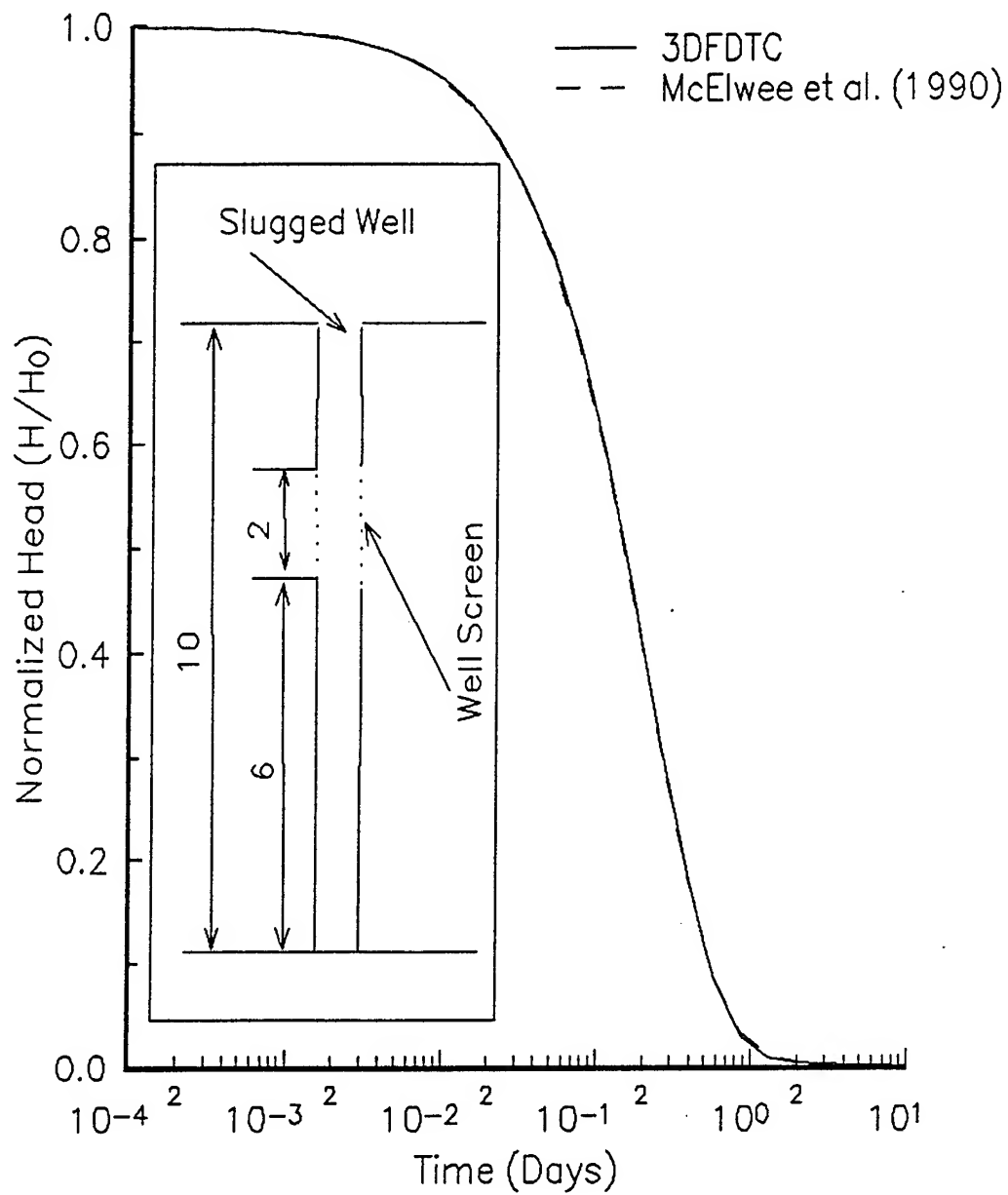


Figure II.A.3 Normalized head (H/H_0) versus time plot comparing McElwee et al. (1990) solution with 3DFDTC results. ($r_w=0.167$, $K=0.1$, $S_s=10^{-6}$; discretization as in Figure II.A.1).

B. IMPROVEMENTS TO SUPRPUMP

Work on improving the well test analysis program SUPRPUMP (Bohling et al., 1990) continued throughout the grant period. In the March-April 1992 issue of *Ground Water*, a paper on the program (Bohling and McElwee, 1992) was published. The development of this program has been an ongoing project for several years. This analysis program has been a very important part of the research effort since much of the field data taken for this project has been analyzed by SUPRPUMP.

During the grant period several well functions were added to the program, including radially-dependent versions of two important slug test functions, that for a finite radius well fully penetrating a confined aquifer (Cooper et al, 1967) and that for a finite radius well with a finite radius well skin (Moench and Hsieh, 1985). These two functions allow an investigator to analyze well test responses not only in the slugged well, but also in nearby observation wells. This greatly enhances the ability to define the storage coefficient of the aquifer (McElwee et al., 1995). Other functions developed and added to the program included a version of the Hvorslev function incorporating a more general expression for the shape factor (and thus a wider range of well geometries) and a nonlinear version of the Hvorslev function accounting for head dependence and frictional losses across the well screen (see section III.D).

Other work on the program included the development of revisions which allow for easier addition of new well functions to the existing library and also enhance program maintainability and portability. The latter modifications include the development of a batch (non-interactive) version of the code. The batch mode version of SUPRPUMP was developed for the sake of greater portability, improved computational reliability, and greater ease in analyzing large data sets or large numbers of closely related well tests. The interactive interface to SUPRPUMP can become tedious to work with when one is analyzing a large number of similar tests, with only slight variations in input specifications. The batch mode program, which reads data and input parameters from ASCII input files, allows the same data set to be analyzed in a number of different ways in one program run. In addition, simple editing changes allow different data sets to be analyzed using the same input parameters, without having to retype repeated information every time the program is run. The batch mode program also uses a more reliable parameter estimation algorithm (Levenberg-Marquardt) than the interactive version. Several new features that have been included in the batch mode program are the ability to 'fit' an unknown boundary (estimate its location), the ability to perform weighted regression (with more reliable data sources being weighted more heavily than less reliable

sources), and the performance of a test for systematic lack of model fit (aiding in the selection of the best of a number of candidate models).

Future work could involve developing a Microsoft Windows interface to the batch mode version of SUPRPUMP. This interactive interface would help the user manage data, set up the input files for and spawn the batch mode program, and provide a 'back-end' interpreter for the output files, including graphical display of results.

C. SENSITIVITY ANALYSIS OF SLUG TESTS

The use of slug tests for site characterization is a common practice in hydrogeology due to the logistical and financial advantage of the procedure. Tests can be performed quickly and inexpensively with a minimum of equipment. Even though slug tests are commonly used and relatively easy to perform, the tests should be planned carefully in order to ensure that the maximum amount of information is obtained. Although a great deal of information about the aquifer hydraulic parameters in the vicinity of the stressed well is contained in slug test data, it is unclear if current practices are actually yielding accurate estimates of those parameters. At the Kansas Geological Survey, we have instituted a program to study heterogeneity in alluvial aquifers. Slug tests are an integral part of that program, so we have undertaken a detailed study of the information provided by slug tests in a variety of situations. Appendices A and B present the first two of a planned series of professional journal articles presenting our results. In appendix A we employ the CBP model (Cooper et al., 1967) for slug tests to demonstrate the use of sensitivity analysis (McElwee, 1987) for designing more effective slug tests. The objective of appendix B is to show that the use of one or more observation wells can vastly improve the parameter estimates, particularly the estimate for storage. The tools we use for this study are sensitivity analysis (McElwee, 1987) and an automated well test analysis package, SUPRPUMP (Bohling and McElwee, 1992), developed at the Kansas Geological Survey.

D. SLUG TESTS IN THE PRESENCE OF A WELL SKIN

Introduction

Slug tests are frequently used to characterize the transmissivity of an aquifer. However, in the presence of heterogeneity it is uncertain how the slug test is averaging the aquifer properties. In this section, we look at the effect of one kind of heterogeneity: a well skin. A well skin can be created by the process of drilling and development of the well, and may have a transmissivity value (T_1) greater or less than that of the aquifer transmissivity (T_2). We have investigated this problem using sensitivity analysis and an automated well-test analysis program we have developed. The sensitivity coefficients for T_1 and T_2 are similar in shape but shifted slightly in time. Thus, it is difficult to obtain good estimates for both T_1 and T_2 due to correlation. The maximum amplitude of the sensitivities is inversely proportional to transmissivity. Varying the skin radius shifts the head response curve along the dimensionless time axis. When fitted to the Cooper-Bredehoeft-Papadopoulos (C-B-P) model, the data show a systematic lack of fit, however, it is not large. The effective transmissivity obtained from the C-B-P fit is a weighted average of T_1 and T_2 and can be predicted with a simple empirical formula. The effective transmissivity is highly weighted by the smallest transmissivity and is a weak function of the skin radius. Addition of observation wells makes little difference in the C-B-P fit results. The value of the effective transmissivity does not depend on the initial slug height. If one attempts a three parameter fit using T_1 , T_2 , and the skin radius (R_s), it is found that T_1 and R_s are usually very highly correlated leading to a nonunique situation. If R_s is assumed known and one tries to solve for T_1 and T_2 , the situation is better, but the fit is still difficult and depends on the initial estimates and the quality of the data. Having copious amounts of accurate data and multiple observation wells is the best situation for obtaining an accurate fit.

Model for Slug Tests With Skin

The physical situation is shown schematically in Figure 1. Mathematically the model is given by the following equations (Moench and Hsieh, 1985):

$$\frac{\partial^2 H_1}{\partial r^2} + \frac{1}{r} \frac{\partial H_1}{\partial r} = \frac{S_1}{T_1} \frac{\partial H_1}{\partial t} \quad r_w \leq r \leq R_s \quad (\text{II.D.1})$$

$$\frac{\partial^2 H_2}{\partial r^2} + \frac{1}{r} \frac{\partial H_2}{\partial r} = \frac{S_2}{T_2} \frac{\partial H_2}{\partial t} \quad r \geq R_s \quad (\text{II.D.2})$$

At the well bore

$$\pi r_c^2 \left(\frac{\partial H_1}{\partial t} \right)_{r_w} = \left(2\pi r T_1 \frac{\partial H_1}{\partial r} \right)_{r_w} \quad r_c \equiv \text{casing radius} \quad (\text{II.D.3})$$

Initial conditions:

$$\begin{aligned} H_1 &= H_2 = 0 \quad \text{at } t = 0 \text{ for } r > r_w \\ H_1 &= H_0 \quad \text{at } t = 0 \text{ for } r = r_w \end{aligned} \quad (\text{II.D.4})$$

The boundary conditions between the skin and aquifer are

$$\begin{aligned} H_1 &= H_2 \text{ at } r = R_s \\ T_1 \frac{\partial H_1}{\partial r} &= T_2 \frac{\partial H_2}{\partial r} \text{ at } r = R_s \end{aligned} \quad (\text{II.D.5})$$

Far away from the slugged well

$$H_2 = 0 \quad \text{at } r = \infty \quad (\text{II.D.6})$$

Sensitivities for T_1 and T_2

The sensitivities for T_1 and T_2 are very similar in shape as shown in Figure 2. However, the sensitivity for T_2 is shifted slightly to larger time values. Figure 2 shows the sensitivity to the skin region when it has the same value for transmissivity as the aquifer. Figure 3 shows the sensitivities when the skin transmissivity is an order of magnitude smaller. Note that the maximum amplitude of the sensitivity is inversely proportional to the transmissivity. The lower sensitivity for T_2 coupled with the similarity in shape (meaning correlation is high) indicates that it is going to be very difficult to get accurate estimates for T_2 . Away from the slugged well there is some difference in shape between sensitivities for T_1 and T_2 , however, the amplitude decays rapidly making it difficult to utilize these differences.

Effect of Varying the Skin Radius

Varying the skin radius shifts the head response curve along the dimensionless time axis for both the slugged well and observation wells. Figure 4 shows the normalized head in the slugged well for various skin radii. Figure 5 is a similar plot for an observation well located at 100 well radii away from the slugged well. Increasing the skin radius shifts the head response curve to larger dimensionless time (beta) when $T_1 \ll T_2$. This is true for both the slugged well and the observation well. However, the response in the observation well declines with increasing skin radius for $T_1 \ll T_2$.

Fitting Well Skin Data to the C-B-P Model

Many times the C-B-P model (Cooper et al., 1967) is used to fit slug test data. The obvious question is: What is the effective transmissivity when a well skin is present? Figure 6 shows a resulting fit with SUPRPUMP (Bohling and McElwee, 1992). The fitted data show a systematic deviation which may be diagnostic. The skin data is greater than the C-B-P model for early time and less than the C-B-P model for larger times, when $T_1 \ll T_2$. In general, the effective transmissivity resulting from the application of the C-B-P model to well skin data is an average of the skin and aquifer transmissivities. We have found that a good empirical equation for the effective transmissivity is

$$\frac{1}{T_{eff}} = \left[\frac{\ln(R_s / r_w)}{T_1} + \frac{\ln(r_{eff} / r_w) - \ln(R_s / r_w)}{T_2} \right] \left[\ln(r_{eff} / r_w) \right]^{-1} \quad (\text{II.D.7})$$

r_{eff} = effective radius influenced by the slug test.

$$r_{eff} / r_w = [C / S]^{1/2} \quad 1 \leq C \leq 2 \quad (\text{II.D.8})$$

S = storage coefficient.

The result given by this equation is highly weighted by T_1 and has a weak dependence on the skin radius when $T_1 \ll T_2$. In general, the lowest value of transmissivity (whether it is the aquifer or the skin) will be the dominant factor in determining the effective transmissivity. Table 1 gives some typical results for effective transmissivity for varying skin radii and transmissivity distributions. As one might expect the effective transmissivity is independent of initial slug height.

Table 1
Effective Transmissivities in the Presence of a Skin

T_1	T_2	R_s/r_w	T_{eff} C-B-P	C (emp.)	T_{eff} (emp.)
0.1	1.0	5	.205	2	.208
0.1	1.0	10	.155	2	.155
0.1	1.0	20	.126	2	.124
1.0	0.1	5	.175	1	.172
1.0	0.1	10	.260	1	.250
1.0	0.1	20	.456	1	.456

The storage coefficient was 10^{-3} for all the above simulations and an observation well was used at $100 r_w$.

Steady-State Derivation

Consider an aquifer with two transmissivity zones. T_1 is the skin transmissivity and T_2 is the regional transmissivity. Radial flow considerations require the steady-state solution to be of the following form,

$$\begin{aligned}
 h_1 &= -\frac{Q}{2\pi T_1} \ln\left(\frac{r}{r_w}\right) + h_w & r_w \leq r \leq R_s \\
 h_2 &= -\frac{Q}{2\pi T_2} \ln\left(\frac{r}{R_s}\right) + h_{R_s} & R_s \leq r \leq \infty
 \end{aligned}
 \tag{II.D.9}$$

where Q is the flow rate. Boundary conditions must be applied to the solution. If we require that h_2 is approximately zero at r_{eff} and that the solutions match at the boundary R_s , then equation (II.D.9) becomes

$$h_1 = -\frac{Q}{2\pi T_1} \ln\left(\frac{r}{r_w}\right) - \frac{Q}{2\pi} \left[\frac{\ln\left(\frac{R_s}{r_{eff}}\right)}{T_2} + \frac{\ln\left(\frac{r_w}{R_s}\right)}{T_1} \right] \quad r_w \leq r \leq R_s \quad (\text{II.D.10})$$

$$h_2 = -\frac{Q}{2\pi T_2} \ln\left(\frac{r}{r_{eff}}\right) \quad R_s \leq r \leq \infty$$

An effective transmissivity can be defined in the usual way requiring the same inner and outer boundary conditions.

$$h_{eff} = -\frac{Q}{2\pi T_{eff}} \ln\left(\frac{r}{r_w}\right) + h_w \quad r_w \leq r \leq r_{eff} \quad (\text{II.D.11})$$

At $r = r_{eff}$ the head is effectively zero by assumption, so equation (II.D.11) can be solved for the effective transmissivity.

$$\frac{1}{T_{eff}} = \frac{2\pi}{Q} \left[\ln\left(\frac{r_{eff}}{r_w}\right) \right]^{-1} h_w$$

$$\frac{1}{T_{eff}} = - \left[\frac{\ln\left(\frac{r_w}{R_s}\right)}{T_1} + \frac{\ln\left(\frac{R_s}{r_{eff}}\right)}{T_2} \right] \left[\ln\left(\frac{r_{eff}}{r_w}\right) \right]^{-1} \quad (\text{II.D.12})$$

The quantity h_w has been identified by simply comparing (II.D.9) and (II.D.10) and substituted into the first line of (II.D.12) to yield the final result. It is seen that this formula for the effective transmissivity is identical with (II.D.7), after some minor algebra manipulation.

Derivation Under Hvorslev Assumptions

The derivation in the preceding section assumes steady state conditions which are not correct during the performance of a slug test. We may relax this assumption by making a Hvorslev type of approximation for the time dependence. Assume that the equations of the preceding section hold at any instant but that the Q is varying as the slug test is carried out. This assumes a kind of instantaneous steady state with a varying Q , which in effect is ignoring the effect of storage. However, it is less restrictive than the steady state assumption and should be valid when a Hvorslev type of analysis is appropriate. Q can be written as

$$Q = -\frac{dh_w}{dt} \pi r_w^2 . \quad (\text{II.D.13})$$

Using equation (II.D.13) for Q and evaluating (II.D.10) at $r = r_w$ gives

$$h_w = \frac{dh_w}{dt} r_w^2 \frac{A}{2}$$
$$A = \left[\frac{\ln\left(\frac{r_w}{R_s}\right)}{T_1} + \frac{\ln\left(\frac{R_s}{r_{eff}}\right)}{T_2} \right] \quad (\text{II.D.14})$$

Integrating this equation gives the normal Hvorslev-type solution.

$$\ln(h_w) = \frac{2t}{Ar_w^2} + Constant \quad (\text{II.D.15})$$

In a similar way the effective radial head equation (II.D.11) can be evaluated at r_{eff} and solved for the head at the well to yield

$$h_w = \frac{Q}{2\pi T_{eff}} \ln\left(\frac{r_{eff}}{r_w}\right). \quad (\text{II.D.16})$$

Using the expression for variable Q (II.D.13) gives the final form

$$h_w = \frac{dh_w}{dt} r_w^2 \frac{\ln\left(\frac{r_w}{r_{eff}}\right)}{2T_{eff}}, \quad (\text{II.D.17})$$

which can be integrated to also give a Hvorslev-type solution.

$$\ln(h_w) = \frac{2T_{eff}}{r_w^2 \ln\left(\frac{r_w}{r_{eff}}\right)} t + \text{Constant} \quad (\text{II.D.18})$$

Comparing (II.D.15) and (II.D.18) allows the same expression for effective transmissivity to be identified as in equations (II.D.7) and (II.D.12).

In fact we do not need to require that the head goes to zero at some effective radius, it is sufficient to simply require that the head there be a small fraction of the head at the well

$$h(r_{eff}) = \epsilon h_w \ll h_w. \quad (\text{II.D.9})$$

In this case the preceding analyses go through as before, allowing the same expression for effective transmissivity to be defined. However, the decay in time is modified slightly. A factor of $1/(1-\epsilon)$ must multiply the right hand side of equations (II.D.14) and (II.D.17). This results in the Hvorslev decay rate being modified slightly; however, as long as ϵ is small the effect is negligible.

We have shown that the formula (II.D.7) may be more general than would be supposed at first glance. In particular, it seems to hold well for situations adequately described by the Hvorslev type of model. Our experience is that it also works well for the C-B-P model. The effective radius is not a strong function of the aquifer parameters. It

may be possible to define some empirical rules for selecting the effective radius in certain cases. In that case, the effective transmissivity obtained from analysis of slug test data might be more useful in estimating the regional transmissivity, especially in those situations where the radius of the skin may be estimated from independent data such as the diameter of the auger flights. Analysis of slug tests in the presence of a skin is a very difficult problem and will require ongoing research in order to gain additional insight.

Parameter Estimation with the Well Skin Model

The well skin model of Moench and Hsieh has been implemented in SUPRPUMP and can be used to look at sensitivities and to fit the data. Figure 7 is a plot of the sensitivities to T_1 and R_s . The sensitivity to R_s is smaller than to T_1 and is of opposite sign. However, the shape of the two sensitivities in Figure 7 is almost identical and very high correlation is the general rule. Away from the slugged well there is some difference in shape between sensitivities for T_1 and R_s , however, the amplitude decays rapidly making it difficult to utilize these differences. Therefore, it is extremely difficult to obtain good estimates for both T_1 and R_s . Usually there will be many pairs of values of T_1 and R_s that will give equally good results. In tests we have run, the high correlation persists even if observation wells are available and used. In some cases the approximate value for the skin radius may be known from the diameter of the hole made by the drilling equipment; in this case one can try holding R_s constant and just fitting T_1 and T_2 .

Three Parameter Fit

Table 2 shows the output from the SUPRPUMP package used in design mode for the three parameter fit (T_1 , T_2 , and R_s) of the Moench and Hsieh well skin solution. Four observation wells were used at r/r_w of 1, 25, 50 and 100 for 56 time measurements between .01 and 1000. units of dimensionless time (BETA). The 95% confidence limits show that T_1 and T_2 could be determined within about $\pm 40\%$, however, the skin radius (R_s) is very poorly determined. The root causes of these results can be seen by looking at the matrix of normalized sensitivities, the sensitivity correlation matrix, and the parameter correlation matrix in Table 2. The diagonal elements of the matrix of normalized sensitivities shows that T_1 has the highest sensitivity by far. The sensitivity correlation matrix and the parameter correlation matrix shows that the correlation between T_1 and R_s is greater than .99. These results are for perfect model data with an assumed accuracy of $\pm .025$ Ho. In the real world things are likely to be much worse.

Alluvial Aquifer Example

Figures 8 and 9 show a real example of a slug test performed in the Kansas River valley near Lawrence, Ks. Figure 8 shows the fit of the data to the C-B-P model. There is a systematic deviation present and we thought it might be explained by a skin effect. Figure 9 shows the same data fit to the Moench and Hsieh model. The fit is much better, but it was difficult to obtain and is very sensitive to the number of parameters fit and the initial estimates for those parameters. Many of the analyses did not converge. Consequently, even though the fit is much better, we do not believe very much accuracy can be ascribed to the estimated aquifer conductivity. On the other hand, the effective conductivity from the C-B-P model and the skin conductivity from the Moench and Hsieh model agree fairly well and can probably be used with some confidence. Unfortunately, it is the aquifer conductivity that is of greatest interest.

Summary

We have investigated the problem of a slugged well having a well skin using sensitivity analysis and an automated well-test analysis program we have developed. The sensitivity coefficients for T_1 and T_2 are similar in shape but shifted slightly in time. Thus, it is difficult to obtain good estimates for both T_1 and T_2 due to correlation. The maximum amplitude of the sensitivities is inversely proportional to transmissivity. Varying the skin radius shifts the head response curve along the dimensionless time axis. When fitted to the Cooper-Breidehoeft-Papadopoulos (C-B-P) model, the data show a systematic lack of fit, however, it is not large. The effective transmissivity obtained from the C-B-P fit is a weighted average of T_1 and T_2 and can be predicted with a simple empirical formula. The effective transmissivity is highly weighted by the smallest transmissivity and is a weak function of the skin radius. If one attempts a three parameter fit using T_1 , T_2 , and the skin radius (R_s), it is found that T_1 and R_s are usually very highly correlated leading to a nonunique situation. If R_s is assumed known and one tries to solve for T_1 and T_2 , the situation is better, but the fit is still difficult and depends on the initial estimates and the quality of the data. Having copious amounts of accurate data and multiple observation wells is the best situation for obtaining an accurate fit.

TABLE 2
SUPRPUMP OUTPUT
THREE PARAMETER FIT

The estimated root-mean-squared residual is .2500E-01

The parameter values with approximate 95% confidence intervals are:

Parameter	Value	Lower Bound	Upper Bound
TRANSMISS. OF AQUIFER	1.000	.6227	1.377
TRANSMISS. OF SKIN	.1000	.5668E-01	.1433
SKIN RADIUS	10.00	-1.459	21.46

For the following arrays:

Col-Row 1 represents TRANSMISSIVITY OF AQUIFER (T2)

Col-Row 2 represents TRANSMISSIVITY OF SKIN (T1)

Col-Row 3 represents SKIN RADIUS (Rs)

Raw crossproducts matrix of normalized sensitivities:

	1	2	3	
1	.2357E-01	.8306E-01	-.3155E-01	This matrix shows that T1 has the highest sensitivity by far.
2	.8306E-01	1.093	-.4113	
3	-.3155E-01	-.4113	.1566	

The reciprocal condition number of the
sensitivity crossproducts matrix is .1079E-02

Sensitivity correlation matrix:

	1	2	3	
1	1.000	.5174	-.5192	-----Very high correlation between T1 and Rs.
2	.5174	1.000	-.9940	
3	-.5192	-.9940	1.000	

Covariance matrix of normalized parameter variations:

	1	2	3
1	.3630E-01	-.6035E-03	.5727E-02
2	-.6035E-03	.4787E-01	.1256
3	.5727E-02	.1256	.3349

Parameter correlation matrix:

	1	2	3	
1	1.000	-.1448E-01	.5194E-01	-----Very high correlation between T1 and Rs.
2	-.1448E-01	1.000	.9918	
3	.5194E-01	.9918	1.000	

Figure 1. Schematic of a slug test in a well with a skin.

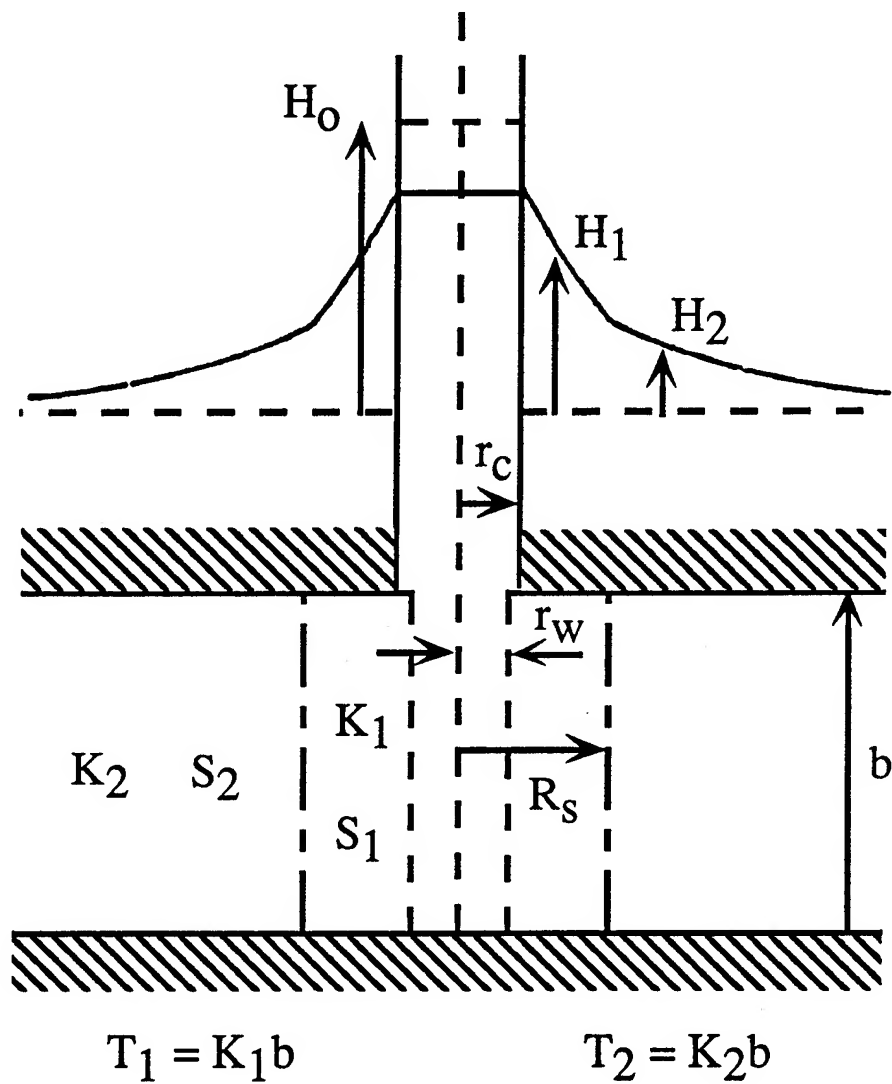


Figure 2.
Variation of u'_T With Time at the Slugged Well

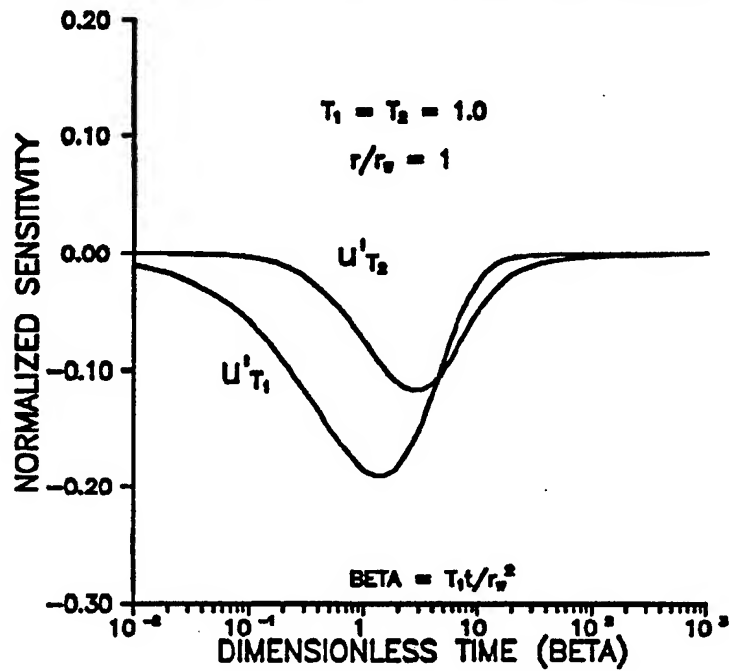


Figure 3.
Variation of u'_T With Time at the Slugged Well

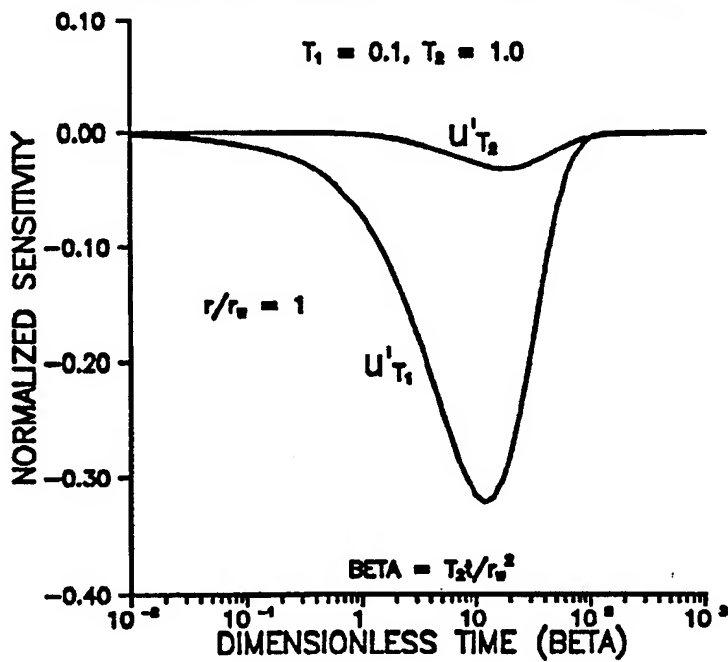


Figure 4.
Variation of Head in Slugged Well With Skin Radius

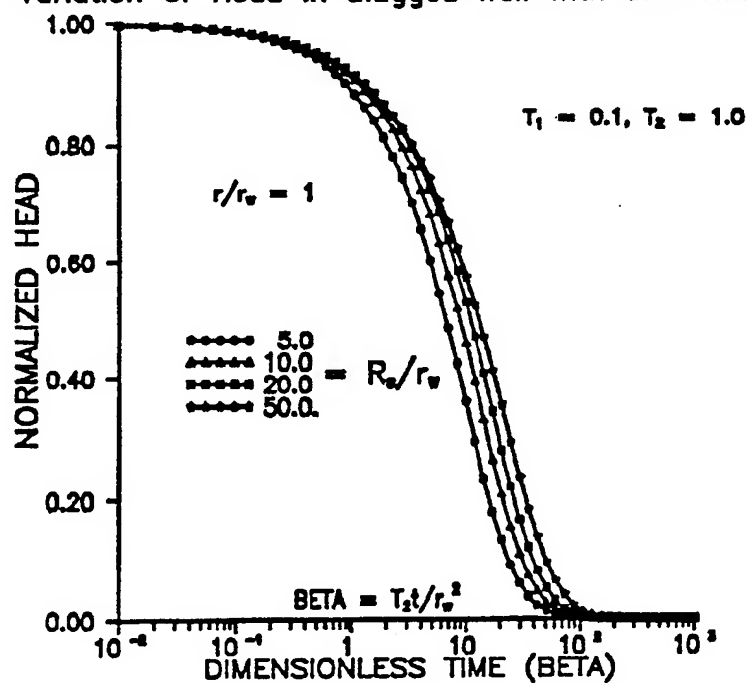


Figure 5.
Variation of Head in Obs. Well With Skin Radius

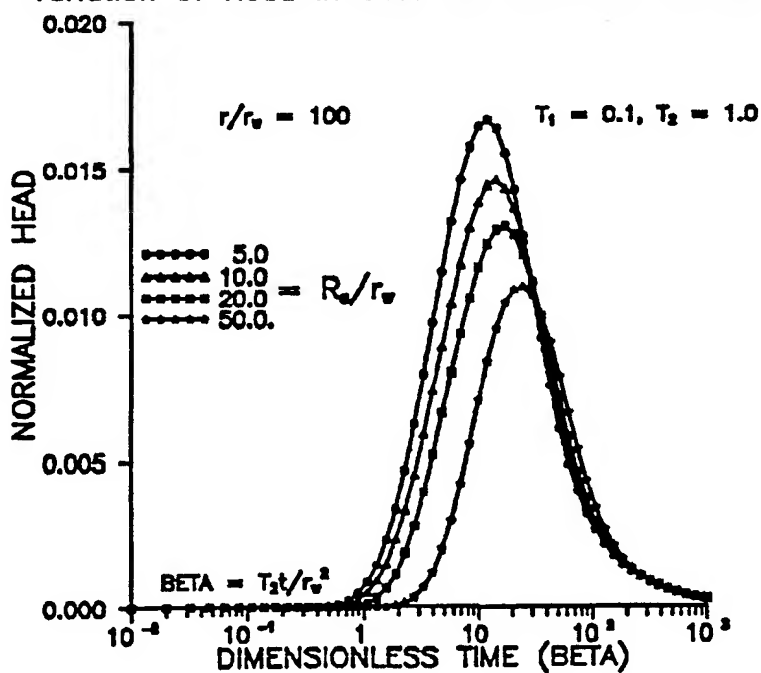


Figure 6.
Fit of Well Skin Data to the C-B-P Model

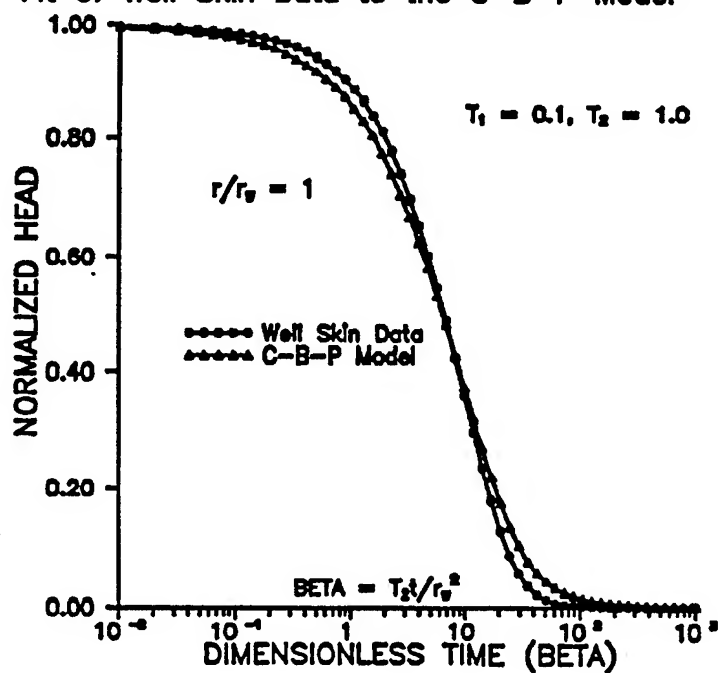


Figure 7.
Comparison of u'_{T_1} and u'_{R_0} at the Slugged Well

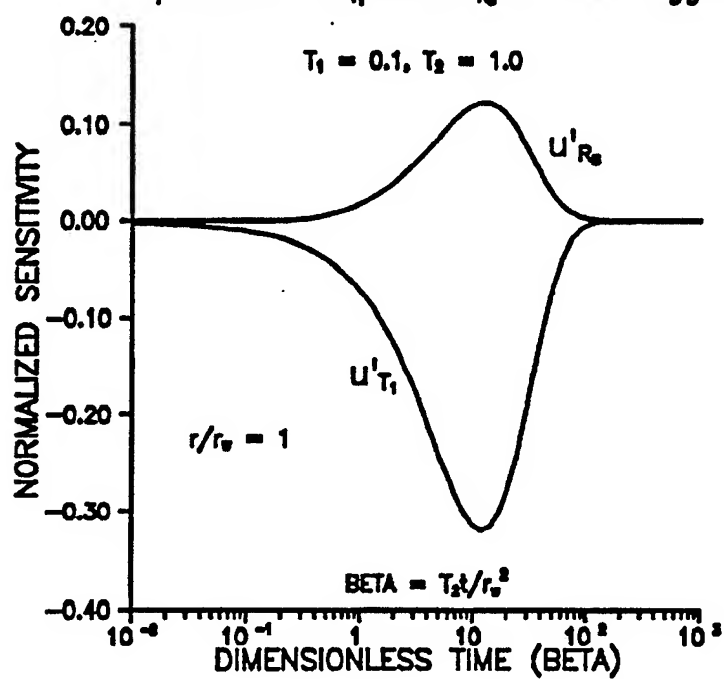


Figure 8.

Analysis of an Alluvial Aquifer Slug Test
With the C-B-P Model

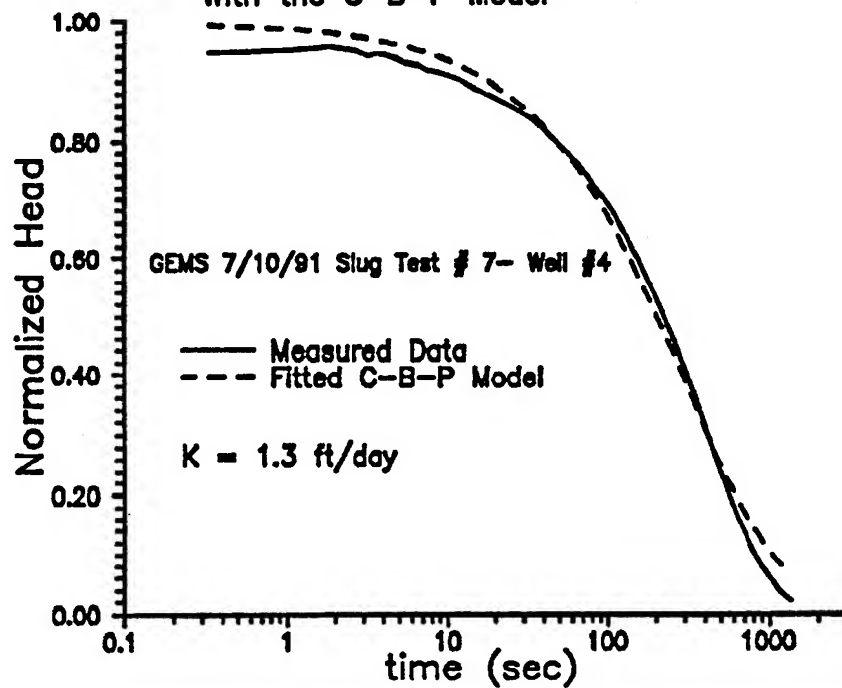
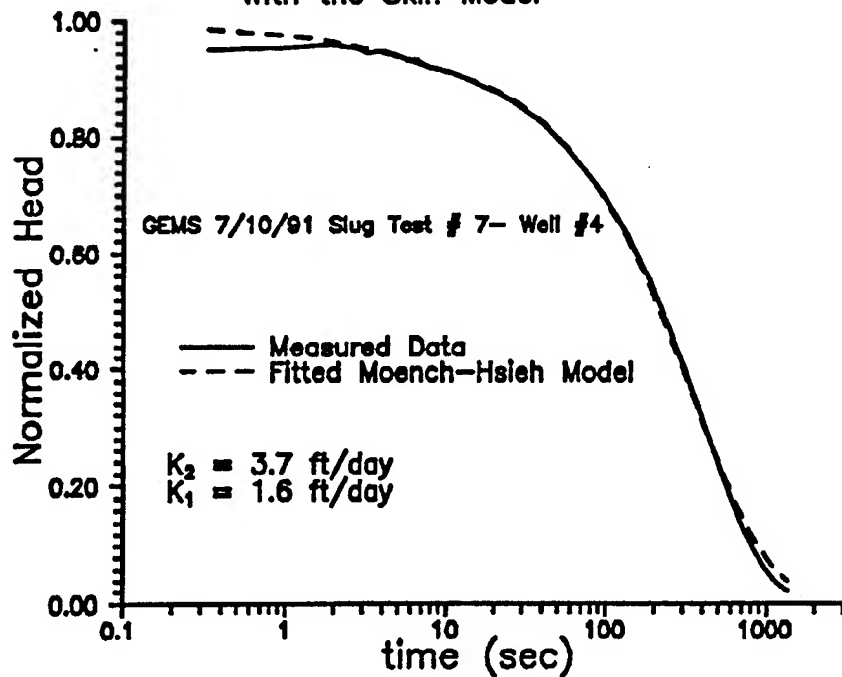


Figure 9.

Analysis of an Alluvial Aquifer Slug Test
With the Skin Model



E. SLUG TESTS IN PARTIALLY PENETRATING WELLS

Appendix C presents a recently published professional journal article in which a semianalytical solution to a mathematical model describing the flow of groundwater in response to an instantaneous change in water level at a well screened in a porous formation is described. The model incorporates the effects of partial penetration, anisotropy, finite-radius well skins of either higher or lower permeability than the formation as a whole, and upper and lower boundaries of either a constant-head or an impermeable form. This model can be employed for the analysis of data from slug tests in a wide variety of commonly met field configurations in both confined and unconfined formations. The major purpose of appendix C is to use the semianalytical solution to quantify the error that is introduced into parameter estimates as a result of using currently accepted practices for the analysis of response data from slug tests. The magnitude of the error arising in a variety of commonly met field configurations serves as the basis for practical guidelines that can be utilized by field practitioners.

F. THE USE OF SLUG TESTS TO DESCRIBE VERTICAL VARIATIONS IN HYDRAULIC CONDUCTIVITY

There are still many unanswered questions about the usefulness of the information provided from multilevel slug tests under conditions commonly faced in the field, where anisotropy, layering, and well skins of either higher or lower permeability than the undamaged formation may be influencing the measured response data. Appendix D presents a recently published professional journal article in which many of these questions are addressed in the context of a theoretical assessment of the potential of multilevel slug tests to provide information about vertical variations in hydraulic conductivity in the vicinity of the well bore. Since no general analytical solution has been developed for the case of slug tests in layered aquifers, this assessment will be performed through numerical simulation. The major objectives of this work are 1) to assess possible techniques for the analysis of slug tests in layered systems; 2) to evaluate the effects of various geologic features (e.g., density of layering, anisotropy within layers, distance from boundaries, etc.) and well-construction features (e.g., well skins, length of the test interval, etc.) on the parameters estimated from slug-test data; 3) to explore the nature of vertical averaging in slug tests in layered aquifers; 4) to assess the effects of packer length and determine under what conditions packer circumvention may be an important mechanism; and 5) to make recommendations for the performance of multilevel slug tests in layered systems that can be utilized by the field practitioner.

G. HYDRAULIC TOMOGRAPHY

Introduction

Some of the important early papers on the groundwater inverse problem, such as those by Nelson [1960, 1961, 1968] and Neuman [1973], pointed out the relationship between this problem and the one-dimensional Cauchy problem. If heads and source and sink values are known at every point in a one-dimensional problem, then the conductivity at every point in the domain can be determined uniquely as long as either conductivity or flux is known at one point in the domain. This same result can be applied along streamtubes or streamlines in a two-dimensional flow problem. This leads to a direct inverse solution for conductivities based on flow net analysis, as in Nelson [1968], and more recently in Scott [1992]. In both of these works the flow net is created by interpolating from observed head values, in one way or another.

The hydraulic tomography method presented here is essentially an iterative least squares solution of the Cauchy problem, with streamlines being iteratively identified based on a computed head field, rather than from observed data. The head drop between any two points on a streamline is given by a line integral of the flux along the streamline multiplied by the hydraulic resistivity, which is the inverse of hydraulic conductivity. Streamline trajectories and flux integrals are computed from a finite difference solution for head based on an estimate of the resistivity distribution. Computing flux integrals along a number of streamlines with known heads at each end results in a system of linear equations which can be solved for an updated set of resistivities. Heads and flux integrals are recomputed and the process repeats until the resistivity estimates converge.

Flow Path Within a Finite Difference Cell

Figure 1 is a sketch of a finite difference cell with one possible flow path passing through it. This diagram and the development of the equations describing the flow path trajectory are taken from Pollock [1988], with minor modifications. Using a block-centered formulation, with computational nodes at the center of the cell and flux values computed at the cell faces, the flux field within the cell can be approximated using bilinear interpolation. The x-component of the specific flux, for example, is given by linear interpolation between q_{x1} on the left face and q_{x2} on the right face, and similarly for the y-component. Given this description of the flux field it is straightforward to work out the trajectory of a particle traveling through the cell, from its entry point (x_p, y_p) , to its exit point, (x_e, y_e) . The flux field is in steady state here, not varying with time. However, any given particle will encounter varying fluxes as it travels along its flow path. Also

note that this development uses Darcy velocity or specific flux in place of actual flow velocity. The time variable employed is not real-world travel time, but is travel time scaled by the value of porosity. Time is used only as a convenient variable of integration, however, and the scaling by porosity does not have any effect on the final results.

Flux Field Within Cell

Using a local coordinate system ranging from $-\Delta x/2$ to $+\Delta x/2$ and from $-\Delta y/2$ to $+\Delta y/2$ within each cell, where Δx and Δy are the cell dimensions, the equations describing the flux field within the finite difference cell are:

$$q_x(x) = q_{x0} + A_x x \quad q_y(y) = q_{y0} + A_y y \quad (\text{II.G.1})$$

with

$$q_{x0} = \frac{(q_{x2} + q_{x1})}{2} \quad q_{y0} = \frac{(q_{y2} + q_{y1})}{2} \quad (\text{II.G.2})$$

and

$$A_x = \frac{(q_{x2} - q_{x1})}{\Delta x} \quad A_y = \frac{(q_{y2} - q_{y1})}{\Delta y} \quad (\text{II.G.3})$$

The locations of the cell-face fluxes, q_{x1} , q_{x2} , q_{y1} and q_{y2} , are shown on Figure 1. In the current implementation of the method, the fluxes at the cell faces are calculated from differences of computed head values in adjacent finite difference cells. Thus the flux gradient terms, A_x and A_y , are computed from differences of differences of computed head values. This is a potential source of problems, since differences of computed values can be in error by arbitrarily large amounts regardless of the accuracy of the original computed values. However, every inverse algorithm depends in some way on computation of head gradients, if not higher-order differences, so this problem is not unique to this particular method.

Particle Trajectory Within Cell

As a particle travels through a cell, it follows a flow path determined by the following two ordinary differential equations:

$$\frac{dq_x(t)}{dt} = A_x q_x(t) \quad \frac{dq_y(t)}{dt} = A_y q_y(t) \quad (\text{II.G.4})$$

Again, t is the real-world travel time scaled by porosity. The equation on the left states that the time rate of change in x -component flux experienced by a particle is given by the flux gradient, A_x , multiplied by the current flux value, q_x . This is an application of the chain rule -- A_x is dq/dx and q_x is dx/dt . The first integral gives the two flux components as exponential functions of travel time through the cell:

$$q_x(t) = q_{xp} \exp(A_x t) \quad q_y(t) = q_{yp} \exp(A_y t) \quad (\text{II.G.5})$$

where q_{xp} and q_{yp} are the flux components at the point where the particle enters the cell. The second integral gives the particle trajectory, x and y coordinates as functions of travel time:

$$x(t) = \frac{1}{A_x} (q_{xp} \exp(A_x t) - q_{x0}) \quad y(t) = \frac{1}{A_y} (q_{yp} \exp(A_y t) - q_{y0}) \quad (\text{II.G.6})$$

The actual travel time through the cell is determined by testing the potential travel time to each cell face. The minimum positive value gives the travel time through the cell, t_c . The coordinates of the particle's exit point, x_e and y_e , are then obtained by plugging the travel time into the trajectory equations. The particle moves into an adjacent cell and the algorithm continues to trace this path through successive cells until it reaches a boundary and exits the model domain.

Constant Hydraulic Resistivity Solution

Figure 2 shows the head contours and pathlines traced by the algorithm for flow through a square domain with a constant hydraulic resistivity of 1.0. The model domain, nine units on a side, was discretized into a 45X45 grid of finite difference cells for this and following examples. For this particular run the five cells between $y=4$ and $y=5$ on the left and right sides were given specified heads of plus and minus one, with zero-flux boundaries elsewhere. Note that the nine streamlines shown actually appear to the program as 18 streamlines. The starting points are nine data points in the middle of the model, located where the streamlines intersect the 0-head contour. Two streamlines start from each data point, one moving forward through the flux field to the right-hand boundary, and the other moving backward through the flux field to the left-hand boundary. The program works this way because, in the tomographic equations, head drops computed from flux integrals are compared to differences between head values

measured at points within the model domain and head values at the boundaries. Thus, the path-tracing algorithm will start at any arbitrary point in the domain, representing a measurement point, and trace both an upstream and a downstream path until each encounters a boundary.

Natural Log of Hydraulic Resistivity Field

Figure 3 shows the synthetic spatially-varying resistivity field used for the next example. The natural log of the resistivity field is shown. Low values of resistivity correspond to high values of conductivity, so that the lighter band above the middle of the model represents a more conductive flow path. Each constant-resistivity block shown here represents a 5X5 block of grid cells. The range of resistivities is from about 0.2 to about 12.

Variable Hydraulic Resistivity Solution

Figure 4 shows the head contours and streamlines computed using the variable-resistivity field and the same boundary conditions as for the constant-resistivity case. The same nine points in the middle of the model are used as the starting points for the streamlines. The general configuration of the flow field is, of course, determined by the boundary conditions, so the variable-resistivity case looks like a wrinkled version of the constant-resistivity case. This seemingly trivial observation is actually fairly important to the success of the tomographic inversion scheme. The flux integrals used in the inverse process are computed along the flow paths derived from the current estimate of the hydraulic resistivity distribution. If the flow path trajectories changed radically with variations in the resistivity values, the iteration process would wander hopelessly. As it is, computed trajectories are fairly similar from one iteration to the next.

Tomographic Equations

The tomographic equations result from applying an integral version of Darcy's law along each streamline leading from a data point to a boundary. Viewed along each streamline, Darcy's law reduces to the simple ordinary differential form

$$q_s(s) = -K(s) \frac{dh}{ds} \quad (\text{II.G.7})$$

where s represents displacement along the streamline, $K(s)$ is the conductivity as a function of that displacement, and dh/ds is the head derivative along the streamline.

Rearranging this and integrating along the length of the streamline, from 0 to L, shows that the head drop along the streamline, H, can be derived directly from the hydraulic resistivity and flux values encountered along that streamline:

$$H = \int_0^L R(s)q_s(s)ds \quad (\text{II.G.8})$$

If the model is discretized into N cells, each of constant resistivity, R_i , then the head drop is given by the sum of the discrete resistivity values, each multiplied by the flux integral along the streamline of interest within the corresponding cell:

$$H = \int_0^L R(s)q_s(s)ds = \sum_{i=1}^N \left(R_i \int_{s_i} q_s(s)ds \right) \quad (\text{II.G.9})$$

The flux integrals along each streamline within each cell can be collected into a coefficient matrix, with rows corresponding to streamlines and columns corresponding to model cells. The cells can be collected into constant-resistivity zones to reduce the number of unknown resistivities and thus the number of columns of the coefficient matrix. This coefficient matrix will contain quite a few zeroes, since each streamline passes through a relatively small number of cells or zones. Multiplying this flux integral coefficient matrix times the vector of zonal resistivities produces a vector of computed head drops, with each element representing the head drop between a particular data point and a boundary. The differences between these computed head drops and observed head drops form a vector of head drop residuals. Linear least squares can then be used to produce a vector of resistivity correction values which will reduce the sum of squared head drop residuals. These correction values are added to the current resistivity estimates, flow path trajectories and flux integrals are recomputed based on the new resistivities, and the process continues until the resistivity estimates converge. This is very similar to the algorithms used in seismic tomography (Peterson et al., 1985).

Flux Integral Within Cell

The flux integral along a given streamline in a cell is simplified by converting it to an integral over time, using the relationship between the spatial increment, ds , and the time increment, dt , $ds = q(s)dt$. Applying this substitution leads to a convenient simplification, since the integral over time breaks down into two pieces, each involving the square of either q_x or q_y :

$$\int_{s_i} q_s(s) ds = \int_0^{t_c} q_s^2(t) dt = \int_0^{t_c} q_x^2(t) dt + \int_0^{t_c} q_y^2(t) dt \quad (\text{II.G.10})$$

Since we already have simple analytical expressions for q_x and q_y as functions of time, it is straightforward to evaluate these integrals. The general result for q_x is:

$$\int_0^{t_c} q_x^2(t) dt = \frac{q_x^2}{2A_x} (\exp(2A_x t_c) - 1) \quad \text{if } A_x \neq 0 \quad (\text{II.G.11})$$

A special case occurs when either q_x or q_y is constant over the cell. In this case the integral is given simply by the square of the flux component multiplied by the travel time in the cell:

$$\int_0^{t_c} q_x^2(t) dt = q_{x0}^2 t_c \quad \text{if } A_x = 0 \quad (\text{II.G.12})$$

Layered Aquifer

The numerical examples are based on simulated experiments using the simple layered aquifer shown in Figure 5. The values are shown directly in terms of hydraulic resistivity. First, a sequence of nine tests was simulated, with each test involving a pair of specified head intervals, one on each end of one of the constant-resistivity layers. For example, for the first test the five grid cells at the left end of the bottom layer were set at a head of +1 and the five grid cells at the right end of the bottom layer were set at a head of -1. The same nine points in the middle of the model were used as observation points, generating 18 streamlines per test (one forward, one backward for each point), for a total of 162 streamlines over all nine tests. Running the program in forward mode using the true resistivity distribution shown here generated the data used in the inverse run. The heads computed at the data points by the finite difference model were taken as the observed heads at those points. Also, the flux value at each specified head boundary cell was computed. The flux values for the right-hand intervals were averaged over the five nodes in the interval and these averaged flux values were used for the boundary conditions on the right side when the inverse run was performed. There has to be at least one specified flux boundary condition along each streamline in order to obtain a unique solution for the resistivities. In the inverse run, the differences between the head values

computed at the interior data points and the known head values at the boundary intervals on the left and right served as the observed head drops.

Except for the fact that a linear, rather than radial, flow problem is being solved here, this experiment simulates the way we envision applying this method in the field. The data obtained from stressing different vertical intervals between a pumping well and an injecting well would be combined in order to estimate the conductivity distribution in the vertical plane between the two wells.

Nine-Test Results

Figure 6 shows the results of the nine-test inverse run. In this case the model was zoned into layers corresponding exactly with the layers in the true model. The true resistivity values are shown by the solid line and the estimates are shown by the dashed line. Starting from an initial resistivity value of 1.0 for every layer, the model converged to the solution shown here in 7 iterations, with the largest relative change in a resistivity value being about 6.5%. Overall the estimated resistivities are reasonable, with the estimates for each layer tending to be influenced somewhat by the resistivities of adjacent layers as well. After the seventh iteration the ratio changes in the resistivities continued to decrease slightly, but the sum squared head drop residual went up just slightly.

Five-Test Results

Figure 7 shows the results of a set of five simulated tests in the same layered aquifer. Each test involved stressing a nine-node interval, with specified head values at the left and right sides of the interval, as before. The aquifer in this case was zoned into five layers, corresponding with the stressed intervals. Thus, the assumed layering is coarser than the actual layering. As shown here, the overall pattern of estimated resistivities still preserves the general character of the actual resistivities.

Fifteen-Test Results

Figure 8 shows the results of stressing fifteen consecutive three-node intervals, with the aquifer being zoned into fifteen corresponding layers. Again, the estimates preserve the overall character of the actual resistivity variation. You may note that the resistivity of the upper portion of the top layer is significantly underestimated. This upper layer is a fairly high resistivity (or low conductivity) layer sandwiched between the no-flow boundary above and a higher conductivity layer below. These conditions cause the flow to avoid this upper layer as much as possible, leading to a relatively small amount of information on its properties and a poor estimate of its resistivity.

Concluding Remarks

Two advantages of this method have not been emphasized earlier. One advantage is that the model responses, the estimated head drops, are given by linear combinations of the model parameters, the hydraulic resistivities. Thus, in the hypothetical case that you knew the true model, the parameter covariance matrix would give an exact description of parameter confidence intervals, not just linear approximations of nonlinear confidence intervals, as in most inverse procedures. Although this hypothetical case is not achievable in real world applications, at least the effects of nonlinearity should be fairly small when the estimated parameters are near the optimal parameters for a given zonation.

In addition this method iteratively identifies the streamlines, or the characteristics of the flow system, as described by Neuman [1973]. Again, if the true model were known with certainty, the head drop along each streamline would be only a function of the resistivities along that streamline, completely independent of resistivity values elsewhere in the flow domain. Since, in reality, the estimated solution does depend on the resistivity estimates throughout the domain, this independence is not completely realized. However, this method should produce fairly low correlations among the parameter estimates as the resistivities approach the optimal values. Preliminary results show that this seems to be the case.

Ongoing work is addressing some problems encountered so far on this project. One problem has been the dependence of the results on the computed flux gradient terms, A_x and A_y . As mentioned before, these values are computed from differences of differences of computed head values and, in some cases, can be in error by large amounts. Frind and Matanga [1985] suggest that flux estimates derived from a stream function solution tend to be more accurate than those derived from a head solution. Work on recasting the program in terms of a stream function solution is underway.

Another problem encountered so far is that the head drops computed from flux integrals tend to underestimate the head drops computed from taking differences of the heads computed by the finite difference model. This inconsistency between the finite difference model and the flux integral results leads to convergence problems for the estimation algorithm. This could result from the use of harmonic averages of adjacent cell conductivities to represent the conductivity at each cell face. Desbarats [1993] pointed out that these harmonic averages underestimate the distribution of actual cell values. Thus the finite difference model sees a lower distribution of conductivities and

predicts higher head drops than the flux integral formulation. Therefore, the program is being recast in terms of a point-centered finite difference formulation, with conductivities being averaged arithmetically at cell faces (resistivities in the stream function formulation).

In addition, we still need to work out how to approach this problem in radial coordinates. A simple logarithmic coordinate transformation can be used to recast the single-well radial case in a form that is identical to the linear flow case presented here. However, modeling a well pair or dipole is not as straightforward. This is an important case, since we envision using a recharge-discharge pair in field applications of this method.

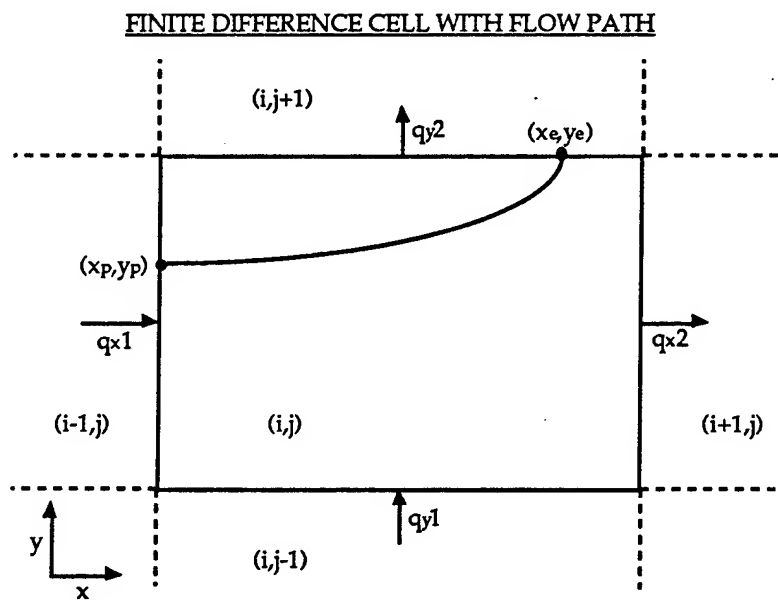


Figure 1.

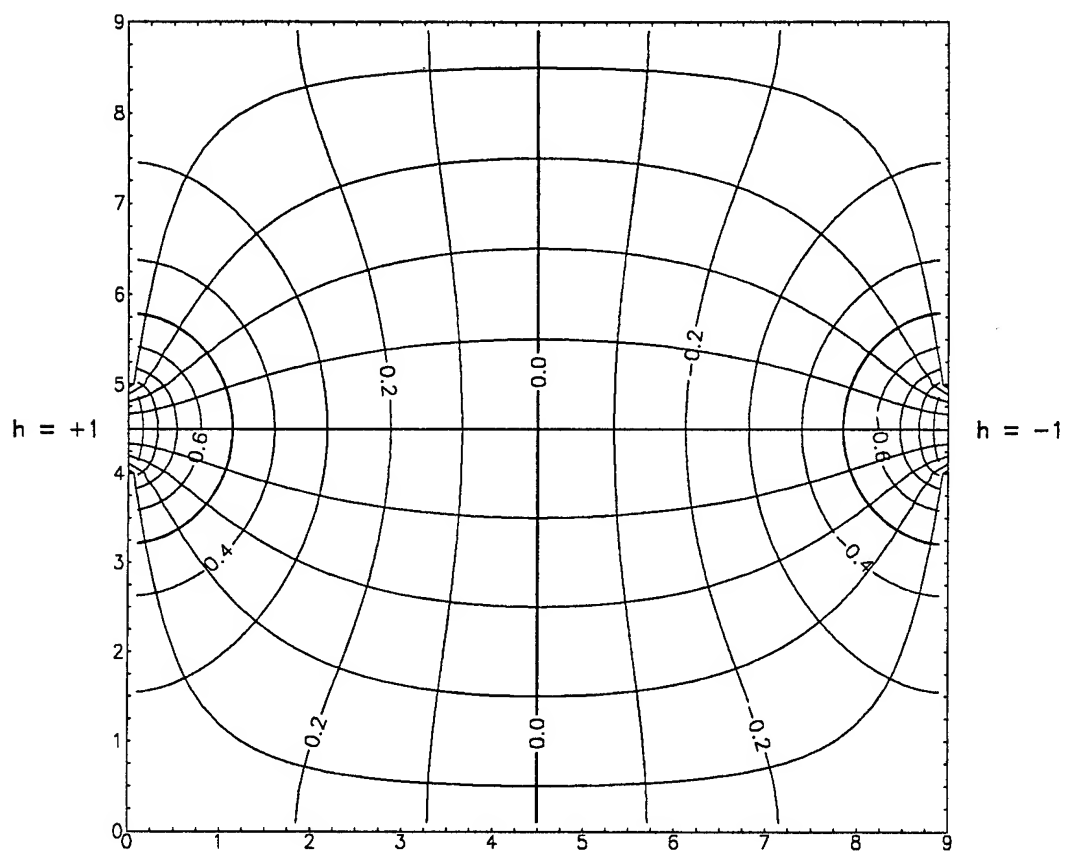


Figure 2. Constant hydraulic resistivity solution.

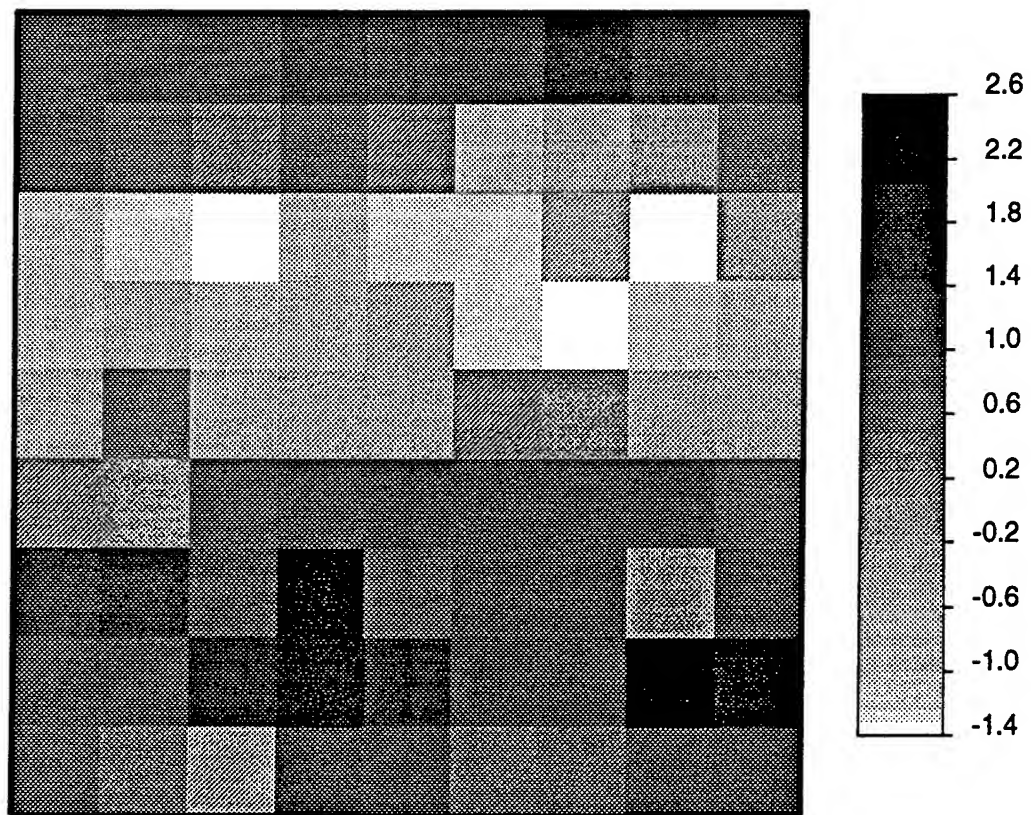


Figure 3. Natural log of hydraulic resistivity.

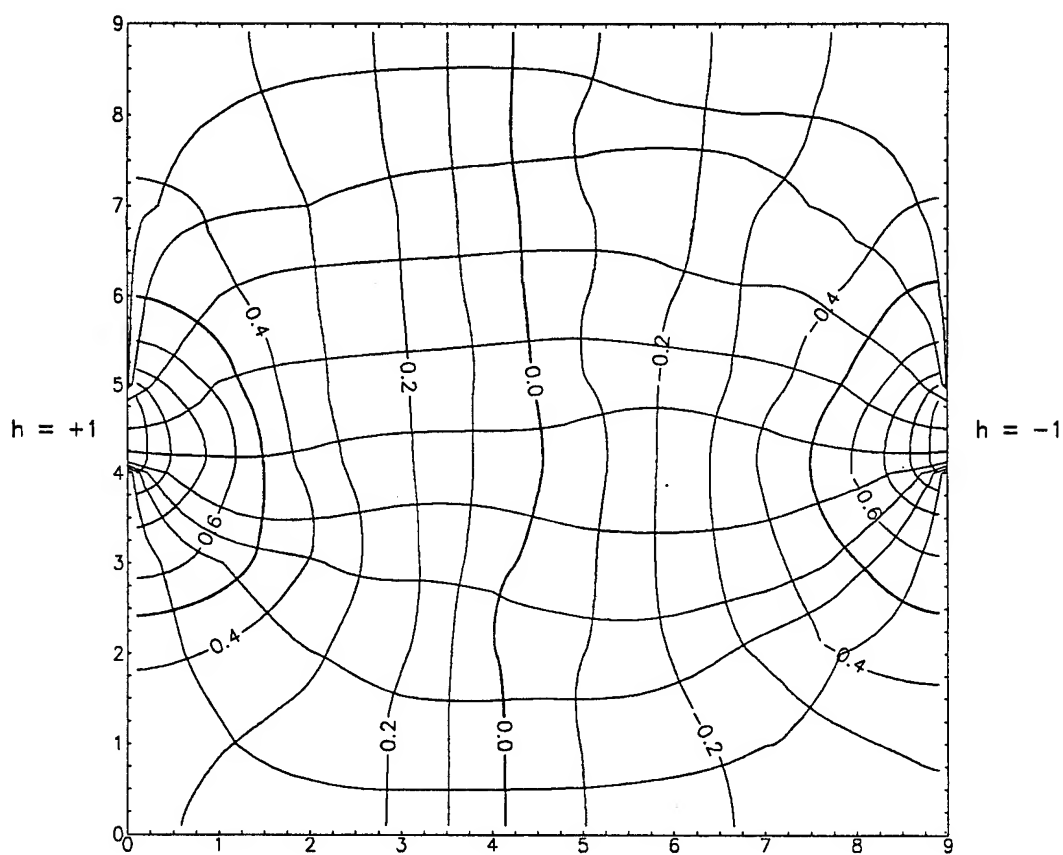


Figure 4. Variable hydraulic solution.



Figure 5. Hydraulic resistivity.

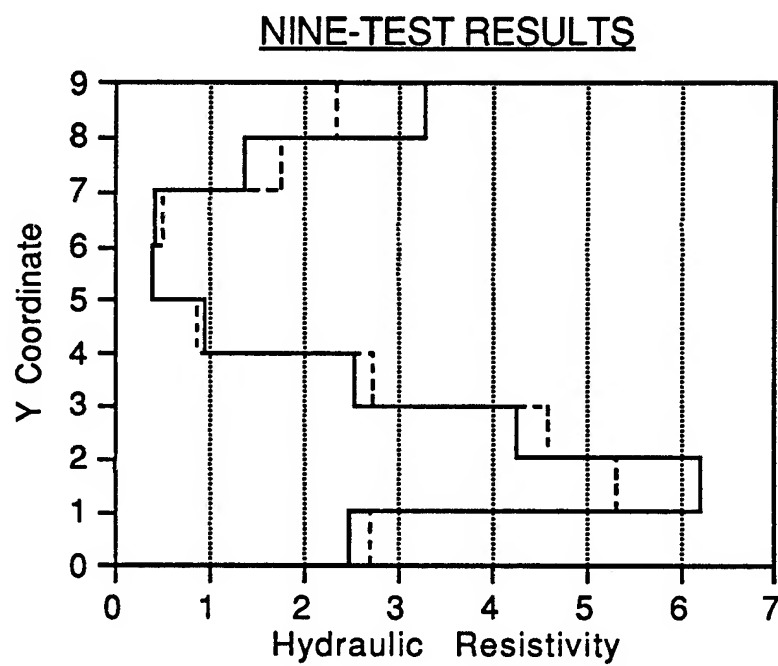


Figure 6. Nine-test results.

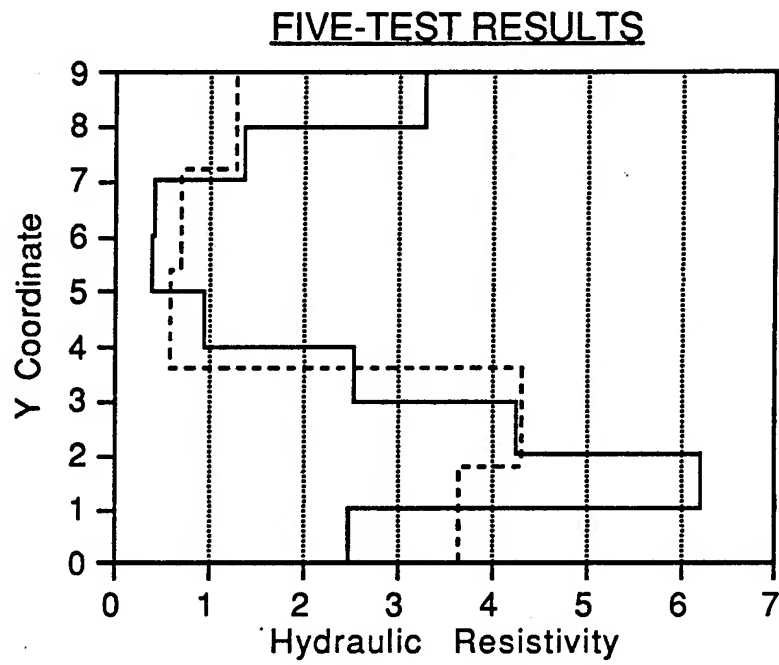


Figure 7. Five-test results.

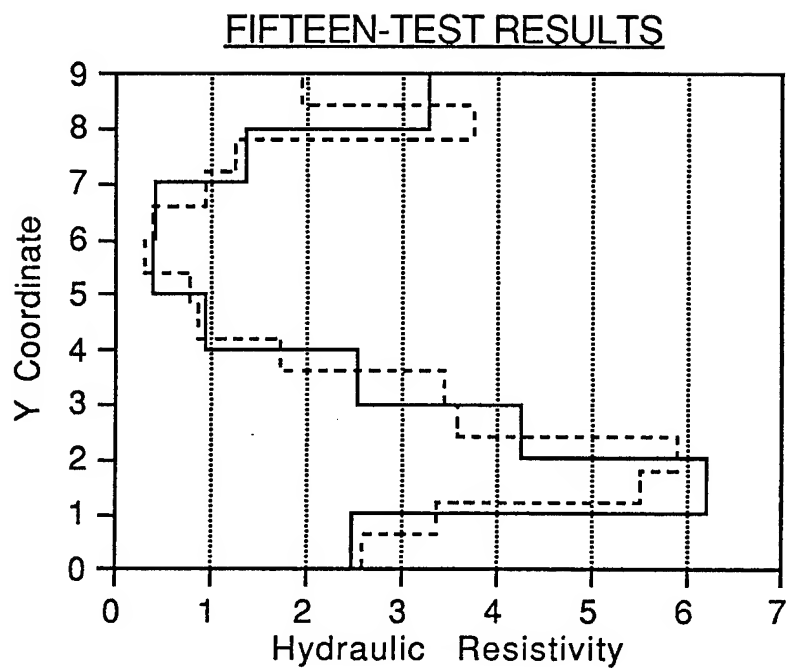


Figure 8. Fifteen-test results.

H. PULSE-TESTING IN HETEROGENEOUS FORMATIONS

Introduction

Time-varying pumping signals have been reported to yield promising information about lateral inhomogeneities of the hydraulic parameters of an aquifer (Johnson et al., 1966; Vela and McKinley, 1970; Butler and McElwee, 1990). In order to assess if periodically time-varying perturbations of the hydraulic head can be used to identify lateral heterogeneities of the hydraulic conductivity field of an aquifer, an analytical one-dimensional solution for the hydraulic head in a two-zone aquifer subjected to sinusoidal time-varying Dirichlet boundary conditions was developed. The analytical structure of the solution was then compared to the head-solution for a homogenous aquifer to investigate whether or not effective parameters (that is, appropriately averaged hydraulic parameters leading to a system response identical to that of a homogeneous aquifer) can be derived for such a simple heterogeneous case like a two-zone aquifer.

Next we have concentrated on two issues: 1) when extended to the radial case will a sinusoidal signal propagate significant distances, and 2) can the amplitude and phase of the observed signal be used to infer something about heterogeneous aquifers? The work on pulse testing has been extended to the radial case by using numerical solution techniques. The Theis equation has been coupled to an equation describing the borehole. This formulation allows us to answer the first question about propagation distances in the radial model and will be the first subject of this subsection. The question about how diagnostic measurements of amplitude and phase can be when trying to delineate heterogeneities will then be taken up. The preliminary analysis on amplitude and phase was done with the analytical one-dimensional two-zone model developed last year. As a check, these results were evaluated with a numerical model. The numerical model was extended to five zones to see if the results could be generalized.

Analytical Solution for Two-Zone Model

The flow processes in the two-zone model aquifer are governed by two mass balance equations of the form :

$$\begin{aligned} \frac{d^2 h_1}{dx^2} &= \frac{1}{v_1} \frac{dh_1}{dt} & v_1 &= \frac{T_1}{S_1} \\ \frac{d^2 h_2}{dx^2} &= \frac{1}{v_2} \frac{dh_2}{dt} & v_2 &= \frac{T_2}{S_2} \end{aligned} \tag{II.H.1}$$

h_1 and h_2 are the head solutions in the first and the second zone of the aquifer, T_1 , T_2 , S_1 , S_2 denote the transmissivities and storage coefficients of both zones. With x_B , representing the boundary between both zones, the boundary conditions for the system are :

$$\begin{aligned} h_1(0, t) &= h_0 \sin\left(\frac{2\pi t}{t_0}\right) = h_0 \sin(\omega t) \\ h_1(x_B, t) &= h_2(x_B, t) \end{aligned} \quad (\text{II.H.2})$$

$$T_1 \frac{dh_1}{dx} \Big|_{x=x_B} = T_2 \frac{dh_2}{dx} \Big|_{x=x_B}$$

$$h_2(\infty, t) = 0$$

The solution of equations (II.H.1) subject to the boundary conditions (II.H.2) can be seen to be of the following complex form :

$$\begin{aligned} h_1(x, t) &= [Ae^{\beta_1 x} + Be^{-\beta_1 x}] e^{i(\omega x - \pi/2)} \\ h_2(x, t) &= Ce^{-\beta_2 x} e^{i(\omega x - \pi/2)} \end{aligned} \quad (\text{II.H.3})$$

with :

$$\beta_1 = \left[\frac{1}{\sqrt{2}} + \frac{i}{\sqrt{2}} \right] \sqrt{\frac{\omega}{v_1}}$$

$$\beta_2 = \left[\frac{1}{\sqrt{2}} + \frac{i}{\sqrt{2}} \right] \sqrt{\frac{\omega}{v_2}}$$

The constants A, B, and C are to be determined from the first three boundary conditions in (II.H.2). The physically meaningful part of equations (II.H.3), that is, the respective real parts of the solutions (II.H.3), will then take the final form :

$$h_1(x, t) = \text{Re} \left\{ \left[h_0 e^{\beta_1 x} - \frac{gh_0}{f} e^{\beta_1(x_B + x)} + \frac{gh_0}{f} e^{\beta_1(x_B - x)} \right] e^{i(\omega x - \pi/2)} \right\}$$

$$\begin{aligned} h_2(x, t) &= \text{Re} \left\{ \left[\frac{h_0 - gh_0 e^{\beta_1 x_B}}{f} e^{(\beta_1 + \beta_2)x_B} e^{-\beta_2 x} \right. \right. \\ &\quad \left. \left. + \frac{gh_0}{f} e^{\beta_1(x_B - x)} \right] e^{i(\omega x - \pi/2)} \right\} \end{aligned}$$

with :

$$g = T_1\beta_1 + T_2\beta_2$$

$$f = 2[T_1\beta_1 \cos(\beta_1 x_B) + iT_2\beta_2 \sin(\beta_1 x_B)]$$

A solution of system (II.H.1) subject to boundary condition (II.H.2) can also be obtained by using a fully real representation of h_1 and h_2 :

$$\begin{aligned} h_1(x, t) = & h_0 e^{-Ax} [(1 - F) \sin(\omega t - Ax) + G \cos(\omega t - Ax)] \\ & + h_0 e^{Ax} [F \sin(\omega t + Ax) - G \cos(\omega t + Ax)] \end{aligned} \quad (\text{II.H.4})$$

$$h_2(x, t) = h_0 e^{-Cx} [D \sin(\omega t - Cx) + E \cos(\omega t - Cx)]$$

Again, the constants A, F, G, C, D, and E have to be determined from the first three boundary conditions in (II.H.2). The resulting expressions for those constants are :

$$A = \sqrt{\omega S_1 / 2T_1}$$

$$C = \sqrt{\omega S_2 / 2T_2}$$

$$\begin{aligned} F = \frac{e^{-Ax_B}}{U} \left(1 - \frac{AT_1}{CT_2}\right) [SINEXP * \sin(Cx_B - Ax_B) \\ - COSEXP * \cos(Cx_B - Ax_B)] \end{aligned}$$

$$U = COSEXP^2 + SINEXP^2$$

$$\begin{aligned} SINEXP = & e^{-Ax_B} \left(1 - \frac{AT_1}{CT_2}\right) \sin(Cx_B - Ax_B) \\ & - e^{Ax_B} \left(1 + \frac{AT_1}{CT_2}\right) \sin(Cx_B + Ax_B) \end{aligned}$$

$$\begin{aligned} COSEXP = & -e^{-Ax_B} \left(1 - \frac{AT_1}{CT_2}\right) \cos(Cx_B - Ax_B) \\ & + e^{Ax_B} \left(1 + \frac{AT_1}{CT_2}\right) \cos(Cx_B + Ax_B) \end{aligned}$$

$$\begin{aligned}
& (1-F)e^{-Ax_B} \left(1 - \frac{AT_1}{CT_2}\right) \sin(Cx_B - Ax_B) \\
& + Fe^{Ax_B} \left(1 + \frac{AT_1}{CT_2}\right) \sin(Cx_B + Ax_B) \\
G = & \frac{-e^{-Ax_B} \left(1 - \frac{AT_1}{CT_2}\right) \cos(Cx_B - Ax_B) \\
& + e^{Ax_B} \left(1 + \frac{AT_1}{CT_2}\right) \cos(Cx_B + Ax_B)}{
\end{aligned}$$

$$\begin{aligned}
D = \frac{AT_1}{CT_2} e^{Cx_B} \{ & e^{-Ax_B} [(1-F) \cos(Cx_B - Ax_B) \\
& - G \sin(Cx_B - Ax_B)] - e^{Ax_B} [F \cos(Cx_B + Ax_B) \\
& - G \cos(Cx_B + Ax_B)] \}
\end{aligned}$$

$$\begin{aligned}
E = \frac{AT_1}{CT_2} e^{Cx_B} \{ & e^{-Ax_B} [(1-F) \sin(Cx_B - Ax_B) \\
& + G \cos(Cx_B - Ax_B)] - e^{Ax_B} [F \sin(Cx_B + Ax_B) \\
& - G \cos(Cx_B + Ax_B)] \}
\end{aligned}$$

Specifically, if $T_1 = T_2 = T$ and $S_1 = S_2 = S$: $F = G = E = 0$, $D = 1$, and $A = C = \sqrt{\omega S / 2T}$ so that equation (II.H.4) reduces to the one-zone solution (Ingersoll et al. 1948):

$$h(x, t) = h_0 e^{-x\sqrt{\omega S / 2T}} \sin(\omega t - x\sqrt{\omega S / 2T}) \quad (\text{II.H.5})$$

In the case of only small variations in the transmissivities and storage coefficients, that is, for $T_1 \sim T_2$ and $S_1 \sim S_2$, a simplification of the constants A , C , D , E , F , and G leads to the following approximate expressions for the two-zone solutions:

$$h_1(x,t) = h_0 e^{-Ax} \sin(\omega t - Ax) \quad (\text{II.H.6})$$

$$h_2(x,t) = h_0 \frac{AT_1}{CT_2} e^{-C(x-x_B)-Ax_B} \sin(\omega t - Cx)$$

This result shows that the amplitude decay is a function of the spatially weighted average of the parameters :

$$\text{Amp} \propto f(e^{-\sqrt{\frac{\omega S_2}{2T_2}}(x-x_B) - \sqrt{\frac{\omega S_1}{2T_1}}x_B}) \quad (\text{II.H.7})$$

Effect of Initial Estimates on Parameter Estimation

Solutions to (II.H.4) were investigated in conjunction with the Levenberg-Marquardt algorithm to inversely estimate the transmissivities and storage coefficients of both zones for predefined model situations. To uncover the influence of the particular set of initial parameter guesses on the estimated transmissivities and storage coefficients, eight Monte Carlo simulations were performed, each simulation based on a slightly altered set of initial guesses. Every Monte Carlo simulation is based on 800 single simulations. For each single simulation the initial transmissivities and storage coefficients were taken from predefined parameter intervals in the form of a uniform deviate. The estimation was then performed by incorporating synthetic data which were generated by using the analytical two-zone solution in conjunction with a defined parameter set of the hydraulic aquifer parameters. As there are five parameters to be estimated for this model (two transmissivities, two storage coefficients, and the boundary separating both aquifer zones), five observation positions were chosen at which the synthetic data were generated. Two observation positions were located within the first zone and three observation positions were located within the second zone. The sequences of observation data were generated at lateral distances of 4.3, 7.2, 11.0, 14.8, and 19.3 meters from the origin at which sinusoidal head boundary conditions were specified. The boundary between both zones is located at $x_B = 10.0$ meters from the origin. The synthetic observation data were generated by (II.H.4) at times $t=n*dt$, $n=0,1,2,3,\dots$ according to the following parameter setup :

$$\begin{aligned} T_{10} &= 1.5535\text{E-}3 \text{ m}^2/\text{sec} \\ S_{10} &= 1.3300\text{E-}5 \\ T_{20} &= 9.9678\text{E-}3 \text{ m}^2/\text{sec} \\ S_{20} &= 4.7200\text{E-}4 \end{aligned}$$

$t_0 = 1800 \text{ sec.}$	period of input signal
$h_0 = 1.0 \text{ m}$	amplitude of input signal
$dt = 90.0 \text{ sec}$	time step
$T_{\max} = 27000 \text{ sec}$	max. simulation time
$t = n * dt$	
$\omega = 2 * \pi / t_0$	

The eight Monte Carlo simulations are numbered from 3 to 10. For Monte Carlo simulation no. 3 the following set of initial parameters was chosen :

$T_1 = T_{10} + 0.5 * u * T_{10}$;	$T_{10} = 1.5535E-3 \text{ m}^{**2}/\text{sec}$
$S_1 = S_{10} + 0.5 * u * S_{10}$;	$S_{10} = 1.3300E-5$
$T_2 = T_{20} + 0.5 * u * T_{20}$;	$T_{20} = 9.9678E-3 \text{ m}^{**2}/\text{sec}$
$S_2 = S_{20} + 0.5 * u * S_{20}$;	$S_{20} = 4.7200E-4$
$x_{B.} = x_{B.0} + u * 0.9999$;	$x_{B.0} = 10.0 \text{ m}$

T_{10} , S_{10} , T_{20} , S_{20} , and $x_{B.0}$ are the initial values with which the synthetic data at the observation positions were generated. u is a uniform deviate with values between -1 and +1. The initial parameters for Monte Carlo simulation no. 4-10 were chosen to be the same as for Monte Carlo simulation no. 3 with the exception of the T_2 parameters. Those parameters were chosen as follows :

Monte Carlo simulation #	$T_2 \text{ (m}^{**2}/\text{sec)}$
4	$T_2 = T_{20}/1.5 + 0.5 * u * T_{20}$
5	$T_2 = T_{20}/2.0 + 0.5 * u * T_{20}$
6	$T_2 = T_{20}/2.5 + 0.5 * u * T_{20}$
7	$T_2 = T_{20}/3.0 + 0.5 * u * T_{20}$
8	$T_2 = T_{20}/3.5 + 0.5 * u * T_{20}$
9	$T_2 = T_{20}/4.0 + 0.5 * u * T_{20}$
10	$T_2 = T_{20}/5.0 + 0.5 * u * T_{20}$

Thus, the interval from which the uniformly distributed T_2 parameters for the 800 single simulations of each Monte Carlo simulation were drawn, is shifted to smaller and smaller values. The averages of the 800 estimates of the parameters of each Monte Carlo simulation are summarized in table 1, the respective standard deviations are given in table 2.

Figures 1, 2, 3, and 4 show selected histograms of the estimated transmissivities of the second zone of Monte Carlo simulation no. 3, 4, 8, and 9. Those histograms reveal that the relative errors of the arithmetic averages of the estimated T_2 value stays within 35% of the true one as long as the deviation of the centroid of the interval from which the transmissivities of the second zone were drawn does not exceed 50% of the true value used to generate the synthetic data (the histograms for the remaining parameters (not

shown) exhibited exactly the same behavior). If the centroid deviates more than 50% from the original value, then the error of the average estimated S_2 -value quickly rose to several 100% (Figure 8). The growth of the relative errors of the averages of estimated transmissivities and storage coefficients is shown in Figures 5, 6, 7, and 8. In a typical real application we would not be able to bracket expected real parameter values with the required precision as outlined above, therefore we can conclude that, although we might arrive at reasonable convergence properties of the employed inverse algorithm, it would be difficult to relate the calculated results reliably to true physical parameters, when all five parameters are estimated simultaneously. To evaluate if better estimations of the true parameters would be obtained when using more observation wells, for example, we would have to perform more extensive numerical investigations. Note that the present results required a CPU-time of approximately 15 days on a 486 personal computer with a mathematical coprocessor. Therefore, any attempts to use a numerical groundwater flow model to estimate the aquifer parameters when using pulse testing with many observation wells at GEMS would require appropriate computer resources.

Table 1: Average estimated transmissivities, storage coefficients, and boundary between both aquifer zones of Monte Carlo simulation no. 3 - 10.

Simulation	Av. T_1	Av. S_1	Av. T_2	Av. S_2	Av. X_{boundary}
3	1.4128E-3	1.2096E-5	9.0656E-3	4.2928E-4	10.0000
4	1.3027E-3	1.1153E-5	8.3585E-3	3.9580E-4	10.0000
5	1.1848E-3	1.0143E-5	7.6021E-3	3.6000E-4	10.0000
6	1.1130E-3	1.0159E-5	6.9098E-3	1.5012E-3	10.0564
7	1.1341E-3	1.1336E-5	6.0792E-3	3.0164E-3	10.0738
8	1.0572E-3	1.2036E-5	5.9890E-3	3.4456E-3	10.1055
9	1.0727E-3	1.0899E-5	5.4940E-3	3.9800E-3	10.1536
10	1.1245E-3	1.1124E-5	5.2809E-3	3.3926E-3	10.1516

Table 2: Standard deviations of estimated transmissivities, storage coefficients, and boundary between both aquifer zones of Monte Carlo simulation no. 3 - 10.

Simulation	Std. T_1	Std. S_1	Std. T_2	Std. S_2	Std. X_{boundary}
3	1.3001E-7	9.5299E-12	5.3528E-6	1.2000E-8	0.0000E0
4	1.2540E-7	9.1915E-12	5.1628E-6	1.1576E-8	0.0000E0
5	1.5688E-7	1.1499E-11	6.4587E-6	1.4482E-8	0.0000E0
6	5.8629E-7	6.2613E-11	9.5502E-6	7.6498E-5	6.0784E-2
7	1.8181E-6	2.8913E-10	1.2730E-5	2.5131E-4	1.3800E-1
8	2.0577E-6	1.9830E-9	1.3282E-5	2.1593E-4	1.3473E-1
9	5.1606E-6	5.6008E-10	1.4629E-5	2.2780E-4	1.8718E-1
10	1.0355E-5	2.3900E-10	3.1645E-5	1.5293E-4	2.0820E-1

Parameter Estimation with SUPRPUMP

The major difficulty in simultaneously estimating all five parameters stems from high correlations between them. It can be directly inferred from equations (II.H.1) that high correlations between T_1 and S_1 and T_2 and S_2 are to be expected as those parameters are comprised within the two diffusivities v_1 and v_2 which might be viewed as the actual two parameters governing groundwater flow described by (II.H.1). To investigate the estimation properties when keeping fixed four of the five parameters, the two-zone solution was implemented into SUPRPUMP. In a first step 30 simulations were performed to test the convergence properties of each physical parameter. Within each of those 30 simulations only one parameter (either one transmissivity value or one storage coefficient) was estimated. The boundary between both zones was always kept fixed at a value of 10m. The initial guesses for the transmissivities covered the parameter range from $4.8\text{m}^2/\text{sec}$ to $5.22 \cdot 10^{-7}\text{m}^2/\text{sec}$, the initial guesses for the storage coefficients covered a parameter range of $3.3 \cdot 10^{-2}$ to $3.9 \cdot 10^{-8}$. Convergence of the estimation procedure was always achieved after at most 21 iterations. In all cases the respective estimated parameter excellently matched the true one. In a further study 47 simulations were performed in which two parameters were now simultaneously estimated again keeping the boundary between both zones fixed as well as the two remaining parameters. 25 simulations were designed to simultaneously estimate T_1 and T_2 , 11 simulations were designed to simultaneously estimate S_1 and T_2 , and 11 simulations were designed to simultaneously estimate T_2 and S_2 . The initial guesses for the transmissivities lay within a range of $10^{-2}\text{m}^2/\text{sec}$ to $10^{-6}\text{m}^2/\text{sec}$, those for the storage coefficients lay in the range of 10^{-3} to 10^{-6} . Again convergence was always achieved within at most 22 iterations with an excellent match of estimated and true parameters. Problems, however, arose when trying to simultaneously estimate two physical parameters and also the boundary location or when trying to simultaneously estimate all four physical parameters keeping the boundary location fixed. In the former case 16 of 24 performed simulations did not converge. In the later case the estimated storage coefficient of the second zone always became unrealistically small (10^{-20}) and convergence to the true parameters could never be achieved. In comparison to the estimations performed by employing a Monte Carlo simulation in conjunction with the Levenberg-Marquardt technique we see that the convergence behavior of the Newton-like estimation technique as implemented in SUPRPUMP might be due to worse convergence properties of the latter method. Similar observations were stated elsewhere (e.g. Sacher 1983, Schwarz 1986).

Parameter Estimation Using Approximate Solution

We note that the application of the approximate expressions (II.H.6), although of intuitive interest, must be applied cautiously to situations for which the assumptions inherent in the derivation of (II.H.6) do not hold, that is, to aquifers showing significant variabilities in the hydraulic parameters. 13 Monte Carlo simulations were performed to support this statement. The same initial parameter setup was chosen for those simulations as was for the Monte Carlo simulations 4-10. In the present case, however, the storage coefficients were kept fixed as was the boundary location $x_B,0$. Only the transmissivities were disturbed by a uniform deviate u according to the following scheme :

Monte Carlo simulation #	T_1 (m**2/sec)	T_2 (m**2/sec)
11	$T_1 = T_{10} + 0.5*u*T_{10}$	$T_2 = T_{20} + 0.5*u*T_{20}$
12	$T_1 = T_{10} + 0.5*u*T_{10}$	$T_2 = T_{20}/3.0 + 0.5*u*T_{20}/3.0$
13	$T_1 = T_{10} + 0.5*u*T_{10}$	$T_2 = T_{20}/6.0 + 0.5*u*T_{20}/6.0$
14	$T_1 = T_{10} + 0.5*u*T_{10}$	$T_2 = T_{20}/9.0 + 0.5*u*T_{20}/9.0$
15	$T_1 = T_{10} + 0.5*u*T_{10}$	$T_2 = T_{20}/12.0 + 0.5*u*T_{20}/12.0$
16	$T_1 = T_{10} + 0.5*u*T_{10}$	$T_2 = T_{20}/15.0 + 0.5*u*T_{20}/15.0$
17	$T_1 = T_{10} + 0.5*u*T_{10}$	$T_2 = T_{20}/30.0 + 0.5*u*T_{20}/30.0$
18	$T_1 = T_{10}/3.0 + 0.5*u*T_{10}/3.0$	$T_2 = T_{20} + 0.5*u*T_{20}$
19	$T_1 = T_{10}/6.0 + 0.5*u*T_{10}/6.0$	$T_2 = T_{20} + 0.5*u*T_{20}$
20	$T_1 = T_{10}/9.0 + 0.5*u*T_{10}/9.0$	$T_2 = T_{20} + 0.5*u*T_{20}$
21	$T_1 = T_{10}/12.0 + 0.5*u*T_{10}/12.0$	$T_2 = T_{20} + 0.5*u*T_{20}$
22	$T_1 = T_{10}/15.0 + 0.5*u*T_{10}/15.0$	$T_2 = T_{20} + 0.5*u*T_{20}$
23	$T_1 = T_{10}/30.0 + 0.5*u*T_{10}/30.0$	$T_2 = T_{20} + 0.5*u*T_{20}$

Again each Monte Carlo simulation consists of 800 single simulations. The chosen scheme once again realizes a systematic shift of the intervals from which the initial transmissivities were drawn. For simulation 11-17 the T_2 -interval was systematically shifted to smaller transmissivity values, for simulation 18-23 the T_1 -interval from which the initial transmissivities were drawn was continuously shifted to smaller values. The averages of the 800 estimated parameters of each Monte Carlo simulation are listed in table 3. The values significantly deviate from the true parameters T_{10} and T_{20} .

Table 3: Average estimated transmissivities of Monte Carlo simulation
no. 11 - 23.

Simulation	Av. T ₁	Av. T ₂
11	1.6828E-2	1.3903E-3
12	1.7725E-2	1.2081E-3
13	1.7725E-2	1.2081E-3
14	1.7725E-2	1.2081E-3
15	1.7725E-2	1.2081E-3
16	1.7725E-2	1.2081E-3
17	1.7725E-2	1.2081E-3
18	2.3654E-3	2.5691E-3
19	3.0087E-4	1.4255E-3
20	3.2287E-4	8.8096E-4
21	3.7956E-4	6.1106E-4
22	1.0763E-3	4.5610E-4
23	2.4751E-3	1.9340E-3

Application of a Kalman Filter for Hydraulic Parameter Estimation

Today, the use of a Kalman filter (Kalman 1960, Kalman & Bucy 1961) is well known for yielding improved estimates not only of the respective state variables but also of the associated parameters. Lim & Lee (1992), for example, use a Kalman filter to predict the growth of *Trichoderma viride* grown on glucose while simultaneously estimating the kinetic parameters of the underlying Monod model. Geer (1982, 1984) applied the Kalman filter algorithm to design monitoring networks in the Netherlands, and Sen (1984) based a Kalman filter on the Theis-equation to estimate the hydraulic parameters of an aquifer. For the present work the two-zone solution developed above was employed as a base-model for a Kalman filter. To derive a suitable state equation, the system describing equations for the two-zone aquifer must be compiled appropriately. Assuming that the transmissivities, storage coefficients, and the boundary between both aquifer zones shall not depend on the time, the governing system equations have the form:

$$\begin{aligned}
 \frac{dh_1}{dt} &= f_1(T_1, S_1, T_2, S_2, x_B.) & \frac{dh_6}{dt} &= \frac{dT_1}{dt} = 0 \\
 \frac{dh_2}{dt} &= f_2(T_1, S_1, T_2, S_2, x_B.) & \frac{dh_7}{dt} &= \frac{dS_1}{dt} = 0 \\
 \frac{dh_3}{dt} &= f_3(T_1, S_1, T_2, S_2, x_B.) & \frac{dh_8}{dt} &= \frac{dT_2}{dt} = 0
 \end{aligned}$$

$$\frac{dh_4}{dt} = f_4(T_1, S_1, T_2, S_2, x_B.)$$

$$\frac{dh_9}{dt} = \frac{dS_2}{dt} = 0$$

$$\frac{dh_5}{dt} = f_5(T_1, S_1, T_2, S_2, x_B.)$$

$$\frac{dh_{10}}{dt} = \frac{dx_B.}{dt} = 0$$

Here the f_i , which stem from the time-derivative of the two-zone aquifer solutions h_i , are functions in the free parameters T_1, S_1, T_2, S_2 , and $x_B.$ as are the h_i :

$$h_i = h_i(T_1, S_1, T_2, S_2, x_B., x_i, t) \quad i=1, \dots, 5 ; x_i - \text{observation node}$$

h_i - two-zone solution

Using a local linear approximation to the derivative of these equations the system equations can be summarized by an augmented dynamic equation of the form :

$$\left. \frac{d\vec{h}}{dt} \right|_{t+\Delta t} = \left. \frac{d\vec{h}}{dt} \right|_t + \Delta t \left[\underline{\underline{A}} \frac{d\vec{h}}{dt} \right]_t \quad (\text{II.H.8})$$

where $\mathbf{h} = (h_1, \dots, h_{10})$ and $\underline{\underline{A}}$ is the Jacobian of the process which is given by :

$$A = \begin{bmatrix} \frac{d\dot{h}_1}{dh_1} & \frac{d\dot{h}_1}{dh_2} & \frac{d\dot{h}_1}{dh_3} & \frac{d\dot{h}_1}{dh_4} & \frac{d\dot{h}_1}{dh_5} & \frac{d\dot{h}_1}{dT_1} & \frac{d\dot{h}_1}{dS_1} & \frac{d\dot{h}_1}{dT_2} & \frac{d\dot{h}_1}{dS_2} & \frac{d\dot{h}_1}{dx_B.} \\ \frac{d\dot{h}_2}{dh_1} & \frac{d\dot{h}_2}{dh_2} & \dots & \dots & & & & & \dots & \frac{d\dot{h}_2}{dx_B.} \\ \vdots & \vdots & & & & & & & & \vdots \\ \frac{d\dot{T}_1}{dh_1} & \frac{d\dot{T}_1}{dh_2} & \dots & \dots & & & & & \dots & \frac{d\dot{T}_1}{dx_B.} \\ \vdots & \vdots & & & & & & & & \vdots \\ \frac{d\dot{x}_B.}{dh_1} & \frac{d\dot{x}_B.}{dh_2} & \frac{d\dot{x}_B.}{dh_3} & \frac{d\dot{x}_B.}{dh_4} & \frac{d\dot{x}_B.}{dh_5} & \frac{d\dot{x}_B.}{dT_1} & \frac{d\dot{x}_B.}{dS_1} & \frac{d\dot{x}_B.}{dT_2} & \frac{d\dot{x}_B.}{dS_2} & \frac{d\dot{x}_B.}{dx_B.} \end{bmatrix}$$

$\underline{A} \in \mathbb{R}^{10 \times 10}$. The vector $\vec{h} = (h_1, \dots, h_{10})$ represents not only the time dependent two-zone solutions of the hydraulic heads h_1, \dots, h_5 at the five observation wells but also a state representation h_6, \dots, h_{10} of the five aquifer parameters T_1, S_1, T_2, S_2 , and x_{Boundary} which are simultaneously estimated during the filter process. The time derivative of vector \vec{h} is given by :

$$\frac{d\vec{h}}{dt} = \left[\frac{dh_1}{dt}, \frac{dh_2}{dt}, \frac{dh_3}{dt}, \frac{dh_4}{dt}, \frac{dh_5}{dt}, \frac{dT_1}{dt}, \frac{dS_1}{dt}, \frac{dT_2}{dt}, \frac{dS_2}{dt}, \frac{dx_{B.}}{dt} \right]$$

Rearranging equation (II.E.8) yields :

$$\left. \frac{d\vec{h}}{dt} \right|_{t+\Delta t} = [\underline{I} + \Delta t \underline{A}]_t \left. \frac{d\vec{h}}{dt} \right|_t \quad \underline{I} \in \mathbb{R}^{10 \times 10}$$

where \underline{I} is the identity matrix. Multiplying both sides of this equation formally by dt and replacing $d\vec{h}$ by $\Delta\vec{h}$ gives the final state equation which was used in a Kalman filter :

$$\Delta\vec{h} \Big|_{t+\Delta t} = (\underline{I} + \Delta t \underline{A})_t \Delta\vec{h} \Big|_t \quad (\text{II.H.9})$$

Note that generally only the upper right 5×5 -submatrix of \underline{A} is different from zero, the transition matrix $(\underline{I} + \Delta t \underline{A})_t$ of the process, however, is never zero as the identity is added to the product $\Delta t \underline{A}$. Assuming that the state vector $\Delta\vec{h} = 0$, that is assuming that all states and parameters are known at the beginning of the filter process, the parameters for times $t > 0$ are modeled as time independent. For example, equation (II.E.8) results in the following expression for parameter T_1 : $T_1|_{t+\Delta t} = T_1|_t + \Delta h_6|_t$. As $\Delta h_6|_{t=0} = 0$, the transmissivity of the first aquifer zone is modeled as independent of time. Analogous equations hold for the remaining system parameters.

Initial attempts to estimate parameters with the Kalman filter technique have not been successful. The reason is unknown at this time. A reformulation of the proposed methodology and a reprogramming of the Kalman filter program could be pursued to include the ε -technique described by Gelb (1974).

Radial Pulse-Test Model

In order to analyze pulse tests with a radial model, we extended an approach of Kabala et al. (1985) who developed a slug-test model based on the momentum equation for the water in the well coupled to the Theis equation for the aquifer. Our approach employs an additional sinusoidal external forcing function representing any desired pumping scheme. The governing ordinary differential equation for the displacement of water (x , positive upward) in the well with an effective water column (H_e) then reads :

$$(H_e + x) \frac{d^2 x}{dt^2} + \beta g \int_0^t \left(\frac{dx}{d\tau} + \frac{Q_0}{\pi r_w^2} \sin(\omega\tau) \right) \frac{e^{-\alpha/(t-\tau)}}{t-\tau} d\tau + gx + \frac{3}{4} \left[\frac{dx}{dt} \right]^2 = 0 \quad (\text{II.H.10})$$

which is identical to eq. (9) in Kabala et al. (g is the acceleration of gravity), with the exception of the flow through the screen which is here assumed to be:

$$Q_{screen} = Q_{pumpage} + \pi r_w^2 \frac{dx}{d\tau} = Q_0 \sin(\omega\tau) + \pi r_w^2 \frac{dx}{d\tau} \quad (\text{II.H.11})$$

where r_w is the well radius and Q_0 is the amplitude of the sinusoidal pumping stress. The quantities α and β used in equation (II.H.10) are defined as

$$\alpha = \beta S$$

$$\beta = \frac{r_w^2}{4T}$$

where S is the storage coefficient and T is the transmissivity.

The numerical solution to equation (II.H.10) can be obtained in an analogous way to that outlined in section (III.D) by means of a point iterative method and yields as the solution x as a function of time in the well.

$$(H_e + x^n) \frac{x^{n+1,m+1} - 2x^n + x^{n-1}}{\Delta t^2} + \beta g \left(Term_1(x^{n+1,m}) + Term_2 \right) + \frac{3}{4} \left(\frac{x^{n+1,m+1} - x^{n-1}}{2\Delta t} \right) \left(\frac{x^{n+1,m} - x^{n-1}}{2\Delta t} \right) + gx^n = 0 \quad (\text{II.H.12})$$

where n is the time index and m is the iteration index. Term₁ and Term₂ are two expressions stemming from the discretization of the integral in equation (II.H.10). Term₁ is dependent on $x^{n+1,m}$, the new x value, whereas Term₂ is completely known at the beginning of a new time step, since it depends only on old values of x as shown below. Since equation (II.H.12) is nonlinear and can not be solved explicitly for x , an iterative solution technique must be used. Multiplying the latter equation by $(\Delta t)^2$ and solving for $x^{n+1, m+1}$ the final equation for the solution at time level $n+1$ becomes

$$x^{n+1, m+1} = \frac{(H_e + x^n)(2x^n - x^{n-1}) - (\beta g \text{Term}_2 + g x^n) \Delta t^2}{(H_e + x^n) + \frac{3}{16}(x^{n+1, m} - x^{n-1})} + \frac{\frac{3}{16} x^{n-1} (x^{n+1, m} - x^{n-1}) - \beta g \text{Term}_1(x^{n+1, m})}{(H_e + x^n) + \frac{3}{16}(x^{n+1, m} - x^{n-1})} \quad (\text{II.H.13})$$

Equation (II.H.13) must be solved iteratively for x until there is little change in x between successive iterations.

The explicit form of the two expressions Term₁ and Term₂ can be obtained by discretizing the integral in (II.H.10) as follows :

$$\begin{aligned} \int_0^{t_{n+1}} \left(\frac{dx}{d\tau} + \frac{Q_0}{\pi r_w^2} \sin(\omega \tau) \right) \frac{e^{-\alpha/(t_{n+1}-\tau)}}{t_{n+1} - \tau} d\tau \\ = \sum_{i=0}^n \int_{t_i}^{t_{i+1}} \left(\frac{dx}{d\tau} + \frac{Q_0}{\pi r_w^2} \sin(\omega \tau) \right) \frac{e^{-\alpha/(t_{n+1}-\tau)}}{t_{n+1} - \tau} d\tau \\ = \frac{1}{2\Delta t} \sum_{i=0}^{n-2} \left[x^{i+2} - x^i + \frac{Q_0}{\pi r_w^2} \sin(\omega t_{i+1}) \right] \frac{e^{-\left[\frac{\alpha}{(n+1-i-1)\Delta t}\right]}}{(n+1-i-1)} \\ + \frac{1}{2\Delta t} \left[x^{n+1} - x^{n-1} + \frac{Q_0}{\pi r_w^2} \sin(\omega t_n) \right] e^{-\frac{\alpha}{\Delta t}} \end{aligned} \quad (\text{II.H.14})$$

where we have assumed all Δt_i are equal.

The two terms introduced earlier may now be identified. We must introduce the iteration index m on the x at the new time level $n+1$.

$$Term_1(x^{n+1,m}) = \frac{1}{2\Delta t} \left[x^{n+1,m} - x^{n-1} + \frac{Q_0}{\pi r_w^2} \sin(\omega t_n) \right] e^{-\frac{\alpha}{\Delta t}} \quad (\text{II.H.15})$$

$$Term_2 = \frac{1}{2\Delta t} \sum_{i=0}^{n-2} \left[x^{i+2} - x^i + \frac{Q_0}{\pi r_w^2} \sin(\omega t_{i+1}) \right] \frac{e^{-\left[\frac{\alpha}{(n+1-i-1)\Delta t}\right]}}{(n+1-i-1)} \quad (\text{II.H.16})$$

With these definitions equation (II.H.13) can be solved for x in the borehole as a function of time. However, we want to look at the propagation of the wave away from the borehole. In order to do this, we must solve an additional equation (Kabala et al., 1985).

$$s(r,t) = \frac{1}{4\pi T} \int_0^t \left[\pi r_w^2 \frac{dx}{d\tau} + Q_0 \sin(\omega\tau) \right] \frac{e^{-\left[\frac{r^2 S}{4T(t-\tau)}\right]}}{t-\tau} d\tau \quad (\text{II.H.17})$$

The observation point is at r , an arbitrary distance from the borehole, and the drawdown (s) is given by equation (II.H.17). Since we are using a sinusoidally varying pumpage rate, we would expect the drawdown to be sinusoidal also with an amplitude and phase differing from the signal at the borehole. In general, the solution for this equation would also be done numerically.

Although any arbitrary external discrete forcing function can be used for pumpage, we chose the sinusoidal function outlined above for the first investigations of the behavior of signals transmitted into the aquifer. Figure 9 shows a simulation for which static conditions were initially specified in the borehole (aquifer parameter values are given in Table 4). It can be observed that the peaks of transmitted pulses are phase-shifted with regard to the signal within the well. This is expected according to existing theories (e.g., Streltsova, 1988). Also, the amplitudes decay steadily as one moves away from the well. However, Figure 9 shows that in this case a usable signal has propagated

more than 40 meters from the well. This implies that indeed we should be able to propagate sinusoidal signals over significant distances in aquifers.

Table 4

Simulation	: Fig.	: T ₁ (m ² /s)	: T ₂ (m ² /s)	: S ₁	: S ₂	: X _{Boun.} (m)
No.0	: 1	: 3.0E-2	:	: 1.0E-5	:	:
Case 4	: 3	: 3.0E-2	: 4.9E-2	: 1.0E-5	: 1.0E-5	: 20.0
Case 5	: 4	: 5.9E-2	: 2.9E-2	: 1.0E-5	: 1.0E-5	: 20.0
Case 6	: 5	:	: 4.9E-2	:	: 1.0E-5	:
Case 1	: 6	: 3.0E-2	:	: 1.0E-5	:	:

Finally, the implemented pulse-test code has been validated against SUTRA (Voss, 1984). A precise match of the simulated drawdown with that produced by SUTRA, when specifying equivalent time-dependent boundary flux conditions for the numerical simulator, is shown in Figure 10 (the two curves practically overlies one another) and confirms that the pulse-test code is working correctly.

Amplitude and Phase Information

This approach is based upon applying the following homogenous aquifer solution for a propagating sine wave

$$h(x,t) = h_0 \exp\left(-\sqrt{\frac{S\omega}{2T}}x\right) \sin(\omega t - \sqrt{\frac{S\omega}{2T}}x) + const. \quad (II.H.18)$$

to observation data taken from heterogeneous aquifers. If we introduce two terms, $lag = \sqrt{S\omega / 2T}$ and $AMP = h_0 \exp(-\sqrt{S\omega / 2T}x)$, a plot of $\ln(AMP) = \ln(h_0 * \exp(-lag * X_{Obs})) = \ln(h_0) - lag * X_{Obs}$ versus the respective observation location X_{Obs} clearly will yield a straight line for a homogenous formation. For a heterogeneous formation, however, the situation might be expected to be different.

Before discussing this approach, some additional analytical manipulations of the two-zone heterogeneous solution presented earlier in this section will be very useful to understand how the parameters to be estimated (lag and AMP) depend on the observation point location x . From equation II.H.4, the analytical solution in the first-zone is

$$h_1(x,t) = h_0 e^{-Ax} [(1-F) \sin(\omega t - Ax) + G \cos(\omega t - Ax)] \\ + h_0 e^{Ax} [F \sin(\omega t + Ax) - G \cos(\omega t + Ax)] \quad (\text{II.H.19})$$

This equation can be rewritten by employing the addition rules for trigonometric functions to yield

$$h_1(x,t) = h_0 e^{-Ax} \sqrt{(1-F)^2 + G^2} \sin(\omega t - Ax + \tan^{-1}(\frac{G}{1-F})) \\ + h_0 e^{-Ax} \sqrt{F^2 + G^2} \sin(\omega t + Ax - \tan^{-1}(G/F)) \quad (\text{II.H.20})$$

which shows that the solution in the first zone consists of the superposition of two waves traveling in opposite directions. Equation (II.H.20) can be further manipulated by the cosine law to cast the first-zone solution into a compact form involving only one sine function term. The respective amplitude factor in front of this trigonometric term becomes

$$AMP = h_0 \sqrt{e^{-2Ax} [(1-F)^2 + G^2] + e^{2Ax} (F^2 + G^2)} \quad (\text{II.H.21})$$

Therefore, the analytical expression for the logarithm of the amplitude for the first zone is

$$\ln(AMP) = \ln(h_0) - Ax + 0.5 \ln[(1-F)^2 + G^2 + e^{4Ax} (F^2 + G^2)] \quad (\text{II.H.22})$$

which shows that there is generally no linear dependence of $\ln(AMP)$ with respect to the observation location x . A similar analysis allows us to cast the second-zone solution into the form

$$h_2(x,t) = h_0 e^{-Cx} \sqrt{D^2 + E^2} \sin(\omega t - Cx + \tan^{-1}(\frac{E}{D})) \quad (\text{II.H.23})$$

so that the phase lag and logarithm of the amplitude are given by

$$Lag = -Cx + \tan^{-1}(E/D) \quad (II.H.24)$$

$$\ln(AMP) = \ln(h_0 \sqrt{D^2 + E^2}) - Cx \quad (II.H.25)$$

Equations (II.H.24) and (II.H.25) clearly show that the phase and $\ln(AMP)$ should plot as straight lines when plotted versus distance for zone 2.

First, we investigated the analytically amenable heterogeneous two-zone case. Figures 11 and 12 show the logarithm of the amplitudes $AMP = h_0 \exp(-lag * X_{obs})$ calculated from fitting equation (II.B.9) to the generated two-zone data. The fitted parameters were $lag = \sqrt{S\omega / 2T}$ and h_0 . ω was always kept fixed (assumed known) at the value used to generate the observation data. Table 4 shows the parameter specifications with which the respective two-zone data were generated. It is interesting to note that in each zone the fitted logarithm of the amplitude appears to decay in a linear fashion showing different slopes for both zones which is due to relatively small variations in the transmissivities T_1 and T_2 . The slope of the best fit straight line representing the second zone is identical to the slope of an equivalent homogeneous case (compare Figure 11 and Figure 13) which is in accord with equation (II.H.25), where $C = \sqrt{S_2 \omega / 2T_2}$ represents the slope within the second zones of Figures 11 and 12. Also, when calculating the amplitude intercept value from equation (II.H.25) at $x=0m$ we get exactly the same values as those determined in Figures 11 and 22 by fitting. On the other hand, the slope of the best fit straight line representing the first zone is different from that of an equivalent homogeneous case (compare Figures 11 and 14). This is again in accord with the analytical solution of the two-zone aquifer indicating that generally we can expect first-zone slopes produced by the suggested fitting procedure to carry information of aquifer zones located further away from the well than where the signal is measured. For the n-zone case the slopes might be expected to carry some weighted information of the hydraulic parameters of those other zones further out from the measurement location. However, an interesting feature of Figures 11 and 12 is that the discrete boundary between zone 1 and zone 2 is easily seen in the plots of the logarithm of the amplitude versus observation distance. This technique could be of good use in some field situations, the main drawback being the necessity of having several observation wells at various distances from the stressed well.

Although not shown here, plots of the phase lag versus observation distance are many times very close to straight line segments with breaks in slope associated with discrete boundaries in aquifer properties. Therefore, plots of phase lag are also good

indicators of boundaries and may have some value for field application where sufficient observation wells exist.

In order to investigate whether or not this behavior can also be observed for the one-dimensional n-zone case we resorted to numerical methods and generated oscillatory data for a heterogeneous model aquifer composed of five zones using the finite element program SUTRA (Voss, 1984). Fig. 15 shows the fitted logarithms of the amplitudes versus observation distance which are obtained from fitting the observation data generated with the finite element program. First of all, it should be noted that in more complex systems the overall form of the fitted curve of the logarithm of the amplitude will generally not be stepwise linear. However, the estimation procedure again clearly identifies regions of differing aquifer parameters by showing a significant discontinuity of the slope at the boundaries. In Figure 15, these regions are approximately located at $x=50\text{m}$, $x=120\text{m}$, $x=180\text{m}$, and $x=300\text{m}$. In comparison, the locations of the boundaries of the five aquifer patches had been placed at $x=50.4\text{m}$, $x=116.0\text{m}$, $x=180.0\text{m}$, and $x=304.0\text{m}$ for observation data generation with the finite element program. The close reproduction of the boundaries is remarkable. One would suspect that the application of the fitting procedure outlined here might prove very useful in some field applications for identification of changing aquifer properties and in particular the location of fairly discrete boundaries.

Conclusion

An analytical solution for a simple heterogeneous aquifer configuration was developed and combined with statistical estimation techniques to investigate how reliable the respective aquifer parameters might be inversely estimated using pulse-test data. Although the Levenberg-Marquardt algorithm always led to good convergence properties of the estimation processes, the averaged parameter estimates deviated significantly from the true ones when the initial guesses of the parameters were chosen too far off the true parameters.

For the case of only small variations in the hydraulic parameters the analytical solution of the two-zone model can be simplified to yield significant insight into the averaged aquifer properties which determine the signal amplitude of pulse-test data. However, real situations are usually characterized by strong variations in the hydraulic conductivity field. The approximate solution for small variations in the parameters may have limited application to such situations. The analytical structure of the exact two-zone solution is complex. The expansion of this solution to more complicated heterogeneous

systems would be very difficult. Consequently, numerical studies will be used in further work to investigate the potential of pulse testing to delineate aquifer heterogeneity.

Currently pulse-testing as presented in the literature has only been used for the identification of physical aquifer parameters, specifically for the determination of the spatial distribution of hydraulic diffusivities. Typically, the analysis of pulse test data is based on the analysis of transmitted pulse test signals at one specific observation well assuming a homogenous formation between observation well and pulsed well. A diffusivity value is then assigned to the midpoint of both wells thereby yielding a cartographic interpolation for the hydraulic parameters. Our investigations have revealed the potential of the method to also map the locations of boundaries between aquifer regions having different hydraulic parameters. However, it is necessary to have several observation wells.

The work on pulse testing has been extended to the radial case by using numerical solution techniques. The Theis equation has been coupled to an equation describing the borehole. The purpose was to see if a sinusoidal signal could be transmitted reasonable distances in a radial model. The results of this analysis indicate that a sinusoidal signal generated at a central well can be transmitted large distances relative to those of interest in most contaminant site investigations. The next step was to see if the sinusoidal signal could be analyzed for amplitude and phase to yield some information about heterogeneities it has passed through. The preliminary analysis was done with an analytical, one-dimensional, two-zone model and the results were checked with a numerical model and extended to the case of 5 zones. The preliminary results indicate that plotting amplitude and phase versus distance can yield useful information about heterogeneities, in particular the location of fairly discrete boundaries.

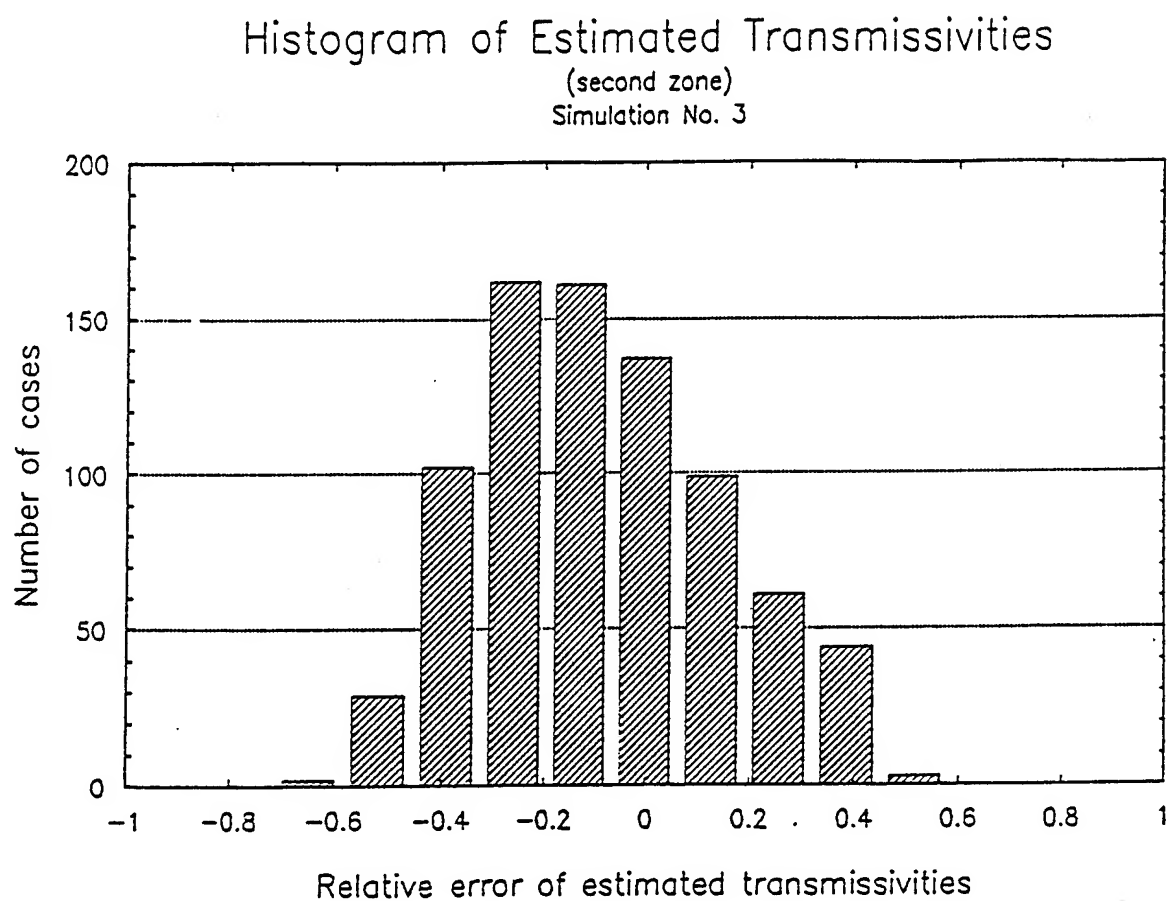


Figure 1. Histogram of the relative errors of the estimated transmissivities of the second zone (Monte Carlo simulation no. 3).

Histogram of Estimated Transmissivities
(second zone)
Simulation No. 4

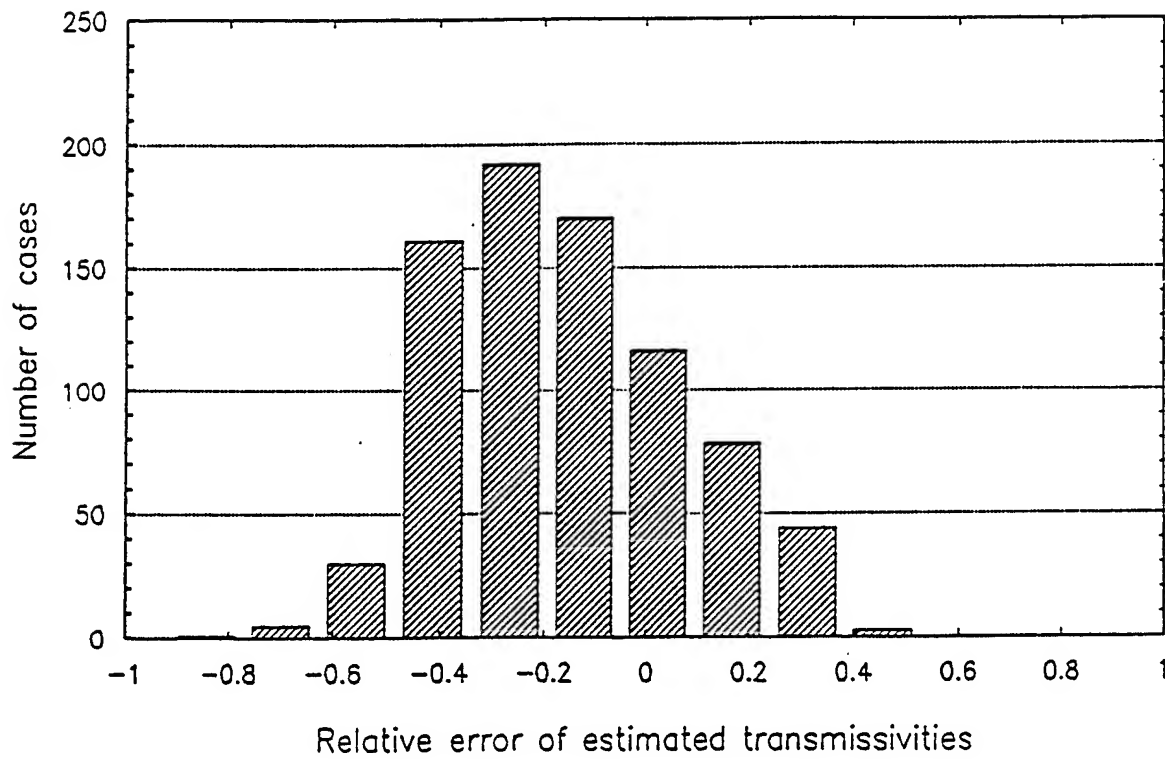


Figure 2. Histogram of the relative errors of the estimated transmissivities of the second zone (Monte Carlo simulation no. 4).

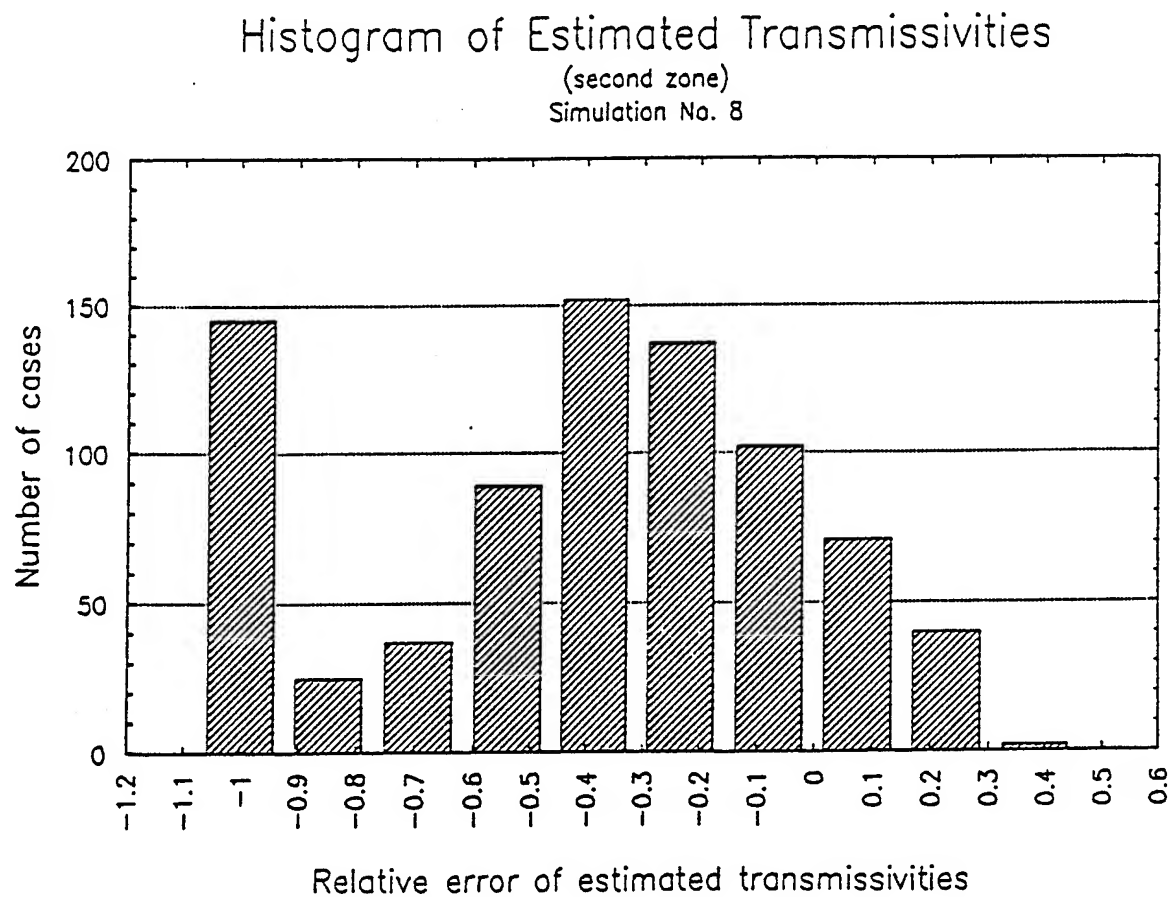


Figure 3. Histogram of the relative errors of the estimated transmissivities of the second zone (Monte Carlo simulation no. 8).

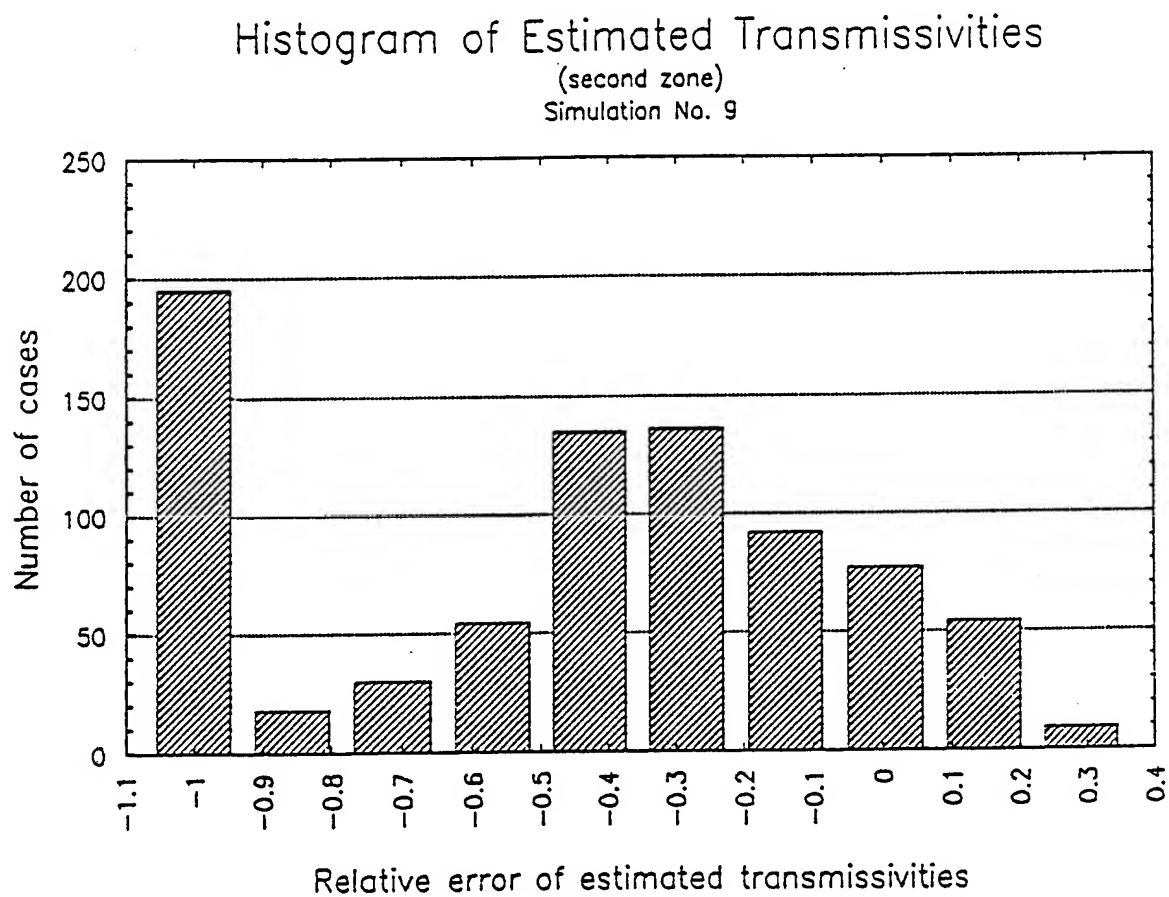


Figure 4. Histogram of the relative errors of the estimated transmissivities of the second zone (Monte Carlo simulation no. 9).

Monte Carlo Simulation No. 3 - 10

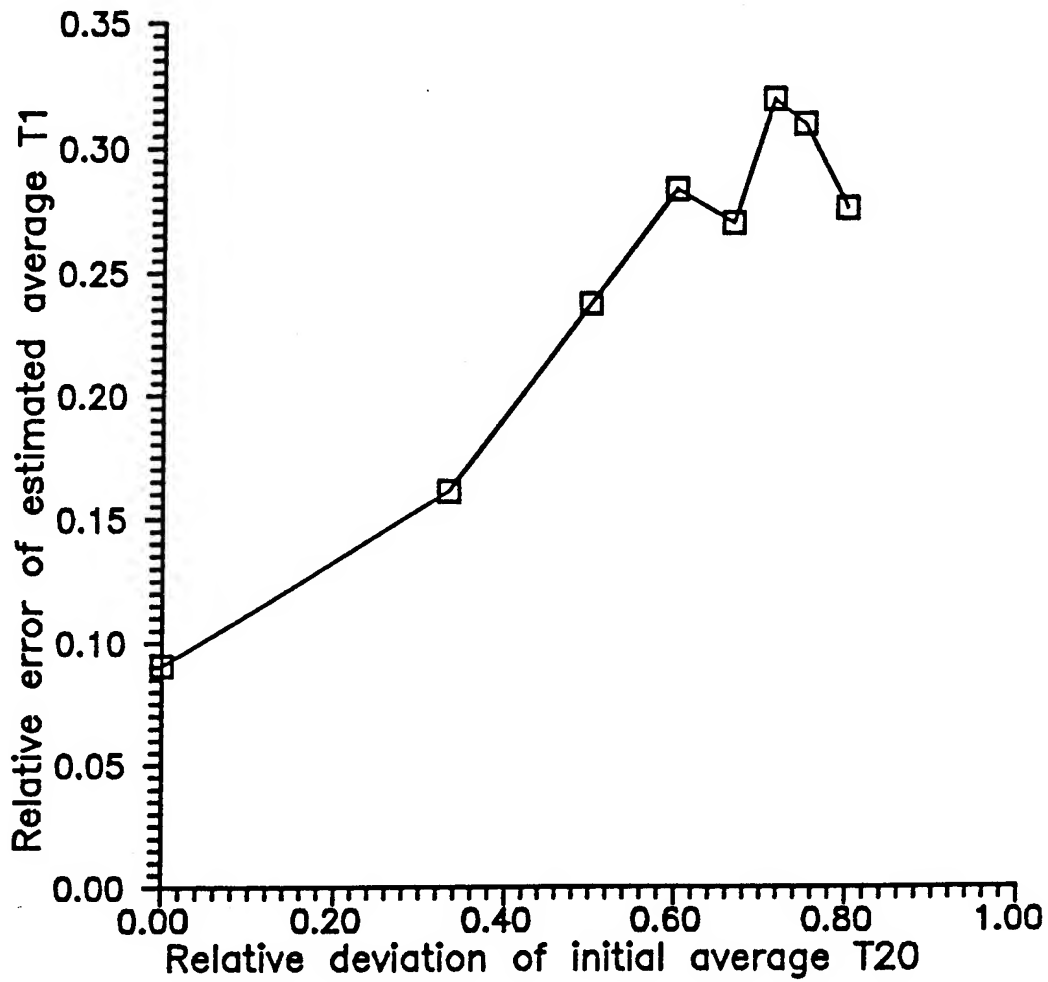


Figure 5. Relative errors of average estimated transmissivities of the first zone plotted versus the relative location of the centroid of the interval from which the initial guesses of the transmissivities of the second zone were drawn.

Monte Carlo Simulation No. 3 - 10

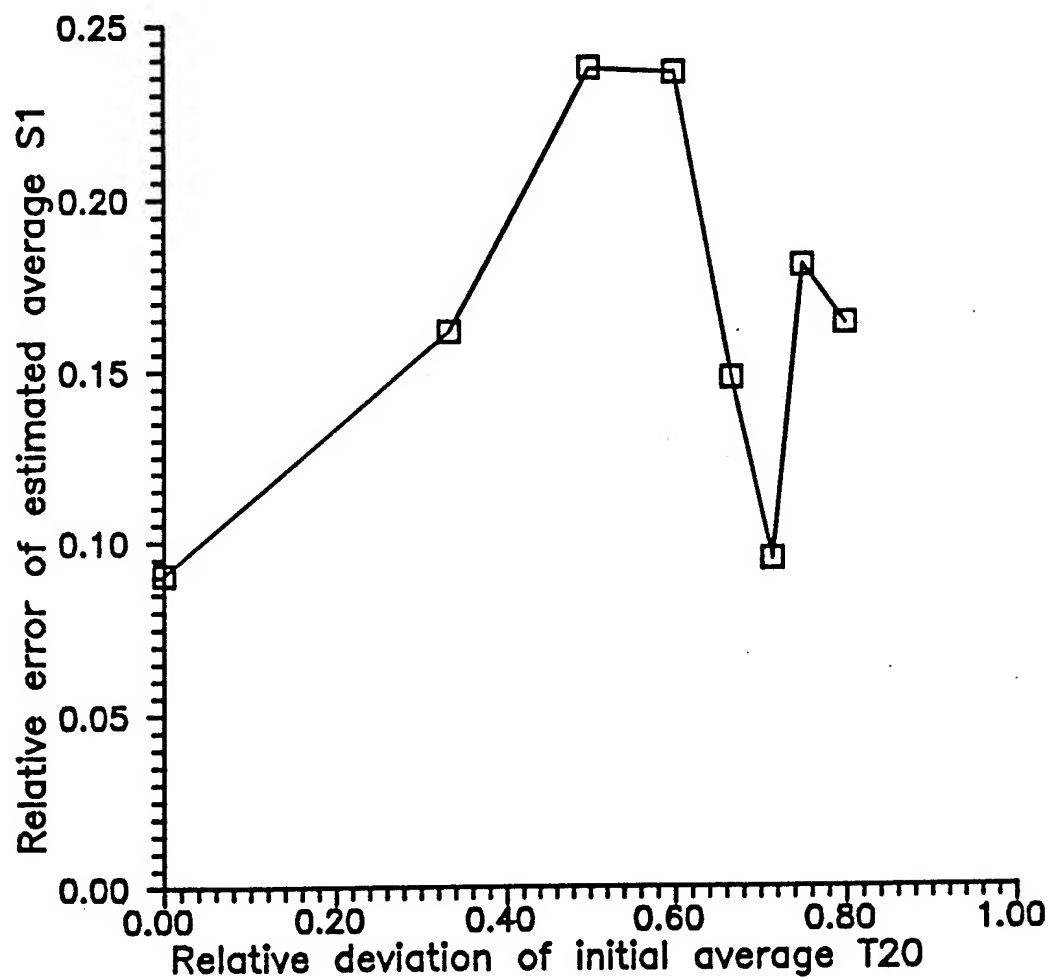


Figure 6. Relative errors of average estimated storage coefficients of the first zone plotted versus the relative location of the centroid of the interval from which the initial guesses of the transmissivities of the second zone were drawn.

Monte Carlo Simulation No. 3 - 10

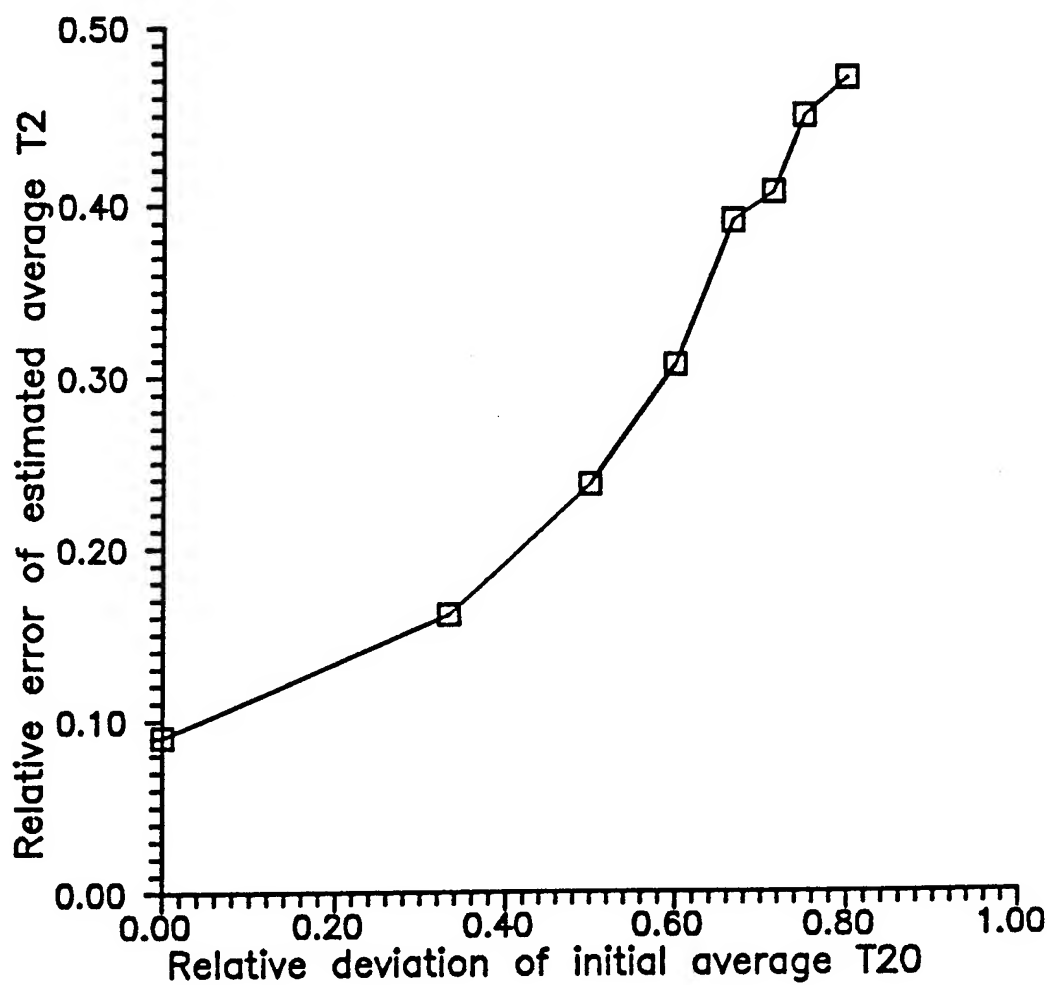


Figure 7. Relative errors of average estimated transmissivities of the second zone plotted versus the relative location of the centroid of the interval from which the initial guesses of the transmissivities of the second zone were drawn.

Monte Carlo Simulation No. 3 - 10

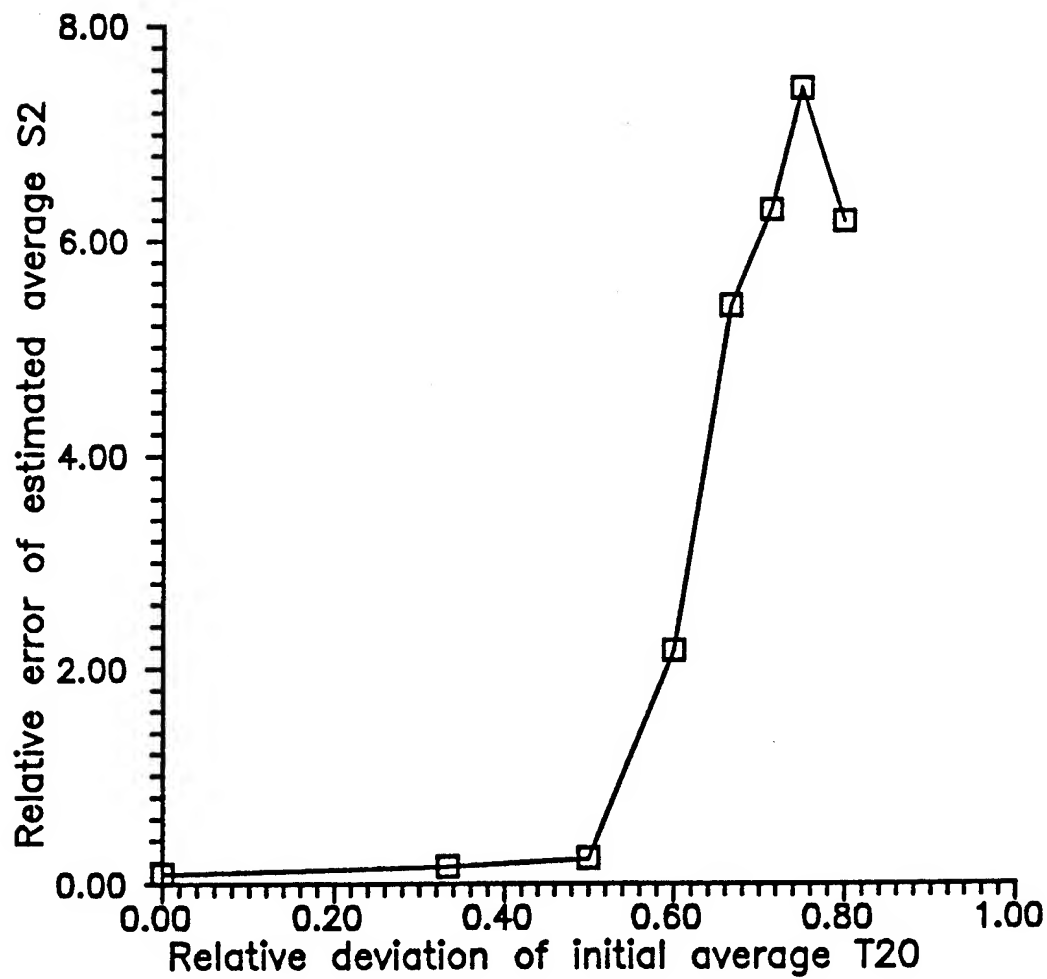


Figure 8. Relative errors of average estimated storage coefficients of the second zone plotted versus the relative location of the centroid of the interval from which the initial guesses of the transmissivities of the second zone were drawn.

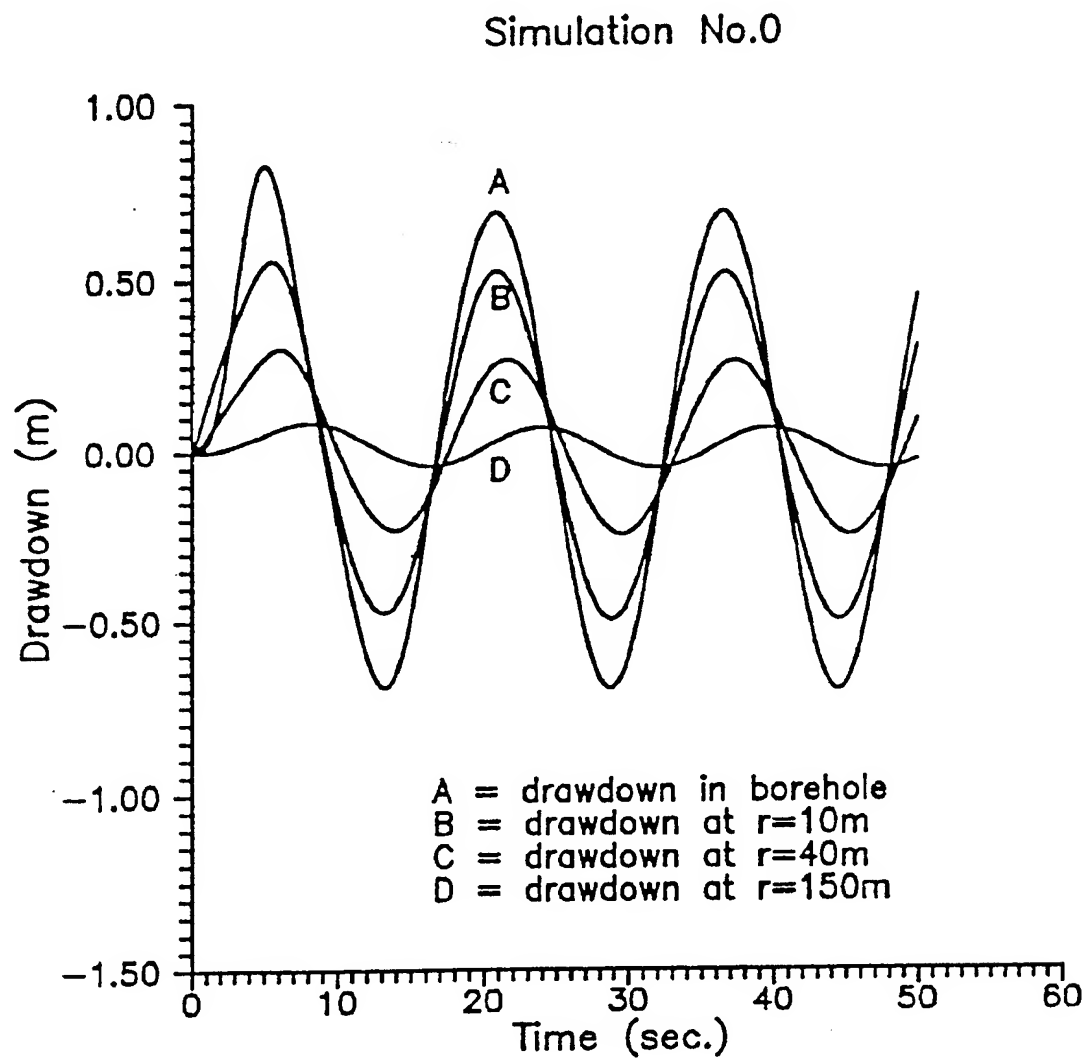


Figure 9. Simulation of pulse test data in a homogenous aquifer with initially static conditions in the borehole.

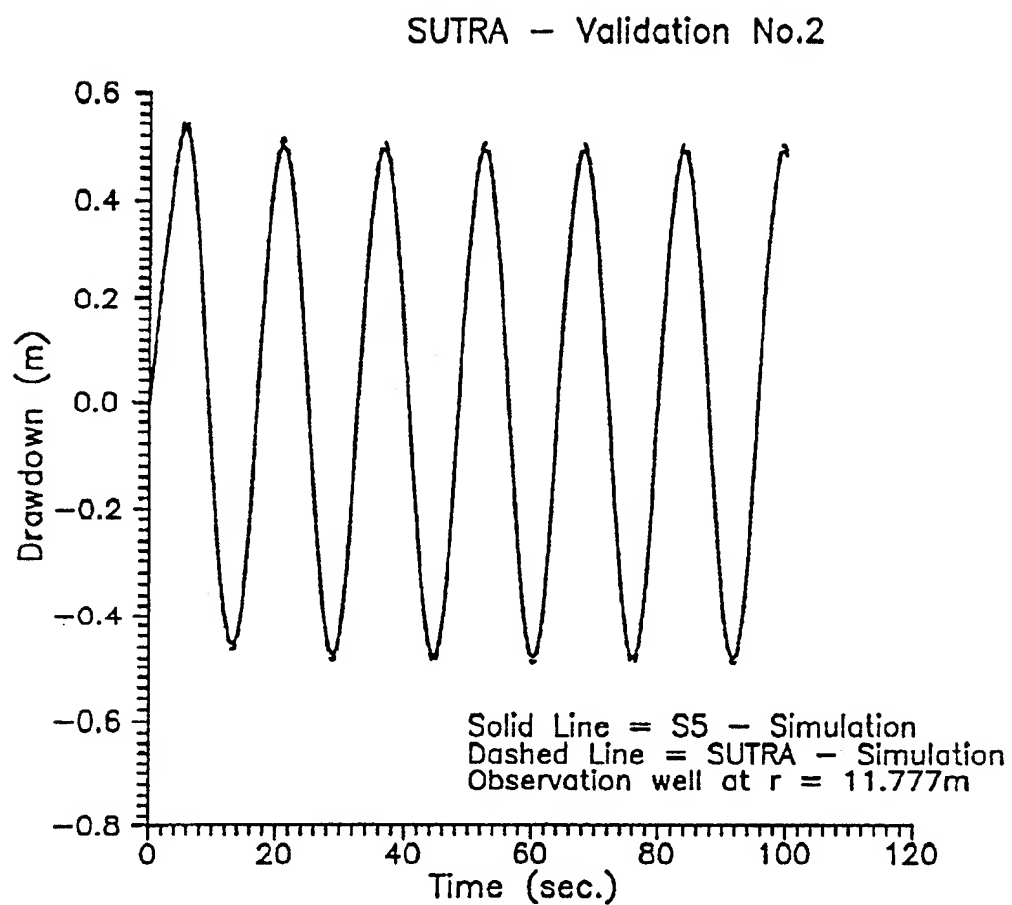


Figure 10. Validation of computer implementation of pulse test program against SUTRA (Voss, 1984).

Case No.4

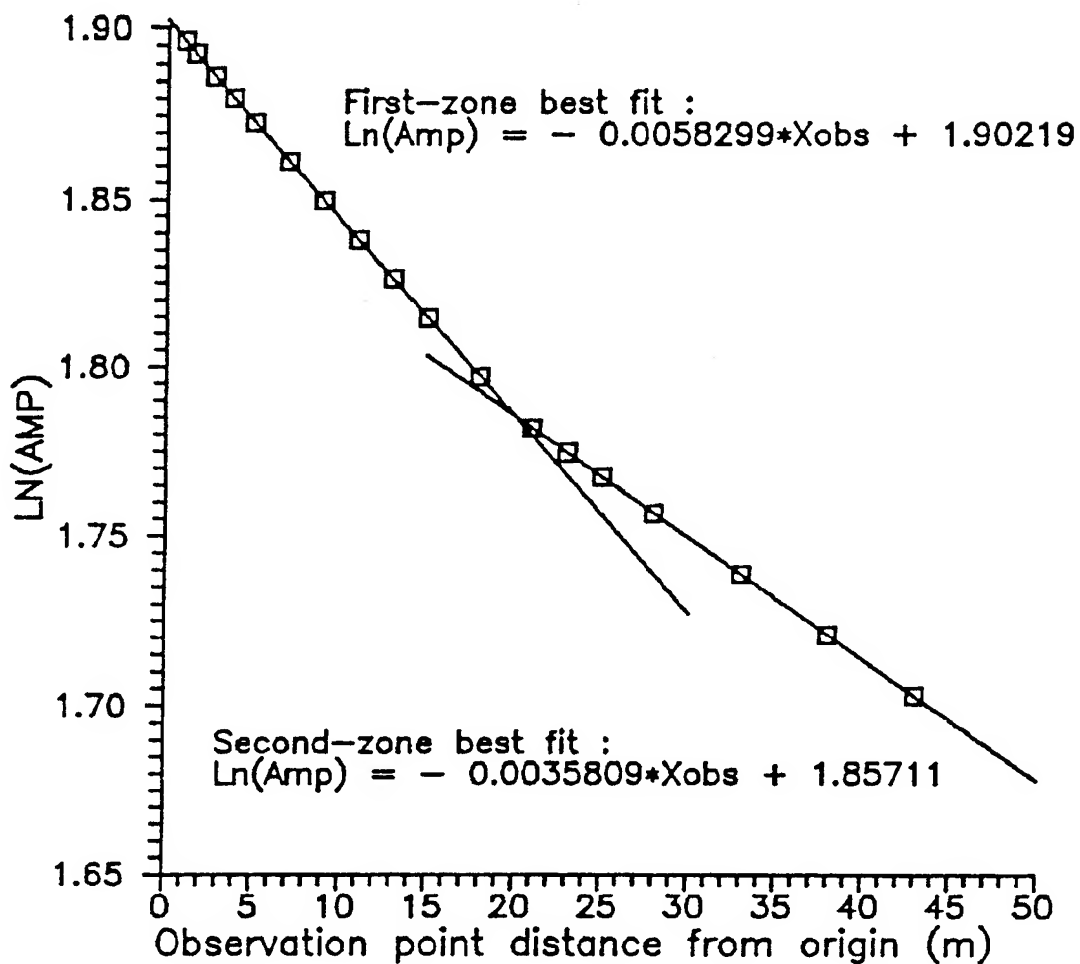


Figure 11. Fitted amplitude $\text{AMP} = h_0 \cdot \exp(-\text{lag} \cdot X_{\text{obs}})$ versus observation point location for two-zone quasi-steady state data.

Case No.5

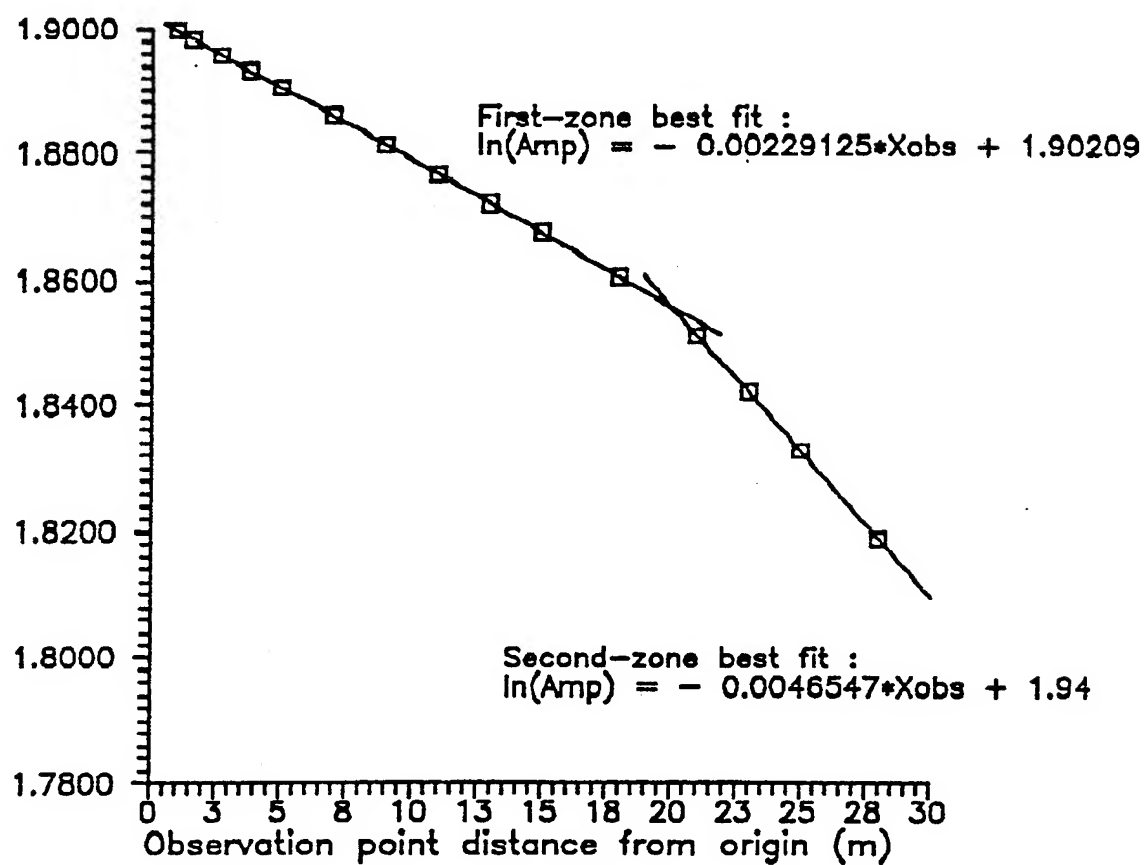


Figure 12. Fitted amplitude $\text{AMP} = h_0 \cdot \exp(-\text{lag} \cdot X_{\text{obs}})$ versus observation point location for two-zone quasi-steady state data.

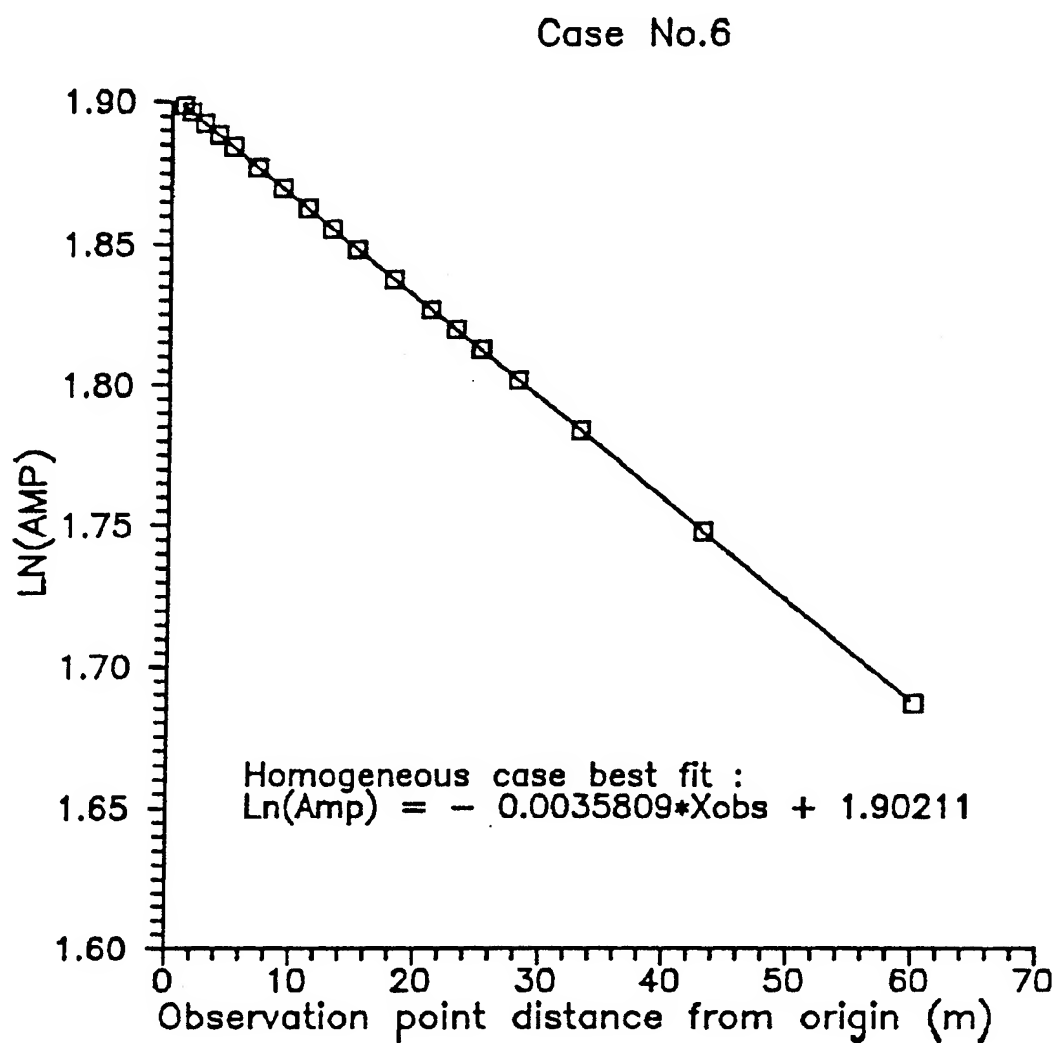


Figure 13. Fitted amplitude $\text{AMP} = h_0 \cdot \exp(-\text{lag} \cdot \text{Xobs})$ versus observation point location for homogenous case data. Physical parameters are the same as for the second zone of two-zone case in figure 3.

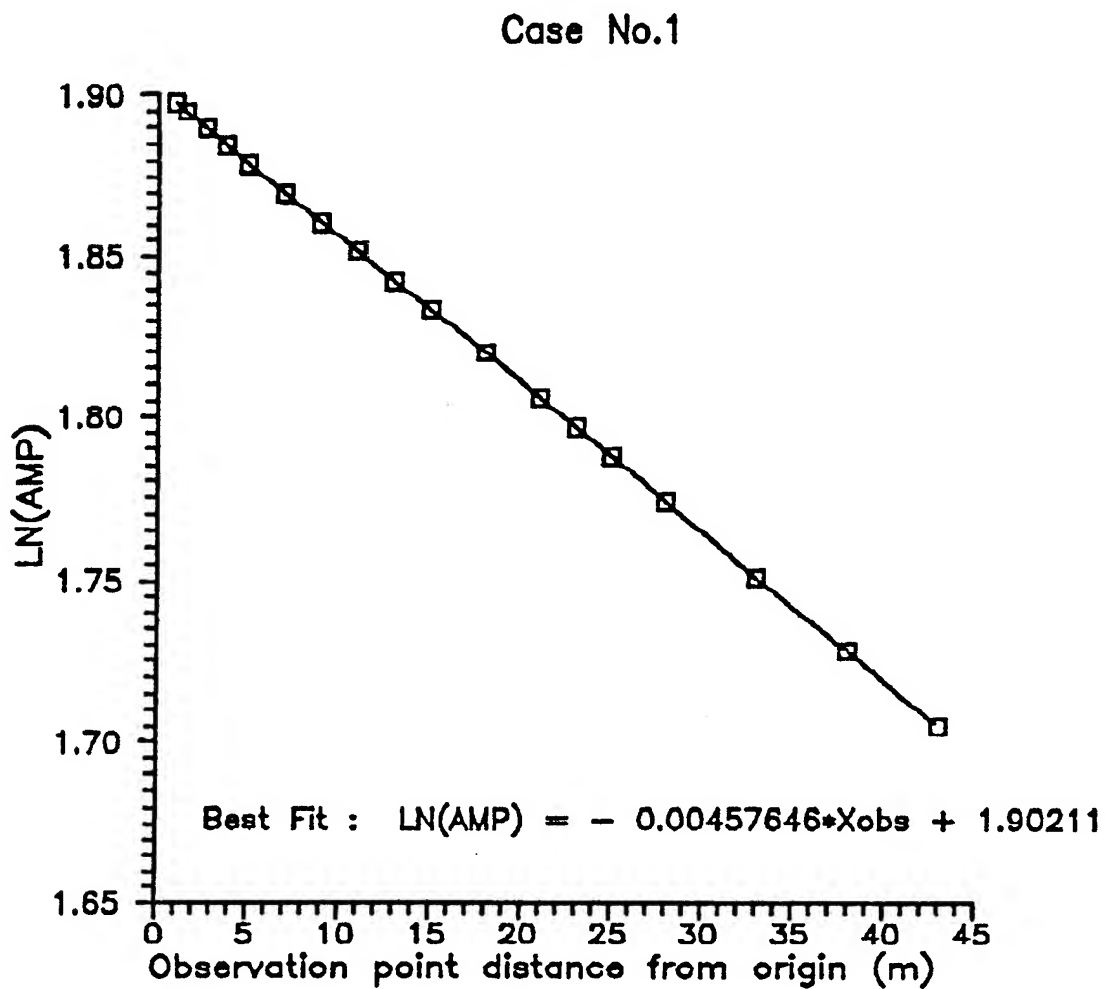


Figure 14. Fitted amplitude $\text{AMP} = h_0 \cdot \exp(-\text{lag} \cdot X_{\text{obs}})$ versus observation point location for homogenous case data. Physical parameters are the same as for the first zone of two-zone case in figure 3.

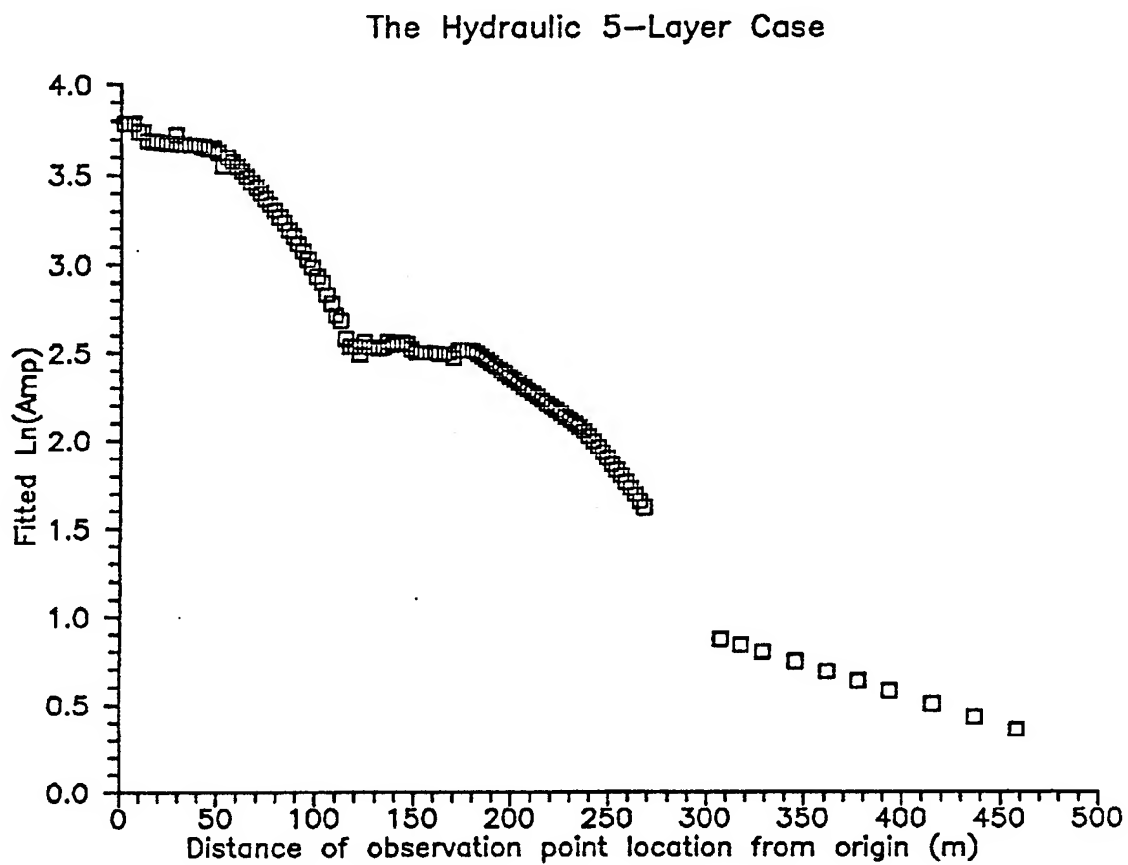


Figure 15. Fitted amplitude $AMP = h_0 \cdot \exp(-lag \cdot X_{obs})$ versus observation point location for the 5-zone case data generated with SUTRA (Voss 1984).

I. NUMERICAL SIMULATION OF INDUCED GRADIENT TRACER TESTS

Introduction

This section describes modeling efforts which contributed to the design of the October 1994 tracer test (GEMSTRAC1) at GEMS. The network design and other tracer test design parameters were chosen based on a combination of theoretical and practical considerations. The design modeling presented here helped to determine the hydraulic format of the tracer test (radially convergent versus dipole), the method of tracer introduction (instantaneous versus continuous), and the amount of tracer mass to introduce. In addition, these results gave us an estimate of the amount of time required to conduct the test and of the necessary sampling frequency.

The final network configuration is shown in Figure 1. This map uses the injection well location (IW) as the origin of the coordinate system. The discharge well (DW) is 46.5 feet south 20° east from the injection well. Both IW and DW are essentially fully screened. The observation well TMO-1 has two screens, one extending from about 0.17 feet to 1.96 feet above the bottom of the aquifer, and the other extending from about 8.52 feet to 10.41 feet above the bottom of the aquifer. All the multilevel samplers east (TME, TMEE) and west (TMW, TMWW) of the centerline are 'regular' samplers, with a two-foot interval between each pair of ports. Thus the 17 ports extend throughout the 35-foot thickness of the aquifer. The odd-numbered samplers along the centerline (TMC) are also regular samplers. However, the even-numbered centerline samplers are 'detailed' samplers, with ports at one-foot intervals, except for a two-foot interval, between ports 9 and 10, to accommodate a coupler between sections of PVC. Thus, the ports for the detailed samplers extend only through approximately the bottom half of the aquifer. See section V for details of the MLS construction. Figure 2 displays the locations of sample ports along the centerline, along with the locations of well screens for IW, DW, and TMO-1. The elevations are in terms of feet above datum, where datum corresponds roughly with the bottom of the aquifer.

Pre-test site characterization

In August and September of 1994, several pumping tests and slug tests were performed using wells in the tracer test network (IW, DW, and TMO-1, along with two observation wells located near TMWW-5). The purpose of these tests was to determine aquifer parameters to use in tracer test design modeling, in order to estimate expected travel times and concentration magnitudes for a given pumping rate and injection scheme. However, the results of these tests raised more questions than they answered. In addition,

while the vertical distribution of relative horizontal hydraulic conductivity has a profound influence on tracer test results, transport in a stratified, steady state flow field is unaffected by the absolute value of hydraulic conductivity. Therefore the bulk conductivity estimate yielded by a pumping test is in some respects irrelevant to tracer test design decisions. Slug tests can potentially yield useful information on the vertical variation of hydraulic conductivity (Butler et al., 1994). However, the results of GEMSTRAC1 were clearly influenced by a very fine scale of conductivity variation. It is unclear as yet whether slug tests at the site can be configured to resolve such a fine scale. A further analysis of these issues will be the subject of future work.

The most important result of the pumping tests performed in August and September of 1994 was that they were clearly affected by the pumping of nearby rural water district (RWD) wells. This led us to perform some longer-term continuous monitoring of the head variation at the site, using pressure transducers in several wells. Figure 3 shows the head variation observed in well 0-1 over a two-day period from the afternoon of September 28, 1994, until the afternoon of September 30, 1994. These results clearly show the influence of the two rural water district wells, which are pumped alternately. It was estimated that each well was pumping approximately 30% of the time, with the nearer well (designated RWD1 in this report) pumping at approximately 305 gpm and the farther well (RWD2) pumping at approximately 315 gpm. RWD1 and RWD2 are approximately 1200 feet and 1750 feet, respectively, roughly due west of the network centerline. The locations of the RWD wells were estimated using an aerial photograph and a pace estimate of the distance between RWD1 and RWD2. The locations of these wells relative to the network centerline are shown in Figure 4. The location of GEMS well 0-8 is also included in this plot, since this well was ultimately used as a 'hydraulic compensator' to attempt to correct for the expected influence of the RWD wells, as discussed below.

Modeling of the Influence of RWD Wells

Theoretical modeling was used to help identify an appropriate test format. Based on some initial design modeling and consideration of field logistics, we had originally decided to perform a radially convergent tracer test, with a zero fluid injection rate at the tracer injection well. That is, no water would be introduced at the injection well other than that which was necessary to introduce the tracer. The results would then be analyzed under the assumption that the tracer was transported in a radial flow field, considering the hydraulic effects of the injection process to be negligible. The alternative format would have been to inject water continuously at the injection well, setting up a dipole flow field

between the two wells. The tracer mass would then be introduced over a much longer period with the injected fluid. This test format creates a teardrop-shaped envelope of streamlines emanating from the injection well and flowing to the discharge well. This results in the tracer being spread out over a much larger area, compared to the radially convergent test. Due to the spreading of tracer mass over both time and space, the dipole test with continuous (or long-term) tracer injection will have much lower concentrations for a given mass of tracer than the radially convergent test with pulse injection. In the latter test most of the tracer mass will remain near the line between the injection and discharge wells and should be contained in packets of relatively limited longitudinal extent, due to the pulse nature of the input. We had hoped that by performing a pulse-injection radially convergent test we would be able to focus our sampling efforts on the samplers along the network centerline and would also increase our chances of obtaining measurable concentrations at most ports sampled. In addition, results of a radially convergent tracer test could be analyzed with an existing semianalytical solution for transport in a radially convergent flow field (Moench, 1989, 1991).

The discovery of the potential influence of the RWD wells led us to reconsider a dipole format test, in hopes that a nonzero (fluid) injection rate would help to compensate for the tendency for the RWD wells to draw the tracer away from the centerline to the west. The design modeling presented here demonstrates that a dipole format does little to reduce the deflection of flowlines caused by the RWD wells. Instead, an alternative scheme, involving pumping at a low rate at a GEMS well to the east of the network centerline (well 0-8) seems to compensate for the deflection caused by the RWD wells while still allowing us to perform a radially convergent test.

The computation of flow lines for different pumping scenarios is accomplished by performing a numerical integration of analytical expressions for the x- and y-components of pore fluid velocity due to a number of point sources and sinks superimposed on a uniform regional flow field. These expressions can be found in Javandel et al. (1984). If u_x and u_y are the x- and y-components of the regional pore fluid velocity and Q_i is the pumping rate (positive for extraction, negative for injection) at well i , located at (x_i, y_i) , then the x- and y-components of the pore fluid velocity are given by

$$\frac{dx}{dt} = v_x(x, y) = u_x - \sum_{i=1}^N \frac{Q_i}{2\pi b\phi} \frac{(x - x_i)}{(x - x_i)^2 + (y - y_i)^2}$$

$$\frac{dy}{dt} = v_y(x, y) = u_y - \sum_{i=1}^N \frac{Q_i}{2\pi b\phi} \frac{(y - y_i)}{(x - x_i)^2 + (y - y_i)^2}$$

where b is the aquifer thickness and ϕ is the porosity. Flowlines for a given scenario are computed by using a fourth-order adaptive stepsize Runge-Kutta algorithm (Press et al, 1992) to integrate the above expressions from time zero at a specified starting point (x_s, y_s) .

In the following scenarios the steady state flow field for the tracer tests is computed under the assumption that the influence of the RWD wells can be represented using their overall average pumping rates. That is, since each well is on about 30% of the time, the overall average pumping rate at RWD1 is $0.3 \times (305 \text{ gpm}) = 91.5 \text{ gpm}$ and the pumping at RWD2 is $0.3 \times (315 \text{ gpm}) = 94.5 \text{ gpm}$. The temporal variations in the actual pumping rates should not significantly influence the overall trajectory of the tracer cloud, but will instead produce somewhat greater apparent transverse dispersion than might occur otherwise due to the shifting of the hydraulic gradient as the RWD wells turn on and off.

Unfortunately, we are unable to obtain a useful measurement of the regional hydraulic gradient at the site; the differences in hydraulic head across the site due to the regional gradient are probably of the same magnitude as the errors in our measurements of the relative elevations of the tops of the well casings. Therefore the following computations will be based on the assumption that u_x and u_y are negligible in comparison to the pore velocities induced by pumping. At this point we have no way of confirming the validity of this assumption.

The pumping rate at the discharge well will be fixed at 70 gpm, about the maximum rate obtainable with our equipment, for all simulations. Figures 5 and 6 show the computed flowlines for an injected pulse of two different widths, 6 feet and 8 feet, respectively, with a zero fluid injection rate at IW and no pumping at well 0-8, that is, with no attempts to compensate for the influence of the RWD wells. The middle line represents the trajectory of the center of the plume from the injection well at (0,0) to the discharge well at (46.5 ft, 0). The two outer lines are the trajectories of the outer edges of the plume based on the given injection width and assuming negligible transverse dispersion. The anticipated diameter of the injected pulse was about six feet (3-foot radius) assuming a uniform distribution of mass throughout the 35-foot thickness of aquifer and assuming a porosity of about 0.3. It is clear that the plume is deflected significantly from the network centerline in these simulations. With a six-foot injected width, the simulated plume is just grazing the network centerline for approximately the final 15 feet of travel to the discharge well. This would potentially lead to low concentrations along the network centerline and also substantial systematic deviations from the behavior predicted by a radially convergent transport model. With an eight-foot

injected width, the potential for 'missing' the injected plume is reduced but not entirely alleviated and the problem of a systematic deviation from a radially convergent transport model is unchanged.

Figures 7, 8, and 9 show the computed flowlines for dipole tests with three different fluid injection rates at well IW. The flowlines emanate from starting points located around a circle of one-foot radius surrounding IW. There are eight flowlines shown for the 1 gpm injection rate simulation (Figure 7) and twelve flowlines for the 5 gpm and 10 gpm injection rate simulations (Figures 8 and 9). A model for transport in a dipole flow field would be the appropriate one to use to analyze observed concentrations in this case. However, it is clear that a non-zero injection rate at IW does little to reduce the deflection caused by pumping at the RWD wells. This would result in a systematic deviation from behavior predicted by a dipole transport model (based on the purely dipole flow field caused solely by the pumping and injection at DW and IW). In addition, the dipole format would require a much higher injected mass relative to the radially convergent format due to the spreading of tracer over a larger area and the longer time period of injection.

Since fluid injection at IW does little to compensate for the deflection of flowlines caused by the RWD wells, an alternative compensation scheme was proposed: pumping at a low rate in a well in the 0 nest, approximately due east of the discharge well. Well 0-8, shown in Figure 4, was selected as the potential 'compensator' well. Figure 10 shows the flowlines computed using a 10 gpm flow rate at well 0-8 with a zero fluid injection rate at IW and assuming a 6-foot injection width. The computed flowlines are nearly identical to those computed for a purely radial flow field. The eastward velocity components due to pumping at well 0-8 nearly cancel the westward components due to pumping at the RWD wells. Thus, the transport problem could reasonably be modeled using a radially convergent transport model. Figures 11 and 12 show the sensitivity of the computed flowlines to our estimates of the average pumping rates at the RWD wells. Figure 11 shows the flowlines computed assuming 20% higher pumping rates at the two RWD wells, with the same pumping rate (10 gpm) at well 0-8. The effects of a 20% lower pumping rate at the RWD wells are demonstrated in Figure 12. In both cases the center of the plume still remains reasonably close to the network centerline and the flow is nearly radially convergent. Based on these simulations, we decided to pump well 0-8 at about 10 gpm during the tracer test.

Simulated Breakthrough Curves

The Moench (1989, 1991) semianalytical solution for radially convergent, conservative transport, discussed in Section IV.D, was used to simulate breakthrough curves at the pumping well and at three multilevel samplers along the network centerline in order to help determine the expected duration of the test, the necessary sampling frequency, and the amount of injected mass required to obtain reasonable concentrations at most ports. The computed concentrations are in terms of mg/l per kg of injected Br⁻. Breakthrough curves for a range of dispersivity values, from 0.5 feet to 8.0 feet were computed. This range of values was selected based on dispersivities reported for tracer experiments in sand and gravel aquifers (see Gelhar et al., 1992, for a review of such experiments). It was anticipated that smaller dispersivity values would represent 'local' dispersivities and thus more accurately predict breakthrough curves at individual ports whereas larger dispersivity values would represent 'whole-aquifer' dispersivities appropriate for modeling vertically averaged concentrations. Thus the breakthrough curves for smaller dispersivities are appropriate for estimating the sampling frequency necessary to define breakthrough curves at individual ports while the breakthrough curves for larger dispersivities are appropriate for determining the expected duration of the test.

Breakthrough curves computed at the discharge well are shown in Figure 13. These results are computed using a pumping rate of 70 gpm and assuming a porosity of 0.28. Since the pumping well concentration represents a vertically mixed sample, the breakthrough curves for larger dispersivities are probably more appropriate in this case. These curves give some indication of the expected duration of the test. The curve for the largest dispersivity, 8 feet, would seem to indicate that negligible tracer mass would remain in the aquifer after about three weeks of pumping.

Figures 14 through 16 show the breakthrough curves computed for TMC-7, TMC-4, and TMC-1. As discussed in Section IV.D, the concentrations computed from Moench's solution must be adjusted by a geometrical factor in order to be appropriate for observations at locations other than the pumping well. The injected pulse travels in a narrow wedge from the injection well to the pumping well, where it is then diluted by mixing with a large amount of fresh water. At the pumping well, the observed concentrations are insensitive to the angular distribution of tracer and thus the injected mass can be treated as if it were initially distributed uniformly around a circle of radius r_L , the distance from the injection well to the discharge well. Moench's solution for concentrations at arbitrary observation radii are also stated in terms of an angularly averaged concentration. However, this is not appropriate for describing actual concentrations, which will be large at observation points within the wedge of tracer and

zero outside that wedge. Assuming that the mass is initially distributed uniformly across a pulse of transverse width Δy , then the concentrations computed from Moench's solution must be multiplied by the factor $2\pi r_l/\Delta y$ in order to be appropriate for concentrations observed within the tracer plume. This is the primary reason for the large difference in concentration scales between Figure 13 (for the pumping well) and for Figures 14 through 16 (for the three multilevel samplers).

The breakthrough curves for TMC-7 (Figure 14) are fairly sharp for all dispersivity values, due to the limited travel distance (10.9 feet) from the injection well to TMC-7. For the smallest dispersivity, 0.5 feet, the breakthrough occurs over a period of about three days. A good data density will be somewhat arbitrarily defined here as meaning at least 15 samples within the non-negligible portion of the breakthrough curve. Thus, about five sample rounds per day would be required to clearly define this peak. The breakthrough curve for a dispersivity of 8 feet, more indicative of the 'whole-aquifer' behavior, indicates that non-negligible concentrations would be expected to occur in some ports of TMC-7 over a period of 10 to 12 days.

Figure 15 contains the breakthrough curves computed for TMC-4, approximately in the middle of the network (25.6 feet from the injection well, 20.9 feet from the discharge well). Here the sharpest peak occurs over a period of about four to five days, requiring a sampling frequency of three or four times per day for good definition. The breakthrough curve for the largest dispersivity indicates that non-negligible concentrations would be expected to occur in some ports over a period of about two weeks. The breakthrough curves computed for TMC-1 (Figure 16), 5.8 feet from the discharge well, are of a similar duration as those computed for TMC-4, requiring approximately the same sampling frequency and duration.

In all cases, measurable concentrations are computed at all sampler locations given one kilogram of injected bromide. Due to the possibility that a large portion of the mass could enter a few zones, an injected mass of a few kilograms of bromide would probably be appropriate, in order to increase the chances of obtaining measurable concentrations at most ports.

Discussion and Conclusions

The validity of the above design modeling can now be discussed in retrospect by comparing the above predictions to the actual tracer test results, described in Section IV.D. In some respects the design modeling was quite successful. A number of the breakthroughs at individual ports did indeed occur over a period of several days and, in general, vertically averaged breakthroughs at most samplers were approximately

complete after a period of about two weeks. However, we failed to take into account the full ramifications of the stratified flow model implicit in our analyses. The 'whole-aquifer' dispersion is created primarily by differential advection between different vertical zones of the aquifer, with faster flow occurring at some levels and slower flow occurring at other levels. If the breakthrough curves computed above for larger dispersivities are taken as representing concentrations that are vertically averaged across these different flow zones, then the steep early rise in these curves represents contributions from very rapidly moving, sharp fronts at certain levels in the aquifer. Note, for example, that the breakthrough curve for a dispersivity of 8 feet at TMC-1 (Figure 16) indicates that substantial amounts of mass could have moved all the way along the centerline by just two days into the test. In fact, this is exactly what occurred in the actual tracer test: large quantities of tracer mass entered narrow, highly permeable zones and moved rapidly toward the discharge well. We did not anticipate such rapid movement downgradient and focused our sampling efforts on those samplers near the injection well during the first couple days of the test. Thus, peak concentrations had already passed some ports in samplers further downgradient by the time we sampled them. In retrospect, it is clear that we should have incorporated some design modeling runs using a range of flow rates and small ('local') dispersivities, appropriate for modeling the transport in individual zones, in order to anticipate the effects of the vertical variation in flow velocity. However, the tracer test results revealed that the magnitude of this variation was much greater than we would have anticipated based on prior work at the site.

Figure 1: Tracer network map with Injection Well as origin

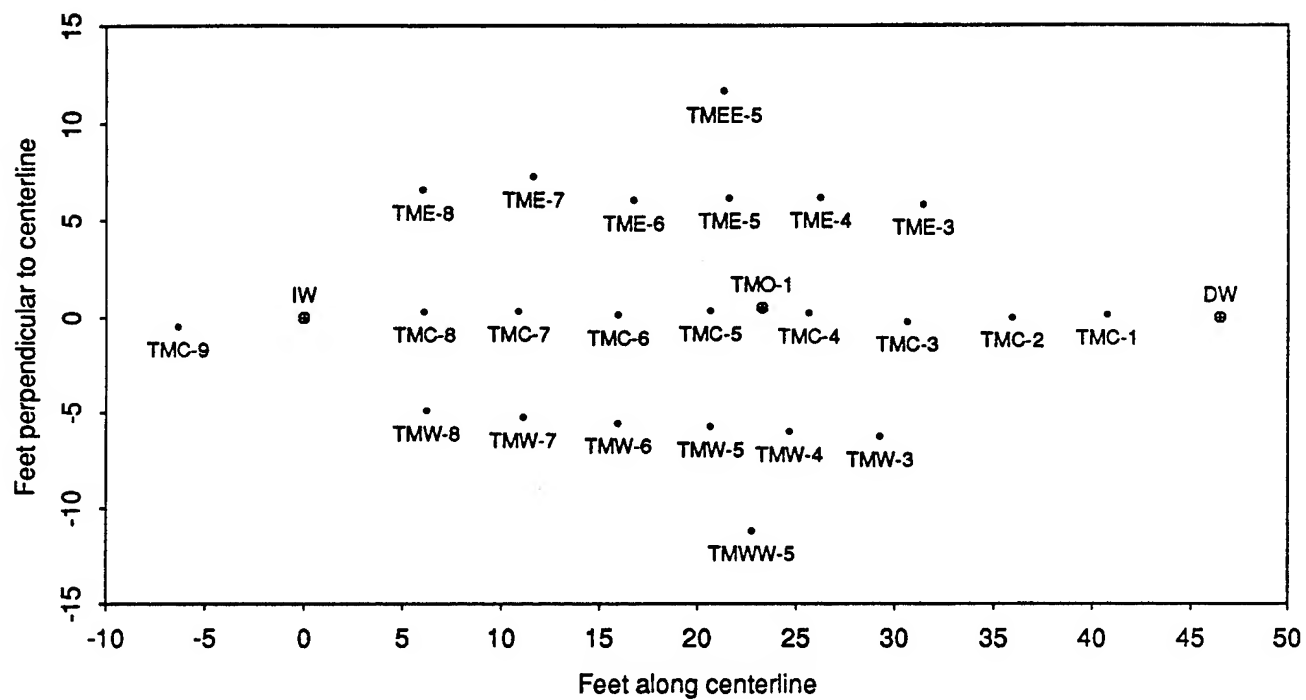


Figure 2: Locations of Sampling Ports Along Centerline

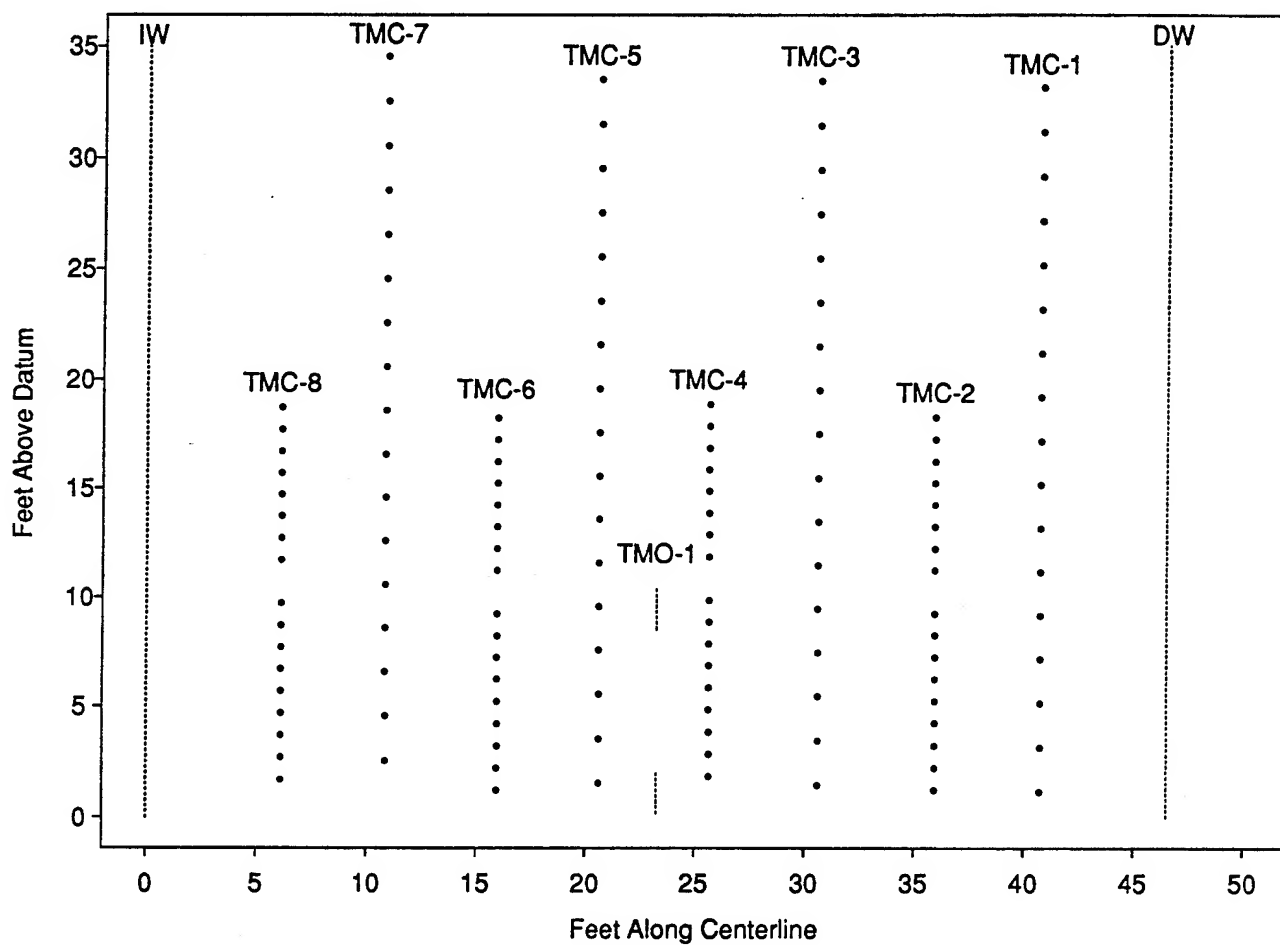


Figure 3: Head variation at well 0-1, 9/28/94-9/30/94

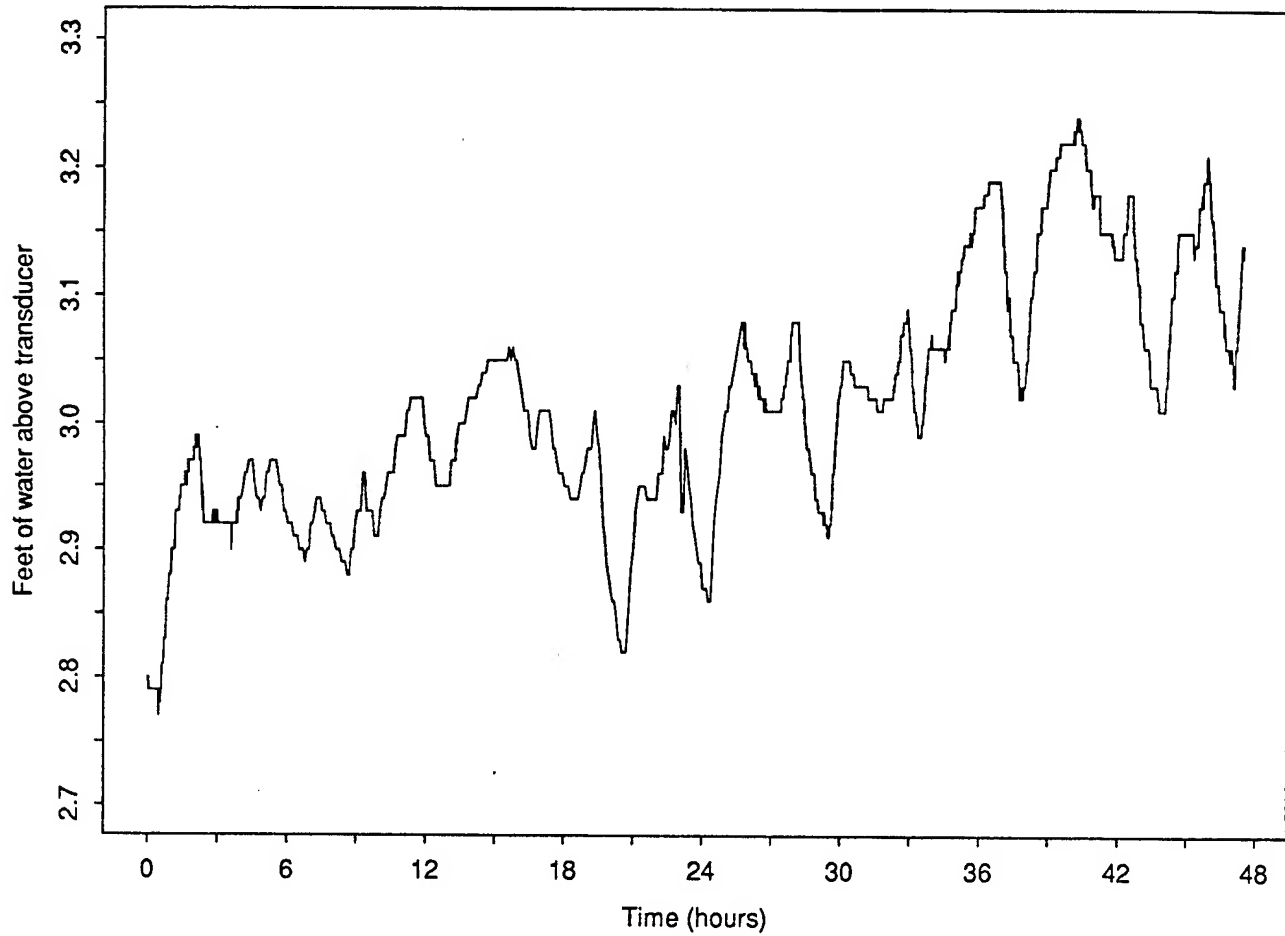


Figure 4: Locations of Rural Water District Wells

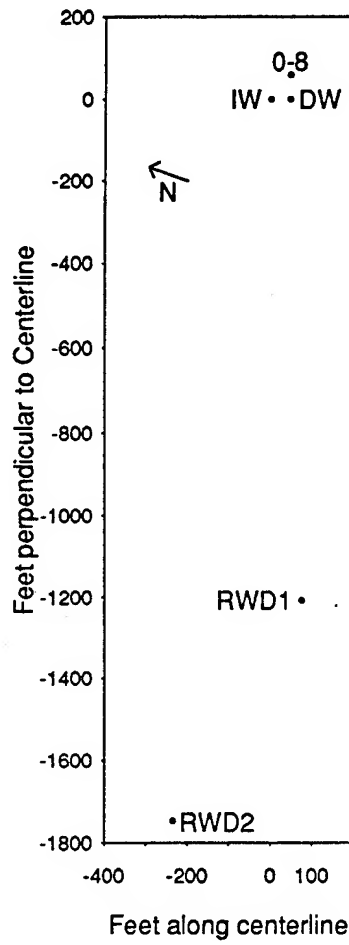


Figure 5: Flowlines with 0 injection rate, 6-foot initial width

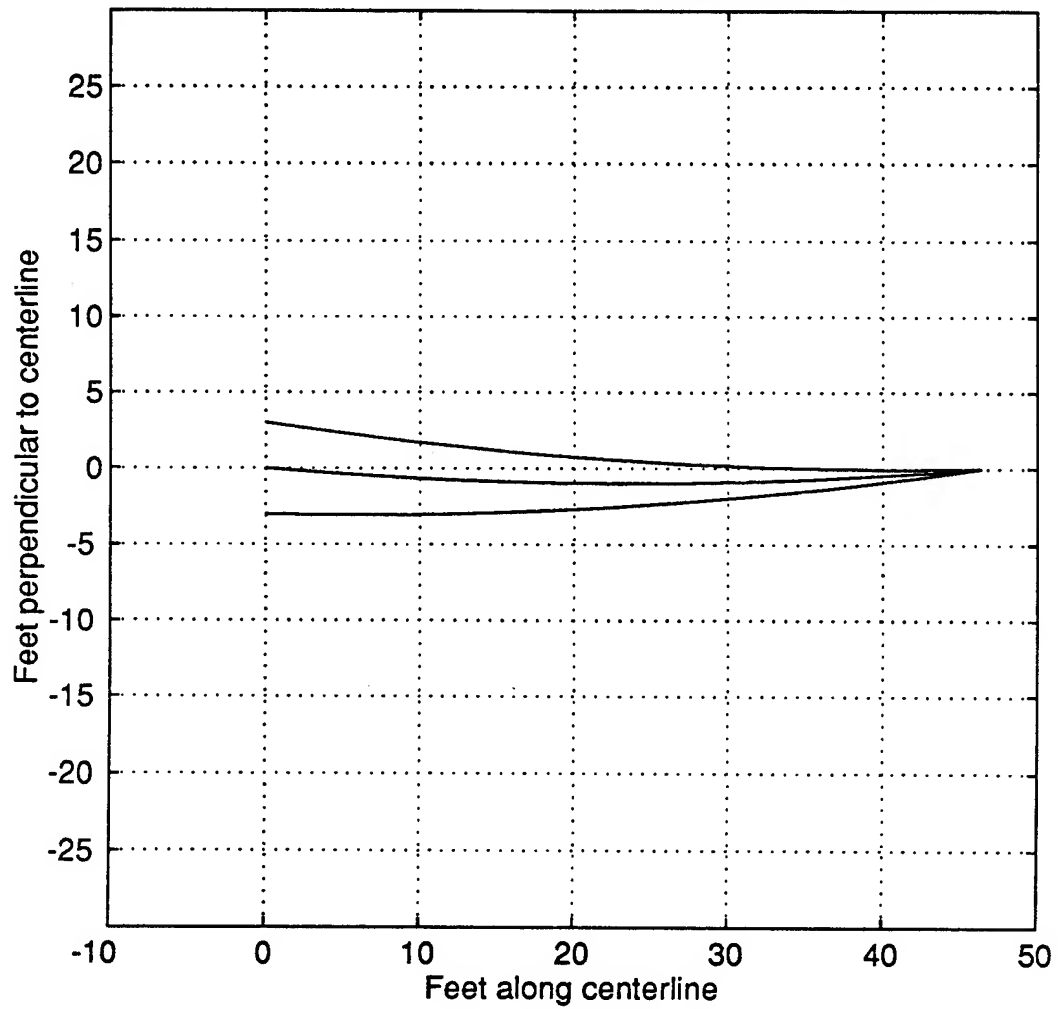


Figure 6: Flow lines with 0 injection rate, 8-foot initial width

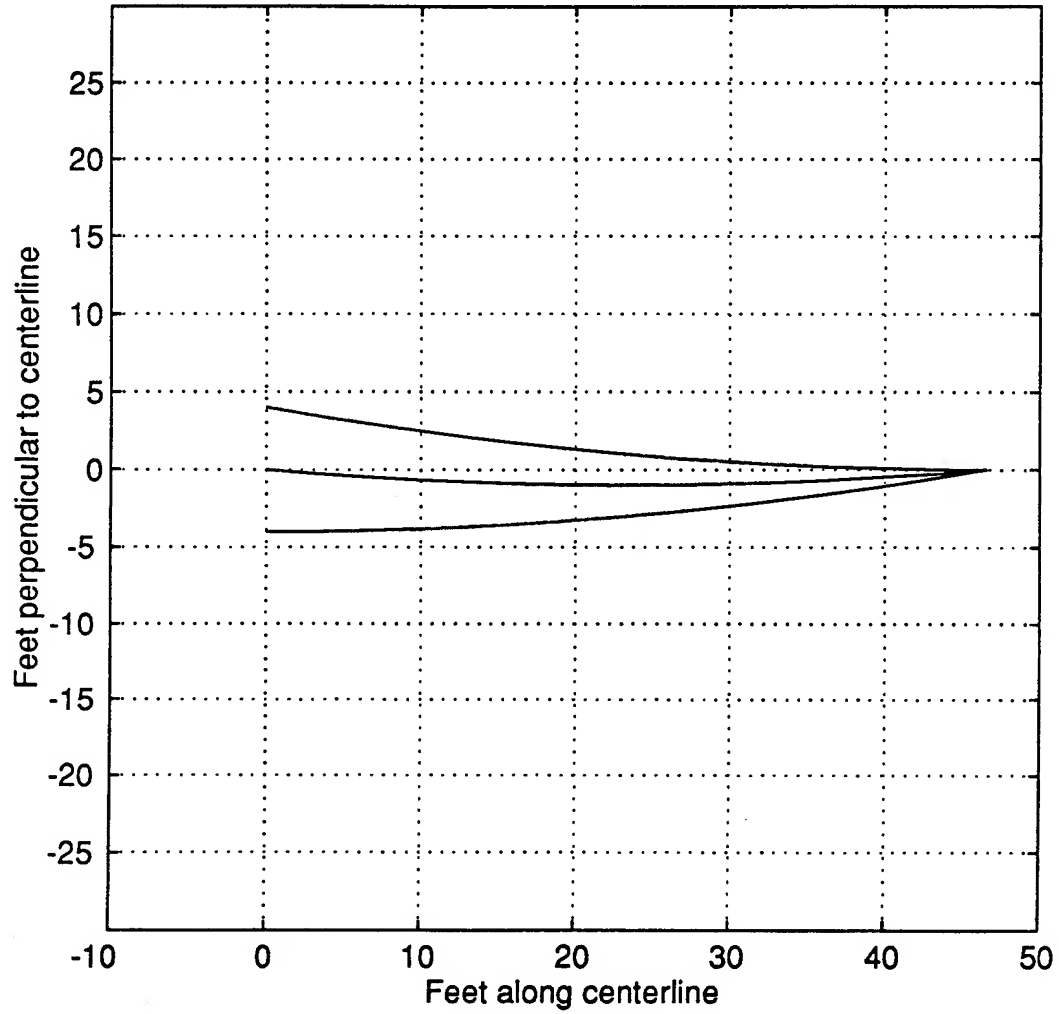


Figure 7: Flowlines with 1 gpm injection rate

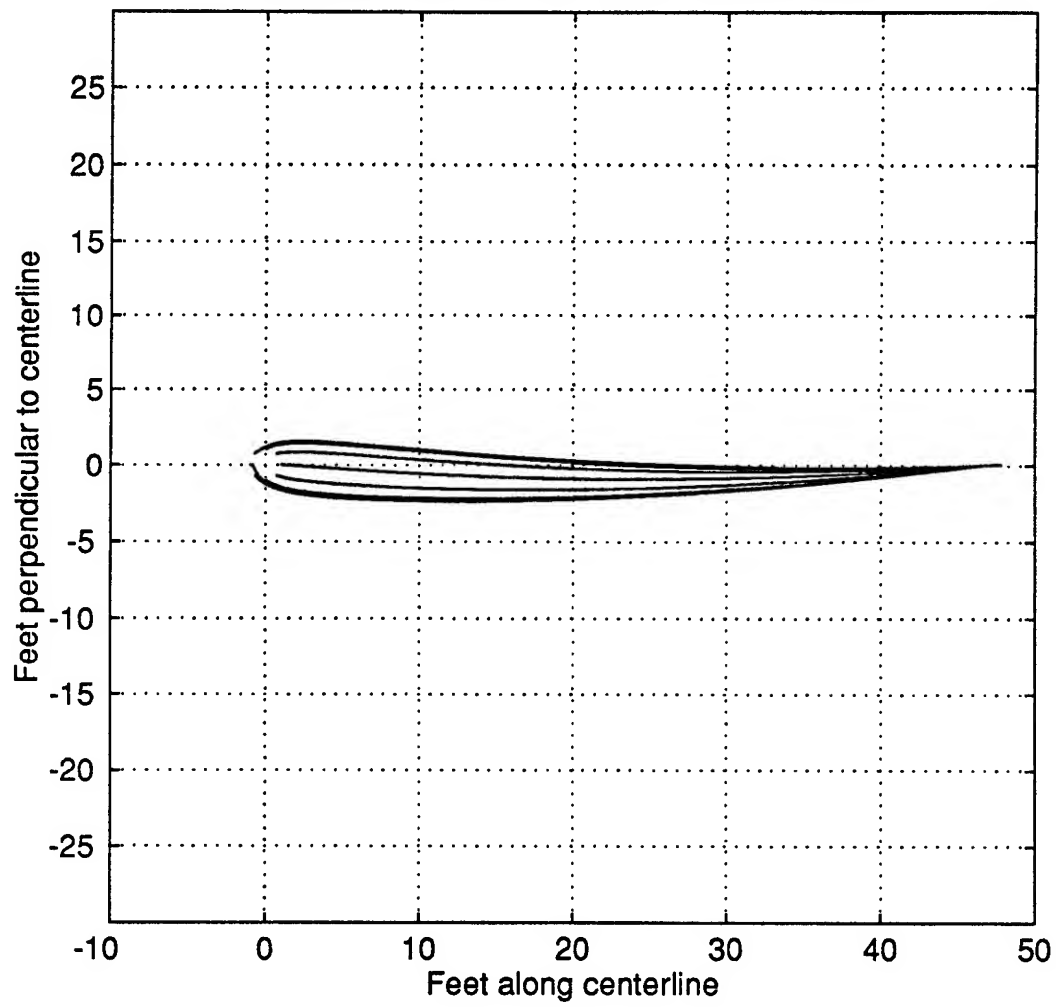


Figure 8: Flowlines with 5 gpm injection rate

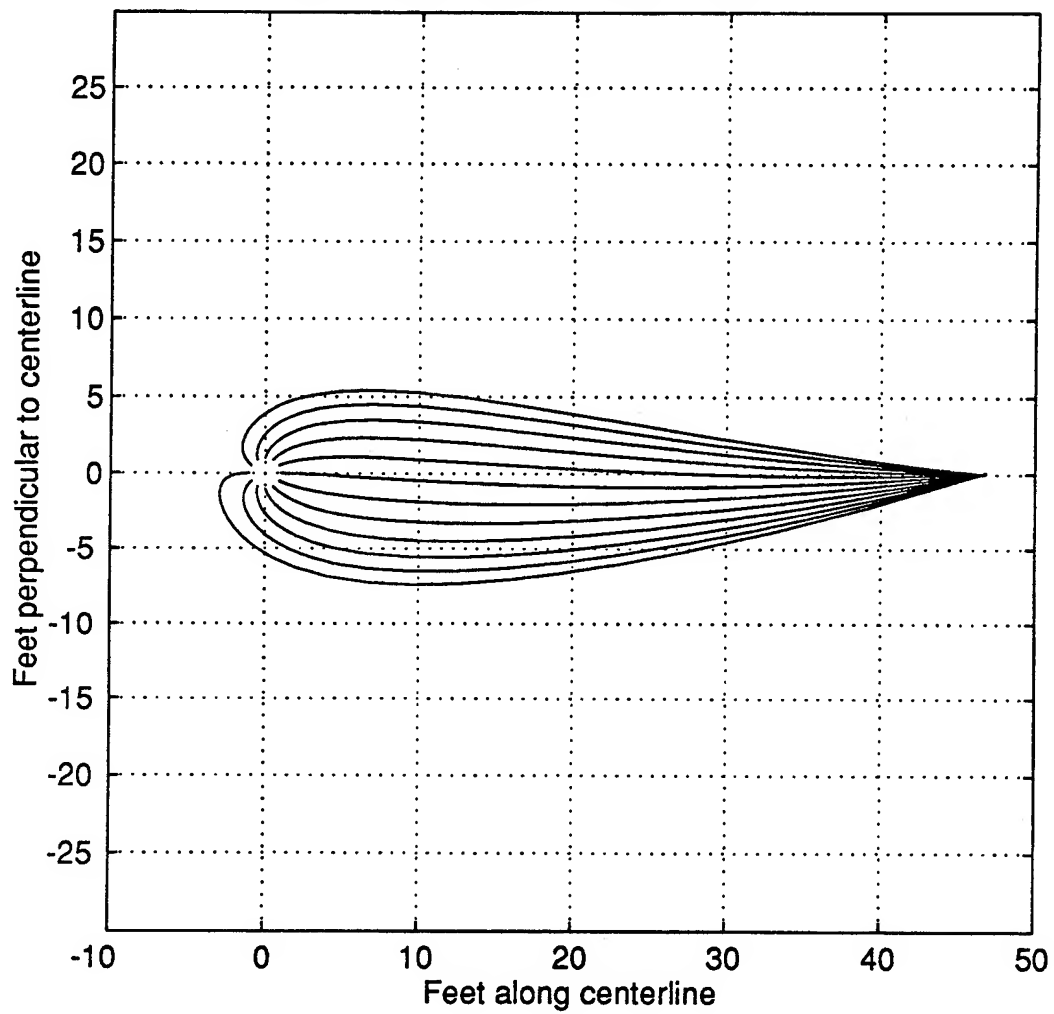


Figure 9: Flowlines with 10 gpm injection rate

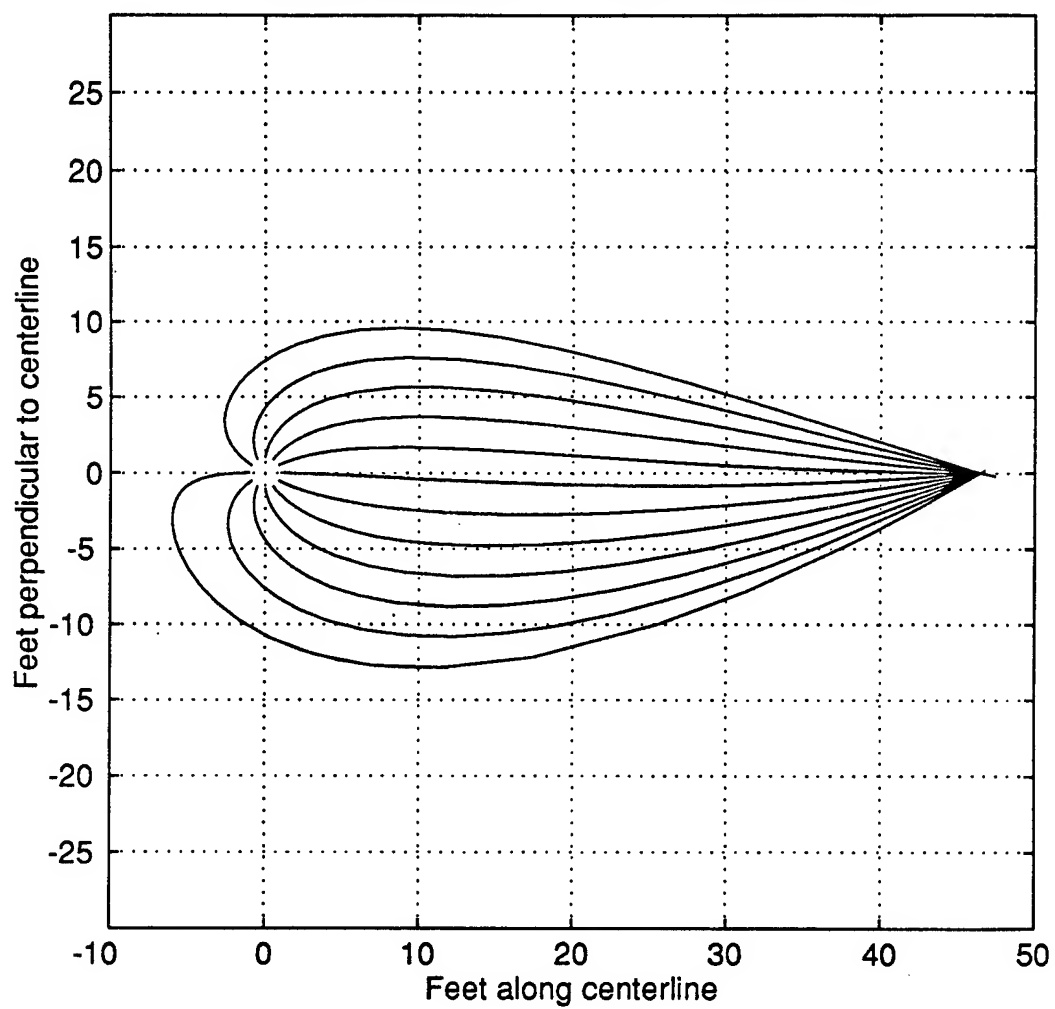


Figure 10: Flowlines with 10 gpm pumping at well 0-8

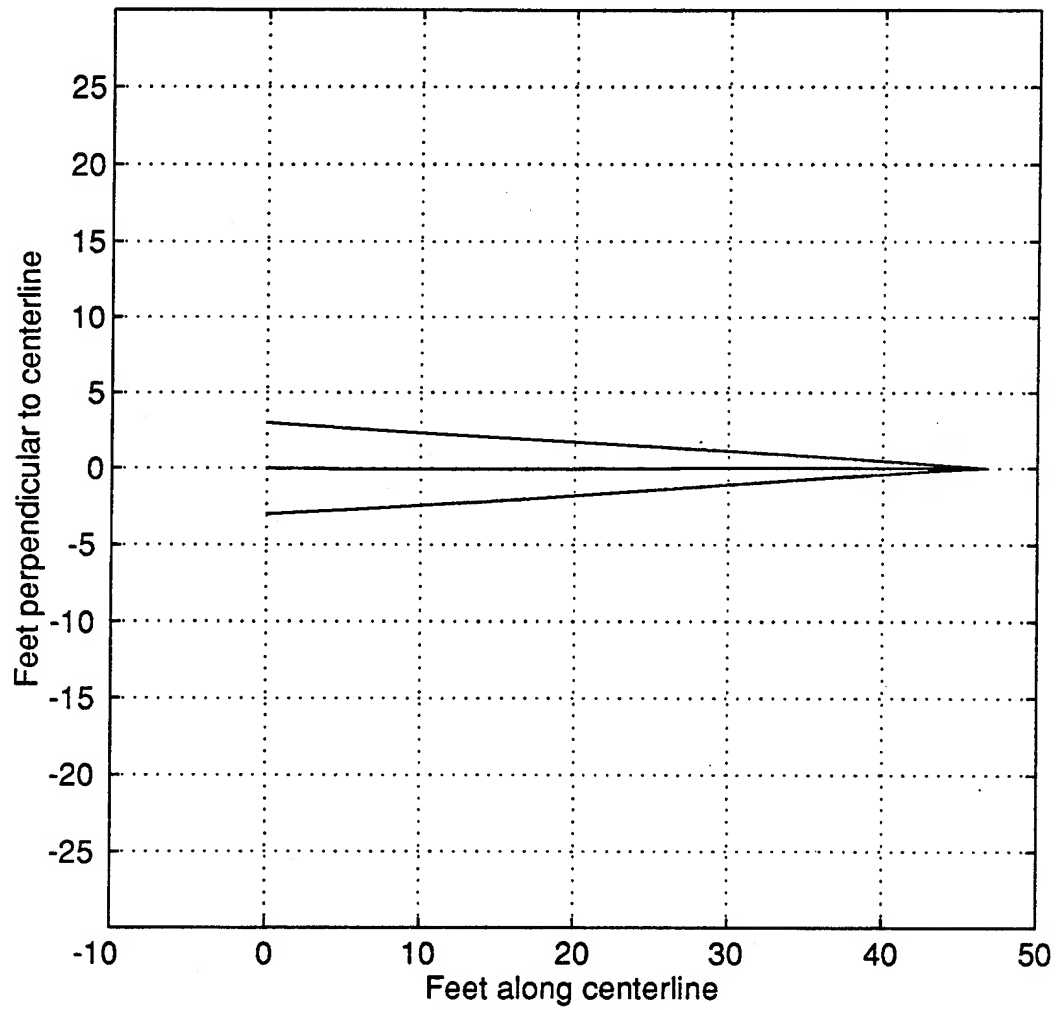


Figure 11: Flowlines with 20% higher pumping rates at RWD wells

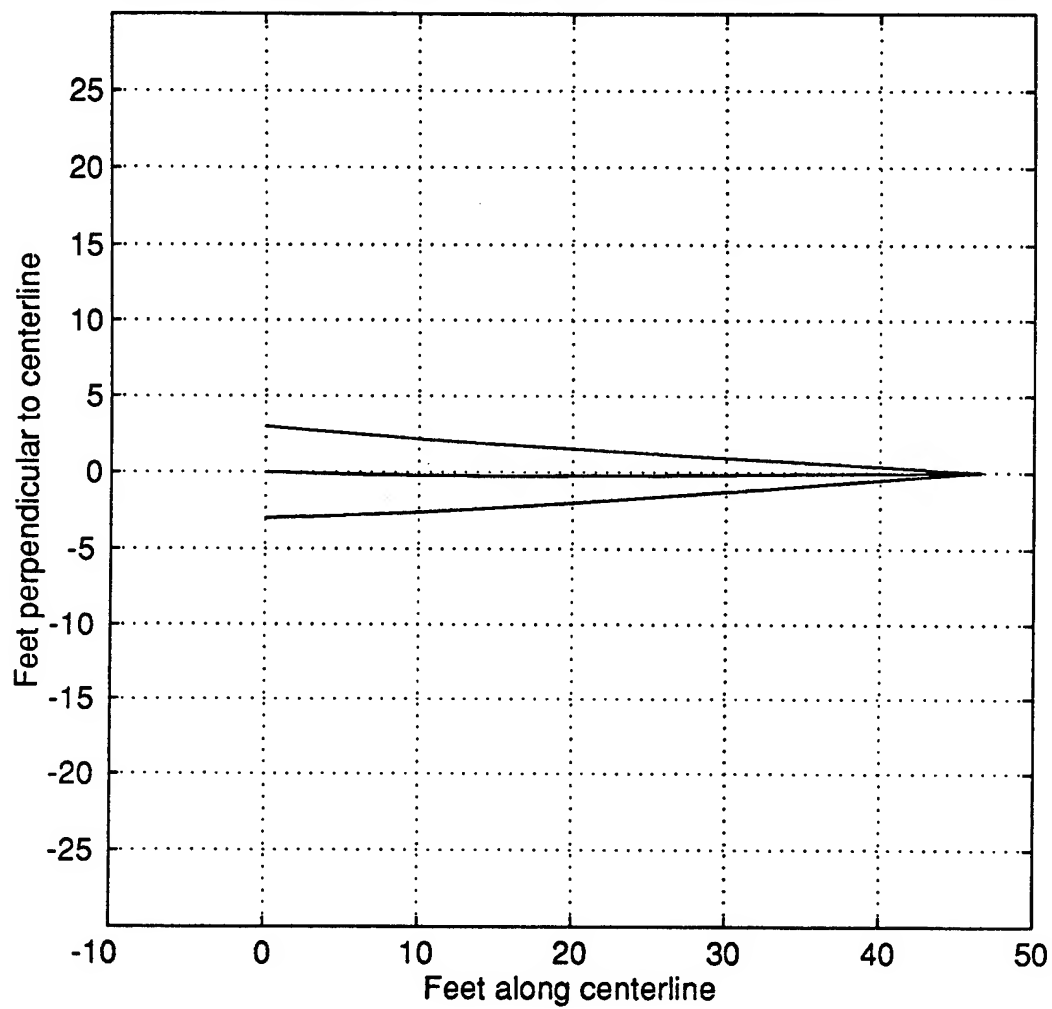


Figure 12: Flowlines with 20% lower pumping rates at RWD wells

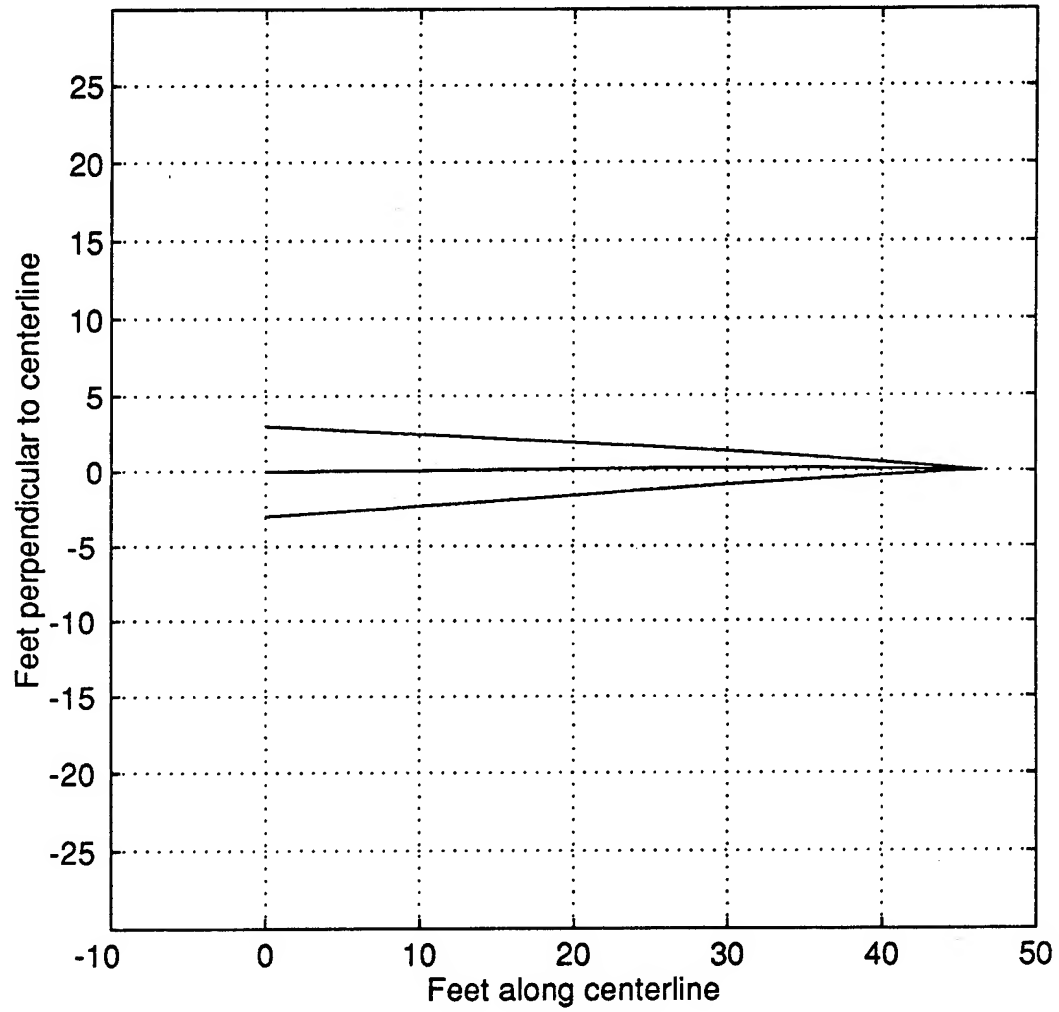


Figure 13: Breakthrough curves at pumping well

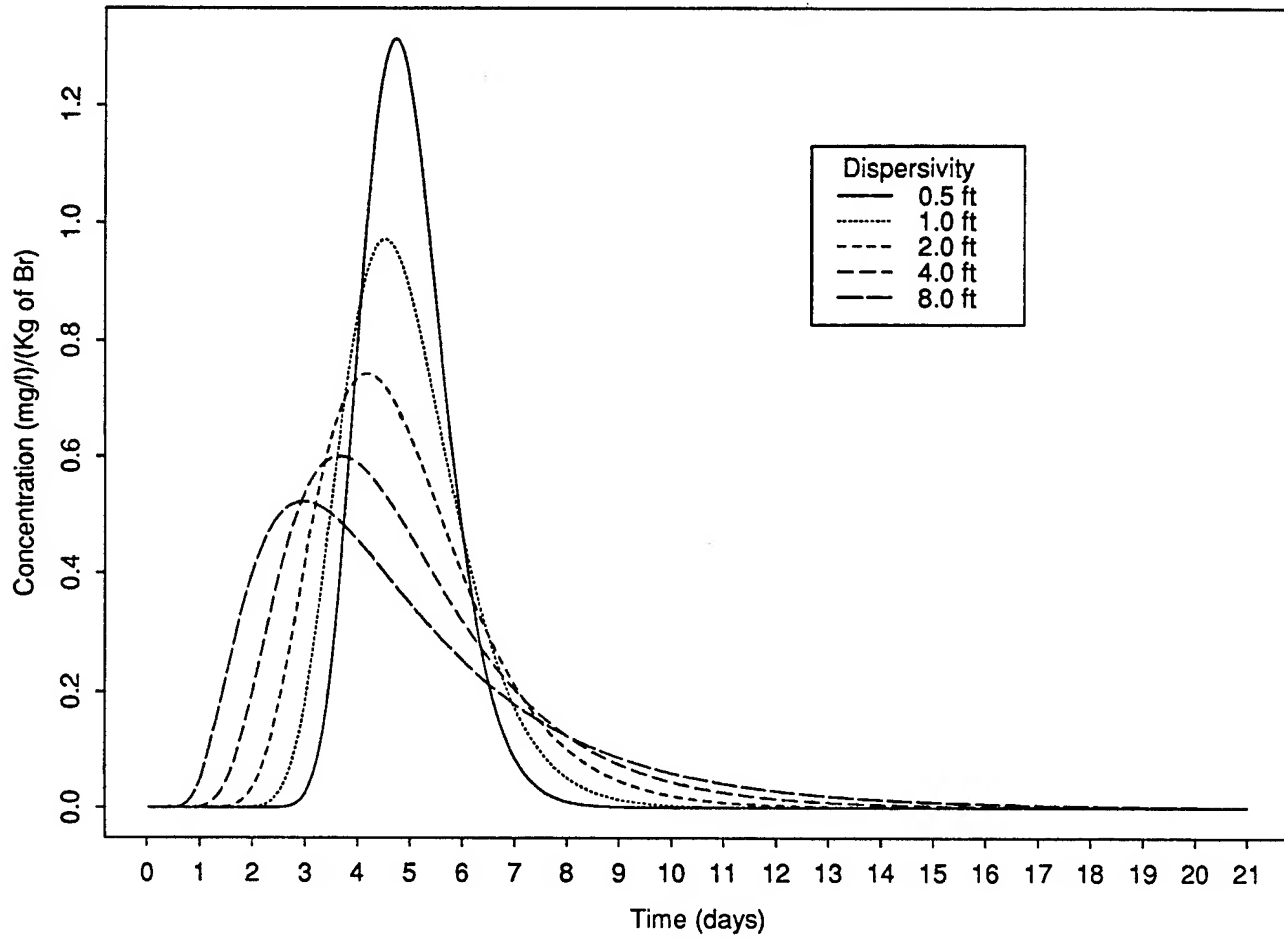


Figure 14: Breakthrough curves at TMC-7

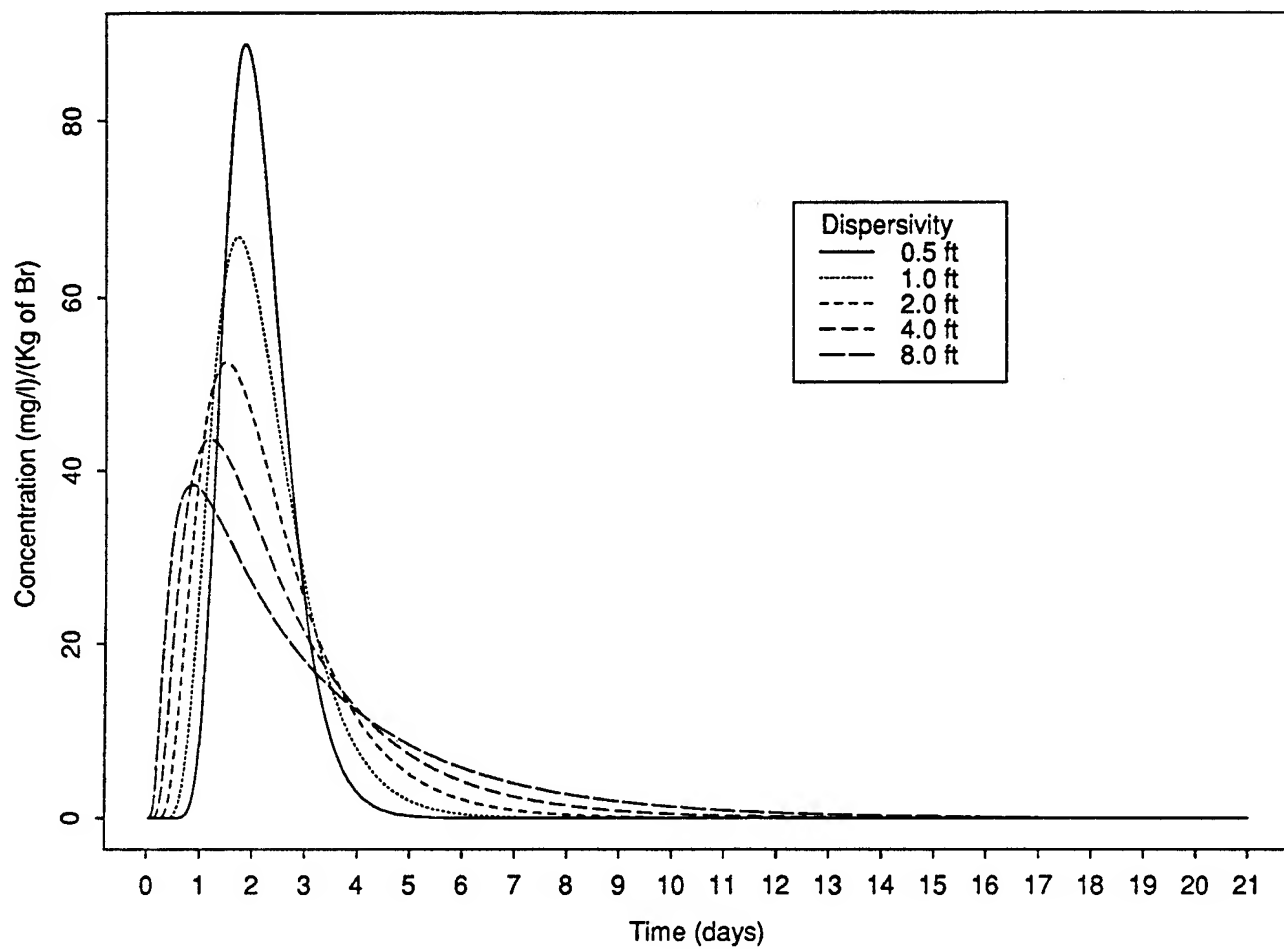


Figure 15: Breakthrough curves at TMC-4

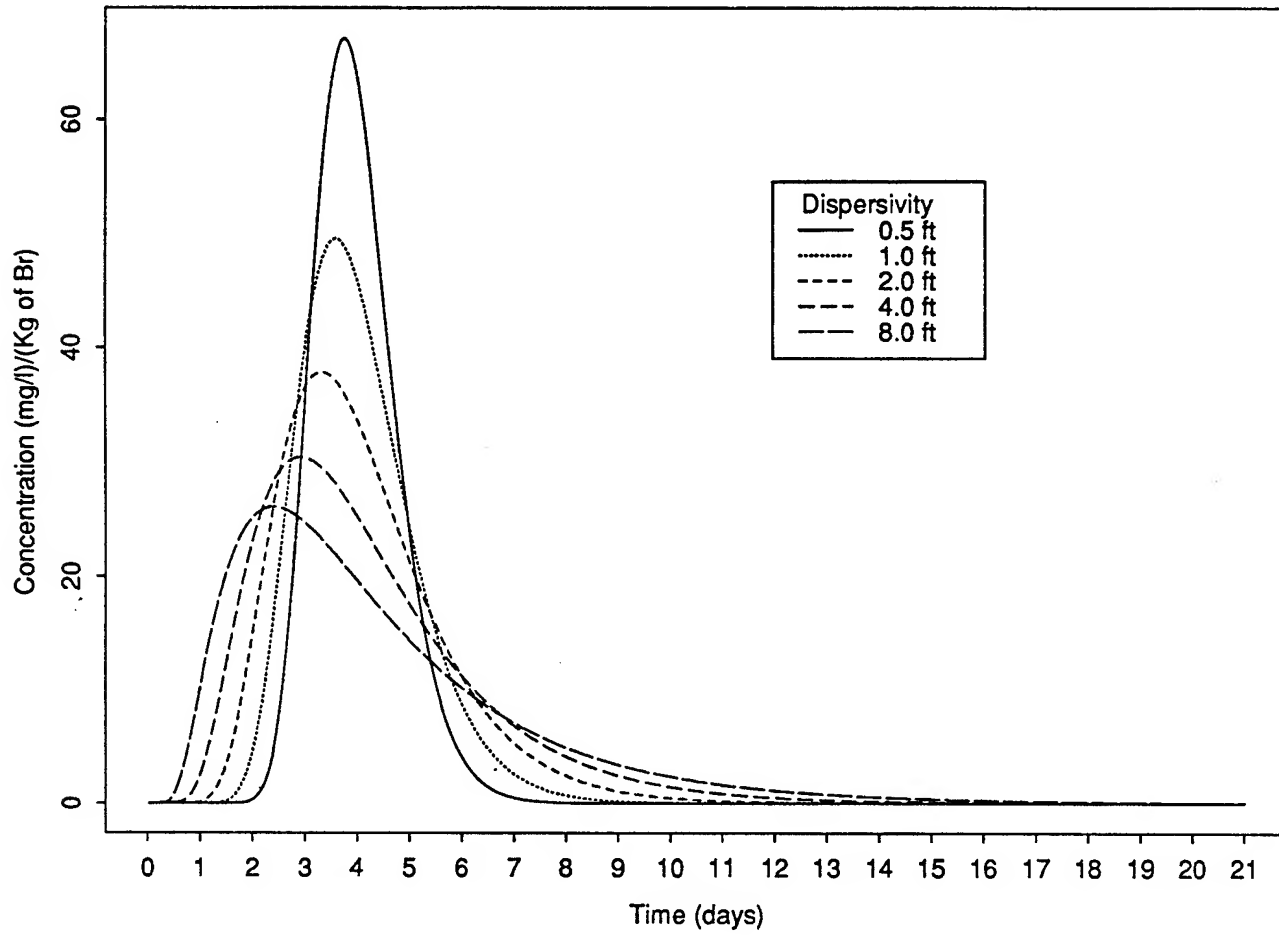
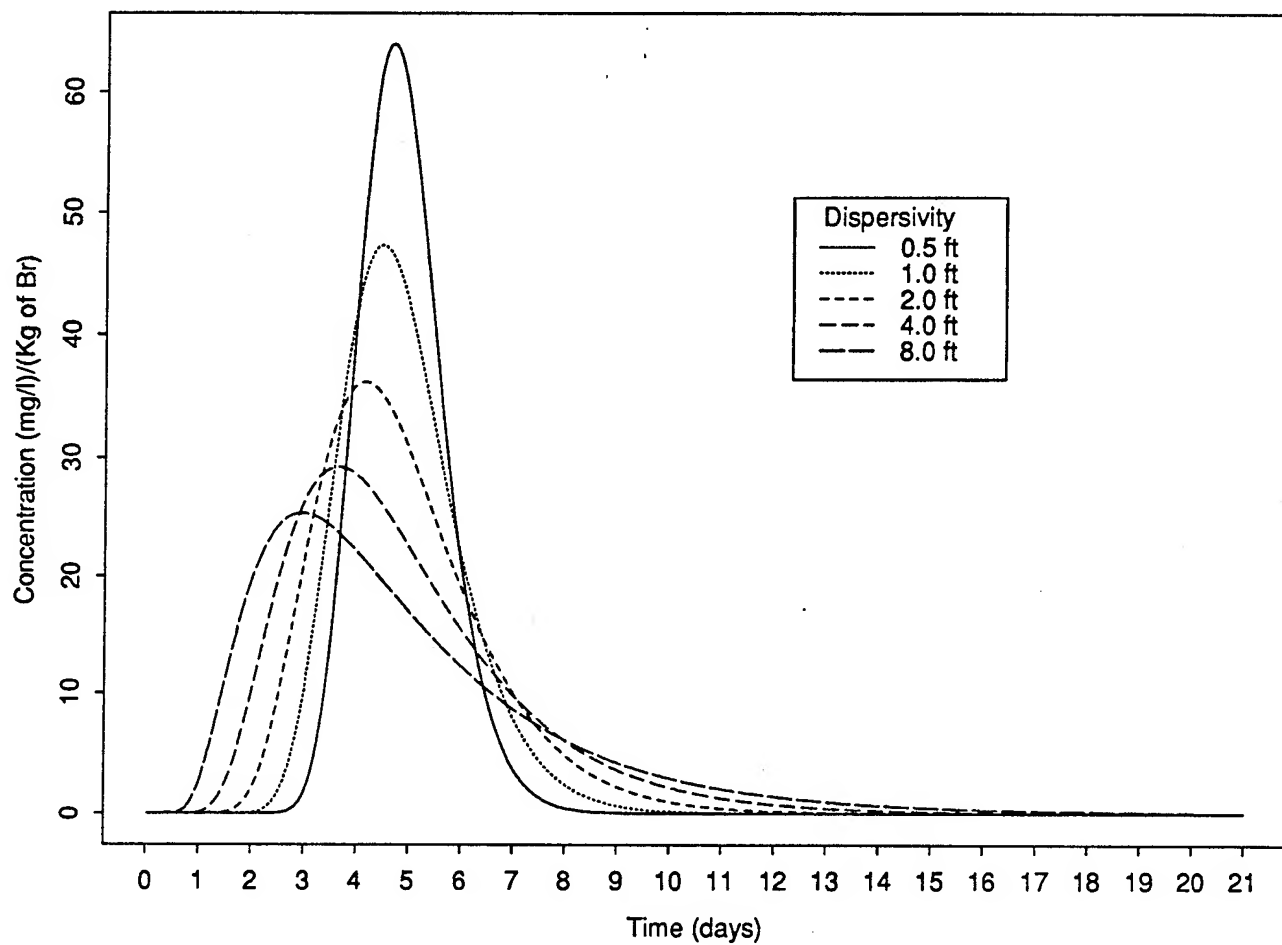


Figure 16: Breakthrough curves at TMC-1



III. FIELD INVESTIGATIONS OF MULTILEVEL SLUG TESTS

A. KGS MULTILEVEL SLUG-TEST SYSTEM

In 1989, a slug-test system was developed at the KGS for the purpose of performing slug tests in wells of small diameters (.05 m ID) located in highly permeable alluvial units (McElwee and Butler, 1989). This equipment served as the basis of a multilevel slug test system that is being developed for the research described in this report. A prototype straddle-packer system for multilevel slug tests has been constructed at the KGS. The prototype system consists of two packers (each approx. .67 m in length when fully inflated) that are used to seal off the test interval from the adjacent screen. A section of .025 m ID PVC (SCH 40) pipe is connected to the central flow-through pipe of the top packer of the pair. A series of sections of the .025 m ID PVC pipe runs to a third packer located above the top of the screened interval. This pipe allows the pressure pulse initiating a slug test to be confined to the straddle-packer interval. The central flow-through pipe of the middle packer is closed off prior to testing. A slug test is initiated by adding or removing water to the casing above the third packer and then opening the central flow-through pipe in the middle packer. As with the original KGS slug-test system (McElwee and Butler, 1989), the central flow-through pipe is opened by the mechanical lowering of a plug attached to pump rods. Although the test interval can be up to several meters in length, it cannot be less than .29 m in the present configuration.

After the completion of testing at one level, the packers are deflated and the string of packers and pipes is moved until the straddle-packer interval is opposite the next zone to be tested. The string can be moved until the top of the third packer is raised above the static water level or lowered below the top of the screen. At that point, a section of PVC pipe must be either removed or added, respectively, to the pipe string connecting the straddle packer to the top packer before testing can be continued. In this manner, a series of multilevel slug tests can be readily performed across the entire screened interval of a well in a relatively short period of time. At shallow depths the string of packers and pipes can be lifted manually, while at deeper depths a special tripod and winch arrangement that was constructed during the first year of this project is employed. Note that the packers used in this system were designed and constructed at the KGS. Commercially available packers for use in .05 m ID wells have central flow-through pipes

that are .0125 m ID or smaller. Packers with larger flow-through pipes (.025 m and .019 m) were designed in an effort to ensure that the parameters estimated from the response data would be reflective of properties in the aquifer, and not the diameter of the flow-through pipe.

As stated above, slug tests are initiated by adding or removing water from the cased section of the well above the third packer. In all cases, pressure transducers (PS7000 and PS9000 series, Instrumentation Northwest, Inc.) placed above the third packer are employed to measure water-level recoveries in the slugged well. During the field season, the transducers are calibrated in the laboratory on a monthly to bimonthly basis as described in section IV.E. Between laboratory calibrations, transducer functioning is checked in the field by measuring the height of the column of water above the transducer using an electric tape (Model 101 flat tape water meter, Solinst Canada Ltd.). The transducers are connected to one of two types of data acquisition devices: a datalogger (21X datalogger, Campbell Scientific, Inc.), or a data acquisition card (WB-FAI-B high speed interface card, Omega Engineering, Inc.). Note that the data-acquisition card has been placed in the expansion chassis of a 12 MHZ laptop computer (Supersport 286 Portable Computer, Zenith Data Systems Corp.).

In the following section, the use of this equipment in an initial series of multilevel slug tests at GEMS is described.

B. MULTILEVEL SLUG TESTS AT GEMS

Multilevel Tests at GEMS 2-5

The prototype KGS multilevel slug-test system was employed in a series of multilevel slug tests at GEMS. GEMS well 2-5 (depth = 20.67 m, screen length = 9.14 m), which is screened essentially through the entire sand and gravel section at the site, was used for these tests. An initial series of tests was run in which the slug consisted of the volume of water required to raise water levels 3.07 meters in the cased section of the well ($H_0=3.07$ m). As shown in Figure III.B.1, the slug-test responses measured at the different depths were very similar. Note that Table III.B.1 lists the depths corresponding to each test interval. Although the variation in the hydraulic conductivity values calculated from the core samples taken from GEMS 2-5 at these same depths was also small (Butler et al., 1991), the decision was made to repeat the series of slug tests using H_0 's of different magnitudes to see if greater discrimination between test zones would be possible using a different H_0 . Figure III.B.2 shows a plot for slug tests over the same intervals as Figure III.B.1 using a H_0 of approximately 1.65 m. A comparison of the two figures shows that, although there is little difference between tests using the same H_0 , there is a considerable difference between tests using different H_0 's. Normalized plots of the slug-test responses from a series of tests with differing H_0 's in the third test interval are presented in Figure III.B.3. Note the dramatic dependence of the slug-test responses on magnitude of H_0 . Dependence relationships of this form were seen in all the tested intervals. Table III.B.1 summarizes the parameters calculated from the slug-test responses for a subset of the tested intervals. In all cases, the higher the H_0 , the lower the calculated conductivity. The inverse relationship between the magnitude of H_0 and the calculated conductivity does not appear to require a threshold value for H_0 . Experiments have shown that differences in H_0 as small as .03 meters will still produce conductivity differences in the direction predicted from this relationship. Thus, the small difference in H_0 that exist between the slug tests shown on Figure III.B.1 or Figure III.B.2 could easily explain the differences displayed on those plots. Note that when special care was taken to ensure that the same volume was used for the slug in repeat tests at a given interval, the plots of the responses for the repeat tests coincided.

It is important to note that the theory from which the conventional methodology used for slug-test analysis (e.g., the CBP or Hvorslev models) was developed holds that

the slug-test responses should be independent of H_0 . In other words, plots of slug-test responses from tests using differing H_0 normalized by the H_0 used in each test should coincide. Clearly, the multilevel slug tests at GEMS are being affected by processes not considered in the standard theory.

The dependence of slug-test responses on H_0 was not the only anomalous behavior observed during the multilevel slug testing at GEMS. Figures III.B.1 - III.B.3 are plots of slug-test responses given in the format of the Hvorslev method (log heads versus arithmetic time). Note the concave downward form of the curves. Conventional theory dictates that these plots should be concave upward or straight lines (Chirlin, 1989; McElwee et al., 1990). Nothing in the conventional theory would allow for concave downward plots. Additional indications that the multilevel slug tests at GEMS are being affected by processes not considered in the standard theory are seen in Figures III.B.4 and III.B.5, where the slug-test data are fitted using conventional approaches (CBP and Hvorslev techniques). The systematic deviation displayed on these plots between the fitted model and the data are characteristic of the behavior observed in every multilevel slug test performed in GEMS well 2-5.

Clearly, the processes that are producing these anomalous responses need to be explained before much useful information can be obtained from multilevel slug tests at GEMS. The decision was made to suspend multilevel slug testing and to concentrate on trying to explain the observed behavior. The objective of the work thus shifted to the definition of the underlying mechanisms causing the anomalous behavior and the incorporation of these mechanisms into a general theory that can be the basis of new techniques for slug-test analysis. In the following pages, a series of field experiments, which were performed in an attempt to define the relevant processes, are described. These experiments led to the development of a nonlinear flow model that is described in a later section.

Field Experiments to Explain Anomalous Behavior

A series of field experiments were designed to assess the role of several possible factors in explaining the observed behavior. Factors that could be important in explaining the observed behavior include the following: 1) Frictional flow losses - these could occur in the cased region of the well above the top packer, within the PVC pipe

connecting the straddle packer to the top packer, within the packer flow-through pipes, and within the well screen; 2) Non-Darcian flow within the aquifer in the vicinity of the well screen; 3) Aquifer heterogeneities; and 4) Measured pressure not reflective of water level position - the transducers used in the field tests are measuring pressure, which may not always equate to the position of the water level.

The first of the above factors was considered the most likely, although there was no reason to immediately rule out the possibility of non-Darcian flow. Simulations that were performed as part of the theoretical work described in Appendix D indicated that the third factor (aquifer heterogeneities) is not going to produce a dependence on H_0 in perfectly stratified systems. Even in a system of discontinuous layers, one would not expect that aquifer heterogeneities would always produce the inverse relationship between H_0 and slug-test parameters that is seen in all tests at GEMS. The fourth factor may be important in the initial period of a test (e.g., the first one or two seconds of the data shown in Figure III.B.4 displays some oscillations in pressure that we suspect are due to water hammer effects and not actual movement of the water column), but should not affect data in the middle and latter portions of a test.

A series of field experiments was designed to test the possibility of frictional flow losses in each of the components of the system listed above. In order to simplify the testing procedure, the multilevel slug-test system was not used for these experiments. Instead, all experiments were carried out using a single packer inflated in the cased region of a well with a short screened interval. This configuration allows for a long length of well casing between the top of the packer and the static water level.

GEMS well 10-1 (depth = 17.25 m, screen length = .76 m) was selected for the initial series of tests. The packer was placed just above the screened region and two transducers were placed in the well above the packer. One transducer was placed immediately above the packer (7.59 m below static water level) and one was placed slightly below the static water level (.58 m below static water level). Thus, there was 7.01 m of casing separating the two transducers. If there are significant flow losses within the casing, normalized plots of the transducer data should differ. Figure III.B.6 displays data from two tests of this series: Test 1, which employed an H_0 of 1.07 m, and Test 6, which employed an H_0 of 6.83 m. Note that on both plots the early-time data display pressure oscillations that are attributed to the water hammer effects accompanying the opening of the flow-through pipe in the packer. In both plots, the transducer closest to the packer displays the largest early-time pressure oscillation, consistent with a water

hammer explanation (Parmakian, 1963). After the early-time pressure transients have passed, there is little to no difference between the normalized pressure measurements from the transducers. Thus, frictional flow losses within the cased region of the well do not appear to be an important mechanism for these tests. Note that Figure III.B.6 clearly indicates that the dependence of slug-test responses on H_0 is seen with the single packer setup. Note also that a Hvorslev plot of the tests of Figure III.B.6 will display a marked concave downward curvature. Thus, the same behavior was observed in the single packer tests as in the multilevel packer tests. This would imply that the PVC pipe employed in the multilevel system is not primarily responsible for the observed behavior.

The next series of field tests was designed to assess whether frictional losses within the flow-through pipe of the packer could be an explanation for the observed behavior. In order to test the importance of this mechanism, a transducer must be placed below the packer and isolated from the region above the packer. Unfortunately, there is not enough room in a .05 m ID well to place such a transducer-packer arrangement. Therefore, work was shifted to GEMS well 0-6 (depth = 24.69 m, screen length = 1.52 m, radius = .127 m), which is currently the only large-diameter observation well at the site. Unfortunately, GEMS 0-6 is screened in the bedrock underlying the alluvial deposits, so the velocity of the slug-test induced flows is considerably lower than in the wells sited in the sand and gravel section of the alluvium. Preliminary testing, however, did reveal that the slug-test responses at this well displayed a similar dependence on H_0 . In addition, a slight downward curvature was seen on Hvorslev plots of tests when a very large H_0 (7.39 m) was employed. Thus, even a well sited in material of lower permeability displayed much of the same anomalous behavior.

A simple transducer-packer arrangement was constructed at the KGS for this set of experiments. The transducer cable was run through the central flow-through pipe of the packer to the bottom of the packer, a short distance above the location of the plug used to initiate the slug tests, at which point it passes out of the flow-through pipe at a T connection. A compression fitting was placed on the cable at the T connection to ensure that no water leaked into the flow-through pipe along the transducer cable. This setup enabled the transducer sensor to be placed below the packer, isolated from the region above the packer. A series of experiments was performed in the field and laboratory to ensure a watertight seal was obtained with the compression fitting and that the transducer was truly isolated from the cased region above the packer. Neither in these experiments nor in any of the following tests was there any indication of leakage

in this system.

Figure III.B.7 displays the head data from a test ($H_0 = 6.88$ m) in the first series using the transducer-packer arrangement. The upper transducer is located above the packer, .46 m below the static water level. The lower transducer is located below the packer, 11.88 m below the static water level (total distance between the two transducers is 11.42 m). The plotted data show that there are differences between the two transducers in the early portions of the test. These differences, however, become negligible later in the test. Some flow losses do seem to occur within the packer flow-through pipe, but, since the differences do not extend through the entire test, they are probably not the primary reason for the observed anomalous behavior. A comparison of Figures III.B.6 and III.B.7 shows that recovery to the static water level in the bedrock well takes much longer than in the wells sited in the sand and gravel section. The velocities in the flow-through pipe in the wells in the sand and gravel section are clearly much greater than in the bedrock well and thus the effect of frictional losses in the flow-through pipe should be larger. However, given that a similar dependence on H_0 is observed in the bedrock and alluvial wells, frictional losses in the flow-through pipe are probably still not the primary mechanism producing the anomalous responses.

In order to further assess the possible role of the packer in the production of the observed behavior, an additional series of experiments was run in which the packer arrangement was not employed. Instead, PVC pipes (.06 m OD) of differing lengths (1.60 and 3.10 m), which had been filled with sand and sealed at both ends, were used to perform the slug tests. A slug test was initiated by rapidly lowering a PVC pipe below the static water level, causing a rise in water levels. Pipes of different lengths cause the H_0 's to be different ($H_0 = .36$ m for short pipe and $= .69$ m for large pipe). Figure III.B.8 displays the results from two tests of this series. As with tests using the packer, a dependence on H_0 is observed. Thus, flow losses in the central flow-through pipe in the packer do not appear to be the primary mechanism producing the observed dependence on H_0 .

Frictional losses in the well screen appear to be the most likely source of the observed behavior. Unfortunately, there is not an easy way of testing the importance of this mechanism in the field. An initial attempt at assessing the importance of frictional losses in the well screen was made using the transducer-packer arrangement discussed earlier. In this case, a piece of well screen (1.52 m in length) was screwed on to the bottom end of the flow-through pipe. The transducer situated below the packer was

located outside this section of screen. The idea was to mount a piece of screen whose slot size was smaller than that used in the well screen at GEMS 0-6. The screen with the smallest slot size should be the feature with the most resistance to flow in the system. If frictional losses in this screen are important, measurements from the transducer located below the packer outside the mounted screen should differ from the measurements from transducers above the packer. A series of experiments with screens of two different slot sizes were performed. In all cases, the responses were similar to those of Figure III.B.7. There were no additional losses of any significance. We suspect, however, that this result may be more of a function of experimental design (i.e. slot sizes of mounted screen are too large, slots of screen in well are encrusted with mud, etc.), so further tests are planned both in the laboratory and field in an attempt to better assess the importance of this mechanism.

Summary

An initial series of multilevel slug tests was performed at a well sited in the sand and gravel section at GEMS. The data from this series of tests indicated that the slug-test responses at this well were being affected by mechanisms not accounted for in the conventional theory. An inverse relationship between the magnitude of the induced slug (H_0) and the estimated conductivity, a concave downward curvature to data plotted in the Hvorslev format, and systematic deviations between the test data and the best-fit conventional models were the most obvious indications of these mechanisms. Additional experiments indicated that some of these processes also affect slug-test responses in a well in the less permeable bedrock underlying the alluvial section at GEMS.

A large number of field experiments were performed in an attempt to identify the relevant mechanisms producing the observed behavior. The results of these experiments indicated that frictional flow losses in the well casing, in the PVC pipe string used in the multilevel slug-test system, and in the flow-through pipe in the packer were not the primary mechanisms producing the observed responses. Experiments to assess the importance of frictional flow losses within the well screen produced ambiguous results. Further work is needed to assess the role of flow losses within the well screen and possible non-Darcian flow in the aquifer.

Although the work described here is ongoing, an important recommendation can be made about the performance and analysis of slug tests. A series of slug tests at a well should always be performed using at least two different H_0 's (preferably differing by at

least .5 m). If plots of the response data normalized by the corresponding H_0 all coincide, then one can feel confident that some variant of the conventional approach for analysis of slug-test data can be employed. As shown in the experiments described in this section, the use of only one H_0 in a series of slug tests could lead to considerable error in the estimated parameters. It is important to note that the behavior described here has, to the best knowledge of the authors, never been reported on in the literature. This is not especially surprising due to the fact that H_0 is almost never varied during a program of slug testing and that most slug tests are performed and analyzed in a rather approximate fashion. However, if our ability to predict contaminant movement in the subsurface is to be improved, it is essential that the error being introduced into the modeling analyses by the use of incorrect parameter values be diminished.

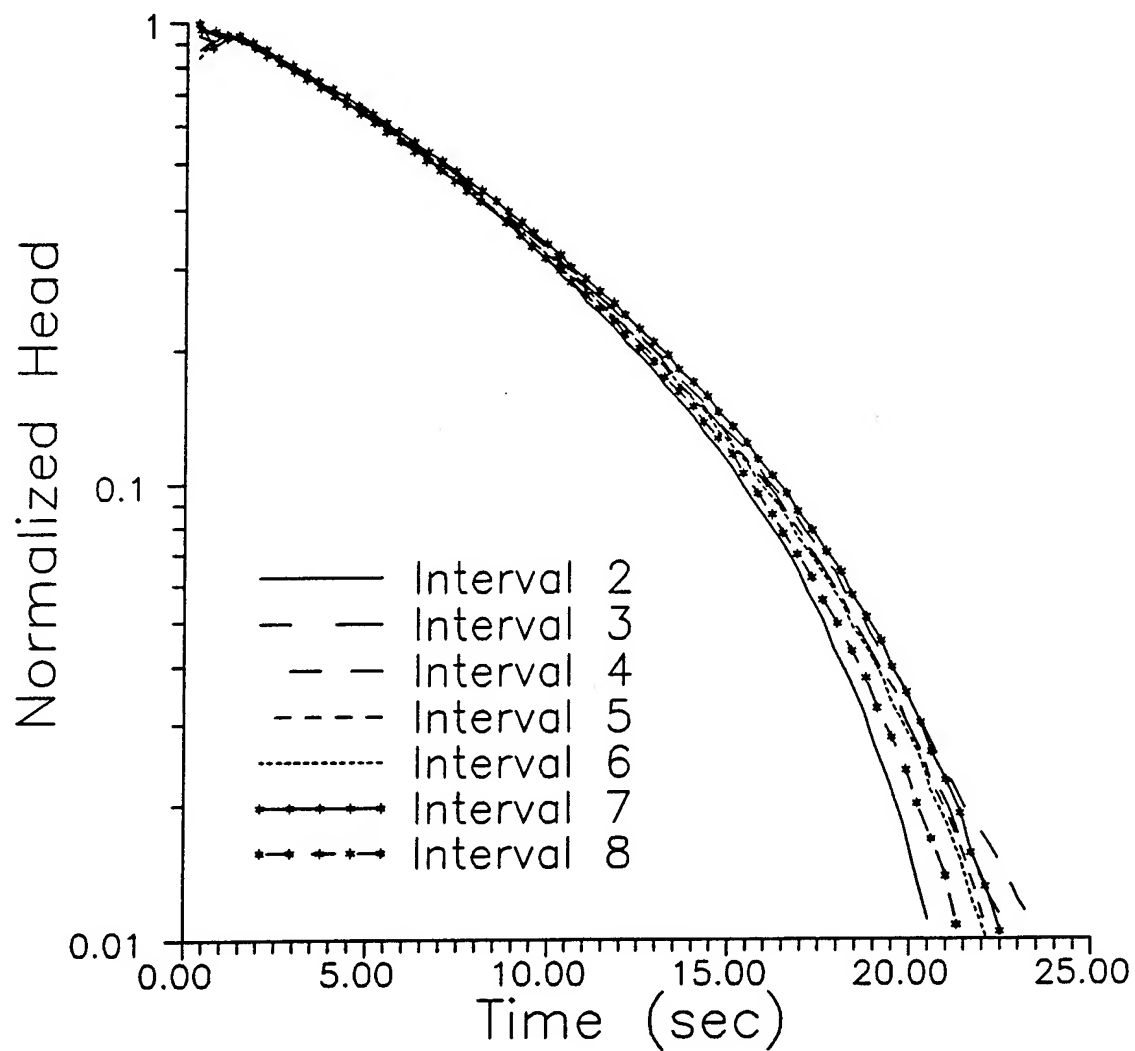


Figure III.B.1 - Normalized head (H/H_0) versus time plots for slug tests in seven intervals of GEMS well 2-5 ($H_0 = 3.07$ m). See Table III.B.1 for depths corresponding to each interval.

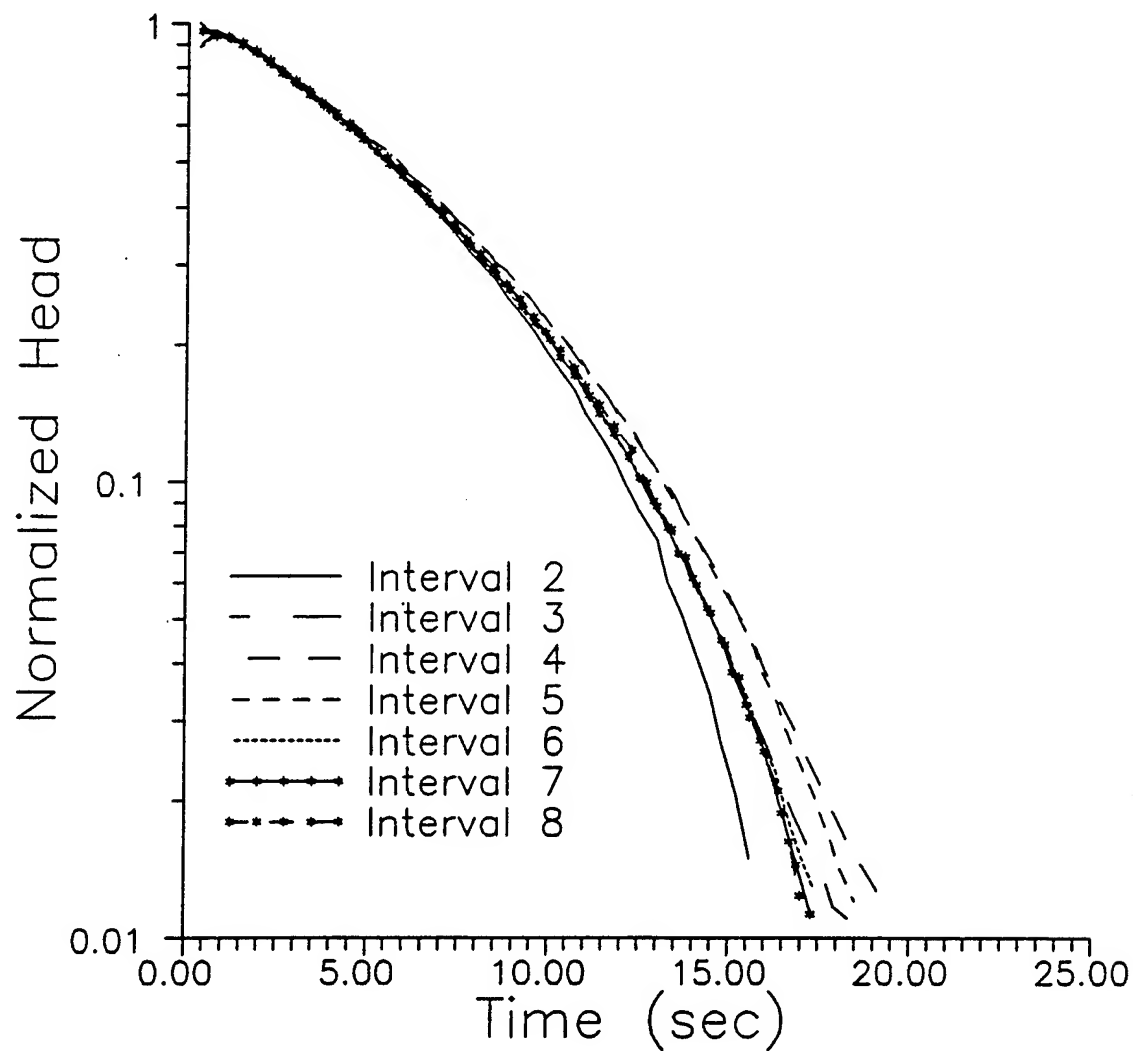


Figure III.B.2 - Normalized head (H/H_0) versus time plots for slug tests in seven intervals of GEMS well 2-5 ($H_0 = 1.65$ m). See Table III.B.1 for depths corresponding to each interval.

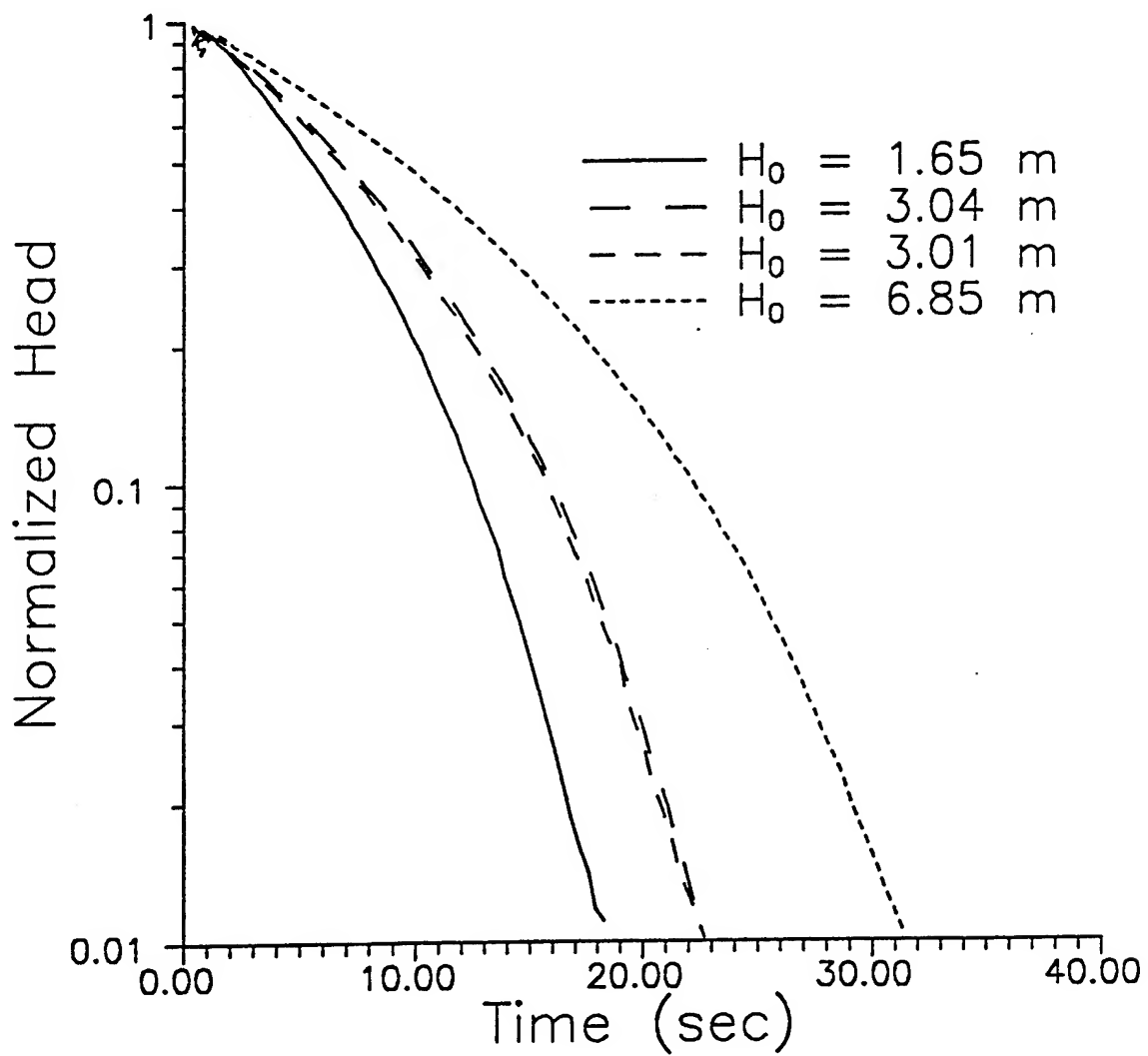


Figure III.B.3 - Normalized head (H/H_0) versus time plots for slug tests in the third interval (19.77-20.05 m) of GEMS well 2-5 using H_0 's of different magnitudes.

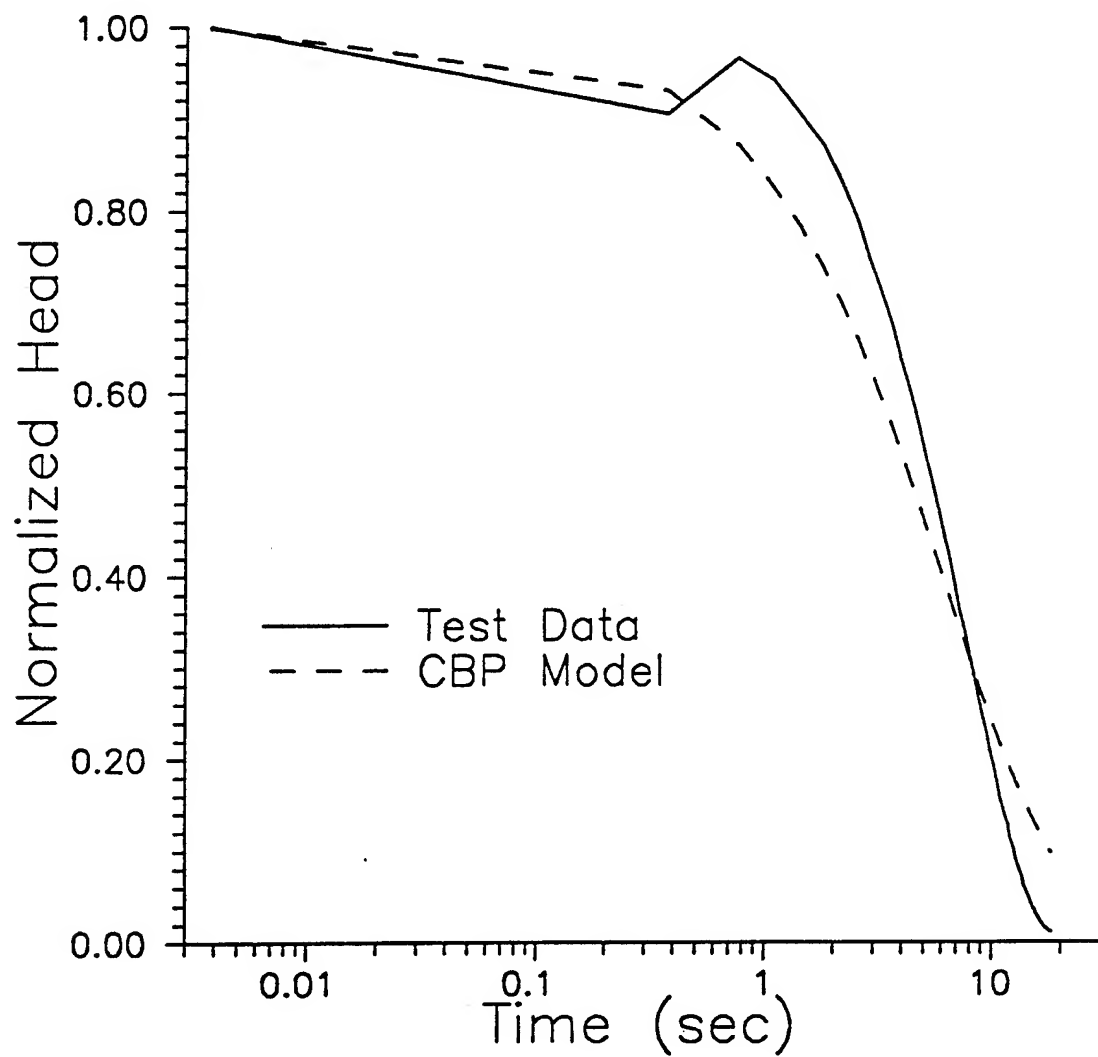


Figure III.B.4 - Normalized head (H/H_0) versus time plots of slug-test data from interval 3 (19.77-20.05 m) of GEMS well 2-5 and the best-fit CBP model.

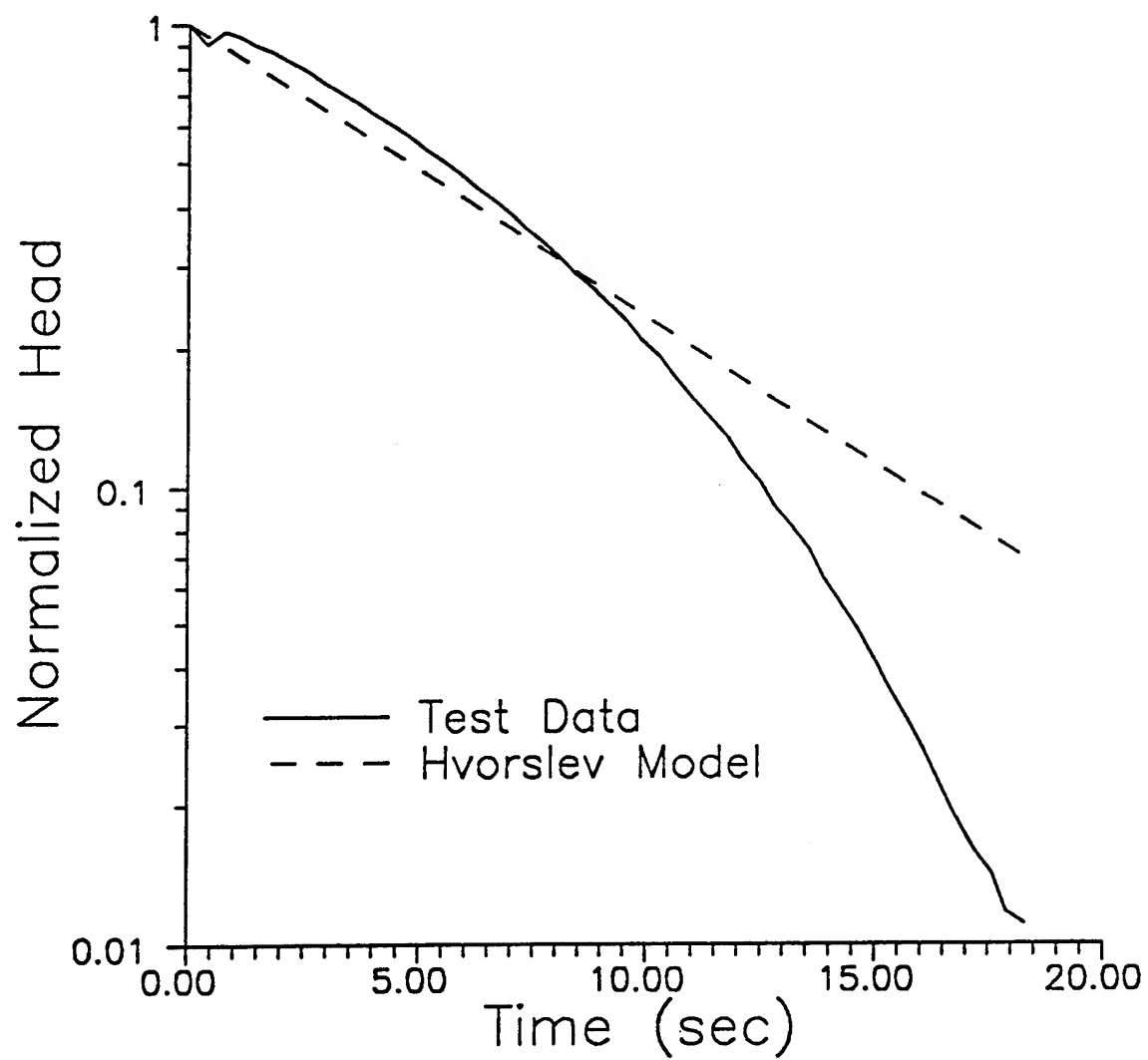


Figure III.B.5 - Normalized head (H/H_0) versus time plots of slug-test data from interval 3 (19.77-20.05 m) of GEMS well 2-5 and the best-fit Hvorslev model.

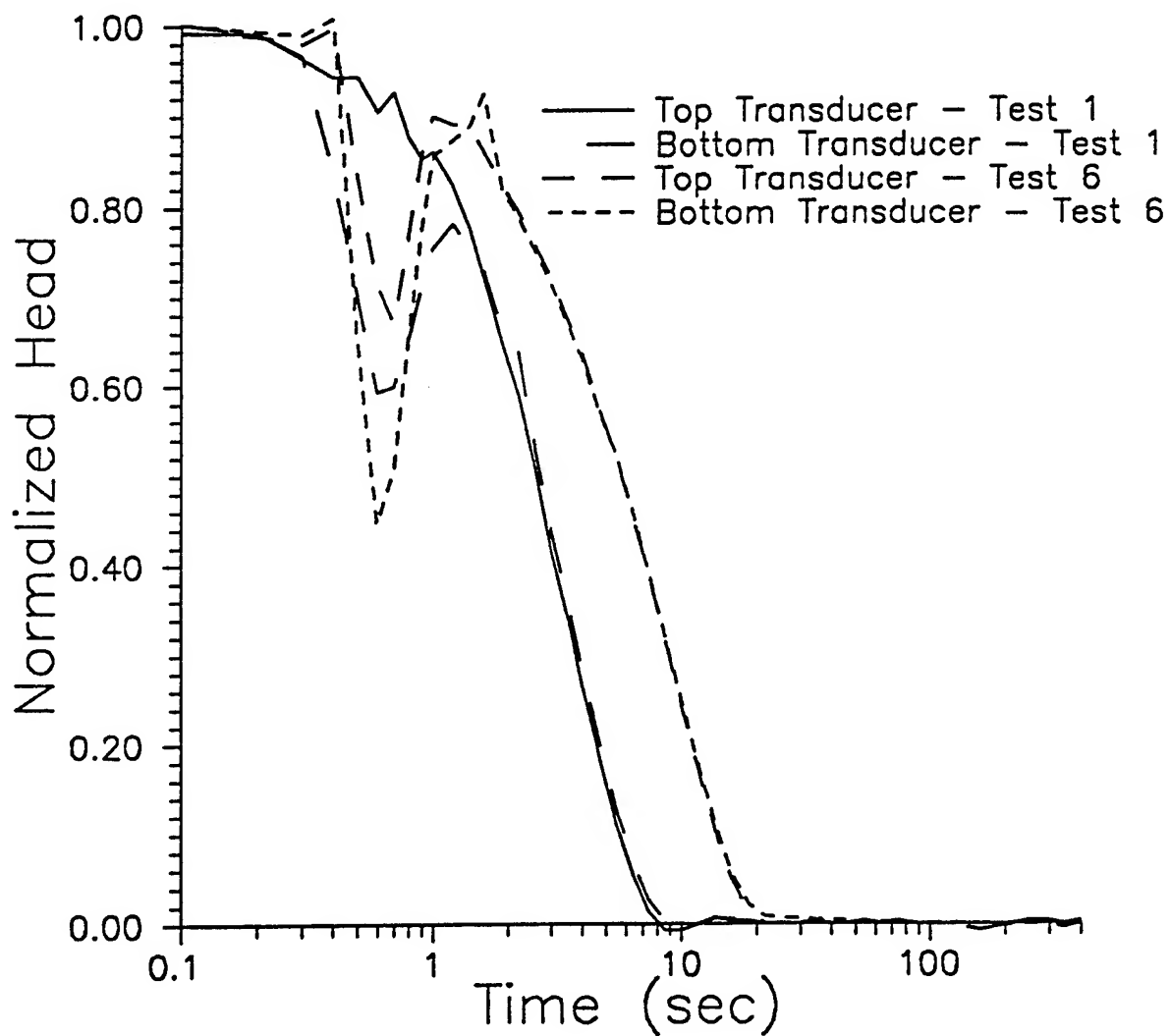


Figure III.B.6 - Normalized head (H/H_0) versus time plots for two slug tests at GEMS well 10-1 ($H_{01} = 1.07$ m; $H_{06} = 6.83$ m). Note that two transducers were used in each test.

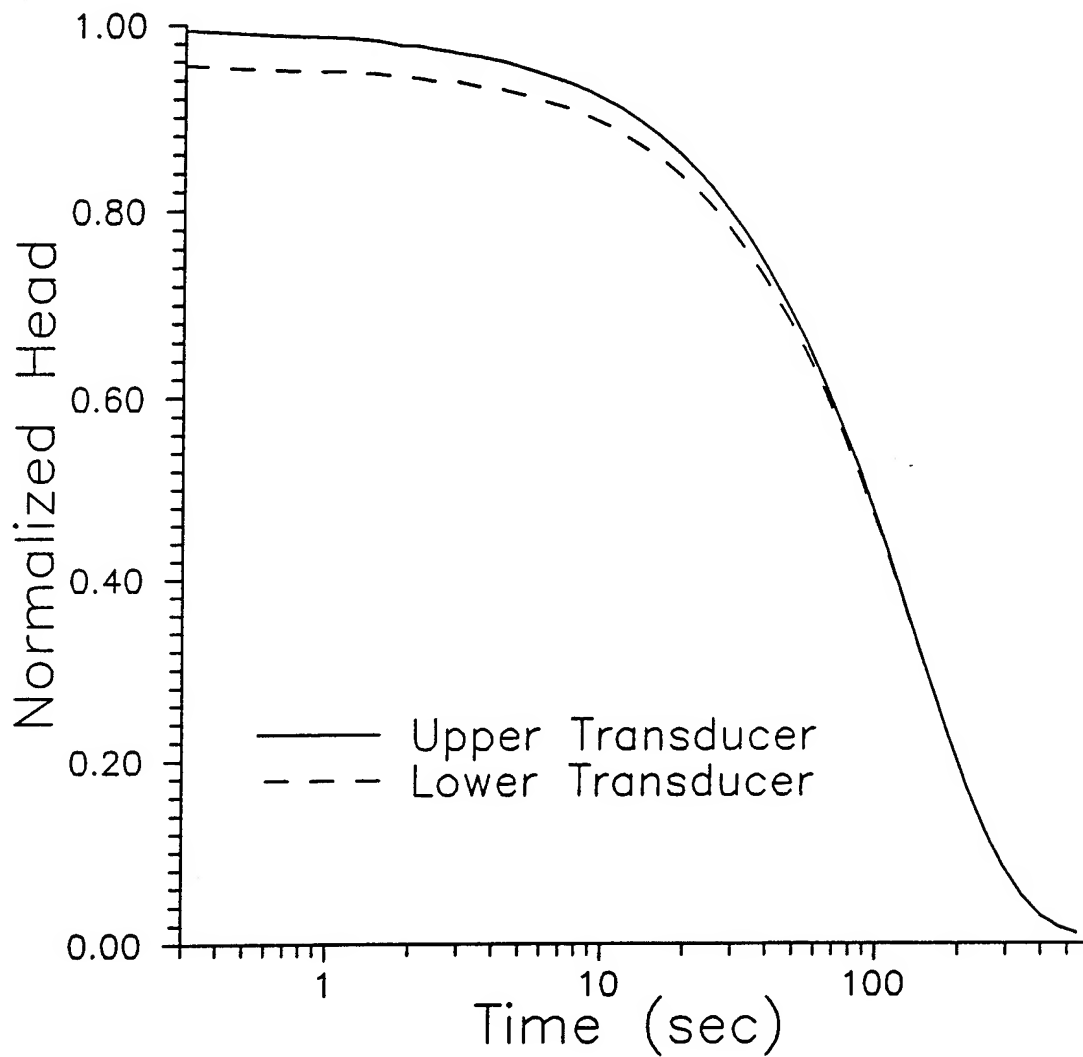


Figure III.B.7 - Normalized head (H/H_0) versus time plots for slug test at GEMS well 0-6 ($H_0 = 6.88$ m). Note that the transducer-packer arrangement described in the text was used in this test.

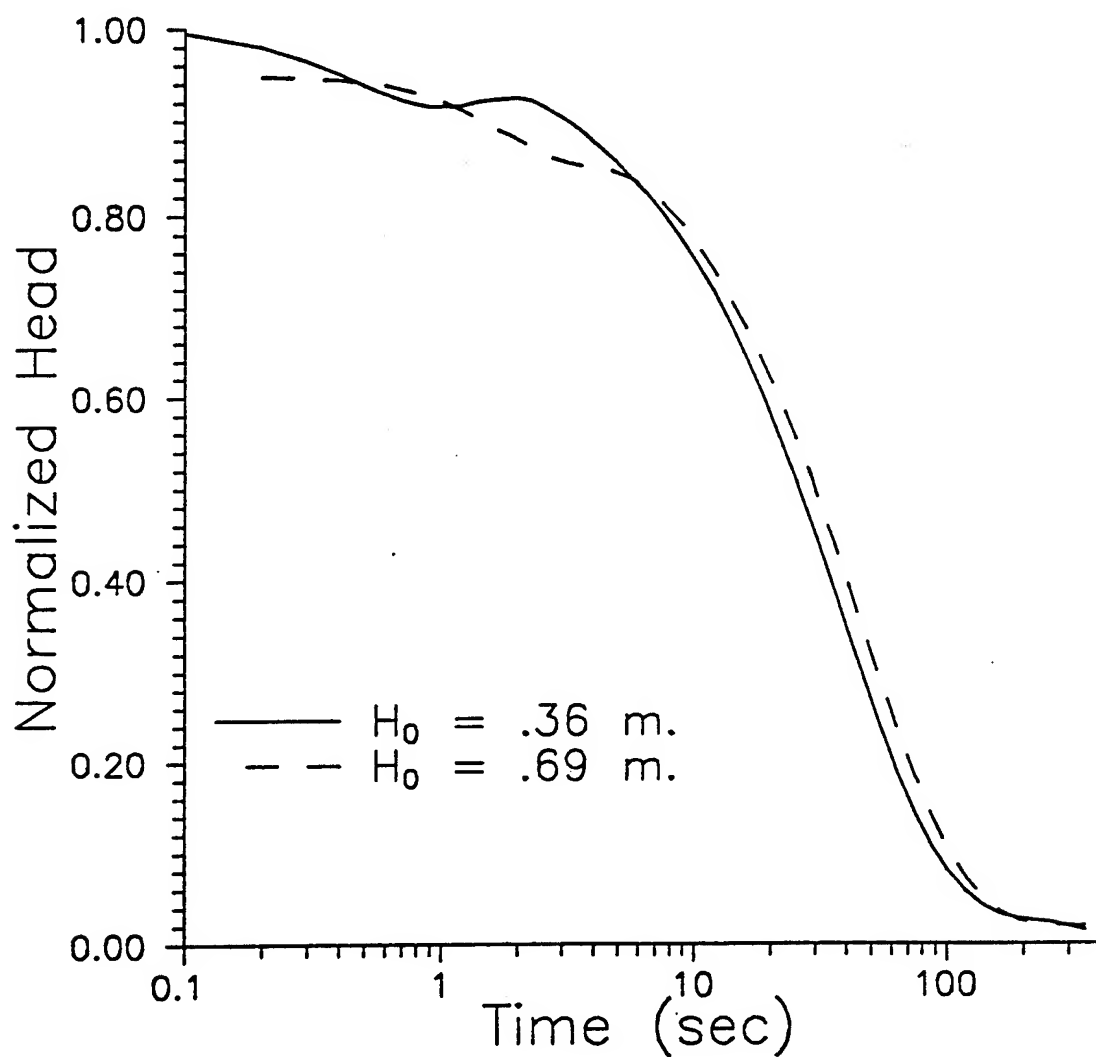


Figure III.B.8 - Normalized head (H/H_0) versus time plots for two slug tests at GEMS well 0-6 ($H_{01} = 0.36$ m; $H_{02} = 0.69$ m). Note that these slug tests were initiated using the PVC pipes described in the text.

Interval (m)	K_{HV} (10^{-3} m/s)	K_{CBP} (10^{-3} m/s)	H_0 (m)
20.07 - 20.36	0.2105	0.0682	6.88
20.07 - 20.36	0.2136	0.0693	6.86
20.07 - 20.36	0.3499	0.1124	1.66
20.07 - 20.36	0.2856	0.0921	3.06
20.07 - 20.36	0.2960	0.0956	3.12
19.77 - 20.05	0.3499	0.1135	1.65
19.77 - 20.05	0.2785	0.0904	3.04
19.77 - 20.05	0.2881	0.0938	3.01
19.77 - 20.05	0.2045	0.0664	6.85
19.46 - 19.74	0.3377	0.1098	1.74
19.46 - 19.74	0.2797	0.0911	3.05
19.46 - 19.74	0.2805	0.0913	3.03
19.46 - 19.74	0.2074	0.0676	6.86
19.15 - 19.43	0.3347	0.1085	1.62
19.15 - 19.43	0.2823	0.0917	3.04
19.15 - 19.43	0.2673	0.0864	3.28
19.15 - 19.43	0.2011	0.0652	6.85
18.83 - 19.12	0.3539	0.1177	1.58
18.83 - 19.12	0.2839	0.0922	3.03
18.83 - 19.12	0.2777	0.0900	3.19
18.83 - 19.12	0.2031	0.0660	6.87
18.52 - 18.81	0.3481	0.1124	1.60
18.52 - 18.81	0.2723	0.0882	3.23
18.52 - 18.81	0.2908	0.0943	2.94
18.52 - 18.81	0.2068	0.0672	6.90
18.22 - 18.50	0.3441	0.1111	1.69
18.22 - 18.50	0.2868	0.0929	3.01
18.22 - 18.50	0.2941	0.0955	2.99
18.22 - 18.50	0.2117	0.0688	6.92

Table III.B.1 - Results of Hvorslev (K_{HV}) and CBP (K_{CBP}) analyses for the multilevel slug tests using different initial heads (H_0). Interval nos. increase down table (top is no.2).

C. SLUG TESTS WITH OBSERVATION WELLS

Introduction

Traditionally, slug tests have been performed using the central test well as both the site of the stress and the site at which measurements are taken. In Appendix B, theoretical and field results are reported that demonstrated the benefits of using observation wells other than the stressed well in slug tests. The most noteworthy of the reported results is the finding that the reliability of the parameter estimates can be improved through the use of observation wells. In the case of the storage parameter, the improvement is quite dramatic. The field experiment described in Appendix B involved wells approximately 6.5 meters apart. The transmission of the slug-induced pressure disturbance over that distance indicates that the estimated parameters from slug tests are reflective of conditions over a much larger volume of the formation than is normally considered to be influencing the results of a slug test. In cases where large volumetric averages of formation parameters are desired, slug tests may provide an alternative to pumping tests. Clearly, slug tests present several advantages to the conventional pumping tests. As discussed in Appendix C, these include the small amount of equipment and manpower required to perform a test, the relatively short duration of the test, and the need for only a small amount of water (if any) to be added/removed from the well during the course of the test. The advantage of being able to initiate a slug test without adding or removing water from the well is very important for testing at sites of known or suspected contamination. However, if information about the hydraulic boundaries of a flow system is desired, the slug test does not provide a viable alternative to pumping tests.

To date, there has been very little work on the use of observation wells with slug tests (henceforth designated as multiwell slug tests). One of the few contributions in this area outside of the research of this project has been the work of Novakowski (1989) in which he presents an analytical solution for the response in an observation well to a pressure disturbance introduced instantaneously at a central well. Both the observation well and the stressed well are assumed to be fully screened across the aquifer. Well-bore storage is accounted for at the stressed well and, in an approximate fashion, at the observation well. Recently, van Dyke et al. (1993) describe the use of multiwell slug tests at a monitoring site in New Jersey. Unfortunately, the method that they employ for the analysis of the response data ignores well-bore storage effects at the stressed and observation wells, thereby introducing a large amount of error into the parameter

estimates.

In this section, additional field and theoretical work concerning multiwell slug tests is reported. A program of multiwell slug tests at the Geohydrologic Experimental and Monitoring Site (GEMS) is described. The estimated parameters from these tests were considerably larger than expected. A theoretical examination of multiwell slug tests using the analytical solution discussed in Appendix C is then presented. The results of this theoretical examination provide one explanation for the larger than expected parameter estimates.

Field Testing at GEMS

Well 10-1 (depth 17.32 m, screen length 0.76 m) was selected as the test well for a program of multiwell slug tests because of its proximity to several groups of wells that could be used as observation wells (see Figure 1 of Section IV.A). The tests reported here involved using well 6-2 (depth = 21.55 m, screen length = 11.55 m, distance from 10-1 = 5.62 m) and well 00-1 (depth = 17.04 m, screen length = 0.76 m, distance from 10-1 = 6.61 m). In all cases, the slug test was initiated at 10-1 using the slug-test packer system described in Appendix III.A. Measurements at the observation wells were taken using a transducer attached to the bottom of a packer located beneath the static water level in the well. The packer enabled effects associated with wellbore storage at the observation well to be kept very small. The response data could thus be analyzed without considering the effects of wellbore storage at the observation well.

Figures III.C.1 and III.C.2 display the responses observed at wells 6-2 and 00-1, respectively, for a slug test performed at well 10-1. In all cases, the responses at the stressed well exhibited the nonlinear behavior discussed in Section III.D of this report. Note the very low normalized heads measured at the two observation wells. The head changes at the observation wells were so small that the effective resolution of the transducers produced a stepped pattern in the measured responses. Note that the responses at well 6-2 were approximately 33% smaller than those at 00-1, even though 6-2 is one meter closer to 10-1 than 00-1. Several explanations can be advanced for the difference between the responses at 6-2 and 00-1: 1) the well at 6-2 is screened for a considerable length, so head increases at the same vertical interval as the stressed well are dampened by vertical movement of water in the well; 2) the resolution of the transducers causes the measured difference in the responses to be greater than the actual difference; and 3) spatial variations (heterogeneities) in flow properties produce a lower diffusivity (K/S) between wells 10-1 and 6-2 than that between wells 10-1 and 00-1. Additional testing with a higher resolution pressure transducer and use of additional wells

is currently being carried out to evaluate which of these explanations is the most reasonable.

Figures III.C.3 and III.C.4 display the results of an analysis of the response data using the fully penetrating slug-test model of Cooper et al. (1967). Note that although the fits appear relatively good (especially considering the stepped nature of the measured responses), the parameter estimates are much larger than the results obtained from the single-well slug tests discussed in Section III.D of this report. In addition, the parameter values exceed the maximum values that would be plausible for the sand and gravel aquifer at GEMS. In an attempt to explain the anomalously high parameter values that were obtained in the field testing, a further theoretical investigation of multiwell slug tests was initiated. The results of the initial portion of this work are reported below.

Theoretical Investigation of Multiwell Slug Tests

The Cooper et al. model that was used in the analysis of the responses at wells 6-2 and 00-1 is based on the assumption that both the stressed well and the observation well are fully screened across the aquifer. Since well 10-1 is screened for only .76 meters of a 10.7 meter sequence of sands and gravels, the fully screened assumption of the Cooper et al. model is clearly being violated. In order to assess the error that is introduced into parameter estimates through use of partially penetrating wells in multiwell slug tests, the partially penetrating slug test solution presented in Appendix C was extended to the case of observation points at other than the stressed well. The head at an observation point anywhere in the aquifer for the case of a slug test performed in a well with a finite-radius well skin in an anisotropic confined aquifer can be written in a non-dimensional form as

$$\phi_1(\xi, \eta, p) = \frac{\frac{\gamma}{\alpha} F_c^{-1}(F_c(\omega) f_2)}{[1 + \frac{\gamma}{\alpha} p F_c^{-1}(F_c(\omega) f_1)]}, \quad \xi \leq \xi_{sk} \quad (\text{III.C.1a})$$

$$\phi_2(\xi, \eta, p) = \frac{\frac{\gamma}{\alpha} F_c^{-1}(F_c(\omega) f_3)}{[1 + \frac{\gamma}{\alpha} p F_c^{-1}(F_c(\omega) f_1)]}, \quad \xi_{sk} \leq \xi \quad (\text{III.C.1b})$$

where the notation is as in Appendix C except for

$$f_2 = \frac{[\Delta_2 K_0(\nu_1 \xi) - \Delta_1 I_0(\nu_1 \xi)]}{\nu_1 [\Delta_2 K_1(\nu_1) + \Delta_1 I_1(\nu_1)]};$$

$$f_3 = \frac{N[K_0(\nu_1 \xi_{sk}) I_1(\nu_1 \xi_{sk}) + K_1(\nu_1 \xi_{sk}) I_0(\nu_1 \xi_{sk})] K_0(\nu_2 \xi)}{\gamma \nu_1 [\Delta_2 K_1(\nu_1) + \Delta_1 I_1(\nu_1)]}.$$

Note that the inverse Fourier transforms in the numerator of Equations (III.C.1a) and (III.C.1b) are performed for η in the screened interval of the observation well, while the inverse Fourier transforms in the denominator are performed for η in the screened interval of the well at which the test is initiated.

Equation (III.C.1b) was employed to simulate a series of slug tests in a hypothetical aquifer with a hydraulic conductivity of $1.0\text{e-}3$ m/s and a specific storage of $1.0\text{e-}5$ /m. For the initial analysis discussed here, the well skin was assumed to have the same properties as the aquifer and the formation was considered isotropic with respect to hydraulic conductivity. This series of tests was designed to examine the effect of the fully screened assumption of Cooper et al. A slug test was simulated in which the well was assumed to be fully screened across a one-meter thick aquifer. A second simulation was performed in which a slug test was done in a well, with a screen one meter in length, that is at the center of a very thick aquifer. Figure III.C.5 displays the simulated responses for an observation point located ten meters in the radial direction from the stressed well. In both cases, the observation point is at the same vertical position as the center of the screen. Note that the responses in the partially penetrating case are close to an order of magnitude smaller than those in the fully penetrating case. An analysis of the partially penetrating responses using the Cooper et al. model produced the results displayed in Figure III.C.6. Note that the estimated hydraulic conductivity and specific storage are 7.8 and 33 times, respectively, larger than the actual parameters employed in the simulations. Clearly, the misapplication of the Cooper et al. model to data from a partially penetrating well can produce parameter estimates that are much larger than the actual parameters for that site.

Given this result, it is clear that the data from the multiwell slug tests at GEMS must be reanalyzed using the partially penetrating slug test model (designated as the KGS model). Figure III.C.7 displays the results of the reanalysis of the test at well 00-1. Note that the estimated hydraulic conductivity and specific storage values are 22 and 38 times, respectively, smaller than the parameters obtained in the fully penetrating case. Note also that the estimated conductivity of $3.4\text{e-}4$ m/s (29.4 m/d) is in keeping with the results of the core analyses reported in Section IV.B.

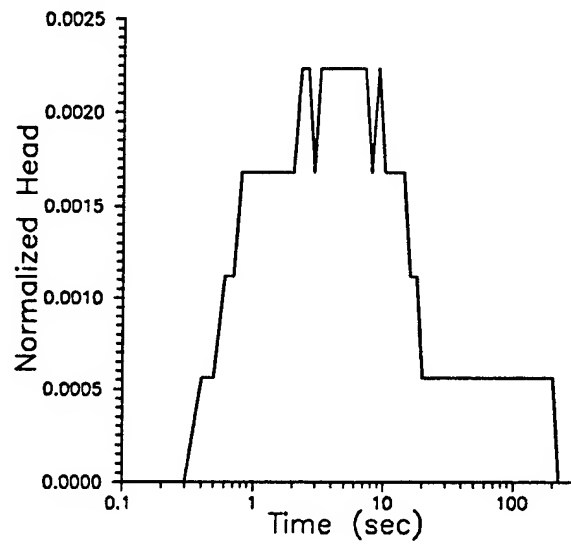


FIGURE III.C.1 - Normalized head ($h(t)/H_0$) versus time plot for well 6-2.

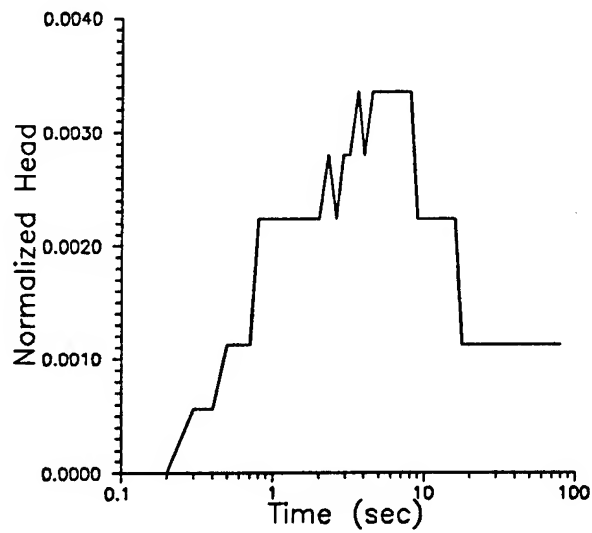


FIGURE III.C.2 - Normalized head ($h(t)/H_0$) versus time plot for well 00-1.

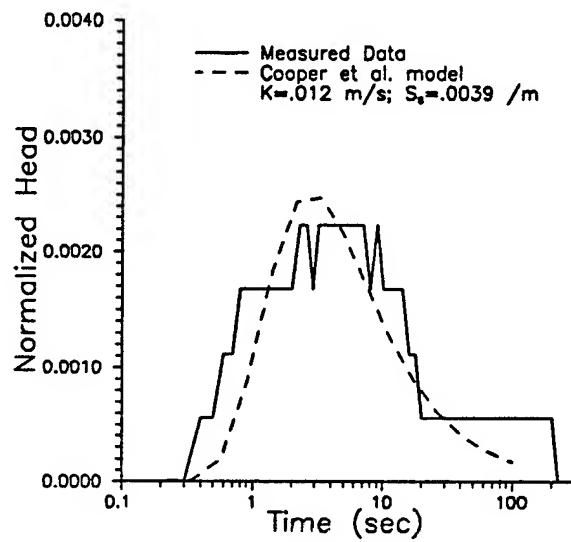


FIGURE III.C.3 - Normalized head versus time plot and the best-fit Cooper et al. model for well 6-2.

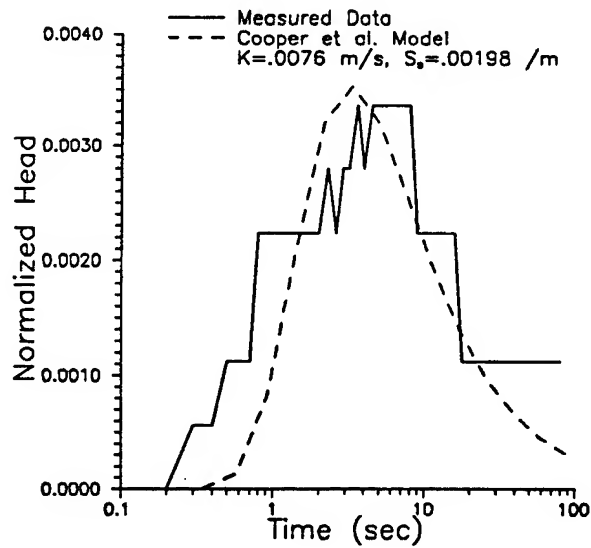


FIGURE III.C.4 - Normalized head versus time plot and the best-fit Cooper et al. model for well 00-1.

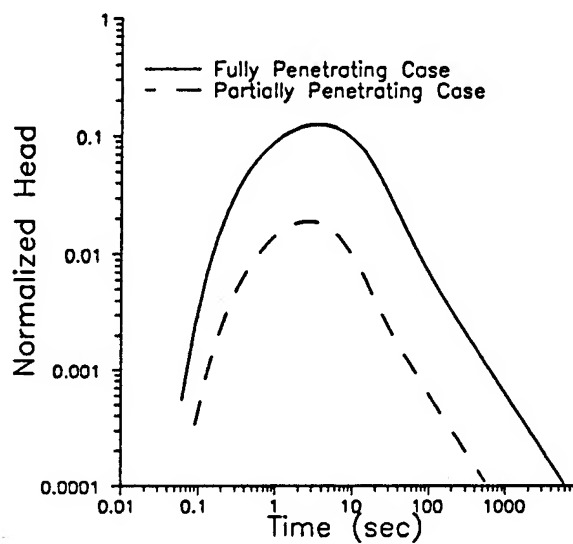


FIGURE III.C.5 - Normalized head versus time plot of simulated slug-test data (simulations employ the partially penetrating slug test model of Appendix C).

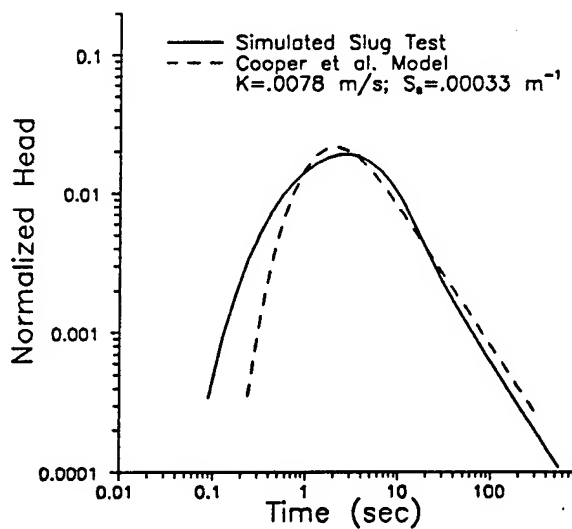


FIGURE III.C.6 - Normalized head versus time plot and the best-fit Cooper et al. model for the simulated partially penetrating well data of Figure III.C.5.

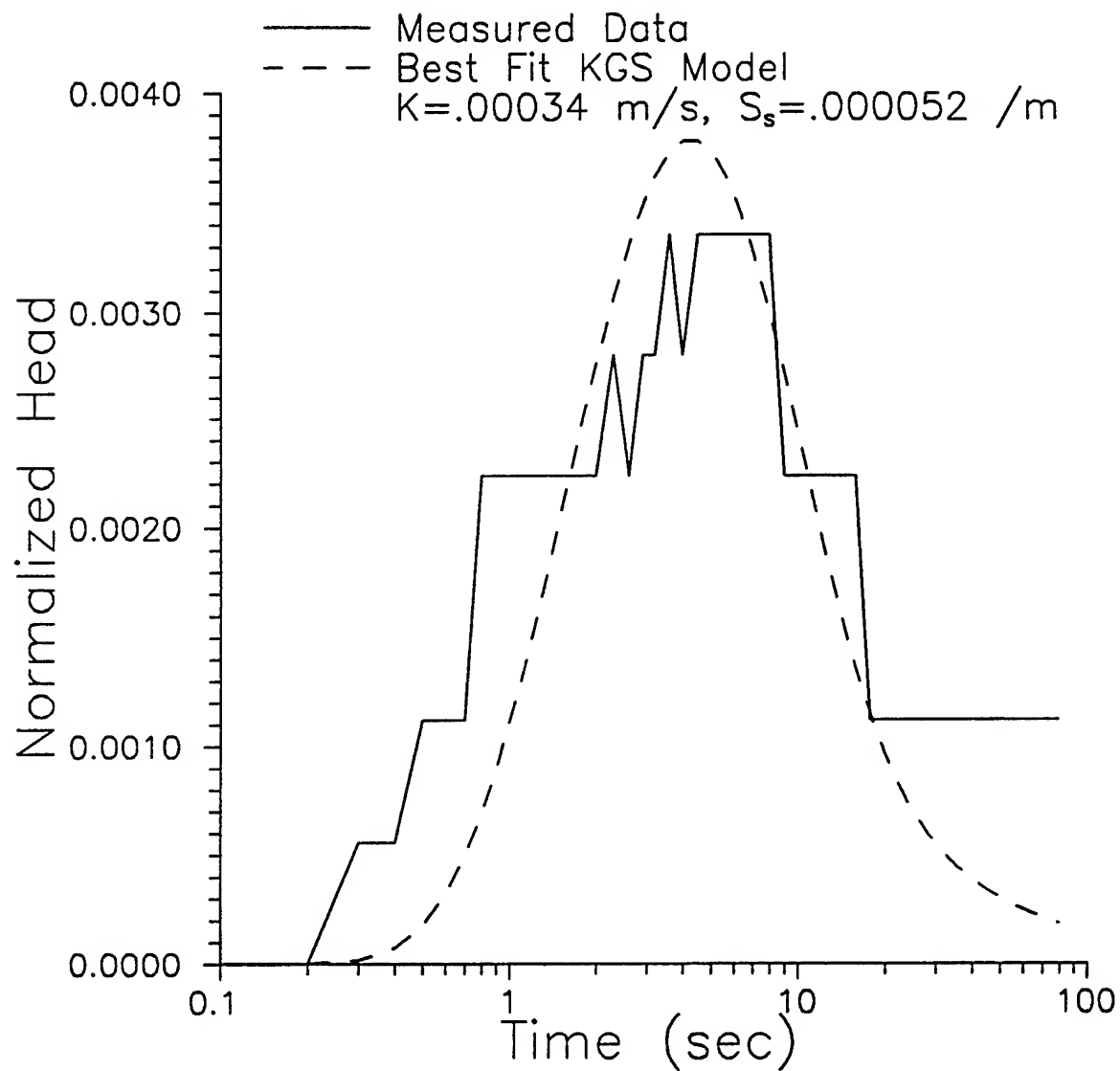


FIGURE III.C.7 - Normalized head versus time plot and the best-fit KGS model (partially penetrating slug test model of Appendix C) for well 00-1.

D. A GENERAL NONLINEAR MODEL FOR ANALYSIS OF SLUG-TEST DATA

Introduction

Slug tests are frequently used to characterize the transmissivity of an aquifer. However, in highly permeable aquifers, problems arise when the conventional analytical techniques are applied. In an aquifer consisting of coarse sand and gravel overlain by silt and clay, we have consistently seen deviations from the expected response of linear theoretical models. For example, in the Hvorslev (1951) method, the log of the slugged head in the well is plotted against time on a linear scale (e.g., Figure 1). Ideally this plot is a straight line, the slope of which is proportional to the hydraulic conductivity of the aquifer. Typically, we do not see a straight line on this plot, but rather a concave downward curve (e.g., Figure 2). Also, we see a dramatic dependence of the duration of the slug test on the initial height. If the slug-test data are normalized to the initial height, conventional models predict that all curves for different initial heights should be the same. We find that the curves are dramatically shifted to larger times for our field data (see section III.B). The sand and gravel at our field site is so coarse that the slug tests generally only last a few tens of seconds. This means that the water velocity is much faster than in finer sediments. We have investigated three non-linear variants of the Hvorslev model. One considers frictional effects caused by the flow of water in the casing and through the screen. We assume this frictional effect is proportional to a power of the velocity. Another model assumes non-Darcian flow, with the hydraulic gradient proportional to the first and second powers of velocity. A third model considers a modification of Darcy's law, adding in an inertial term proportional to the acceleration. With the addition of this extra term we have a fairly general model for slug tests that unifies several phenomena. There are three parameters in the model: one is the hydraulic conductivity, another is related to the nonlinearity, and the last is a parameter representing inertial effects. We have developed a numerical solution for this general model and have found that the solutions do exhibit downward curvature and do show the correct form of dependence on initial head. We have applied these models to field data and have found that the downward curvature and the dependence on head can be fit very well. Initial findings are that the hydraulic conductivity can be determined with good consistency, at a given well, for tests with different initial heads. However, a traditional Hvorslev analysis gives very different results for the hydraulic conductivity with these same data.

Field Data

When we plot field data (Figure 2) on a Hvorslev-type plot, concave downward curves are seen. Chirlin (1989) has shown that for the transient C-B-P model (Cooper et al., 1967) concave upward curves should result. Also, we see a dramatic dependence of the duration of the slug test on the initial height. If the slug-test data are normalized to the initial height, conventional models predict that all curves for different initial heights should be the same. We find that the curves are dramatically shifted to larger times for our field data (see section III.B).

Nonlinear Models

The sand and gravel at our field site is so coarse that the slug tests generally only last a few tens of seconds. This means that the water velocity is much faster than in finer sediments. We have investigated three nonlinear variants of the Hvorslev model. One considers frictional effects caused by the flow of water in the casing and through the screen. The Hvorslev approximation for the flow during a slug test is

$$Q(t) = \pi r_c^2 \frac{\partial H(t)}{\partial t} = -FK \cdot h(t) \quad (\text{III.D.1})$$

where

$Q(t)$ = flow of water into aquifer

$H(t)$ = height of water in well at any time,

$h(t)$ = head of water just outside the screen in the aquifer,

K = hydraulic conductivity,

F = Hvorslev geometric factor, and

r_c = casing radius.

Equation (III.D.1) is the usual equation used to start the Hvorslev derivation, except that the right hand side contains $h(t)$ which may be different from the head in the casing due to frictional effects. Assume a loss in head across the screen due to friction

$$Q(t) = \left(\frac{H(t) - h(t)}{R} \right) \quad (\text{III.D.2})$$

R is the resistance factor. The flow through the screen [$Q(t)$ in equation (III.D.2)] is assumed to be proportional to the head loss in the casing and screen and inversely

proportional to a resistance factor (R). Replacing $h(t)$ in equation (III.D.1) with equation (III.D.2) gives

$$\pi r_c^2 \frac{\partial H(t)}{\partial t} = -FK \cdot (Q(t)R + H(t)) \quad (III.D.3)$$

which involves only the head in the casing $H(t)$. $Q(t)$ can be replaced by using equation (III.D.1) again.

R is an empirical resistance factor that we have introduced. We assume this factor is proportional to a power of the velocity.

$$R = A \cdot |V| = A \left| \frac{dH(t)}{dt} \right| \quad (III.D.4)$$

where A is an assumed constant of proportionality. Equation (III.D.4) assumes that R is proportional to the first power of the velocity. A is a measure of the nonlinearity (nonlinear factor), if $A = 0$ then we have the usual Hvorslev solution. Replacing R in equation (III.D.3) yields

$$\frac{dH(t)}{dt} \left[1 + FKA \left| \frac{dH(t)}{dt} \right| \right] = -\frac{FK}{\pi r_c^2} H(t). \quad (III.D.5)$$

It is clear that equation (III.D.5) is a nonlinear equation which must be solved for the head in the casing, $H(t)$.

There is other work in the literature that suggests the frictional effects may be proportional to higher powers of the velocity (Barker and Herbert, 1992; Singh and Shakya, 1989). The generalization for any power (N) of the velocity is:

$$R = A \cdot |V|^N = A \left| \frac{dH(t)}{dt} \right|^N. \quad (III.D.6)$$

Similarly, the generalization of equation (III.D.5) is:

$$\frac{dH(t)}{dt} \left[1 + FKA \left| \frac{dH(t)}{dt} \right|^N \right] = -\frac{FK}{\pi r_c^2} H(t). \quad (III.D.7)$$

Consequently, equations (III.D.6) and (III.D.7) give the generalization to the case when R is proportional to the Nth power of the velocity.

The second model we shall employ assumes non-Darcian flow, with the hydraulic gradient proportional to the first and second powers of velocity (Bear, 1972; Guppy et al., 1982).

$$\frac{\partial h}{\partial r} = -\frac{1}{K}V + bV^2 \quad (\text{III.D.8})$$

where b is a constant. After some algebra the result is the same as for the resistive loss case with $N = 1$, even though they represent different physical processes.

$$\frac{dH(t)}{dt} \left[1 + FKA \left| \frac{dH(t)}{dt} \right| \right] = -\frac{FK}{\pi r_c^2} H(t), \quad (\text{III.D.9})$$

where the relationship between A and b is

$$A = \frac{br_c^2}{4\pi L^2 r_w}. \quad (\text{III.D.10})$$

L is the length of the well screen and r_w is the screen radius. b is the nonlinear factor in equation (III.D.8). Again if $b = 0$ we have the usual Hvorslev solution.

From here on, we shall use only A for the nonlinear factor, realizing that two different physical models can be represented for $N = 1$. There are two parameters in the models that may be fitted: one is the hydraulic conductivity (K), and the other is the nonlinear factor (A). We have also done some analysis with the $N = 2$ case but preliminary results indicates that the $N = 1$ model is more consistent with the data and it has the advantage of representing both physical models discussed here.

Numerical Solution of Nonlinear Models

The two physical models can be represented by the same nonlinear equation (III.D.5) in the variable $H(t)$. In general, it can not be solved in closed form. Using an iterative numerical solution technique, one obtains the following form:

$$H^{n+1(m+1)} = H^n - \frac{\frac{\Delta t}{2t_0}(H^{n+1(m)} + H^n)}{\left[1 + FKA \left| \frac{H^{n+1(m)} - H^n}{\Delta t} \right|^N\right]} \quad (\text{III.D.11})$$

where we have also used the usual definition of the Hvorslev time lag

$$t_0 = \frac{\pi r_c^2}{FK} \quad (\text{III.D.12})$$

and $H^{n(m)}$ is the m^{th} iteration value at the n^{th} time level. Equation (III.D.11) must be iterated for each time step until there is relatively little difference in the $H(t)$ for consecutive iterations. Equation (III.D.11) can be used for sequential time steps to generate the entire nonlinear type curve.

Figure 3 shows some of these type curves for typical parameters that might occur at the GEMS site. The solutions do exhibit downward curvature and do show the correct form of dependence on initial head. As the initial head increases the length of the test increases also. This implies that, when all data are given equal weight and a normal Hvorslev analysis is applied, one will estimate a lower hydraulic conductivity for tests with larger initial heads. However, looking carefully at the type curves in Figure 3, one can see that the large time behavior of all the curves for differing initial heads become parallel with a slope that is proportional to the hydraulic conductivity. Therefore, the late time data is more sensitive to the hydraulic conductivity, while the early time behavior may be heavily influenced by the nonlinear behavior.

Fitting and Editing Considerations

Figures 4 and 5 show some data from a 2 inch PVC well at GEMS with approximately 2.5 feet of screen. The initial slug height is about 23 feet. The field data are shown by asterisks and the solid curves are fitted by using an equal weight regression program (Bohling and McElwee, 1992). There are problems in fitting both the traditional Hvorslev model (Figure 4) and the nonlinear model (Figure 5) using an equal weight regression program. First of all, the late-time data are small in magnitude so its effect on the least squares fit is minimized. This shows up as a substantial deviation of the data from the curve at late time. Of course, the deviation in Figures 4 and 5 is emphasized by taking the log of the head. The second problem in fitting the field data centers about the fact that field data will be dominated by noise at late time when the head has decayed to

nearly the static level. Unfortunately, the late-time data are most sensitive to the hydraulic conductivity, so these two problems must be dealt with carefully in order to achieve the best estimate of hydraulic conductivity. First of all the late-time data can be emphasized by fitting the log of the slugged head; this tactic will give greater weight to the late-time data. Secondly, careful editing of the log of the slugged head must be done before fitting, since taking the log of the slugged head emphasizes the importance of the late-time data. We must be certain that the signal level of all late-time data used in the fit is substantially above the ambient noise level. The last data points in both Figures 4 and 5 are examples of data that is not substantially above the ambient noise level and should be edited out.

Figure 6 shows field data from four slug tests with varying heights from well GEMS 02, which is a 2 inch PVC well that is approximately 45 feet deep with a screen length of approximately 2.5 feet. Clearly, the late-time data must be edited. The edit line we used is shown in the figure. It is uncertain what causes all the ambient noise (some sites will be noisier than others due to cultural effects), however, part of the late time noise level comes from elastic effects which are probably greater for larger initial heads.

Results

We have applied the nonlinear models to carefully edited field data and have found that the downward curvature and the dependence on head can be fit very well to the log of the slugged head. The data in Figure 7 are also from GEMS 02; the initial head is 8.62 feet. The fit is good; the early time curvature and late time behavior are well represented by the nonlinear models. Fits for other values of initial head are similar. However, the systematic deviations from the model fit seem more pronounced at early time for the smaller values of initial head (not actually shown here).

Analysis of eight separate slug tests at GEMS 02 are summarized in Table 1. The initial heads range from 2.75 feet to 23.1 feet. This table shows that the hydraulic conductivity can be determined with some consistency at this well, for tests with different initial heads. The fitted hydraulic conductivity (K) varies from .00485 ft./sec. to .00296 ft./sec., with an average value of .00388 ft./sec. The nonlinear factor (A) varies from 177 to 63.9, with an average of 108. We revisited this well several months after the first round of testing when differing hydraulic conditions existed: the water table was several feet higher due to a very wet spring. Another set of eight slug tests with varying initial heads was performed and analyzed with the nonlinear model and the results were very consistent with the values given in Table 1. Ideally, K and A should be constant within the limitations of the data noise level, if the physical model is correctly describing the

test. It is clear that there are some systematic trends in Table 1; K and A both decrease as the initial head is increased. This systematic trend indicates that our physical model is still not quite correct. In addition, in some recently conducted slug tests in other wells, we have observed some oscillatory behavior at late time. These nonlinear models do not predict any such oscillatory behavior, so clearly there is additional work to be done to completely describe the results of slug tests at GEMS.

Need For a General Model

Figure 8 shows some typical slug test data from a GEMS well that does not oscillate; however, the conventional theories do not adequately explain this data. The main problems shown in the data of Figure 8 are: first, the response is dependent on the initial head and second, the Hvorslev (1951) and Cooper, Bredehoeft, and Papadopoulos (CBP, 1967) models show a systematic lack of fit. In all linear theories the normalized responses for various initial slug heights should collapse onto one curve. Clearly, this is not the case in Figure 8. As discussed earlier, a typical Hvorslev plot of the field data does not yield a straight line, but instead we see a pronounced downward curvature. This is in contrast to the upward curvature plot Chirlin (1989) shows should result from the transient CBP model. The implication is that this well is exhibiting behavior in the "critically damped" region. The Hvorslev and CBP theories are supposed to be valid in the "overdamped" region. These concepts will be discussed later in the section in connection with the theory presented.

In some wells we have also observed oscillatory behavior (Figure 9). Although there are some theories describing oscillatory behavior in slug tests, until now it has been difficult to analyze tests which are in the so-called "critically damped" region. One of the earliest attempts to analyze oscillatory data was by van der Kamp (1976); however, he invoked a number of assumptions to make the theory linear. Kipp (1985) has also dealt with the linear theory of oscillatory slug test responses by using Laplace transforms and numerical inversions to calculate type curves. Kabala et al. (1985) are among the first to consider the use of a nonlinear equation to describe the oscillatory slug test behavior. However, after considerable numerical study, they state that "the linear model is sufficiently accurate in all practical cases." The data in Figure 9 show that their conclusion is not valid for this well. Very recently Stone and Clarke (in press) have used a nonlinear model to study hydraulic properties in glacial flow systems.

We have developed a unified model for slug tests that includes the effects of nonlinear terms, inertia, turbulence (spatial velocity distributions), viscosity and differing casing and screen radii. We have developed a numerical solution under Hvorslev type

assumptions that should be valid over the whole range from "overdamped" to "underdamped" conditions. There are a couple of surprises that come to light in analyzing the GEMS data. First, most investigators (van der Kamp, 1976; Kabala et al., 1985; and Stone and Clarke) find that the effective water column height may be different than that measured in the field. We think we may have found an explanation for this phenomenon. Second, some nonlinear effects are much stronger than most investigators have suggested and the magnitude of their strength is not easily predicted with the theory. For this reason, we use the magnitude as a fitted parameter.

Navier-Stokes Equation for the Borehole

The motion of the water in the borehole can be described by the Navier-Stokes equations (Eskinazi, 1967). If we consider the borehole as a streamtube with average flow in the z direction the z component equation is

$$\frac{\partial V}{\partial t} + V \frac{\partial V}{\partial z} = -g - \frac{\nabla P}{\rho} + \frac{\mu}{\rho} \nabla^2 V \quad (\text{III.D.13})$$

V is the average velocity of the water in the borehole in the z direction, g is the acceleration of gravity, P is the pressure, ρ is the density and μ is the viscosity. This equation is basically a force balance equation per unit fluid mass and can be integrated in the z direction over the length of the borehole shown in Figure 10 to obtain an energy or work balance equation. We assume that the length of the screen (b) is negligible in comparison with the water column length,

$$b \ll z_o + h(t) \quad (\text{III.D.14})$$

$$\int \frac{\partial V}{\partial t} dz + \int V dV = -g(h + z_o + b) - \int \frac{dP}{\rho} + \int \frac{\mu}{\rho} \nabla^2 V dz \quad (\text{III.D.15})$$

We will assume that the water is incompressible (ρ is constant) and that the viscosity is constant. Integrating from the bottom of the screen to the top of the water in the borehole gives

$$\int \frac{\partial V}{\partial t} dz + \frac{V_T^2 - V_s^2}{2} = -g(h + z_o + b) + \frac{P_s - P_a}{\rho} + \int \frac{\mu}{\rho} \nabla^2 V dz \quad (\text{III.D.16})$$

P_s and P_a are the pressures at the screen and the top of the water column, respectively, and V_T and V_s are the water velocities at the top of the column and at the screen, respectively. These velocities are related by the conservation of mass flow while the average velocity at the top of the water column is simply dh/dt .

$$\pi r_c^2 V_T = \pi r_c^2 \frac{dh}{dt} = 2\pi r_s b V_s, \quad (\text{III.D.17})$$

r_c and r_s are the casing and screen radii, respectively. Using equation (III.D.17) in equation (III.D.16) results in

$$\int \frac{\partial V}{\partial t} dz + \frac{1}{2} \left[1 - \left(\frac{r_c^2}{2r_s b} \right)^2 \right] \left(\frac{dh}{dt} \right)^2 = -g(h + z_o + b) + \frac{P_s - P_a}{\rho} + \int \frac{\mu}{\rho} \nabla^2 V dz \quad (\text{III.D.18})$$

The first and last terms of equation (III.D.18) require a little more explanation.

The last term in equation (III.D.18) is the work done by viscous forces in the fluid column. Writing out the Laplacian operator gives

$$\int \frac{\mu}{\rho} \nabla^2 V dz = \frac{\mu}{\rho} \int \left[\frac{\partial^2 V}{\partial r^2} + \frac{1}{r} \frac{\partial V}{\partial r} + \frac{1}{r^2} \frac{\partial^2 V}{\partial \theta^2} + \frac{\partial^2 V}{\partial z^2} \right] dz \quad (\text{III.D.19})$$

If we assume that the flow is unchanging in the θ direction and that the cross section of the borehole is uniform and the fluid is incompressible then

$$\frac{\partial^2 V}{\partial \theta^2} = 0, \quad \frac{\partial^2 V}{\partial z^2} = 0 \quad (\text{III.D.20})$$

and equation (III.D.19) becomes

$$\int \frac{\mu}{\rho} \nabla^2 V dz = \frac{\mu}{\rho} \int \left[\frac{\partial^2 V}{\partial r^2} + \frac{1}{r} \frac{\partial V}{\partial r} \right] dz \quad (\text{III.D.21})$$

Of course if we have varying radii in the borehole due to changes in casing radius or the presence of an obstruction such as a packer or other equipment, then equation (III.D.20) is no longer true and additional terms need to be added to equation (III.D.21) due to viscous work being performed at those locations. If we assume a parabolic distribution of velocities across the borehole radius as shown in Figure 11, we can write

$$V = V_o \left[1 - \frac{r^2}{r_c^2} \right]. \quad (\text{III.D.22})$$

This allows equation (III.D.21) to be written as

$$\int \frac{\mu}{\rho} \nabla^2 V dz = -\frac{4\mu}{r_c^2 \rho} V_o \int dz = -\frac{4\mu}{r_c^2 \rho} V_o (h + z_o + b) \quad (\text{III.D.23})$$

The average vertical water velocity is given by the rate of change of the height of the water column and is related to the maximum of the parabolic velocity distribution as follows

$$Q = \pi r_c^2 \frac{dh}{dt} = \int V dA = 2\pi \int_0^{r_c} V_o \left[1 - \frac{r^2}{r_c^2} \right] r dr = \frac{\pi r_c^2 V_o}{2} \quad (\text{III.D.24})$$

$$V_o = 2 \frac{dh}{dt}$$

where Q is the rate of water flow through the borehole. The final form for equation (III.D.23) is

$$\int \frac{\mu}{\rho} \nabla^2 V dz = -\frac{8\mu}{r_c^2 \rho} (h + z_o + b) \frac{dh}{dt} \quad (\text{III.D.25})$$

The first term in equation (III.D.18) can be manipulated as follows

$$\int \frac{\partial V}{\partial t} dz = \frac{\partial}{\partial t} \int V dz = \frac{\partial}{\partial t} \left[\frac{dh}{dt} \int \frac{\pi r_c^2}{A(z)} dz \right] \quad (\text{III.D.26})$$

by remembering that conservation of water flow requires that

$$\pi r_c^2 \frac{dh}{dt} = A(z)V(z) \quad (\text{III.D.27})$$

where dh/dt is the average velocity in the casing with normal radius r_o and $V(z)$ is the average velocity where the cross sectional area is $A(z)$. If the cross sectional areas do not change with time and if the cross sectional area is uniform in the z direction then equation (III.D.26) becomes

$$\int \frac{\partial V}{\partial t} dz = (h + z_o + b) \frac{d^2 h}{dt^2} \quad (\text{III.D.28})$$

Additional acceleration work terms must be added to this equation if there are significant restrictions in the cross sectional area in the borehole. Our calculations show that these additional terms are usually negligible if the restrictions in cross sectional area are not too great.

Using equations (III.D.28) and (III.D.25) in equation (III.D.18) allows us to write the form

$$(h + z_o + b) \frac{d^2 h}{dt^2} + \frac{1}{2} \left[1 - \left(\frac{r_c^2}{2r_s b} \right)^2 \right] \left(\frac{dh}{dt} \right)^2 = -g(h + z_o + b) + \frac{P_s - P_a}{\rho} - \frac{8\mu}{r_c^2 \rho} (h + z_o + b) \frac{dh}{dt} \quad (\text{III.D.29})$$

which is an ordinary differential equation for the height of the water column in the borehole as a function of time. Notice that the equation is nonlinear in h .

Borehole and Aquifer Interaction

The pressure at the screen will depend on the head in the aquifer, which in turn depends on the aquifer parameters. If $H(r)$ is the head in the aquifer relative to the static level shown in Figure 10, we can write

$$P_s = P_a + g\rho[H(r_s, t) + z_o + b] \quad (\text{III.D.30})$$

(assuming that b is small so that the pressure across the screen is nearly constant in the vertical). With the use of equation (III.D.30) in equation (III.D.29) we obtain the final form for the borehole equation which couples to the aquifer equation through $H(r,t)$.

$$(h + z_o + b) \frac{d^2 h}{dt^2} + \frac{1}{2} \left[1 - \left(\frac{r_c^2}{2r_s b} \right)^2 \right] \left(\frac{dh}{dt} \right)^2 + \frac{8\mu}{r_c^2 \rho} (h + z_o + b) \frac{dh}{dt} + g[h - H(r_s, t)] = 0 \quad (\text{III.D.31})$$

The general aquifer equation

$$\nabla \cdot [bK \nabla H(r, t)] = S \frac{\partial H}{\partial t} \quad (\text{III.D.32})$$

must be solved for $H(r,t)$ concurrently with equation (III.D.31) to obtain the complete solution, where K and S are the aquifer conductivity and storage, respectively. The screen is the boundary between these two solutions and the following boundary condition applies.

$$Q(t) = -\pi r_c^2 \frac{dh(t)}{dt} = -2\pi bK \left[r \frac{\partial H(r, t)}{\partial r} \right]_{r_s} \quad (\text{III.D.33})$$

Hvorslev Style Approximation

The system of equations (III.D.31)-(III.D.33) is difficult to solve in general, so an approximation which simplifies the solution would be welcome. In the spirit of the Hvorslev (1951) and Bouwer and Rice (1976) methods, we can assume that the storage in the aquifer is negligible and consider the aquifer as going through a series of quasi steady states in response to the slug in the borehole. With this assumption, equation (III.D.33) can be taken to hold at any radius, not just at the screen. In that case the following equation describing $H(r,t)$ can be obtained by integrating equation (III.D.33) over r .

$$H(r, t) = \left(\frac{r_c^2}{2bK} \right) \left(\frac{dh}{dt} \right) \ln \left(\frac{r}{r_c} \right) \quad (\text{III.D.34})$$

r_e is an empirical parameter, which is the effective radius at which the effect of the slug goes to zero. Evaluating equation (III.D.34) at r_s and substituting in equation (III.D.31) gives a single ordinary differential equation which must be solved for $h(t)$.

$$(h + z_o + b) \frac{d^2 h}{dt^2} + \frac{1}{2} \left[1 - \left(\frac{r_c^2}{2r_s b} \right)^2 \right] \left(\frac{dh}{dt} \right)^2 + \left[\frac{8\mu}{r_c^2 \rho} (h + z_o + b) + g \left(\frac{r_c^2}{2bK} \right) \ln \left(\frac{r_e}{r_s} \right) \right] \left(\frac{dh}{dt} \right) + gh = 0 \quad (\text{III.D.35})$$

Equation (III.D.35) is the nonlinear equivalent to the usual linear Hvorslev equation. Dropping the nonlinear, inertial, and viscous terms in equation (III.D.35) gives

$$\left[g \left(\frac{r_c^2}{2bK} \right) \ln \left(\frac{r_e}{r_s} \right) \right] \left(\frac{dh}{dt} \right) + gh = 0 \quad (\text{III.D.36})$$

which is equivalent to the Hvorslev equation

$$Q = -\pi r_c^2 \frac{dh}{dt} = FK h \quad (\text{III.D.37})$$

if we identify the Hvorslev form factor (F) as

$$F = \frac{2\pi b}{\ln \left(\frac{r_e}{r_s} \right)} \quad (\text{III.D.38})$$

Both F and r_e are empirical factors, so it does not matter which we use. In order to stay consistent with the Hvorslev theory which is widely used, we will write equation (III.D.35) as

$$\begin{aligned}
(h + z_o + b) \frac{d^2 h}{dt^2} + \frac{1}{2} \left[1 - \left(\frac{r_c^2}{2r_s b} \right)^2 \right] \left(\frac{dh}{dt} \right)^2 \\
+ \left[\frac{8\mu}{r_c^2 \rho} (h + z_o + b) + g \left(\frac{\pi r_c^2}{FK} \right) \right] \left(\frac{dh}{dt} \right) + gh = 0
\end{aligned}
\tag{III.D.39}$$

This equation only has one unknown parameter which is K, if we use the usual Hvorslev expressions for F. The rest of the physical parameters in equation (III.D.39) can be measured directly in the field or laboratory. Therefore, a least squares fit of the numerical solution of equation (III.D.39) to field data for $h(t)$ should yield a value for K, the aquifer conductivity.

To conserve writing effort we use the usual definition of the Hvorslev time lag

$$t_o = \frac{\pi r_c^2}{FK} \tag{III.D.40}$$

and define two more quantities

$$A = \frac{\left[1 - \left(\frac{r_c^2}{2r_s b} \right)^2 \right]}{2g\pi r_c^2} \tag{III.D.41}$$

and

$$M = \frac{8\mu}{gt_o r_c^2 \rho} \tag{III.D.42}$$

With these definitions and dividing by gt_o , equation (III.D.39) can be written as

$$\frac{(h + z_o + b)}{gt_o} \frac{d^2 h}{dt^2} + FKA \left(\frac{dh}{dt} \right)^2 + [M(h + z_o + b) + 1] \left(\frac{dh}{dt} \right) + \frac{h}{t_o} = 0 \tag{III.D.43}$$

When the acceleration term is negligible and $M=0$ this is the same model as presented in equation (III.D.5) for the non oscillating case.

Limiting Case Solutions

Analytical solutions to equation (III.D.43) can be obtained in a couple of limiting cases. At $t=0$ the water column is at rest and $dh/dt = 0$. The velocity of the water column will be small at early times, so the velocity dependent terms of equation (III.D.43) can be dropped to give

$$(h_o + z_o + b) \frac{d^2 h}{dt^2} + gh_o = 0 \quad (\text{III.D.44})$$

where h_o is the initial height. Equation (III.D.44) can only be used for very early times before the water column has moved much because we are assuming the height is approximately constant at h_o . With these assumptions the solution to equation (III.D.44) is

$$h = h_o - \frac{g}{2} \left(\frac{h_o}{h_o + z_o + b} \right) t^2. \quad (\text{III.D.45})$$

This is simply the normal equation for a falling body under the action of gravity; however, the acceleration is not g but some fraction based on the quantities h_o , z_o , and b . In the case where $h_o \gg z_o + b$, the column acceleration approaches g at early times.

Dropping only the velocity squared term (assuming small velocities) in equation (III.D.43) gives

$$(h + z_o + b) \frac{d^2 h}{dt^2} + gt_o [M(h + z_o + b) + 1] \left(\frac{dh}{dt} \right) + gh = 0 \quad (\text{III.D.46})$$

which would be the usual damped harmonic oscillator equation except for the expression $(h + z_o + b)$ which occurs in the coefficients and makes the equation nonlinear. In the case where $h_o \ll z_o + b$ (initial displacements are small), equation (III.D.46) can be approximated by

$$(z_o + b) \frac{d^2 h}{dt^2} + gt_o [M(z_o + b) + 1] \left(\frac{dh}{dt} \right) + gh = 0 \quad (\text{III.D.47})$$

which is exactly the damped harmonic oscillator equation (Kreyszig, 1983). Three cases can be identified. The overdamped case is the classical one usually treated in older geohydrology papers and texts.

$$g^2 t_o^2 [M(z_o + b) + 1]^2 > 4g(z_o + b) \quad (\text{III.D.48})$$

In this case the water column does not oscillate at all. In these overdamped cases the viscosity effects represented by M are usually much smaller than the damping due to the low aquifer conductivity, and can usually be ignored. If the quantities on both sides of equation (III.D.48) are equal, then critical damping is said to occur and there is no oscillation.

The third case to be identified is underdamping and occurs when

$$g^2 t_o^2 [M(z_o + b) + 1]^2 < 4g(z_o + b) \quad (\text{III.D.49})$$

In this case we have an exponentially decaying oscillation given by

$$h(t) = C \text{Exp}[-\alpha t] \cos(\omega^* t - \delta) \quad (\text{III.D.50})$$

where

$$\alpha = \frac{gt_o [M(z_o + b) + 1]}{2(z_o + b)} \quad (\text{III.D.51})$$

and

$$\omega^* = \sqrt{\frac{g}{z_o + b} - \alpha^2} \quad (\text{III.D.52})$$

C and δ are given by the initial conditions on the displacement and the velocity of the water column. If $\alpha = 0$ in equation (III.D.52), which corresponds to no damping either by viscous forces or the aquifer, then ω^* is just the natural frequency of an undamped water

column. A number of papers in recent years have dealt with the underdamped case (Van der Kamp, 1976; Kabala et al., 1985; etc.). However, little has been done to treat the general case which might lie anywhere in the domain from overdamped to underdamped. Clearly what is needed is a general solution to equation (III.D.43).

Numerical Solution

Since the fully nonlinear equation (III.D.43) can not be solved analytically, we must resort to numerical techniques. Evaluating equation (III.D.43) at time n and using central difference formulas for the time derivatives results in

$$\begin{aligned} \frac{(h^n + z_o + b)}{gt_o} \left[\frac{h^{n+1} - 2h^n + h^{n-1}}{\Delta t^2} \right] + FKA \left(\frac{h^{n+1} - h^{n-1}}{2\Delta t} \right)^2 + \\ [M(h^n + z_o + b) + 1] \left(\frac{h^{n+1} - h^{n-1}}{2\Delta t} \right) + \frac{h^n}{t_o} = 0 \end{aligned} \quad (\text{III.D.53})$$

We have had good results applying a point iterative method to equation (III.D.53). In order to apply this iterative method an iteration index $(m+1)$ will be introduced as a superscript in all single appearances of h at time level $n+1$. In all terms where h squared at time level $n+1$ appears we must evaluate one h at the new iteration level $(m+1)$ and one h at the old iteration level (m) .

$$\begin{aligned} \frac{(h^n + z_o + b)}{gt_o} \left[\frac{h^{n+1(m+1)} - 2h^n + h^{n-1}}{\Delta t^2} \right] \\ + FKA \left(\frac{h^{n+1(m)} - h^{n-1}}{2\Delta t} \right) \left(\frac{h^{n+1(m+1)} - h^{n-1}}{2\Delta t} \right) \\ + [M(h^n + z_o + b) + 1] \left(\frac{h^{n+1(m+1)} - h^{n-1}}{2\Delta t} \right) + \frac{h^n}{t_o} = 0 \end{aligned} \quad (\text{III.D.54})$$

Rearranging equation (III.D.54) gives

$$h^{n+1(m+1)} = \frac{\text{coef}(n-1, m)h^{n-1} + \text{coef}(n)h^n}{\text{coef}(n+1, m)} \quad (\text{III.D.55})$$

where

$$coef(n+1, m) = \left[1 + \left(M + \frac{2}{gt_o \Delta t} \right) (h^n + z_o + b) + FKA \left(\frac{h^{n+1(m)} - h^{n-1}}{2 \Delta t} \right) \right], \quad (III.D.56)$$

$$coef(n-1, m) = \left[1 + \left(M - \frac{2}{gt_o \Delta t} \right) (h^n + z_o + b) + FKA \left(\frac{h^{n+1(m)} - h^{n-1}}{2 \Delta t} \right) \right], \quad (III.D.57)$$

and

$$coef(n) = \left[\frac{4(h^n + z_o + b)}{gt_o \Delta t} - \frac{2 \Delta t}{t_o} \right]. \quad (III.D.58)$$

Equation (III.D.55) can now be solved iteratively for h at the new time level $n+1$.

This numerical solution has been incorporated into SUPRPUMP, the well-test analysis package described in section II.B. As mentioned earlier there is really only one parameter available for fitting in equation (III.D.43); and that is K , the hydraulic conductivity of the aquifer. We discovered a number of things when we tried to fit the field data. First of all, it was impossible to fit the overall shape of the oscillatory field data with only one available parameter. The values of A and M calculated by equations (III.D.41) and (III.D.42) were quite small and did not seem to represent the field data. The value of A calculated from equation (III.D.41) for our field data was about .7 sec^2/ft^2 , while the kinematic viscosity (μ/ρ) is about $10^{-5} \text{ ft}^2/\text{sec}$. Therefore, neither of these parameters played an important role in the analysis of our data. We decided to treat A as an adjustable parameter to be determined by fitting the data. Earlier in this section we had pretty good success using this kind of model when no oscillating water column was observed. Unfortunately, when applied to oscillatory data, the model with two parameters (A and K) still did not give a good overall fit to the shape of the curve and, most troubling of all, a constant set of values for A and K did not seem to predict the head dependence of the slug test properly. In the process of trying to fit the data it was observed that if the length of the water column in the borehole was adjusted to larger

values the general shape of the field data could be fit much better. So, it seemed that something was missing in the physical model.

Revision of the Model

An alternate method of deriving the equation of motion of the water column in a slug test can be obtained by considering an energy balance equation (Hansen, 1967). Consider the water column inside the borehole (Figure 10) to be a control volume. The change of energy within the control volume over time is determined by the work done at the free surface and the amount of energy that flows out the screen. In equation form this is

$$\frac{d}{dt} \int_{V_{cv}} \left(\frac{V^2}{2} + gz \right) \rho dV_{cv} + \int_{A_s} \left(\frac{P_s}{\rho} + \frac{V_s^2}{2} \right) V_{rn} \rho dA_s + \int_{A_T} P_a V_a dA_T = 0 \quad (\text{III.D.59})$$

The first term is the rate of change of kinetic and potential energy in the borehole (control volume, V_{cv}). The second term is the rate at which energy flows out the screen area (A_s) due to a radial velocity (V_{rn}), where P_s and V_s are the screen pressure and velocity respectively. The third term is the rate at which work is done by atmospheric pressure (P_a) on the moving upper surface. This equation neglects viscous forces.

Assume that the pressure is constant over the screen area ($2\pi r_s b$) and on the upper surface (πr_c^2). In addition, assume that the velocity is uniform over the screen area (V_s) and the upper free surface (V_a). If we consider the water incompressible, the average screen velocity is related to the average borehole velocity (dh/dt).

$$V_s = -\frac{r_c^2}{2r_s b} V_a = -\frac{r_c^2}{2r_s b} \frac{dh}{dt} \quad (\text{III.D.60})$$

Using the mean value theorem to average equation (III.D.59) over the control volume gives the result

$$\begin{aligned} \frac{d}{dt} \left\{ \left[\frac{\overline{V^2}}{2} + \frac{g}{2}(h + z_o + b) \right] \pi r_c^2 \rho (h + z_o + b) \right\} \\ - \left\{ \frac{P_s}{\rho} + \left(\frac{r_c^2}{2r_s b} \right)^2 \frac{1}{2} \left(\frac{dh}{dt} \right)^2 \right\} \left(\frac{r_c^2}{2r_s b} \frac{dh}{dt} \right) 2\pi r_s b \rho + P_a \pi r_c^2 \frac{dh}{dt} = 0 \end{aligned} \quad (\text{III.D.61})$$

The term involving $\overline{V^2}$ is the average kinetic energy per unit volume of the borehole and needs further consideration. In actual fact there will be other velocity components inside the borehole other than the average vertical velocity describing the drop of the water column. These velocity components may be random in nature (turbulence) or axially circular (curl of velocity not zero) but when averaged over the borehole they do not contribute to the net flow of water out the screen. However, these velocity components may carry significant energy and must be considered when averaging the kinetic energy over the control volume, which is the entire borehole. Assume that the velocity field can be represented by a vertical component and a random component.

$$V = V_z + V_r \quad (\text{III.D.62})$$

Using this form for the velocity in equation (III.D.61) gives

$$\begin{aligned} \overline{V^2} \rho \pi r_c^2 (h + z_o + b) &= \int_{V_{cv}} V^2 \rho dV_{cv} = \int_{V_{cv}} (V_z + V_r)^2 \rho dV_{cv} \\ &= \int_{V_{cv}} (V_z^2 + 2V_z V_r + V_r^2) \rho dV_{cv} \end{aligned} \quad (\text{III.D.63})$$

Since V_r is a random velocity component, we assume that the following integral will average to zero over the control volume.

$$\int_{V_{cv}} V_z V_r \rho dV_{cv} = 0 \quad (\text{III.D.64})$$

Assume that V_z is given by a radial velocity distribution defined by equations (III.D.22) and (III.D.24).

$$V_z = 2 \frac{dh}{dt} \left[1 - \frac{r^2}{r_c^2} \right] \quad (\text{III.D.65})$$

The first term in equation (III.D.63) can now be evaluated. The last term in equation (III.D.63) requires some addition assumptions about the random component. Since the

random component is zero in a static situation and could logically be expected to increase proportionally to the average vertical velocity, it is reasonable to assume that

$$V_r = \alpha \frac{dh}{dt} \quad (\text{III.D.66})$$

With these assumptions equation (III.D.63) can be written as

$$\begin{aligned} \overline{V^2} \rho \pi r_c^2 (h + z_o + b) &= \left(\frac{dh}{dt} \right)^2 \int_{V_{cv}} \left(4 \left[1 - \frac{r^2}{r_c^2} \right]^2 + \alpha^2 \right) \rho dV_{cv} \\ &= \left(\frac{dh}{dt} \right)^2 \left[\frac{4}{3} + \alpha^2 \right] \rho \pi r_c^2 (h + z_o + b) \end{aligned} \quad (\text{III.D.67})$$

which shows that the average square velocity is larger than the square of the average velocity by a factor greater than one.

$$\overline{V^2} = \left(\frac{dh}{dt} \right)^2 \left[\frac{4}{3} + \alpha^2 \right] \quad (\text{III.D.68})$$

This implies that the kinetic energy of the water column can be significantly larger than one might suspect based on the average vertical velocity (dh/dt).

With the above considerations, equation (III.D.61) can now be written as

$$\begin{aligned} \frac{d}{dt} \left\{ \left[\frac{1}{2} \left(\frac{dh}{dt} \right)^2 \left(\frac{4}{3} + \alpha^2 \right) + \frac{g}{2} (h + z_o + b) \right] \pi r_c^2 \rho (h + z_o + b) \right\} \\ - \left\{ \frac{P_s}{\rho} + \left(\frac{r_c^2}{2r_s b} \right)^2 \frac{1}{2} \left(\frac{dh}{dt} \right)^2 \right\} \left(\frac{r_c^2}{2r_s b} \frac{dh}{dt} \right) 2\pi r_s b \rho + P_a \pi r_c^2 \frac{dh}{dt} = 0 \end{aligned} \quad (\text{III.D.69})$$

Performing the differentiation and rearranging slightly shows that this is identical to equation (III.D.29) except for the viscous terms which have been neglected and the factor multiplying the kinetic energy term.

$$\left(\frac{dh}{dt} \right) \left\{ (h + z_o + b) \left[\frac{4}{3} + \alpha^2 \right] \frac{d^2 h}{dt^2} + \frac{1}{2} \left[\frac{4}{3} + \alpha^2 - \left(\frac{r_c^2}{2r_s b} \right)^2 \right] \left(\frac{dh}{dt} \right)^2 + g(h + z_o + b) - \frac{P_s - P_a}{\rho} \right\} = 0 \quad (\text{III.D.70})$$

By considering an energy based equation we have derived the same basic equations as are obtained starting from the Navier-Stokes equation; however, the kinetic energy contribution of velocity components other than those in the vertical direction may be considerable and a new parameter (α) has been added to the model. The generalization of equation (III.D.70) to include a viscous term or the addition of the factor multiplying the acceleration term into equation (III.D.29) gives the final form for the mathematical model.

$$(h + z_o + b) \left[\frac{4}{3} + \alpha^2 \right] \frac{d^2 h}{dt^2} + \frac{1}{2} \left[\frac{4}{3} + \alpha^2 - \left(\frac{r_c^2}{2r_s b} \right)^2 \right] \left(\frac{dh}{dt} \right)^2 + g(h + z_o + b) - \frac{P_s - P_a}{\rho} + \frac{8\mu}{r_c^2 \rho} (h + z_o + b) \frac{dh}{dt} = 0 \quad (\text{III.D.71})$$

The definition of A given in equation (III.D.41) now needs to be changed slightly, with the 1 in the numerator replaced by $4/3 + \alpha^2$. Since A is used as an empirical factor which is fitted to the field data, this redefinition of A does not change the form of the earlier model.

Data Analysis

The numerical method presented earlier can easily be adapted to the model presented by equation (III. D.71) simply by adding the factor which multiplies the acceleration term. The point iterative formula for the head at the latest time level is still given by equation (III.D.55).

$$h^{n+1(m+1)} = \frac{\text{coef}(n-1, m)h^{n-1} + \text{coef}(n)h^n}{\text{coef}(n+1, m)} \quad (\text{III.D.55})$$

Only the coefficients are changed slightly.

$$\begin{aligned} coef(n+1, m) = 1 + \left(M + \frac{2\left(\frac{4}{3} + \alpha^2\right)}{gt_o \Delta t} \right) (h^n + z_o + b) \\ + FKA \left(\frac{h^{n+1(m)} - h^{n-1}}{2\Delta t} \right) \end{aligned} \quad (III.D.72)$$

$$\begin{aligned} coef(n-1, m) = 1 + \left(M - \frac{2\left(\frac{4}{3} + \alpha^2\right)}{gt_o \Delta t} \right) (h^n + z_o + b) \\ + FKA \left(\frac{h^{n+1(m)} - h^{n-1}}{2\Delta t} \right) \end{aligned} \quad (III.D.73)$$

and

$$coef(n) = \frac{4\left(\frac{4}{3} + \alpha^2\right)(h^n + z_o + b)}{gt_o \Delta t} - \frac{2\Delta t}{t_o} \quad (III.D.74)$$

The model represented by equation (III.D.55) and equations (III.D.72)-(III.D.74) has three parameters (α , A, K) which may be adjusted to fit the field data. We have had good results fitting this model to the GEMS data. Figures 12 and 13 show the fitted theoretical values as stars on the field data plots. The theory describes the head dependence and general shape of the field data very well. Both the non oscillatory (Figure 12) and oscillatory (Figure 13) data are predicted very well with the fitted values. Field data for a variety of initial slug heights are reproduced well for a single set of parameters (α , A, K). Models presented earlier in this section fit the non oscillatory data pretty well but the parameters had some dependence on the initial slug height. In general, the effect of the viscosity term in the model appears to be insignificant. The factor $(4/3 + \alpha^2)$ in the model implies that the velocity components not in the z direction carry about

15% of the kinetic energy since $\alpha = .5$ is the best fit value. The $4/3$ arises from the assumption that there is a parabolic distribution of velocities in the radial direction. Any other radial distribution will give a slightly different result; however, the important point is that the column is usually carrying more kinetic energy than would be predicted by simply using the average vertical velocity (dh/dt). These two contributions together increase the kinetic energy about 60% over the uniform velocity case. The other parameter, A , was fitted with a magnitude of 55-70 for this field data. This is much larger than would be calculated from equation (III.D.41) for A . Clearly, some physical mechanism has been left out of the model, apparently with the same mathematical form as the term involving A in equation (III.D.43), but with a much larger magnitude. Further research is needed to shed light on the nature of this mechanism.

Figures 14 and 15 are simply single plots of the field data and theory for one particular value of the initial slug height. These plots allow one to better assess the quality of the fit of theory to experiment. In general the fit is very good. Figure 16 is a Hvorslev type plot of the field data and theory for the non oscillatory well. Notice that the data is becoming very noisy after about 12 seconds, so little quantitative information is available in that region. Also notice that the theory curve is approaching a straight line whose slope is proportional to K at large time (McElwee et al., 1992). However, there is no hope that data could ever be collected in this region since the response is so small. Only in the overdamped case will this straight line portion move into the range where it is measurable. In the case of wells in the critically damped region, we will always see this characteristic downward curvature on a Hvorslev plot. In that case an appropriate model must be used to analyze the data.

Summary and Conclusions

In summary, some slug tests in highly permeable aquifers seem to exhibit non-linear behavior. Field data show a downward curvature when plotted in the normal Hvorslev fashion and that the duration of the slug test in field data is dependent on the value of the initial head. Models based on frictional loss, non-Darcian flow, or inertial effects seem to explain the gross features of this noted field behavior. Through careful editing and fitting the log of the slugged head, reasonable consistency in hydraulic conductivity values for various initial heads can be obtained. Further refinement of the non-linear models is needed because systematic trends in the fitted parameters with initial head are observed and recently some late time oscillatory behavior has been observed in some wells. We have developed a more general model incorporating nonlinear and inertial effects.

The general model has shown that the effects of viscosity and changing casing-screen radii are negligible on slug test responses. However, the effects of nonlinearities, inertia, and velocity distributions can be quite important. The nonlinear terms make slug test results dependent on the initial head, inertial effects are important when oscillatory behavior is observed, and nonuniform velocity distributions cause the effective water column length to be greater than expected. We have developed a general model incorporating all these features. This general model can be reduced to a Hvorslev type model by assuming no storage in the aquifer. We have obtained an iterative numerical solution to this model and have applied it to field data from our research site. The results are quite good both for oscillatory and non oscillatory situations and give consistent values of the physical parameters for various initial displacements. The theory predicts the general shape and head dependence observed in the field data. Further research is needed to identify the source of the strong nonlinearity represented by one parameter.

Table 1. Summary of Eight Slug Tests at Well GEMS 02

INITIAL HEAD	HYDRAULIC COND.	NON-LINEAR FACTOR
2.88 ft.	.00450 ft./sec	177.
6.63	.00414	116.
8.81	.00349	103.
23.1	.00308	77.0
2.75	.00485	131.
7.14	.00430	108.
8.62	.00376	85.6
23.1	.00296	63.9
Average	.00388	108.

Typical Hvorslev Analysis

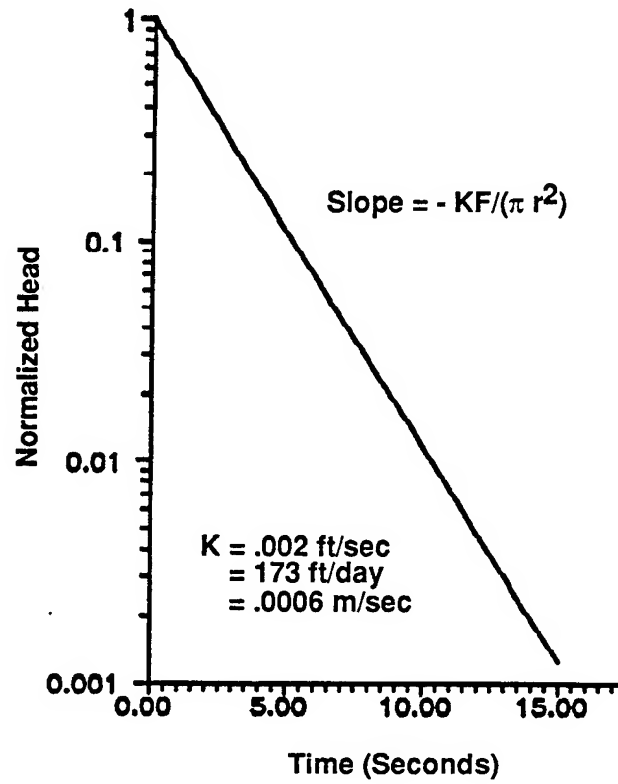


Figure 1. Plot showing typical Hvorslev analysis.

Typical GEMS Field Data

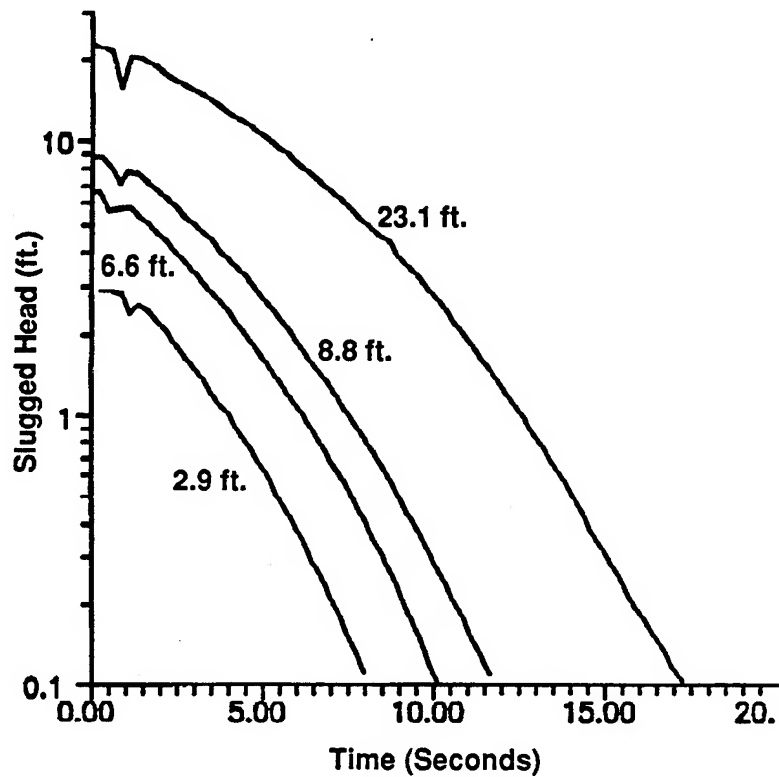


Figure 2. Typical GEMS field data.

Theoretical Nonlinear Solutions

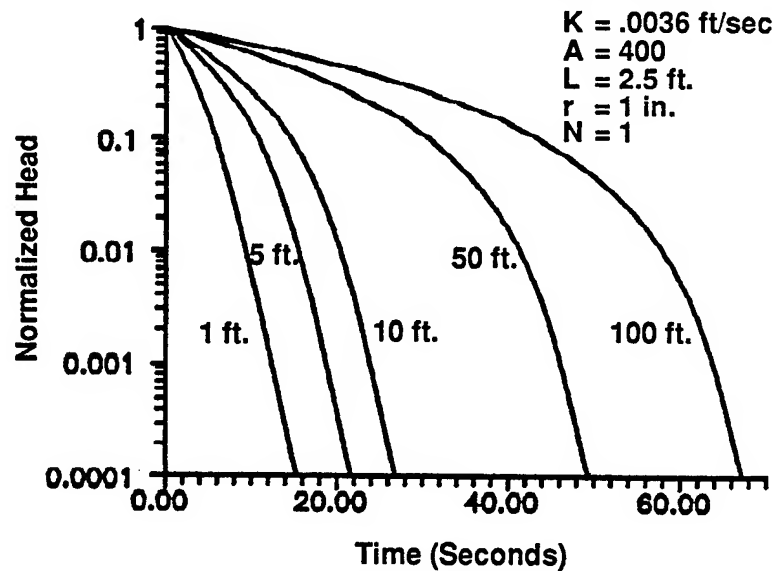


Figure 3. Examples of theoretical nonlinear solutions.

Regression Fit of Head to Hvorslev Model

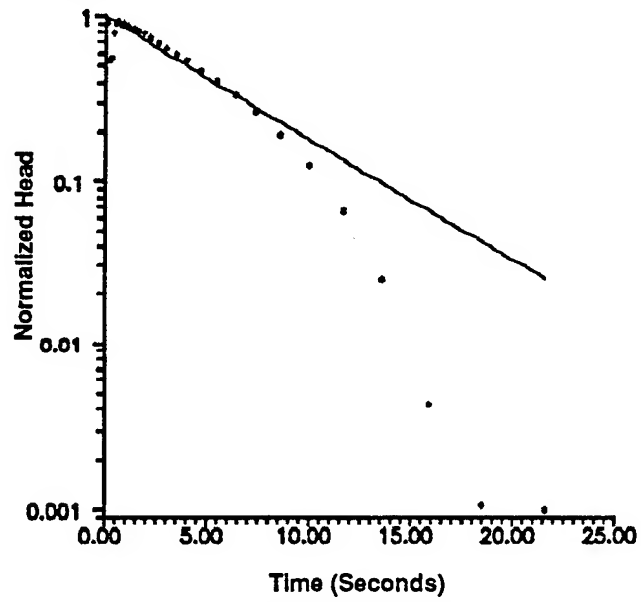


Figure 4. Regression fit of nonlinear data to the Hvorslev model.

Regression Fit of Head to Nonlinear Model

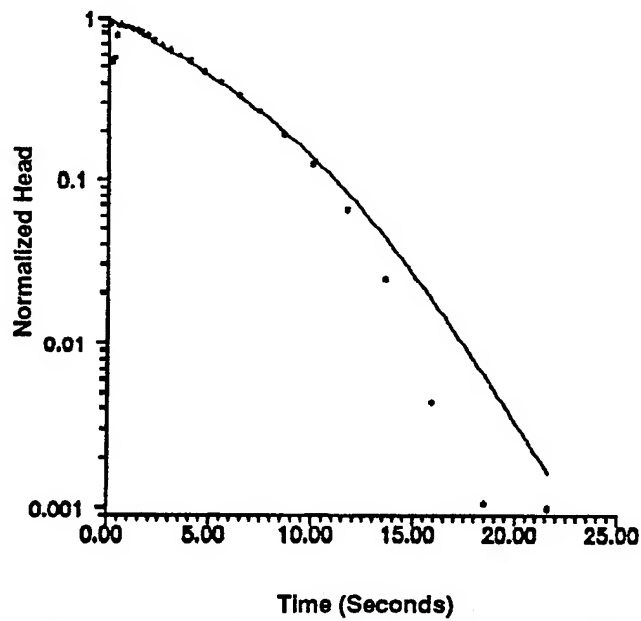


Figure 5. Regression fit of nonlinear data to the nonlinear model.

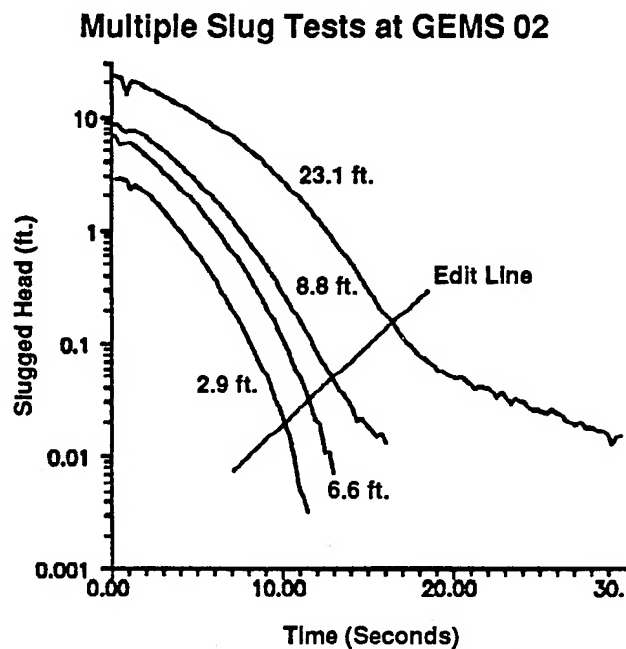


Figure 6. Data from multiple slug tests at GEMS well 02.

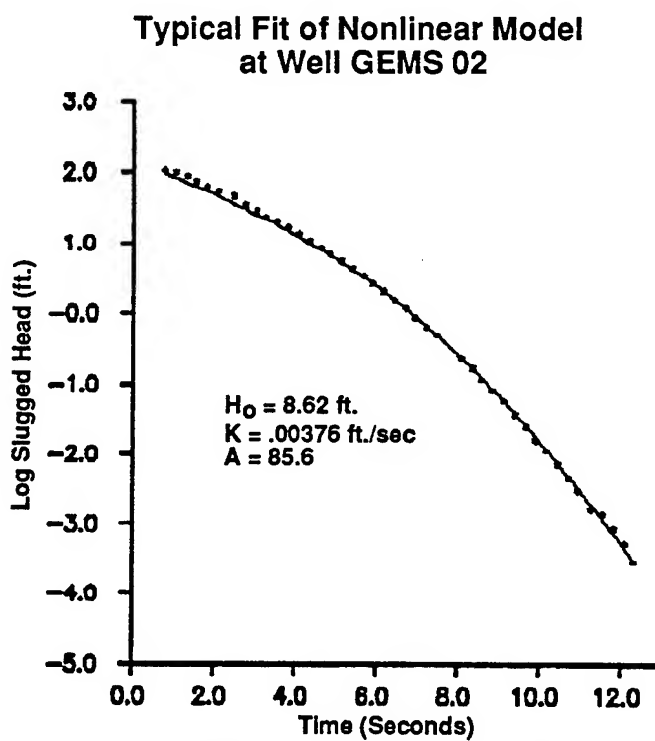


Figure 7. Typical fit of nonlinear Model at GEMS well 02.

Slug Test Response at GEMS Well 02

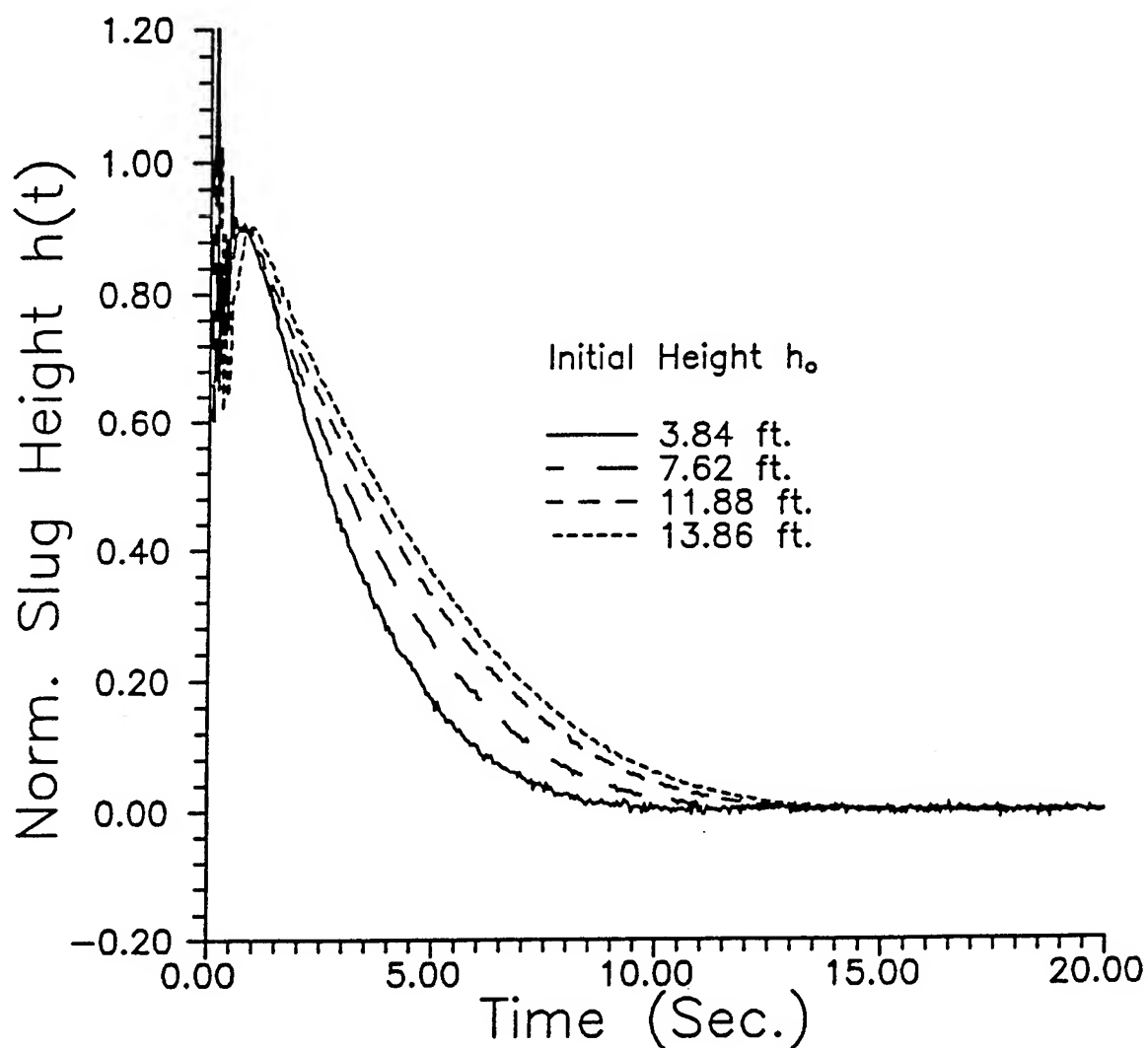


Figure 8. Slug test response at GEMS well 02.

Slug Test Response at GEMS Well 07

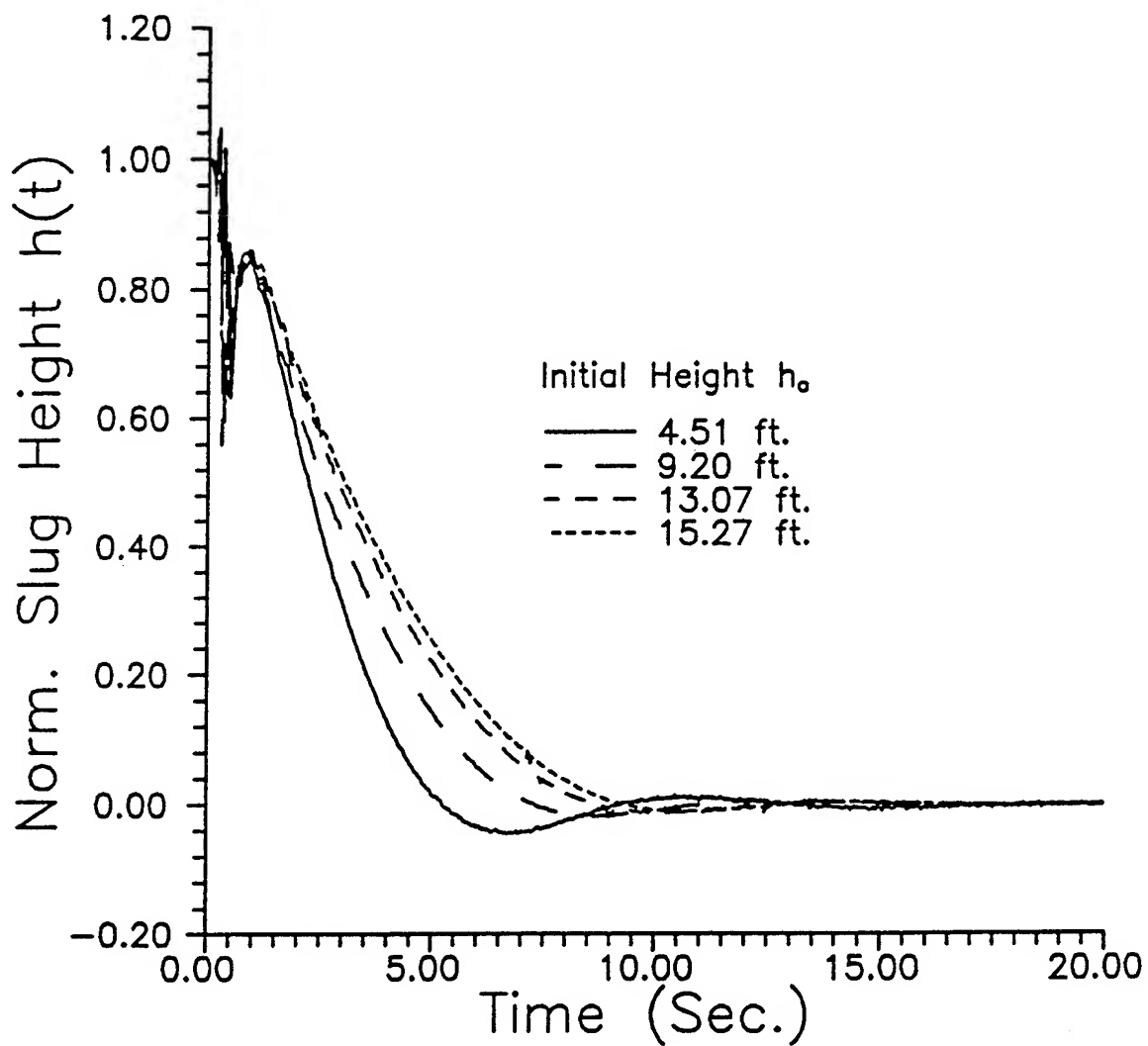
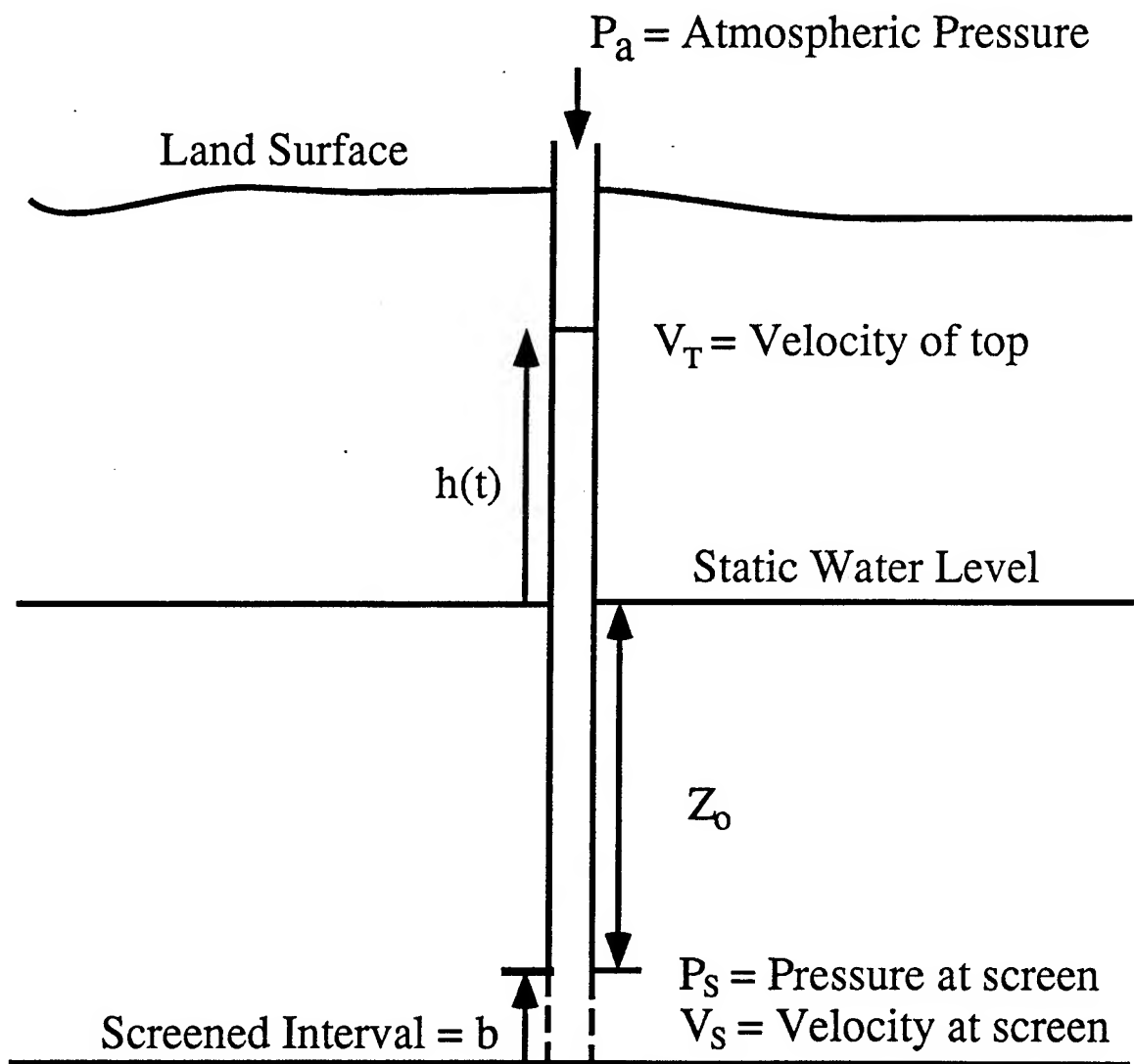


Figure 9. Slug test response at GEMS well 07.

Figure 10. Schematic of the Slug Test Wellbore



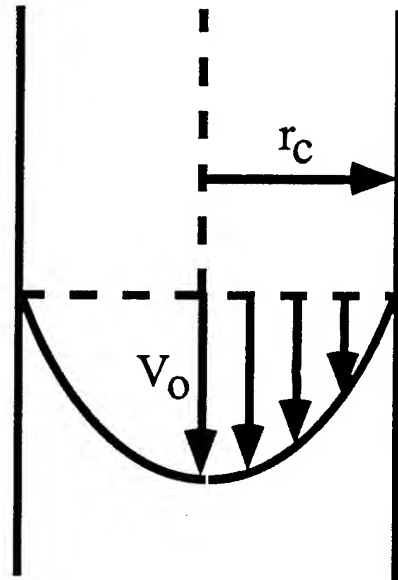


Figure 11. Assumed Radial Velocity Distribution

Slug Test Response at GEMS Well 02

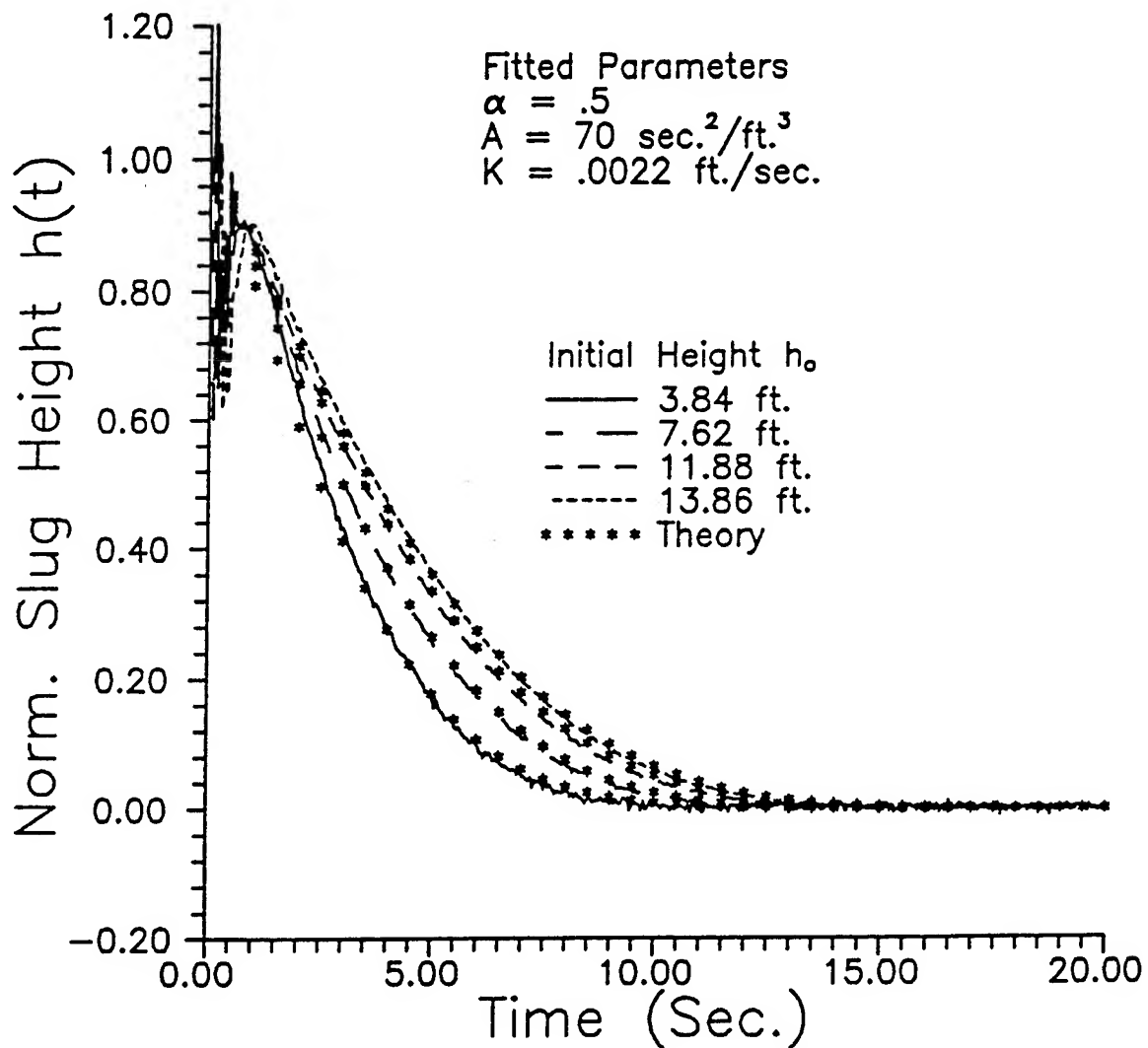


Figure 12. Fitted slug test responses at GEMS well 02.

Slug Test Response at GEMS Well 07

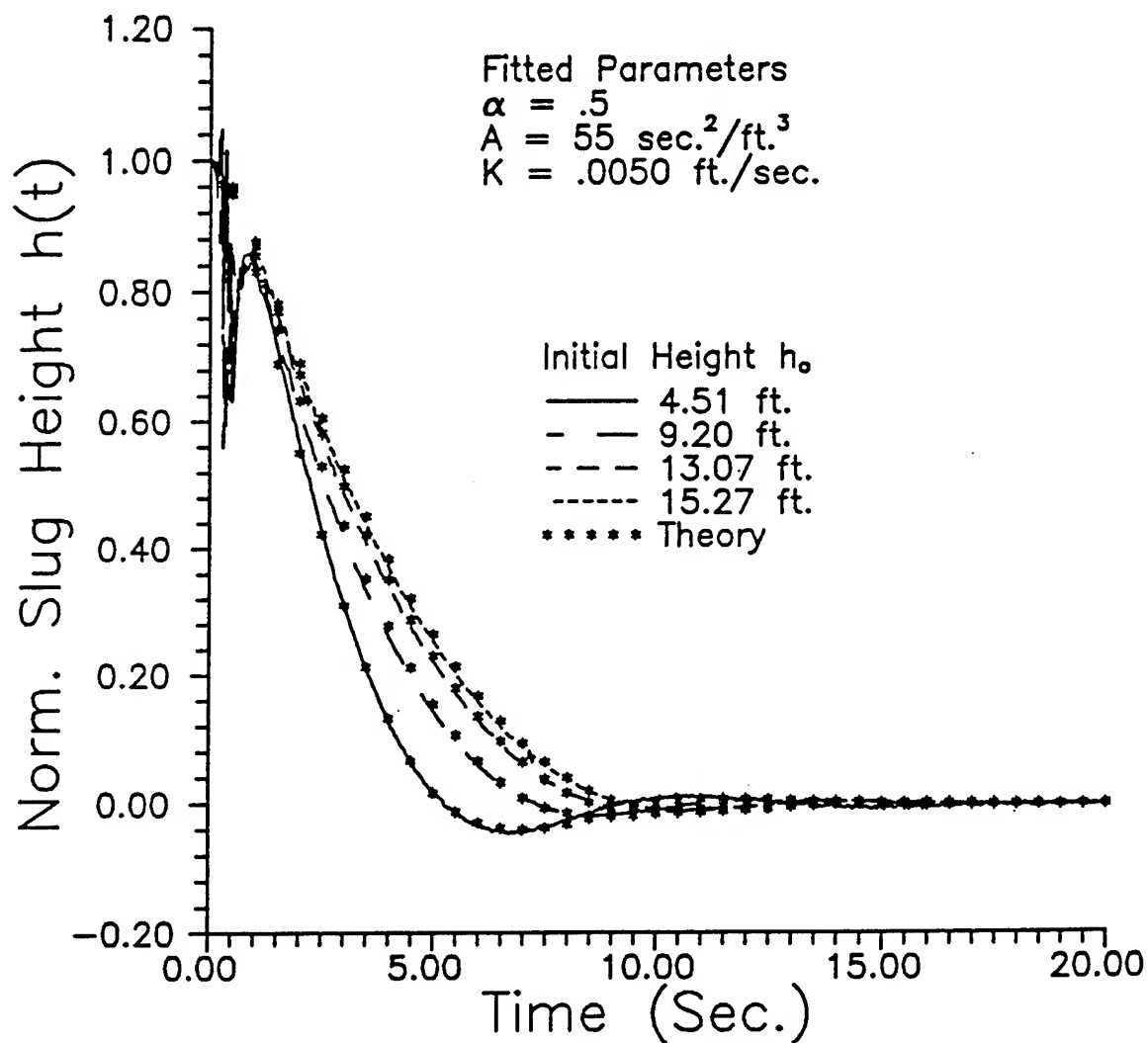


Figure 13. Fitted slug test responses at GEMS well 07.

Slug Test Response at GEMS Well 02

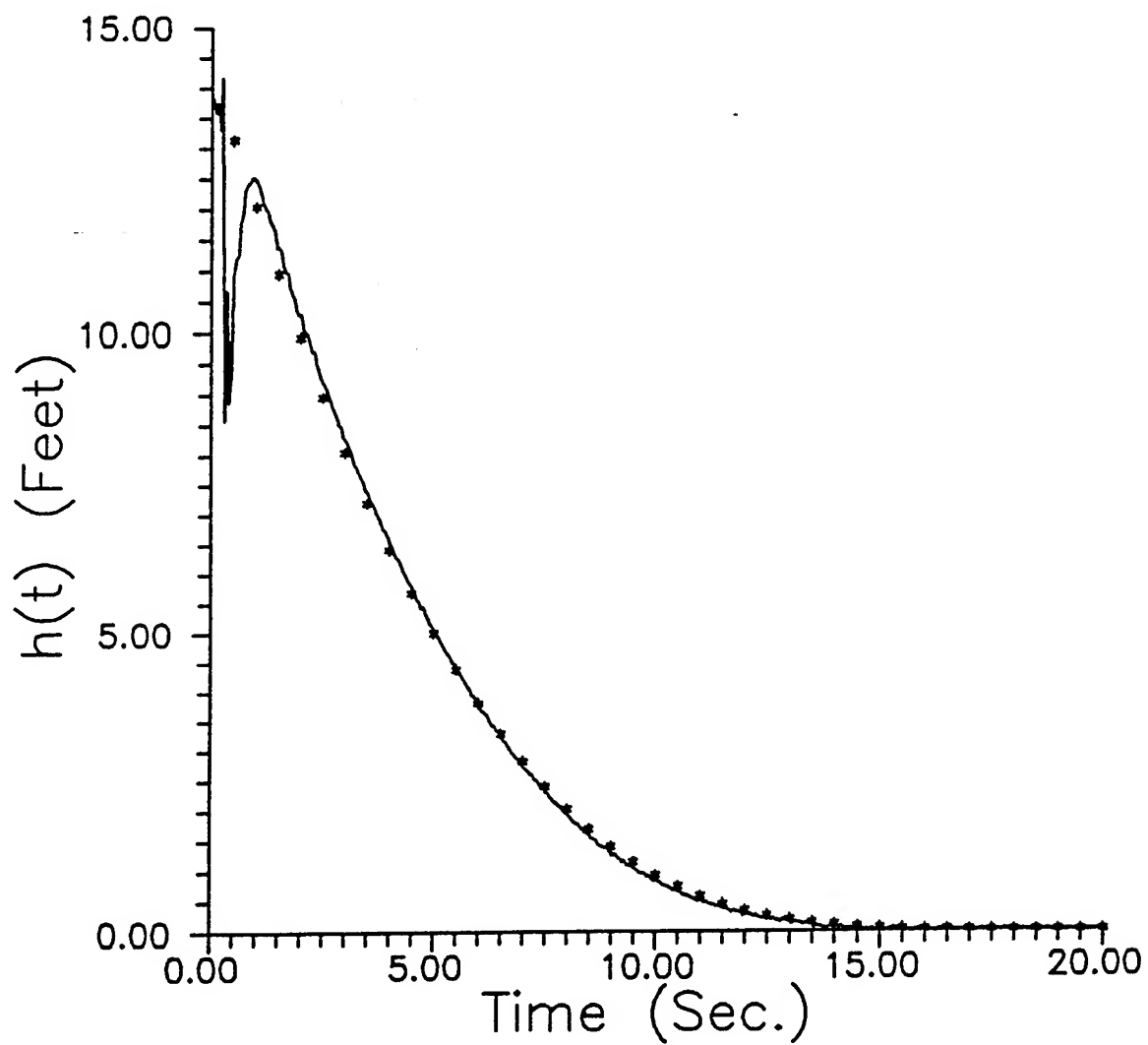


Figure 14. Fit of one slug test response at GEMS well 02.

Slug Test Response at GEMS Well 07

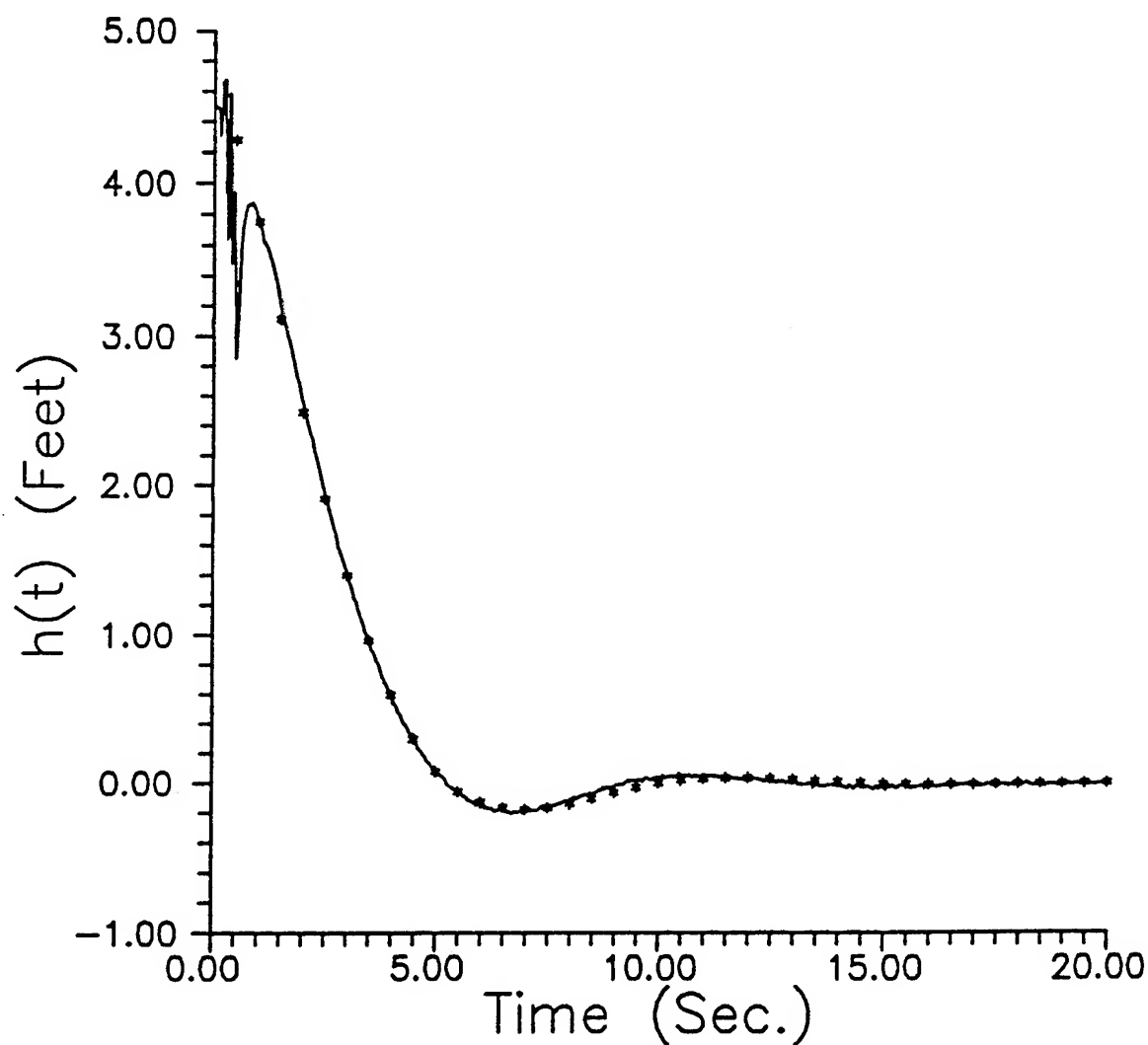


Figure 15. Fit of one slug test response at GEMS well 07.

Slug Test Response at GEMS Well 02

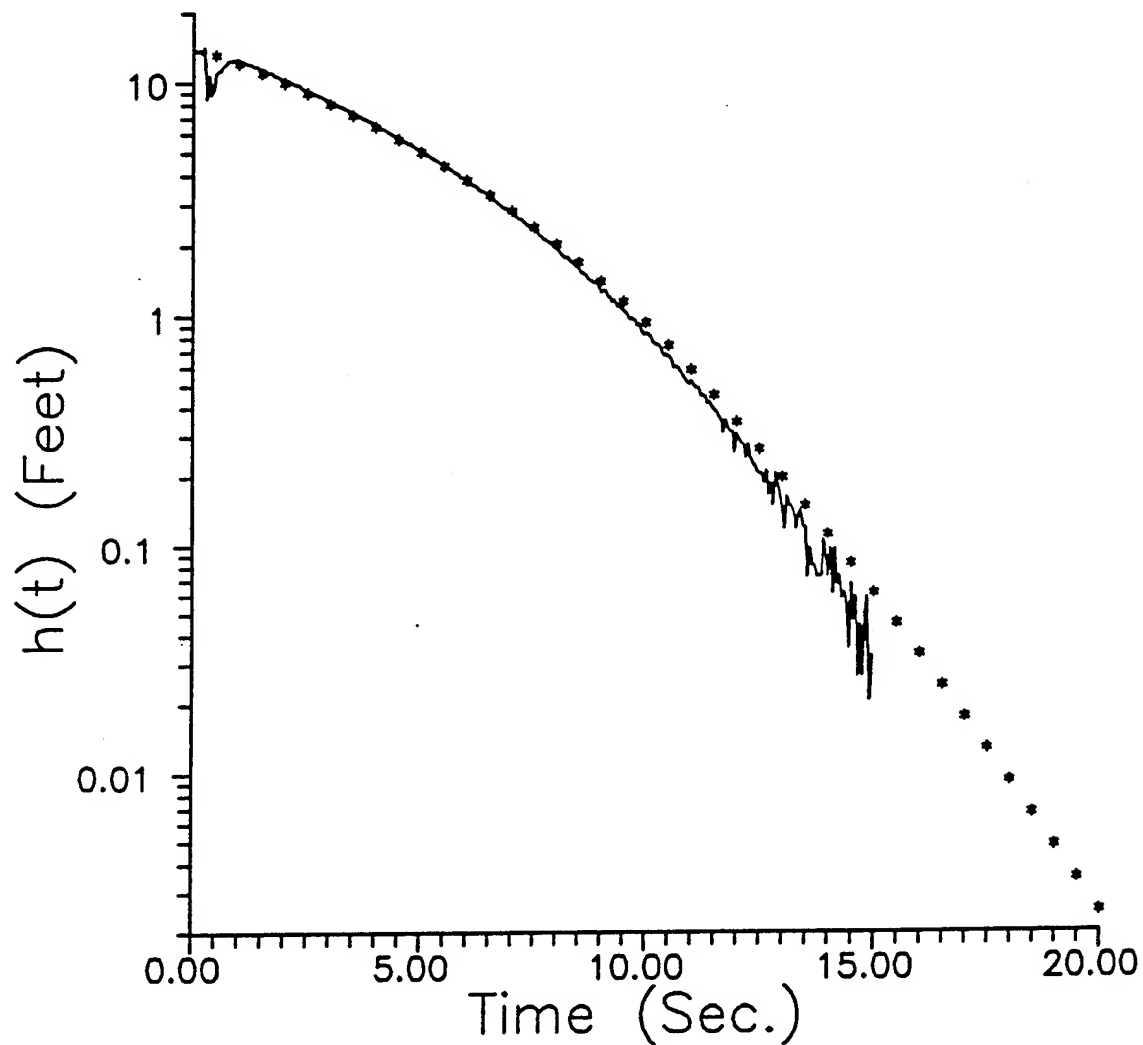


Figure 16. Log plot of one slug test response at GEMS well 02.

E. IMPROVING THE RELIABILITY OF PARAMETER ESTIMATES OBTAINED FROM SLUG TESTS

The slug test is a widely used technique for the in-situ estimation of hydraulic conductivity at sites of suspected groundwater contamination. Parameter estimates obtained from slug tests can be used for a variety of purposes including prediction of contaminant transport, design of large-scale pumping tests and remediation schemes, etc. Recently, however, this technique has received a considerable amount of criticism in the groundwater literature. A primary cause of this criticism is the discrepancy that is often observed between estimates obtained from slug tests and those obtained from other information collected as part of the site investigation. Although spatial variability and the different scales at which the various information was obtained can explain a portion of the observed discrepancy, a significant component of this difference undoubtedly arises as a result of the somewhat casual attitude that is often directed at the performance and analysis of slug tests. Since slug tests have considerable logistical and economic advantages over alternative approaches, it is imperative that these tests be done in such a manner so as to yield parameter estimates of as high a reliability as possible. Appendix E presents a recently accepted professional journal article in which practices for the performance and analysis of slug tests that should increase the reliability of the resulting parameter estimates are proposed. Since 1989, the Kansas Geological Survey (KGS) has pursued extensive theoretical and experimental research on slug tests in porous formations. A major component of this effort has been a thorough examination of currently accepted practices. This work has resulted in the definition of a series of guidelines for the performance and analysis of slug tests. We have found that adherence to these guidelines will greatly improve the reliability of the parameter estimates obtained from slug testing. Appendix E describes the most significant of these guidelines. Tests from a variety of KGS field sites are used as examples to demonstrate the importance of the proposed guidelines.

IV. SITE CHARACTERIZATION ACTIVITIES

A. DRILLING AND CORE SAMPLING ACTIVITIES

Introduction

Geologic site characterization is an important issue that must be addressed if details of contaminant transport in the subsurface are to be understood and predicted. Ideally, the formation heterogeneities at a site must be characterized at several scales. This section deals with the smallest practical scale: core samples with cross-sectional dimensions of a few inches. Historically, there has been great difficulty in obtaining relatively undisturbed cores of unconsolidated coarse sand and gravel. Prior to 1991, twenty five wells had been installed at GEMS in the Kansas River alluvium with hollow stem auger techniques. Six of these wells were cored through about 30 feet of coarse sand and gravel at depths of 40-70 feet using various techniques. A modified Waterloo sampler (Zapico, 1987; Zapico et al., 1987) was employed with good success, using drilling mud in the auger flights to control heave and help retain the sample. However, the use of heavy drilling mud has disadvantages (potential to contaminate the aquifer and cores) and recovery without sample loss is difficult since the procedure is very sensitive to vibration and other mechanical forces. Without the use of drilling mud, the modified Waterloo sampler design was unsatisfactory because of relatively low recovery percentages. In order to address this limitation, new sampler designs were developed and field tested. The most promising design did not require drilling mud, achieved a very high recovery percentage, and was not as sensitive to vibration and mechanical forces during recovery. The new design (McElwee et al., 1991) incorporates an inflatable bladder, located in the drive shoe, which closes off the end of the sampler. The deflated rubber bladder lies behind a plastic sample liner as the core begins to enter the sampler. Near the end of the 5 foot sample drive, a piston extension triggers a release mechanism and allows a four inch retraction of the plastic liner, resulting in the bladder being in direct contact with the sediment. The bladder is then inflated from the surface with nitrogen gas, closing off the bottom of the sampler and allowing recovery with minimal opportunity for sediment loss. Using this sampler, we usually have been able to achieve about 85% recovery out of a possible 90% (drive shoe loss is .5 feet out of 5 feet due to bladder length and placement). The remaining 5% loss is due to compaction, premature piston movement, or wall friction preventing material movement into the sampler. After recovery the cores are taken to the laboratory for storage until analysis for hydraulic conductivity, porosity, density and particle-size fraction can be done.

Drilling Procedure

All except one of the monitoring wells at GEMS have been installed with hollow-stem auger techniques (one bedrock well was installed with mud rotary techniques). A review of hollow-stem auger techniques and equipment is given by Hackett (1987). Auger flights with 3 1/4 inch inside diameter and 6 5/8 inch outside diameter were used for most wells. New larger diameter auger flights were purchased during the course of this project, which have an inside diameter of 6 1/2 inches and an outside diameter of 10 inches. The deepest alluvial wells at the site are about 70 feet. One bedrock well is about 80 feet deep and extends into bedrock about 10 feet. A typical installation would proceed by drilling to about 35 feet with a knock-out plate installed in the auger head in place of a pilot bit (Perry and Hart, 1985; Hackett, 1987). At that point, the plate would be knocked out by the pilot bit attached to drill rods or an overshot mechanism, then drilling and sampling could proceed to the desired depth. If no sampling is intended for that well, the plate may be left in until the completion depth is achieved. Alternately, if samples of the first thirty-five feet of silt and clay are desired, a split-spoon sampler with an overshot mechanism for attachment inside the auger flights may be used. Typically, these split-spoon samplers are two feet in length and must be retrieved after every two feet of drilling.

Heaving sands or sandblows (Minning, 1982; Perry and Hart, 1985; Keely and Boateng, 1987; and Hackett, 1987) are a severe problem at this site in the zone of sand and gravel (35-70 ft.). It is absolutely essential to maintain greater hydrostatic pressure inside the auger flights than in the formation when coring in heaving sands. The water level inside the auger flights is maintained higher than the ambient water table by adding water at critical times (mainly when tools are moved within the flights or the flights are moved). If a greater hydrostatic head within the auger flights is not maintained at critical times, several feet of sediment may quickly enter the flights, with the result that the possibility of obtaining an undisturbed sample at that depth is lost. Adding water to maintain a higher head in the flights may affect the chemistry and biota of an aquifer, so an investigator must balance this concern with the need to control heaving sands.

At GEMS, we are mainly interested in the sand and gravel aquifer (although we have taken continuous silt and clay samples for the first thirty-five feet at four of the well locations scattered over the site). Before knocking the plate out of the auger head at about 35 feet, the auger flights are filled with water from existing wells at the site. There is no known contamination at GEMS, so we simply pump water from a nearby well into the flights. Thus, we are not adding water of a dramatically different chemical

composition to the aquifer. Below 35 feet, we typically want to obtain continuous samples. The sampler is designed to obtain a five foot core. Sampling occurs over the five foot interval in front of the auger head before drilling down the next flight. Before sampling, the pilot bit must be withdrawn and the sampler inserted and driven beyond the auger head. Figure 1 summarizes the steps involved in obtaining a sample. Due to the close fit of the pilot bit and the sampler in the flights, there is great potential to induce heaving sands during removal of the pilot bit and retrieval of the sampler, so water is added to the flights at these critical times.

During the last year of this project we instituted a new drilling procedure for the installation of the multilevel sampling (MLS) wells used in the tracer test. The first part is similar to the old procedure in that we drill to 35 feet with a pilot bit in the end of the auger flights. At this point, we add water and pull the pilot bit slowly to obtain an open hole. We then place a plastic end cap on the 3 inch drive casing and proceed to drive it to bedrock (about 70 feet) with a pneumatic jack hammer. The endcap keeps the inside of the drive casing clean and is much better than trying to wash out an open ended drive string after it has been driven (an earlier version of this installation procedure). With the plastic cap on or near bedrock, drill rods are lowered into the casing to gently push out the plastic cap as the drill casing is raised slightly. When the casing is free of the plastic cap we pull the drill rods while adding water to prevent heaving sands. The MLS wells are made of 1 1/4 inch PVC pipe with 17 polyethylene tubes (1/4 inch O.D.) running through the middle to each port location (see section V for construction details). After the drill rods are out, an MLS well is lowered into place ten feet at a time. Each section must be screwed together and the small tubing threaded through each higher section (the first few ten foot sections containing ports are threaded with the small tubing at construction time, the others are threaded on site as lowered). This lowering and threading procedure is awkward and required a crew of four or five people to be done efficiently. When the MLS well is in place we add water and carefully pull the drive casing from around the MLS. We only had one problem with heaving sands locking the MLS into the drive casing and we were able to wash it out. The auger flights are then pulled after all the drive casing has been retrieved. We can install up to two of these MLS wells per day, although, our long term average is closer to one per day. Others have reported in the literature various installation procedures for MLS wells with either augering techniques or driving techniques (Pickens et al., 1978; Morin et al., 1988; Boggs et al., 1988; and Stites and Chambers, 1991). However, we have refined and combined the two techniques into a procedure that works quite well for us.

Drilling and Core Sampling For 1991-1994

In this total grant period (June 1, 1991 - Dec. 31, 1994), forty three new wells have been drilled at GEMS bringing the total to 68 pumping, observation, monitoring or multilevel sampling wells. Figure 1 is a map of the GEMS area showing the location of all the wells. Table 1 is a summary of pertinent information about all these wells. The absolute elevations relative to sea level were obtained through a cooperative surveying exercise with the 1st Battalion of the 127th Field Artillery of the Kansas Army National Guard in 1991. The elevations and coordinates of all wells with respect to the National Guard Datum were obtained by a detailed survey conducted by the investigators.

Continuous coring of 10 wells (00-1, 1-7, 8-1, 10-1, 5-1, 7-1, 9-1, 11-1, TMO-1, and TME-8) through the sand and gravel aquifer section was completed. Table 2 summarizes the core sample recovery for all holes cored in this time period: 75.5% for 4 wells the first year, 72 % for 4 wells the second year, and 82.6% for 2 wells the third year. The overall percentage recovery was 75.3%.

New wells were drilled at nest 00 (00-2 through 00-7) completing the normal nest complement. These were put in to document the hydraulic properties at different levels in the aquifer and serve various monitoring and testing functions.

Two new 4 inch wells (0-8, 0-9) were added at nest 0 for use in hydraulic testing. These wells were installed with different types of screens to see if screen type had any significant effect on hydraulic testing. These wells have been a good source of water for experiments since their completion because they accept 4 inch pumps.

Twenty four new multilevel sampling (MLS) wells were installed during this grant period. The bromide tracer array consists of 23 of these wells (TM wells). Each of the MLS wells were completed by cutting the casing back to a known distance above the top port. There are two kinds of wells as detailed in the construction section (V); one has two feet spacing between ports (regular) and one has one foot spacing between ports (detailed). The regular MLS wells were cut back to 38 feet above the top port. The detailed samplers were cut back to 53 feet above the top port. The detailed elevation survey that we performed allows us to accurately know the depth of each port relative to the others. After the MLS wells were installed a comprehensive program of developing the ports was begun using multichannel peristaltic pumps (two ten-channel pumps). If a port did not develop quickly and give the desired flow (approximately 150 ml per min.) of clear water then a repeated sequence of backflushing followed by pumping was performed. Of the 408 ports in 24 MLS wells only about 5 ports have problems of insufficient or no flow. Overall we are very pleased with this success rate.

Two 5 inch wells were added, one at each end of the bromide tracer array for injection (IW) and discharge (DW) wells. These wells were carefully developed in an attempt to prevent the formation of a low-permeability skin around the well. Detailed hydraulic testing was conducted in these wells to insure that constant head conditions would prevail throughout the screened interval during conditions similar to those expected during the bromide tracer test. After well development, our highest capacity pump (about 70 gal./min.) was carefully installed a short distance above the screened interval in the discharge well (DW) in readiness for the bromide tracer test.

Table 1
Well Data

Well Number	Elevation (m)	Depth (m/ft)	Screen Length (m/ft)
00-1	252.690	17.04/55.90	0.76/2.5
00-2	252.779	14.41/47.28	0.76/2.5
00-3	252.675	21.37/70.11	NA
00-4	252.660	11.18/36.68	NA
00-5	252.013	9.74/31.96	NA
00-6	252.753	12.91/42.36	NA
00-7	252.731	20.34/66.73	NA
0-1	252.811	21.74/71.32	9.14/30.0
0-2	252.762	14.08/46.19	0.70/2.3
0-3	252.845	11.00/36.09	0.74/2.4
0-4	252.772	7.94/26.05	0.76/2.5
0-5	252.799	19.84/65.09	0.70/2.3
*0-6	252.854	24.66/80.90	1.52/5.0
0-7	252.801	16.57/54.63	0.70/2.3
*0-8	253.178	18.52/60.76	0.76/2.5
*0-9	253.116	17.29/56.74	0.76/2.5
1-1	252.805	14.26/46.78	0.76/2.5
1-2	252.724	11.22/36.81	0.61/2.0
1-3	252.808	8.55/28.05	0.65/2.1
1-4	252.813	6.15/20.18	1.45/4.75
1-5	252.802	20.33/66.70	9.14/30.0
1-6	252.916	17.06/55.97	0.73/2.4
1-7	252.725	21.42/70.28	9.14/30.0
2-1	252.807	11.92/39.11	0.57/1.9
2-2	252.804	14.72/48.29	0.56/1.8
2-3	252.803	8.53/27.98	0.63/2.1
2-4	252.812	6.04/19.82	1.41/4.6
2-5	252.807	21.42/70.28	9.14/30.0
2-6	252.761	20.24/66.40	9.14/30.0
2-7	252.741	17.17/56.33	0.79/2.6
4-1	252.740	21.58/70.80	9.14/30.0
5-1	252.818	21.54/70.67	9.14/30.0
6-1	252.747	20.34/66.73	0.77/2.5
6-2	252.765	21.55/70.70	11.6/38.0
7-1	252.480	17.74/58.20	9.14/30.0
8-1	252.701	17.44/57.22	NA
9-1	252.556	20.93/68.67	13.26/43.5
10-1	253.166	17.32/56.82	NA
11-1	252.453	19.63/64.40	13.72/45.0
A1	252.447	9.91/32.51	0.76/2.5
A2	252.775	7.86/25.79	0.61/2.0

+PW	NA	21.84/71.65	6.10/20.0
Multlvl. sampler	252.277	11.58/38.00	ps2
*Discharge well	252.724	21.53/70.64	10.52/34.5
*Injection well	252.873	21.67/71.09	10.36/34.0
TMC-1	252.584	11.58/38.00	ps2
TMC-2	252.608	16.15/53.00	ps1
TMC-3	252.682	11.58/38.00	ps2
TMC-4	252.803	16.15/53.00	ps1
TMC-5	252.711	11.58/38.00	ps2
TMC-6	252.614	16.15/53.00	ps1
TMC-7	253.016	11.58/38.00	ps2
TMC-8	252.759	16.15/53.00	ps1
TMC-9	252.663	11.58/38.00	ps2
TMO-1	252.686	20.33/66.71	###
TME-3	252.560	11.58/38.00	ps2
TME-4	252.673	11.58/38.00	ps2
TME-5	252.637	11.58/38.00	ps2
TME-6	252.639	11.58/38.00	ps2
TME-7	252.618	11.58/38.00	ps2
TME-8	252.480	11.58/38.00	ps2
TMEE-5	252.590	11.58/38.00	ps2
TMW-3	252.843	11.58/38.00	ps2
TMW-4	252.728	11.58/38.00	ps2
TMW-5	252.746	11.58/38.00	ps2
TMW-6	252.623	11.58/38.00	ps2
TMW-7	252.766	11.58/38.00	ps2
TMW-8	252.580	11.58/38.00	ps2
TMWW-4.5	252.535	11.58/38.00	ps2

KGS Reference Mark (Corps. Stake): Latitude-North 39°00' 55.628" ,
Longitude-West 95°12' 21.272" , Elevation 252.242 m

* - All well diameters are .051m (2 in.); except for wells PW (.254 m/10 in.), Discharge (.127m/5 in.), Injection (.127 m/5 in.), 0-6 (.127 m/5 in.), 0-8 (0.102 m/4 in.), and 0-9 (.102 m/4 in.) which have the denoted diameters.

- Well TMO-1 has .61m (2.0 ft.) of screen at the bottom of the well and .61m (2.0 ft.) of screen starting at 2.6m (8.5 ft.) from the bottom of the casing and extending up.

+PW - High capacity pumping well with 0.254 m (10 in.) screen and casing diameter and 0.102 m (4 in.) drop pipe diameter.

NA - Information not currently available.

ps1 - Detailed sampler port spacing = 1.0 ft. between ports, except 2.0 ft. between 9 and 10

ps2 - Regular sampler port spacing = 2.0 ft. between ports.

Note: All multilevel sampler well depths were measured from top of casing to the first port.

Table 2
Sample Recovery Analysis

Well Number	Sample Number	Sample Length (ft)	Head Space (ft)	% of Sample Length
Procedure: Hydraulic Jackhammer				
00-1	19	5.00	0.20	4.00
00-1	20	5.00	0.29	5.80
00-1	21	5.00	0.35	7.00
00-1	22	4.67	2.88	61.67
00-1	23	5.00	1.32	26.40
00-1	24	5.00	0.21	4.2
00-1	25	4.00	0.68	17.00
00-1 Totals		33.67	5.93	17.61
		Theoretical Recovery		82.39
		Bladder Loss		10.00
		Actual Recovery		72.39
Procedure: Hydraulic Hammer				
1-7	20	4.875	0.32	6.56
1-7	21	4.833	0.38	7.86
1-7	22	5.00	0.32	6.40
1-7	23	5.00	0.33	6.60
1-7	24	5.00	0.40	8.00
1-7	25	5.00	4.33	86.60
1-7	26	5.00	0.50	10.00
1-7	27	5.00	1.34	26.80
1-7 Totals		39.708	7.92	19.94
		Theoretical Recovery		80.06
		Bladder Loss		10.00
		Actual Recovery		70.06
Procedure: Electric Jackhammer				
8-1	20	4.30	0.46	10.70
8-1	21	5.00	0.60	12.00
8-1	22	5.05	0.53	10.50
8-1	23	5.00	0.36	7.20
8-1	24	5.05	0.81	16.04
8-1	25	5.00	0.52	10.40
8-1	26	5.00	0.98	19.60
8-1 Totals		34.40	4.26	12.38
		Theoretical Recovery		87.62
		Bladder Loss		10.00
		Actual Recovery		77.62

Procedure: Air Jackhammer				
10-1	19	5.00	0.21	4.20
10-1	20	5.05	0.17	3.37
10-1	21	Numbering Omission		
10-1	22	5.10	0.24	4.70
10-1	23	5.00	0.46	9.20
10-1	24	4.95	0.23	4.65
10-1	25	4.95	0.46	9.29
10-1	26	4.95	0.79	15.96
10-1		35.00	2.56	7.31
Totals				
		Theoretical Recovery		92.69
		Bladder Loss		10.00
		Actual Recovery		82.69
Yearly Totals		142.78	20.67	14.48
		Theoretical Recovery		85.52
		Bladder Loss		10.00
		Actual Recovery		75.52
Procedure: Pneumatic Jackhammer				
5-1	1	5.00	0.29	5.80
5-1	2	5.00	0.45	9.00
5-1	3	5.00	0.25	5.00
5-1	4	5.00	0.35	7.00
5-1	5	5.00	0.56	11.20
5-1	6	5.00	1.55	31.00
5-1	7	4.54	0.54	12.00
5-1 Totals		34.54	3.99	11.60
		Theoretical Recovery		88.40
		Bladder Loss		10.00
		Actual Recovery		78.40
Procedure: Pneumatic Jackhammer				
7-1	1*	5.00	4.50	90.00
7-1	2	5.00	0.53	10.60
7-1	3	5.00	0.78	15.60
7-1	4	5.00	1.02	20.40
7-1	5	5.00	0.75	15.00
7-1	6	5.00	1.00	20.00
7-1	7	3.00	0.54	18.00
7-1 Totals		33.00	9.10	27.60
		Theoretical Recovery		72.40
		Bladder Loss		10.00
		Actual Recovery		62.40

Procedure: Pneumatic Jackhammer				
9-1	1	5.00	0.35	7.00
9-1	2	5.00	0.27	5.40
9-1	3	4.75*	1.67	35.20
9-1	4	5.00	0.29	5.80
9-1	5	4.83*	0.49	10.10
9-1	6	5.00	0.76	15.20
9-1	7	4.29	1.34	31.20
9-1 Totals		33.87	5.17	15.30
		Theoretical Recovery		84.70
		Bladder Loss		10.00
		Actual Recovery		74.70
Procedure: Pneumatic Jackhammer				
11-1	1	5.00	1.90	38.00
11-1	2	5.00	0.44	8.80
11-1	3	5.00	0.41	8.20
11-1	4	5.00	0.77	15.40
11-1	5	5.00	0.69	13.80
11-1	6	5.00	1.81	36.20
11-1	7	3.35	0.62	18.50
11-1 Totals		33.35	6.64	19.90
		Theoretical Recovery		80.10
		Bladder Loss		10.00
		Actual Recovery		70.10
Yearly Totals		134.76	24.90	18.50
		Theoretical Recovery		81.50
		Bladder Loss		10.00
		Actual Recovery		71.50
Procedure: Pneumatic Jackhammer				
TMO-1	1	5.00	0.95	19.00
TMO-1	2	5.00	0.14	2.80
TMO-1	3	5.00	0.11	2.20
TMO-1	4	5.00	0.58	11.60
TMO-1	5	5.00	0.28	5.60
TMO-1	6	5.00	0.25**	5.00
TMO-1	7	4.27	0.42	9.84
TMO-1 Totals		34.27	2.73	7.97
		Theoretical Recovery		92.03
		Bladder Loss		10.00
		Actual Recovery		82.03

Procedure: Pneumatic Jackhammer				
TME-8	1	4.85	1.29	26.60
TME-8	2	5	0.20	4.00
TME-8	3	No sample was retrieved from the sampler		
TME-8	4	5	0.30	6.00
TME-8	5	5	0.22	4.40
TME-8	6	5	0.00	0.00
TME-8	7	5	0.21	1.75
TME-8 Totals		29.85	2.00	6.70
		Theoretical Recovery		93.30
		Bladder Loss		10.00
		Actual Recovery		83.30
Yearly Totals		64.12	4.73	7.38
		Theoretical Recovery		92.62
		Bladder Loss		10.00
		Actual Recovery		82.62
Project Totals		341.66	50.30	14.72
		Theoretical Recovery		85.28
		Bladder Loss		10.00
		Actual Recovery		75.28

* Mechanical failure produced some anomalous results.

** Head space was measured in laboratory as opposed to the field.

Bladder Loss - 10% of the total sample length, 34.17 ft, is lost due to the bladder mounting dimensions.

B. LABORATORY ACTIVITIES

The Bromide Tracer Test Laboratory Activities

Introduction

A large amount of laboratory work accompanied GMSTRAC1, the induced gradient tracer test performed at GEMS during the fall of 1994 (see section IV.D for a description of the tracer test). The laboratory activities accompanying this test included the preparation of the tracer solution that was injected during the test, and a variety of activities associated with the analysis of the collected water samples. In the following sections, each of these activities is described in detail.

Preparation of Spiking Solutions

Concentrated solutions of KBr were made to be added to an approximately 500-gallon tank which was used as the injection solution. For each of four tank volumes, six liters of a solution containing 188 gms/L KBr were added, resulting in a Br concentration of about 425 mg/L for the solution that was injected into the aquifer. The salt was initially weighed using plastic weighing boats, but the boats were replaced by a Pyrex® beaker when the salt began showing signs of electrostatic attraction and repulsion to the plastic. Aliquots of each batch of stock solution, made in two-liter increments, was reserved for verification of concentration.

Bromide Analysis Procedures

The samples from the October 1994 tracer test (GEMSTRAC1) were analyzed in the lab using Orion bromide-selective electrodes paired with Orion single-junction reference electrodes. When the electrode pair is immersed in a sample solution, the potential developed between the electrodes is approximately proportional to the log of the bromide concentration in the solution, at least over a certain range of concentration values. This potential can be converted to a concentration value by comparing it to the electrode response for calibration solutions of known concentration. The calibration solutions and sample solutions must be about the same temperature, since the electrical potential is also temperature-dependent. In addition, because the electrode response tends to vary over time, the calibration step must be repeated at regular intervals during analysis, if large numbers of samples are being analyzed. For the GEMSTRAC1 test, calibration solutions were prepared using site water so that the samples and standards would have a similar ionic composition and, hopefully, a similar ionic strength (see the

following discussion of preparation of calibration solutions). The electrodes actually respond to ion activity, rather than ion concentration. However, calibrations against standards of known concentration can be used directly as long as the standard solution and sample solution have approximately the same ionic strength.

To keep from running out of sample vials, samples from the field had to be analyzed rapidly and discarded so the vials could be washed and reused (see the following discussion on vial cleaning procedures). Typically, the samples analyzed on a given day were those collected the day before. At the peak of sampling activity, early in the test, this amounted to analyzing at least 408 samples per day. In order to expedite the analysis, we developed a system that allowed us to analyze five samples simultaneously, with the data being recorded electronically for later processing. A device was constructed which held five pairs of electrodes in a sliding rack. A tray containing five sample vials was inserted under the sliding rack and then the electrodes were lowered into the vials. After the electrodes had equilibrated with the solutions (a process taking one to three minutes), the electrode pair potentials were recorded using a Campbell Scientific CR10 data logger attached to a PC. In addition, the readings were recorded by hand on data sheets, as a backup. Each pair of electrodes remained in the same location on the rack and remained connected to the same channel of the data logger throughout the analysis period. As a shorthand, we began referring to the electrode pairs themselves as 'channels', with channel 1 referring to the leftmost electrode pair on the rack and 'channel 5' referring to the rightmost pair, and a set of 5 electrode pairs as a 'bank'. The samples from the seventeen ports of each sampler were always analyzed in the same order, with ports 1-5 analyzed in the first bank of samples, 6-10 in the second bank, 11-15 in the third bank, and finally ports 16 and 17 in the fourth bank (with channels 3 through 5 empty). This created four records on the data file, one for each bank, with a given port always being recorded in the same channel. Two people were required in the lab, one operating the PC controlling the data logger and washing the electrodes between analyses, and the other dealing with the logistics of loading and unloading the sample vials from the tray. Once we became proficient at these tasks, the seventeen samples from one sampler could be analyzed in eight to ten minutes, with the main bottleneck being the time required for the electrodes to equilibrate with the solution.

We calibrated the electrodes every 1.5 to 2 hours, by recording the electrode responses to our standard solutions. Three standard solutions were used, covering the expected range of concentrations: a low standard of 1 mg/l, a medium standard of 50 mg/l, and a high standard of 300 mg/l (see the following discussion of preparation of calibration solutions). The calibration responses for a given channel were then used to

convert the electrode responses for the sample solutions measured in that channel to concentrations. The calibration responses varied over time, most notably for the low concentration standard, sometimes changing quite significantly between successive calibrations. Figures 1 through 3 show the low, medium, and high calibration responses over time for channel five. The calibration responses over a given day could be quite erratic, although the long-term trend over the entire month of analysis is fairly clear. Therefore it was decided to use the median calibration responses for a given day as the 'standards' for that day; that is, all the samples analyzed in channel five on the first day were converted to concentrations using a calibration equation developed from the median low standard response, median medium standard response, and median high standard response for channel five for that day. This particular calibration curve is shown in Figure 4. A similar calibration equation was computed for each of the five channels for each day of analysis.

Calibration Solutions for Br Ion Selective Electrodes

Calibration solutions for the Br ion selective electrodes (ISE's) were made up in GEMS water, using water from well 0-1, a fully-penetrating well in an adjacent well nest. This well was chosen because it would produce a water which was approximately a chemical average of the water at the GEMS site. Because the background Br concentration in GEMS water was found to be as high as about 0.7 mg/L (see section IV.C), calibration standards for the Br ISE's were made up to be 1 mg/L, 50 mg/L and 300 mg/L. Concentrations less than 1 mg/L were thought to be unreliable, because of the possible background effect and electrode response.

Standards were made using GEMS water in order to match the specific conductance of the standards to that of the water produced from the multi-level samplers. By matching the specific conductance of the standards and samples, the problem of ionic-strength adjustment was avoided (Orion Research, 1991), so no ionic-strength adjuster was added during Br determination. It is well known that ionic strength affects the response of ion-selective electrodes (Orion Research, 1991), and this was confirmed during this project (see figure 13 of section IV.C). Other studies have chosen not to use the ionic-strength adjuster because of overall low ion strengths (Garabedian *et al.*, 1988). However, at GEMS, the specific conductance is typically 600 to 700 $\mu\text{S}/\text{cm}$ and the added Br was expected to approximately double the specific conductance, so we chose to matrix-match our samples with standards.

Standards were made from a single stock solution that contained 10 gms Br/L, which was made from KBr in distilled-deionized water. Standards were used once and

then discarded to prevent cross-contamination. Standards were made on 10-4-94, 10-10-94, 10-12-94, 10-19-94, and 11-1-94, either when the previous batch had been consumed or when about two weeks had elapsed. The latter criteria was used to prevent changes in specific conductance of the standards, which would occur if calcite precipitated from the solutions. Previous observations showed that GEMS water at laboratory temperature does not precipitate calcite until about two weeks after removal from the well.

Performance Monitoring of Br ISE's

Br ISE's and reference electrodes were checked every evening during the first nine days of measurement during the tracer test, then every other day for the next eight days, and periodically thereafter. The electrodes were checked by refilling the reference electrodes with outer filling solution as needed, and by performing a slope check on all five electrode pairs. The procedure is outlined in the Orion Instruction Manual (Orion Research, 1991): two aliquots of 100 mL of distilled water treated with two mL of ionic-strength adjuster (5M NaNO₃) were prepared, 1 mL of 1000 ppm Br stock solution was added to one aliquot and 10 mL of Br stock solution to the other. This resulted in Br concentrations in the two solutions of 9.7 mg/L and 89.3 mg/L. The difference in measured potential was considered to be acceptable if it was between -54 to -60 mV at 25°C. After two days of measurement, all electrodes were polished with the polishing strip provided by the manufacturer. Before and after that time, all electrodes stayed within specifications.

Sample Vial Cleaning Procedure

Because all sample vials were reused during the tracer test, it was important that cleaning of the vials was thorough enough to remove all traces of dissolved Br from the vials. All vials were emptied of their contents and stored for up to two days in closed plastic bags. The vials were rinsed five times with distilled water and then inverted and allowed to air dry. Vials with visible staining were first soaked in a 5% HCl solution, rinsed with tap water three times, and then rinsed with distilled water five times and allowed to air dry. After completely dry, the vials were stored in sealed plastic bags until they were reused. This procedure helped minimize contamination by airborne dust or water particles during lab storage, transport to the field site, and in the on-site trailer where they were stored while awaiting use during the tracer test.

Summary

The above laboratory procedures were in support of the bromide tracer test and allowed us to efficiently and accurately conduct the test. Due to the large number of samples that had to be analyzed quickly and accurately, we had to develop methods of mass production, while maintaining maximum reliability. During the course of the tracer test almost 6000 samples were accurately analyzed.

Laboratory Procedures , Methods, and Results - Sand and Gravel Cores

Introduction

The cores recovered from the drilling and sampling activities summarized in section IV.A of this report were taken to the laboratory for measurement of hydraulic conductivity in a constant-head permeameter. Prior to measurement, cores are stored under refrigeration to keep bacterial growth and evaporation to a minimum. The procedures and methods used in analyzing the core samples are essentially the same as those described in Butler et al. (1991) and Jiang (1991), with the exception of the changes noted below.

Laboratory Improvements

A new apparatus was developed to more accurately and efficiently calibrate the pressure transducers used in the permeameter. The calibration apparatus consists of a metal pipe into which pressure transducers can be inserted with an air-tight seal, a rubber bladder to increase the volume of gas within the system, and a high-accuracy pressure transducer (Druck PTX 620 pressure transmitter) to serve as a pressure standard. Nitrogen gas can be introduced into or released from the system in small amounts, simultaneously changing the pressure on both the pressure transducers and the pressure standard, while readings are recorded by a datalogger. The pressure transducers are then calibrated against the pressure standard. This new system can be used to calibrate both the pressure transducers used in the permeameter (0-5 psig) and the pressure transducers used in the field for slug and pumping tests (0-5 psig to 0-25 psig). Up to four pressure transducers can be calibrated at one time.

A Dwyer Series 650-2 temperature transmitter has been installed next to the thermometer in the permeameter. Water temperature is recorded by the datalogger at the same interval as water pressure in the outflow tubes of the permeameter, thus enabling temporal variations in viscosity values to be incorporated into the hydraulic conductivity measurements.

To more accurately determine the head drop over the cores, an instrument incorporating a dial caliper has been constructed and mounted on the permeameter. Water levels in glass-topped manometer tubes, which measure head at the top of each core and at the constant head boundary, can be read to the nearest .001 inch; readings are generally reproducible to better than .05 inch. This device allows us to use smaller head drops over the cores without increasing the percent error in our calculations.

Occasionally, a decrease in head at the constant head boundary is experienced due to lack of flow from the upper reservoir. To reduce the frequency of this occurrence, a new reservoir was installed that drains from the bottom rather than relying on a siphon tube exiting from the reservoir top.

The constant head permeameter used in this work for the measurement of hydraulic conductivity was originally designed to process four cores at one time. The permeameter has now been enlarged to increase the number of cores that can be processed at one time to eight. Most parts of the permeameter that had been composed of opaque PVC have been replaced with clear PVC in order to more easily assess flow of water, transport of fine sediment, and entrapment of air bubbles within the system. The single filter that had been used in the permeameter setup has been replaced by a double filter system. Water first flows through a 5 micron filter to remove most sediment particles and other debris in the water; it then passes through a .5 micron filter that should remove bacteria and virtually all sediment particles.

Laboratory Procedures and Methods

X-rays are taken of each core sample to aid in the determination of changes in grain size and the identification of sedimentary structures. An aluminum filter was used to improve resolution at the edges of the core (Baker and Friedman, 1969). Using the X-rays as a guide, the core is cut into segments which are as homogeneous as possible within the 4 to 8 inch limit on segment size imposed by the permeameter setup. To inhibit organic growth, the core segments are then wrapped in plastic and aluminum foil and refrigerated until they are placed in the permeameter.

In order to keep the Reynolds number below one and reduce the possibility of non-laminar flow, the head drop over the core is kept as small as possible. This also decreases the entrainment of fine material as water moves through the core. The head drop is typically set at approximately .5 inches and increased if no flow occurs after 12 to 24 hours. Using this small head drop, cores take a minimum of 36 hours to saturate and stabilize, with some core segments requiring four to five days.

During the drying process, which precedes particle density analysis and dry sieving, clay-sized particles tend to coat larger grains and form sand-sized aggregates. This will cause the weight percentages of the larger grain sizes to be overestimated at the expense of the fines. To more accurately determine the weight percent of fine material in the core, the samples are wet-sieved with a 53 micron sieve after the particle density analysis. The weight percent of fine material is determined by comparing the dry weight of the sample before removal from the sample tube and after wet sieving. The coarse

fraction is then dry-sieved to complete the grain size analysis. Even though some material is lost during the permeameter tests and the repacking process, this method of determining the amount of fine material should still be reasonably accurate, since most of the material that is lost is clay and silt sized.

No photographs are taken of the sediment before sieving.

Water Chemistry Investigation

A decrease in hydraulic conductivity with time was observed for many of the cores. This may be due to deposition of calcite in pore throats; another possible explanation would be the expansion and/or dispersion of clays, which would also produce a clogging of pore throats. In an attempt to identify the primary mechanism responsible for the observed decreases in conductivity with time, a series of experiments was conducted using a single core in the permeameter. The chemistry of the water prior to passage through the core and after passage through the core was carefully monitored with the assistance of the Analytical Services Section of the Kansas Geological Survey.

The water circulated in the permeameter is obtained from wells at GEMS that are screened close to or over the same interval from which the core was taken. At the time water was collected for use in the permeameter experiments, samples were taken in the field for analysis by the Analytical Services Section. The collected water was then taken to the laboratory where it was allowed to sit for two weeks in order to equilibrate with laboratory temperatures and pressures. Additional water samples were taken during this period in order to assess changes occurring with equilibration to laboratory conditions. Once the water was placed in the permeameter, samples were taken several times a day from the water that had passed through the core and once a day from the permeameter water that had not passed through the core. A subset of these samples was chosen for major cation analysis by the Analytical Services Section using the observed changes in the hydraulic conductivity as the selection criterion. Note that the permeameter setup used here involves recirculating water that has passed through the cores. For these experiments, however, no recirculation was allowed so that any chemistry changes occurring in the water passing through a core could be readily identified.

In addition to the major cation analyses performed by the Analytical Services Section, the pH and dissolved oxygen of the water prior to passage through the core (henceforth designated as permeameter water) and after passage through the core (henceforth designated as outflow-tube water) were monitored in the laboratory. The pH was determined using a CARDY Twin pH meter (Horiba Instruments). Measurement of the pH of the outflow-tube water was done several times a day, while measurement of the

pH of the permeameter water was done at least once a day. Dissolved oxygen (DO) was measured using a K-7512 CHEMets colorimetric kit (CHEMetrics). DO was determined for outflow-tube water once a day and once every 3 to 4 days for the permeameter water.

Sediment samples from the cores used in these experiments were collected for x-ray analysis of clay mineralogy both before and after being processed in the permeameter.

As a result of the findings of the water chemistry and clay analysis, two further modifications have been made to the laboratory procedure: 1) carbon dioxide gas is being bubbled into the water of the upper reservoir to maintain the pH, which is monitored daily, at a level comparable to that of the water at GEMS; and 2) a different biocide (dichlorophene) is being used to inhibit biologic growth in the system.

Core Analysis Results

Graphs of the original and repacked hydraulic conductivities and porosities, the percent fines (<53 microns), and the mean grain size of core segments from 10 wells (00-1, 1-7, 5-1, 7-1, 8-1, 9-1, 10-1, 11-1, TMO-1, and TME-8) are presented in Figures 5 - 62. Due to numerous problems with the grain size data from well 11-1, the graphs for percent fines and mean grain size are not presented.

GEMS 00-1

Hydraulic conductivity values have been obtained for 50 of 51 segments, both in the undisturbed state (Figure 5) and after being dried and repacked (Figure 6). The segment from depth 14.27-14.41 m below datum is composed of material that appears to be wood, so no permeameter test was run on that segment.

The undisturbed cores have an arithmetic mean conductivity of 20.16 m/day, with a sample standard deviation of 24.26 m/day. Values range from a minimum of .06 m/day to a maximum of 94.28 m/day. There is no apparent trend in hydraulic conductivity with depth.

The repacked cores exhibit a higher mean conductivity and greater variability than the undisturbed cores. Values range from .04 m/day to 185.43 m/day with a mean of 44.82 m/day and standard deviation of 44.65 m/day.

For 45 of the 50 segments, the repacked hydraulic conductivity is greater than the original measurement. This is most likely due to the elimination of fine layers and redistribution of fine material during the repacking process, i.e. the repacked cores are generally more homogeneous than the undisturbed cores. In some cases, it is possible that the repacked cores could be less homogeneous than the undisturbed cores. Layers can be created within the core if a poorly sorted sediment is not sufficiently mixed while

being repacked into the sample tube. For example, a one centimeter layer of fine material was noted at the top of the repacked sample 001-24-7 (depth 20.37- 20.56 m).

Porosity values were calculated for both the original and repacked cores from the particle density, bulk density and core volume. The original cores from well 00-1 have porosities ranging from 23.2% to 37.4% with an arithmetic mean of 28.4% and a standard deviation of 3.1% (Figure 7). The porosity of the repacked cores ranges from 23.8% to 35.8% with an arithmetic mean of 28.8% and a standard deviation of 2.7% (Figure 8).

The differences between the original and repacked porosities from well 00-1 range from 0.03% to 3.22% with an arithmetic mean of 1.23%. For 35 of the 49 cores, the repacked porosity is greater than the original porosity; 14 of the repacked cores have lower porosities than the original cores. The primary reasons for differences between the original and repacked porosities are 1) inability to repack the cores to exactly the same volume as the original cores, and 2) loss of sediment during the repacking process.

The percent fines (<53 microns) was also calculated for each core. The percent fines for the segments from well 00-1 exhibit a range from .2% to 40.6% with an arithmetic mean of 2.9% and a standard deviation of 6.1% (Figure 9).

The mean phi grain size was calculated for each core using the method of moments. The phi sizes for well 00-1 range from -1.02 to 2.55 with an arithmetic mean of -0.02 and a standard deviation of .65 (Figure 10).

GEMS 1-7

Wells 1-7 shows some overlap between the top two samples where an interval was resampled during core recovery.

The undisturbed cores of well 1-7 have an arithmetic mean conductivity of 16.43 m/day, with a sample standard deviation of 20.47 m/day (Figure 11). Values range from a minimum of 0.83 m/day to a maximum of 129.03 m/day. There is a general increase in hydraulic conductivity with depth.

The repacked cores exhibit a higher mean conductivity and greater variability than the undisturbed cores (Figure 12). Values range from 0.39 m/day to 171.28 m/day with a mean of 58.26 m/day and a standard deviation of 38.11 m/day. For 52 of the 54 processed segments, the repacked hydraulic conductivity is greater than the original measurement.

The original cores from well 1-7 have porosities ranging from 23.1% to 33.1% with an arithmetic mean of 28.2% and a standard deviation of 2.0% (Figure 13). The porosity of the repacked cores ranges from 23.2% to 32.5% with an arithmetic mean of 28.6% and a standard deviation of 2.1% (Figure 14).

The differences between the original and repacked porosities from well 1-7 range from 0.00% to 5.07% with an arithmetic mean of 0.98%. For 36 of the 54 processed cores, the repacked porosity is greater than the original porosity; 17 of the repacked cores have lower porosities than the original cores and one core has identical original and repacked porosities.

The percent fines for the segments from well 1-7 ranges from .01% to 20.3% with an arithmetic mean of 2.1% and a standard deviation of 3.7% (Figure 15).

The phi sizes for well 1-7 range from -1.19 to 2.24 with an arithmetic mean of -0.05 and a standard deviation of .69 (Figure 16).

GEMS 5-1

Well 5-1 shows some overlap between the top two samples where an interval was resampled during core recovery. Grain size and porosity data for segment #4, sample #1 (11.51-11.69 m) from well 5-1 are not available because some of the sediment was lost during sieving. Information for several other segments is missing because those segments were suspected of having very low permeabilities and thus were saved to be processed in the Brainard-Kilman permeability cell (see the following discussion of low permeability core analysis).

The undisturbed cores of well 5-1 have an arithmetic mean conductivity of 14.05 m/day, with a sample standard deviation of 13.40 m/day (Figure 17). Values range from a minimum of .12 m/day to a maximum of 65.32 m/day. There is no apparent trend in hydraulic conductivity with depth.

As was observed for well 1-7, the repacked cores of well 5-1 have a higher mean conductivity and greater variability than the undisturbed cores (Figure 18). Values range from 4.97 m/day to 159.61 m/day with a mean of 38.11 m/day and a standard deviation of 34.05 m/day. For 44 of the 47 processed segments, the repacked hydraulic conductivity is greater than the original measurement.

The original cores from well 5-1 have porosities ranging from 20.6% to 32.3% with an arithmetic mean of 27.2% and a standard deviation of 2.4% (Figure 19). The porosity of the repacked cores ranges from 22.2% to 36.2% with an arithmetic mean of 27.7% and a standard deviation of 2.6% (Figure 20).

The differences between the original and repacked porosities from well 5-1 ranged from 0.01% to 5.36% with an arithmetic mean of 1.19%. For 30 of the 47 processed cores, the repacked porosity is greater than the original porosity; 17 of the repacked cores have lower porosities than the original cores.

The percent fines for the segments from well 5-1 ranges from .1% to 8.6% with an arithmetic mean of 1.8% and a standard deviation of 1.9% (Figure 21).

The phi sizes for well 5-1 range from -1.05 to 2.44 with an arithmetic mean of 0.26 and a standard deviation of .78 (Figure 22). All profiles show a general fining upward sequence.

GEMS 7-1

Sample #1 was not recovered due to the sampler malfunctioning.

The undisturbed cores of well 7-1 (not including the cores through which no water flowed) have an arithmetic mean hydraulic conductivity of 32.38 m/day, with a sample standard deviation of 48.85 m/day (Figure 23). Values range from a minimum of 0.28 m/day to a maximum of 261.78 m/day. There is no apparent trend in hydraulic conductivity with depth. There was no flow through three segments from this well: sample #6, segments #1, #4, and #5 (18.41-18.56 m, 18.86-19.01 m and 19.01-19.17 m).

The repacked cores of well 7-1 have a higher mean conductivity but less variability than the undisturbed cores (Figure 24). Values range from 0.18 m/day to 153.65 m/day with a mean of 39.91 m/day and a standard deviation of 36.94 m/day. For 27 of the 35 processed segments, the repacked hydraulic conductivity is greater than the original measurement. Sample #5, segment #7 (17.93-18.09 m) and the three cores mentioned in the preceding paragraph were not repacked because of their very low original permeability.

The original cores have porosities ranging from 19.8% to 36.4% with an arithmetic mean of 25.8% and a standard deviation of 3.4% (Figure 25). The porosity of the repacked cores ranges from 20.2% to 36.0% with an arithmetic mean of 26.5% and a standard deviation of 3.3% (Figure 26).

The differences between the original and repacked porosities range from 0.01% to 2.83% with an arithmetic mean of 0.87%. For 25 of the 35 processed cores, the repacked porosity is greater than the original porosity; 10 of the repacked cores have lower porosities than the original cores.

The percent fines for well 7-1 ranges from 0.4% to 20.28% with an arithmetic mean of 3.3% and a standard deviation of 4.1% (Figure 27).

The phi sizes for well 7-1 range from -0.73 to 0.98 with an arithmetic mean of 0.02 and a standard deviation of 0.45 (Figure 28). Grain size data are not available for segments that have not yet been repacked.

GEMS 8-1

The undisturbed cores of well 8-1 have an arithmetic mean hydraulic conductivity of 33.19 m/day, with a sample standard deviation of 34.83 m/day (Figure 29). Values range from a minimum of 0.08 m/day to a maximum of 207.71 m/day. There is a general increase in hydraulic conductivity with depth.

The repacked cores of well 8-1 have a higher mean conductivity and greater variability than the undisturbed cores (Figure 30). Due to an error, no repack was run for sample #21, sample #7 (13.11-13.31 m). Values range from 2.06 m/day to 279.27 m/day with a mean of 79.45 m/day and a standard deviation of 66.35 m/day. Of the 52 segments for which both original and repacked hydraulic conductivity data was collected, 43 have repacked hydraulic conductivities greater than the original measurement.

The original cores have porosities ranging from 23.0% to 47.8% with an arithmetic mean of 29.7% and a standard deviation of 4.6% (Figure 31). The porosity of the repacked cores ranges from 25.0% to 40.3% with an arithmetic mean of 30.0% and a standard deviation of 2.9% (Figure 32).

The differences between the original and repacked porosities range from 0.05% to 9.14%. For 38 of the cores, the repacked porosity is greater than the original porosity; 14 of the repacked cores have lower porosities than the original cores.

The percent fines for well 8-1 ranges from 0.22% to 8.83% with an arithmetic mean of 1.78% and a standard deviation of 2.01% (Figure 33).

The phi sizes for well 8-1 range from -1.01 to 2.45 with an arithmetic mean of -0.08 and a standard deviation of 0.69 (Figure 34). Grain size data are not available for sample #20, segment #1 (10.74-10.91 m), and sample #26, sample #6 (20.39-20.54 m).

Mistakes made in measuring the lengths of sample #24, segments #5-7, and sample #26, segments #5-7, may have resulted in incorrect porosity and hydraulic conductivity calculations.

GEMS 9-1

The undisturbed cores of well 9-1 have an arithmetic mean hydraulic conductivity of 27.19 m/day, with a sample standard deviation of 32.59 m/day (Figure 35). Values range from a minimum of 0.19 m/day to a maximum of 134.73 m/day.

The repacked cores of well 9-1 have a higher mean conductivity and greater variability than the undisturbed cores (Figure 36). Values range from 0.16 m/day to 233.27 m/day with a mean of 49.19 m/day and a standard deviation of 43.36 m/day. For 44 of the 47 processed segments, the repacked hydraulic conductivity is greater than the

original measurement. Sample #1, segment #1 was not repacked because it was used for x-ray analysis of clay mineralogy.

The original cores have porosities ranging from 21.3% to 36.3% with an arithmetic mean of 26.4% and a standard deviation of 2.8% (Figure 37). The porosity of the repacked cores ranges from 21.5% to 37.2% with an arithmetic mean of 27.6% and a standard deviation of 3.0% (Figure 38).

The differences between the original and repacked porosities range from 0.05% to 4.74% with an arithmetic mean of 1.51%. For 35 of the 47 processed cores, the repacked porosity is greater than the original porosity; 12 of the repacked cores have lower porosities than the original cores.

The percent fines for the segments from well 9-1 ranges from 0.2% to 33.43% with an arithmetic mean of 2.7% and a standard deviation of 5.9% (Figure 39). The phi sizes for well 9-1 range from -1.05 to 2.07 with an arithmetic mean of 0.19 and a standard deviation of 0.69 (Figure 40). Grain size and porosity data for sample #1 segment #1 (10.81-10.98 m) are not available because the core was used for x-ray analysis of clay mineralogy. Grain size data for sample #2, segment #3 are not included in the calculations since an error was made in the sieve analysis.

GEMS 10-1

Hydraulic conductivity, porosity and grain size values were not obtained for 5 segments which were too rich in clay to analyze on the permeameter: sample # 20, segment #8 (13.39-13.53m); sample #24, segments #8 and #9 (17.97-18.12 m and 18.12-18.28 m); and sample #25, segments #5 and #7 (19.18-19.37 m and 19.49-19.68 m).

The undisturbed cores of well 10-1 have an arithmetic mean hydraulic conductivity of 19.55 m/day, with a sample standard deviation of 23.29 m/day (Figure 41). Values range from a minimum of 0.13 m/day to a maximum of 123.44 m/day.

The repacked cores of well 10-1 have a higher mean conductivity and greater variability than the undisturbed cores (Figure 42). Values range from 0.32 m/day to 225.18 m/day with a mean of 35.36 m/day and a standard deviation of 35.36 m/day. For 43 of the 51 processed segments, the repacked hydraulic conductivity is greater than the original measurement.

The original cores have porosities ranging from 23.42% to 32.35% with an arithmetic mean of 27.94% and a standard deviation of 2.07% (Figure 43). The porosity of the repacked cores ranges from 22.63% to 33.38% with an arithmetic mean of 28.45% and a standard deviation of 2.29% (Figure 44).

The differences between the original and repacked porosities range from 0.01% to 7.34%. For 48 of the 51 processed cores, the repacked porosity is greater than the original porosity; 3 of the repacked cores have lower porosities than the original cores.

The percent fines for the segments from well 10-1 ranges from 0.46% to 11.01% with an arithmetic mean of 2.47% and a standard deviation of 2.98% (Figure 45). The phi sizes for well 10-1 range from -0.88 to 1.34 with an arithmetic mean of 0.13 and a standard deviation of 0.52 (Figure 46).

GEMS 11-1

The undisturbed cores of well 11-1 have an arithmetic mean hydraulic conductivity of 29.6 m/day, with a sample standard deviation of 32.51 m/day (Figure 47). Values range from a minimum of 0.41 m/day to a maximum of 118.57 m/day. Hydraulic conductivity values were not obtained for sample #1, segments #1, #2 and #5 (10.92-11.07, 11.07-11.19 and 11.47-11.61 m); sample #5, segment #6 (17.66-17.81 m); and sample #6, segment #1 (18.50-18.64 m), as there was no flow through these cores under the head gradient produced in the permeameter.

The repacked cores of well 11-1 have a higher mean conductivity and greater variability than the undisturbed cores (Figure 48). Values range from 1.20 m/day to 166.72 m/day with a mean of 63.93 m/day and a standard deviation of 45.26 m/day. For 30 of 36 processed segments, the repacked hydraulic conductivity is greater than the original measurement. The samples mentioned in the preceding paragraph, as well as sample #6, segments #5 and #6, were not repacked and were set aside to process in the low permeability cell. Sample #3, segment #3 and sample #5, segments #3 and #8 were not repacked because they were used for x-ray analysis of clay mineralogy. The repack information from sample #3, segment #4; sample #4 segments #1, #4 and #7; sample #5, segment #4; and sample #7, segment #3 were not included in the graphs and statistics, since a mistake was made when the method of securing the cores in the permeameter was modified, and the sediment from these cores was repacked to a length approximately 1 to 2 cm longer than the original cores.

The original cores have porosities ranging from 22.2% to 33.0% with an arithmetic mean of 26.4% and a standard deviation of 2.7% (Figure 49). The porosity of the repacked cores ranges from 21.2% to 31.7% with an arithmetic mean of 26.8% and a standard deviation of 3.7% (Figure 50).

The differences between the original and repacked porosities range from 0.09% to 2.03% with an arithmetic mean of 1.06%. For 20 of the 29 cores considered, the

repacked porosity is greater than the original porosity; 9 of the repacked cores have lower porosities than the original cores.

Due to numerous as yet unresolved problems, grain size data for well 11-1 is not presented.

GEMS TMO-1

Hydraulic conductivity, porosity and grain size values were not obtained for 4 segments which were too rich in clay to analyze on the permeameter: sample # 1, segments #1-3 and #5 (10.71-11.21 m and 11.56-11.70 m). There was also a gap in sample #1 from 11.21 to 11.4 m.

The undisturbed cores of well TMO-1 have an arithmetic mean hydraulic conductivity of 45.31 m/day, with a sample standard deviation of 41.46 m/day (Figure 51). Values range from a minimum of 0.04 m/day to a maximum of 166.79 m/day.

The repacked cores of well TMO-1 have a lower mean conductivity and less variability than the undisturbed cores (Figure 52). Values range from 0.25 m/day to 179.98 m/day with a mean of 41.73 m/day and a standard deviation of 34.94 m/day. For 30 of the 57 processed segments, the repacked hydraulic conductivity is greater than the original measurement.

The original cores have porosities ranging from 18.88% to 35.54% with an arithmetic mean of 28.02% and a standard deviation of 2.60% (Figure 53). The porosity of the repacked cores ranges from 22.45% to 37.98% with an arithmetic mean of 28.56% and a standard deviation of 3.23% (Figure 54).

The differences between the original and repacked porosities range from 0.00% to 9.17%. For 53 of the 57 processed cores, the repacked porosity is greater than the original porosity; 3 of the repacked cores have lower porosities than the original cores and one has the same porosity.

The percent fines for the segments from well TMO-1 ranges from 0.01% to 15.34% with an arithmetic mean of 2.24% and a standard deviation of 2.73% (Figure 55). The phi sizes for well TMO-1 range from -0.81 to 1.39 with an arithmetic mean of 0.05 and a standard deviation of 0.54 (Figure 56). Due to laboratory errors in processing the samples, grain size data from sample #5, segments #2 and #3, and sample #6, segment #10 are not included in these statistics.

GEMS TME-8

Hydraulic conductivity, porosity and grain size values were not obtained for 18 segments which were too rich in clay to analyze on the permeameter: all eight segments

of sample # 1, sample #2, segments #3-8 (12.65-13.42 m); sample #6, segment #1 (18.37-18.52m); and sample #7, segments #4, #6, and #8 (20.29-20.41 m, 20.53-20.66 m, and 20.84-21.03 m).

The undisturbed cores of well TME-8 have an arithmetic mean hydraulic conductivity of 83.26 m/day, with a sample standard deviation of 74.02 m/day (Figure 57). Values range from a minimum of 5.85 m/day to a maximum of 327.9 m/day.

The repacked cores of well TME-8 have a lower mean conductivity and less variability than the undisturbed cores (Figure 58). Values range from 1.48 m/day to 205.08 m/day with a mean of 44.41 m/day and a standard deviation of 44.59 m/day. For only 6 of the 30 processed segments was the repacked hydraulic conductivity greater than the original measurement.

The original cores have porosities ranging from 25.12% to 37.76% with an arithmetic mean of 29.73% and a standard deviation of 3.09% (Figure 59). The porosity of the repacked cores ranges from 25.26% to 37.78% with an arithmetic mean of 29.94% and a standard deviation of 3.02% (Figure 60).

The differences between the original and repacked porosities range from 0.01% to 1.87%. For 29 of the 30 processed cores, the repacked porosity is greater than the original porosity; 1 of the repacked cores has a lower porosity than the original core.

The percent fines for the segments from well TME-8 ranges from 0.42% to 6.12% with an arithmetic mean of 2.21% and a standard deviation of 1.61% (Figure 61). The phi sizes for well TME-8 range from -0.98 to 1.50 with an arithmetic mean of 0.32 and a standard deviation of 0.62 (Figure 62).

Summary Core Statistics

Values for original and repacked hydraulic conductivity, original and repacked porosity, percent fines, and mean grain size in phi units were calculated for approximately 450 core segments from 10 wells. The segments have a mean original hydraulic conductivity of 29.9 m/day with values ranging from .04 m/day to 327.9 m/day. The mean repacked hydraulic conductivity value is 49.93 m/day with a low of .04 m/day and a high of 279.27 m/day. The mean porosity for undisturbed cores is 27.86% (values range from 18.88% to 47.8%) with the repacked cores having a slightly higher mean of 28.39% (values range from 20.2% to 40.3%). The percent fines ranged from .01% to 40.6% with a mean of 2.36% over all cores. The mean phi size is .09 with values ranging from -1.19 to 2.55 phi units.

Core Chemistry Analyses

We have found that for many cores hydraulic conductivity increases (as the core completely saturates), reaches a maximum, and then decreases as the test continues. An example of this phenomenon for one core segment is illustrated in Figure 63. Possible explanations for this decrease in conductivity include biological growth, movement of fines, and mineral deposition. Maintaining the concentration of a biocide and employing as low a flow rate through the core as practical should reduce the influence of the first two possible factors. Calcite deposits have been observed on the plastic tubing, thermometer, and temperature transmitter of the permeameter, so a simulation using PHREEQE (Parkhurst et al., 1980) was run to determine the nature and amount of mineral material that might be deposited during the hydraulic conductivity tests.

The water in use in the permeameter is taken from the same site and depth from which the cores are taken to ensure as much as possible that the water will be in chemical equilibrium with the cores during the permeameter experiments. The water does experience some changes, however, before it is used in the permeameter: increased temperature, decreased partial pressure of PCO_2 , and, during the first years of this project, addition of Thymol. These changes may cause the water to precipitate mineral material in order to regain equilibrium.

Chemical analyses of water samples from GEMS are available from the fall of 1990 and the summer of 1991, and two of these samples are from the same depth from which water for the permeameter is collected. Both samples have similar chemical characteristics.

The PHREEQE simulation was performed by first creating a solution matching the temperature, pH and chemical composition of the two well water samples. Alkalinity was input as HCO_3^- , aqueous nitrogen gas was removed from the data base, and the p_e was set at 9.0. The p_e and pH were allowed to be determined by the reaction. The most abundant constituents of the coarse fraction in the cores are quartz and K-feldspar, so the saturation indices of quartz and microcline were adjusted to match the silica and potassium contents of the water samples. This resulted in the solution being slightly oversaturated with respect to quartz and undersaturated with respect to microcline. The solution was then equilibrated with laboratory temperatures (22 degrees C) and surface partial pressure of PCO_2 ($\log \text{PCO}_2 = -3.5$). Thymol was added as a reaction to the computer simulated solution, and the solution was equilibrated with calcite to determine the amount of calcium carbonate that might be deposited.

The changes in alkalinity, pH, and p_e that take place in the water according to the PHREEQE simulation are shown in Figure 64. The changes in the saturation index ($\log \text{IAP/KT}$) of calcite are shown in Figure 65. The simulation shows that when well water is

equilibrated with surface temperatures and pressures, calcite should precipitate. Calculations indicate that ten gallons of GEMS well water (approximately the amount used in the permeameter at one time) precipitate 3.56 cubic centimeters of calcite. What is not presently known is the kinetics of the situation. PHREEQE assumes all reactions reach equilibrium instantaneously. It is unclear how much of the calcite precipitates during the time the water is left to equilibrate with laboratory conditions (two weeks minimum) and how much is deposited in the cores and on the permeameter.

In this section, a series of experiments are described which were performed to better determine if deposition of calcite in the cores is contributing to the observed decrease in hydraulic conductivity with time. These experiments employed three cores, which were placed one after another in the permeameter apparatus using the setup described earlier in the Laboratory Procedures and Methods portion of this section. The permeameter and outflow-tube water were analyzed for pH, dissolved oxygen, and major cations as described earlier.

The pH of GEMS water measured in the field is approximately 7. Monitoring of the pH of water collected for use in the permeameter did not reveal any trend with time while equilibrating to laboratory conditions over a 19 day period. After the water was introduced into the permeameter, the pH rose fairly rapidly to approximately 8 and fluctuated between 8 and 9 while circulating through the permeameter with no apparent trend with time (Figure 66). There was no significant change in pH after the water had passed through the cores. The measured differences are within the limit of accuracy of the pH meter. The rise in pH when the water started circulating through the permeameter was most likely due to the loss of CO₂. Bubbling CO₂ through the upper reservoir has been successful in maintaining a pH close to 7.

Dissolved oxygen (DO) measurements indicate that the oxygen content of the water increases after the water is placed in the permeameter. Before the water is placed in the permeameter, it has a DO content of 1 to 2 ppm. After the water has been placed in the permeameter, the DO content increases to 5 to 8 ppm. There is no significant change in DO content after the water has passed through a sediment core.

Major cation analyses of the water in the permeameter and outflow-tube for the three cores employed in these experiments indicate that the calcium content of the water generally decreases with time (Figure 67), further demonstrating that precipitation of calcite is occurring within the permeameter apparatus.

The first core placed in the apparatus (GEMS 9-1 sample #1, segment #1) shows a consistently lower calcium content in the outflow-tube water as compared to that in the permeameter (the accuracy of the chemical analysis is better than 1 ppm for calcium).

This indicates that calcite is being precipitated in the core and perhaps contributing to a decrease in hydraulic conductivity. The pH rose at the beginning of the period that this core was in the permeameter and the calcium content of the permeameter water remained fairly high.

GEMS 11-1, sample #5, segment #3 was the next core placed in the permeameter. During the period of time that water was flowing through this core the calcium content of the water decreased. No conclusions concerning the relative calcium content of the outflow tube and permeameter water can be made. Only three analyses of the permeameter water were done, with one having a higher calcium content than the outflow-tube water, one having a lower calcium content, and a third sample (marked by an asterisk) that is probably not representative of the system because circulation had been very slow for some time.

The third core placed in the permeameter for this experiment was GEMS 11-1, sample #3, segment #3. The outflow-tube water from this core had a calcium content consistently higher than that of the permeameter water, suggesting that calcite was being dissolved out of the core. However, the hydraulic conductivity of this core decreased with time, which indicates that deposition of calcite is not the controlling mechanism in reducing hydraulic conductivity during this time period.

X-ray analyses of the clays have determined that the clays are composed primarily of smectite, with some kaolinite and some illite (which is fairly crystalline, bordering on mica). There is no change in the composition of the clays while they are in the permeameter, but there was some deposition of calcite on the clays.

It was noted during preparation of the clays for x-ray analysis, that the clays are easily flocculated and dispersed, and that thymol, which had been used in the system as a biocide, caused the clays to flocculate. This tendency to readily flocculate and disperse could result in the clogging of pore throats and decreases in hydraulic conductivity. Fogler and Vaidya (1993) suggested that if the hydraulic conductivity of a core was reduced due to fines blocking the pore throats, reversing the flow direction through the core should flush out the clogged pore throats and produce an increase in hydraulic conductivity. GEMS 7-1, sample #4, segment #3, which experienced a decrease in hydraulic conductivity, was turned upside down in the permeameter, but no increase in conductivity was observed.

Using a different biocide, dichlorophene, appears to have reduced, but not eliminated, the decreases in hydraulic conductivity with time. Whether this is due to more effective biocidal action in the core (though it appears to be less effective in the

permeameter tubing), or due to the fact that the dichlorophene is not reacting with the clays is unclear at this time.

Summary and Discussion

Values for original and repacked hydraulic conductivity, original and repacked porosity, percent fines, and mean grain size in phi units were measured for approximately 450 core segments from 10 wells. This represents a tremendous resource in terms of a data set characterizing an alluvial aquifer. We have been so occupied with the data collection that we have not yet fully analyzed the data in all the ways that are statistically possible. There is a proliferation of theories in the literature for characterizing heterogeneous aquifers, but few data sets available to fully test these theories. This data set developed in this research project should be invaluable in that regard.

Laboratory Procedures , Methods, and Results - Low Permeability Samples

Introduction

As discussed previously, we found that water would only move extremely slowly through certain cores when those cores were mounted in our permeameter designed for sand and gravel samples. These cores tended to have a very high proportion of clay- and silt-sized material. In order to aid in the analysis of such cores, equipment to measure the hydraulic conductivity of low permeability samples was acquired during the grant period. Since we can only analyze one sample at a time with this equipment and since each analysis may take up to three days (depending on the degree of initial saturation and clay content), we have not completed the analysis of all of the collected cores. However, core analysis is continuing and should be completed in the near future.

Laboratory Procedures and Methods

The equipment for analyzing low-permeability samples consists of the following: a flexible wall permeability cell which can handle samples up to 4" in diameter and about 6" in length (currently the apparatus is set up for samples either 2.5" or 1 3/8" in diameter), a triaxial panel for accurate measurement of volume changes and flow rates with regulators and pipettes, and a digital readout with an RS-232 serial port for electronic data acquisition.

With low permeability samples, the presence of air (either in the permeant fluid or in the sample) can cause erroneous results. For this reason, elaborate procedures are needed to prepare deaired water and to saturate the sample slowly and completely. This can be a time consuming process, taking a day or longer. We prepare deaired water by applying a vacuum to GEMS site water for 1 - 2 hours. The process of preparation and mounting a sample into the permeability cell involves trimming the sample to a length that can be accommodated in the cell, placing end pieces on the cell, and covering the sample and end pieces with a rubber membrane. The permeability cell is then pressurized with water and all lines are carefully flushed with water to remove air. The sample is backpressure saturated by applying pressure to both ends of the sample. The deaired water will absorb any air that is present in the sample, although the process may take a considerable amount of time. Several steps of increased backpressure may be required. Once the sample is considered saturated one can proceed to measure hydraulic conductivity. The flow rate can be measured by observing the rate of rise or fall of the fluid level in the inflow and outflow pipettes. If the outflow pipette's rate of rise is not the same as the inflow pipette's rate of decline, then the sample is not completely

saturated and one should continue the saturation process. One can make a plot of water level in one pipette versus elapsed time, draw the best straight line through the data, and calculate the slope of the line in cm^3 per unit time. This quantity is q in the following formula. The hydraulic conductivity (K) can be calculated using:

$$K = \frac{L}{Ah} q$$

where L is the sample length, A is the sample cross sectional area, h is the head differential across the sample and q is the flow rate measured in one of the pipettes. We repeat this procedure several times to see how the hydraulic conductivity is changing with time. If it is decreasing then we may be moving fine material and clogging pores. If it is constant or very slowly decreasing over 3 - 5 runs then we assume the hydraulic conductivity is adequately measured and the sample may be dismantled.

Results

We have analyzed many of the low permeability samples and the results are shown in Table 1. Some of the samples are almost pure clay and have hydraulic conductivities that are typical of clay. However, some samples are mixtures of sand, silt, and clay with the hydraulic conductivity depending on the relative mixture of the components and how they are distributed in the sample. Processing of samples is continuing and should be completed in the near future. This equipment clearly enhances our laboratory capabilities, as we now can quantify the hydraulic conductivity of even very low permeability samples. Thus, we are able to characterize the hydraulic conductivity of clay stringers that occur in the sand and gravel interval at GEMS and, in addition, to increase our understanding of the hydrology of the overlying silt and clay section.

Table 1.
Summary of Measured Hydraulic Conductivities
for Low Permeability Core Samples

Core ID. No. Well No. (sample no.-seg. no.)	Hydraulic Conductivity Range (m/sec) ΔK	Average value (m/sec) K
TME-8(1-1)	$(2.25 - 2.35) \times 10^{-5}$	2.30×10^{-5}
TME-8(1-2)	$(2.20 - 2.99) \times 10^{-7}$	2.48×10^{-7}
TME-8(1-3)	$(7.37 - 8.05) \times 10^{-8}$	7.70×10^{-8}
TME-8(1-4)	$(1.25 - 1.46) \times 10^{-7}$	1.34×10^{-7}
TME-8(1-5)	$(2.27 - 7.19) \times 10^{-8}$	4.17×10^{-8}
TME-8(1-6)	$(5.36 - 6.50) \times 10^{-8}$	5.84×10^{-8}
TME-8(1-7)	$(.843 - 1.27) \times 10^{-6}$	1.07×10^{-6}
TME-8(1-8)	$(6.12 - 6.45) \times 10^{-5}$	6.25×10^{-5}
TME-8(2-3)	$(1.83 - 1.97) \times 10^{-6}$	1.92×10^{-6}
TME-8(2-4)	$(1.03 - 1.09) \times 10^{-5}$	1.06×10^{-5}
TME-8(2-5)	$(4.78 - 4.82) \times 10^{-6}$	4.80×10^{-6}
TME-8(2-6)	$(.953 - 1.03) \times 10^{-6}$	$.978 \times 10^{-6}$
TME-8(2-7)	$(5.59 - 5.79) \times 10^{-6}$	5.66×10^{-6}
TME-8(2-8)	$(1.74 - 1.80) \times 10^{-5}$	1.77×10^{-5}
TME-8(6-1)	$(4.19 - 5.99) \times 10^{-8}$	5.16×10^{-8}
TME-8(7-4)	$(1.82 - 2.07) \times 10^{-7}$	1.95×10^{-7}
TME-8(7-6)	$(3.68 - 4.67) \times 10^{-8}$	4.27×10^{-8}
TME-8(7-8)	$(2.82 - 3.58) \times 10^{-6}$	3.45×10^{-6}
TMO-1(1-1)	$(1.04 - 1.21) \times 10^{-7}$	1.11×10^{-7}
TMO-1(1-2)	$(7.67 - 8.20) \times 10^{-8}$	7.95×10^{-8}
TMO-1(1-3)	$(2.64 - 2.74) \times 10^{-8}$	2.67×10^{-8}
11-1(1-1)	$(3.18 - 3.53) \times 10^{-8}$	3.40×10^{-8}
11-1(1-2)	$(3.05 - 3.94) \times 10^{-7}$	3.53×10^{-7}

Figure 1: Low Calibration Response Over Time for Channel 5

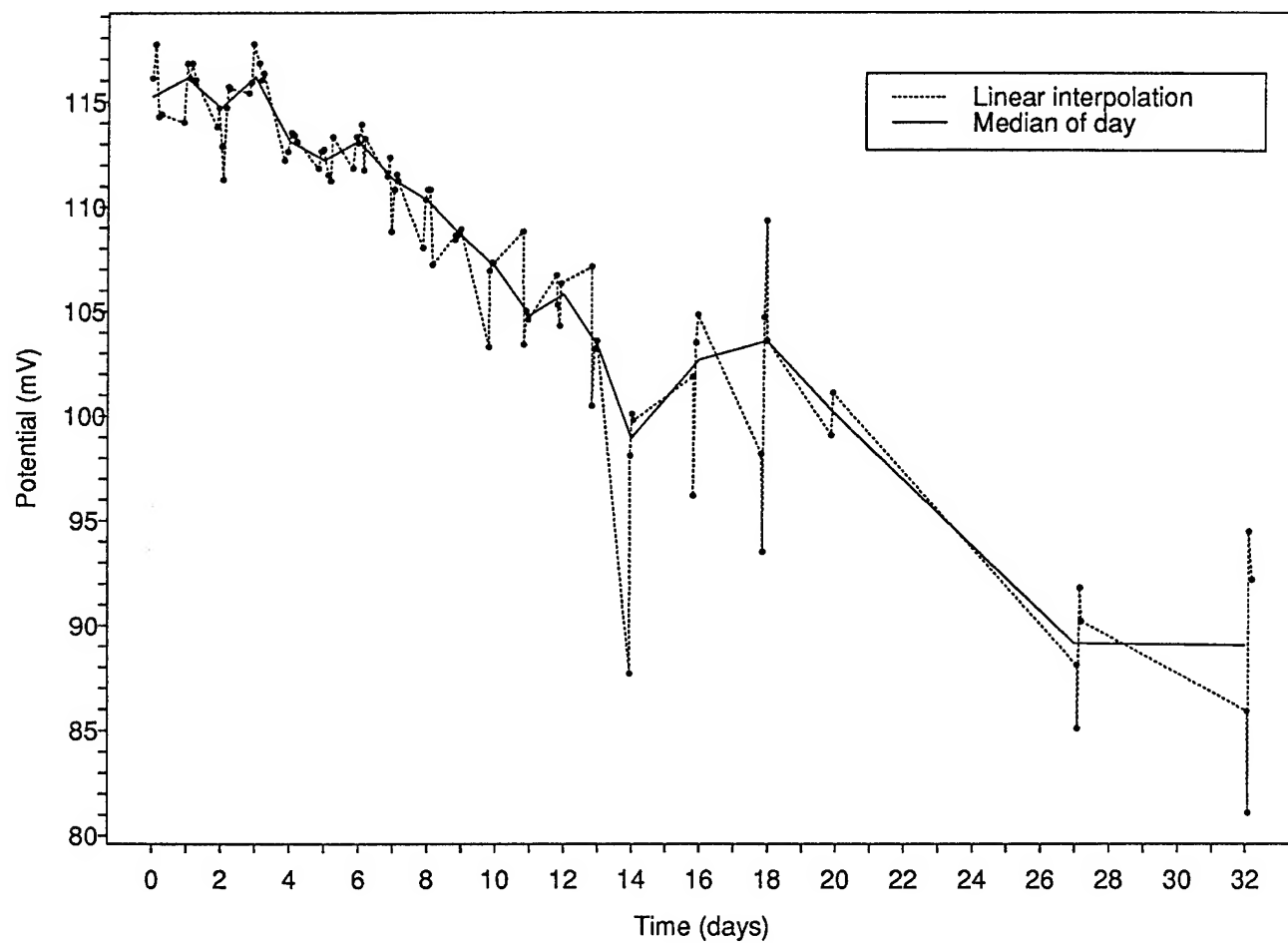


Figure 2: Medium Calibration Response Over Time for Channel 5

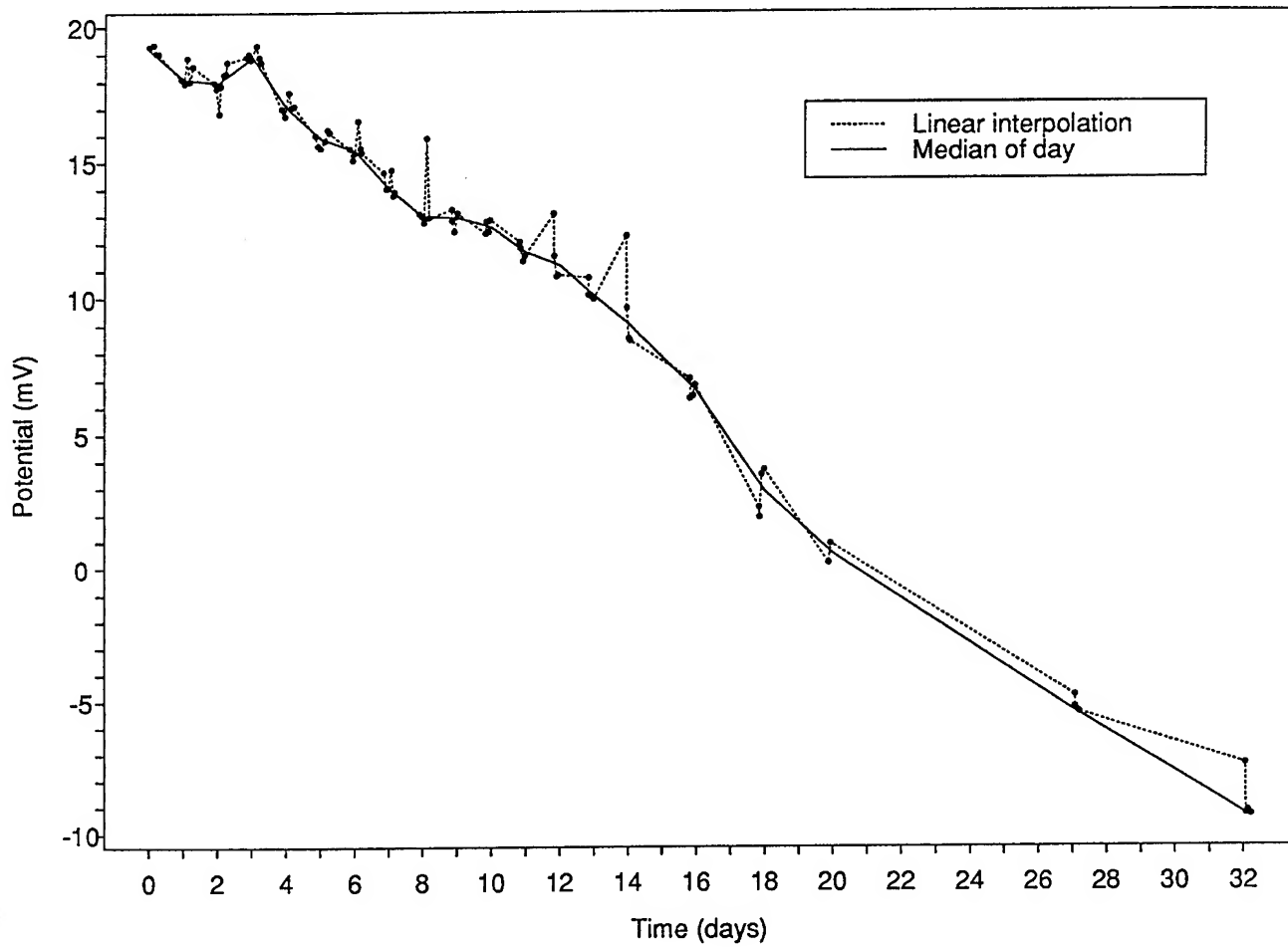


Figure 3: High Calibration Response Over Time for Channel 5

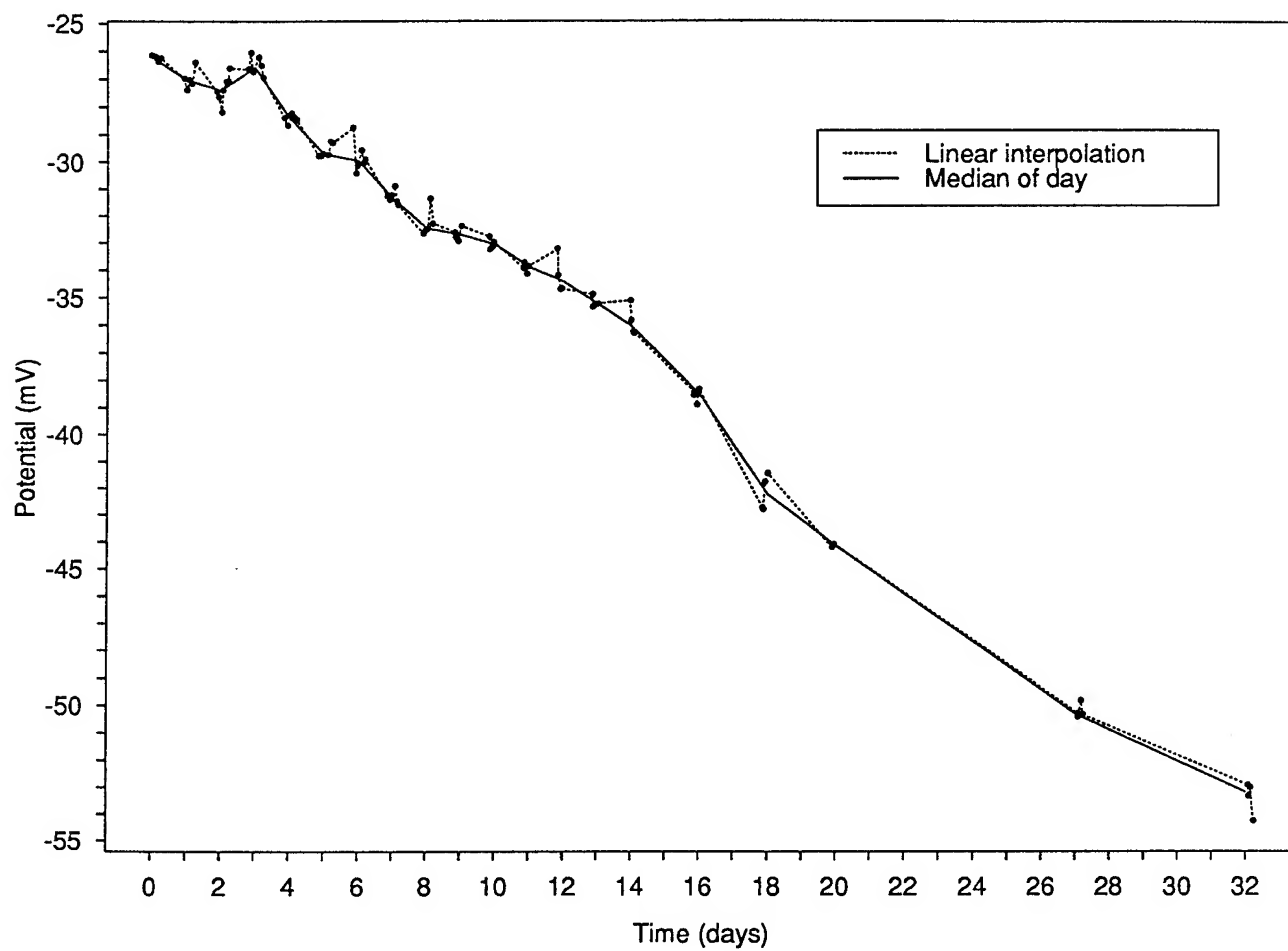
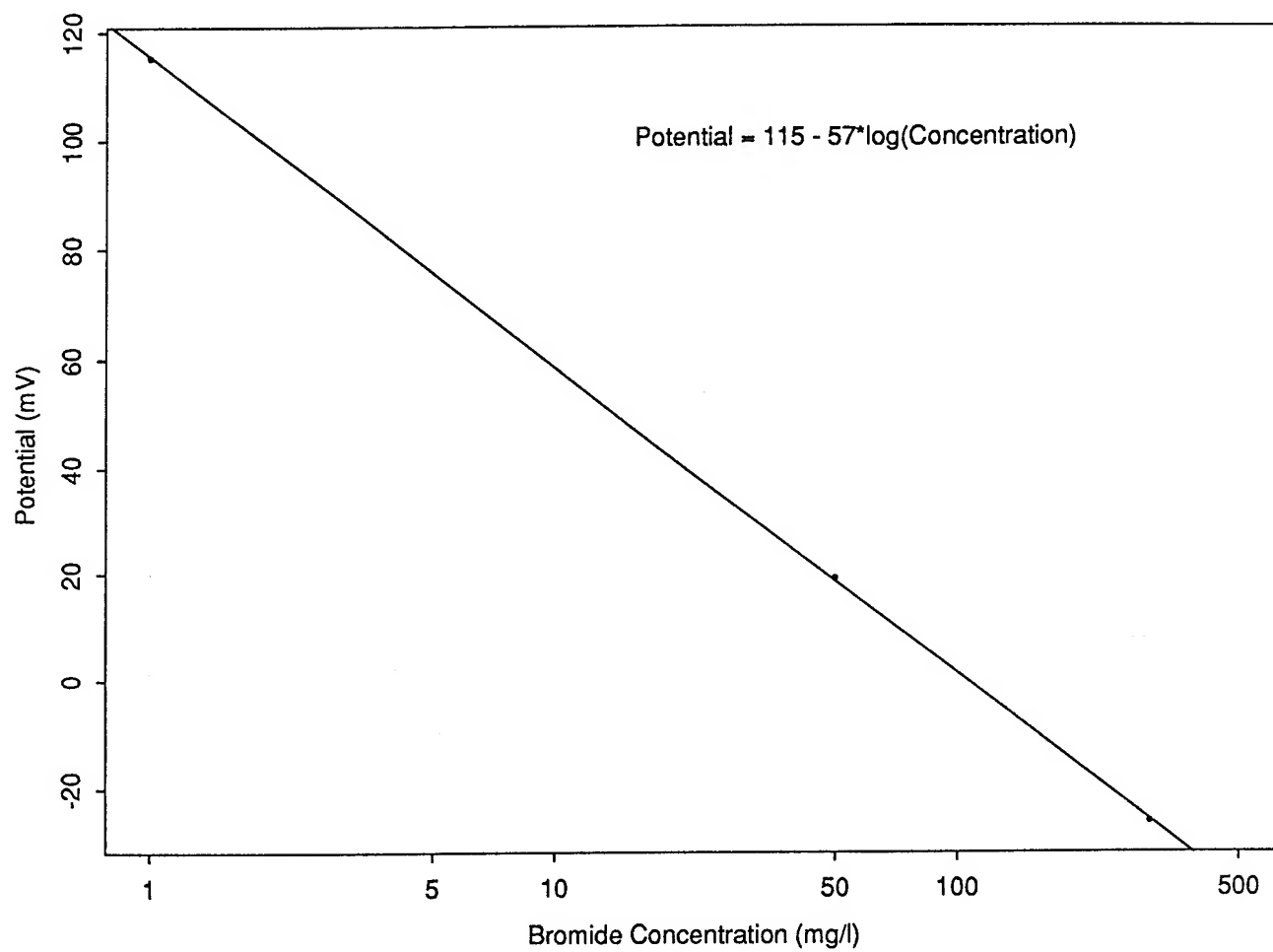


Figure 4: Calibration Curve for Channel 5, 10/8/94



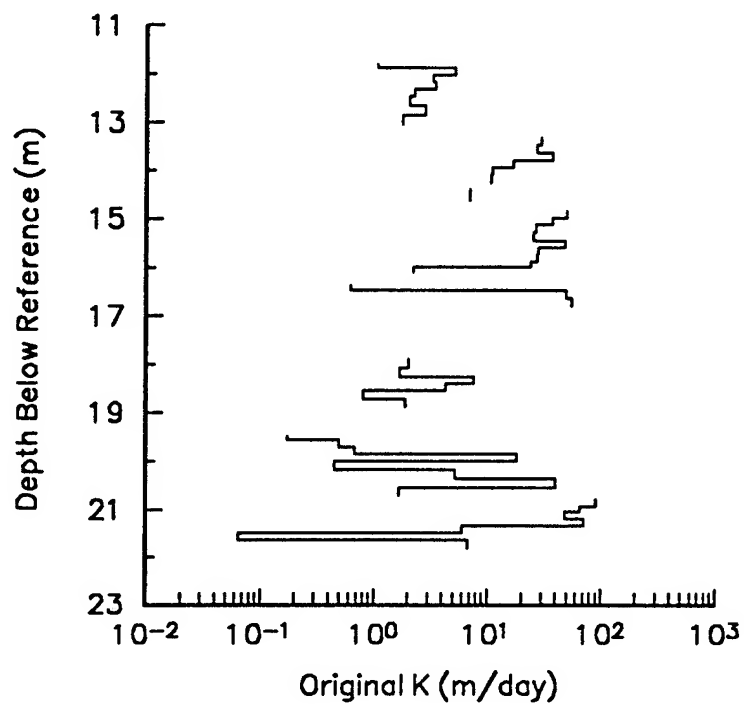


Figure 5. - Original hydraulic conductivity versus depth for GEMS well 00-1.

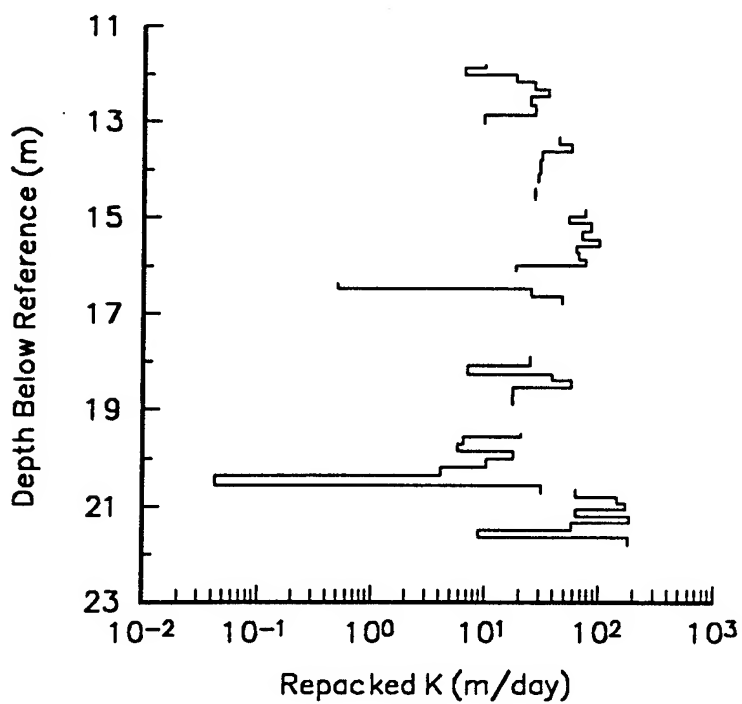


Figure 6. - Repacked hydraulic conductivity versus depth for GEMS well 00-1.

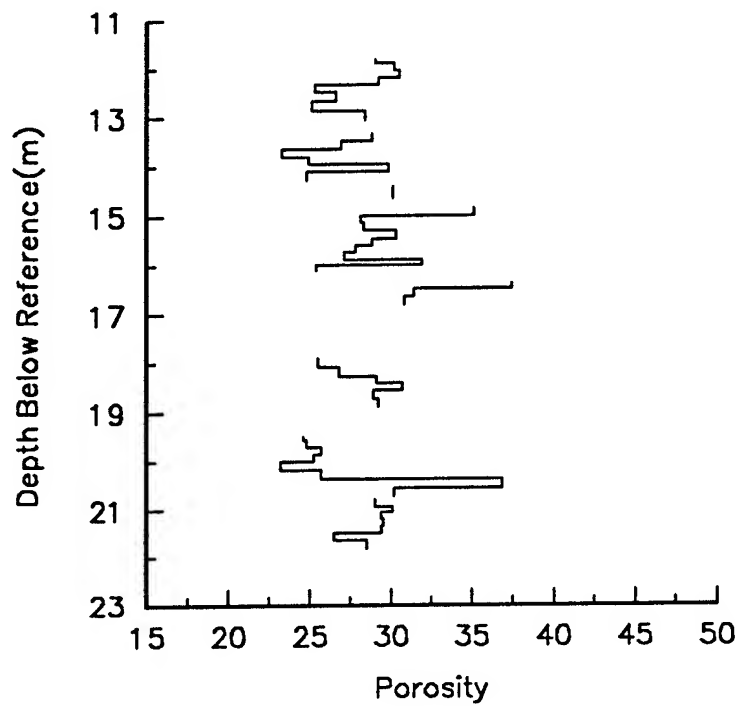


Figure 7. - Original porosity versus depth for GEMS well 00-1.

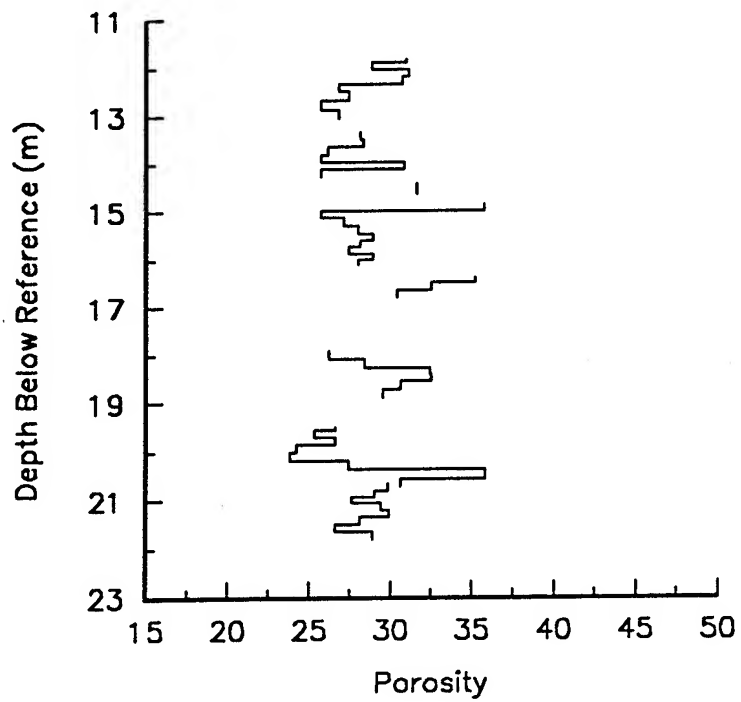


Figure 8. - Repacked porosity versus depth for GEMS well 00-1.

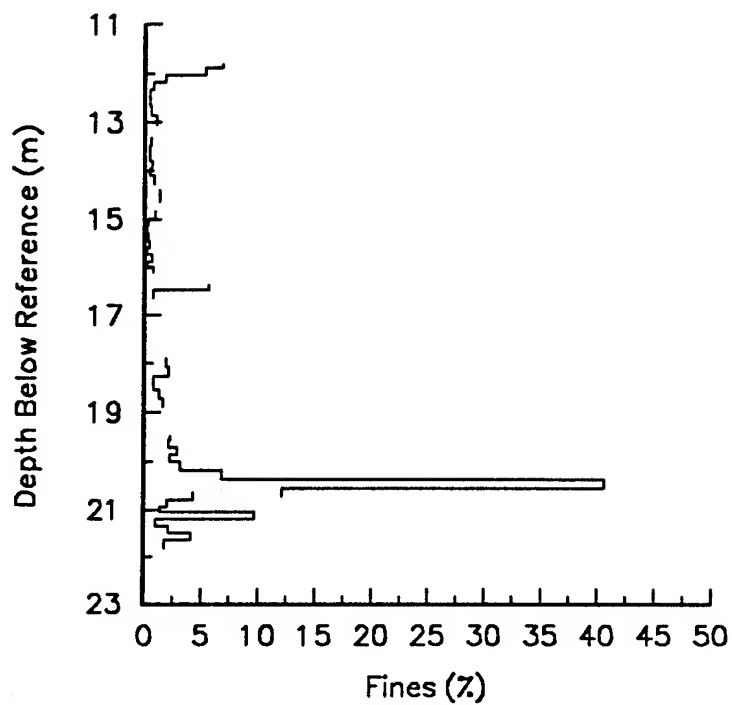


Figure 9. - Percent fines (<.053 mm) versus depth for GEMS well 00-1.

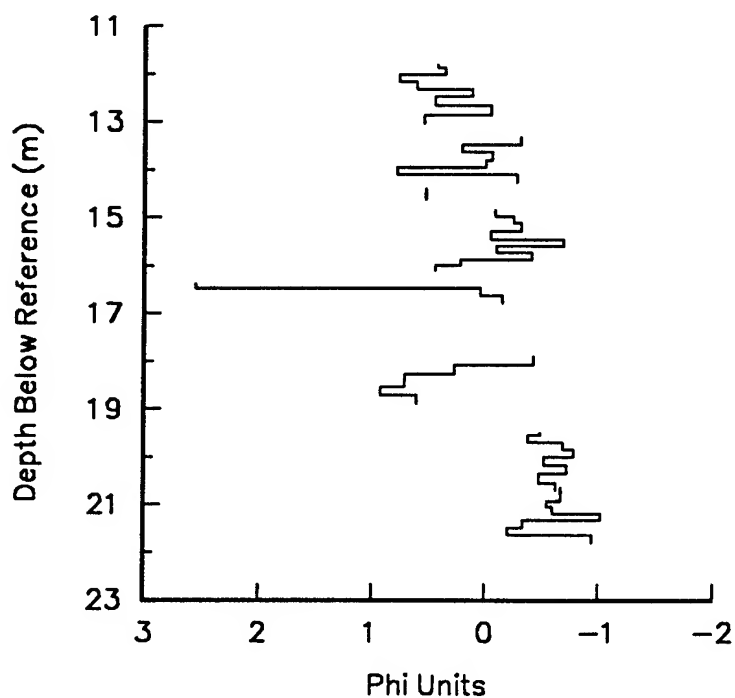


Figure 10. - Mean grain size (in phi units) versus depth for GEMS well 00-1.

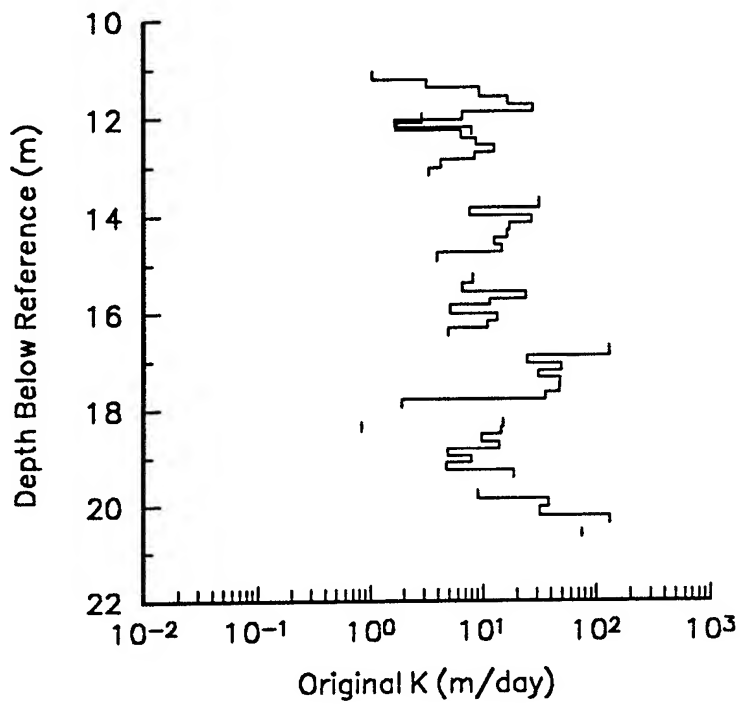


Figure 11. - Original hydraulic conductivity versus depth for GEMS well 1-7.

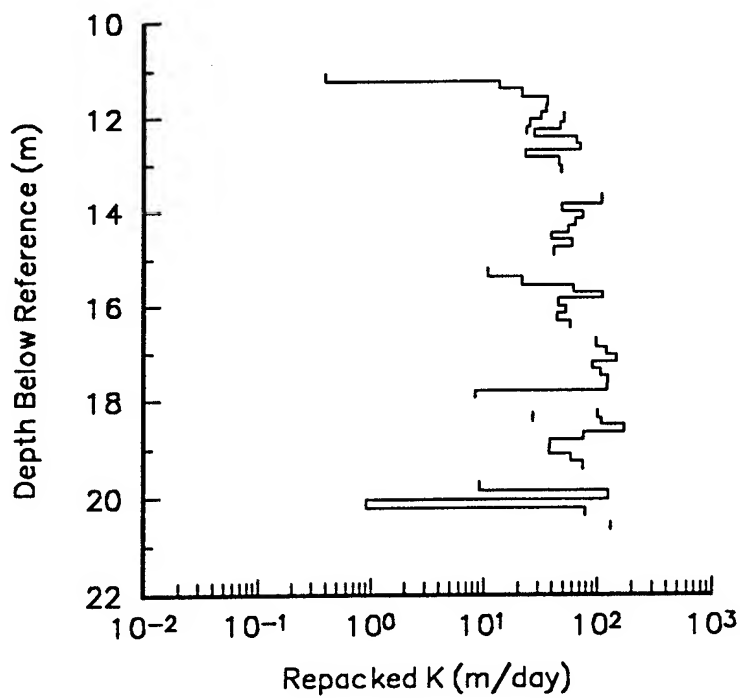


Figure 12. - Repacked hydraulic conductivity versus depth for GEMS well 1-7.

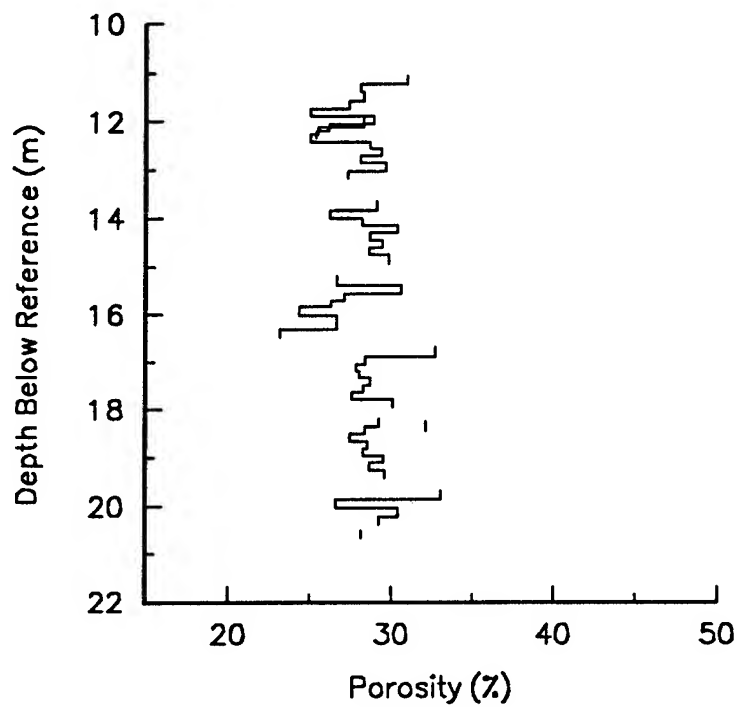


Figure 13. - Original porosity versus depth for GEMS well 1-7.

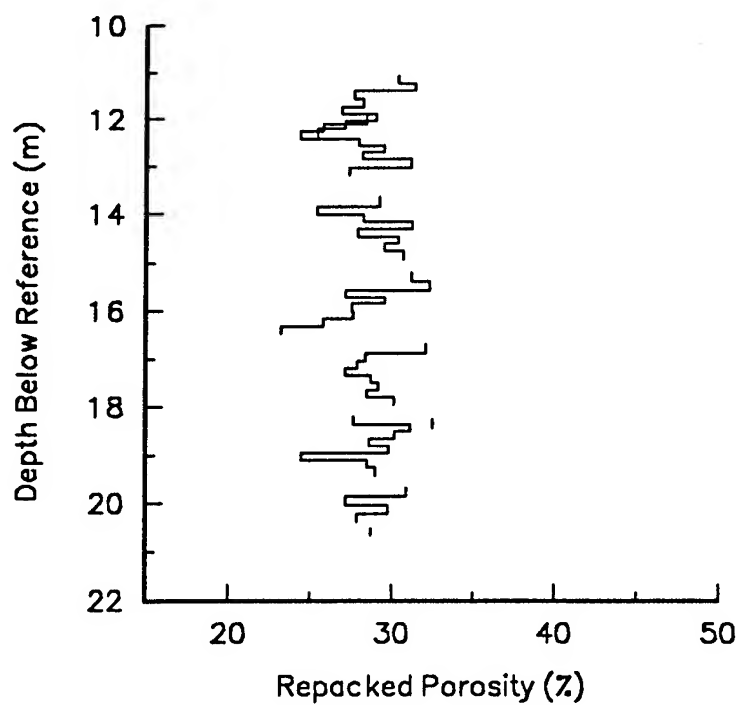


Figure 14. - Repacked porosity versus depth for GEMS well 1-7.

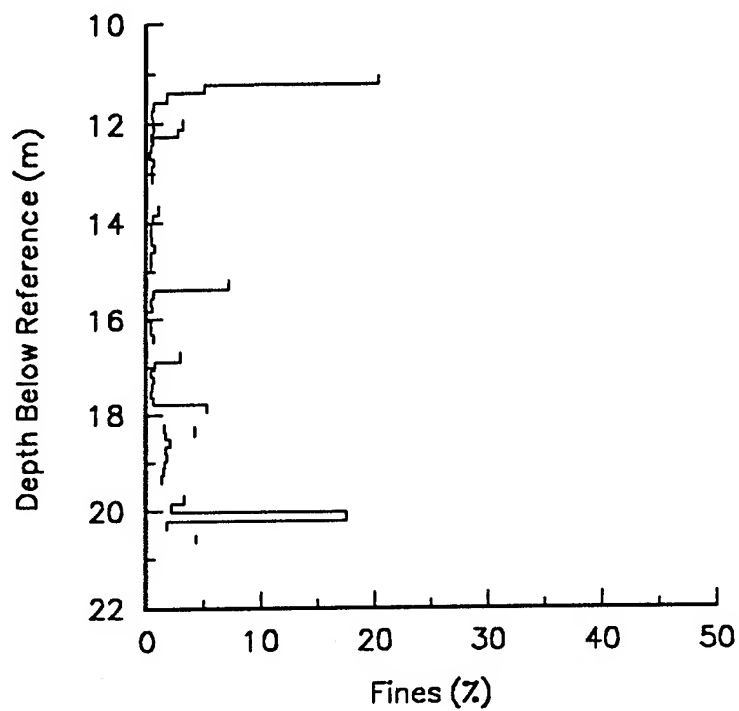


Figure 15. - Percent fines (<.053 mm) versus depth for GEMS well 1-7.

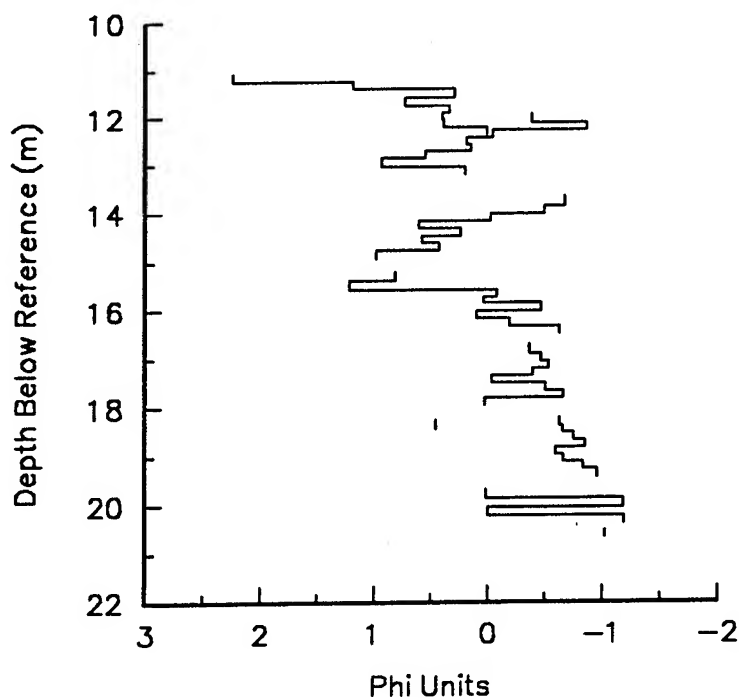


Figure 16. - Mean grain size (in phi units) versus depth for GEMS well 1-7.

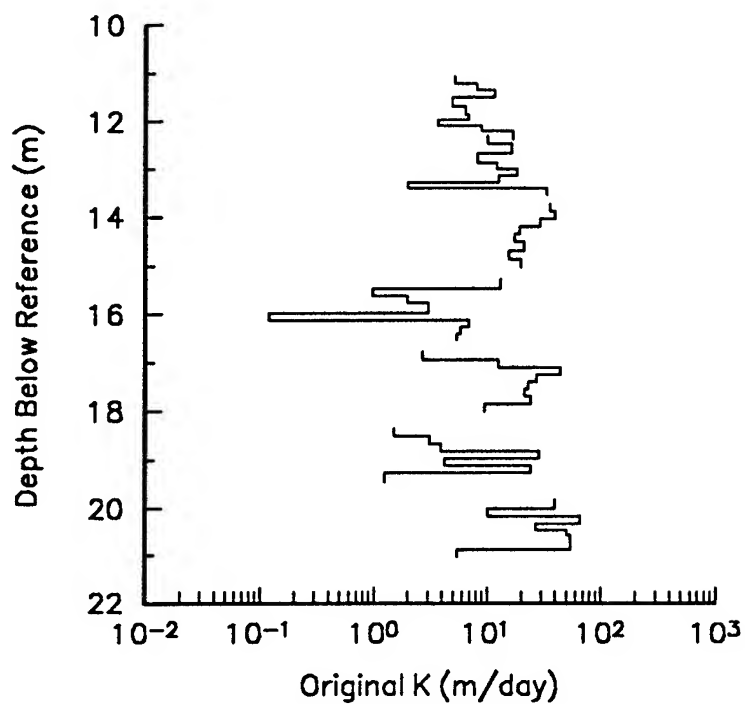


Figure 17. - Original hydraulic conductivity versus depth for GEMS well 5-1.

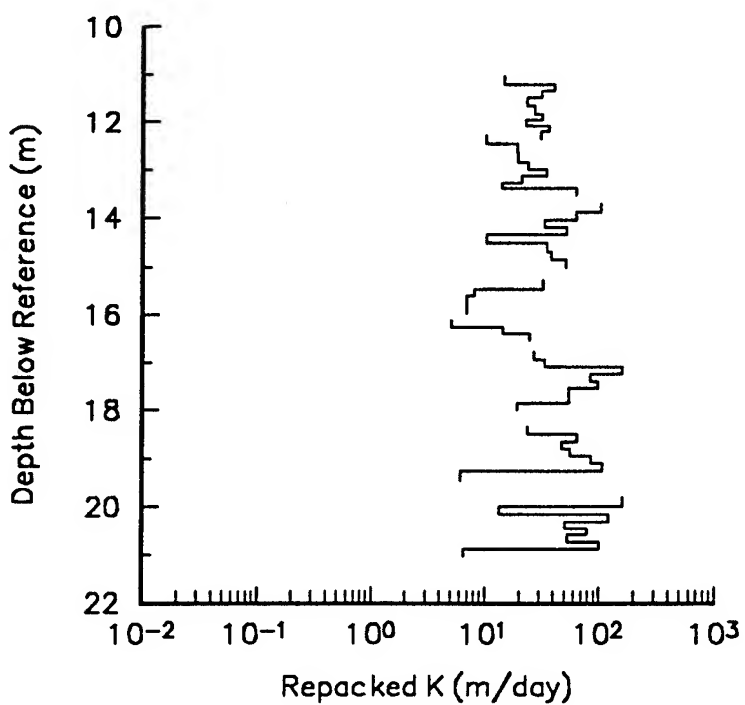


Figure 18. - Repacked hydraulic conductivity versus depth for GEMS well 5-1.

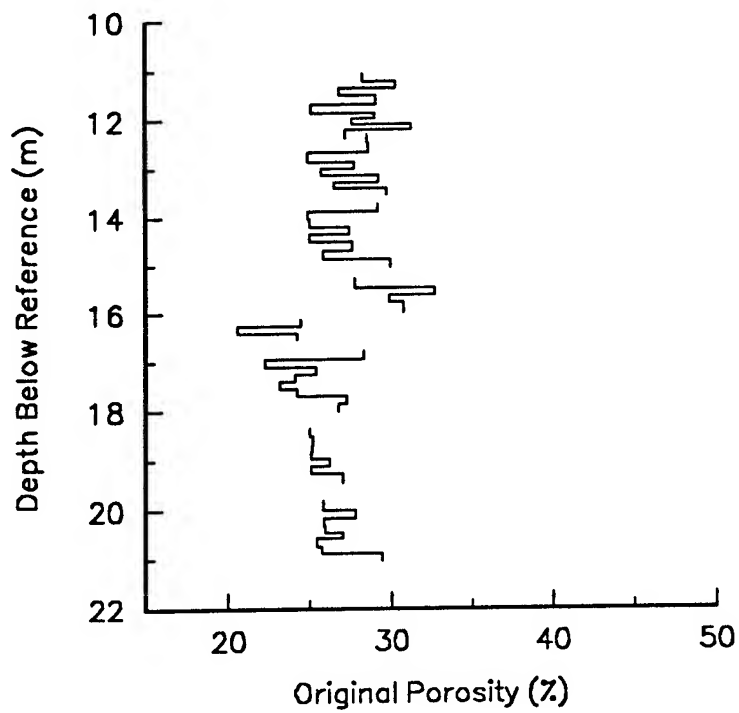


Figure 19. - Original porosity versus depth for GEMS well 5-1.

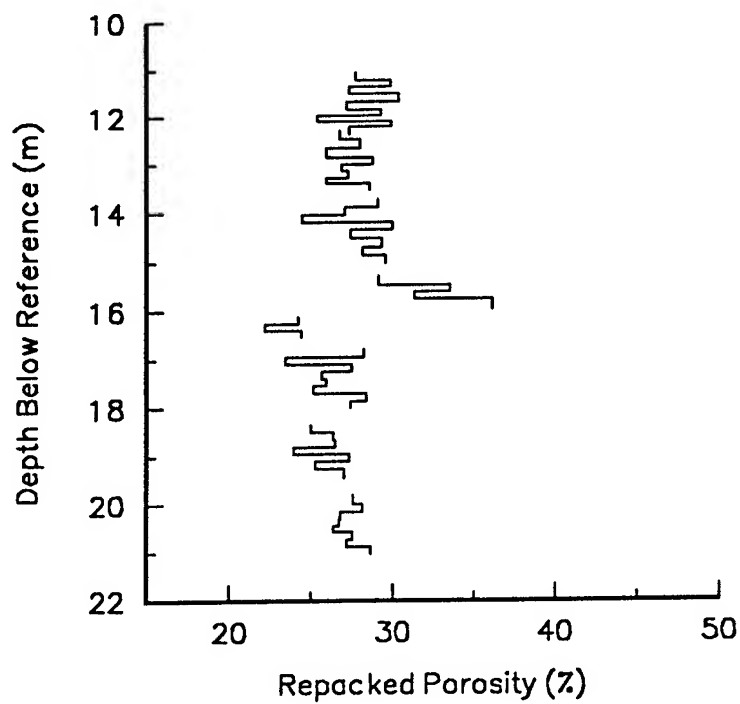


Figure 20. - Repacked porosity versus depth for GEMS well 5-1.

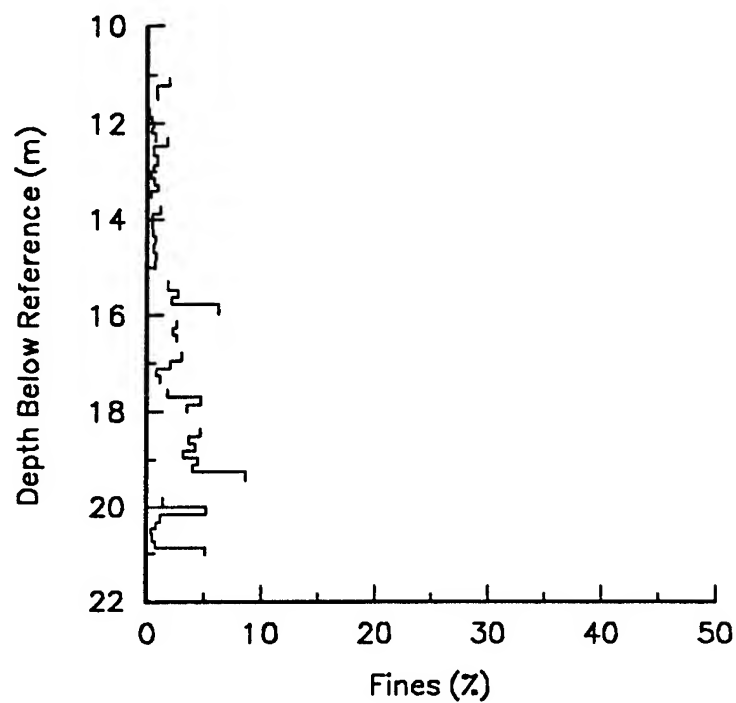


Figure 21. - Percent fines (<.053 mm) versus depth for GEMS well 5-1.

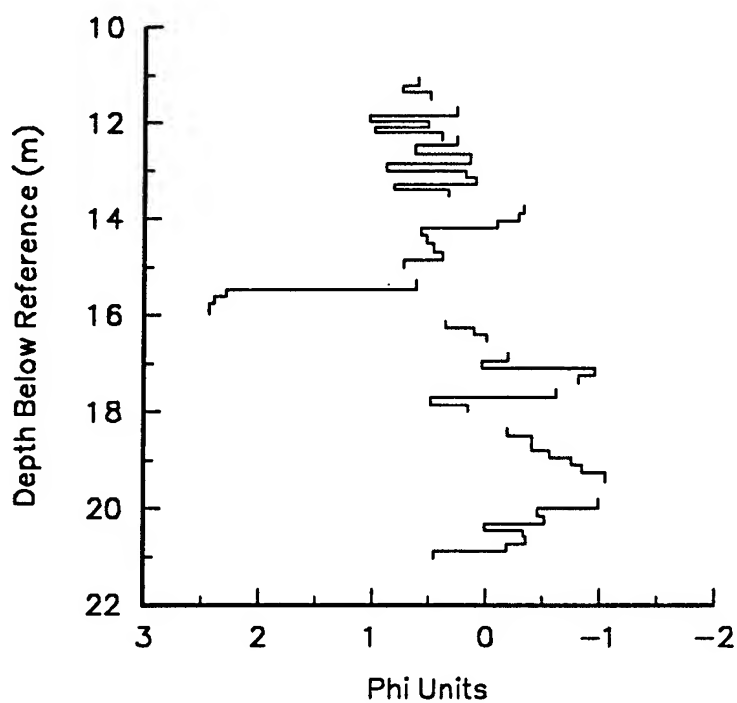


Figure 22. - Mean grain size (in phi units) versus depth for GEMS well 5-1.

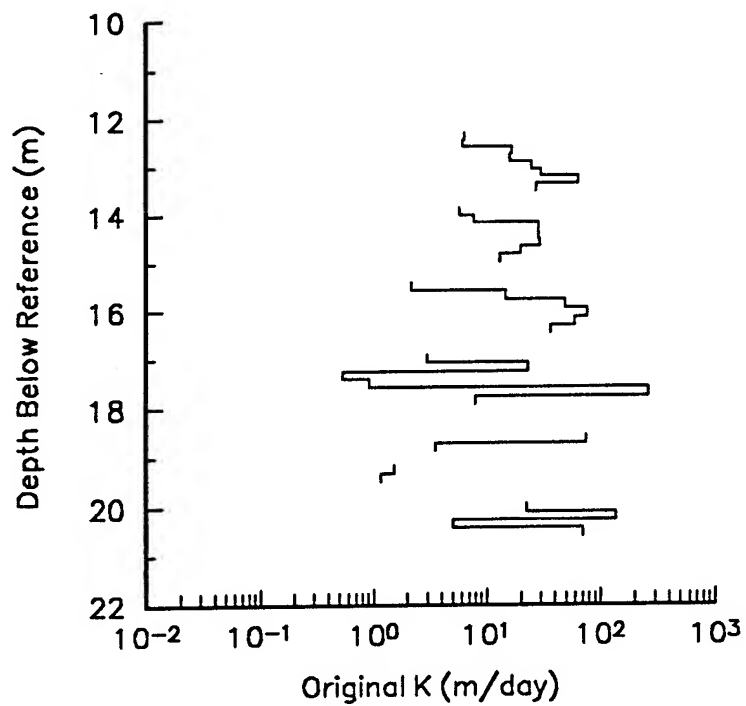


Figure 23. - Original hydraulic conductivity versus depth for GEMS well 7-1.

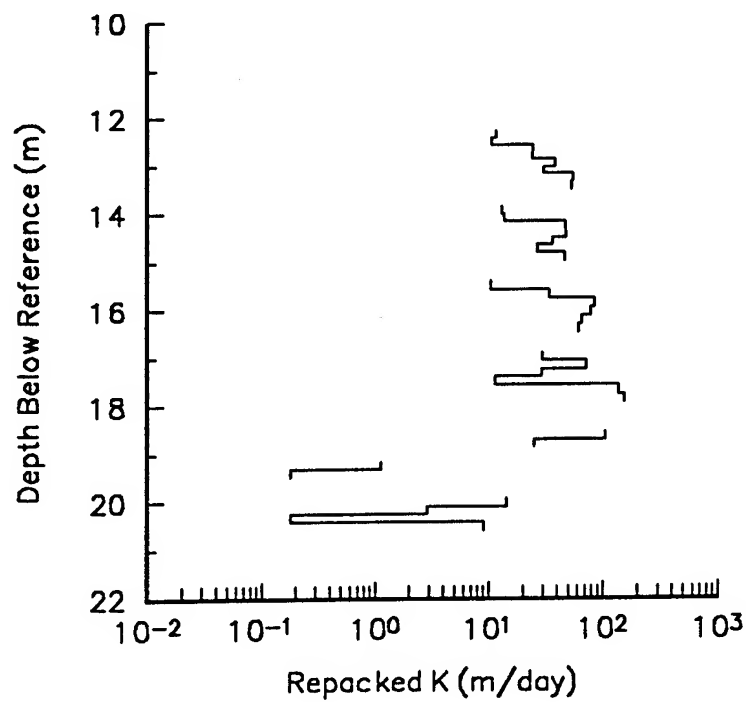


Figure 24. - Repacked hydraulic conductivity versus depth for GEMS well 7-1.

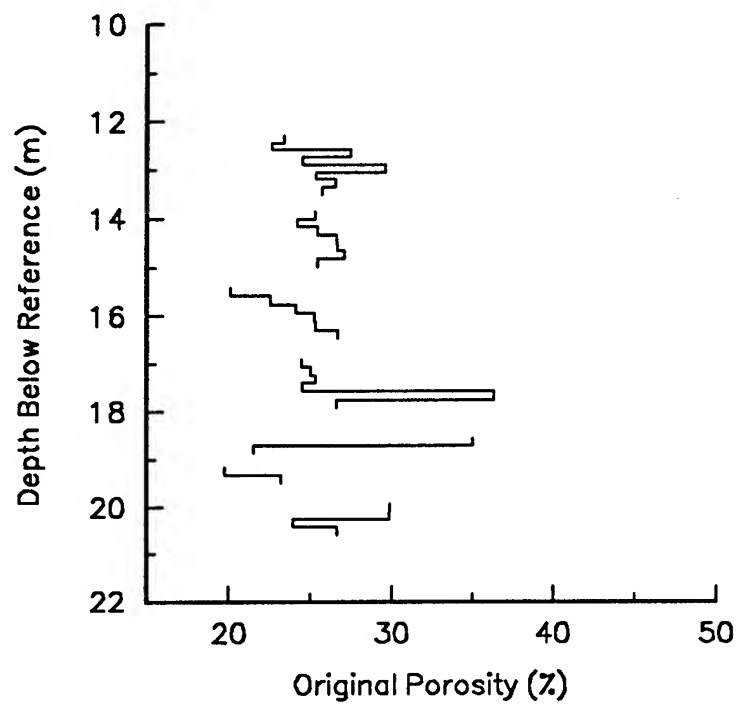


Figure 25. - Original porosity versus depth for GEMS well 7-1.

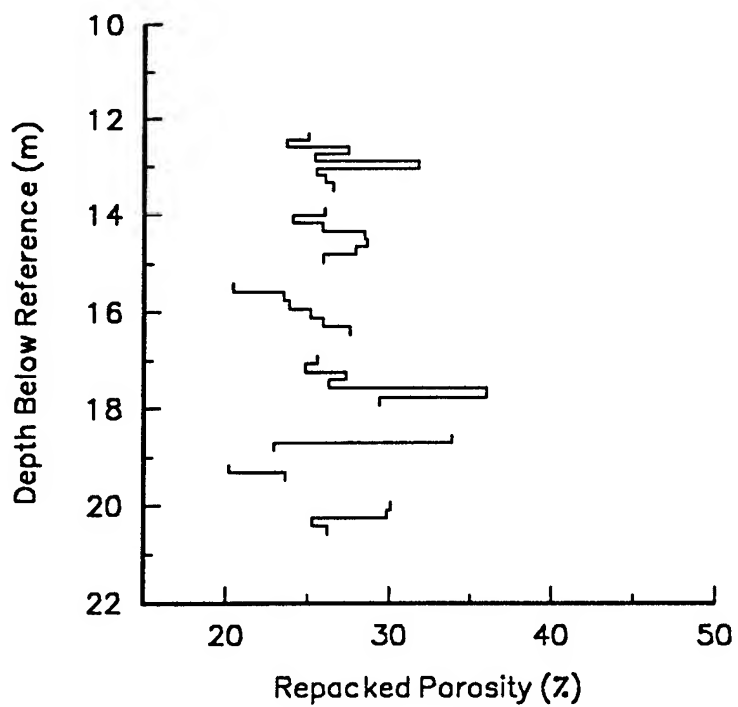


Figure 26. - Repacked porosity versus depth for GEMS well 7-1.

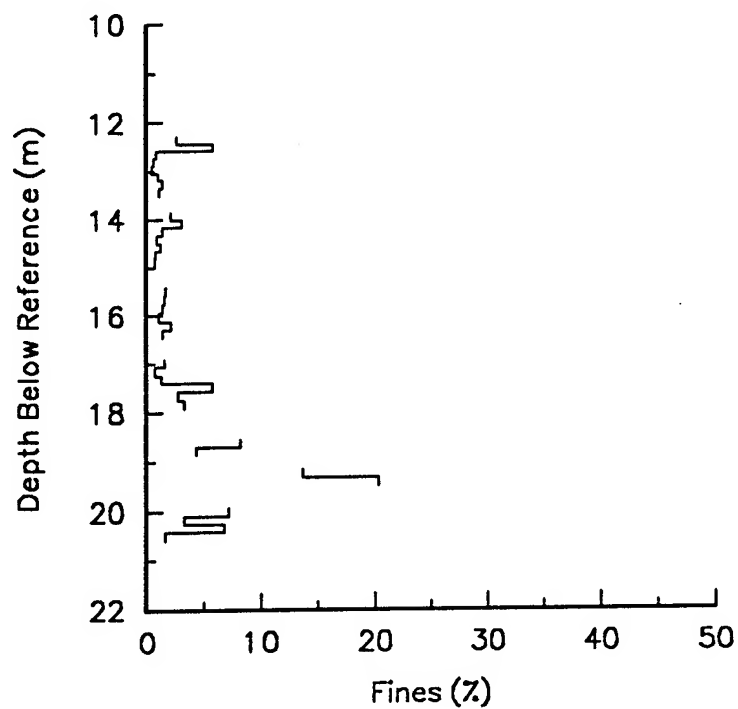


Figure 27. - Percent fines (<.053 mm) versus depth for GEMS well 7-1.

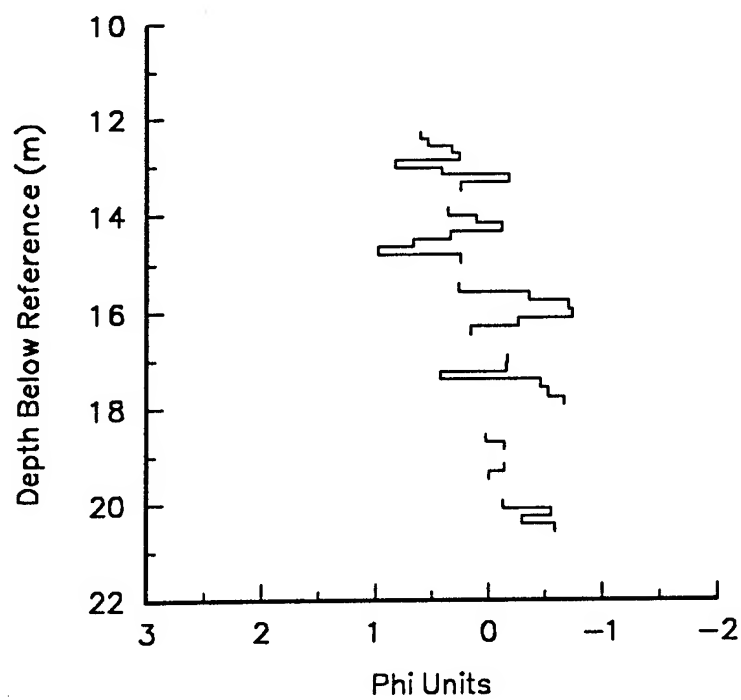


Figure 28. - Mean grain size (in phi units) versus depth for GEMS well 7-1.

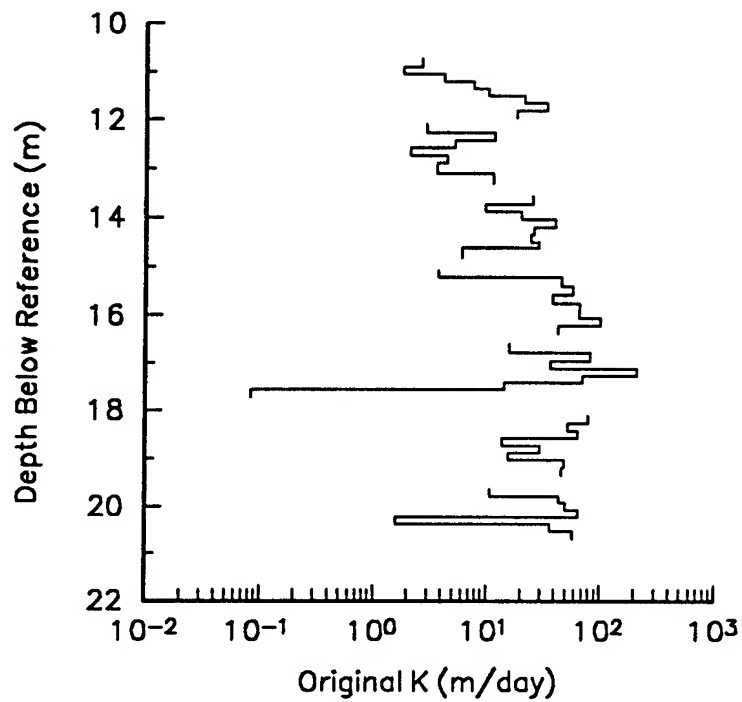


Figure 29. - Original hydraulic conductivity versus depth for GEMS well 8-1.

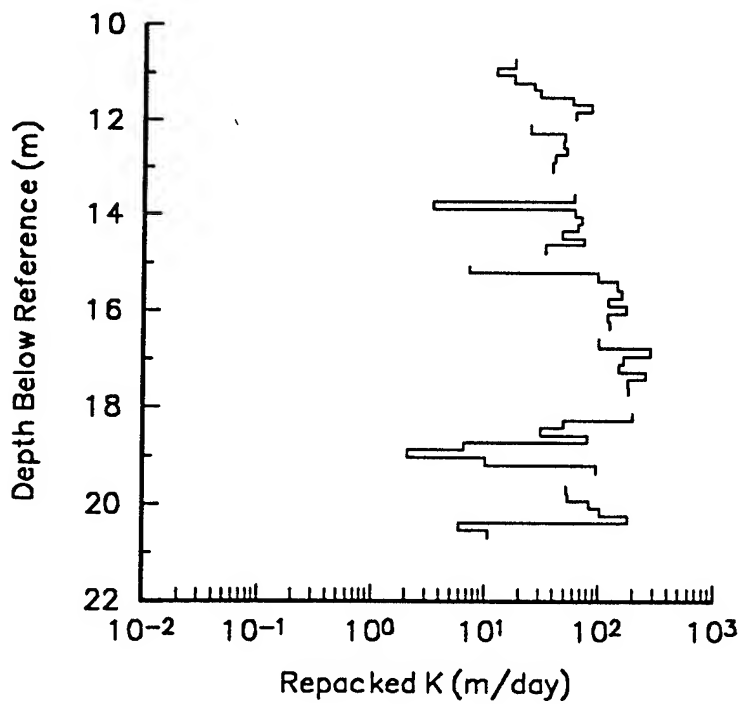


Figure 30. - Repacked hydraulic conductivity versus depth for GEMS well 8-1.

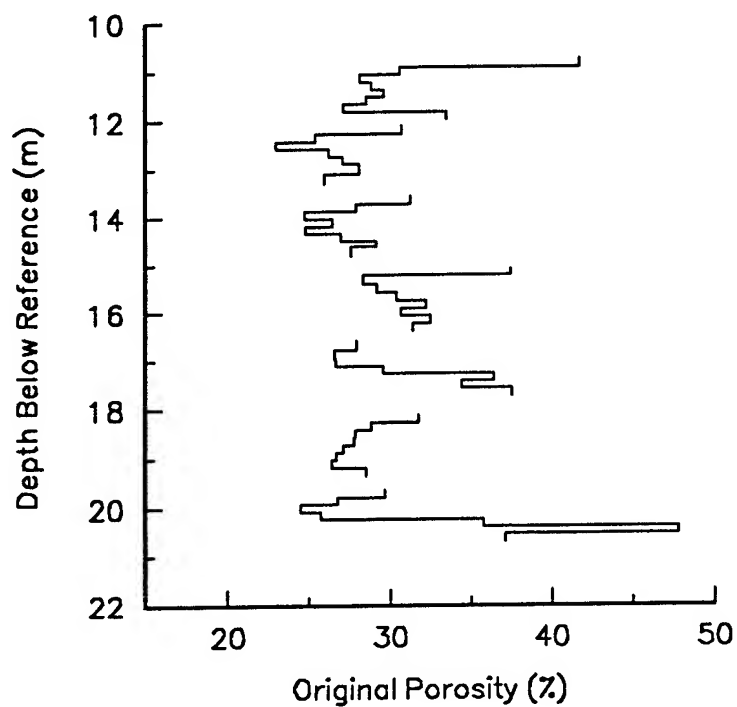


Figure 31. - Original porosity versus depth for GEMS well 8-1.

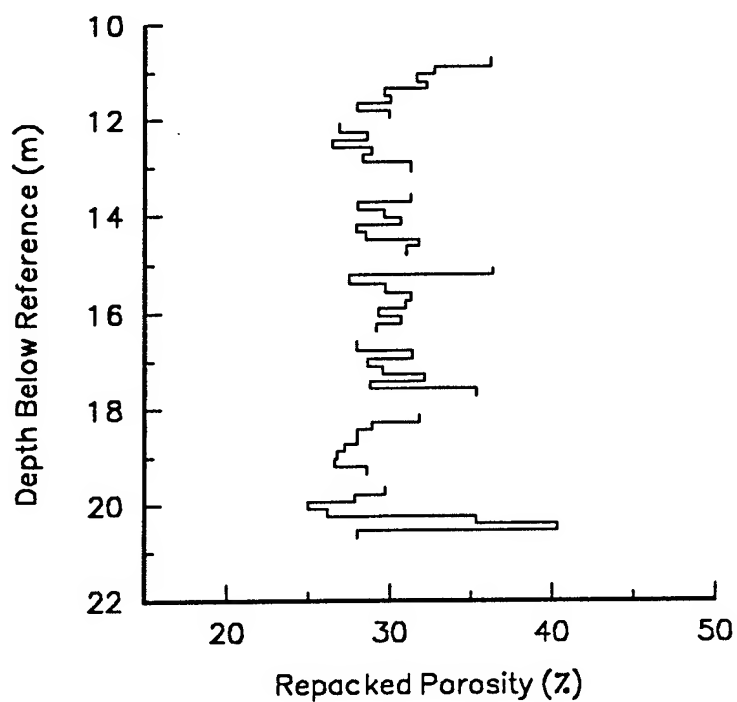


Figure 32. - Repacked porosity versus depth for GEMS well 8-1.

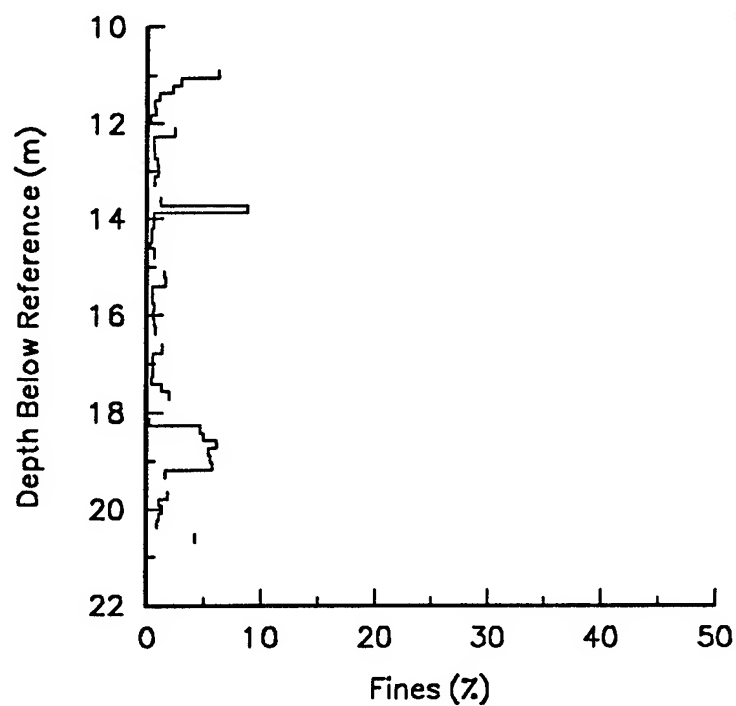


Figure 33. - Percent fines (<.053 mm) versus depth for GEMS well 8-1.

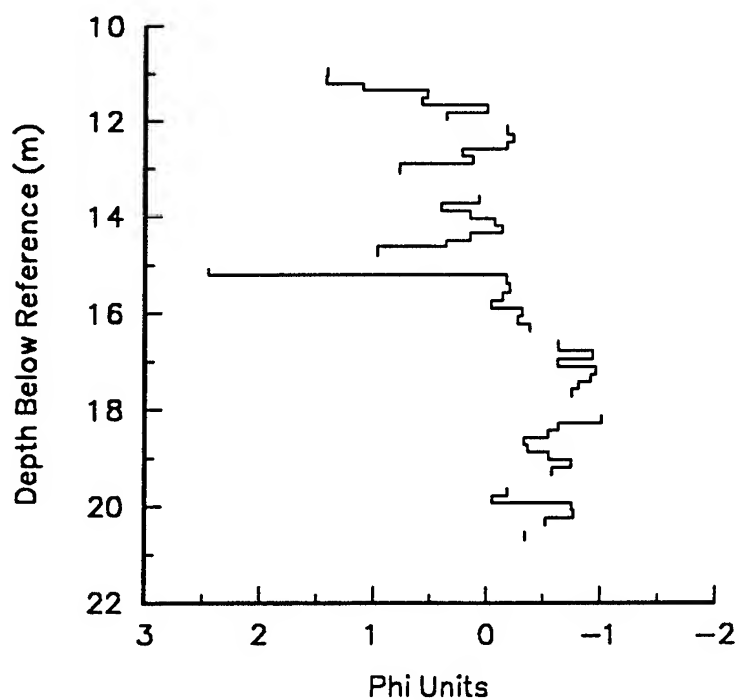


Figure 34. - Mean grain size (in phi units) versus depth for GEMS well 8-1.

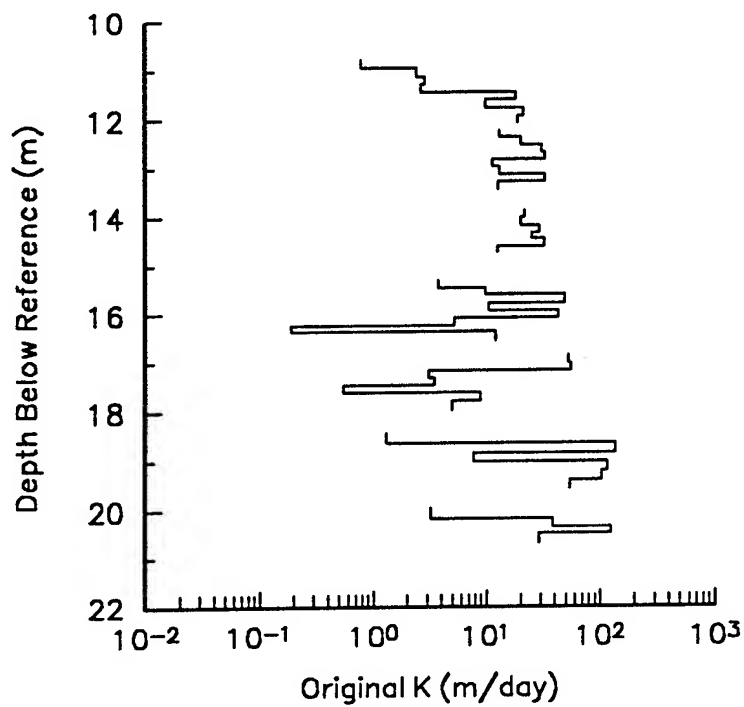


Figure 35. - Original hydraulic conductivity versus depth for GEMS well 9-1.

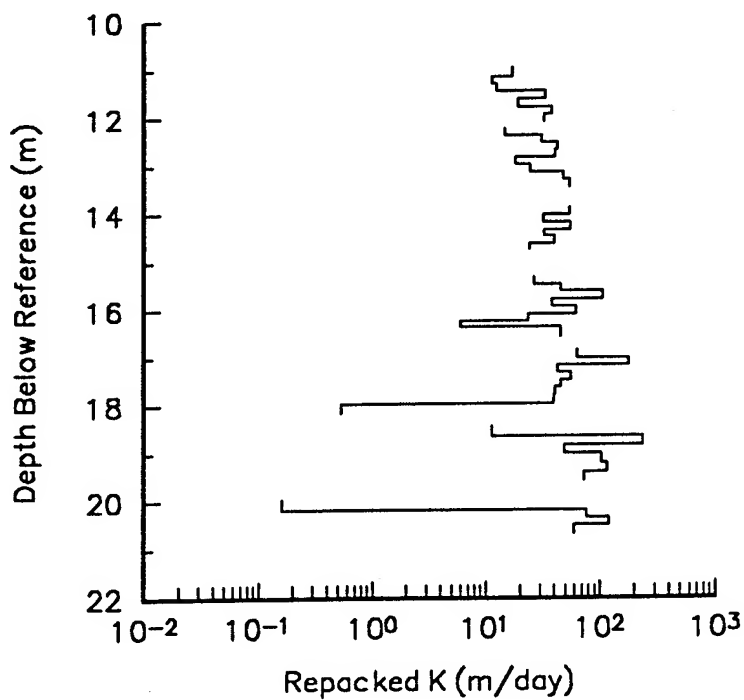


Figure 36. - Repacked hydraulic conductivity versus depth for GEMS well 9-1.

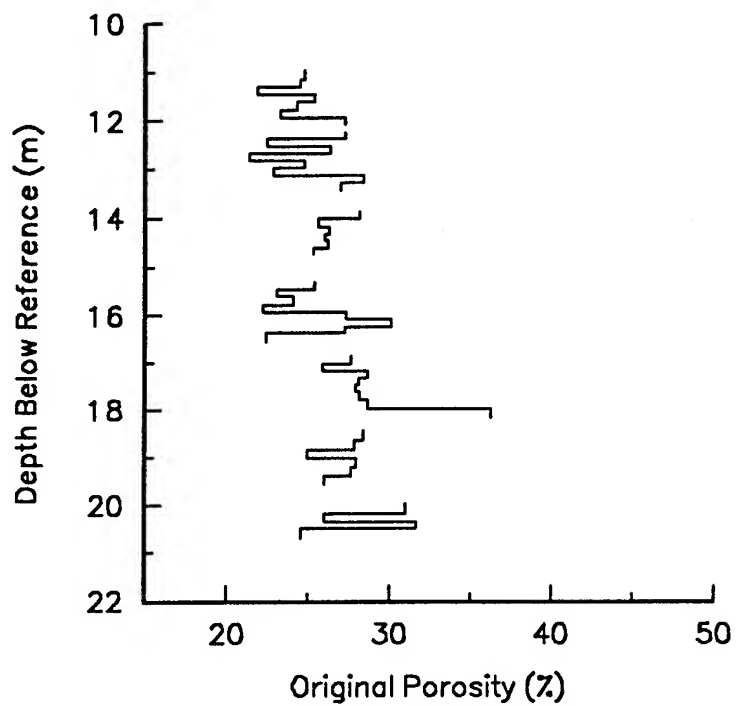


Figure 37. - Original porosity versus depth for GEMS well 9-1.

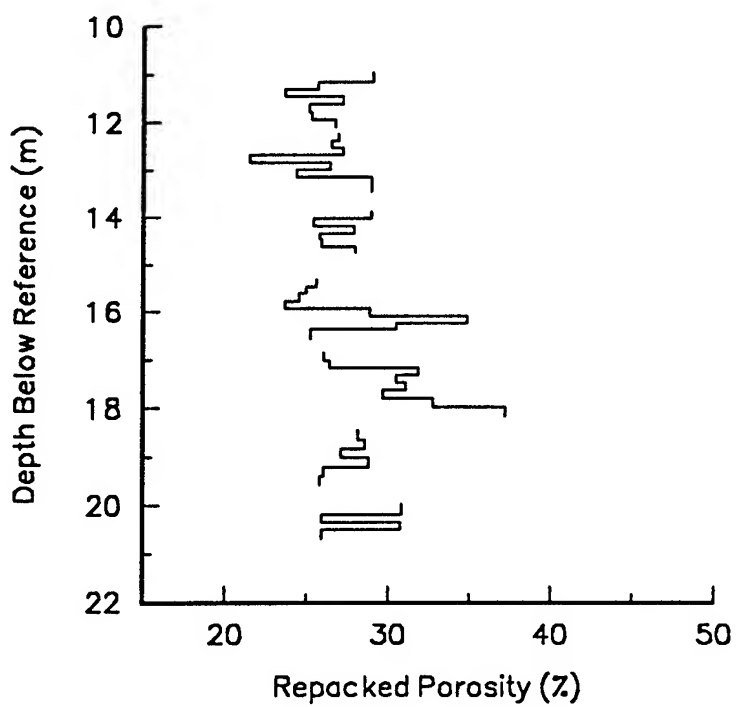


Figure 38. - Repacked porosity versus depth for GEMS well 9-1.

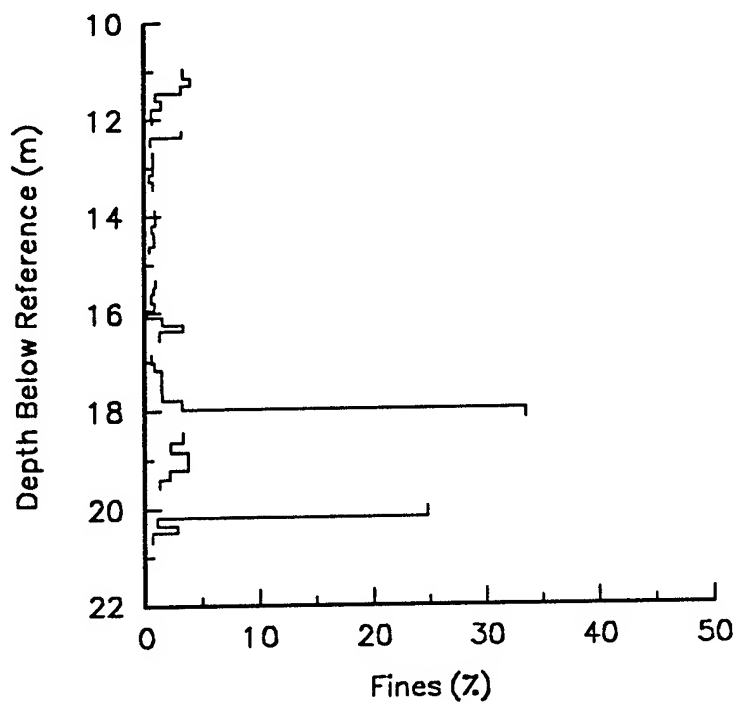


Figure 39. - Percent fines (<.053 mm) versus depth for GEMS well 9-1.

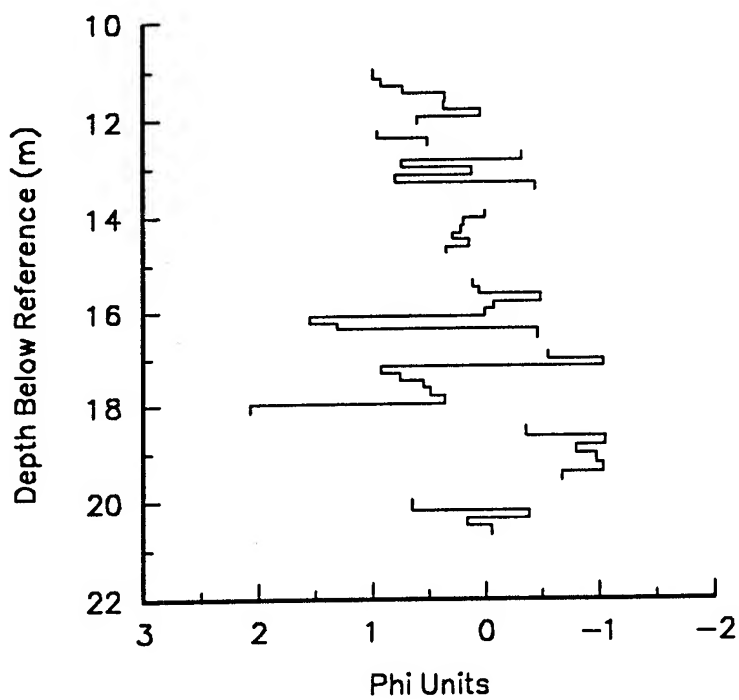


Figure 40. - Mean grain size (in phi units) versus depth for GEMS well 9-1.

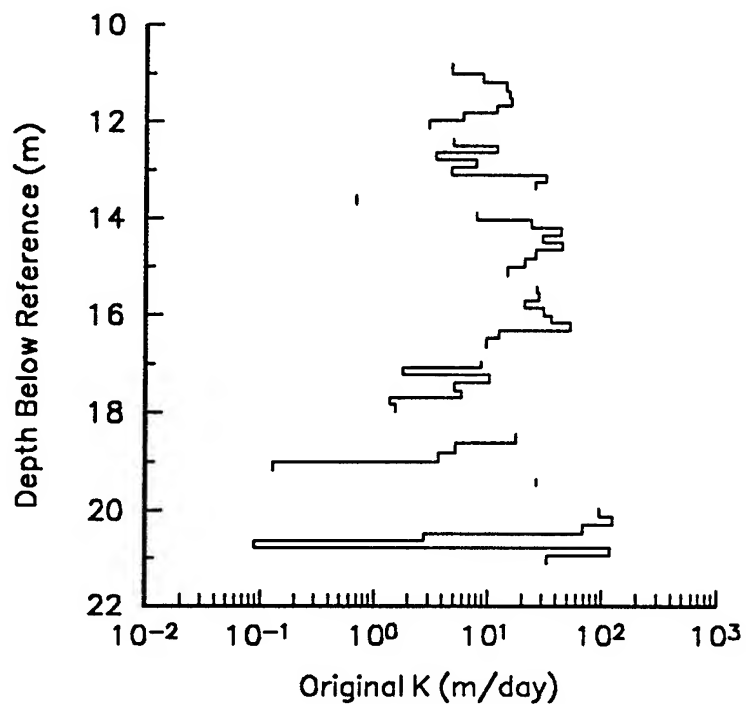


Figure 41. - Original hydraulic conductivity versus depth for GEMS well 10-1.

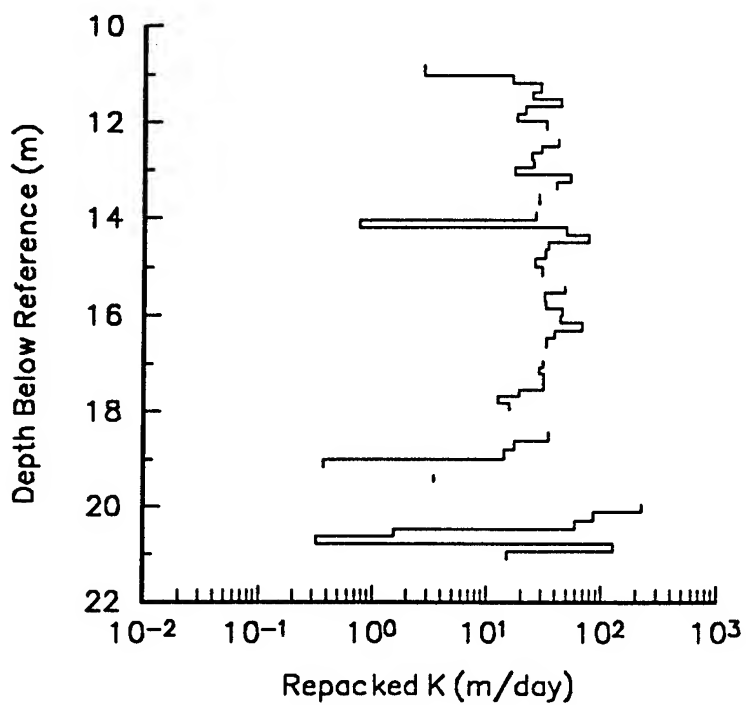


Figure 42. - Repacked hydraulic conductivity versus depth for GEMS well 10-1.

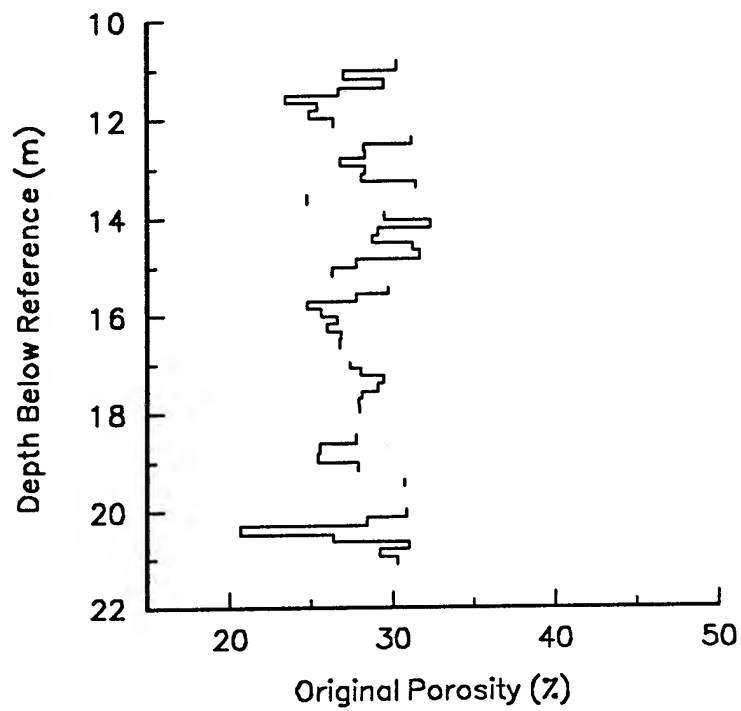


Figure 43. - Original porosity versus depth for GEMS well 10-1.

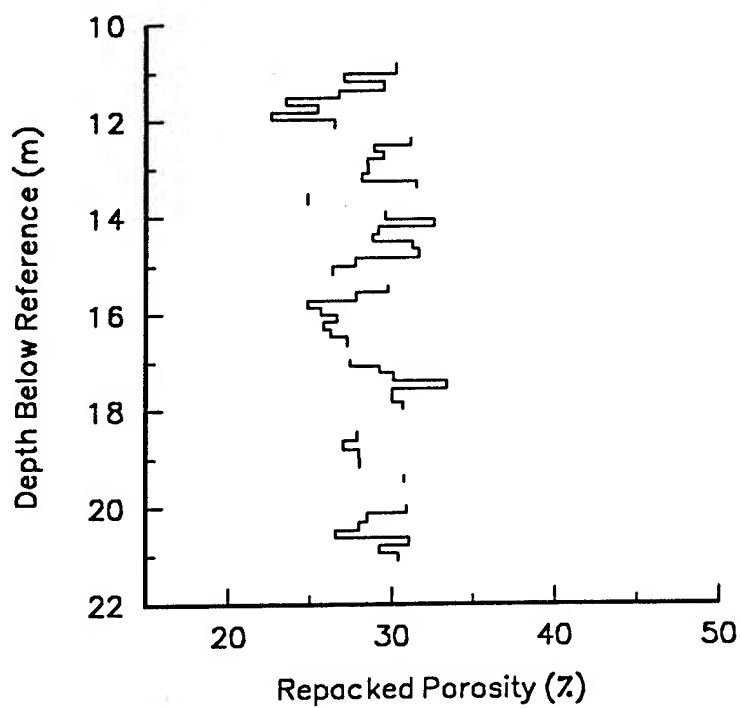


Figure 44. - Repacked porosity versus depth for GEMS well 10-1.

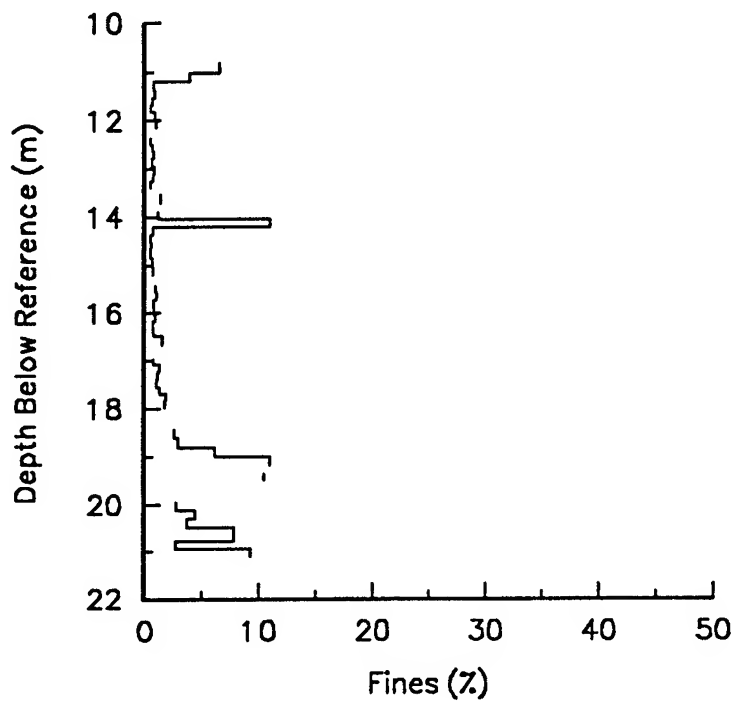


Figure 45. - Percent fines (<.053 mm) versus depth for GEMS well 10-1.

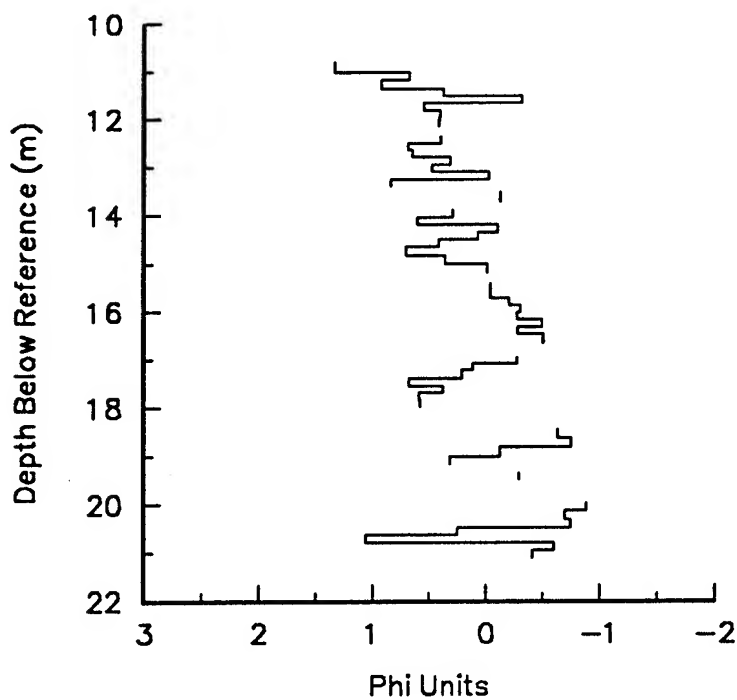


Figure 46. - Mean grain size (in phi units) versus depth for GEMS well 10-1.

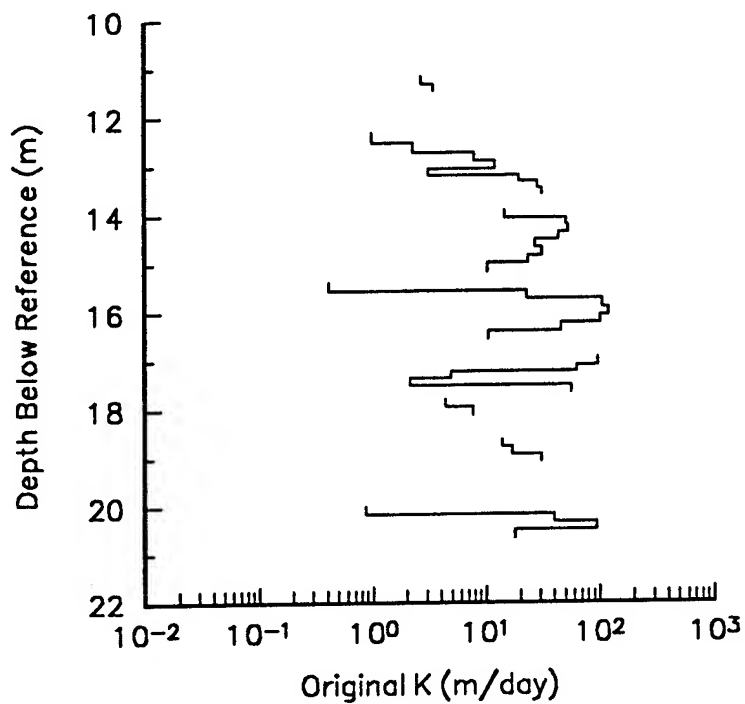


Figure 47. - Original hydraulic conductivity versus depth for GEMS well 11-1.

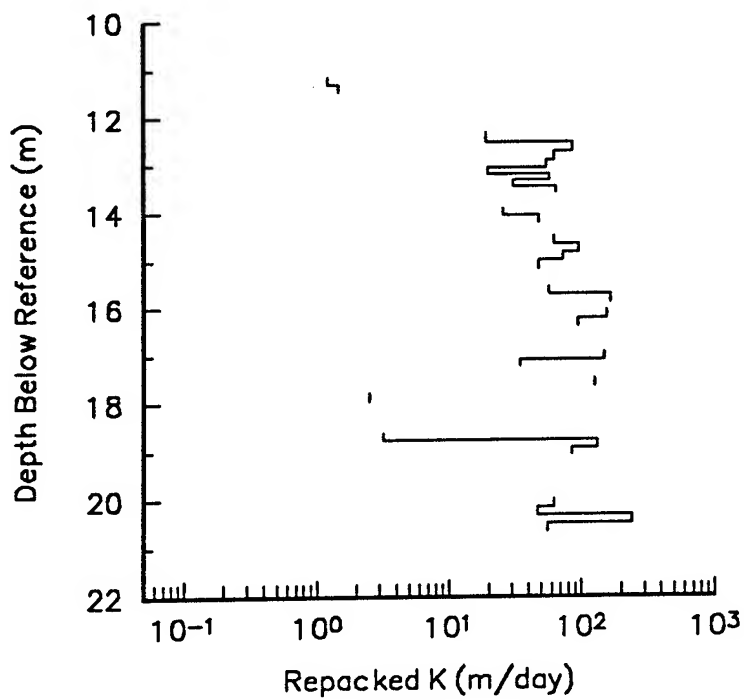


Figure 48. - Repacked hydraulic conductivity versus depth for GEMS well 11-1.

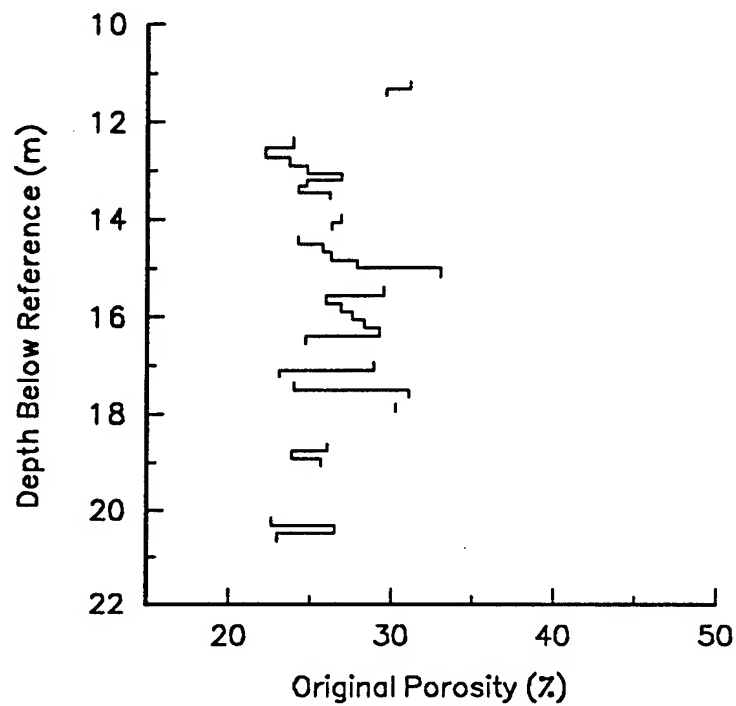


Figure 49. - Original porosity versus depth for GEMS well 11-1.

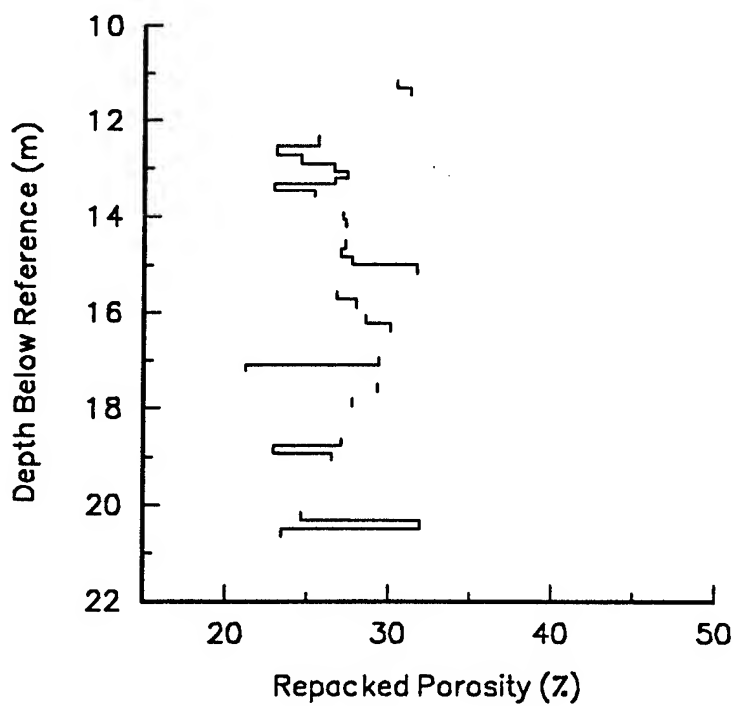


Figure 50. - Repacked porosity versus depth for GEMS well 11-1.

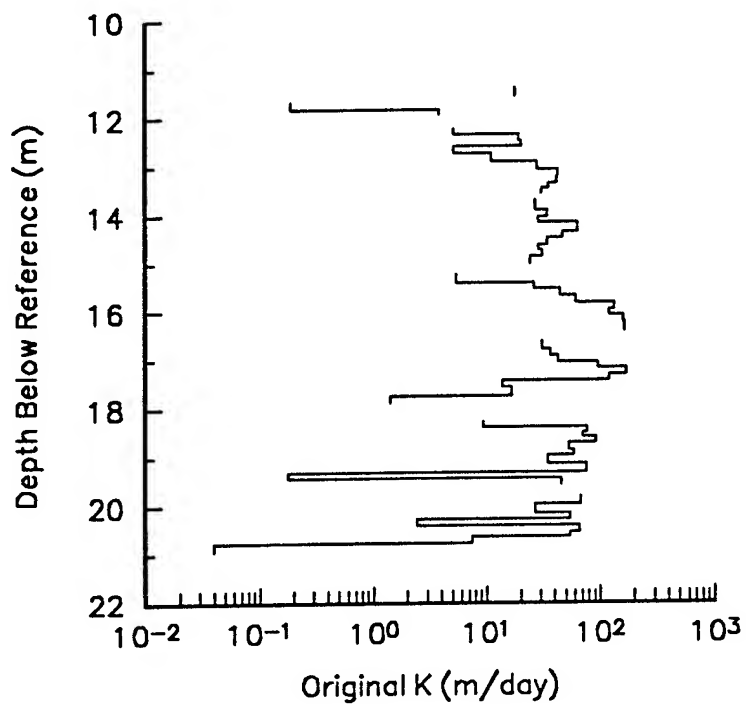


Figure 51. - Original hydraulic conductivity versus depth for GEMS well TMO-1.

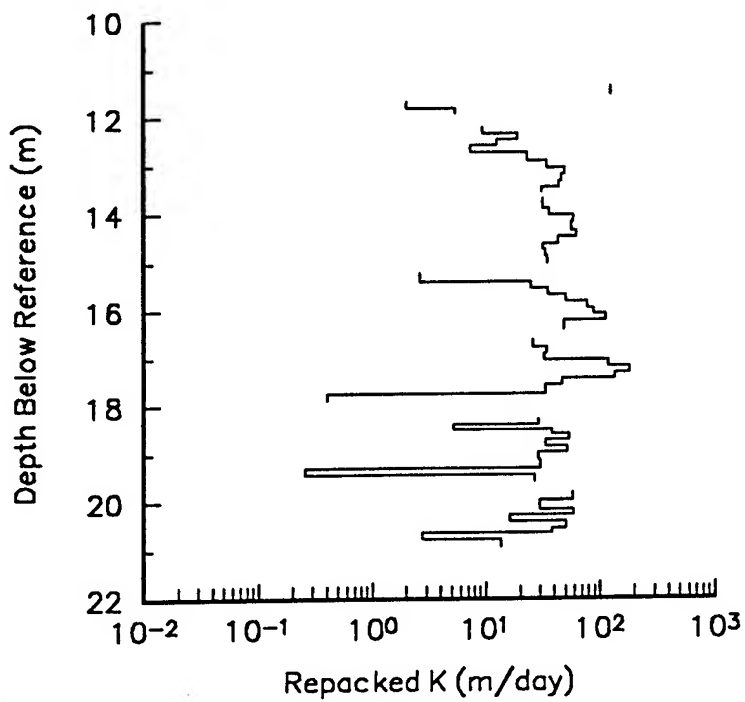


Figure 52. - Repacked hydraulic conductivity versus depth for GEMS well TMO-1.

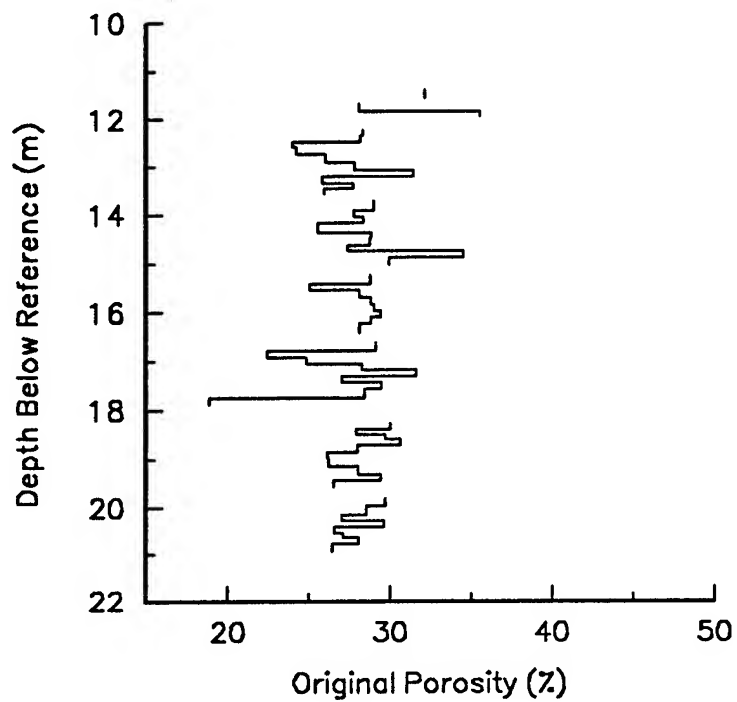


Figure 53. - Original porosity versus depth for GEMS well TMO-1.

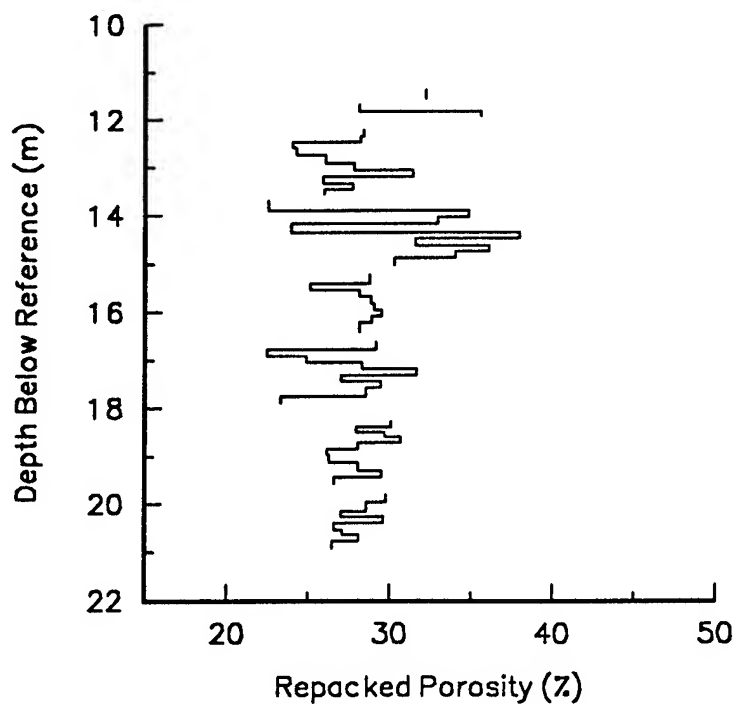


Figure 54. - Repacked porosity versus depth for GEMS well TMO-1.

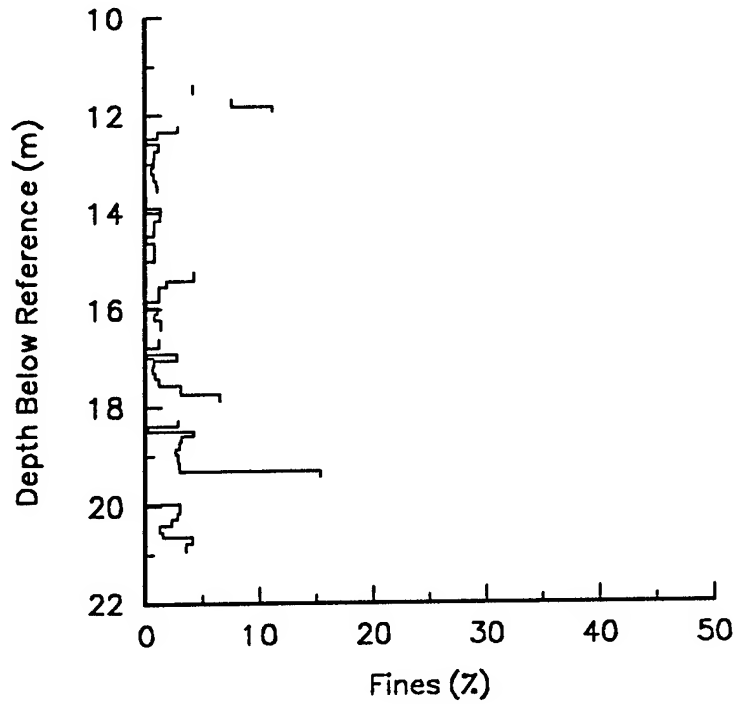


Figure 55. - Percent fines (<.053 mm) versus depth for GEMS well TMO-1.

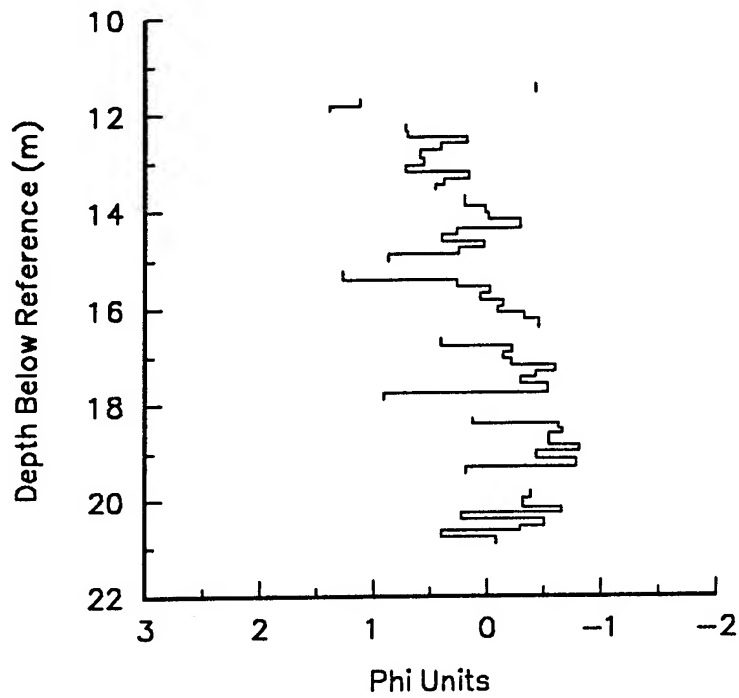


Figure 56. - Mean grain size (in phi units) versus depth for GEMS well TMO-1.

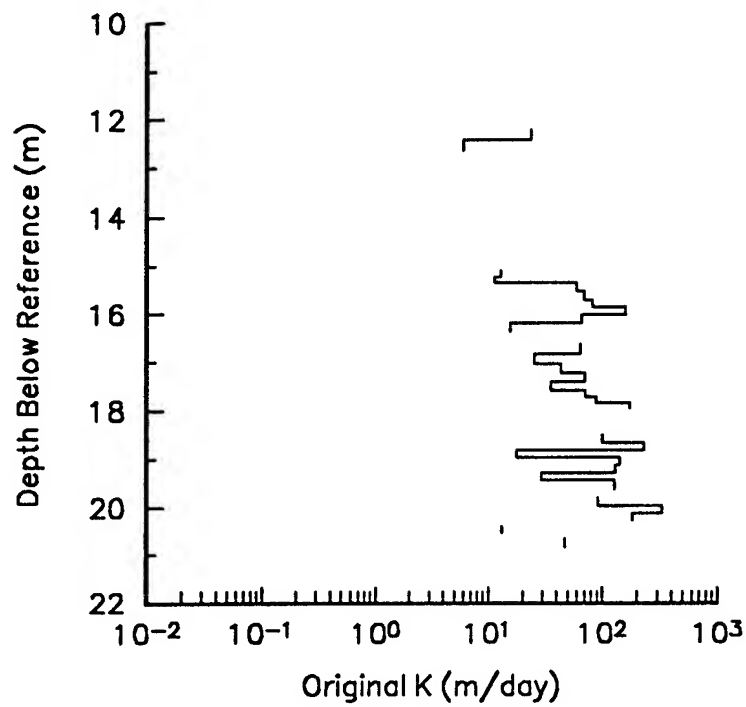


Figure 57. - Original hydraulic conductivity versus depth for GEMS well TME-8.

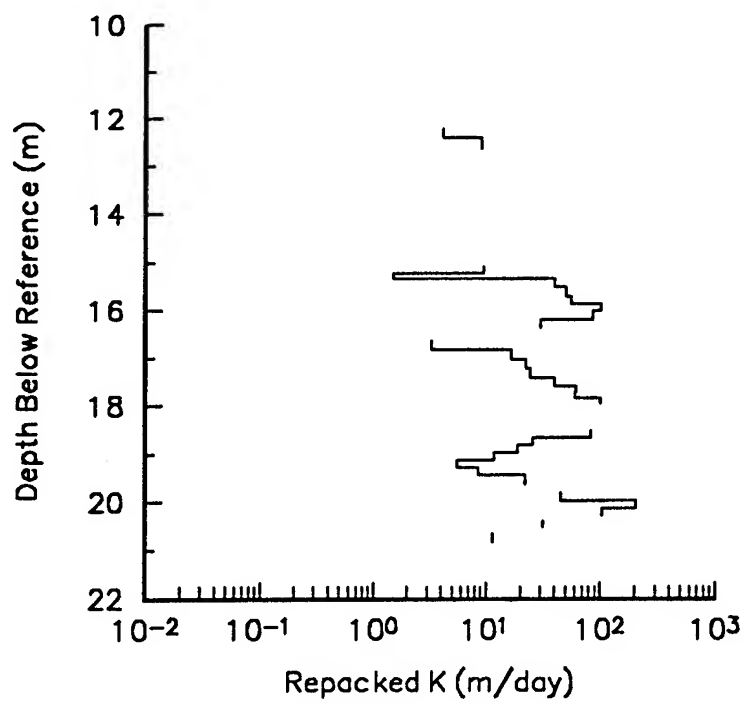


Figure 58. - Repacked hydraulic conductivity versus depth for GEMS well TME-8.

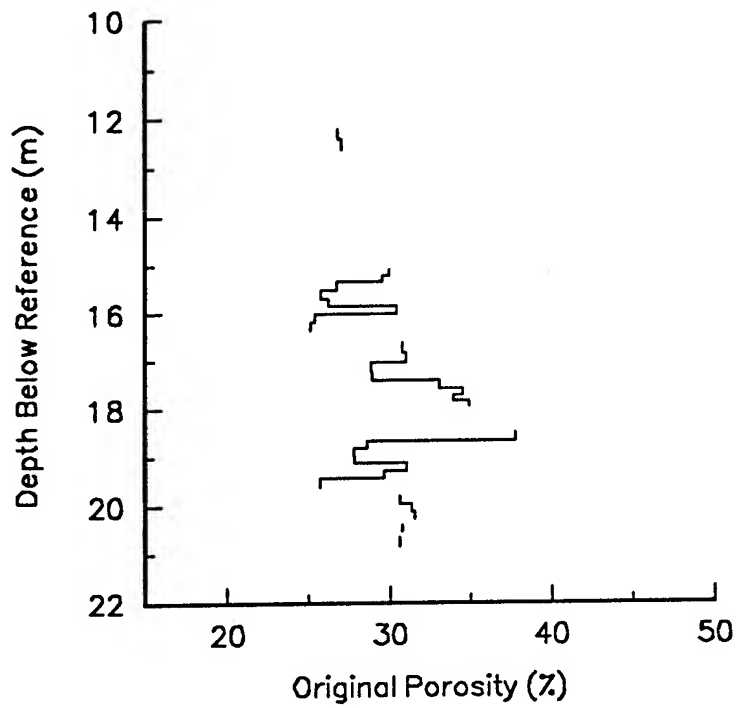


Figure 59. - Original porosity versus depth for GEMS well TME-8.

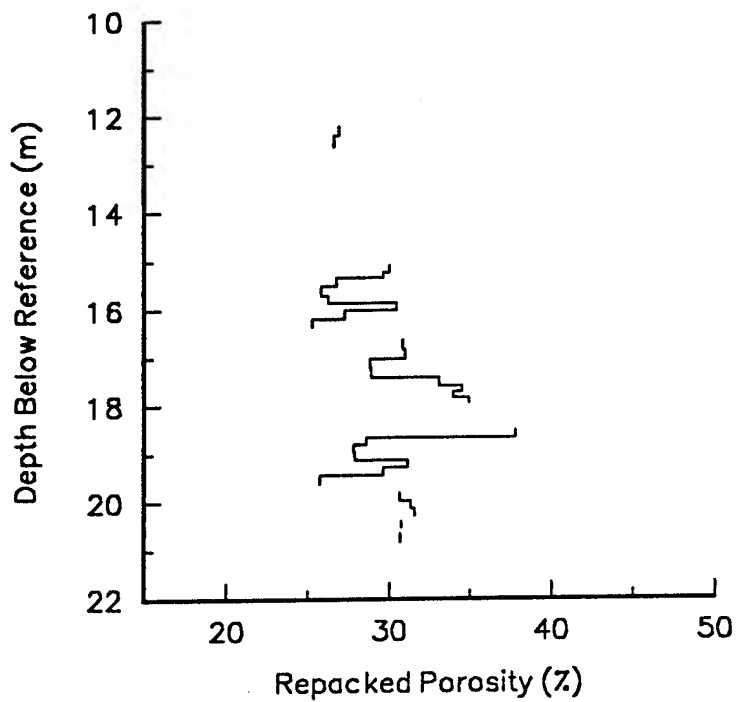


Figure 60. - Repacked porosity versus depth for GEMS well TME-8.

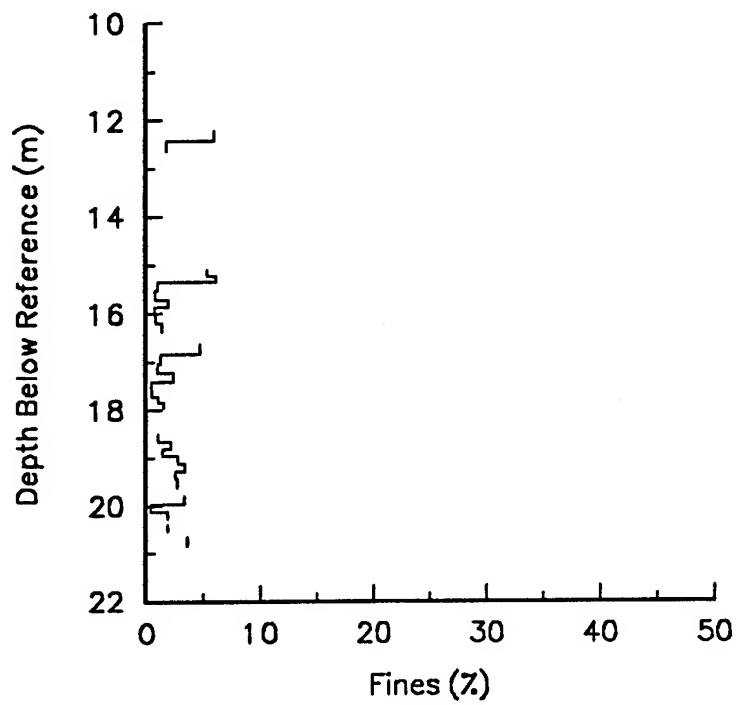


Figure 61. - Percent fines (<.053 mm) versus depth for GEMS well TME-8.

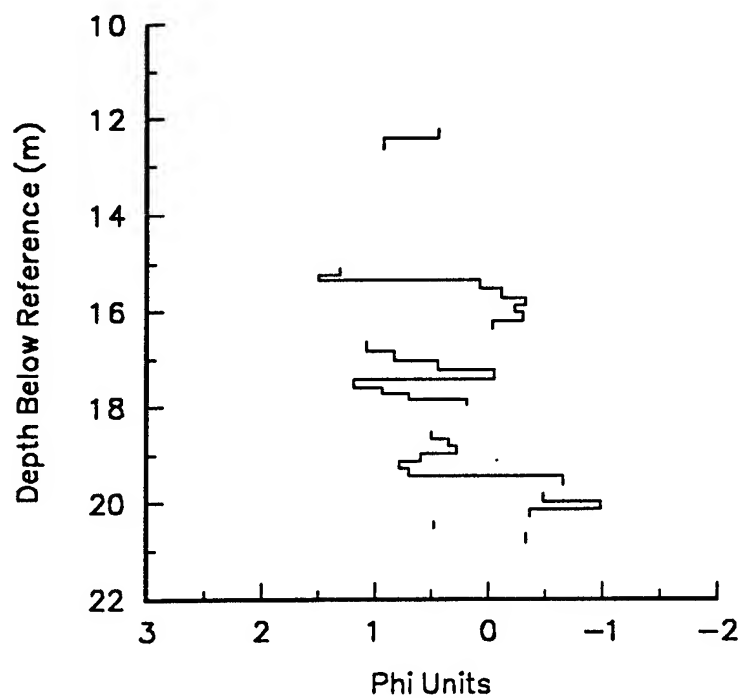


Figure 62. - Mean grain size (in phi units) versus depth for GEMS well TME-8.

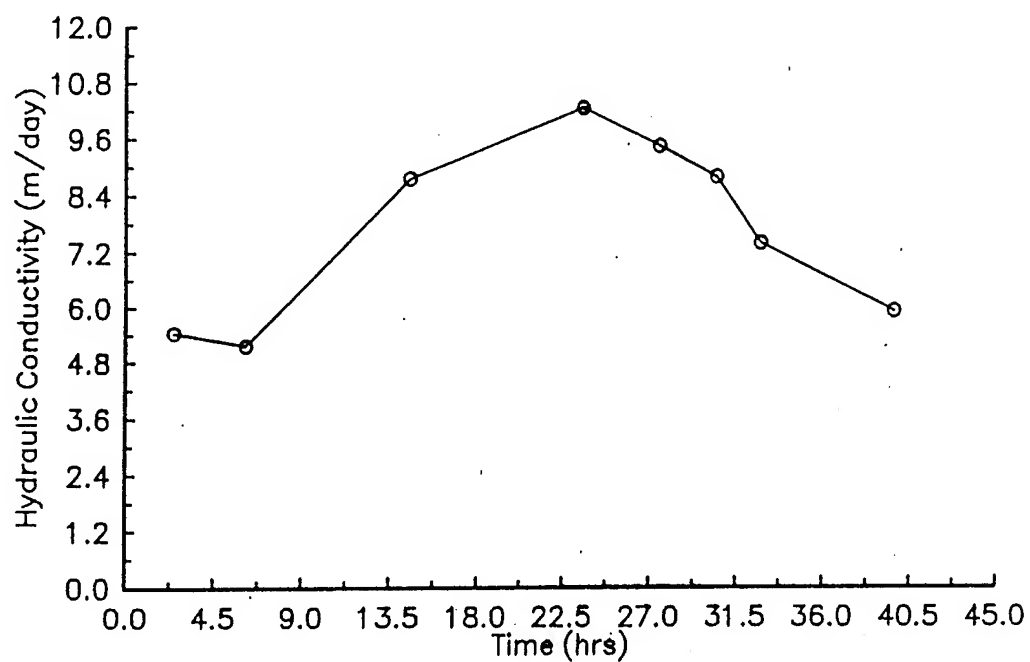


Figure 63. - Changes in hydraulic conductivity with time (Segment 5, sample 24, well 00-1).

Changes in Alkalinity, pH and pe

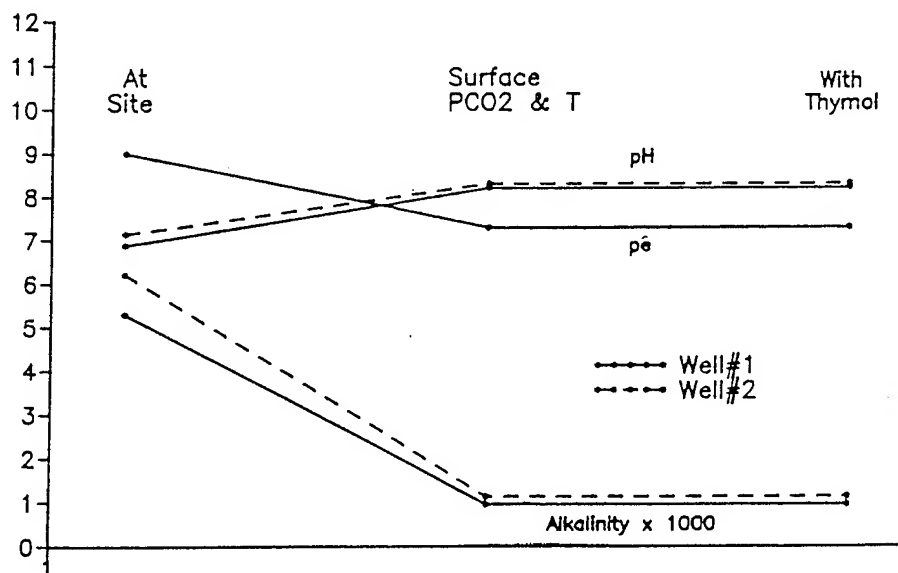


Figure 64. - Changes in alkalinity, pH, and pe.

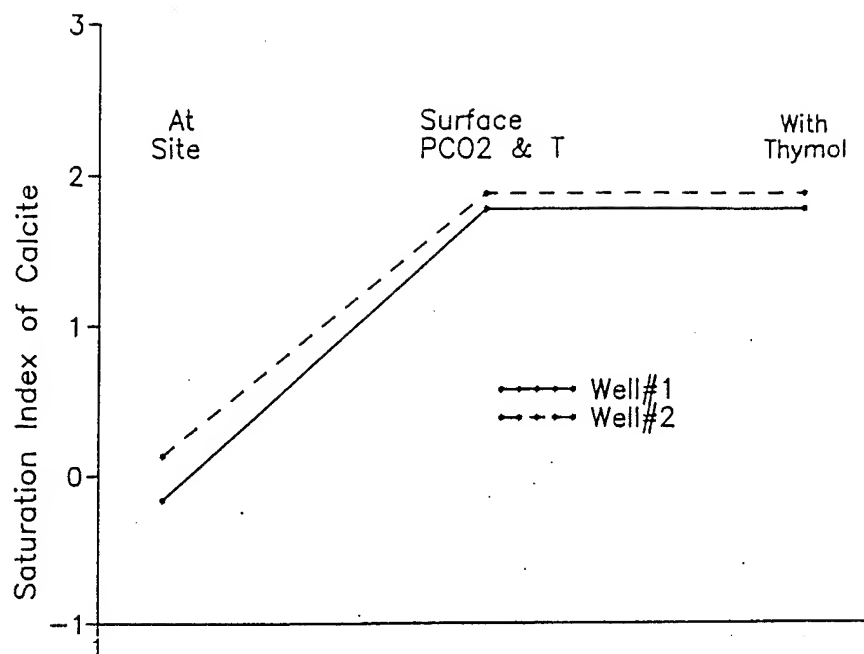


Figure 65. - Changes in the saturation index of calcite.
 (SI = \log ion activity product / equilibrium constant)

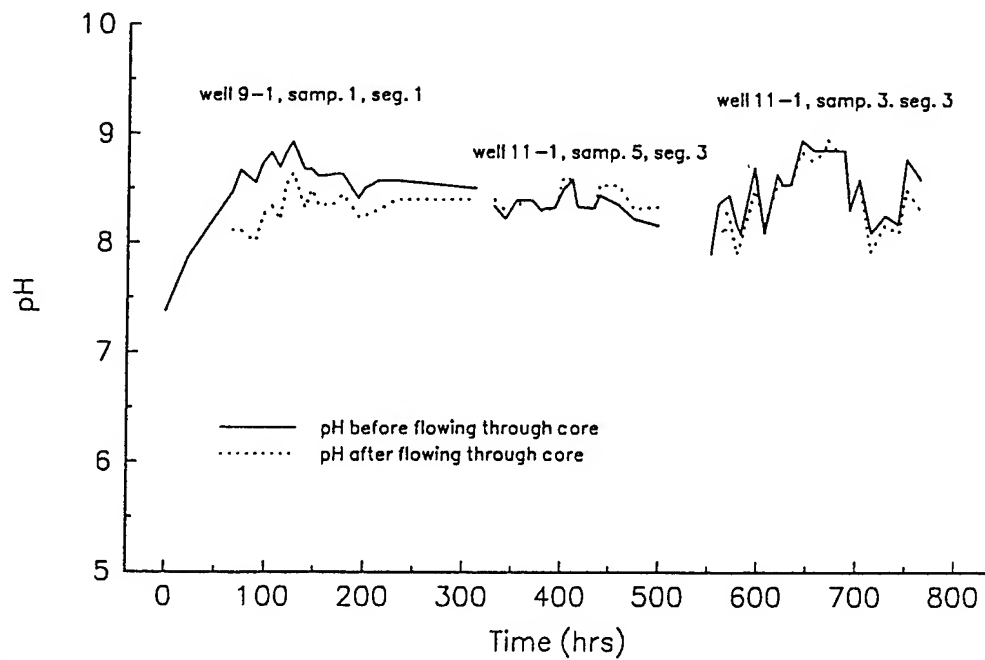


Figure 66. - pH of water versus time.

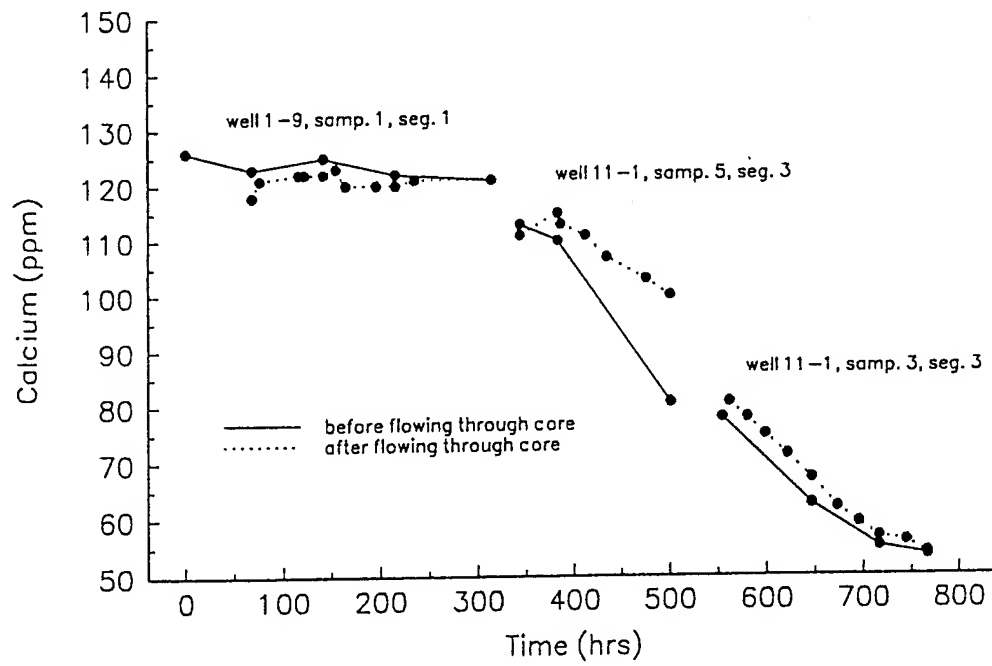


Figure 67. - Calcium content of water versus time.

C. AQUEOUS GEOCHEMISTRY AT GEMS

Introduction

At the Geohydrologic Experimental and Monitoring Site (GEMS) near Lawrence, Kansas, several experiments have been run using the chemistry of the ground water to reveal information about aquifer properties. The experiments were done on the wells and multi-level samplers which are screened at different levels of the 21-m thick Kansas River alluvium and in the underlying bedrock, a Paleozoic sandstone (Shawnee Group). During the summer of 1991, a subset of the wells completed in the alluvium, as well as the bedrock, well served as preliminary test holes to evaluate geochemical variations in the ground water at the site. Based on the results of chemical analyses of these samples, water samples collected during a two-hour pumping test on the bedrock well during April, 1992, were then interpreted in terms of cross flow from the alluvium to the bedrock aquifer. In October, 1992, a longer pumping test was run (seven hours) in order to see if the rate of leakage (as indicated by the ground-water chemistry) from the alluvial aquifer to the bedrock aquifer would stabilize. Also, throughout 1992, a broader geochemical survey was done at the site in order to assess geochemical variability in the ground water. In 1993-4, evaluation of the temporal variations of the ground-water chemistry was accomplished by doing a simple statistical analysis of the variability of the ground-water chemistry and by assessing the implications for the upcoming induced-gradient tracer test. Finally, during the extension period, samples were collected from the newly-installed multi-level samplers (MLS) in order to examine small-scale vertical variations in ground-water chemistry, as well as variations along the length of the multi-level sampler network. In addition, the presence of dissolved Br was found at the site. An evaluation of the amount of Br present was then made because of the implications that it has on the use of KBr as a tracer of ground-water movement during the tracer test.

Conclusions from the various aspects of the geochemical characterization are:

- 1) There is measurable leakage from the alluvial aquifer into the bedrock aquifer after a relatively short pumping time (less than one hour at a pumping rate of about 8 gpm);
- 2) Dissolved nitrate is a good natural tracer of the leakage water at this site because of its absence in the bedrock aquifer;
- 3) There is vertical, spatial, and temporal variability in the ground-water chemistry of the alluvial aquifer at GEMS. Most of the variability is found in the nitrate and sulfate concentrations, and this variability is up to 200% relative standard deviation from the mean;

4) The MLS's provide more detailed and slightly different information about the chemistry of the ground-water at the site because they sample more restricted intervals and do not produce a permeability-weighted water sample, as does a well screened over some finite interval;

5) Low concentrations of dissolved Br are present in parts of the alluvial aquifer. The presence of small amounts of natural Br means that Br concentrations of less than about 1 mg/L Br measured during the tracer test are not interpretable.

This final report summarizes the sampling and analytical methods, and significant results from the various aspects of the geochemical investigation of the site. The methodology for all experiments comprises one section, discussion of chemical variability at the site comprises a second section, discussion of leakage from the alluvial aquifer in the bedrock aquifer comprises a third section, and discussion of background Br concentrations comprises the final section.

Methodology

Water Sampling and On-Site Processing

High-yield wells were pumped until the water temperature stabilized. At this time, approximately 1.5 L of water were collected in a half-gallon polyethylene jug for further processing. The pump was then stopped and temperature and pH measured in a 1000 mL beaker. Low-yield wells were bailed with a Teflon® bailer until nearly dry (less than 0.3 m of water remained) and then allowed to recover for a few hours to overnight. Approximately 1.5 L of water were bailed and stored in a half-gallon polyethylene jug for further processing. All samples were gravity filtered through 0.45 μ filters immediately after collection. A 50-mL aliquot was titrated for total alkalinity using 0.02 N H₂SO₄ while the rest of the sample was filtering during the first sampling; for later samplings, titrations were done in the lab. One or two 250-mL low-density polyethylene bottles (LDPE) were filled completely with water, sealed, and stored on ice. One or two more bottles were filled with 250 mL of sample, 5 mL of concentrated HNO₃ immediately added, and the sealed bottles stored on ice.

Procedures for collecting samples during the pumping tests to assess leakage between the alluvial and bedrock aquifers are similar to those described above, except that duplicate bottles were collected for the filtered samples, and alkalinity titrations were not done.

MLS's were pumped on separate days with a 10-channel peristaltic pump, by pumping first a set of ten and then a set of 7 ports for five to seven minutes. Samples

were then collected into previously marked, clean polypropylene vials, the sample production time taking about 20 to 40 seconds. Samples were immediately filtered through 0.45 μ Acrodisc® syringe filters into clean polypropylene vials. Filtration required one to five syringe filters, depending on the amount of suspended solids in the water. Time elapsed between sample production and finish of filtering for all samples was about 90 minutes for all three multi-level samplers.

Laboratory Methods

Selected samples were titrated with 0.02N H₂SO₄ for alkalinity, the end point of the titration taken as the slope maximum in the vicinity of pH 4.5 on the titration curve. pH was measured in the lab with a Fisher Accumet® Model 955 pH/mV meter with a standard polymer-body gel-filled combination electrode (Ag/AgCl reference). In the field, pH was measured on selected samples with a Corning® PS 15 field pH meter.

Specific conductivity was measured on selected MLS samples in the field using a Horiba® B-173 field conductivity meter. Specific conductance reported on all other samples is calculated from total dissolved solids.

The anions F, Cl, SO₄ and NO₃ were determined in duplicate by ion exclusion chromatography using a Dionex 4000i series ion chromatograph, using an AS4A exchange column, AG4A guard column, and a NG1 guard column. The instrument is equipped with a conductivity detector, and suppression of background conductivity was achieved using an anion micro-membrane suppressor (AMMS-II), continuously regenerated with 25 mM H₂SO₄ at a flow rate of 3 mL/min. The eluent used was 1.8 mM Na₂CO₃ and 1.7 mM NaHCO₃ at a flow rate of 2 mL/min. Sample loop size was 25 μ L. Relative standard deviations (standard deviation/mean) and precisions of the duplicate samples were generally less than 5% except for F and Cl which are strongly affected by the water dip. Spiking the samples with concentrated eluent (EPA, 1984; Test Method 300.0) helped but did not completely eliminate this problem. Tests were also made to assess the linearity of the anion calibration curves below the lower standard used to calibrate the instrument. These tests also show that Cl is difficult to determine at low concentrations (less than 1 mg/L when the lower of two standards is 2 mg/L) either because the water dip results in false positive results or because low levels of Cl are present in the distilled-deionized water used to make up the solutions used in the test. During the second pumping test, samples were reanalyzed two weeks after the first analysis as well, to check for stability of NO₃-N in the samples. There was no significant difference between these two sets of analyses.

The cations Ca, Mg, Na, and K, for the first two years of the project, were determined by atomic absorption spectrometry using a Perkin-Elmer 2380 Spectrophotometer. Routine methods were used (Fishman and Friedman, 1989) and samples were analyzed six times in order to achieve high precision. Subsequent determinations were done by suppressed conductivity using IONPAC CS12 and CG12, and a cation micromembrane suppressor (CMMS-II). Sample loop size was 50 μ L. Eluent was 20 mM HCl and the suppressor was continuously regenerated with 100 mM tetrabutylammoniumhydroxide (TBAOH). Eluent flow rate was 1 mL/min; regenerant flow rate was about 7 mL/min. Duplicate samples were routinely run and precision was typically less than 5% RSD (relative standard deviation) and often less than 3%.

Chemical Variability of Ground-Water at GEMS

Introduction

Ground water chemistry at GEMS is dominated by Ca and alkalinity, with minor to trace amounts of Mg, Na, K, Fe, SO₄, Cl, Br, HPO₄, NO₃-N, and NH₄-N. The total dissolved solids ranges from about 300 to 400 mg/L, and pH is slightly alkaline. Previous work has shown that the chemistry of ground water at GEMS is not steady (Macpherson, 1993; Macpherson and Schulmeister, 1994; McElwee *et al.*, 1994) and that chemistry in one unit may be influenced, during pumping, by leakage from another (McElwee *et al.*, 1992; McElwee *et al.*, 1993). These results are summarized below.

Table 1 is a compilation of all chemical analyses of ground water from the GEMS site, excluding those from the MLS's and the pumping tests. Water samples have been collected primarily from the #0 nest and the #2 nest, with fewer samples collected from the #00 and #1 nests. Sampling dates were September, 1992; May, 1993; August, 1993; November, 1993; and March, 1994. Sampling times include all four seasons (Macpherson and Schulmeister, 1994). Table 2 is a compilation of the water chemistry of samples collected from the MLS's.

The chemical differences in ground water at GEMS have not yet been fully investigated. Geochemical modelling using PHREEQE (Parkhurst *et al.*, 1980) was begun, and preliminary results (as yet unpublished) show that the major-ion chemistries are the result of equilibration with calcite under normal, shallow subsurface partial pressures of CO₂; ion exchange on clay minerals; possible dissolution of dolomite; and possible oxidation of pyrite along with introduction of NO₃.

Chemical Variability in Well-Nest Wells

As discussed in a previous report, the nitrate content of the ground water at GEMS is quite variable, with means from individual wells ranging from less than 0.01 mg/L to nearly 8 mg/L. The coefficient of variations for the means from each of the wells is quite high, and ranges from 12 to 200%. The sulfate content of the ground water at GEMS is much less variable, with means from individual wells ranging from about 30 to 68 mg/L. Excluding a single, probably anomalous sample, means range from about 30 to 47 mg/L. Coefficients of variation are lower than for nitrate, but are still typically greater than 5%, and thus are significant relative to the precision of the method (2%).

The variability in nitrate at GEMS is both spatial (fig. 1) and temporal (fig. 2), and suggests the movement of a slug of nitrate-laden water through part of the aquifer at GEMS at regular times during the year. Other components also are time and space variable. These samples, from wells with short screened intervals (0.76 m), provide one view of the aquifer chemistry. The MLS's extract water from an even smaller interval, providing another view of chemical variations in the alluvial aquifer.

Chemical Variability Deduced from Multi-Level Samplers

Three of the multi-level samplers were chosen to investigate the possibility that stratification exists in the sand and gravel aquifer. The samplers are located at either end of the well network and in the middle (wells TMC-1, TMC-5, and TMC-9), a distribution chosen so that the two-dimensional chemical variability in the aquifer could be assessed. This variability was used to assess whether there might be differential displacement of native fluids by the injected tracer fluid during the tracer test, caused by different densities of native fluids. Table 2 shows the chemical analyses of samples from MLS's collected in August, 1994. Analytical error is reported for species determined by ion chromatography. The analytical error is the highest relative standard deviation (% RSD) of the sample and standard duplicates or of the precision of standards, as calculated from the standards measurements done as unknowns at the beginning and end of analysis period. Charge balance (the ratio of the cation milliequivalents and anion milliequivalents) was calculated for all samples for which alkalinity was determined, and varies between about 97.5% and 101% for all except two analyses.

Vertical plots of the chemistry show that there are distinct vertical variations present at the site but that there is only slight variation in water chemistry among the three multi-level samplers used in this project. The most abundant dissolved species are calcium (Ca) and alkalinity (mostly HCO_3). The profile of calcium with depth (fig. 3) shows that the central part of the aquifer is slightly enriched in calcium relative to the top and bottom, and that TMC-1 may have Ca content which is lower and analytically

distinct from TMC-5 and TMC-9. Alkalinity content increases with depth from 17 m to 23 m, and may also increase between 17 m and 13 m (fig. 4). The magnesium (Mg) content of the ground water (fig. 5) shows a pronounced minimum at about 19 m, nearly coincident with the alkalinity minimum. Sulfate (SO_4) content of the aquifer is nearly constant with depth (fig. 6) except that TMC-5 shows a positive excursion and then retreat at about 21 m depth while TMC-1 and TMC-9 show a steady increase in SO_4 beginning at about depth 21 m and continuing to the deepest port at 23 m. Chloride (Cl) content of the ground water (fig. 7) is at a minimum in the deepest ports and shows two maxima, one at a depth of about 21 m and one at a depth of about 14 m. Bromide (Br) was detected in those samples with the highest Cl content in the upper part of the aquifer only (fig. 7; discussed more fully in next section). Nitrate (reported as $\text{NO}_3\text{-N}$) is found in only very low to undetectable concentrations in the upper part of the sand and gravel aquifer (fig. 8), shows a uniform increase at depths between about 17 m and 19 m, and then is highly variable in the three wells sampled below depths of about 19 m. A comparison of the $\text{NO}_3\text{-N}$ and ammonium ($\text{NH}_4\text{-N}$) distribution in the aquifer (fig. 9) shows that there is an upper, reducing zone in which $\text{NH}_4\text{-N}$ dominates and a lower, oxidizing zone in which $\text{NO}_3\text{-N}$ dominates. In TMC-1, the boundary between the two zones is at a depth of about 16 m (fig. 9).

The calculated total dissolved solids (TDS) content of the samples and the calculated specific conductance (SC; calculated as 60% of TDS) distribution with depth (fig. 10) show that although there are measurable differences in individual chemical species in the aquifer, the change in ground-water density with depth in the aquifer is small.

Implications of the Variable Density of Native Ground Water to the Induced-Gradient Tracer Test

The variation in Ca content, the most abundant cation, is as much as 30% (weight units) throughout a vertical profile in the sand and gravel aquifer, and the Mg content varies as much as 180%. The range in variation of alkalinity, contributing the most abundant anion, is as much as about 30%. The range in TDS (calculated from measured concentrations of dissolved species) and specific conductance (measured), however, is only about 20%, much smaller than that reported by Garabedian (1987). The impact of this level of variation on density is small: a change of this magnitude on a pure Na-HCO_3 fluid, using density-weight percent salt relations reported in Weast (1985) (no similar data are available for Ca-HCO_3 fluids from this source) results in a theoretical density change from 0.998217 to 0.998267, or 0.005%. Thus, it is unlikely that the

density variations in the aquifer could cause uneven displacement of native ground water by the tracer plume.

The amount of KBr salt added to the ground water resulted in a Br concentration of about 400 mg/L or 596 mg KBr/L. Thus, the TDS of the native ground water increased by about 2.5 times because of addition of the tracer. The impact of this density increase on movement through the aquifer during the test was minimized by introducing the tracer in such a way that a fairly uniform cylinder of tracer-spiked fluid, extending from the top to the bottom of the screened interval, was present in the injection well at the beginning of the test. Any other method of sample introduction would have resulted in initial movement of the plume strongly driven by density gradients.

Leakage between Alluvial and Bedrock Aquifers

One of the initial experiments done evaluating the chemistry of ground water at GEMS was to see if leakage from the alluvial aquifer induced during pumpage of the bedrock aquifer could be verified and identified using natural chemical tracers. The following section describes the two pumping tests, the first a two-hour test and the second a seven-hour test. These two tests showed that there is chemical evidence of a hydraulic connection between the two aquifers which results in leakage of water when the aquifer(s) are stressed (pumped). All chemical species analyzed on pumping test samples are in Table 1; anion chemistry is highlighted in Table 3.

The first pumping test of the bedrock well lasted two hours and demonstrated that pumping induces cross-formational flow from the alluvial aquifer into the bedrock. During this test, the pumping rate increased from 6.01 gpm to 8.04 gpm after 60 minutes of pumping making it slightly more difficult to interpret than if the pumping rate had held steady. However, as shown on time versus nitrate concentration plot (fig. 11), $\text{NO}_3\text{-N}$ is not detectable initially but then increases nearly linearly in the last three samples. Some other parameters, which have relatively large differences in concentration in the alluvium and bedrock aquifer, show similar results. Using $\text{NO}_3\text{-N}$ as the best indicator of the "end members" (sand and gravel aquifer water having relatively high $\text{NO}_3\text{-N}$ and the bedrock aquifer have undetectable $\text{NO}_3\text{-N}$), leakage water from the sand and gravel aquifer was produced from the bedrock well after about 38 minutes of pumping. At the end of the test, about 5.6% of the produced water was water from the sand and gravel aquifer and the remaining part from the bedrock aquifer, *if $\text{NO}_3\text{-N}$ concentrations in the sand and gravel aquifer are represented accurately by the sample from well GEMS 01.* Using $\text{NO}_3\text{-N}$ content as an indicator of sand and gravel aquifer water, I predicted the concentrations through time of the other anions in the first year's report (McElwee *et al.*,

1992). These calculations underpredicted that Cl concentrations, the only other major anion with significant differences between the bedrock and alluvial aquifers. The underprediction of Cl suggested that there may be chemical stratification within the sand and gravel aquifer, and that the Cl produced from the GEMS 01 well is lower than Cl in the lower part of the sand and gravel aquifer. Alternately, the NO₃-N in the lower part of the sand and gravel aquifer is lower than that produced from the GEMS 0-1 well, which in turn underpredicted the percentage of sand and gravel water produced from the bedrock well at the end of the pumping test. These predictions were in fact verified by the more detailed chemical sampling described above, in that there are significant vertical and temporal variations in nitrate content of the alluvial aquifer at GEMS.

During October, 1992, a second, longer (seven-hour) pumping test on the bedrock well was run to see if changes in geochemistry corresponded with the earlier, shorter test, and to see if the chemistry of the pumped water would stabilize, indicating attainment of steady-state leakage from the alluvial aquifer into bedrock. The pumping rate during the test was approximately steady at about 6 gallons per minute. A plot of NO₃-N through time (fig.11) shows the chemical change in the produced ground water during the test. No NO₃-N was detected (less than 0.05 mg/L) until about 1.5 hours after pumping began. Thereafter, the NO₃-N content increased almost steadily until the end of the test. Some curvature is apparent in the profile. The differences between the two-hour test, during which detectable nitrate was found in the pumping well after about 40 minutes, and the seven-hour test, during which nitrate was not found until about 1.5 hours of pumping, may be attributed to lower nitrate content of the ground water in the alluvial aquifer and/or a steady, lower pumping rate during the longer test.

Evaluation of the nitrate concentration-time plot from the longer pumping test shows that steady-state leakage (as evidenced by achievement of constant chemical signature) was not attained after 7 hours of pumping. As discussed in McElwee *et al.* (1993), if leakage is not occurring as a point or line source but is evenly distributed along the presumably horizontal interface between the bedrock and overlying sand and gravel, then it is possible to do some simple evaluations of aquifer parameters.

Dispersivity Estimates from Pumping Tests

The pumping test is a simple case of a well penetrating bedrock which, when pumped, causes a cone of depression of the hydraulic head around the well. The maximum radius of this cone of depression is ideally a circle on the plane separating the two units. Flow lines are mostly horizontal, from the bedrock sandstone into the bedrock

well. However, the cone of depression induces downward flow from the alluvium, and this flow moves vertically or obliquely toward the bedrock well.

Assuming the bedrock sandstone is homogeneous and isotropic, it is possible to represent this flow by a vertical plane including the well. The maximum horizontal extent of the cone of depression caused by the pumping test is attained at steady-state, apparently not reached during the October, 1992 test. Flow lines to the well are probably curved, but for purposes of this exercise they are represented as being straight. The length of the path from the boundary between the alluvium and bedrock increases with increasing distance from the well, with the longest path being from the boundary between the two units starting at the maximum diameter of the cone of depression. The shortest path is that path which is vertical or nearly vertical, closest to the well bore. Water from the alluvium traveling along this path will reach the well screen first. Because this path is nearly vertical, it can be treated, as a first approximation, in the same way that column experiments of continuous sources of contaminants are treated. That is, the concentration distribution in the column is described by:

$$D_x \frac{\partial^2 C}{\partial x^2} - v_x \frac{\partial C}{\partial x} = \frac{\partial C}{\partial t}$$

where D_x is the dispersion coefficient in the x direction

C is concentration of a tracer species

x is distance

v_x is flow velocity in the x direction

t is time

Using the boundary and initial conditions that the tracer is a continuous source (or $C(0,t) = C_0$) and that the tracer is not present in the aquifer before the test begins, the above equation is integrated to produce the following solution:

$$C(x,t) = C_0 / 2 \operatorname{erfc} [(x - vt) / 2 (\alpha_x v t)^{0.5}]$$

where α_x is the longitudinal dispersivity

erfc is the complementary error function

v is the linear velocity of the water, assumed to be that of the tracer

The predicted breakthrough curves (vertical profiles of $\text{NO}_3\text{-N}$ with time) vary according to values used for longitudinal dispersivity and velocity. The distance (x) is taken as the distance between the midpoint of the screen in the bedrock aquifer well and the interface between the alluvium and bedrock. Initial $\text{NO}_3\text{-N}$ concentration is taken as

the concentration in the deepest partially screened (20-meter) well in Nest #0. It is not known whether this concentration is representative of water at the base of the alluvium, because there is no partially screened well at the base of the alluvium in Well Nest #0. The concentration of $\text{NO}_3\text{-N}$ used is probably too high, based on extrapolation from the known $\text{NO}_3\text{-N}$ profile in the upper part of the alluvium.

The shapes of the calculated breakthrough curves (fig. 12a, b) differ from that of the observed chemical changes in that the observed curve is concave down, whereas the calculated curves are concave up or nearly linear after the first third of the pumping test. Because the cone of depression grows outward during the pumping test and progressively more ground water from the bedrock aquifer is produced, the observed curve is an integration of an infinite series of breakthrough curves, one for each flow line. Only during the very first part of the test does the simplified situation of vertical flow hold true, and, in fact, vertical flow almost certainly does not hold by the time $\text{NO}_3\text{-N}$ is first detected in the pumped water, about 1.5 hours after pumping began. Figure 12b shows the breakthrough curve during the early part of the test with the calculated curves superimposed. Although there is no unique solution to the equation, because both dispersivity and velocity can be varied and because the shape of the curve during the later part of the test is obscured by dilution from other flow lines, it is apparent that the solutions with larger dispersivities (10 m to 100 m) are better fits than with small dispersivity (1 m). These values are high for the typical range of dispersivity in single well tests (0.03 to 0.3 m; Palmer and Johnson, 1989), and support the statement above that by the time $\text{NO}_3\text{-N}$ arrived in detectable concentrations at the outflow point, the water produced was a mixture from vertical and inclined flow lines from the alluvium into the bedrock aquifer. This is analogous to the difference between breakthrough curves observed at specific points (depths) in a layered aquifer versus the breakthrough curve observed in a fully penetrating well (National Research Council, 1990, p. 119).

Summary. Leakage between Aquifers

Ground water chemistry of the sand and gravel aquifer, the upper silt and clay aquitard, and the lower bedrock aquifer are sufficiently different to be useful as "natural" tracers during pumping tests. The $\text{NO}_3\text{-N}$ content of the alluvium is the best indicator of water sources because it is relatively easy to detect and because the bedrock aquifer does not contain detectable levels. The chemistry survey at GEMS showed that the water chemistry varies spatially, both vertically and horizontally, as well as temporally. This makes it possible to evaluate leakage from the alluvial aquifer into the bedrock aquifer,

but because the chemistry within the alluvial aquifer also varies considerably, these calculations will be extremely complex.

The pumping test on the bedrock aquifer showed that water from the alluvium leaks into the bedrock aquifer during pumping, and calculations from the first test show that the alluvial aquifer water is produced after about 38 minutes of pumping at a pumping rate of about 8 gpm. Arrival time during the second test was longer, probably mostly because of the lower pumping rate (6 gpm). The second bedrock pumping test also showed that steady-state chemistry was not attained after seven hours of pumping. The preliminary assessment of dispersivity and ground-water velocity shows that an evaluation of these parameters is difficult because of the relatively late arrival time of the nitrate ($\text{NO}_3\text{-N}$). Because of the late arrival time of $\text{NO}_3\text{-N}$, the water produced at the time of detectable concentrations of $\text{NO}_3\text{-N}$ is a mixture of many flow lines coming from the alluvium through the bedrock, and is not simple vertical flow. For this reason, the parameters fitted to the one-dimensional advection-dispersion equation are overestimates of dispersivity in this system and should be compared, with caution, to other more sophisticated estimates.

Br in Ground Water at GEMS: Implications to the Induced-Gradient Tracer Test

During this investigation, bromide, the anion to be used as the conservative tracer in the induced-gradient tracer test, was found in measurable concentrations in the alluvial aquifer ground water. The sections below detail the investigation done to assess how much bromide was present in the ground water, where it could be expected to be found, and implications to the tracer-test interpretation.

Verification of the Expected Conservative Behavior of Br at GEMS

The measured pH of ground water at this site is neutral to slightly alkaline, eliminating the need for concern about adsorption of Br onto aquifer materials (Boggs *et al.*, 1992). CaBr_2 was not used as the bromide salt because of the likelihood that oversaturation with respect to calcite would occur when the native ground water was spiked with the salt. The oversaturation would hasten precipitation of calcite which might occur in the mixing tank if the fluid was sufficiently oversaturated, or which might occur in the aquifer pores, changing the hydraulic conductivity of the system. Either NaBr or KBr was considered an acceptable salt, but KBr was preferred because increased K in the ground water, causing cation-exchange reactions to proceed, would not make smectitic clays swell as Na would. Thus, the choice of KBr for the tracer salt was made

to minimize any response of aquifer materials to the tracer salt toward lowering of hydraulic conductivity.

Measuring Low Br Concentrations

Because of the nonlinear response of Br ISE's at low concentrations, an experiment was designed to evaluate low-level Br concentration measurement. The Br ISE mV response to low concentrations either with or without ionic strength adjustor (ISA) is well known, and was reproduced during this study for concentrations less than 1 mg Br/L (fig. 13). Electrode response at mid-levels (1 to 10 mg Br/L) is linear, but is dependent upon ionic strength (fig. 13). The slope relating Br concentration to mV response of the electrodes with and without ISA is different although the correlation coefficient is high for each plot (fig. 14). No ionic strength adjustor was used for determination of Br during the tracer test, and it was known that background levels of Br exist in some parts of the aquifer at GEMS (see below). Furthermore, the lowest Br standard used routinely during calibration of the ISE's was 1 mg/L. To assess the precision and reproducibility of Br concentrations at levels below 1 mg/L, GEMS water and distilled water spiked with Br at levels of 0.2, 0.4, 0.6 and 0.8 mg Br/L were measured five times each. The electrode had undergone the usual calibration at 1, 50 and 300 mg/L. The results (fig. 15) show that ISE-measured Br content of spiked distilled water is consistently low, as expected since the GEMS water used to make the standards contained a small amount of Br. ISE-measured Br content of the GEMS water is consistently high, although it approaches the correct measurement as the spiked Br content approached 1 mg/L. Precision is reported in Table 4, showing that precision of ISE-measured concentrations above 0.8 mg/L is about 3%, precision of concentrations of about 0.6 mg/L is about 10%, and precision at 0.4 mg/L is about 20%. Thus, low concentrations of Br have poor precision by the method of analysis used in this study.

Background Concentrations of Br at GEMS

Initial assessment of the background concentration of Br in ground water at GEMS resulted in an estimate of about 0.7 mg Br/L in fluid produced from TMC5-15, a port located near what appeared to be the point of maximum Br content in the ground water. An experiment done using the method of standard additions was done on the water from GEMS used to make standards for ISE determination of Br. For this experiment, GEMS water was spiked so as to contain about 0.0, 0.2, 0.4, 0.6, 0.8 and 1.0 mg/L Br. The spiked concentration plotted versus the Br concentration measured by the ISE's, projected to intersect the abscissa, gives the Br concentration of the unspiked water

(fig. 16). Each solution was measured six times, resulting in a relative standard deviation (coefficient of variation) ranging from 9.3% (at 0.0 mg Br spike/L) to 1.8% (at 1.0 mg Br spike/L). Because of the non-linear response of the ISE at low concentrations, the measurement at 0.0 mg Br spike/L is ignored, giving a background concentration of about 0.11 mg/L in the GEMS water used to make standards. Thus, concentrations of less than about 1 mg/L measured during the tracer test should not be considered possible indicators of the presence of the tracer fluid.

Summary, Aqueous Geochemistry at GEMS

Ground-water chemistry in the aquifers at GEMS varies laterally, vertically, and temporally. Temporal variations are most evident in $\text{NO}_3\text{-N}$ and SO_4 concentrations, and spatial variations are also evident in these parameters as well as most others. The variation in total dissolved solids is relatively high, but small relative to the increase in TDS resulting from spiking the ground water with the tracer salt used during the induced-gradient tracer test.

Because the alluvial (sand and gravel) aquifer contains measurable $\text{NO}_3\text{-N}$ and the bedrock aquifer does not, the $\text{NO}_3\text{-N}$ concentration of water pumped from the bedrock aquifer has been used to evaluate leakage between the two aquifers. Estimates of dispersivity using the one-dimensional advection dispersion equation are unreasonably high, probably because of the relatively long travel time between the two aquifers, allowing mixing of ground-water moving vertically and obliquely into the well screen of the bedrock well. Further evaluation is needed to improve these estimates, but it is apparent that leakage does occur.

Several laboratory experiments were done in order to evaluate the reliability of Br determination by ISE, and to measure background concentrations of Br at GEMS. Br found in GEMS MLS's was found mostly in the upper part of the aquifer. Concentrations were less than 1 mg/L. In the water spiked with tracer salt for injection during the tracer test, Br content was about 0.11 mg/L. Because of the nonlinear response of the Br ISE's at low concentrations, the low precision at concentrations less than about 0.6 mg/L, and because of the possibility of native dissolved Br existing the ground water, concentrations less than 1 mg Br/L measured in tracer-test samples should not be included in aquifer-parameter calculations.

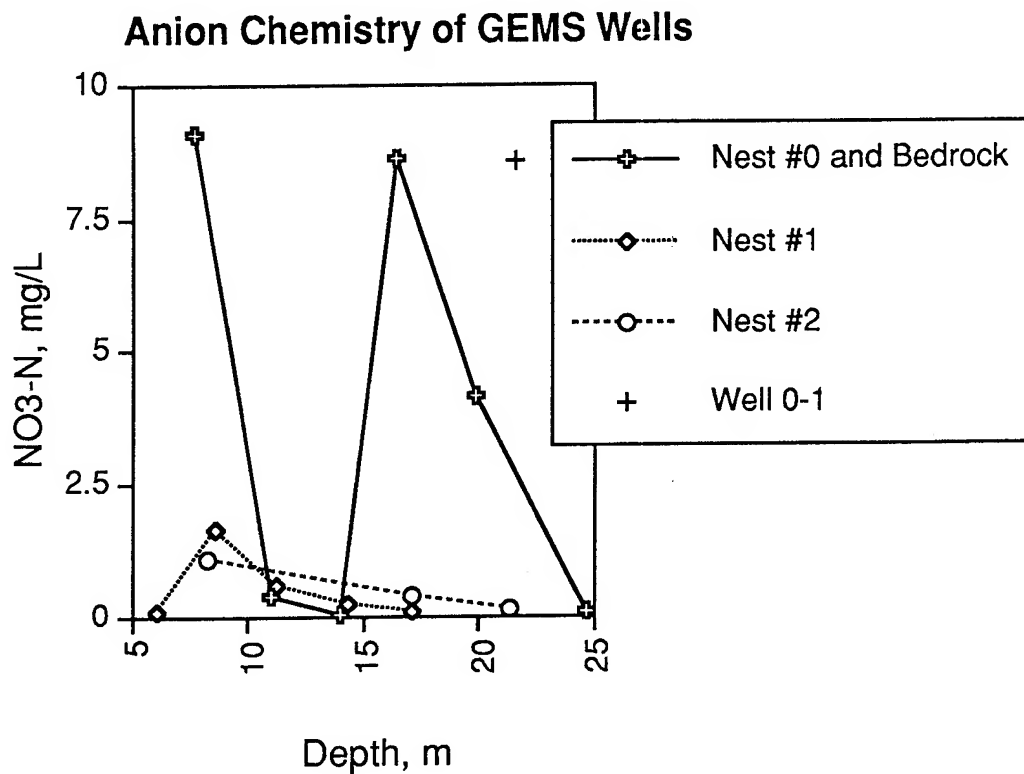


Figure 1: Nitrate concentration versus depth in three well nests at GEMS (from McElwee *et al.*, 1993). The single well completed in Paleozoic bedrock beneath the Kansas River Alluvium is shown as the deepest point on the profile for Nest #0, although it is near but not actually located within that nest. Well #0-1 is shown as a separate point because it is screened over the entire sand and gravel interval (approximately depth 11-21 m), but it is plotted at the depth corresponding to the total depth of the well.

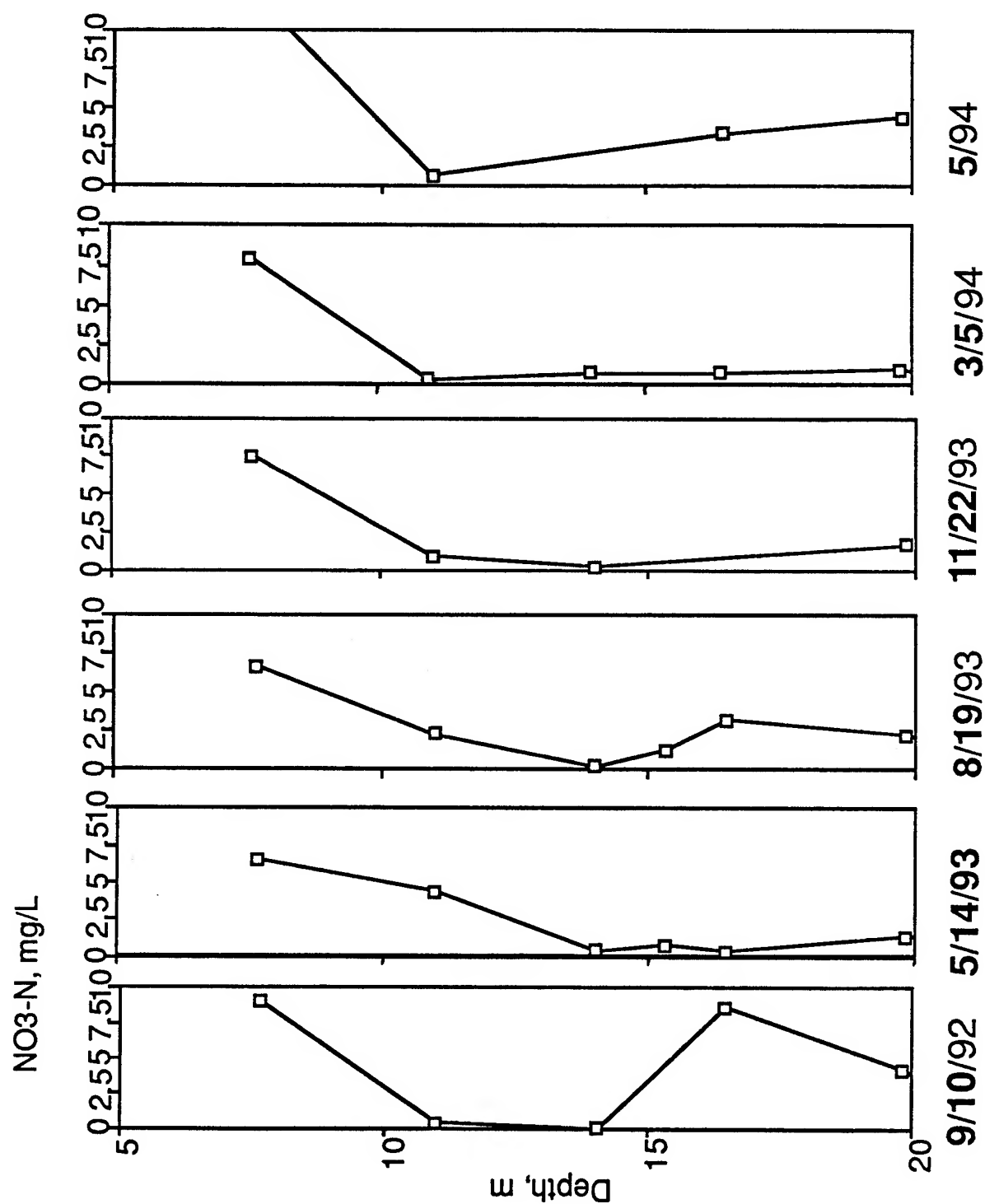


Figure 2: Changes in nitrate concentration with time in nest #0, GEMS. The profiles show that nitrate content varies through time and that there is a slug of nitrate coming through the bottom part of the aquifer periodically.

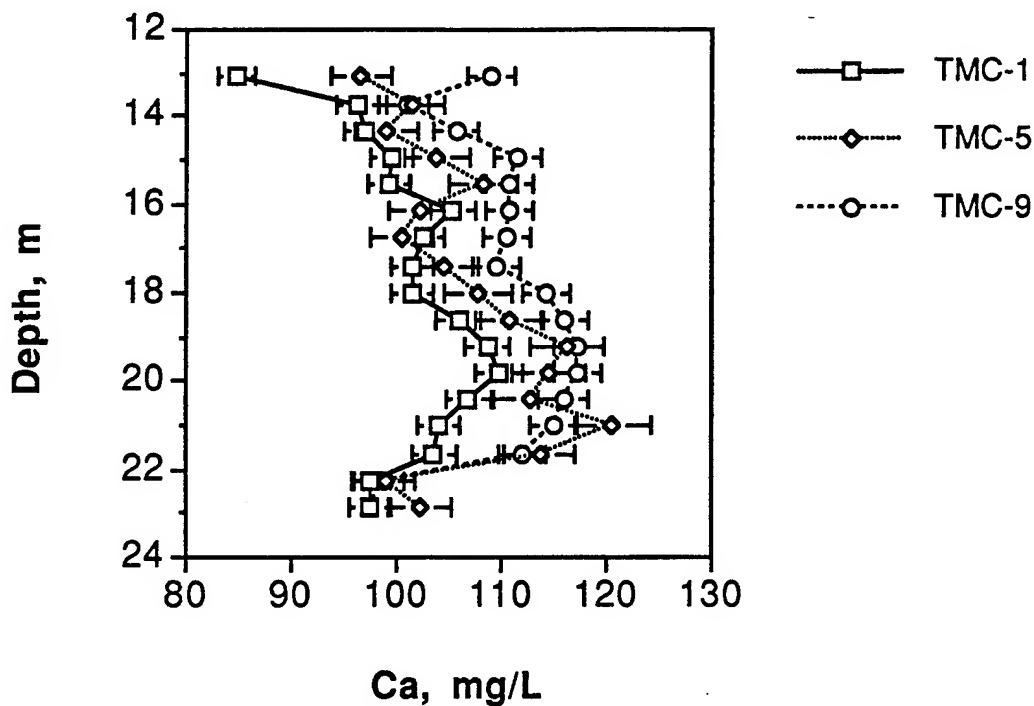


Figure 3: Calcium concentration in ground water in the sand and gravel aquifer at GEMS. Three MLS depth profiles are shown with analytical error bars.

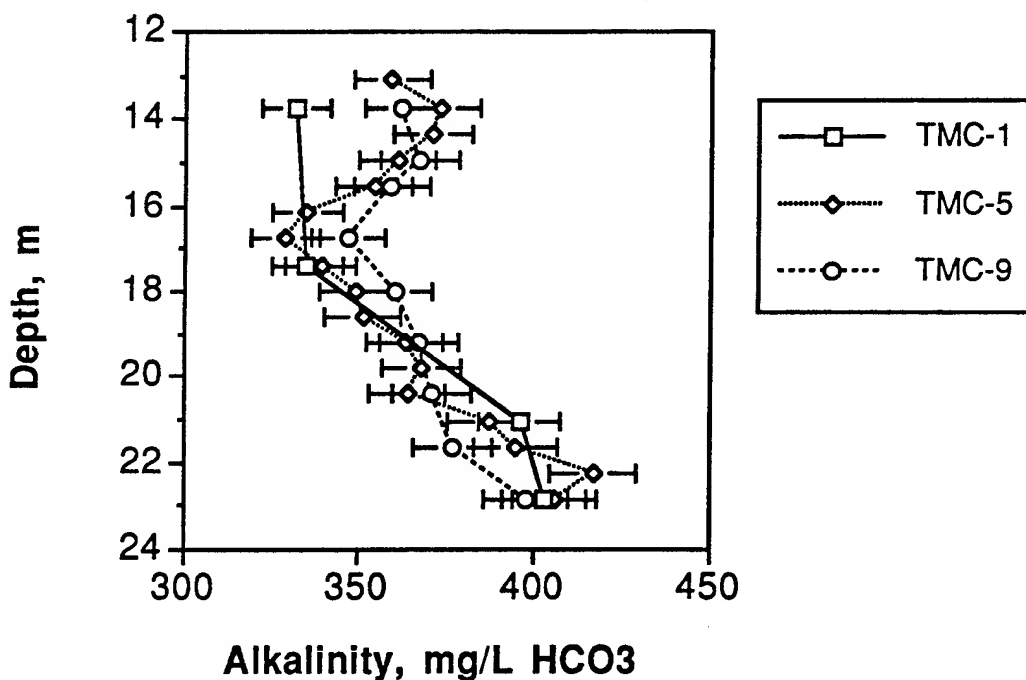


Figure 4: Alkalinity, reported as mg HCO₃/L, in ground water in the sand and gravel aquifer at GEMS. Three MLS depth profiles are shown with analytical error bars.

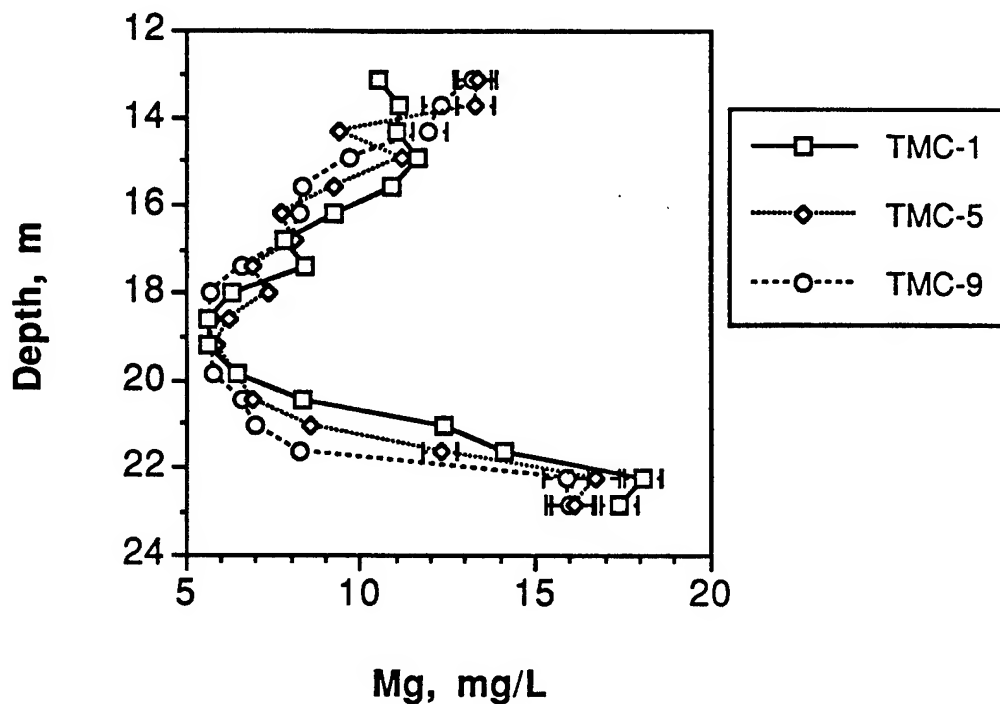


Figure 5: Magnesium concentration in ground water in the sand and gravel aquifer at GEMS. Three MLS depth profiles are shown with analytical error bars.

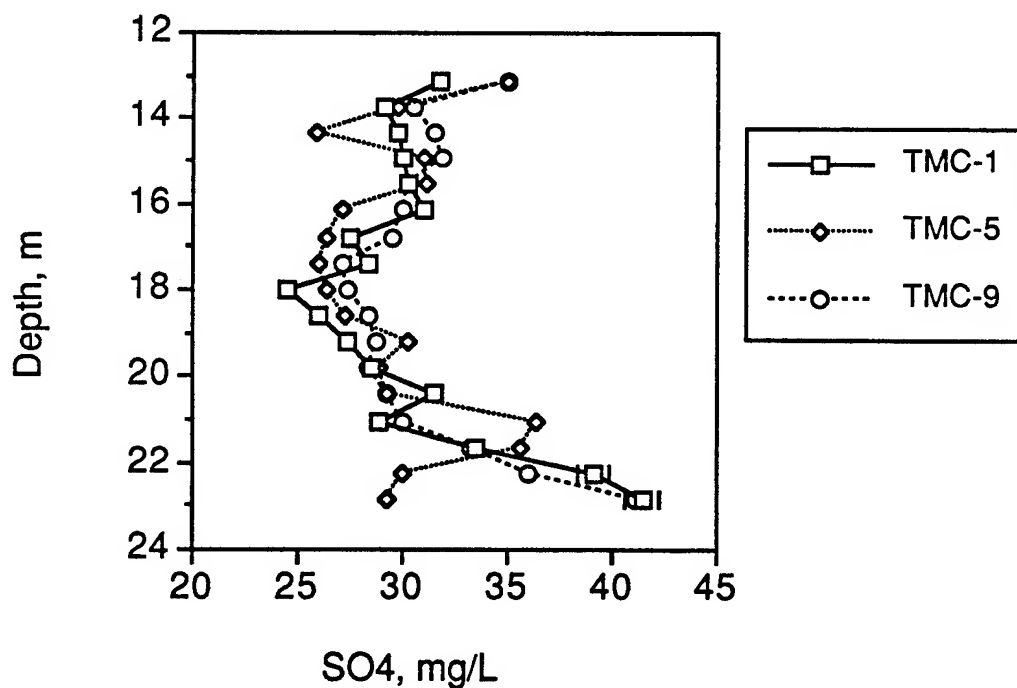


Figure 6: Sulfate concentration in ground water *versus* depth in the sand and gravel aquifer at GEMS. Three MLS depth profiles are shown with analytical error bars.

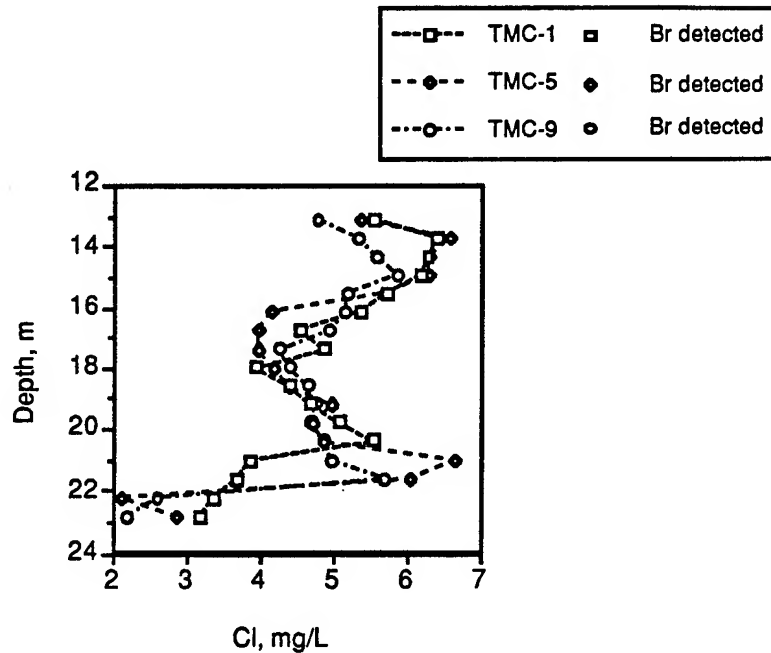


Figure 7: Chloride concentration in ground water *versus* depth in the sand and gravel aquifer at GEMS. Profiles for three multi-level samplers are shown with analytical error bars. Filled data points indicate Br was detected. These points correspond to the highest chloride content in the upper part of the aquifer.

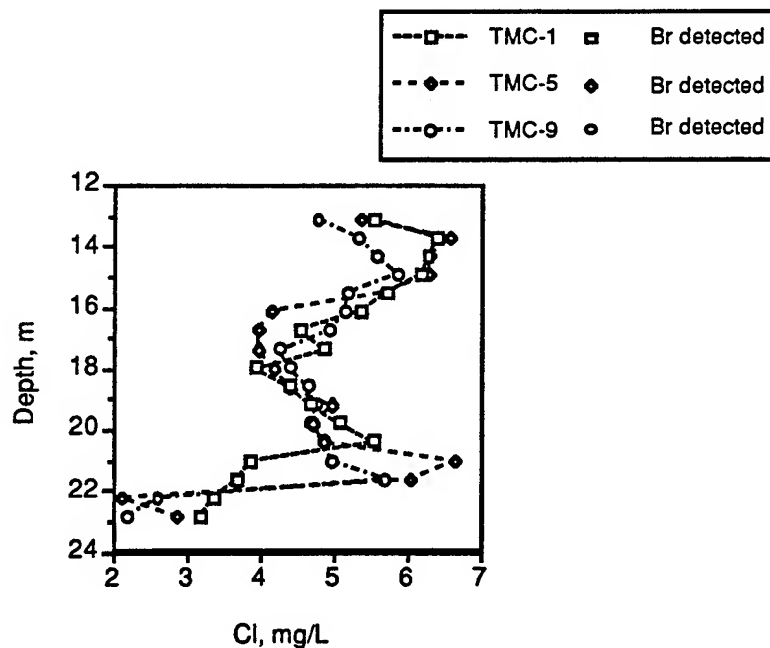


Figure 8: Nitrate concentration in ground water *versus* depth in the sand and gravel aquifer at GEMS. Profiles for three multi-level samplers are shown. Nitrate is found in very low to undetectable concentrations in the upper part of the aquifer, and varies vertically and between wells in the lower part of the aquifer.

Figure 9: Nitrate and ammonium *versus* depth in the sand and gravel aquifer at GEMS. Profiles for three multi-level samplers are shown as separate plots to illustrate the spatial variability. a) TMC-1. b) TMC-5. c) TMC-9.

Fig. 9a:

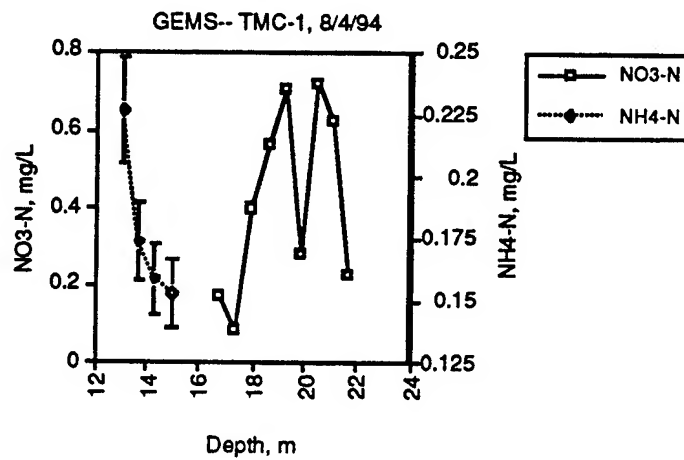


Fig. 9b:

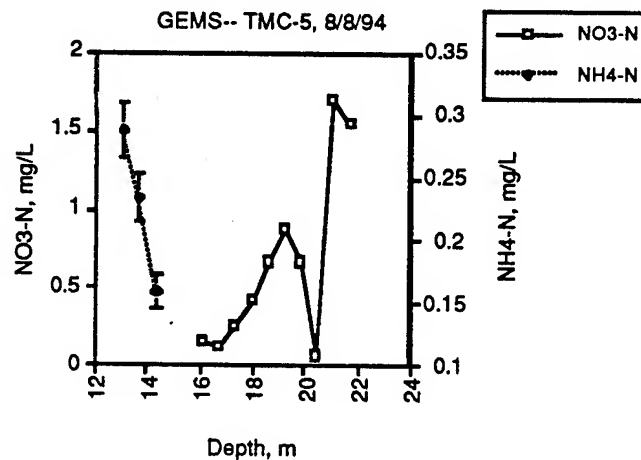
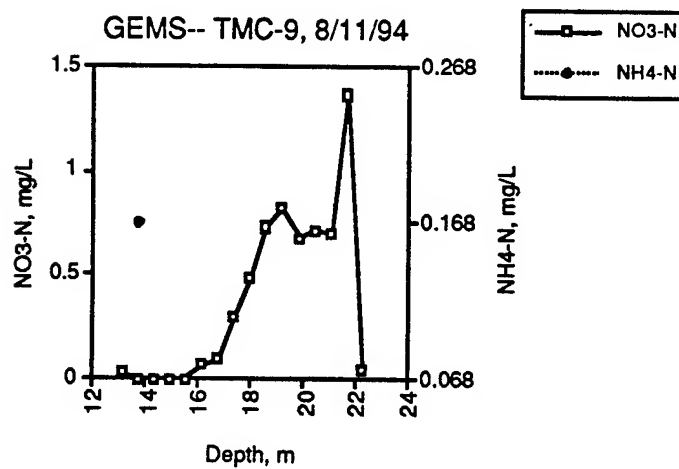


Fig. 9c:



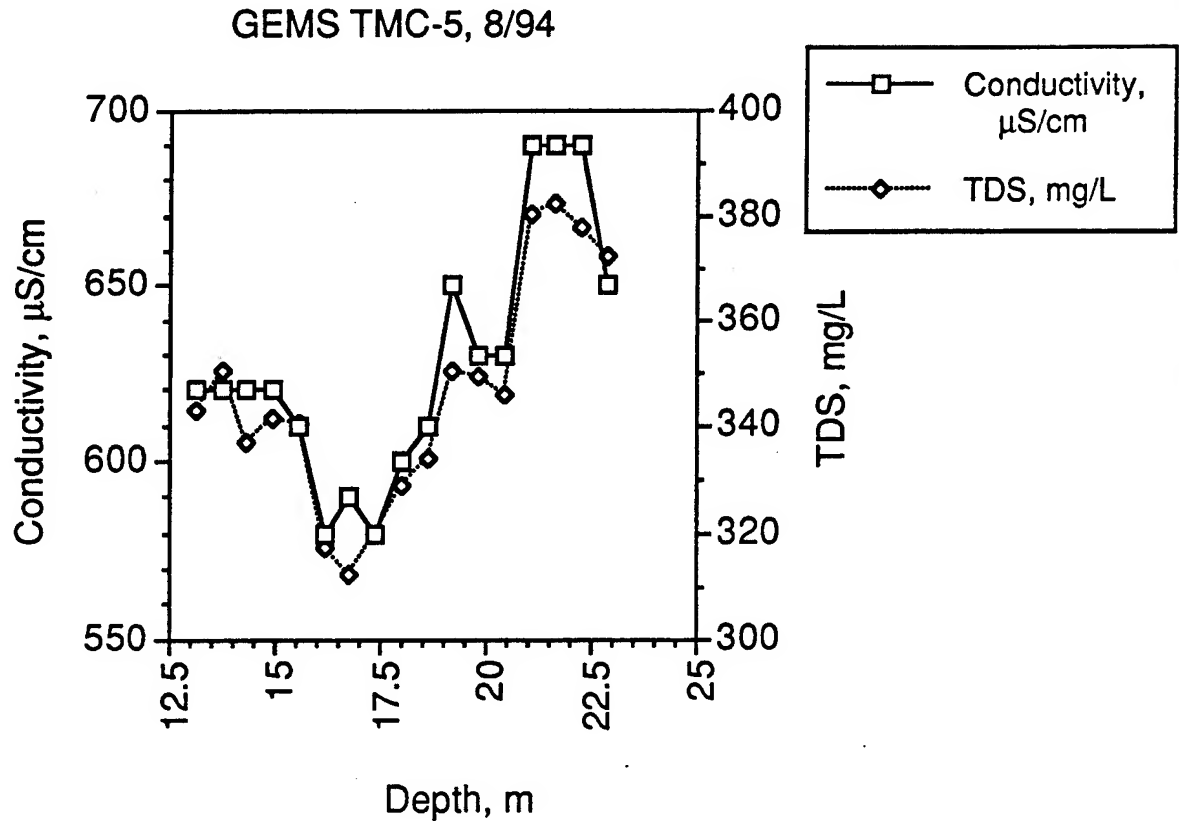


Figure 10: Distribution of total dissolved solids and specific conductivity with depth in one of the MLS's at GEMS.

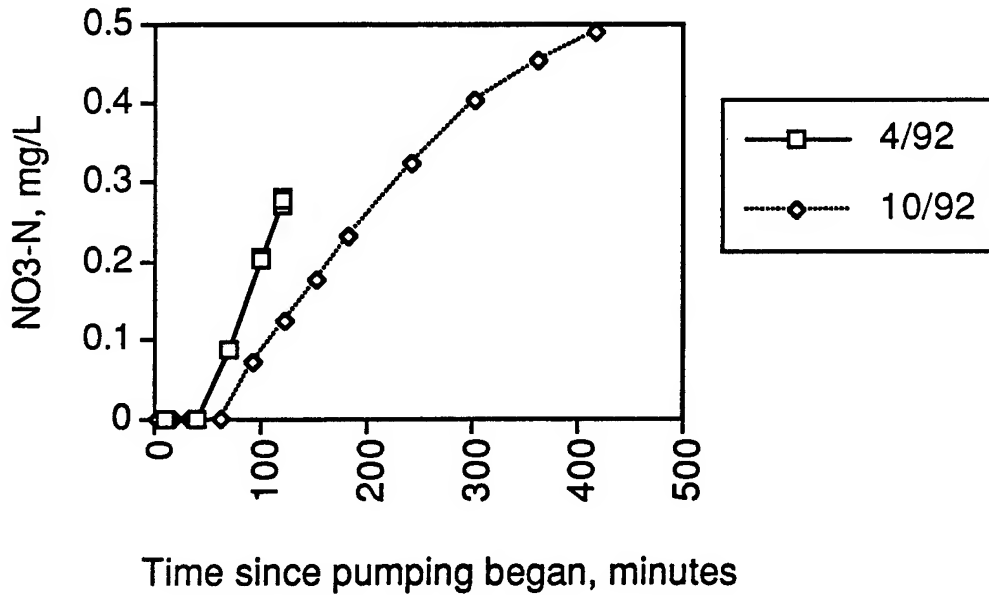


Figure 11: Nitrate content of produced ground water from the bedrock well (0-6) during two pumping tests. Difference in "arrival time" of nitrate at the well may be due to different pumping rates or different nitrate content of the alluvial-aquifer water.

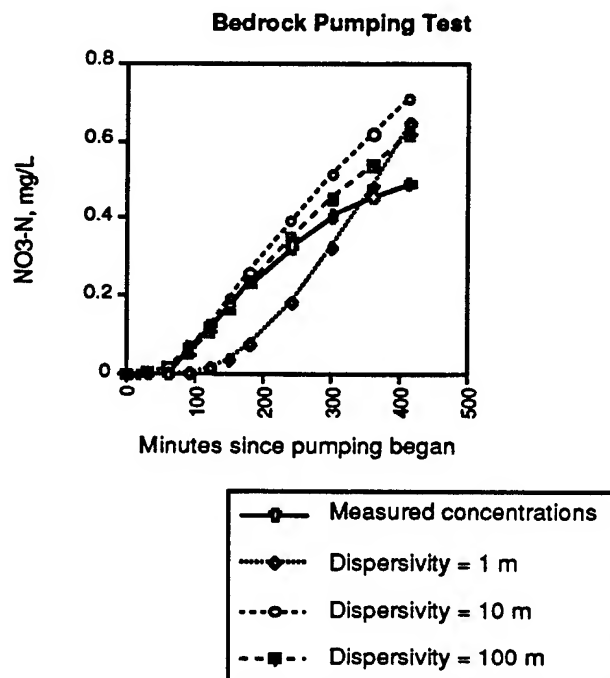


Figure 12a: NO₃-N concentration as measured and several breakthrough curves calculated using the advection-dispersion equation for the entire time of the second bedrock pumping test.

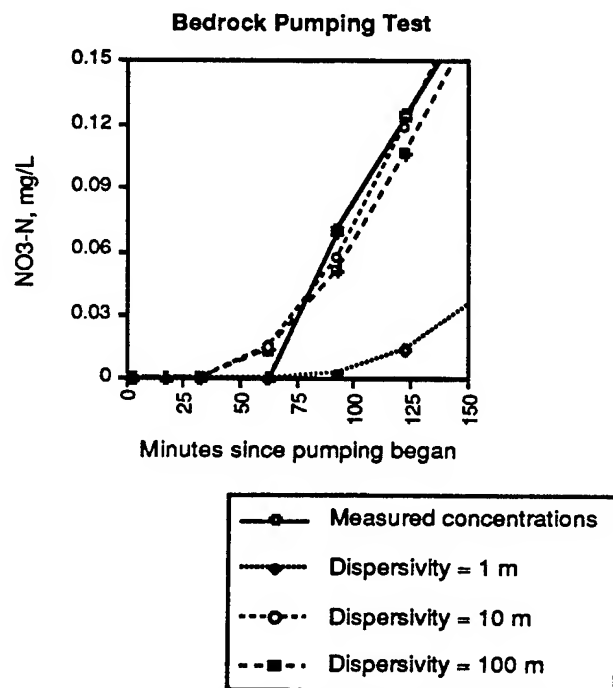


Figure 12b: NO₃-N concentration as measured and calculated for several values of dispersivity and ground-water velocity at the beginning of the second bedrock pumping test.

Low-Level Calibration of Br ISE: 24 Mar '94

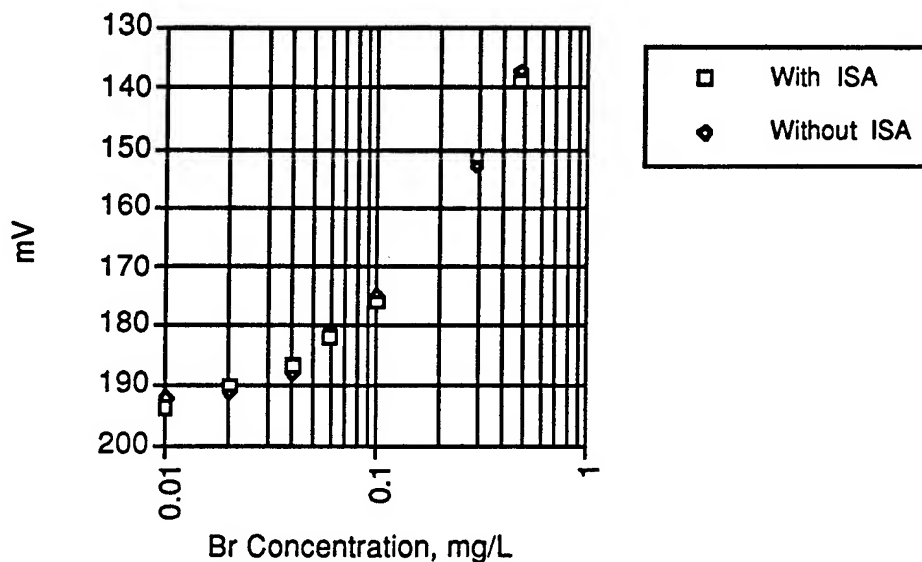


Figure 13: Electrode response at low-Br concentrations.

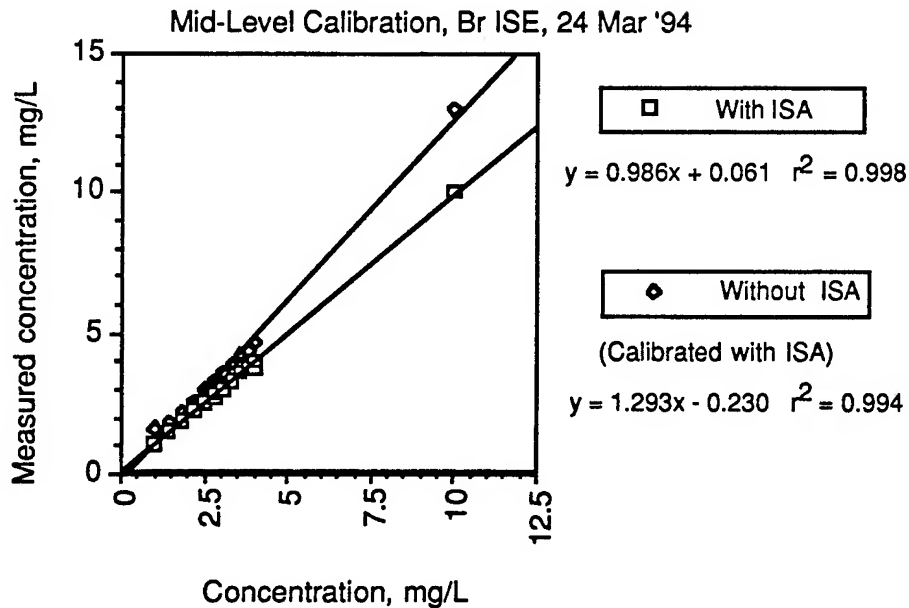


Figure 14: Comparison of measured concentrations at mid-Br content in fluids with and without ionic strength adjustor.

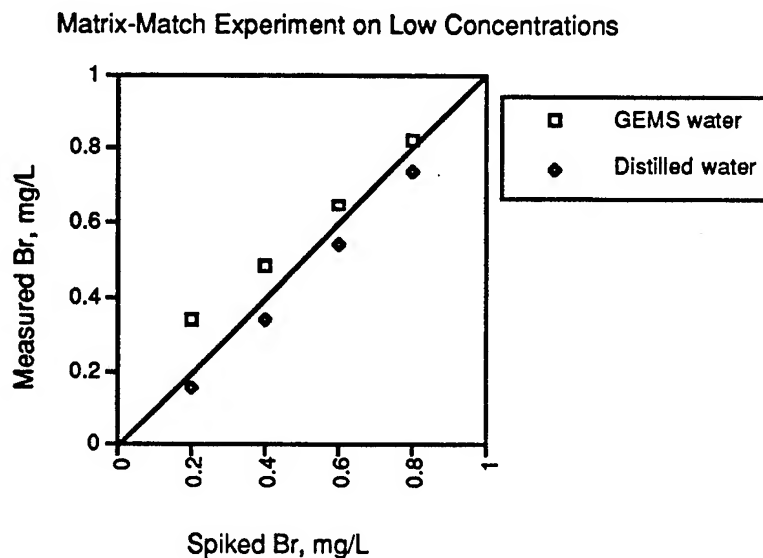


Figure 15: Comparison of measurements of Br concentration in spiked samples of GEMS water and distilled water.

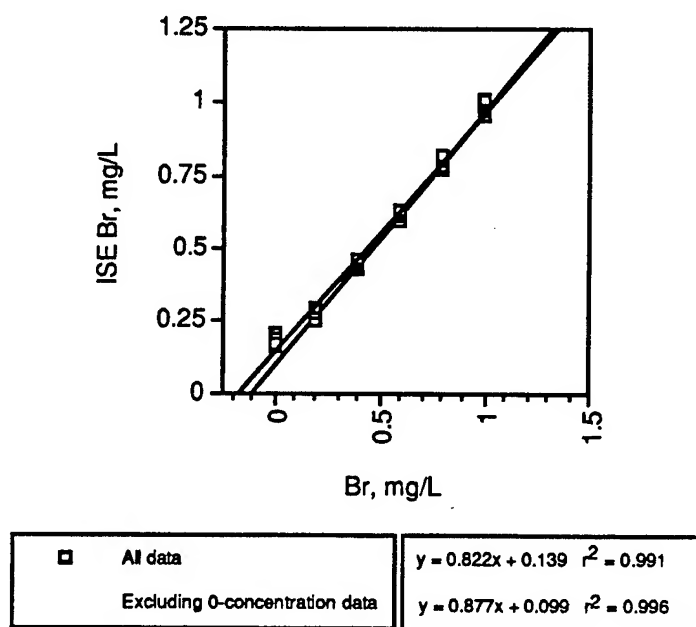


Figure 16: Method of standard additions used to evaluate background Br content of GEMS water.

Well ID	Date	Na	K	Ca	Mg
	(chem.)	mg/L	mg/L	mg/L	mg/L
Mol. Wt		22.9898	39.102	40.08	24.305
Valence		1	1	2	2
Well Survey -- 1991					
0-6 (A)	7/10/91	24.0	1.17	102.6	17.6
0-6 (B)	7/10/91	21.5	1.17	102.6	17.3
0-1 (A)	7/10/91	10.4	1.26	110.3	8.4
0-1 (B)	7/10/91	10.5	1.27	109.3	8.3
0-4 (A)	7/10/91	12.8	1.06	74.1	8.4
0-4 (B)	7/10/91	12.7	1.06	74.2	8.3
0-3 (A)	7/10/91	11.5	1.14	58.7	7.9
0-3 (B)	7/10/91	11.0	1.11	58.1	7.7
1-4	7/10/91	53.4	1.41	98.6	14.7
1-3	7/10/91	49.7	1.47	85.5	11.8
1-2	7/10/91	12.3	1.67	93.2	13.4
Well Survey --1992					
0-1	9/8/92				
0-2	9/8/92				
0-3	9/8/92				
0-4	9/8/92				
0-5	9/8/92				
0-6	9/8/92				
0-7	9/8/92				
1-1	9/8/92				
1-2	9/8/92				
1-3	9/8/92				
1-4	9/8/92				
1-5	9/8/92				
1-6	9/8/92				
2-1	9/8/92				
2-2	9/8/92				
2-3	9/8/92				
2-5	9/8/92				
2-6	9/8/92				
2-7	9/8/92				

Table 1: Chemical Analyses of Samples from GEMS Monitoring Wells.

Well ID	SO4 mg/L	F mg/L	Cl mg/L	NO3-N mg/L	Alkal. mg/L HCO3
Mol. Wt	96.06		35.453		61.017
Valence	-2	-1	-1	-1	-1
Well Survey --					
0-6 (A)	38.0	0.1	3.5	0.00	393
0-6 (B)	38.0	0.1	3.5	0.00	393
0-1 (A)	43.0	0.1	9.7	4.96	324
0-1 (B)	43.0	0.1	9.7	4.96	324
0-4 (A)	29.5	0.1	5.9	8.73	217
0-4 (B)	29.5	0.1	5.9	8.73	217
0-3 (A)	27.5	0.1	6.9	2.42	205
0-3 (B)	27.5	0.1	6.9	2.42	205
1-4					
1-3					
1-2					
Well Survey --					
0-1	26.4			8.60	
0-2	38.8		7.5	0.05	
0-3	26.6			0.36	
0-4	29.6			9.07	
0-5	39.9		9.7	4.11	
0-6	36.5			0.07	
0-7	32.8		6.4	8.61	
1-1	55.2		10.5	0.24	
1-2	45.3			0.56	
1-3	49.2			1.61	
1-4	60.2			0.10	
1-5	39.0		6.1	bdl	
1-6	37.8		11.0	0.09	
2-1	40.8		7.4	bdl	
2-2	38.7		6.9	bdl	
2-3	50.3		5.5	1.09	
2-5	35.5		6.3	0.11	
2-6	40.3		5.7	bdl	
2-7	31.1		4.6	0.36	

Table 1: Chemical Analyses of Samples from GEMS Monitoring Wells (Continued).

Well ID Mol. Wt Valence	pH (field)	T, °C	Chg Bal (Cat/An)	Σcations meq/L	Σanions meq/L
Well Survey --					
0-6 (A)	7.08	16.4	104.21%	7.639	7.331
0-6 (B)	7.08	16.4	102.41%	7.507	7.331
0-1 (A)	6.89	15.7	103.09%	6.679	6.479
0-1 (B)	6.89	15.7	102.25%	6.625	6.479
0-4 (A)	6.77		114.75%	4.977	4.337
0-4 (B)	6.77		114.41%	4.962	4.337
0-3 (A)	6.79		99.42%	4.103	4.127
0-3 (B)	6.79		97.77%	4.035	4.127
1-4				8.490	
1-3				7.437	
1-2				6.332	
Well Survey --					
0-1					
0-2					
0-3					
0-4					
0-5					
0-6					
0-7					
1-1					
1-2					
1-3					
1-4					
1-5					
1-6					
2-1					
2-2					
2-3					
2-5					
2-6					
2-7					

Table 1: Chemical Analyses of Samples from GEMS Monitoring Wells (Continued).

Well ID	Date (chem.)	Na mg/L	K mg/L	Ca mg/L	Mg mg/L
Pump Test, #1					
0 mn	4/24/92	34.2	1.23	97.7	17.2
30 mn	4/24/92	35.4	1.28	98.0	17.3
60 mn	4/24/92	36.9	1.26	97.2	17.6
90 mn	4/24/92	31.7	1.27	99.1	17.6
120 mn	4/24/92	34.5	1.25	99.7	17.6
Pump Test #2					
0 h 2.5 mn	10/28/92	21.9	1.14	95.4	17.2
0 hr 17.5 mn	10/28/92	21.7	1.22	95.0	17.1
0 h 32.5 mn	10/28/92	21.3	1.18	92.5	17.1
1 hr 2.5 mn	10/28/92	22.3	1.17	96.3	17.2
1 hr 32.5 mn	10/28/92	21.8	1.16	95.0	17.4
2 hr 2.5 mn	10/28/92	21.6	1.15	93.9	16.2
2 hr 32.5 mn	10/28/92	21.1	1.15	96.3	17.4
3 hr 0 mn	10/28/92	21.5	1.16	93.2	17.2
4 hr 2.5 mn	10/28/92	23.2	1.16	96.9	17.4
5 hr 2.5 mn	10/28/92	20.8	1.17	97.3	17.2
6 hr 0 mn	10/28/92	22.0	1.16	94.5	17.4
6 hr 56 mn	10/28/92	21.3	1.16	98.3	17.6

Notes:

"bdl" or "0.00" indicates concentration is below detection limit

Table 1: Chemical Analyses of Samples from GEMS Monitoring Wells (Continued).

Well ID	SO4 mg/L	F mg/L	Cl mg/L	NO3-N mg/L	Alkal. mg/L HCO3
Pump Test, #1					
0 mn	38.0	0.1	2.1	0.00	
30 mn	37.7	0.1	2.2	0.00	
60 mn	37.5	0.1	2.3	0.09	
90 mn	37.4	0.1	2.5	0.20	
120 mn	37.5	0.1	2.6	0.28	
Pump Test #2					
0 h 2.5 mn	37.6		2.3	0.00	
0 hr 17.5 mn	37.6		2.6	0.00	
0 h 32.5 mn	37.8		2.6	0.00	
1 hr 2.5 mn	37.5		2.6	0.00	
1 hr 32.5 mn	37.5		2.6	0.01	
2 hr 2.5 mn	37.5		2.7	0.12	
2 hr 32.5 mn	37.5		2.9	0.18	
3 hr 0 mn	37.9		3.1	0.23	
4 hr 2.5 mn	38.0		3.2	0.33	
5 hr 2.5 mn	38.0		3.3	0.40	
6 hr 0 mn	38.0		3.4	0.45	
6 hr 56 mn	38.0		3.5	0.49	

Notes:

"bdl" or "0.00"

Table 1: Chemical Analyses of Samples from GEMS Monitoring Wells (Continued).

Well ID	pH (field)	T, °C	Chg Bal (Cat/An)	Σcations meq/L	Σanions meq/L
Pump Test, #1					
0 mn				7.805	0.851
30 mn				7.884	0.846
60 mn				7.937	0.846
90 mn				7.802	0.848
120 mn				7.959	0.854
Pump Test #2					
0 h 2.5 mn				7.155	0.849
0 hr 17.5 mn				7.120	0.858
0 h 32.5 mn				6.979	0.861
1 hr 2.5 mn				7.216	0.853
1 hr 32.5 mn				7.157	0.855
2 hr 2.5 mn				6.991	0.857
2 hr 32.5 mn				7.184	0.861
3 hr 0 mn				7.030	0.876
4 hr 2.5 mn				7.299	0.882
5 hr 2.5 mn				7.205	0.885
6 hr 0 mn				7.133	0.888
6 hr 56 mn				7.313	0.889

Notes:

"bdl" or "0.00"

Table 1: Chemical Analyses of Samples from GEMS Monitoring Wells (Continued).

Table 2: Chemical Analyses of Water Samples from Three Multi-Level Samplers.

Well ID	Depth, m	Na mg/L	Na error %	K mg/L	K error %	Ca mg/L	Ca error %	Mg mg/L	Mg error %	NH4-II mg/L	NH4 error %
Mol. Wt		22.99		39.10		40.08		24.31		14.01	
Valence		1.00		1.00		2.00		2.00		1	
tmc-1-17	13.11	12.56	1%	1.99	5%	84.87	2%	10.48	3%	0.227	9%
tmc-1-16	13.72	11.20	1%	1.49	5%	96.37	2%	11.10	3%	0.174	9%
tmc-1-15	14.33	10.99	1%	1.69	5%	97.15	2%	11.03	3%	0.159	9%
tmc-1-14	14.94	10.78	1%	1.62	5%	99.63	2%	11.65	3%	0.153	9%
tmc-1-13	15.54	10.32	1%	1.57	5%	99.37	2%	10.84	3%		
tmc-1-12	16.15	10.33	1%	1.44	5%	105.47	2%	9.24	3%		
tmc-1-11	16.76	10.08	1%	1.28	5%	102.64	2%	7.81	3%		
tmc-1-10	17.37	10.44	1%	1.35	5%	101.61	2%	8.40	3%		
tmc-1-09	17.98	10.32	1%	1.19	5%	101.68	2%	6.27	3%		
tmc-1-08	18.59	10.74	1%	1.17	5%	106.03	2%	5.64	3%		
tmc-1-07	19.20	11.48	1%	1.12	5%	108.78	2%	5.59	3%		
tmc-1-06	19.81	12.48	1%	1.16	5%	109.81	2%	6.45	3%		
tmc-1-05	20.42	13.99	1%	1.17	5%	106.91	2%	8.29	3%		
tmc-1-04	21.03	20.52	1%	1.27	5%	104.13	2%	12.34	3%		
tmc-1-03	21.64	23.22	1%	1.31	5%	103.70	2%	14.10	3%		
tmc-1-02	22.25	27.30	1%	1.46	5%	97.71	2%	18.09	3%		
tmc-1-01	22.86	24.52	1%	1.35	5%	97.57	2%	17.40	3%		

Table 2: Chemical Analyses of Water Samples from Three Multi-Level Samplers (Cont.).

Well ID	Sr mg/L	Sr error %	SO4 mg/L	SO4 error %	F mg/L	F error %	Cl mg/L	Cl error %	NO3-N mg/L	N error %
Mol. Wt	87.62		96.06				35.45		14.010	
Valence	2		-2.00		-1.00		-1.00		-1.000	
tmc-1-17			31.65	2%	0.16	17%	5.55	6%		
tmc-1-16			29.07	2%	0.14	17%	6.39	6%		
tmc-1-15			29.64	2%	0.14	17%	6.28	6%		
tmc-1-14			29.92	2%	0.15	17%	6.18	6%		
tmc-1-13			30.25	2%	0.15	17%	5.72	6%		
tmc-1-12			30.94	2%	0.16	17%	5.36	6%	0.172	2%
tmc-1-11			27.47	2%	0.14	17%	4.54	6%	0.087	2%
tmc-1-10			28.36	2%	0.14	17%	4.84	6%	0.401	2%
tmc-1-09			24.48	2%	0.12	17%	3.92	6%	0.571	2%
tmc-1-08			25.94	2%	0.13	17%	4.40	6%	0.708	2%
tmc-1-07			27.31	2%	0.14	17%	4.67	6%	0.280	2%
tmc-1-06			28.48	2%	0.14	17%	5.07	6%	0.727	2%
tmc-1-05			31.46	2%	0.17	17%	5.56	6%	0.629	2%
tmc-1-04			28.82	2%	0.21	17%	3.88	6%	0.229	2%
tmc-1-03			33.39	2%	0.22	17%	3.69	6%		
tmc-1-02			39.06	2%	0.29	17%	3.37	6%		
tmc-1-01			41.42	2%	0.23	17%	3.17	6%		

Table 2: Chemical Analyses of Water Samples from Three Multi-Level Samplers (Cont.).

Well ID	Alkal. mg/L HCO ₃ 61.017	Alk. error %	pH (lab)	pH (field)	TDS, mg/L (Calculated)	Cond. (μS) (Measured)	TDS (mg/L) (calc.; 0.6)	Chg Bal (Cat/An)	Σ cations	Σ anions	I 0.5Σnz ² mmol/L
Mol. Wt Valence											
tmc-1-17					no alk		no sp.cd.	0.00%	5.710	0.815	
tmc-1-16	332		7.12	6.90	319.18	590	354	100.54%	6.260	6.227	9.407237
tmc-1-15					no alk		no sp.cd.	0.00%	6.287	0.794	
tmc-1-14					no alk		no sp.cd.	0.00%	6.451	0.797	
tmc-1-13					no alk		no sp.cd.	0.00%	6.340	0.791	
tmc-1-12					no alk		no sp.cd.	0.00%	6.509	0.795	
tmc-1-11					no alk		no sp.cd.	0.00%	6.235	0.712	
tmc-1-10	335		7.22		319.94		no sp.cd.	100.43%	6.250	6.224	9.413134
tmc-1-09					no alk		no sp.cd.	0.00%	6.069	0.649	
tmc-1-08					no alk		no sp.cd.	0.00%	6.252	0.705	
tmc-1-07					no alk		no sp.cd.	0.00%	6.416	0.751	
tmc-1-06					no alk		no sp.cd.	0.00%	6.583	0.756	
tmc-1-05					no alk		no sp.cd.	0.00%	6.655	0.864	
tmc-1-04	396		7.31		366.52		no sp.cd.	98.52%	7.137	7.244	10.59656
tmc-1-03					no alk		no sp.cd.	0.00%	7.379	0.816	
tmc-1-02					no alk		no sp.cd.	0.00%	7.589	0.908	
tmc-1-01	403		7.49	7.10	383.81	850	510	97.95%	7.402	7.556	11.06055

Table 2: Chemical Analyses of Water Samples from Three Multi-Level Samplers (Cont.).

Well ID	Depth, m	Na mg/L	Na error %	K mg/L	K error %	Ca mg/L	Ca error %	Mg mg/L	Mg error %	NH4-H mg/L	NH4 error %
tmc-5-17	13.11	13.93	1%	1.83	5%	96.69	3%	13.32	4%	0.287	8%
tmc-5-16	13.72	13.23	1%	2.03	5%	101.54	3%	13.28	4%	0.233	8%
tmc-5-15	14.33	11.43	1%	1.82	5%	99.16	3%	9.35	4%	0.16	8%
tmc-5-14	14.94	10.05	1%	1.60	5%	103.90	3%	11.16	4%		
tmc-5-13	15.54	10.30	1%	1.44	5%	108.31	3%	9.21	4%		
tmc-5-12	16.15	9.85	1%	1.25	5%	102.37	3%	7.69	4%		
tmc-5-11	16.76	10.04	1%	1.30	5%	100.72	3%	8.12	4%		
tmc-5-10	17.37	9.88	1%	1.24	5%	104.62	3%	6.93	4%		
tmc-5-09	17.98	9.91	1%	1.32	5%	107.86	3%	7.35	4%		
tmc-5-08	18.59	10.72	1%	1.12	5%	110.91	3%	6.21	4%		
tmc-5-07	19.20	12.18	1%	1.05	5%	116.44	3%	5.87	4%		
tmc-5-06	19.81	11.75	1%	1.18	5%	114.63	3%	6.45	4%		
tmc-5-05	20.42	11.87	1%	1.34	5%	112.85	3%	6.87	4%		
tmc-5-04	21.03	14.94	1%	1.21	5%	120.74	3%	8.58	4%		
tmc-5-03	21.64	17.66	1%	1.21	5%	113.82	3%	12.28	4%		
tmc-5-02	22.25	23.50	1%	1.33	5%	99.01	3%	16.70	4%		
tmc-5-01	22.86	21.23	1%	1.06	5%	102.32	3%	16.11	4%		

Table 2: Chemical Analyses of Water Samples from Three Multi-Level Samplers (Cont.).

Well ID	Sr mg/L	Sr error %	SO4 mg/L	SO4 error %	F mg/L	F error %	Cl mg/L	Cl error %	NO3-N mg/L	N error %
tmc-5-17			34.89	1%	0.19	12%	5.35	4%		
tmc-5-16			29.75	1%	0.27	12%	6.57	4%		
tmc-5-15			25.86	1%	0.23	12%	6.30	4%		
tmc-5-14			30.91	1%	0.16	12%	6.26	4%		
tmc-5-13			31.06	1%	0.15	12%	5.68	4%		
tmc-5-12			27.05	1%	0.12	12%	4.15	4%	0.152	2%
tmc-5-11			26.32	1%	0.12	12%	3.96	4%	0.124	2%
tmc-5-10			25.94	1%	0.12	12%	3.98	4%	0.256	2%
tmc-5-09			26.31	1%	0.13	12%	4.17	4%	0.426	2%
tmc-5-08			27.26	1%	0.12	12%	4.40	4%	0.665	2%
tmc-5-07			30.24	1%	0.13	12%	4.97	4%	0.880	2%
tmc-5-06			28.85	1%	0.13	12%	4.70	4%	0.665	2%
tmc-5-05			29.16	1%	0.13	12%	4.84	4%	0.066	2%
tmc-5-04			36.32	1%	0.17	12%	6.64	4%	1.692	2%
tmc-5-03			35.54	1%	0.18	12%	6.04	4%	1.544	13%
tmc-5-02			29.97	1%	0.18	12%	2.12	4%		
tmc-5-01			29.20	1%	0.20	12%	2.85	4%		

Table 2: Chemical Analyses of Water Samples from Three Multi-Level Samplers (Cont.).

Well ID	Alkal. mg/L HCO ₃	Alk. error %	pH (lab)	pH (field)	TDS, mg/L (Calculated)	Cond. (µS) (Measured)	TDS (mg/L) (calc.; 0.6)	Chg Bal (Cat/An)	Σ cations	Σ anions	I 0.5Σmr ²
tmc-5-17	359		7.24		343.00	620	372	97.53%	6.594	6.761	10.00072
tmc-5-16	373		7.23		350.30	620	372	98.34%	6.803	6.918	10.24983
tmc-5-15	371		7.32		336.73	620	372	92.30%	6.273	6.796	9.662492
tmc-5-14	361		7.36		341.55	620	372	97.69%	6.581	6.737	10.03242
tmc-5-13	354		7.19		340.20	610	366	100.59%	6.647	6.609	10.03254
tmc-5-12	335		7.29		317.35	580	348	100.33%	6.202	6.181	9.343532
tmc-5-11	329		7.11		312.47	590	354	101.70%	6.164	6.061	9.233067
tmc-5-10	339		7.18		319.66	580	348	100.42%	6.252	6.226	9.404889
tmc-5-09	349		7.19		329.07	600	360	100.56%	6.451	6.416	9.700658
tmc-5-08	351		7.37		333.99	610	366	100.75%	6.540	6.492	9.822258
tmc-5-07	363		7.23		350.24	650	390	101.00%	6.849	6.782	10.27674
tmc-5-06	368		7.32		349.30	630	378	99.71%	6.792	6.812	10.22752
tmc-5-05	364		7.29		346.10	630	378	100.50%	6.747	6.714	10.13223
tmc-5-04	387		7.31		380.57	690	414	100.06%	7.411	7.407	11.15259
tmc-5-03	395		7.37		382.49	690	414	99.93%	7.489	7.494	11.20637
tmc-5-02	417		7.47		377.85	690	414	98.05%	7.371	7.518	10.91365
tmc-5-01	406		7.32		372.61	650	390	100.54%	7.382	7.342	10.88191

Table 2: Chemical Analyses of Water Samples from Three Multi-Level Samplers (Cont.).

Well ID	Depth, m	Na mg/L	Na error %	K mg/L	K error %	Ca mg/L	Ca error %	Mg mg/L	Mg error %	NH4-H mg/L	NH4 error %
tmc-9-17	13.11	16.58	2%	2.96	2%	109.15	2%	13.22	4%	0.168	12%
tmc-9-16	13.72	12.62	2%	1.96	2%	101.16	2%	12.29	4%		
tmc-9-15	14.33	10.70	2%	1.75	2%	105.81	2%	11.95	4%		
tmc-9-14	14.94	10.33	2%	1.66	2%	111.62	2%	9.67	4%		
tmc-9-13	15.54	10.28	2%	1.45	2%	110.92	2%	8.34	4%		
tmc-9-12	16.15	10.00	2%	1.37	2%	110.97	2%	8.26	4%		
tmc-9-11	16.76	9.90	2%	1.35	2%	110.57	2%	8.02	4%		
tmc-9-10	17.37	9.87	2%	1.28	2%	109.58	2%	6.57	4%		
tmc-9-09	17.98	10.43	2%	1.13	2%	114.36	2%	5.67	4%		
tmc-9-08	18.59	11.00	2%	1.04	2%	116.16	2%	5.69	4%		
tmc-9-07	19.20	11.48	2%	1.02	2%	117.41	2%	5.78	4%		
tmc-9-06	19.81	11.14	2%	1.11	2%	117.40	2%	5.78	4%		
tmc-9-05	20.42	12.00	2%	1.26	2%	116.01	2%	6.62	4%		
tmc-9-04	21.03	12.35	2%	1.29	2%	115.17	2%	6.99	4%		
tmc-9-03	21.64	15.82	2%	1.15	2%	112.06	2%	8.24	4%		
tmc-9-02	22.25	21.80	2%	1.25	2%	98.90	2%	15.87	4%		
tmc-9-01	22.86	22.11	2%	1.24	2%	97.53	2%	15.97	4%		

Table 2: Chemical Analyses of Water Samples from Three Multi-Level Samplers (Cont.).

Well ID	Sr mg/L	Sr error %	SO4 mg/L	SO4 error %	F mg/L	F error %	Cl mg/L	Cl error %	NO3-N mg/L	N error %
tmc-9-17			34.90	1%	0.21	3%	4.77	4%	0.028	8%
tmc-9-16			30.50	1%	0.19	3%	5.31	4%		2%
tmc-9-15			31.47	1%	0.15	3%	5.56	4%		2%
tmc-9-14			31.86	1%	0.14	3%	5.87	4%		2%
tmc-9-13			30.19	1%	0.14	3%	5.17	4%		2%
tmc-9-12			29.99	1%	0.13	3%	5.14	4%	0.064	2%
tmc-9-11			29.50	1%	0.13	3%	4.95	4%	0.094	2%
tmc-9-10			27.13	1%	0.11	3%	4.25	4%	0.289	2%
tmc-9-09			27.36	1%	0.11	3%	4.39	4%	0.477	2%
tmc-9-08			28.35	1%	0.11	3%	4.65	4%	0.731	2%
tmc-9-07			28.71	1%	0.12	3%	4.74	4%	0.818	2%
tmc-9-06			28.32	1%	0.11	3%	4.67	4%	0.678	2%
tmc-9-05			29.22	1%	0.12	3%	4.84	4%	0.714	2%
tmc-9-04			29.95	1%	0.13	3%	4.97	4%	0.696	2%
tmc-9-03			33.15	1%	0.15	3%	5.69	4%	1.367	2%
tmc-9-02			35.99	1%	0.15	3%	2.60	4%	0.045	2%
tmc-9-01			41.09	1%	0.16	3%	2.20	4%		

Table 2: Chemical Analyses of Water Samples from Three Multi-Level Samplers (Cont.).

Well ID	Alkal. mg/L HCO ₃	Alk. error %	pH (lab)	pH (field)	TDS, mg/L (Calculated)	Cond. (µS) (Measured)	TDS (mg/L) (calc.; 0.6)	Chg Bal (Cat/An)	Σ cations	Σ anions	I 0.5Σmz ²
tmc-9-17					no alk		no sp.cd.	0.00%	7.331	0.863	
tmc-9-16	362		7.30		342.20	610	366	99.30%	6.671	6.718	10.04119
tmc-9-15					no alk		no sp.cd.	0.00%	6.773	0.812	
tmc-9-14	367		7.30		351.60	640	384	100.20%	6.857	6.844	10.36519
tmc-9-13	359		7.30		343.02	610	366	100.72%	6.706	6.658	10.10706
tmc-9-12					no alk		no sp.cd.	0.00%	6.687	0.774	
tmc-9-11	347		7.27		335.12	610	366	103.02%	6.642	6.447	9.940496
tmc-9-10					no alk		no sp.cd.	0.00%	6.470	0.705	
tmc-9-09	360		7.45		340.93	620	372	100.43%	6.656	6.627	10.01309
tmc-9-08					no alk		no sp.cd.	0.00%	6.770	0.774	
tmc-9-07	367		7.58		350.54	630	378	100.81%	6.860	6.805	10.29853
tmc-9-06					no alk		no sp.cd.	0.00%	6.847	0.770	
tmc-9-05	371		7.29		353.20	640	384	100.16%	6.887	6.876	10.35267
tmc-9-04					no alk		no sp.cd.	0.00%	6.892	0.813	
tmc-9-03	377		7.36		362.99	670	402	98.04%	6.987	7.127	10.53688
tmc-9-02					no alk		no sp.cd.	0.00%	7.221	0.826	
tmc-9-01	398		7.45		376.01	690	414	96.43%	7.175	7.440	10.82596
								0.00%	0.000		

Table 3: Anion Chemistry of Pumping Test Samples

April '92 Time† (minutes)	F (mg/L)	Cl (mg/L)	NO3-N (mg/L)	SO4 (mg/L)	Oct. '92 Time†† (minutes)	NO3-N (mg/L)	SO4 (mg/L)	Cl (mg/L)
8	0.088	2.23	0	38.5				
8	0	2.06	0	37.4	2.5	0.000	37.6	2.35
8	0.087	2.14	0	38.6	17.5	0.000	37.6	2.64
8	0	2.12	0	37.4	32.5	0.000	37.8	2.63
38	0.09	2.22	0	38.3	62.5	0.000	37.5	2.59
38	0	2.10	0	37.1	92.5	0.070	37.5	2.64
38	0.082	2.17	0	38.3	122.5	0.124	37.5	2.71
38	0	2.15	0	37.1	152.5	0.176	37.5	2.86
68	0.094	2.28	0.089	37.7	182.5	0.234	37.9	3.09
68	0.094	2.36	0.086	37.4	242.5	0.326	38.0	3.24
68	0.09	2.32	0.089	37.4	302.5	0.404	38.0	3.31
68	0.088	2.31	0.086	37.4	362.5	0.454	38.0	3.43
98	0.083	2.47	0.202	37.3	416	0.490	38.0	3.47
98	0.083	2.50	0.206	37.6				
98	0.093	2.50	0.202	37.5				
98	0.088	2.44	0.202	37.2				
120	0.097	2.58	0.275	37.5				
120	0.096	2.61	0.282	37.5				
120	0.092	2.59	0.271	37.6				
120	0.089	2.55	0.278	37.4				

† Each of four repeat analyses shown in table.

†† Average of two repeat analyses shown in table.

Table 4: Precision and Reproducibility of Measurements of Low Concentrations of Br.

Analysis of low concentrations in GEMS water, 10/21/94

Time	Solution	ch. 1	ch. 2	ch. 3	ch. 4	ch. 5
844	1 mg/l	102.8	105.4	108	108.3	107.1
848	50 mg/l	4.925	9.32	11.22	12.26	10.71
851	300 mg/l	-40.04	-35.51	-34.36	-32.65	-34.89
855	1 mg/l	99.8	102.4	105.5	105.7	100.5
858	50 mg/l	5.007	9.52	10.57	12.17	10.06
901	300 mg/l	-40.5	-35.66	-34.89	-33.27	-35.36
1023	0.2 mg/l	128	131.8	133.5	134.7	131.3
1028	0.4 mg/l	118.3	123	124.9	125.4	124
1032	0.6 mg/l	110.8	116	117.3	118.1	117.8
1036	0.8 mg/l	104.8	110.2	111.5	112.3	111.5
1045	1 mg/l	100.5	105.2	107.2	107.6	103.2
1049	50 mg/l	3.706	9.09	9.75	11.17	10.03
1053	300 mg/l	-41.34	-35.72	-35.43	-33.89	-35.26
1234	1 mg/l	101.7	105.1	107.6	107.9	103.6
1238	50 mg/l	4.463	9.34	10.05	11.28	9.93
1242	300 mg/l	-40.73	-35.62	-35.21	-33.79	-35.23

Median calibrations

log10(mg/l)	ch. 1	ch. 2	ch. 3	ch. 4	ch. 5
0	101.1	105.15	107.4	107.75	103.4
1.699	4.694	9.33	10.31	11.725	10.045
2.477	-40.615	-35.64	-35.05	-33.53	-35.245

Fitted Coefficients

Intercept	101.2584	105.2987	107.5224	107.925	103.7477
Slope	-57.1339	-56.7651	-57.4478	-56.9504	-55.8041

Concentrations (mg/l)

0.340368	0.341304	0.353025	0.33873	0.320824
0.503182	0.487715	0.498318	0.493348	0.433593
0.680763	0.64786	0.675772	0.662728	0.559996
0.866987	0.819704	0.852632	0.837873	0.72624

Known Br, mg/L:	Average	Precision
0.200	0.339	69.43%
0.400	0.483	20.81%
0.600	0.645	7.57%
0.800	0.821	2.59%

D. ANALYSIS OF GEMS TRACER TEST DATA

Introduction

This section presents the data obtained from the GEMSTRAC1 tracer test. Breakthrough curves at a number of multilevel samplers are presented, along with profiles of concentration values along the network centerline for different sampling rounds. Breakthrough curves at some multilevel samplers have been analyzed using a semianalytical solution for conservative transport in a radially convergent flow field, presented by Moench (1989, 1991). This model-fitting exercise should be regarded with some skepticism, due to the clear deviation of tracer test results from model assumptions. Nevertheless, the fitted advective velocities (determined primarily by the time to peak concentration) probably serve as fairly reliable indicators of the vertical distribution of horizontal hydraulic conductivity.

Tracer Injection and Field Operations

The GEMSTRAC1 tracer test began on the morning of Friday, October 7, 1994. Prior to beginning the test a large tent had been set up over the multilevel sampler array to give protection in case of bad weather during the tracer test. Also, extensive head surveys had been run in the discharge and injection wells, to insure that constant head conditions existed throughout the screened intervals for conditions similar to those that would exist during the tracer test. A velocity diffuser was used in the injection well to insure existence of constant head conditions during injection. Approximately 4.5 kg of KBr (3.02 kg of Br^-) was introduced over a two-hour period into the injection well, IW. Pumping at the discharge well, DW, started at 7:32 that morning and was maintained at approximately 69 gpm throughout the duration of the test. It is very likely that an approximately steady state response to this pumping had been established before the start of injection several hours later. Prior to injection, the KBr was mixed with approximately 2000 gallons of water pumped from DW. The discharge from DW was used to fill a 500-gallon tank four times, with portions of the KBr added at regular intervals during each filling. Filling the tank took about 7.5 minutes each time. A jet pump was used to increase circulation in the tank, providing for more uniform mixing of the injectate. The jet pump was started about one minute after the beginning of filling the tank. The jet pump continued to operate in recirculating mode for about 10 minutes after the tank was filled. The outflow from the jet pump was then diverted to a hose leading to the injection well, beginning the injection process. The time required to drain the tank into IW was a little over 16 minutes, implying an injection rate of about 31 gpm. Injection from the first

tank began at 10:13:00 and was completed by 10:29:12. Injection from the second tank began at 10:49:00 and ended at 11:05:05. Tank 3 injection lasted from 11:24:00 to 11:40:06 and injection from the fourth tank lasted from 11:59:00 until 12:15:24.

For the preliminary modeling presented here, all four injections are considered together as one input pulse. In fact, the injection is modeled as a Dirac function, occurring over an infinitesimally short time. This is probably a valid approximation for responses further from the injection well. However, the finite time span of the injection and finite spatial extent of the injected pulse could influence the results at those samplers nearest to the injection well (such as TMC-7 and TMC-8).

At the completion of injection a small pump was started in well 0-8. The pumping at well 0-8 was intended to compensate for the expected influence of pumping at the RWD wells, as described in Section II.I. The pumping rate at well 0-8 was maintained at about 10 gpm throughout the test.

The first sampling round began at about 2:00 in the afternoon on October 7. Initially we performed five sample rounds each day, at four-hour intervals beginning at 6:00 a.m. and ending at 10:00 p.m. The multichannel sampling device described in Section V was used to collect simultaneous samples from all 17 ports at each sampler. The sample tubes were flushed for four minutes prior to sample collection to insure that a fresh sample from the aquifer was collected. The first sample rounds concentrated on the samplers nearest the injection well. We intended to use measured sample concentrations to guide our sampling and gradually extend our collection efforts downgradient. However, the earliest samples indicated that at some levels in the aquifer tracer was moving much more rapidly than we had expected. By the afternoon of Sunday, October 9, we had extended our sampling efforts all the way down the centerline. Sampling frequency gradually decreased, with the sampling strategy being guided by the observed concentrations as the test progressed.

Typically samples gathered on one day were analyzed in the lab on the next day, using the bromide analysis procedures described in Section IV.B. In all, 5967 samples were analyzed.

Observed Breakthrough Curves and Profiles

The map of MLS locations and profile of port locations along the centerline were presented in Section II.I (Figures 1 and 2 of that section). Figures 1 through 12 show the breakthrough curves at all ports for the twelve MLS where data density is great enough to justify plotting curves. Note that time and concentration scales vary from one sampler to

the next. However, the scales are the same for all four panels for one MLS, in order to facilitate comparison between the breakthrough curves at one MLS.

Figures 13 through 30 show profiles of concentration data from samplers along the centerline for selected sample rounds. The sampling time shown for each profile is the average sampling time for that sample round. In some cases sample rounds lasted up to a couple hours, a time that is not insignificant compared to the time between sample rounds, at least early in the test. The vertical scale is in terms of feet above datum. The datum is at an arbitrary level which corresponds very roughly with the bottom of the aquifer. The concentration scale for each sample round is determined by the maximum concentration along the centerline for that sample round. Thus, the concentration scale varies from one figure to the next and some of the apparent variation between sample rounds is simply a result of this scale change. Therefore, care should be taken when comparing these plots. Each one should be regarded as presenting the relative variation in concentration along the centerline for that sample round. The plot for a given sampler is empty if that sampler was not sampled in that round. The data points are connected by lines simply to clarify their vertical order. There is no reason to believe that such a smooth variation actually exists between vertically adjacent ports. Given the concentration contrasts observed between ports even one foot apart, it is quite possible that abrupt changes in concentration can occur between ports; i.e., the scale of vertical variation might be significantly smaller than the vertical sample interval.

A number of conclusions can be drawn directly from the experimental breakthrough curves and profiles. First of all, it is clear that sharp contrasts in concentration between vertically adjacent ports were maintained throughout the test. These contrasts seem to indicate that minimal mixing occurred between ports. Possibly the simultaneous pumping of all 17 ports created flow divides between vertically adjacent ports, minimizing the mixing between zones. Regardless of the exact mechanics, the procedure seems to be quite successful in sampling from isolated zones around each port.

It is also clear that we missed the peak concentrations at a number of ports in samplers TMC-5 through TMC-1 (Figures 4 through 8), and possibly even in TMC-6 (Figure 3). Based on our design modeling we decided to concentrate our sampling efforts on samplers close to the injection well during the first few days of the test. We intended to use results obtained from these early sample rounds to guide further sampling efforts. However, in some zones the tracer moved out much faster than anticipated and peaks had already passed some ports before we extended our sampling down the centerline. By the time we finally sampled all the way along the centerline, about two days into the test, a significant amount of tracer had already moved all the way through the system (Figures 8

and 18). Future tests will include full-centerline sample rounds beginning immediately after tracer injection.

The hydraulic compensation pump in well 0-8 proved to be unnecessary if not detrimental. Large concentrations were observed in some ports in samplers on the east side of the network, the side toward the compensation well, as shown in Figures 9 through 12. Only small concentrations were observed in samplers on the west side, the side toward the rural water district wells, except at TMW-8, where concentrations in a few ports rapidly rose and fell in the first few days of the test. Thus it is likely that the pumping at the RWD wells had little effect on the test while the pumping at the compensation well might even have drawn the plume a little to the east of the centerline. The samplers on the west side were sampled fairly infrequently, based on their apparent lack of activity.

Taken together, the centerline samplers TMC-3, TMC-2 and TMC-1 (Figures 6 through 8) exhibit rather mysterious behavior. All but two ports at TMC-3 and most ports at TMC-2 exhibited negligible concentrations throughout the tracer test. However, non-negligible (though perhaps small) concentrations occurred in most ports at TMC-1, closer to the injection well. The tracer seems to have missed samplers TMC-3 and TMC-2 at most vertical levels in the aquifer. Two possible explanations for this are that a vertically extensive region of low permeability material exists in the vicinity of TMC-2 and TMC-3 or that the hydraulic compensator well actually caused the tracer to follow a curved path (in the horizontal), bypassing TMC-3 and TMC-2, but returning to the centerline before reaching TMC-1. The latter explanation is possibly supported by the anomalous appearance of a very large spike at port 10 in TMC-1 relatively late in the test (peaking at 14 days). No hint of this spike occurs anywhere upgradient along the centerline, or in the samplers in the east line, for that matter. Either this particular packet of tracer is of extremely limited vertical extent and passed between ports in the upgradient centerline samplers TMC-3, TMC-5 and TMC-7 or it is of limited horizontal extent and missed or skirted the centerline until it reached TMC-1.

Fitting of Selected Breakthrough Curves

The radially convergent transport model presented by Moench (1989, 1991) has been used to analyze breakthrough curves from the three centerline wells nearest the injection well, TMC-8, TMC-7 and TMC-6, and from the well nearest the discharge well, TMC-1. This model is not strictly applicable to the GEMSTRAC1 tracer test, due to the clear discrepancy between model assumptions and actual test conditions. Nevertheless, the model can be reinterpreted to be at least approximately applicable to the tracer test.

First of all, Moench presented a solution describing vertically averaged flow and transport in a confined aquifer. We apply the model to essentially point measurements of concentration at particular vertical levels in an aquifer. This approach is valid assuming that flow and transport are stratified, with negligible tracer transfer between vertically adjacent flow 'zones'. Even if it can be considered valid, this assumption raises a number of as yet unanswered questions: What is the typical scale of a flow zone (or the vertical correlation length of the velocity field)? How does that scale compare to the vertical sampling or mixing scale associated with a given port? What is the relationship between the vertical correlation scale of the velocity field and the correlation scales, both horizontal and vertical, of the hydraulic conductivity and dispersivity fields? These questions will be addressed in future work. Without answering them, the fitted parameters can be regarded only as apparent parameters, somehow typifying an unspecified vertical interval surrounding each port and also averaging horizontal property variations between the injection well and the port.

Moench (1989) presents a solution describing radial transport from an injection well to a pumping well, separated by a distance r_L , where the transport is influenced only by advection and longitudinal dispersion. The radius of the pumping well is represented by r_w . The aquifer is assumed to be of constant thickness, h , with a constant porosity, ϕ . Moench uses the symbol q_0 to represent the pumping rate. However, we will use Q to represent the pumping rate and $q_0 = Q/(\phi h)$ to represent the pumping rate per unit thickness of aquifer. In addition, we assume that q_0 varies in the vertical direction as a result of flow stratification, i.e.,

$$Q = \sum_i q_{0i} h_i \phi_i$$

where q_{0i} , h_i , and ϕ_i are the flux rate, thickness, and porosity associated with a given flow zone, i , in the vertical. Presumably the stratification of flow, represented by the vertical variation of q_0 , would be controlled primarily by the vertical variation of the horizontal hydraulic conductivity. Thus we use q_0 as a fitting parameter when analyzing the breakthrough curve at each port, taking the resulting value to reflect the hydraulic conductivity at that level in the aquifer. This is similar to the approach taken by Thorbjarnarson and Mackay (1994) in analyzing an induced gradient tracer test at the Borden site. The value of q_0 for a given layer determines the advective travel time, t_* , from the injection well to the pumping well according to

$$t_a = \frac{\pi(r_L^2 - r_w^2)}{q_0}.$$

The importance of longitudinal dispersion is quantified by the Peclet number, $Pe = r_L/\alpha$, where α is the longitudinal dispersivity. Lower Peclet numbers represent more dispersive transport. Breakthrough curves for high Peclet numbers are sharp, nearly symmetrical peaks, whereas breakthrough curves for low Peclet numbers are more diffuse and skewed, with a slow decline to background concentration levels after the peak concentration has passed.

In dimensionless form, the partial differential equation describing conservative radial transport with longitudinal dispersion is

$$\frac{1}{Pe} \frac{\partial^2 C_D}{\partial r_D^2} + \frac{\partial C_D}{\partial r_D} = \frac{2r_D}{(1 - r_{wD}^2)} \frac{\partial C_D}{\partial t_D}$$

where the dimensionless time and radius are related to the actual time and radius according to

$$t_D = t/t_a$$

$$r_D = r/r_L$$

and, for a slug (Dirac delta) input, the dimensionless concentration, C_D , is related to the actual concentration by

$$C_D = C/C_i$$

with

$$C_i = \frac{M}{\pi h \phi (r_L^2 - r_w^2)}.$$

M is the injected tracer mass. The reference concentration C_i represents the concentration that would exist if the tracer mass were uniformly distributed throughout the entire volume of water between r_w and r_L . As discussed below, this is an appropriate reference concentration to use when analyzing concentrations measured in the pumping well.

However, this definition has to be modified in order to be appropriate for responses at observation wells between the pumping well and the injection well.

In the main body of his 1989 paper, Moench presents a solution describing the time variation of the tracer concentration observed in a pumping well in response to either a pulse or step injection of tracer in an injection well a radial distance r_L away, under the assumption that the injection does not significantly perturb the flow field. The derivation of the solution is simplified by treating the tracer mass as if it were initially distributed uniformly around a ring of radius r_L , rather than concentrated in a small zone around the injection well. A similar approach is used by Welty and Gelhar (1994). This approach is valid for describing the concentrations measured in the pumping well, since these represent an average of concentrations from a full 360 degree arc around the well.

In an appendix Moench presents a solution for an arbitrary observation radius, between the pumping and injection wells. This solution also represents an angularly averaged concentration, treating the tracer mass as if it were initially distributed around a full circle surrounding the pumping well. Moench dismisses this solution as not being of practical use, since only the pumping well captures the entire tracer mass; thus only the pumping well concentrations can be treated using the angularly averaged simplification of the tracer distribution. Responses at observation points outside the pumping well will clearly be influenced by the actual angular distribution of the tracer. This angular distribution will be influenced both by the geometry of the injected pulse and by the subsequent effects of transverse dispersion, which is neglected in the development of the solution. Moench states that while the results at the pumping well are insensitive to transverse dispersion, results at observation wells could be significantly affected by transverse dispersion.

The solution for arbitrary observation radii can be modified to be of practical use under the assumption that transverse dispersion is truly negligible. In the absence of transverse dispersion, the tracer cloud would remain within the streamtube that contained it at the end of injection. Therefore, in a purely radial flow field, the angle (θ) encompassed by the wedge of solute would be determined by the mechanics of the injection process and would not change thereafter. Assuming that the tracer was initially distributed uniformly across the wedge (in the direction transverse to flow), then the concentration in the wedge could be obtained by multiplying the concentration given by Moench's solution by the factor $2\pi/\theta$, the ratio of the two averaging angles involved. If the initial width of the tracer mass transverse to flow is Δy , then the angle encompassed by the tracer is given by

$$\theta \cong \frac{\Delta y}{r_L}.$$

where a small-angle approximation for inverse tangent is used. Thus the concentration in the wedge can be obtained by multiplying the concentration given by Moench's solution by the factor $2\pi r_L/\Delta y$, which is simply the ratio of the circumference of the circle of radius r_L to the transverse width of the injected pulse. Alternatively, this geometric factor could be seen as scaling the reference concentration, C_i , yielding

$$C_i = \frac{2\pi r_L}{\Delta y} \frac{M}{\pi h \phi (r_L^2 - r_w^2)}$$

If transverse dispersion is in fact non-negligible, then analysis with this model will lead to an overestimation of the longitudinal dispersivity, since the effects of transverse dispersion will be attributed to longitudinal dispersion. We assume that transverse dispersion probably had little influence on the GEMSTRAC1 data, due to the advectively-dominant nature of the transport.

The inability to exactly characterize the vertical distribution of tracer immediately after injection is a major source of uncertainty in analyzing the GEMSTRAC1 data. It is quite likely that different amounts of tracer entered different zones and penetrated those zones to different distances. That is, the factor $M/(h\phi\Delta y)$ probably varies considerably in the vertical, leading to considerable vertical variation in C_i . Thus, for the model-fitting results presented here, C_i is treated as an unknown parameter, along with q_0 and α . Unfortunately, this parameterization leads to a highly non-unique model in a number of cases, especially for those ports at which we missed the peak concentration and sampled only the falling limb of the breakthrough curve. In these cases a number of different combinations of C_i , q_0 and α fit the data about equally well. The effects of the non-uniqueness are exacerbated by systematic deviations between the data and the model. Typical systematic deviations observed in the test data are double-peaked behavior and excessive tailing, both discussed further below. These difficulties made it impossible to totally automate the fitting process. Each breakthrough curve had to be treated on an individual basis and analyzed with a fair amount of user-intervention concerning initial parameter estimates and weighting of different segments of data. As a result, fewer breakthrough curves have been analyzed to date than was originally anticipated. So far, data from four samplers (TMC-8, TMC-7, TMC-6, and TMC-1) have been analyzed.

It should be noted that the sampled concentrations have been treated as resident concentrations in the analyses presented here. Samples obtained from a discharge well will tend to be flux-averaged, rather than resident, concentrations (Moench, 1989; Valocchi, 1986; Parker and van Genuchten, 1984). The resident concentration is the actual concentration in the pore fluid, averaged over a certain volume of aquifer material. The flux-averaged concentration, on the other hand, is a characteristic of the transport problem: the ratio of the solute flux density to the fluid flux density. The distinction can be very important in some situations (Parker and van Genuchten, 1984). However, it is not clear what kind of concentration is obtained by pumping from a sampling port. This question is the subject of ongoing investigation.

The code implementing Moench's solution was obtained from the author (Moench, personal communication, 1994). His code implements only the solution at the pumping well. We modified the code to allow modeling of breakthrough curves at observation wells, incorporating the results presented in the Appendix of Moench (1989). In addition, as suggested by Moench (1991), the complex Airy functions in Moench's code were replaced by those from Amos (1986), in order to allow modeling of the very sharp breakthrough curves observed at some ports. As stated in Moench (1991), Moench's original Airy function subroutines allow computation with Peclet numbers up to about 220, whereas the use of Amos's functions extend the range of Peclet numbers up to about 1350 (under IEEE arithmetic). Our experiments with the code bore out these results. The minimum fitted dispersivity was 0.04 feet, corresponding to a Peclet number of 1163, since the distance from the injection well to the pumping well is 46.5 feet. Therefore, the functions from Amos (1986) were required in order to model the breakthrough curves at a number of ports.

For the sake of the fitting, Moench's program was converted into a subroutine then linked into the data analysis package S-Plus (Statistical Sciences, 1993). Several different methods were then used to adjust the three model parameters to produce a least-squares match between the observed and computed breakthrough curve at each MLS port. The exact sequence of operations varied from port to port, but in most cases was the following: 1) Computed and observed breakthrough curves were compared graphically and the parameters were adjusted manually until a reasonable graphical match between the two curves was found. 2) A downhill simplex algorithm was used to further minimize the least-squares deviation between modeled and fitted data, starting from the manually obtained parameters. This algorithm consisted of an S translation of the Fortran subroutine amoeba found in Press et al. (1992). 3) The final step for each port was generally to use the S-Plus function for nonlinear least-squares regression with bounds,

nlregb, to compute the optimal parameters, beginning with the final parameters computed using the simplex algorithm. The nonlinear regression routine seemed to have a tendency to get trapped in local minima, sometimes corresponding to a very poor match to the data. In particular, the regression algorithm never substantially changed the dispersivity from the value supplied as an initial estimate. The final values for q_0 and C_i were influenced by the selected initial value for dispersivity. Thus the first two steps were employed in order to find reasonable starting estimates to use in nlregb. The simplex algorithm, although much less efficient than nlregb, was also much less sensitive to the chosen initial parameter values. In a number of cases variable weighting was used during steps 2 and 3 in order to cause the minimization algorithms to essentially ignore certain portions of the data, such as a small peak superimposed on the shoulder of a larger peak or an excessively heavy tail. Additional modifications were made in certain cases in order to obtain what was considered a reasonable fit.

Figure 31 shows the observed and fitted breakthrough curves for TMC-8, a detailed sampler approximately six feet from the injection well. Fortunately, all the peak breakthroughs were measured at this sampler, and most breakthrough curves can be modeled reasonably well using the radially convergent transport model. Notable exceptions are ports 2, 7, 8, and 17. Port 2 exhibits an early rise with a hint of an early peak, followed by a plateau leading to a second peak. Only this second peak has been fitted, since the first peak is not distinguished clearly enough to be analyzed. The response at port 7 is one of the prime examples of the excessive tailing seen at several ports. The same thing occurs to a lesser extent at port 8. In both these cases the data in the tails have been downweighted in order to produce a reasonable fit in the vicinity of the peak. At port 17, two very sharp and separable peaks occur and each peak has been analyzed separately.

Clearly the validity and meaning of the fitted parameters can be called into question when such systematic deviations are essentially ignored in the fitting process. This approach could be valid assuming that the data could be separated or deconvolved into a number of distinct events and analyzed separately. In the case of double peaked behavior with non-overlapping peaks, each peak could reasonably be fitted separately, each viewed as a single 'event'. The two peaks occurring at port 17 are essentially non-overlapping. However, in general, data corresponding to a given peak would need to be corrected for the influence of overlapping events before being analyzed with the radial transport model. Since we have applied no corrections it is possible that we are overestimating both the reference concentration and the dispersivity, since the peaks

would be both lower in magnitude and sharper if they were separated from overlapping events. Future work will include more careful analysis of these issues.

It should be noted that both double-peaked behavior and excessive tailing have been observed in other transport studies. Li et al. (1994) discuss the effects of local stratification of hydraulic conductivity on transport in soils, examining the idealized case of stratification into two conductivity regimes. They note that the flux-averaged transport (with concentrations averaged across the two layers) in this case is separated into three regimes: 1) short-distance transport characterized by double-peaked behavior, each peak corresponding to transport in one of the layers, 2) transitional transport characterized by a single peak with excessive tailing, as the two peaks begin to overlap due to longitudinal dispersion and mix due to lateral diffusion, and 3) long-distance transport characterized by a single Gaussian peak. Such mechanisms could explain some of the double-peaked and heavy-tailed behavior seen in GEMSTRAC1 data assuming that some ports are yielding samples that represent mixtures from distinct transport zones. There is some evidence that this is occurring. For example, at TMC-8 (Figure 1), port 8 exhibits double-peaked behavior, with the first peak occurring at about the same time as the peak in port 7. Similarly, the first peak at port 17 could correspond with the peak at port 16. Similar behavior was observed by Thorbjarnarson and Mackay (1994) in an induced gradient tracer test at the Borden site.

The fitted parameter values for the breakthrough curves at TMC-8 are shown in Table 1. The number of data points for each breakthrough curve and the root-mean-squared (rms) residual from the fit are included in the table. The rms residual should be judged relative to the fitted C_i , since a poor fit at a port with relatively low concentrations could yield a smaller rms residual than a good fit at a port with higher concentrations. Note that the fitted value for q_0 for the first peak at port 17 does indeed correspond well with that from the peak at port 16.

Figure 32 shows the fitted breakthrough curves at TMC-7 and Table 2 contains the corresponding fitted parameters. Port 16 of TMC-7 never yielded any samples, either due to damage during installation or due to being clogged by and/or adjacent to low permeability sediments. At ports 11 and port 12, an estimated background concentration of 0.2 mg/l (determined simply from visual inspection of the breakthrough data) was subtracted from the concentration values prior to fitting. The low concentration values observed at these locations required this correction. The breakthrough data at several ports (1, 7, 12, 13, and 14) clearly exhibit the excessive tailing mentioned above.

Fitted breakthrough curves for TMC-6 are shown in Figure 33 and the corresponding parameter values are contained in Table 3. A number of these fits are

fairly nonunique, since we failed to sample the rising limbs of the breakthrough curves at a number of ports. Two peaks have been fit at port 8, even though the two peaks overlap a fair amount. Strictly speaking, the data from each peak should have been 'corrected' for the influence of the adjacent peak prior to fitting. Despite the lack of correction, it is hoped that the fitted values of q_0 in this case are still reasonably accurate. The fit at port 13 is actually a combined fit of two peaks, ignoring the narrow gap between them.

The fitted breakthrough curves for TMC-1 are shown in Figure 34, and the fitted parameters are shown in Table 4. The data from ports 2, 11, 12, and 13 are essentially at background levels, with no discernible breakthrough, and so were not analyzed. As shown in Table 4, estimated background concentrations were subtracted from the responses at a number of ports prior to analysis.

Discussion and Conclusions

Despite the preliminary nature of the data analysis to date, some reasonable conclusions can still be drawn from comparing fitted parameters. The fitted values of q_0 at the four samplers are plotted in Figure 35. Two points are shown for those ports at which two peaks were fit (port 17 of TMC-8 and port 8 of TMC-6). The consistency of these results is quite striking, especially when comparing TMC-8 and TMC-6. These results indicate a consistent high permeability zone between about 5 and 8 feet above datum and two more at around 14 and 17 feet above datum. The high permeability zone near 14 feet above datum is not reflected in the results at TMC-7; it could simply occur between ports 6 and 7 at this sampler. There seems to be a slight downward shift to the vertical locations of high permeability zones between TMC-6 and TMC-1. This downward shift should be better characterized after analysis of the data from intervening samplers.

The fitted values of reference concentration, C_i , are shown in Figure 36. Generally they correlate well across the samplers. Also, it is clear from comparing Figures 35 and 36 that higher permeability zones have a tendency to have higher C_i values. This is not surprising, since the higher permeability zones would be expected to take more of the injected tracer than lower permeability zones. The results give the strong impression that very little tracer entered the upper half of the aquifer, above about 19 feet above datum. This results essentially in an undersampling of the permeability distribution in the top half of the aquifer. For future tests we will consider how to create an injected pulse with a more uniform vertical distribution of tracer, hopefully allowing us to observe more significant breakthroughs in higher ports. Nevertheless, it is clear that the identification and characterization of narrow, high permeability zones is crucial to

adequate assessment of transport problems, since these zones can transport large portions of the contaminant mass rapidly downgradient.

Figure 37 shows the fitted dispersivities at all four samplers. Again, these seem to correlate reasonably well across the site, but the correlation is much less striking than that for the other two parameters. There is a general tendency for the fitted dispersivity to increase with increased transport distance. A number of investigators have proposed that dispersivity might increase with transport distance, due, for example, to the solute encountering increasing scales of heterogeneity as it is transported. A review of such investigations is found in Gelhar et al. (1992). Our results should not be taken as a decisive indication of a scale effect in the dispersivity, however. The current analyses are quite preliminary and it is possible that the apparent increase in dispersivity with distance is at least partly due to neglect of other transport processes (such as lateral dispersion). In addition, the nonuniqueness of the fitting process could contribute to this apparent increase.

Figure 1: Breakthrough Curves at TMC-8

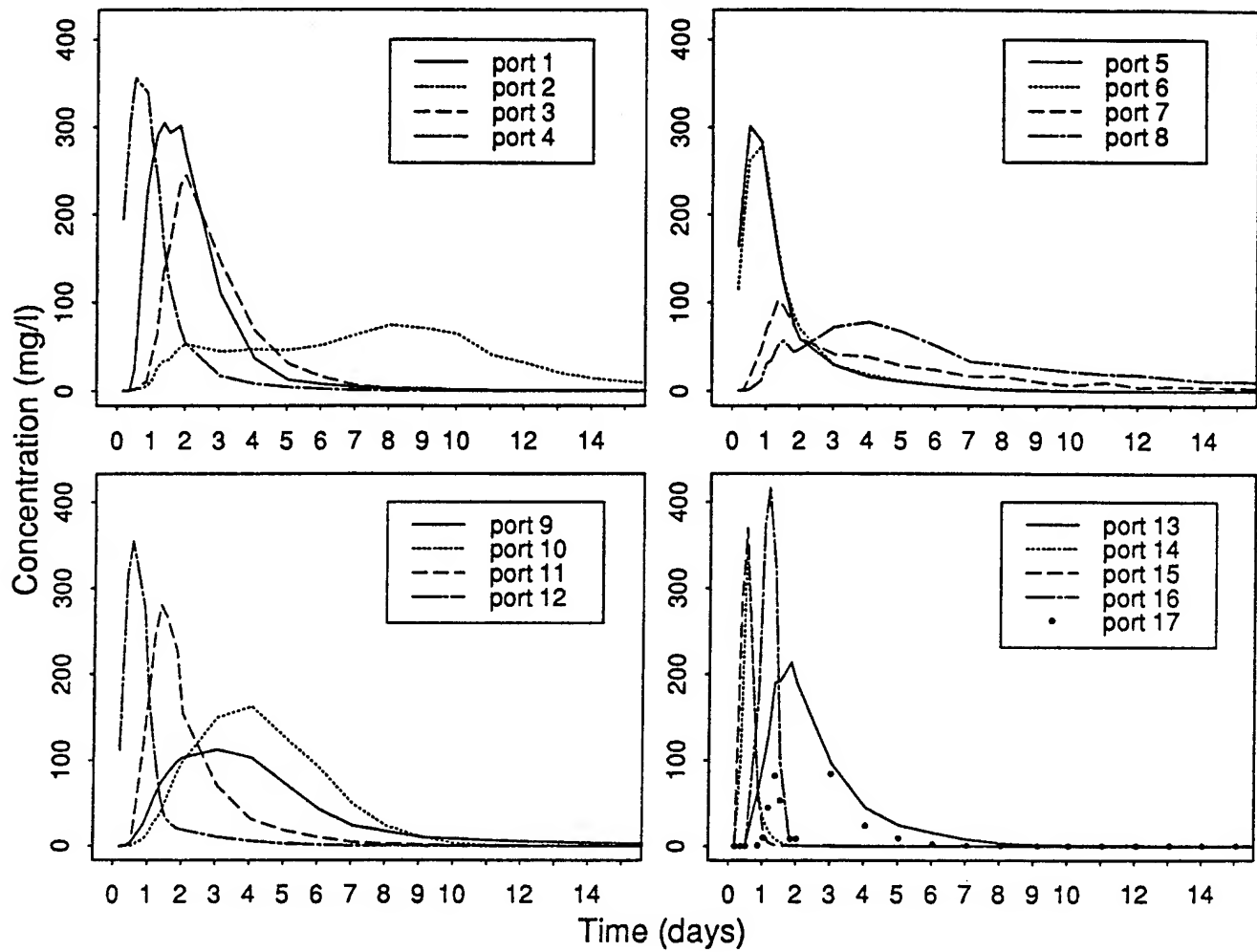


Figure 2: Breakthrough Curves at TMC-7

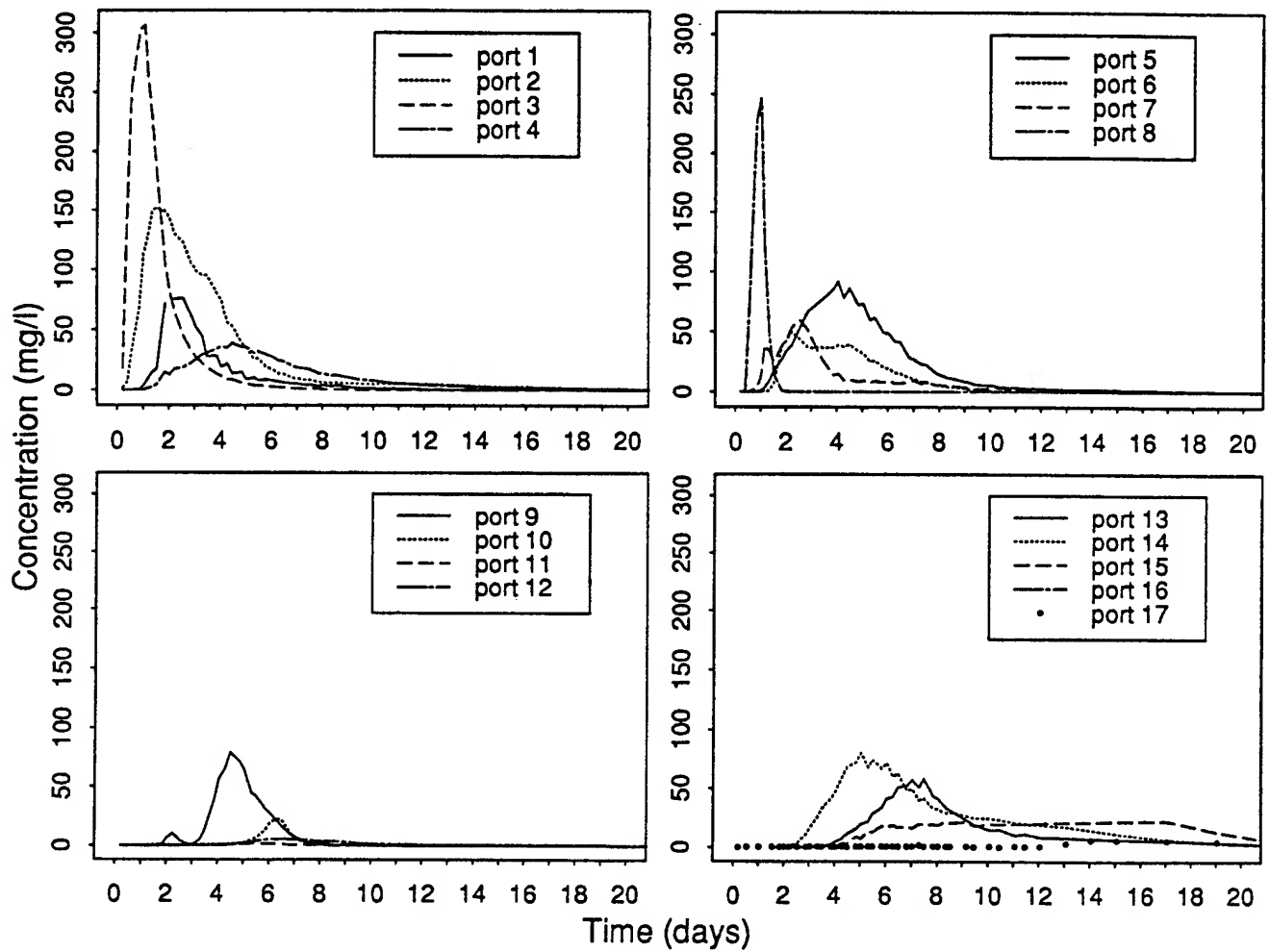


Figure 3: Breakthrough Curves at TMC-6

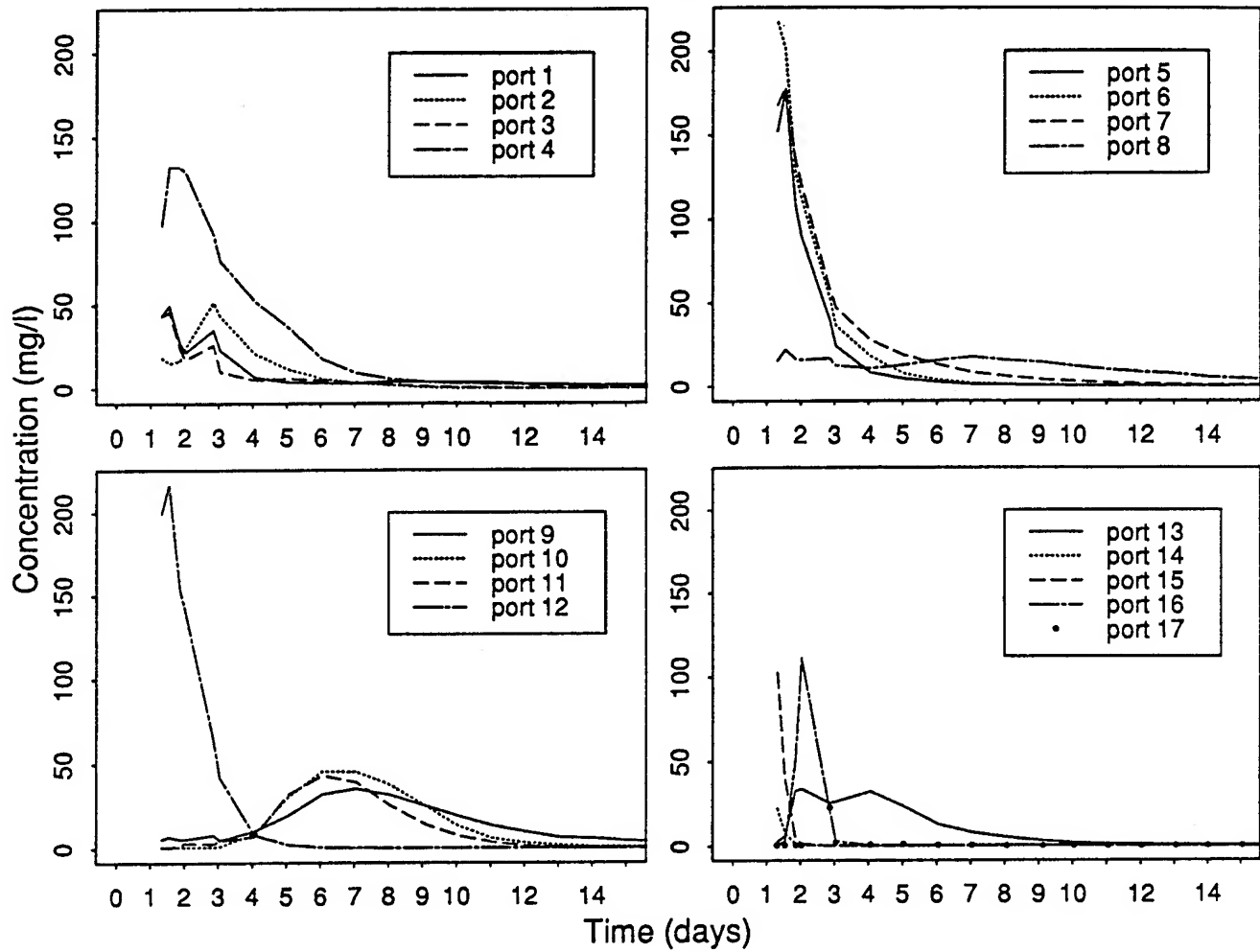


Figure 4: Breakthrough Curves at TMC-5

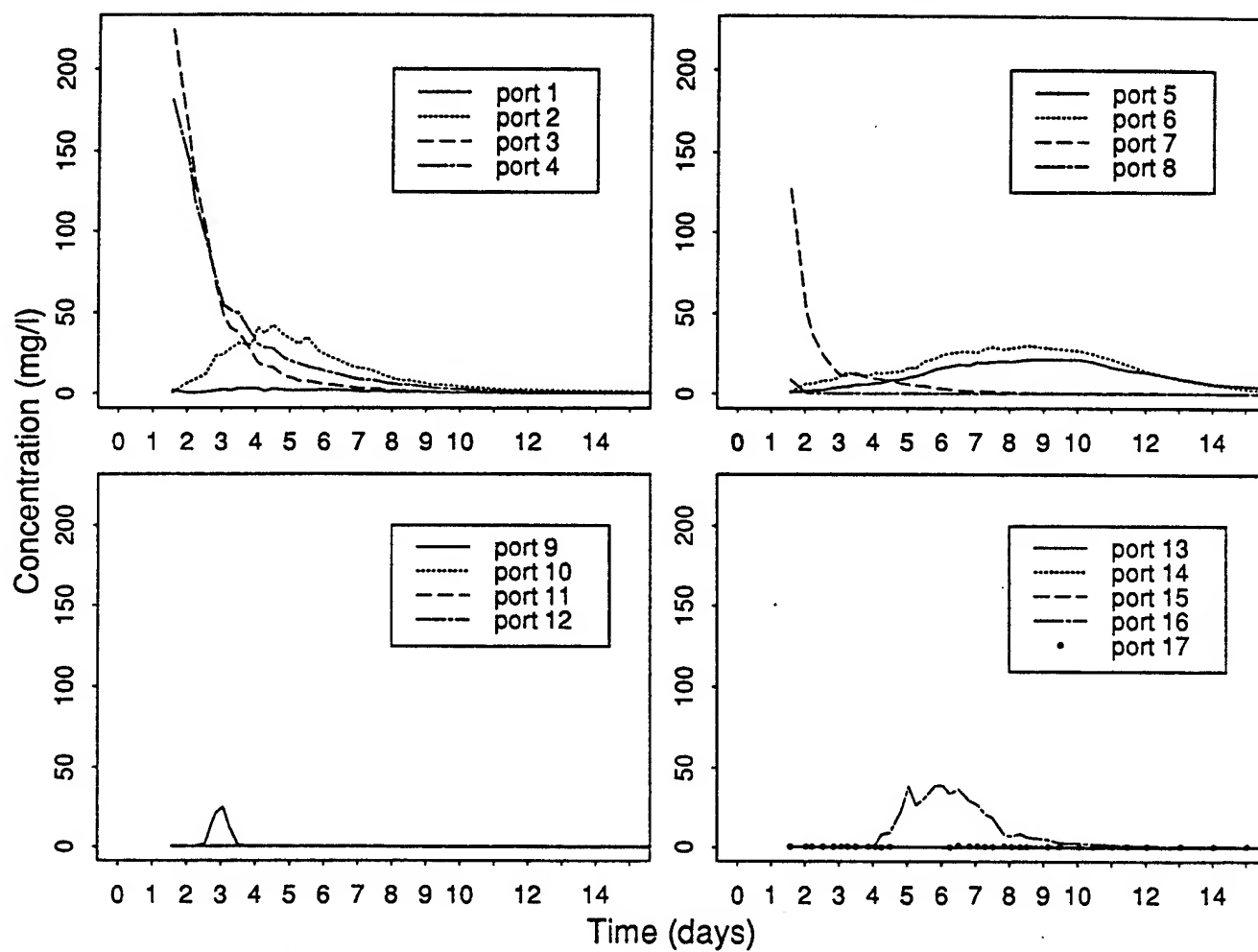


Figure 5: Breakthrough Curves at TMC-4

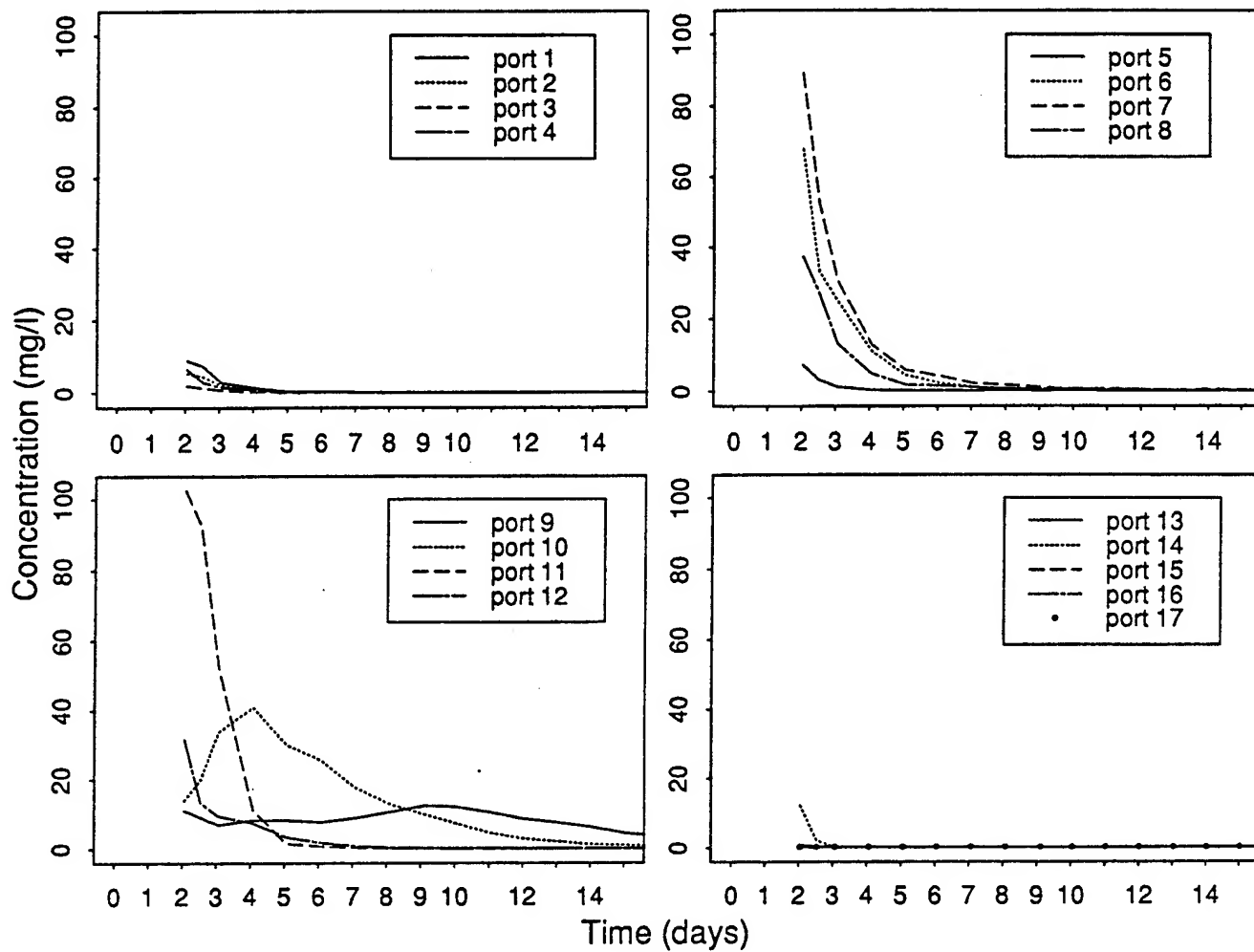


Figure 6: Breakthrough Curves at TMC-3

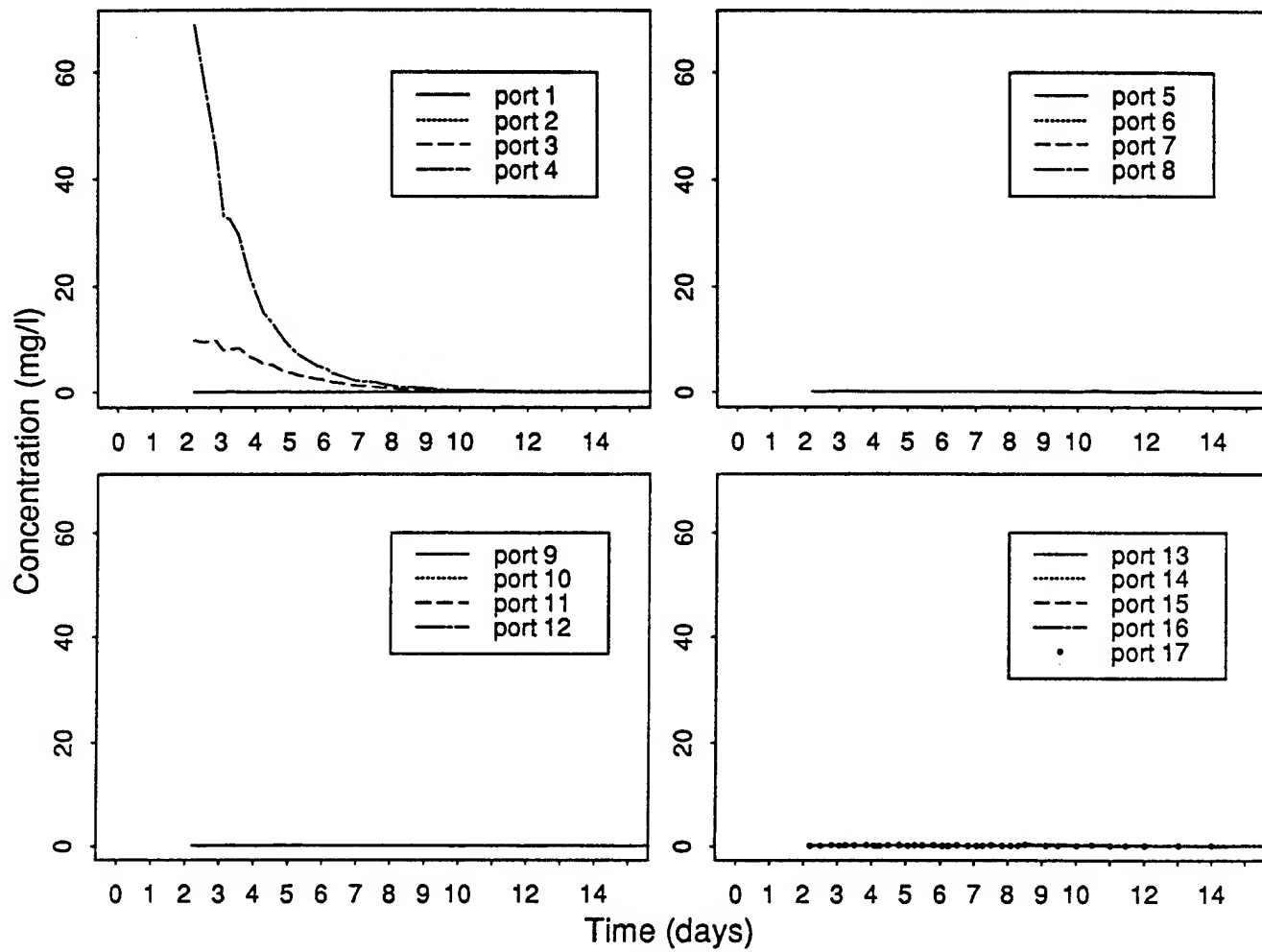


Figure 7: Breakthrough Curves at TMC-2

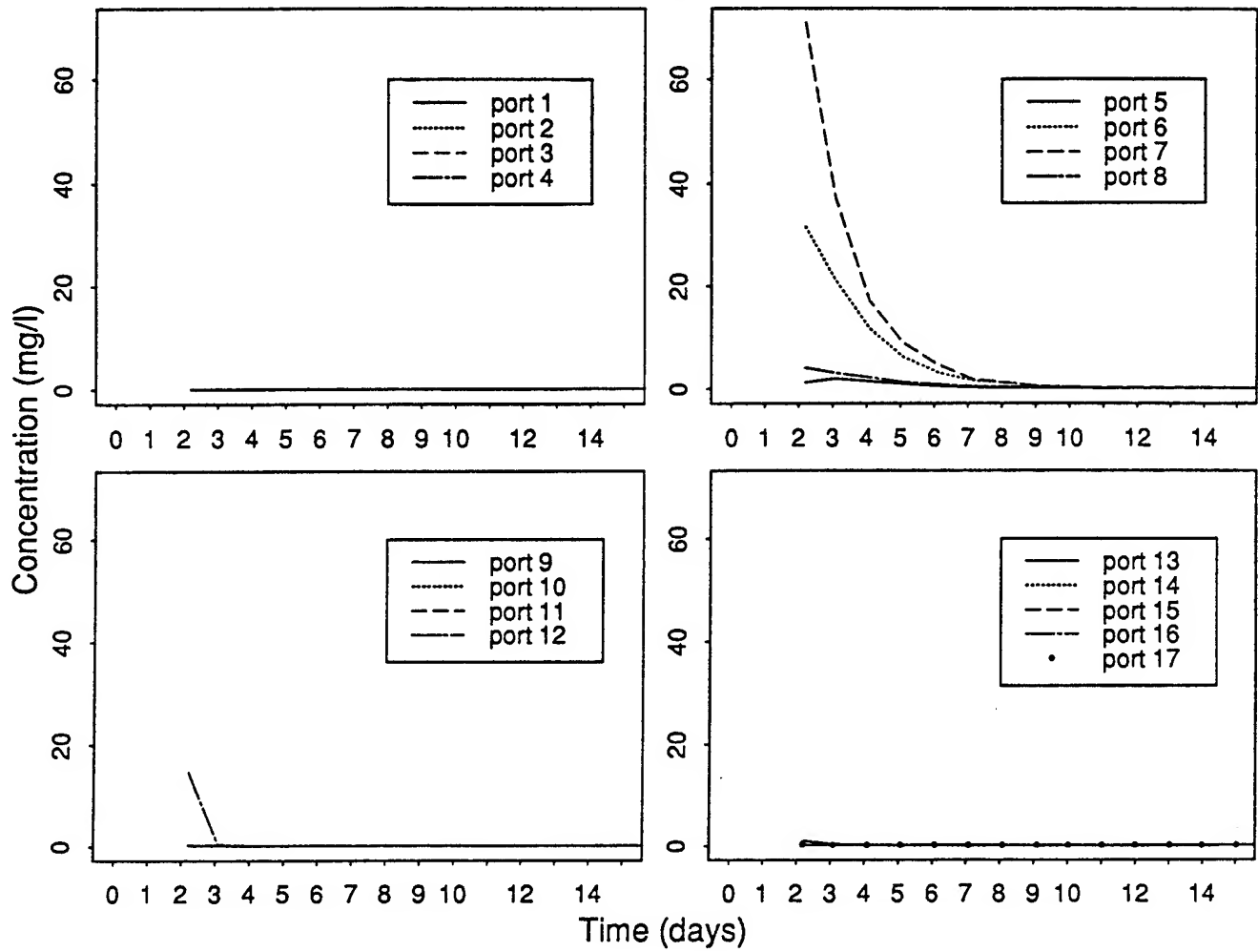


Figure 8: Breakthrough Curves at TMC-1

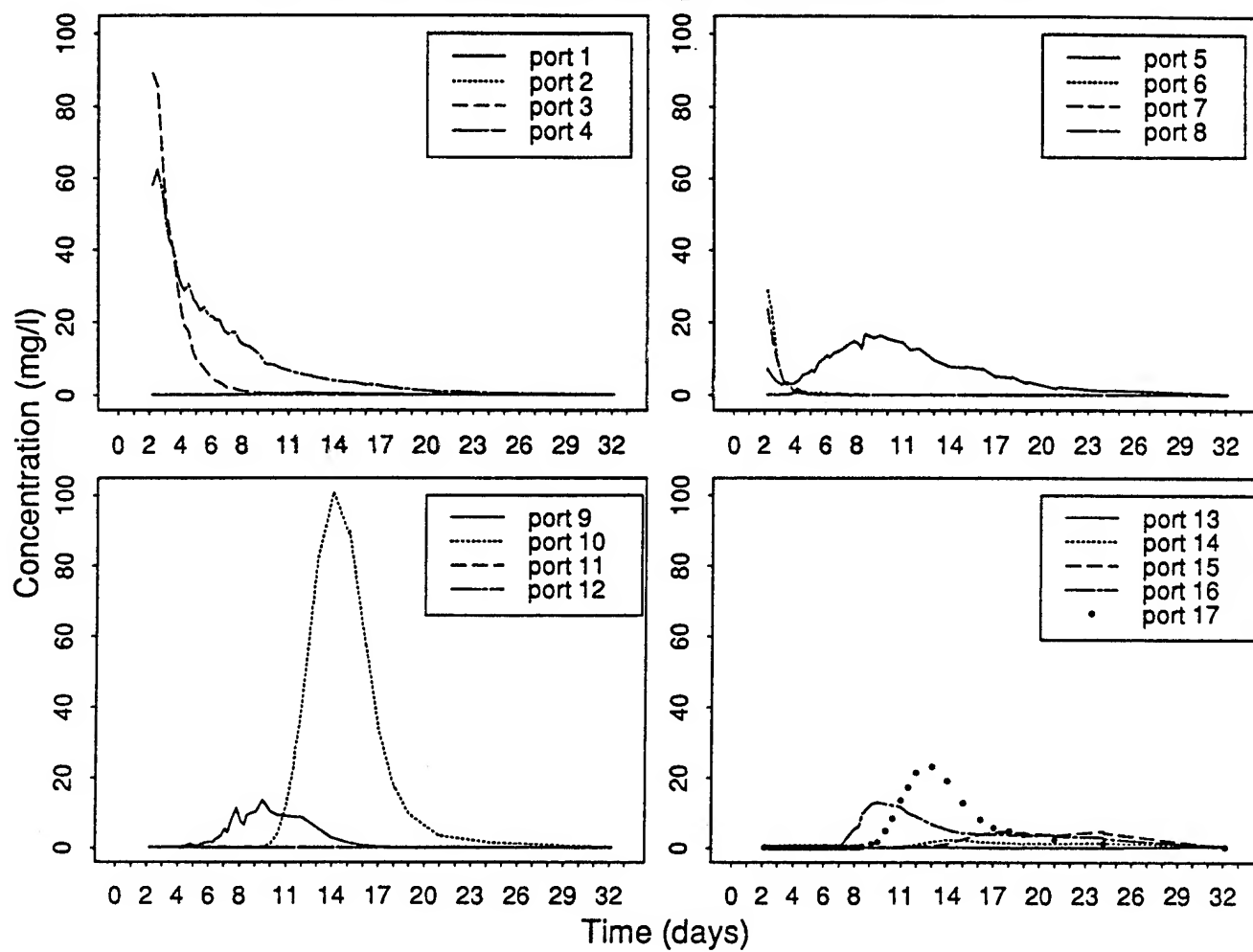


Figure 9: Breakthrough Curves at TME-6

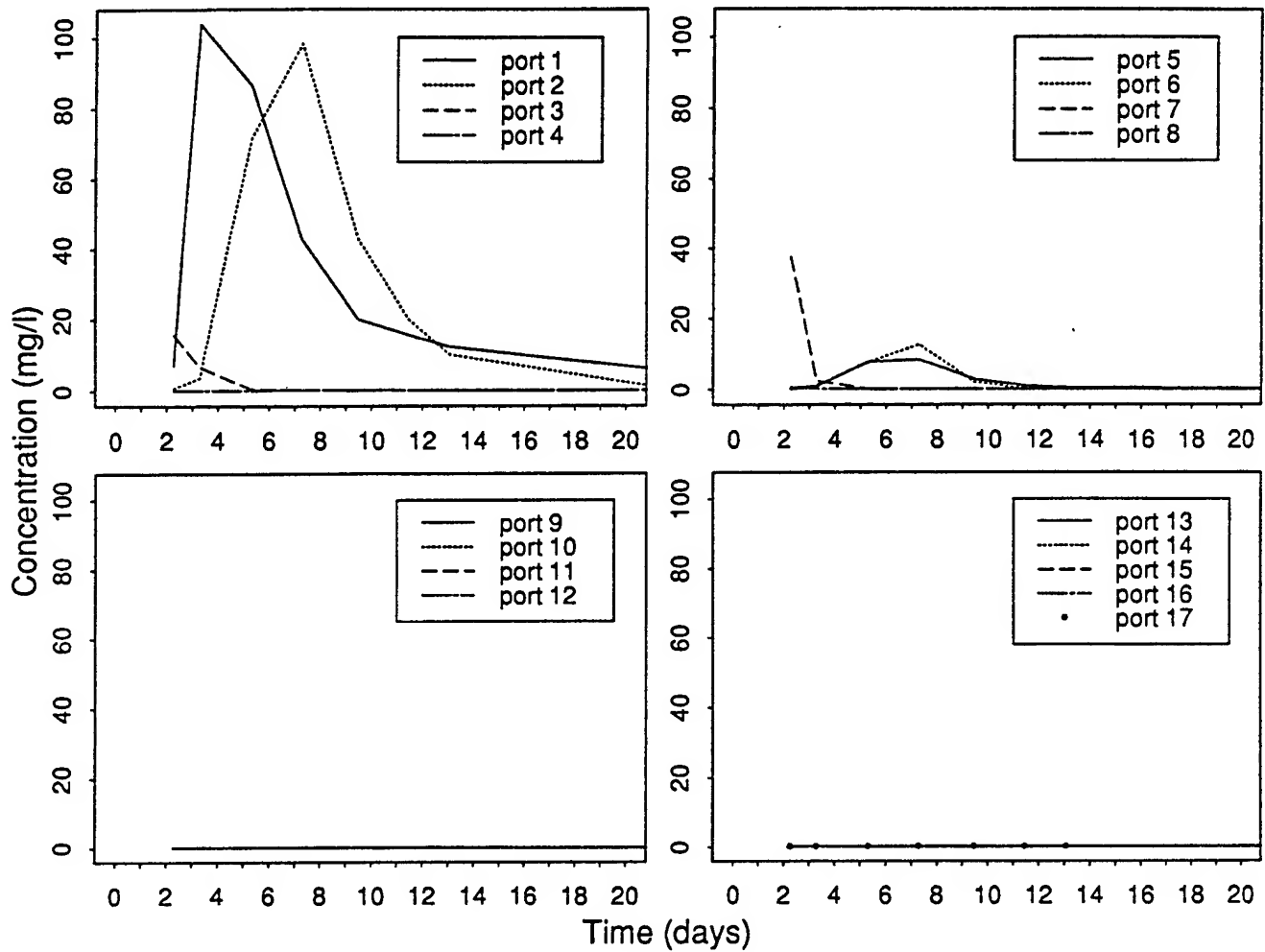


Figure 10: Breakthrough Curves at TME-5

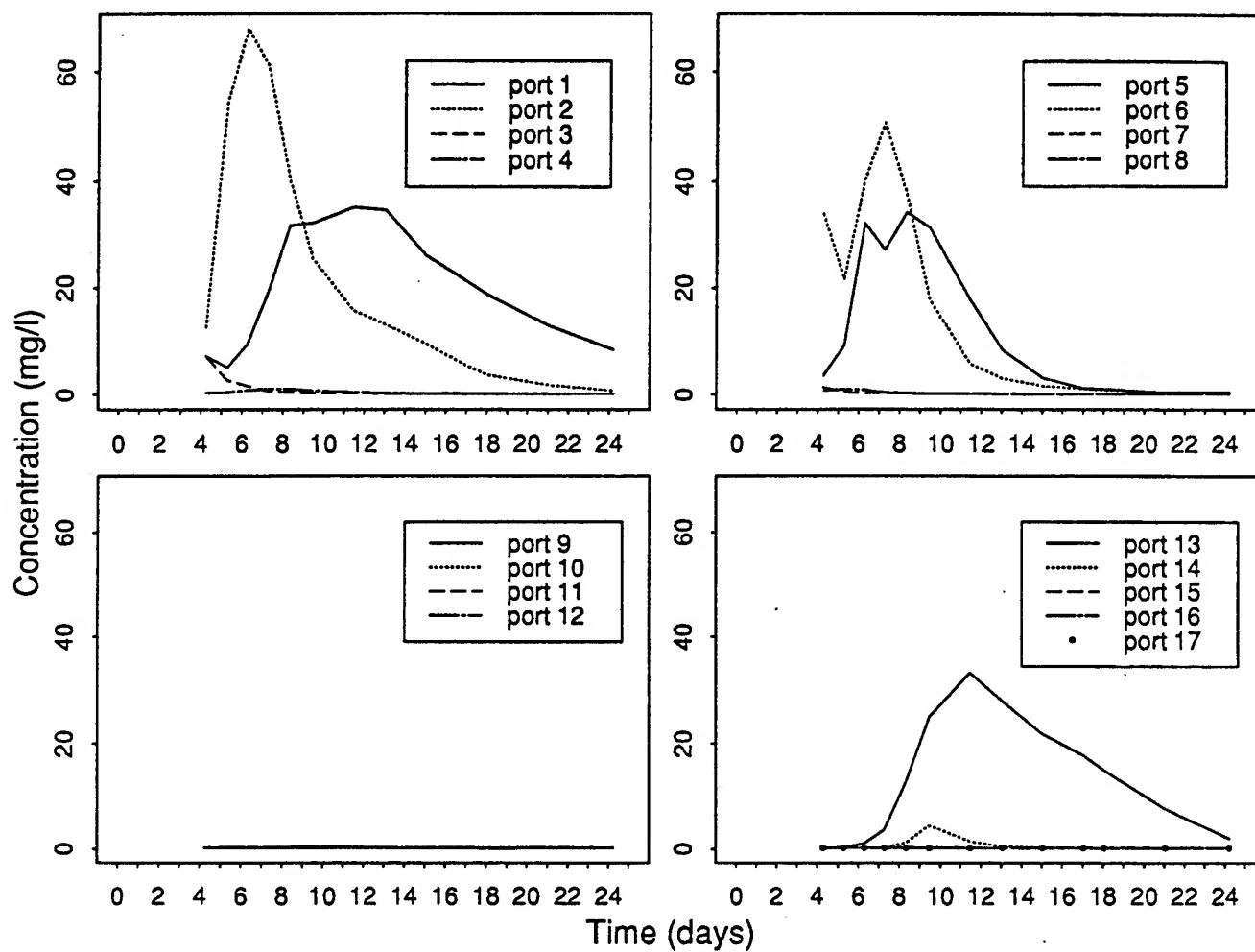


Figure 11: Breakthrough Curves at TME-4

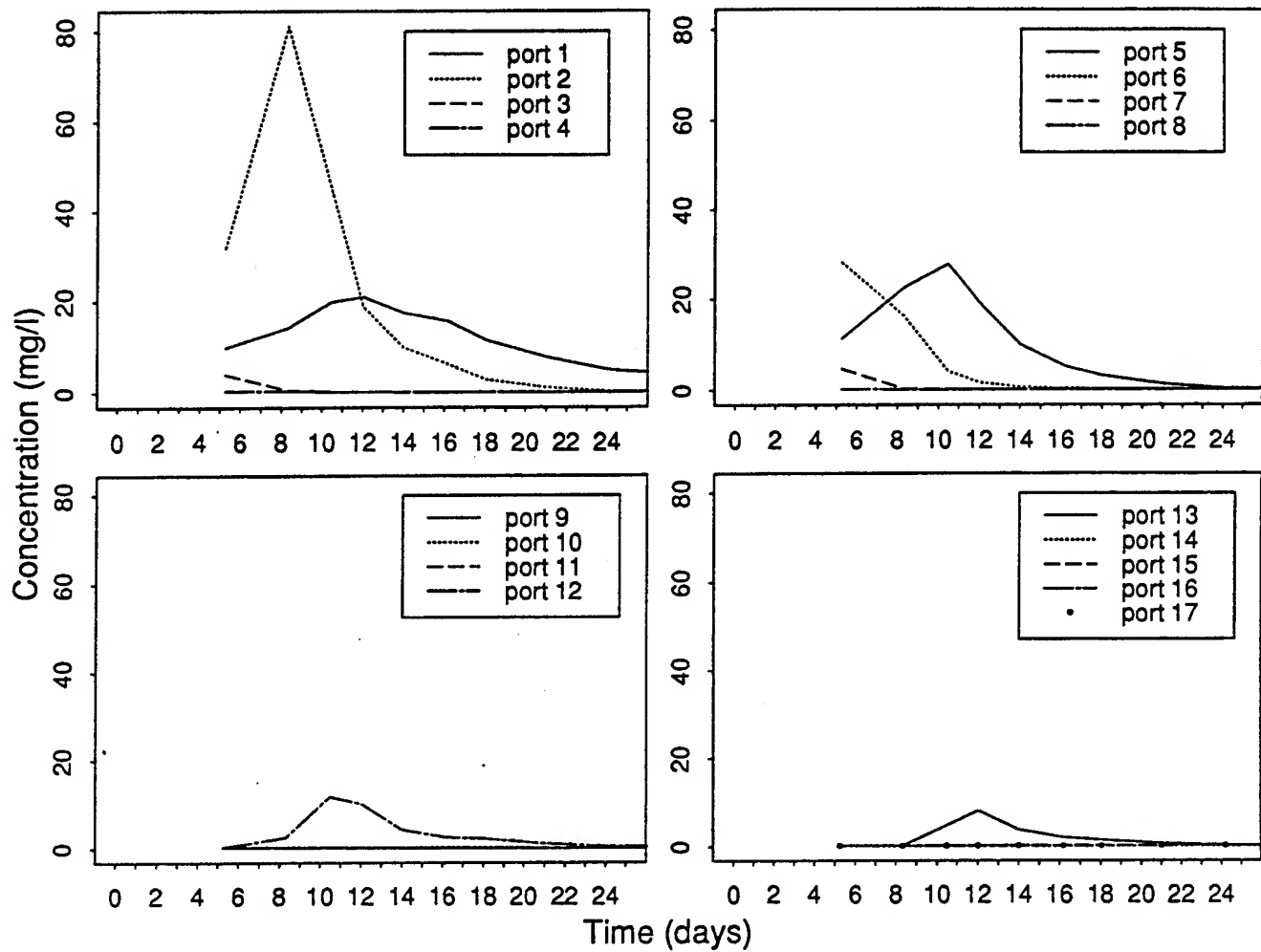


Figure 12: Breakthrough Curves at TME-3

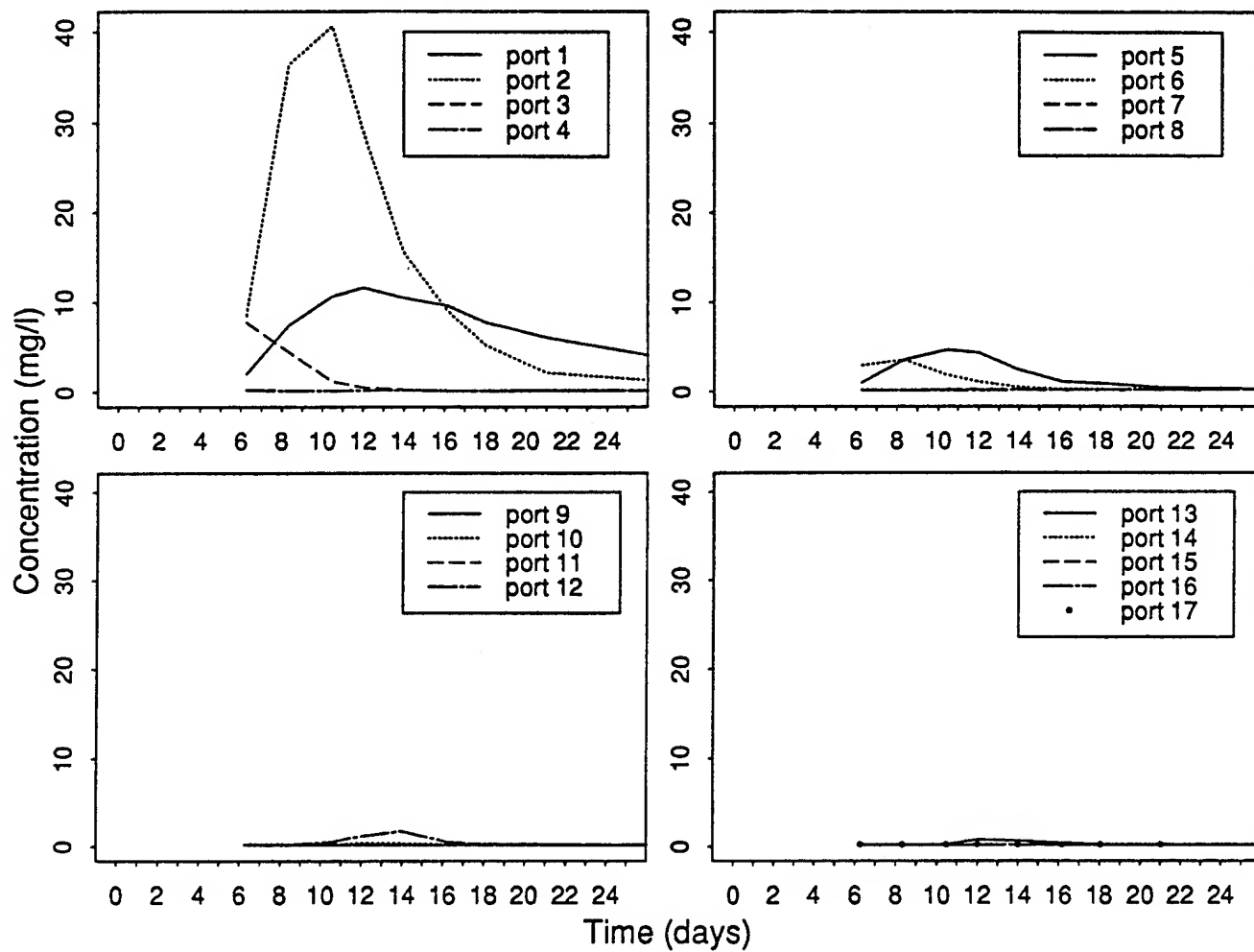


Figure 13 : Profile at 0.52 days (sample round 3)

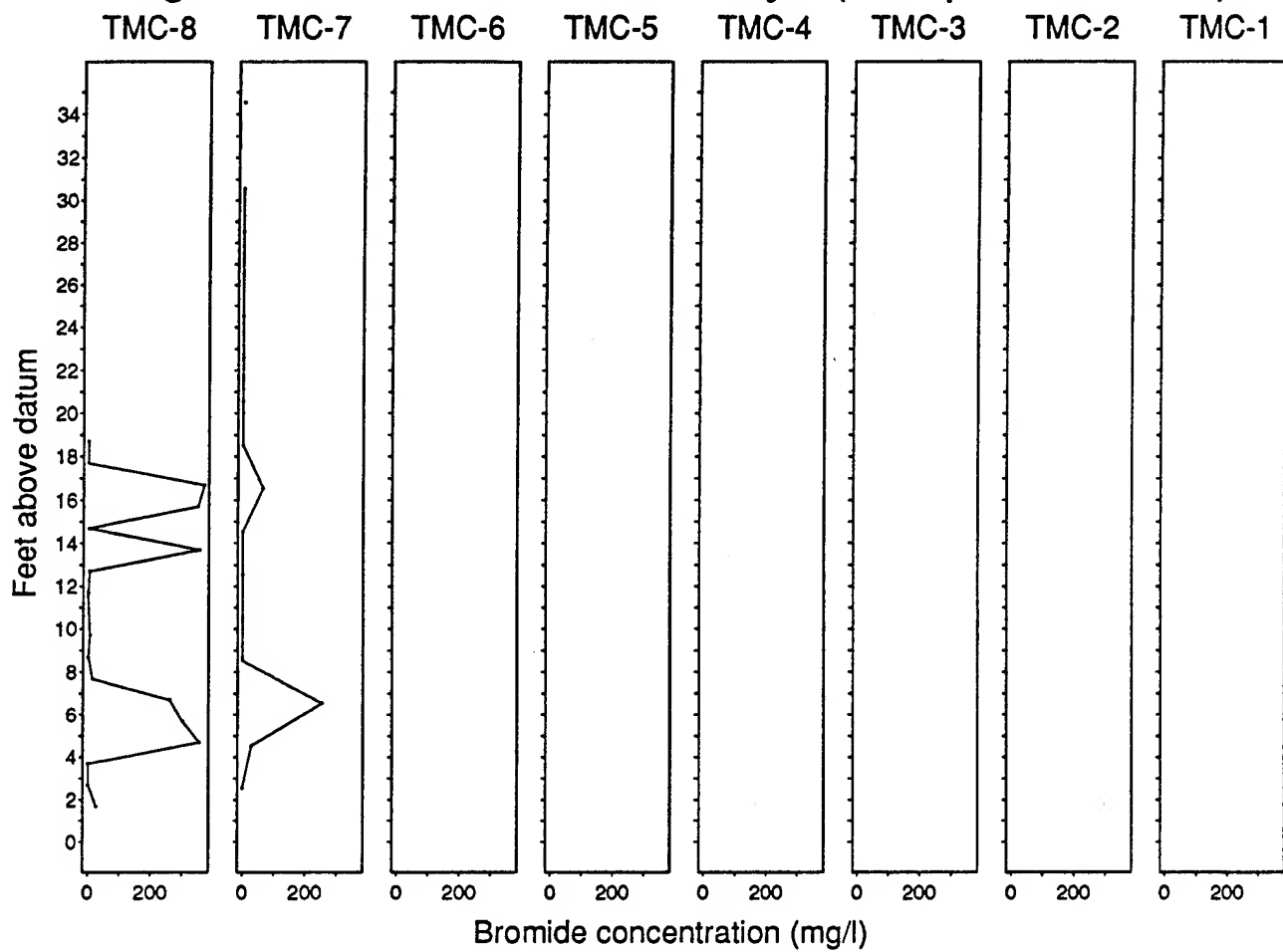


Figure 14 : Profile at 1.02 days (sample round 5)

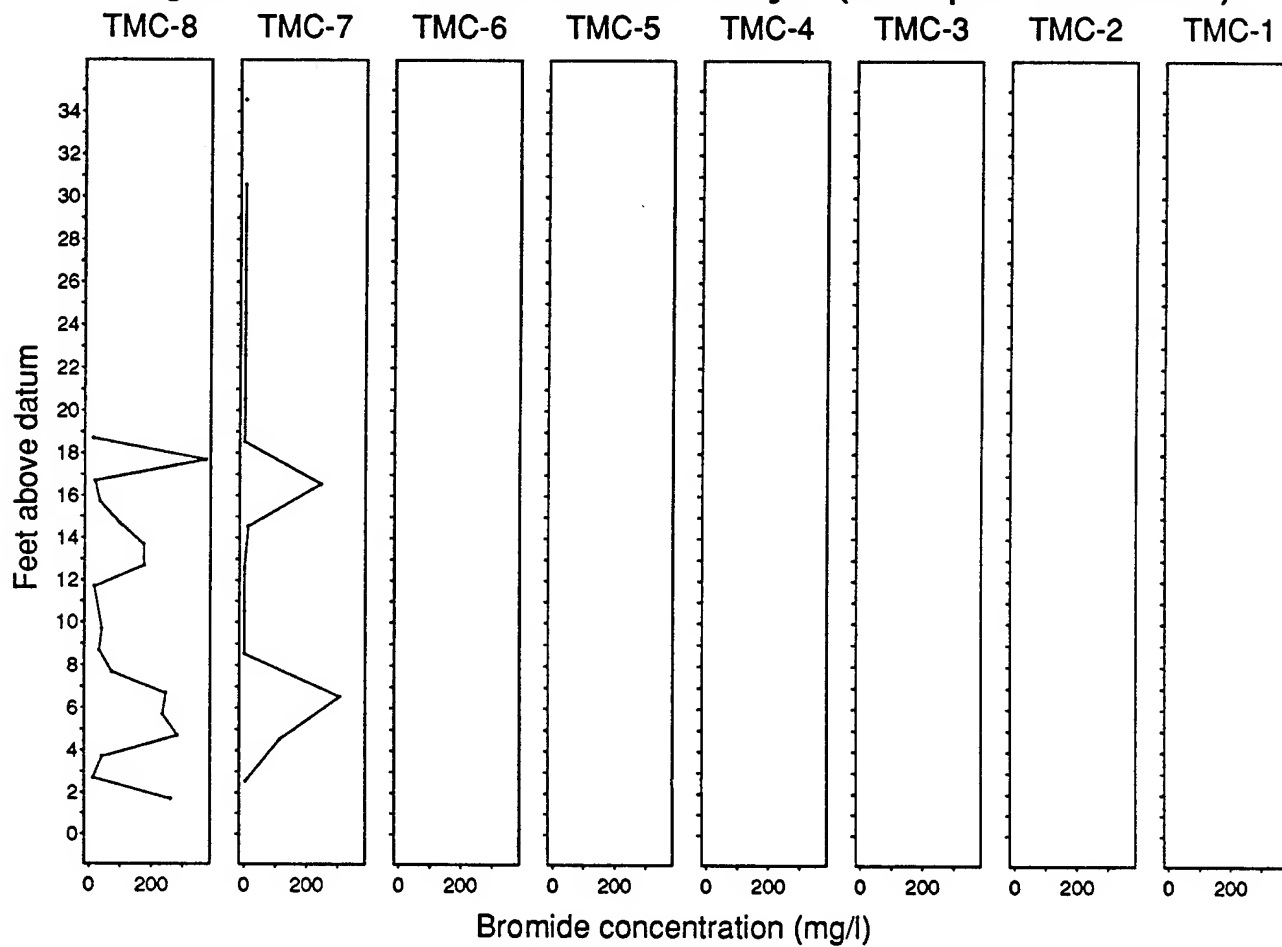


Figure 15 : Profile at 1.18 days (sample round 6)

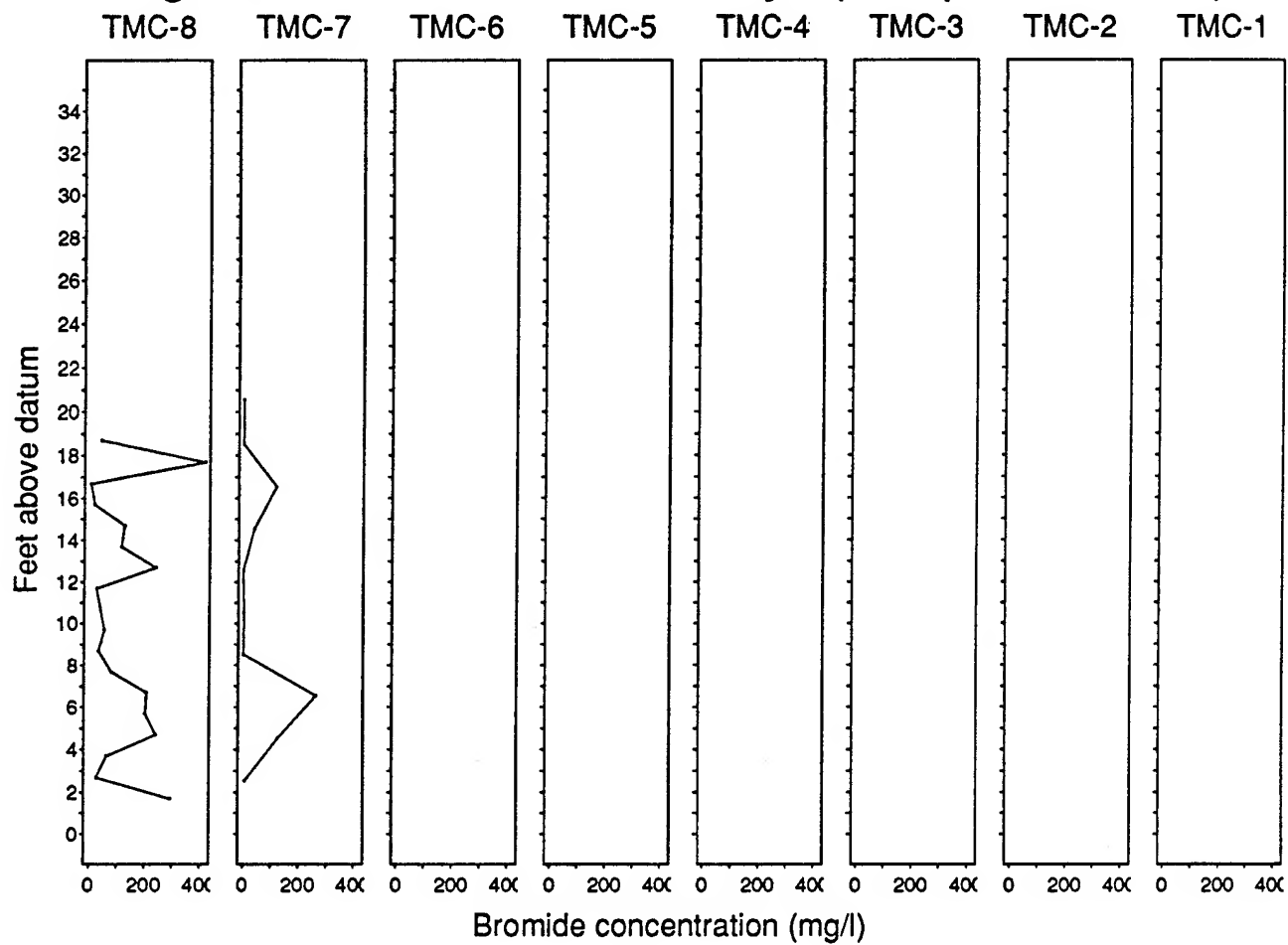


Figure 16 : Profile at 1.53 days (sample round 8)

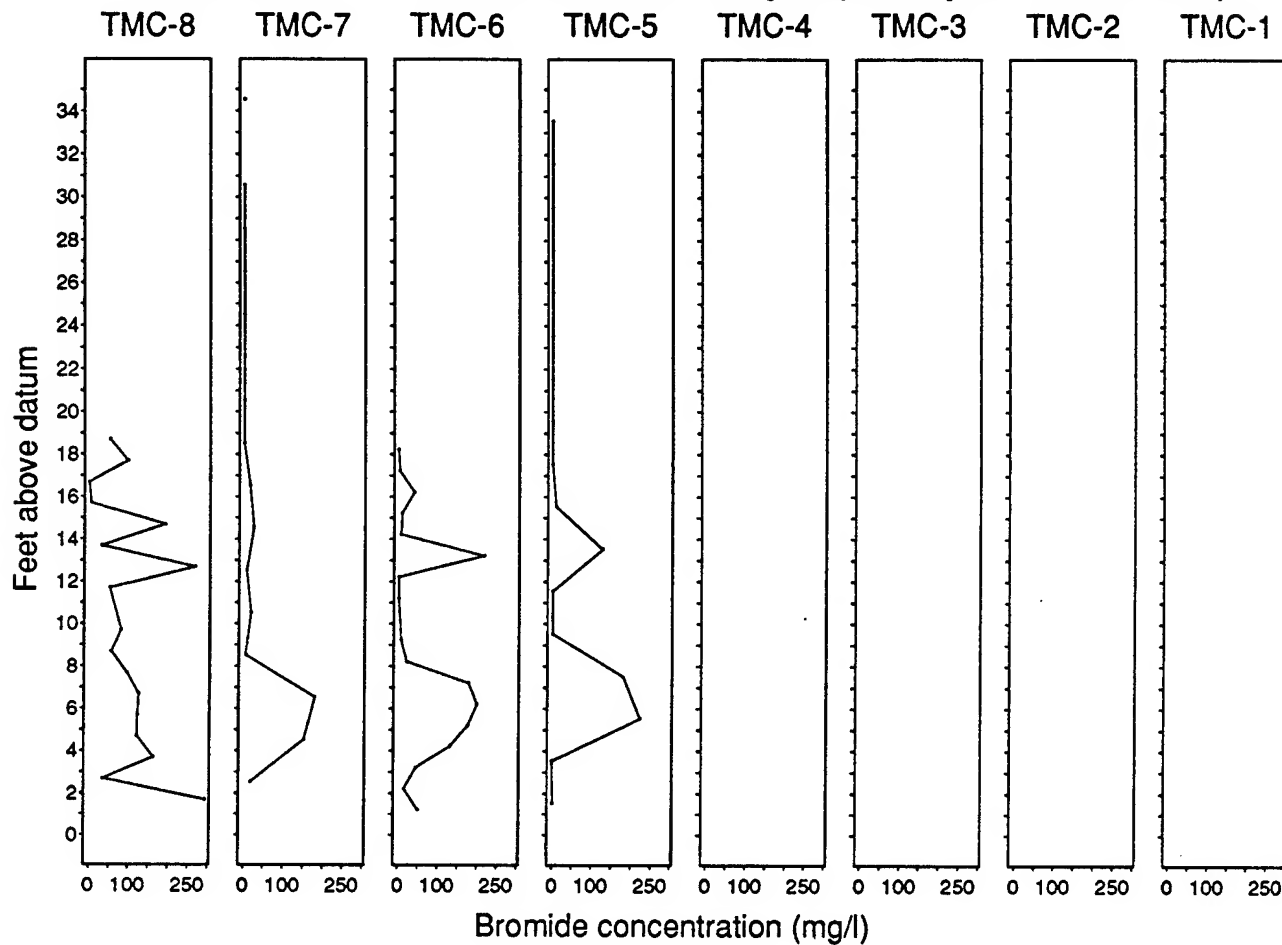


Figure 17 : Profile at 2.02 days (sample round 10)

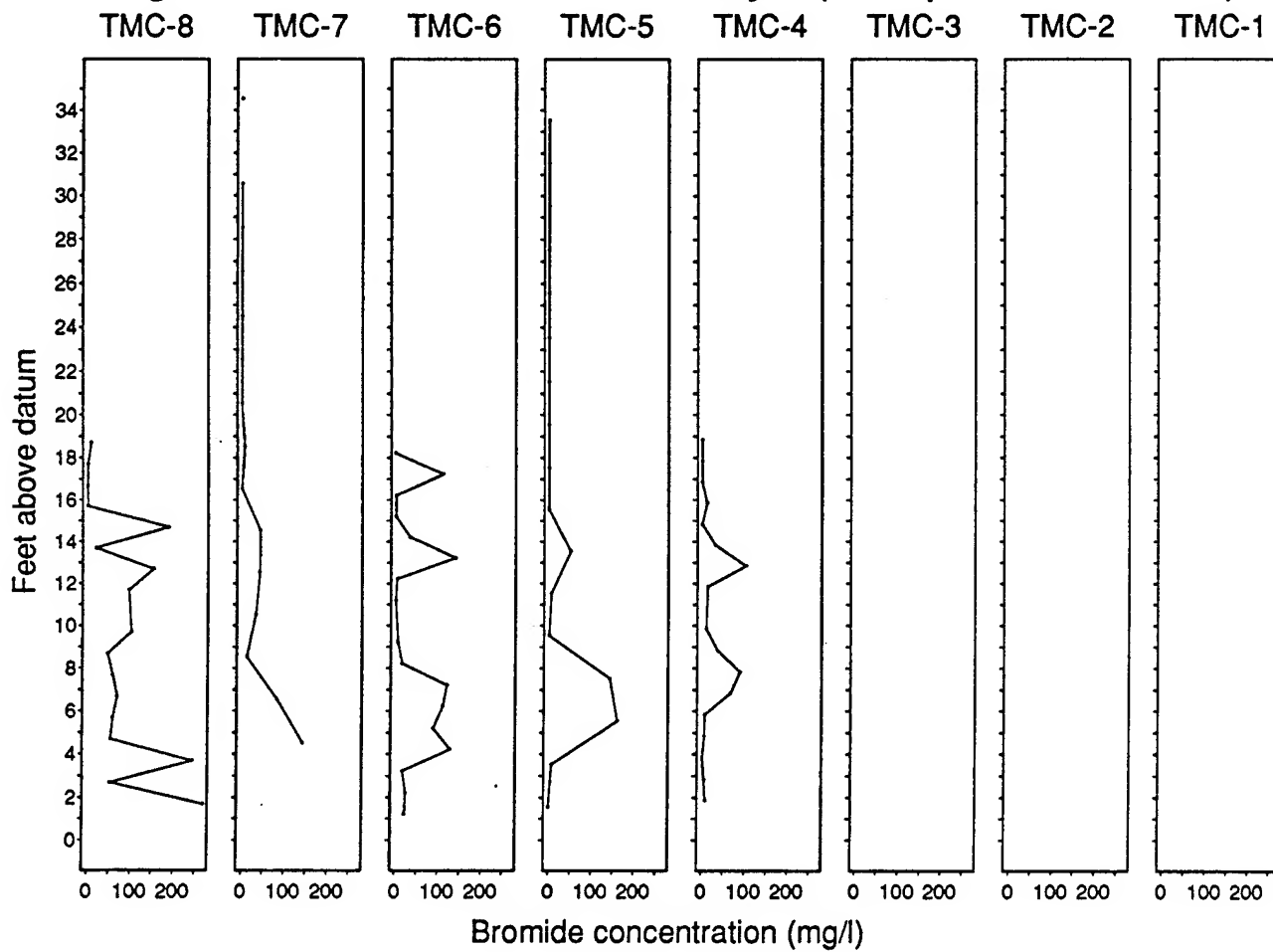


Figure 18 : Profile at 2.22 days (sample round 11)

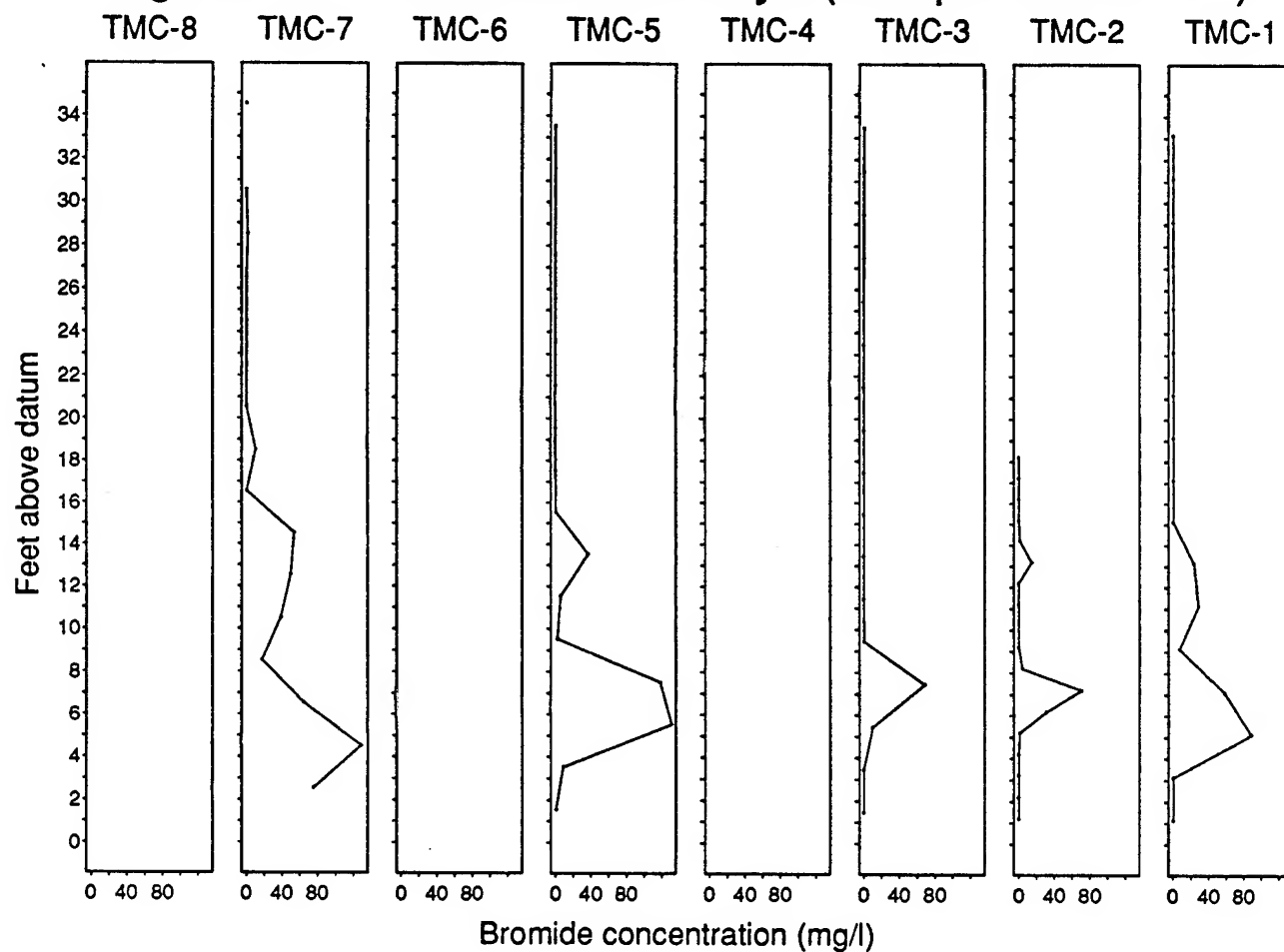


Figure 19 : Profile at 3.06 days (sample round 14)

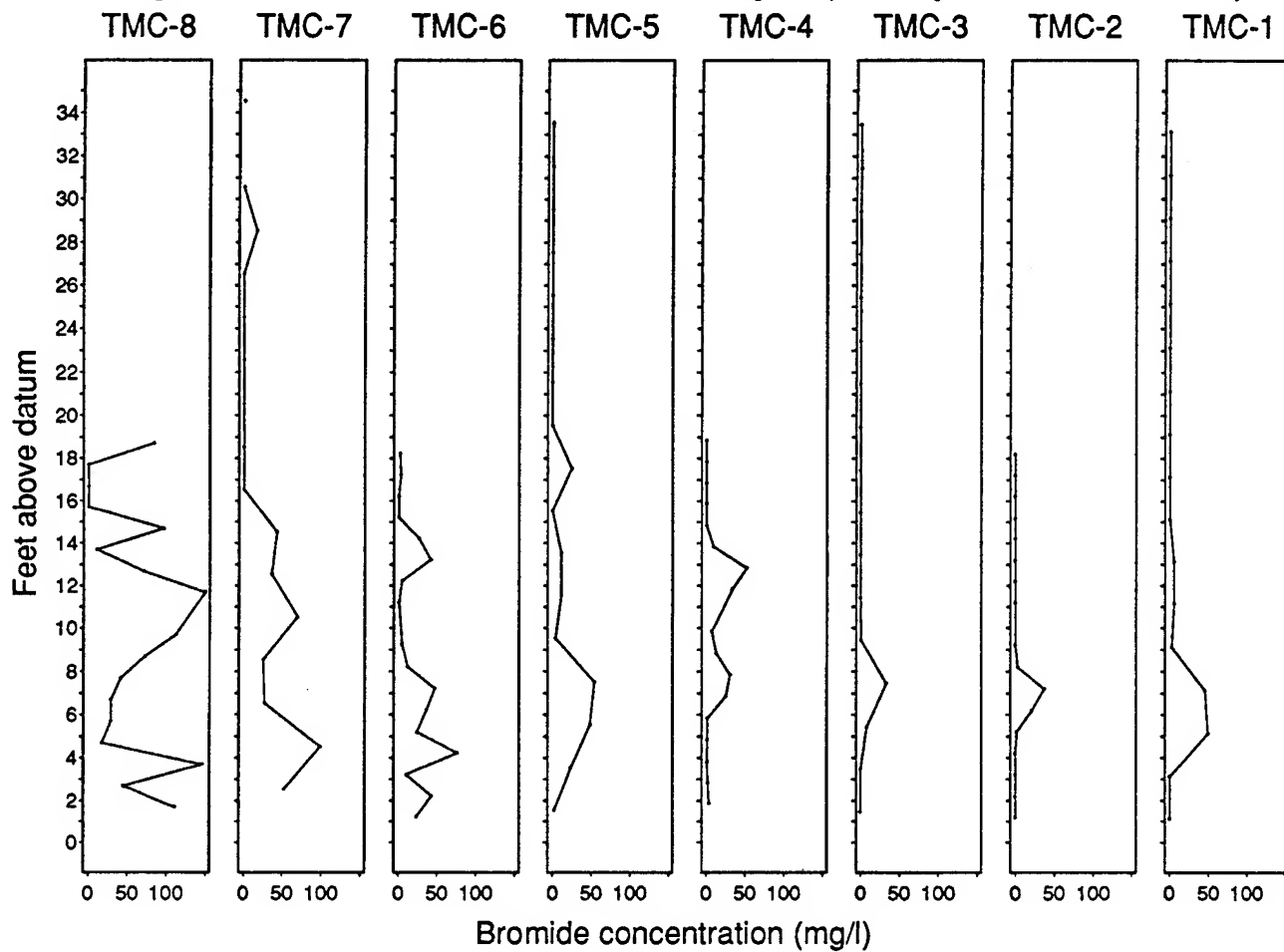


Figure 20 : Profile at 4.07 days (sample round 18)

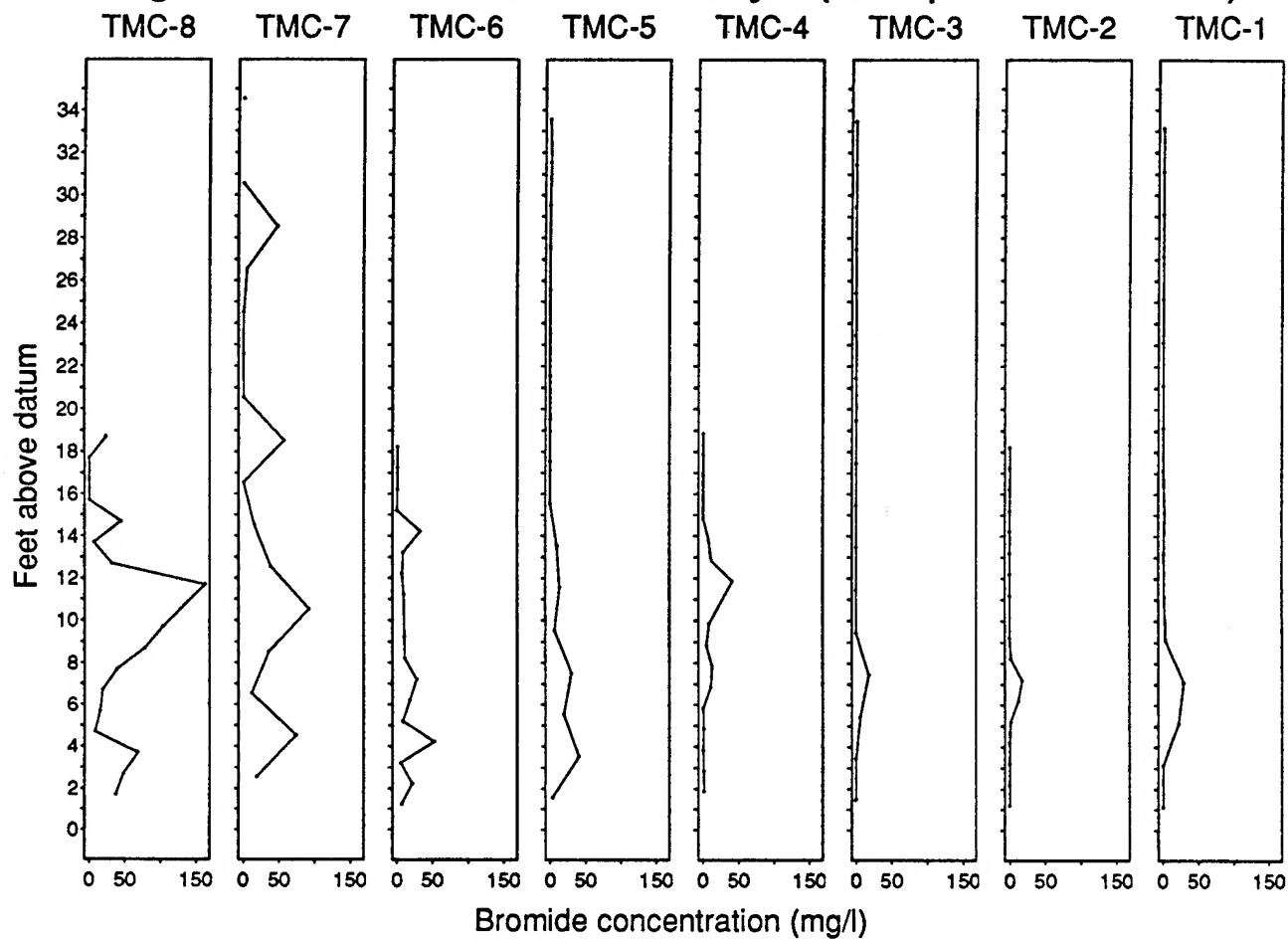


Figure 21 : Profile at 5.06 days (sample round 22)

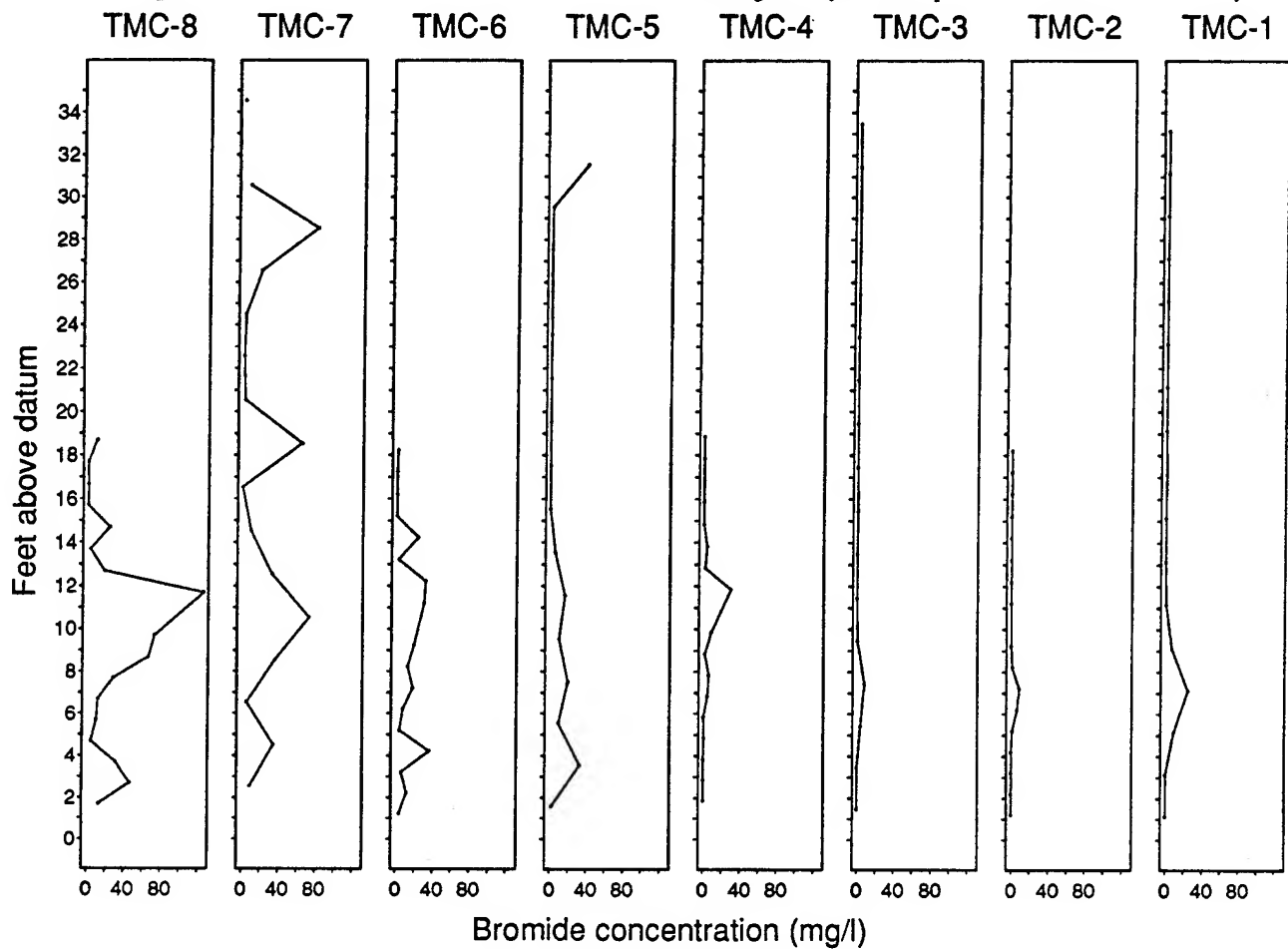


Figure 22 : Profile at 6.06 days (sample round 26)

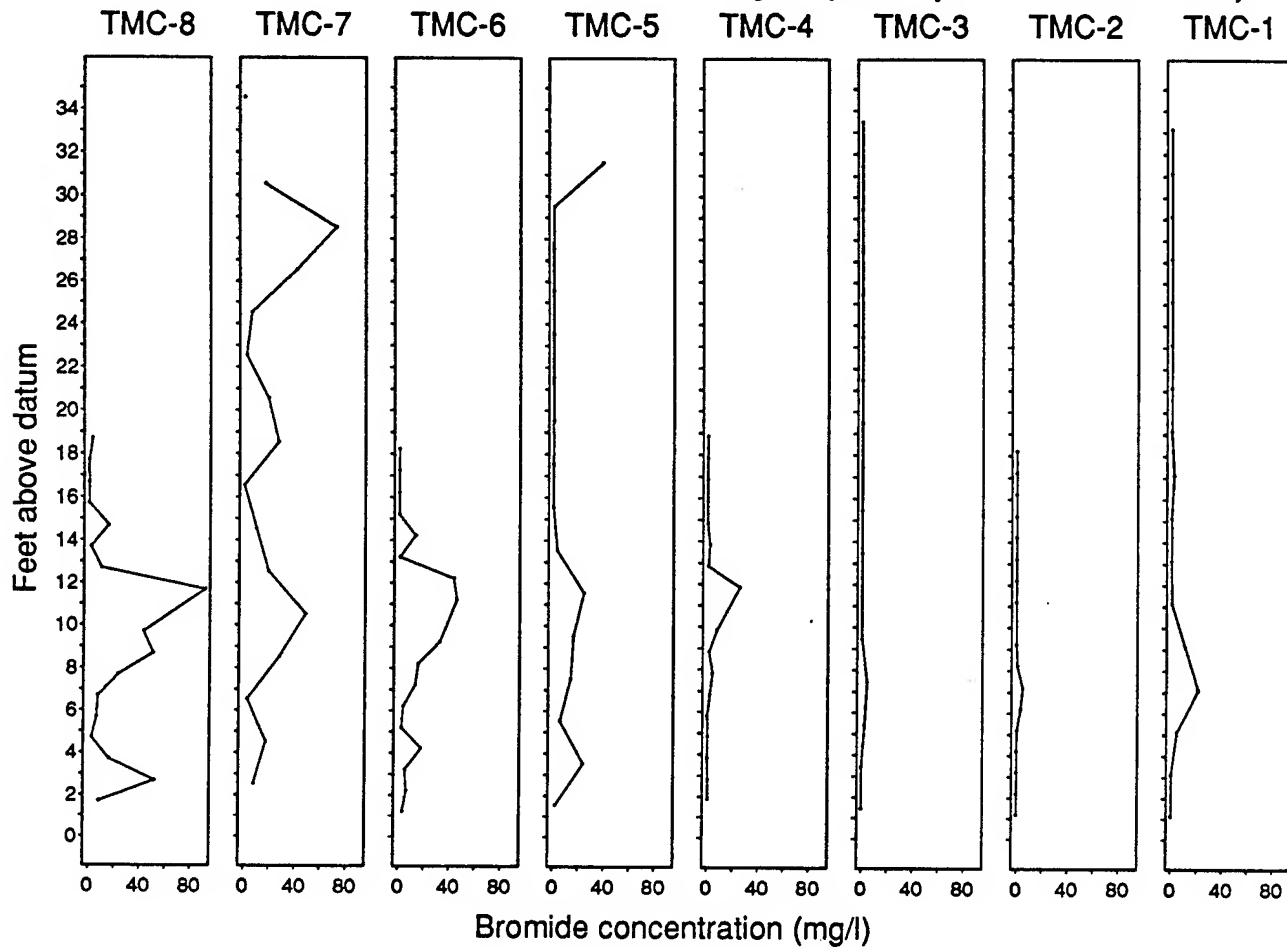


Figure 23 : Profile at 7.06 days (sample round 30)

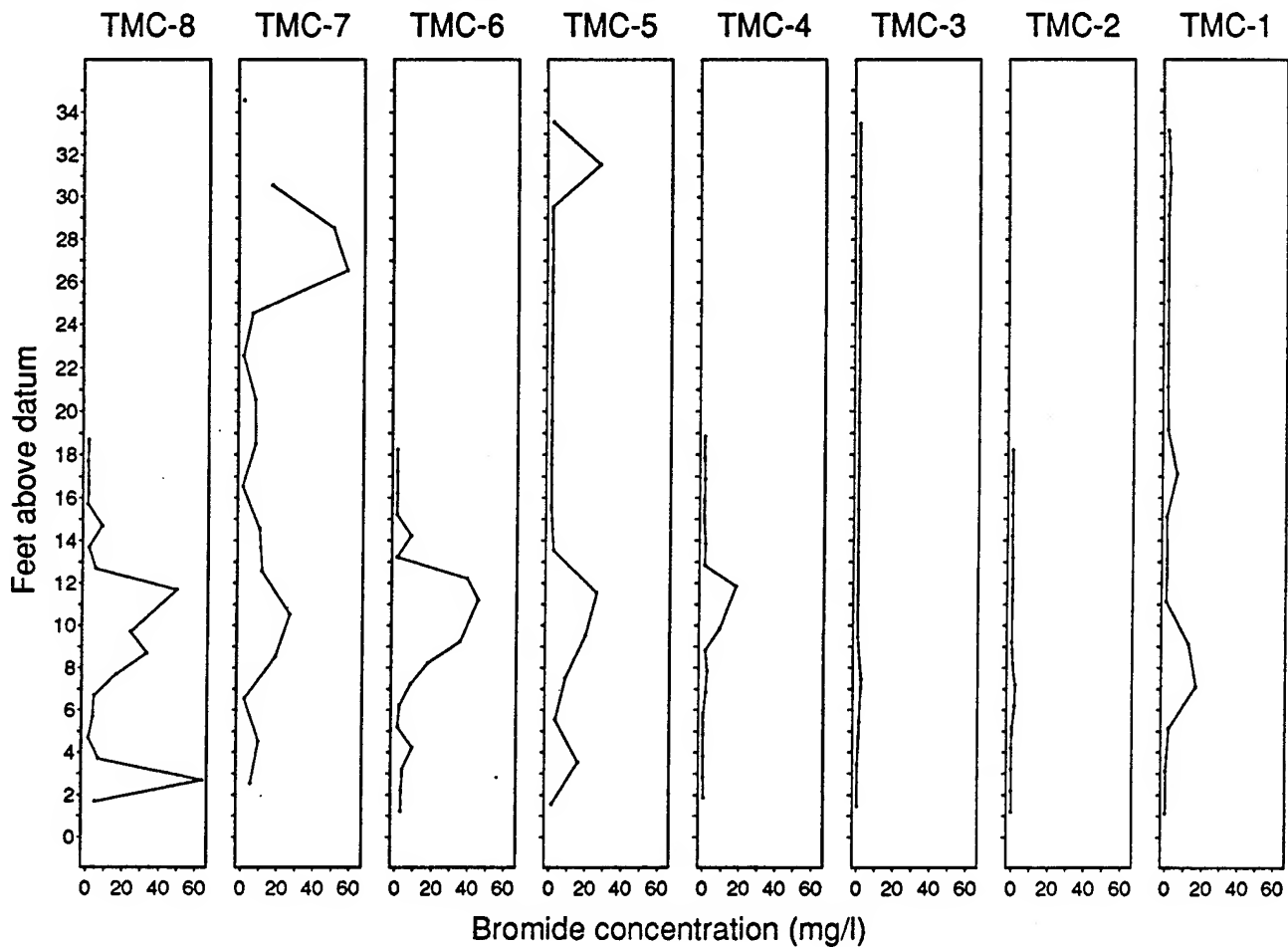


Figure 24 : Profile at 8.07 days (sample round 34)

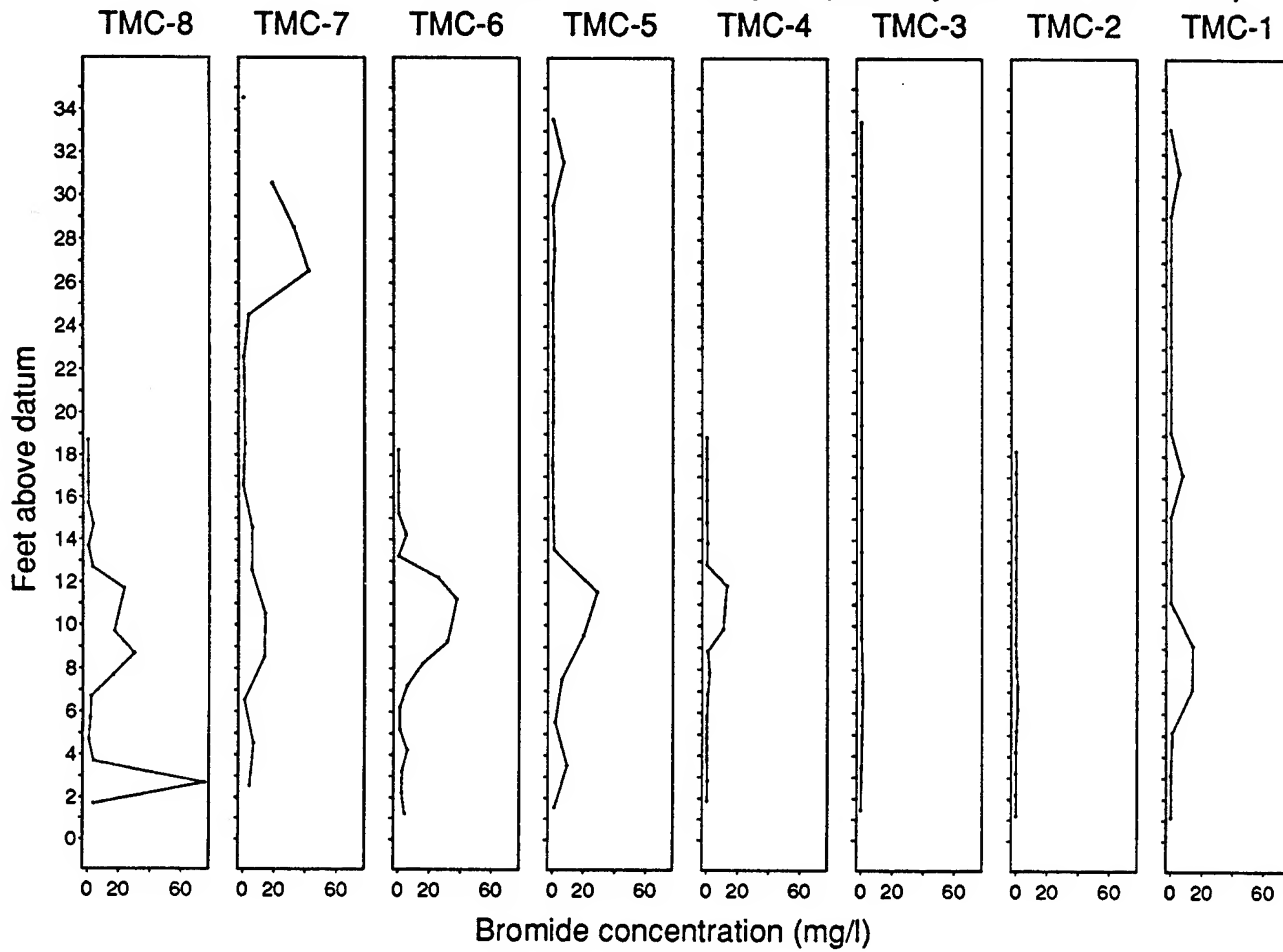


Figure 25 : Profile at 10.04 days (sample round 39)

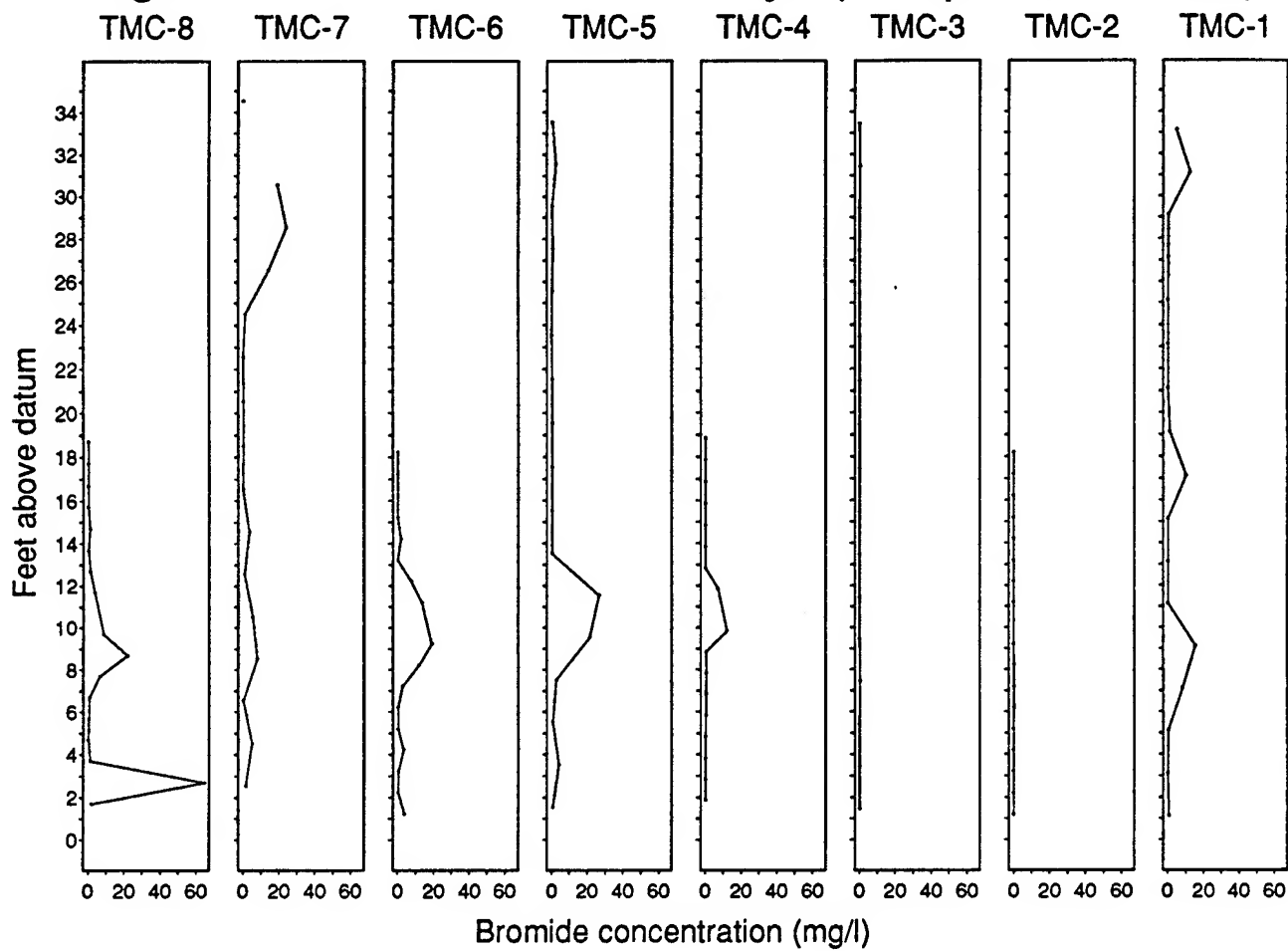


Figure 26 : Profile at 12.02 days (sample round 43)

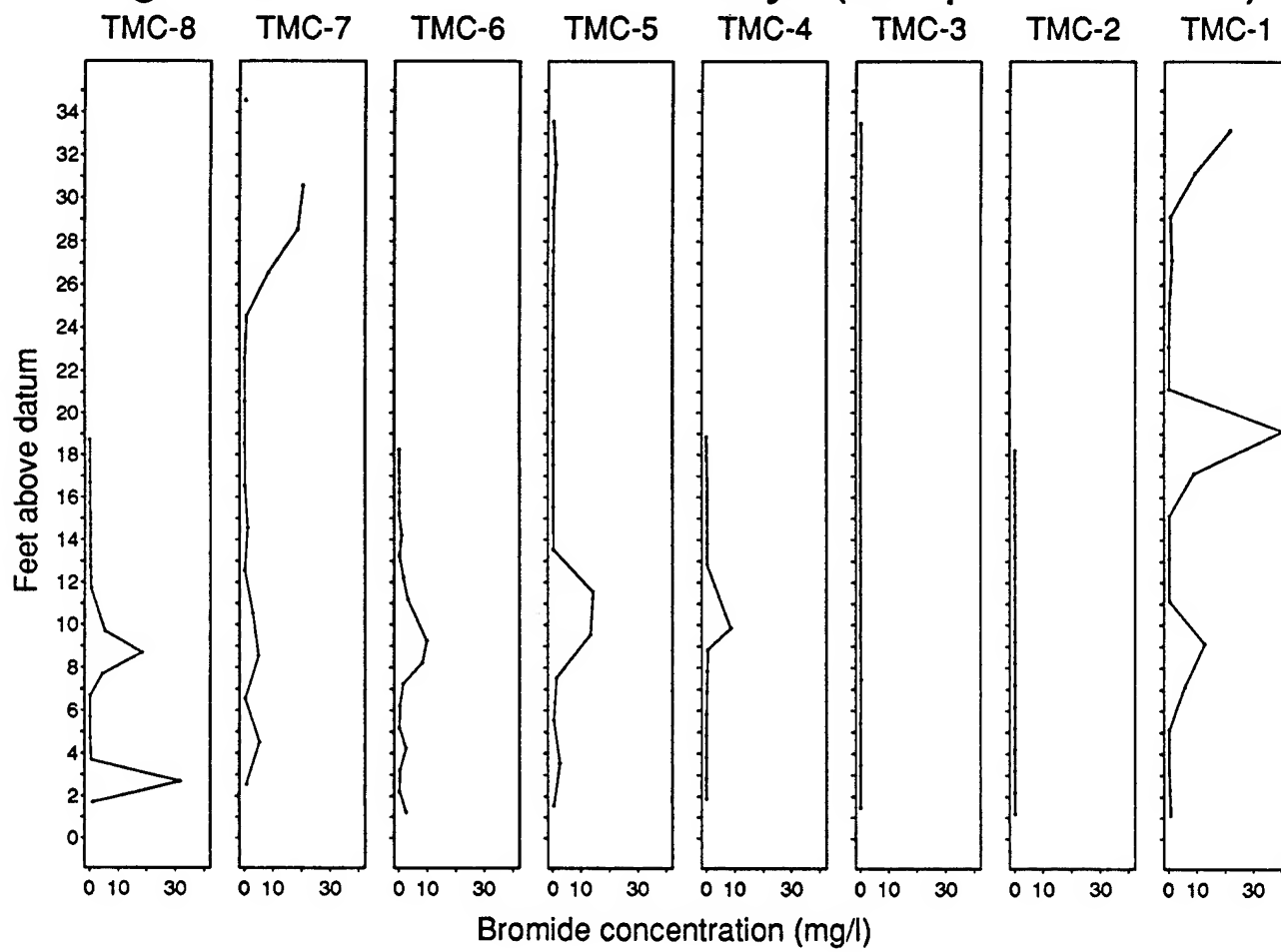


Figure 27 : Profile at 14.01 days (sample round 45)

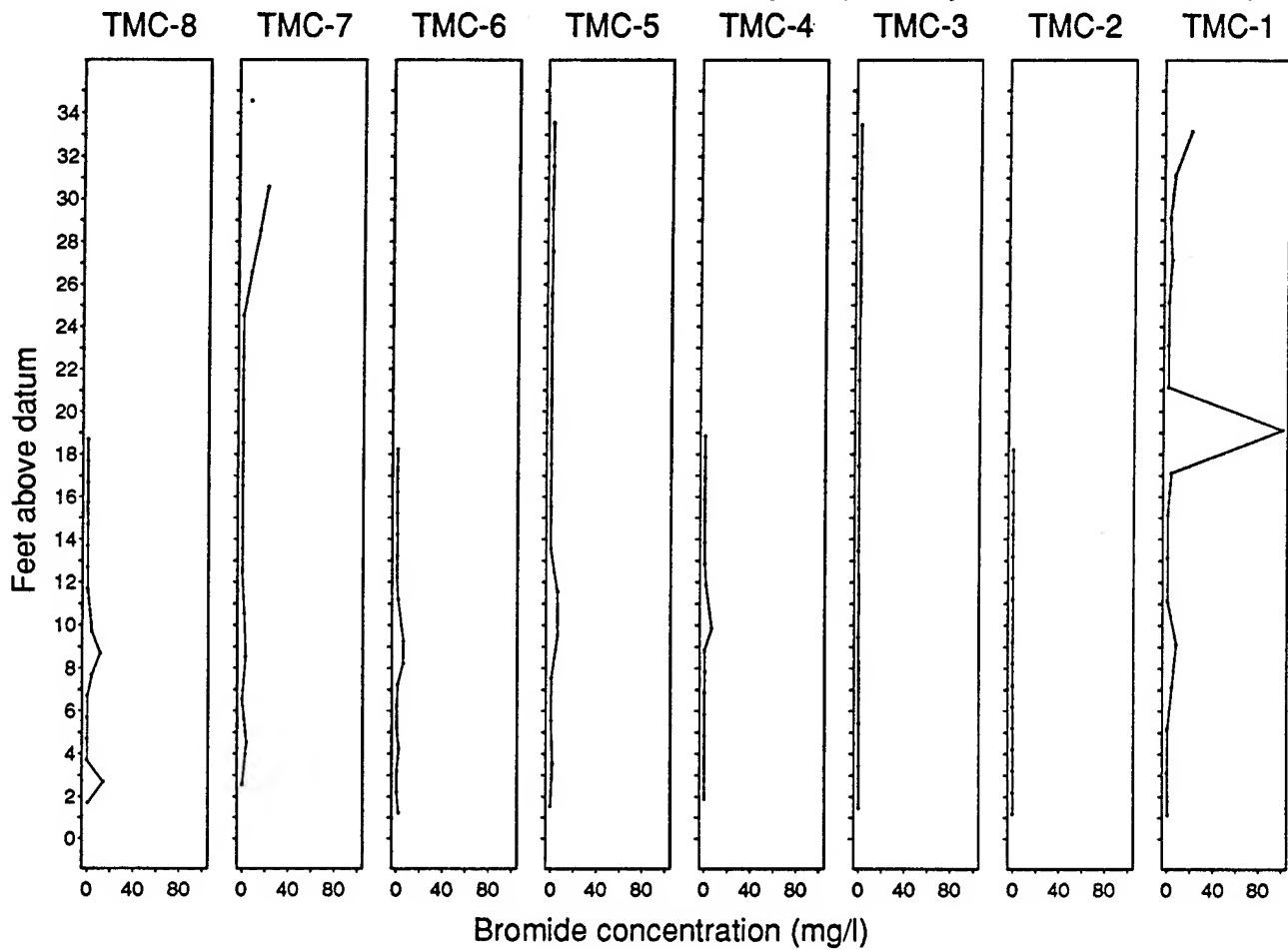


Figure 28 : Profile at 19.01 days (sample round 50)

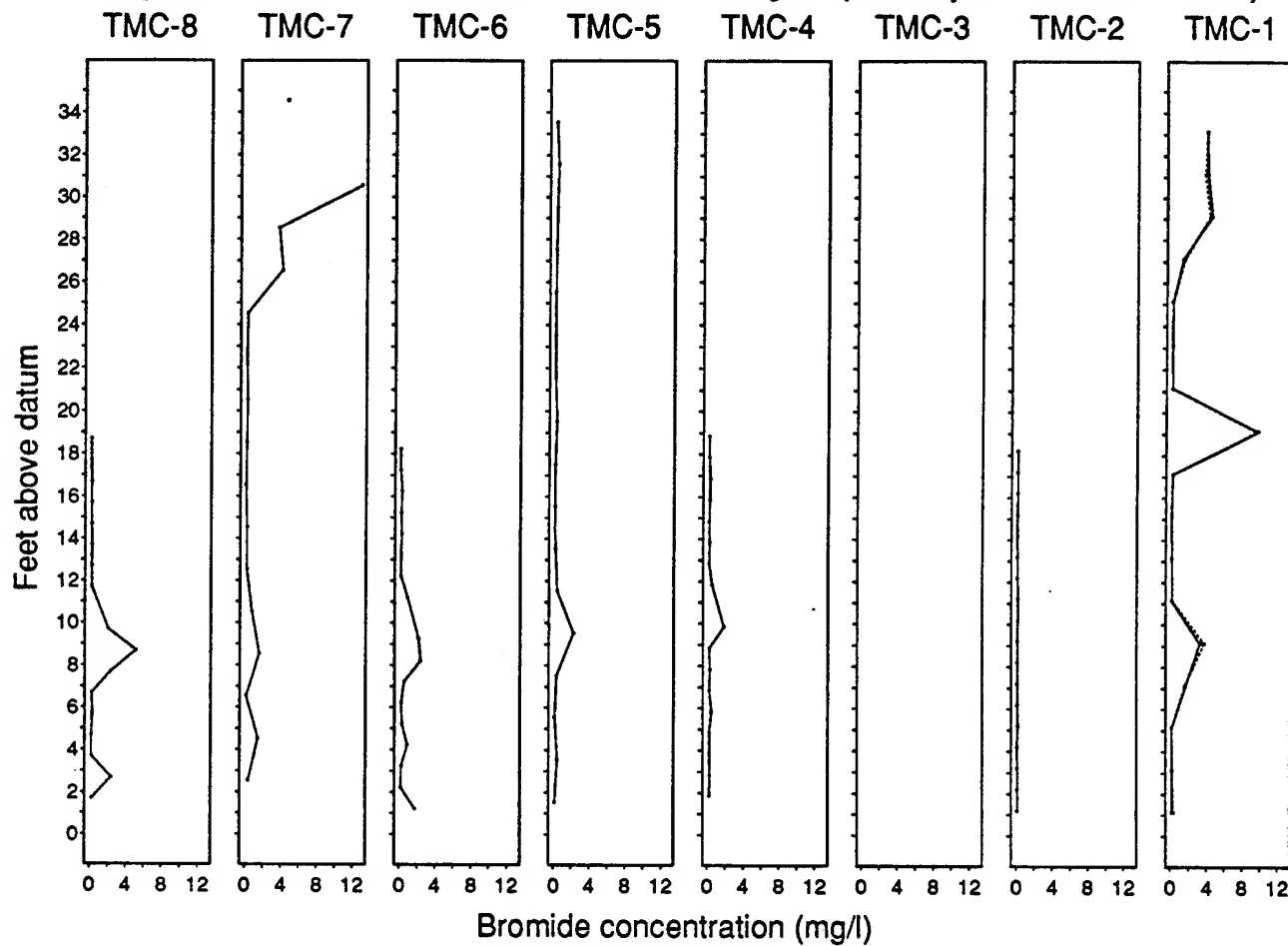


Figure 29 : Profile at 24.2 days (sample round 52)

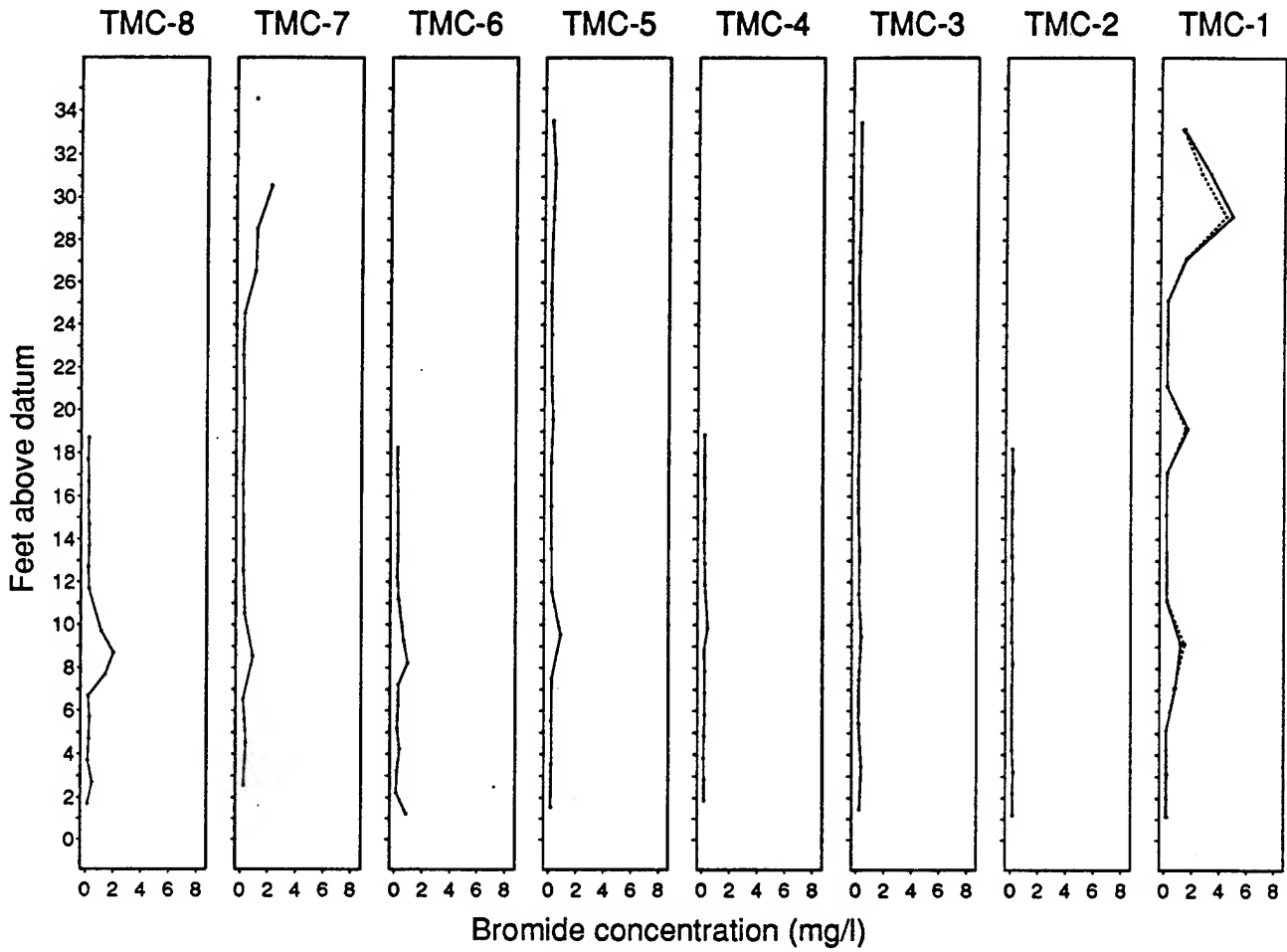


Figure 30 : Profile at 32.18 days (sample round 53)

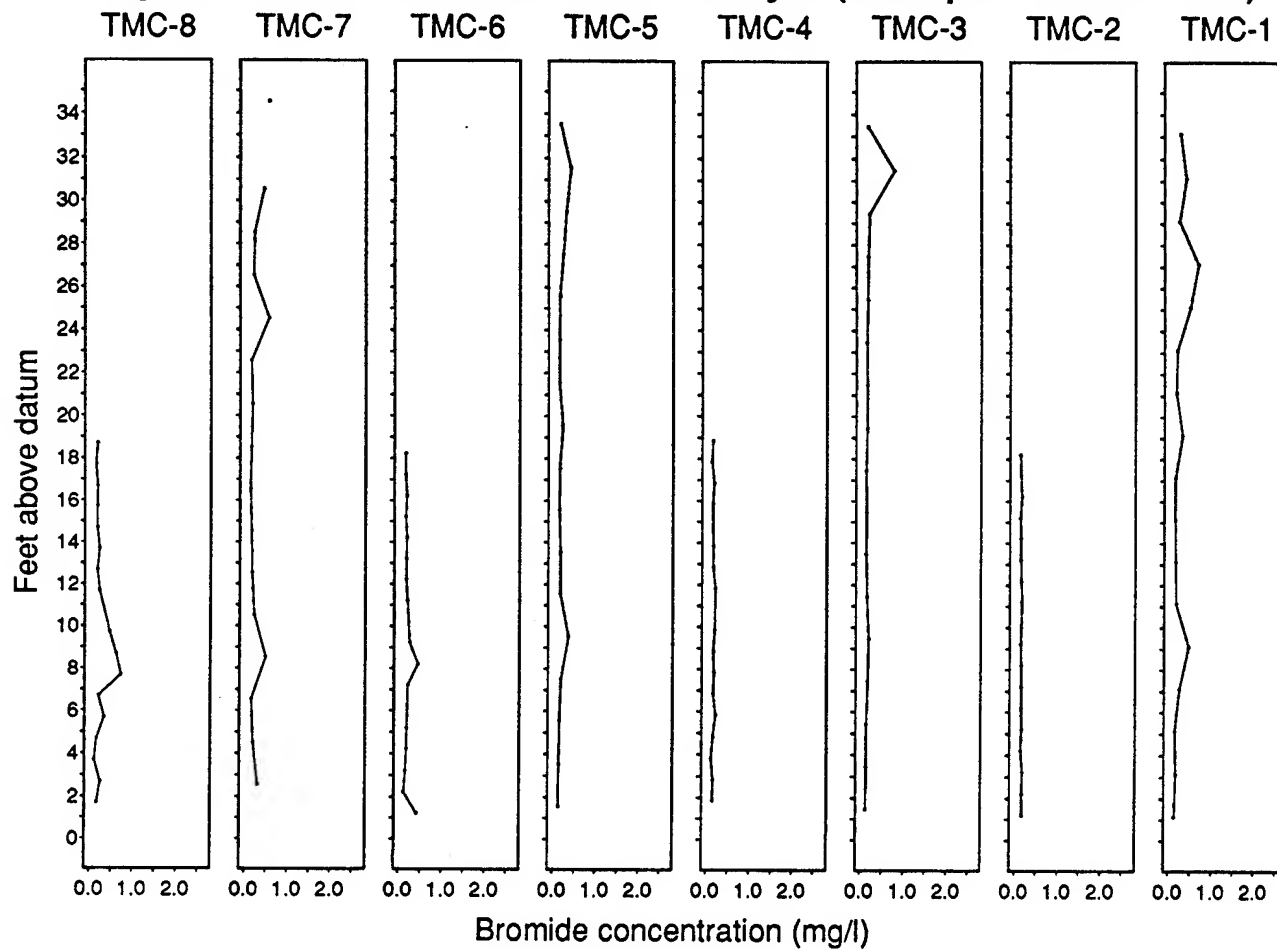


Figure 31: Fitted Breakthrough Curves for TMC-8

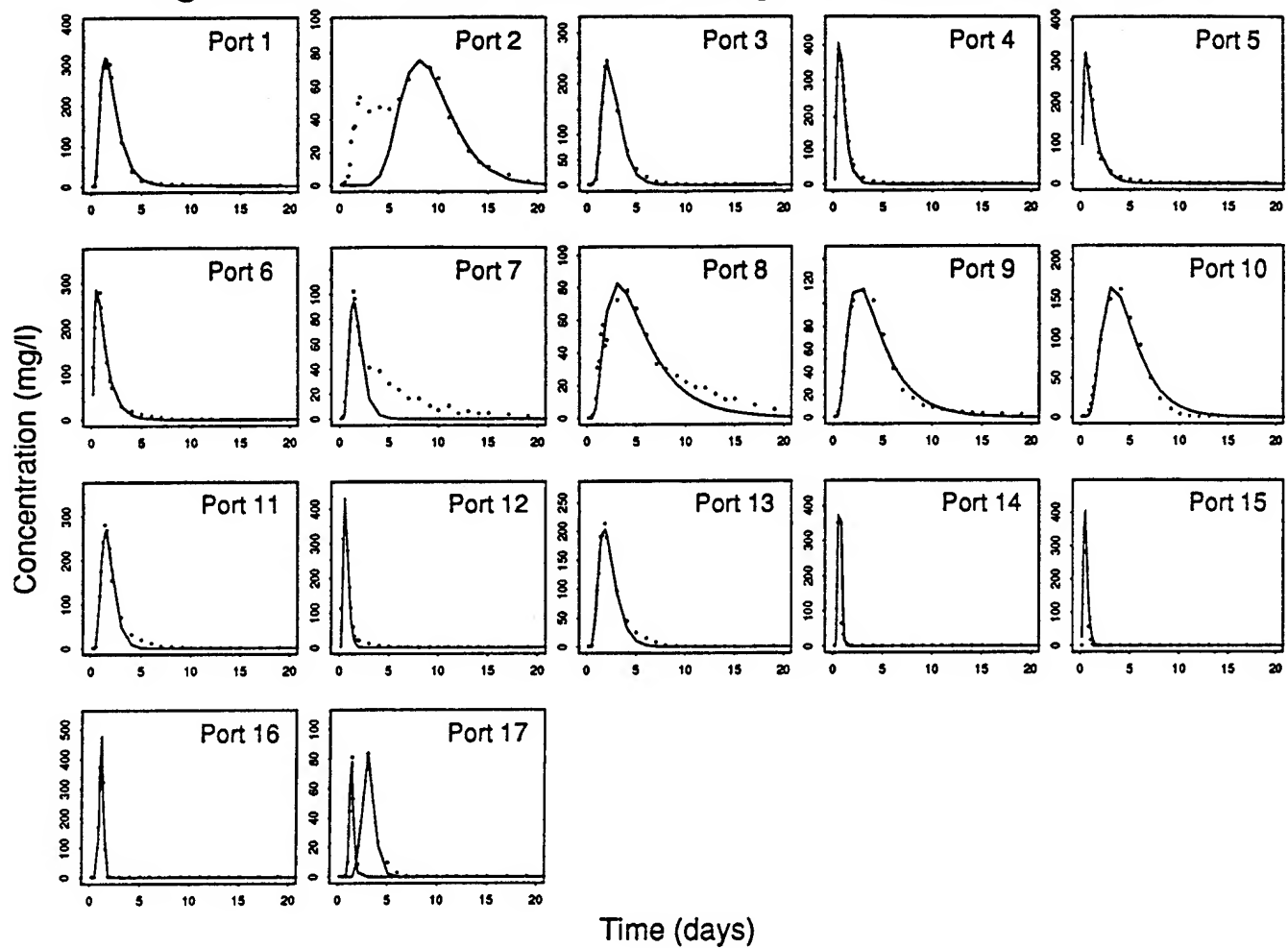


Figure 32: Fitted Breakthrough Curves for TMC-7

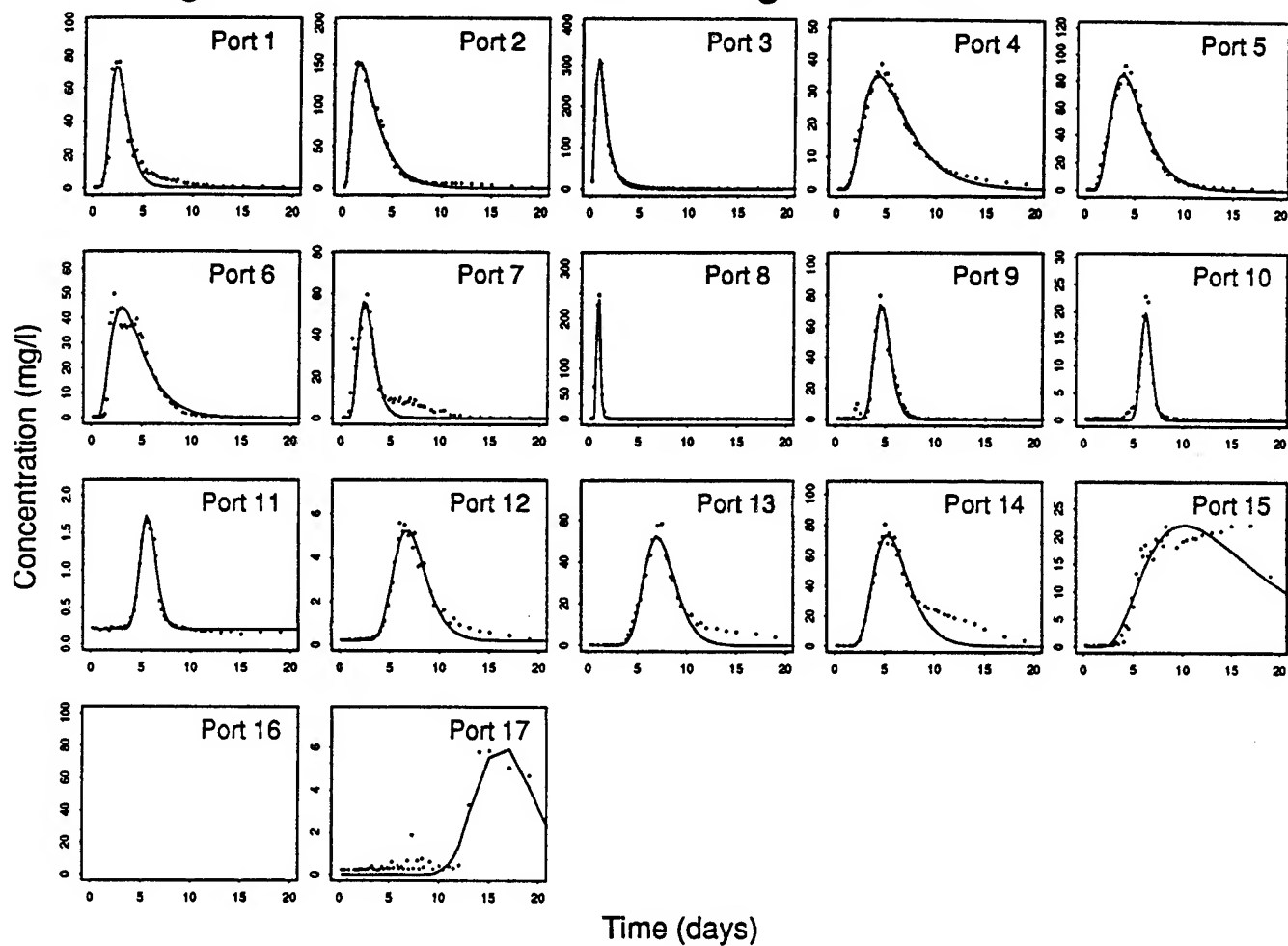


Figure 33: Fitted Breakthrough Curves for TMC-6

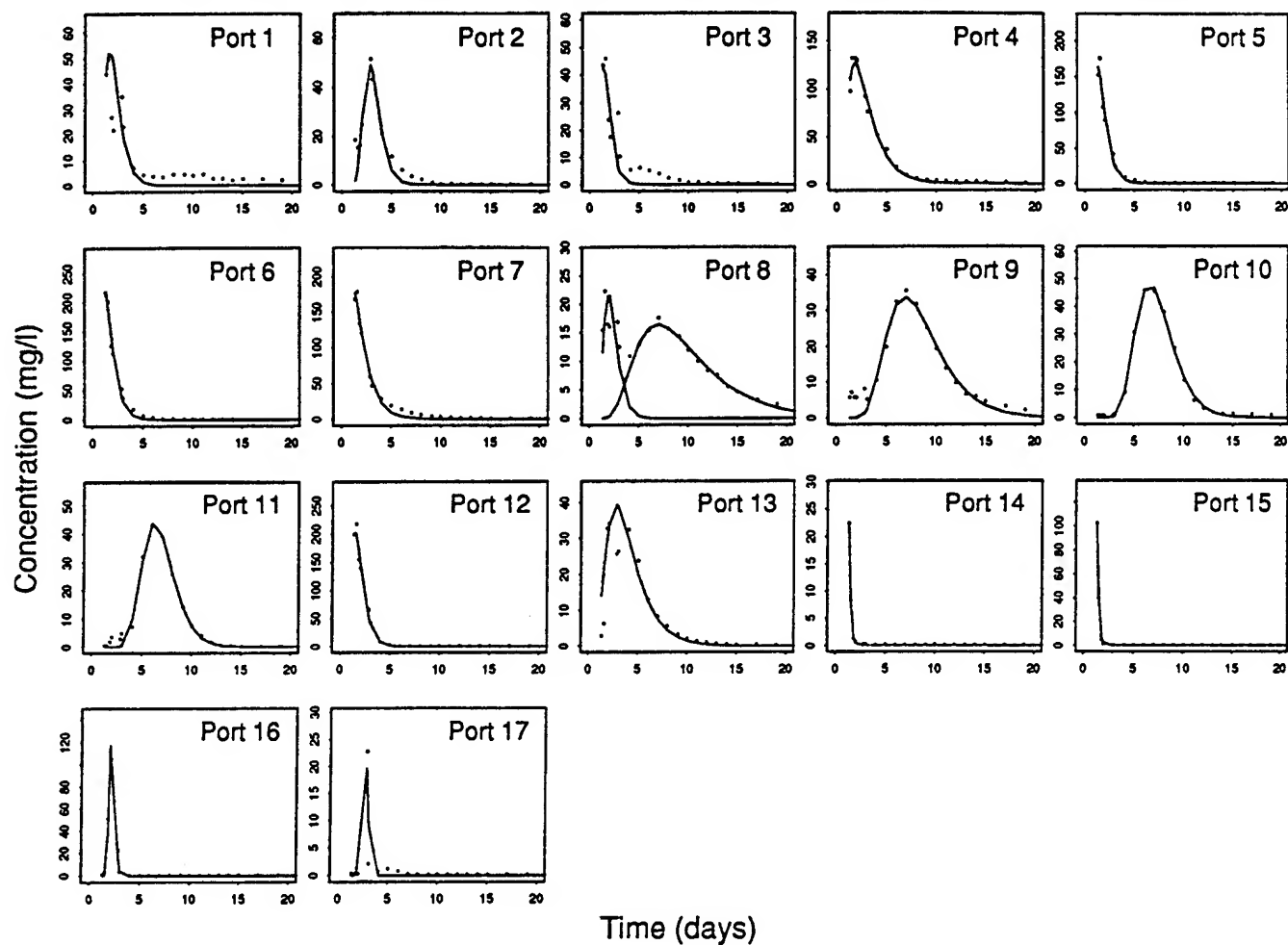


Figure 34: Fitted Breakthrough Curves for TMC-1

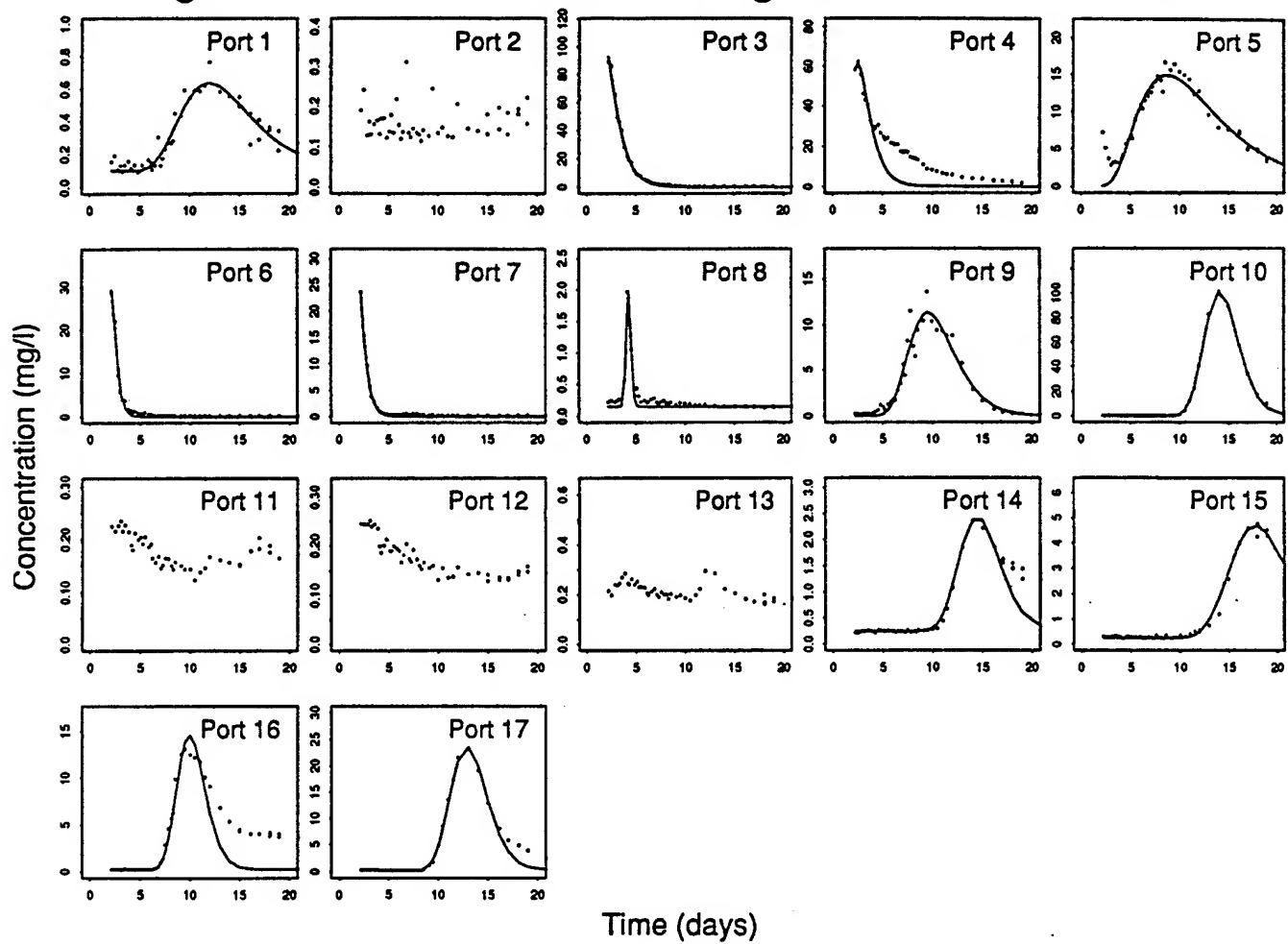


Figure 35: Fitted Advective Velocities

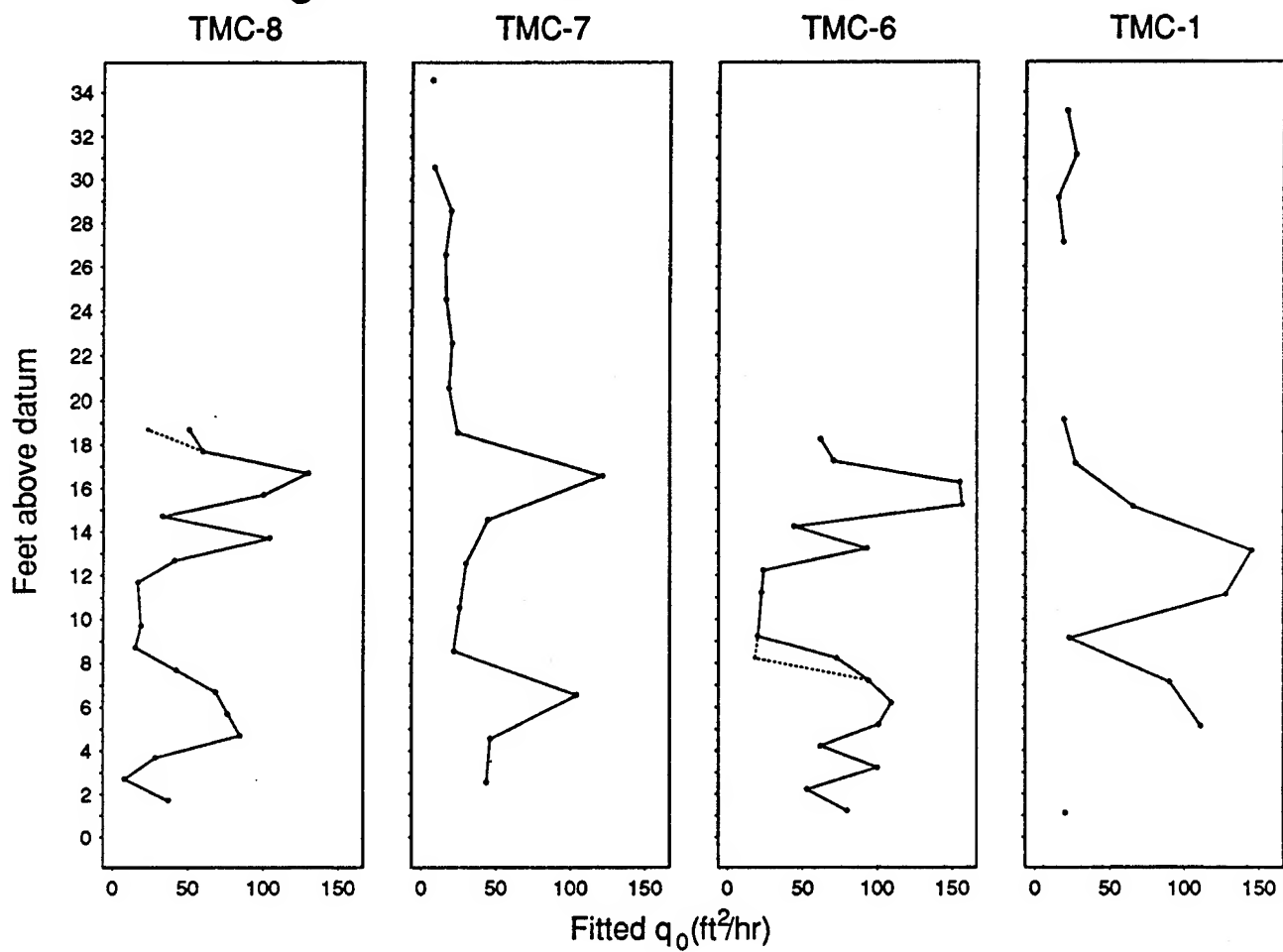


Figure 36: Fitted Reference Concentrations

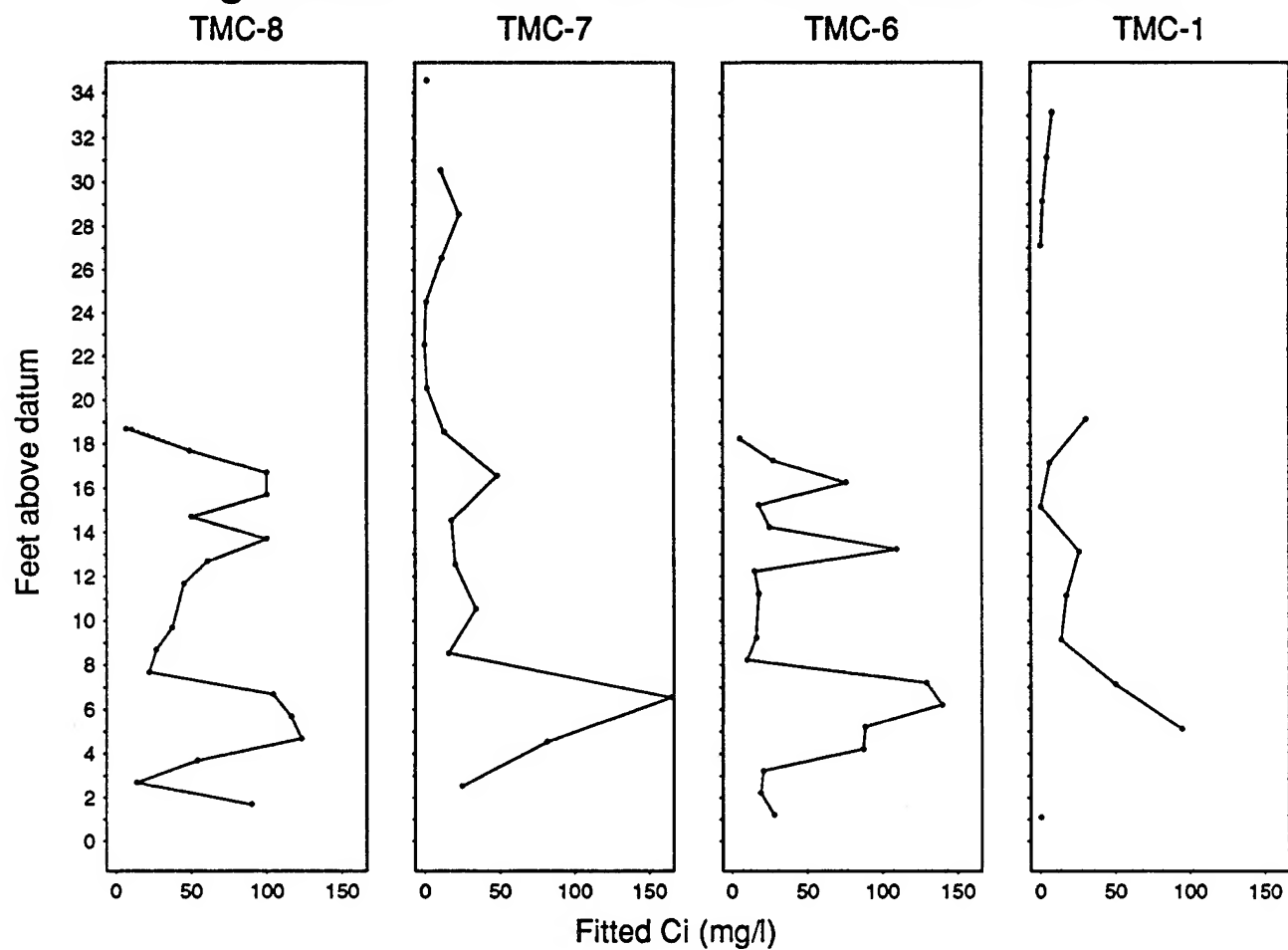


Figure 37: Fitted Dispersivities

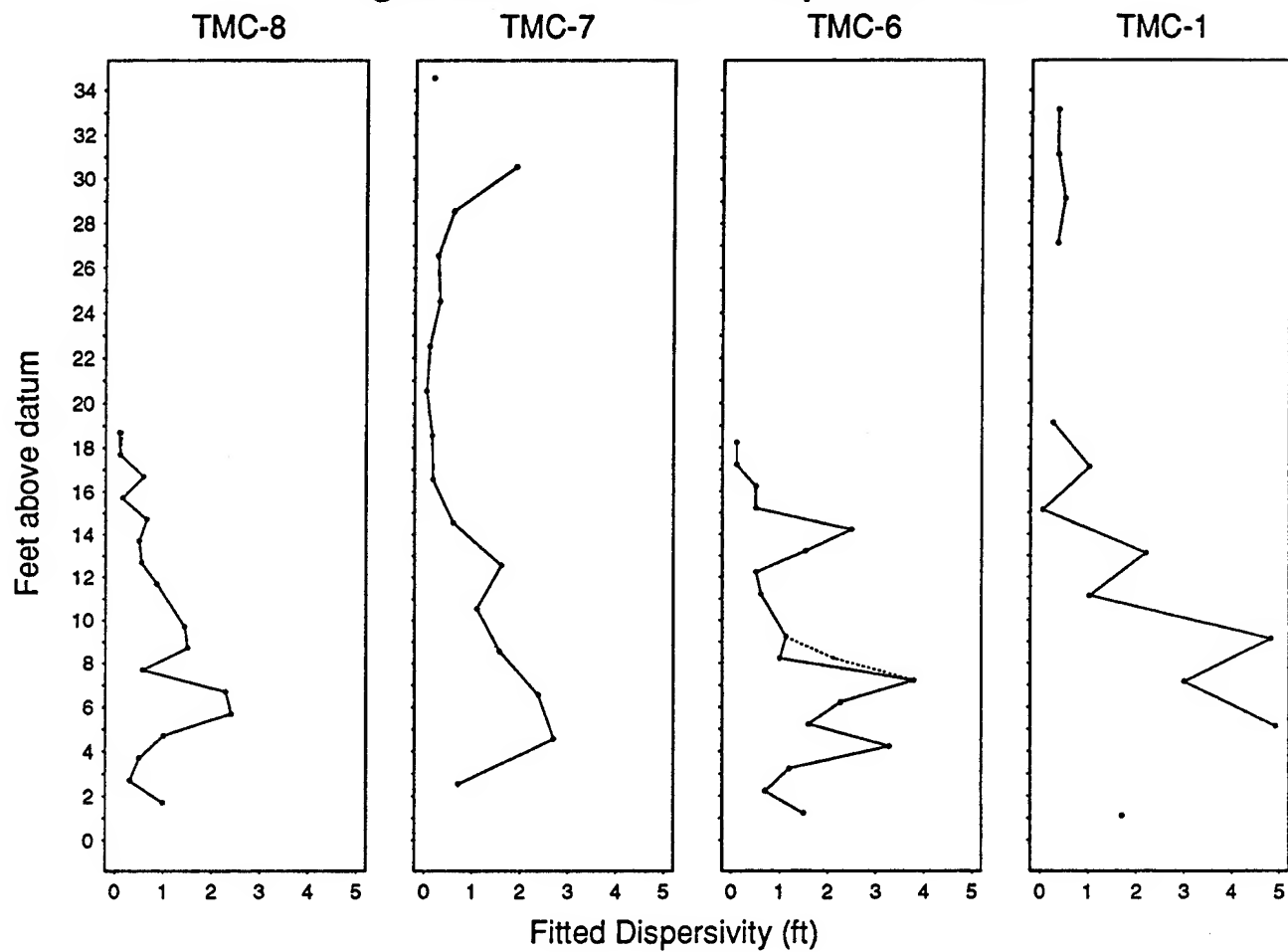


Table 1: Fitted parameter values for breakthrough curves at TMC-8; n is the number of data points and rmsr is the root-mean-squared residual. Note that two peaks have been fit at port 17.

port	C_i (mg/l)	q_p (ft ² /hr)	α (ft)	n	rmsr
1	89.81	37.02	0.99	28	8.82
2	13.51	7.80	0.30	28	22.85
3	53.77	28.12	0.50	28	5.51
4	122.90	84.58	1.00	28	40.17
5	116.24	76.45	2.40	28	18.32
6	104.10	68.25	2.29	28	16.51
7	21.90	42.00	0.57	28	13.20
8	26.58	15.09	1.50	28	9.20
9	37.37	18.64	1.44	28	4.54
10	45.00	16.52	0.86	28	6.97
11	60.61	41.06	0.54	28	11.16
12	100.02	104.09	0.50	28	35.43
13	50.11	32.91	0.65	28	6.30
14	99.96	100.04	0.15	28	40.34
15	100.10	129.62	0.59	28	25.83
16	48.64	59.84	0.10	28	19.38
17	6.94	50.49	0.08	28	17.62
17	10.63	23.16	0.14	28	21.43

Table 2: Fitted parameter values for breakthrough curves at TMC-7; n is the number of data points, $rmsr$ is the root-mean-squared residual, and C_b is the estimated background concentration.

port	C_i (mg/l)	q_p (ft ² /hr)	α (ft)	n	$rmsr$	C_b (mg/l)
1	24.78	43.71	0.70	50	4.86	0.00
2	81.45	46.09	2.70	51	5.26	0.00
3	164.68	104.13	2.38	51	5.09	0.00
4	15.79	21.63	1.58	51	1.90	0.00
5	33.86	25.75	1.10	51	3.71	0.00
6	20.32	29.78	1.61	51	4.42	0.00
7	17.83	44.68	0.60	51	7.49	0.00
8	48.15	121.08	0.18	51	9.50	0.00
9	12.76	24.34	0.16	51	2.74	0.00
10	1.72	18.55	0.04	51	0.99	0.00
11	0.22	20.51	0.11	47	0.05	0.20
12	1.21	16.35	0.32	47	0.31	0.20
13	11.72	15.89	0.28	47	3.48	0.00
14	23.09	19.77	0.60	47	7.14	0.00
15	10.73	8.45	1.91	47	2.46	0.00
16	---	---	---	0	---	---
17	1.10	6.96	0.17	47	0.46	0.00

Table 3: Fitted parameter values for breakthrough curves at TMC-6; n is the number of data points, rmsr is the root-mean-squared residual, and C_b is the estimated background concentration. Note that two peaks have been fit at port 8.

port	C_i (mg/l)	q_0 (ft ² /hr)	α (ft)	n	rmsr
1	28.00	80.00	1.50	23	7.26
2	19.28	52.87	0.70	23	4.93
3	20.73	100.23	1.20	23	5.85
4	87.18	61.94	3.28	23	5.27
5	88.70	100.68	1.60	23	7.13
6	139.73	109.27	2.27	23	6.07
7	129.43	94.48	3.79	23	6.00
8	9.78	72.97	1.00	23	9.49
8	9.85	18.11	2.12	23	8.75
9	16.10	20.15	1.13	23	3.37
10	17.78	22.54	0.61	23	0.91
11	15.09	24.05	0.51	23	1.58
12	109.68	93.04	1.54	23	5.76
13	25.00	44.50	2.50	23	6.02
14	17.62	156.45	0.50	23	0.20
15	76.30	154.80	0.50	23	0.69
16	27.51	70.79	0.10	23	1.95
17	5.15	62.20	0.10	23	1.85

Table 4: Fitted parameter values for breakthrough curves at TMC-1; n is the number of data points, $rmsr$ is the root-mean-squared residual, and C_b is the estimated background concentration.

port	C_i (mg/l)	q_p (ft ² /hr)	α (ft)	n	$rmsr$	C_b (mg/l)
1	0.36	20.29	1.70	51	0.06	0.10
2	---	---	---	51	---	---
3	94.15	110.61	4.93	51	1.36	0.00
4	50.00	90.00	3.00	51	2.50	0.00
5	13.80	22.79	4.82	51	1.62	0.00
6	17.34	127.53	1.03	51	0.59	0.00
7	25.98	144.94	2.20	51	0.27	0.00
8	0.26	65.65	0.06	51	0.08	0.15
9	6.26	26.72	1.03	51	0.95	0.00
10	30.69	19.23	0.27	51	1.12	0.00
11	---	---	---	51	---	---
12	---	---	---	51	---	---
13	---	---	---	51	---	---
14	0.75	18.70	0.35	51	0.39	0.25
15	1.80	15.00	0.50	51	0.75	0.25
16	4.90	27.19	0.35	51	2.26	0.25
17	8.00	21.00	0.35	51	1.25	0.25

E. GEMS SLUG-TEST SURVEY

As part of the effort to describe the spatial variations in hydraulic conductivity in the subsurface at GEMS, slug tests were performed in most of the wells screened in the sand and gravel section. In all cases, the KGS single-packer slug-test system (McElwee and Butler, 1989) was used to perform these tests. As discussed in Section III.B, the slug-test response data from wells at GEMS have displayed anomalous features that prevent ready analysis by conventional methods. In Section III.D, a nonlinear variant of the Hvorslev (1951) model was developed in an attempt to account for the observed phenomena. Although this model does not completely explain all the physical mechanisms that are affecting the slug-test data at GEMS, it does seem to do a better job than any other presently existing model. Thus, the data from this series of slug tests were analyzed by the non oscillating nonlinear Hvorslev model (see Fig. III.D.3 for an example fit using data from this series of tests).

Table IV.E.1 summarizes the estimated parameter values determined from this program of testing. Note that in Sections III.B and III.D considerable attention was given to the issue of the dependence of estimated parameters on the magnitude of H_0 . In order to minimize the error that might be introduced by this dependence, a calibrated container of known volume was used to add the water utilized as the slug at each well. Thus, the slug introduced at each well consisted of approximately the same volume of water. The actual H_0 did differ somewhat between wells (H_0 range was .67-.93 m) mainly as a result of the differences in the schedules (thicknesses of pipe wall) of the PVC casing used at wells at the site. The conductivity values listed on Table IV.E.1 are quite high, but they are not surprising given the coarse sand and gravel deposits underlying GEMS. As discussed in Section III.D, the non oscillating nonlinear Hvorslev model does not fully account for the dependence of the physical parameters on H_0 . Thus, the values reported in Table IV.E.1 must be considered somewhat approximate. However, by controlling H_0 to within narrow bounds, the error due to the H_0 dependence should be similar between wells. Thus, the variations between the values reported on in Table IV.E.1 should be a reasonable reflection of the actual natural variability within the sand and gravel section at the site. Note that slug tests within the overlying clay and silt deposits and the underlying bedrock yielded conductivity values considerably lower than those of the sand and gravel section.

Well #	A (10^4 sec^2/m^3)	K (10^{-3} m/sec)	K (m/day)
0-1	1.577	0.893	77.13
0-2	0.676	0.984	84.98
0-5	0.411	0.499	43.11
0-7	2.250	5.19	448.22
1-1	0.527	0.735	63.55
1-5	3.764	1.69	146.21
1-7	3.212	1.84	158.67
2-2	0.142	0.506	43.69
2-5	1.164	0.537	46.43
2-6	4.022	0.730	63.07
2-7	3.124	4.71	406.61

Table IV.E.1 - Summary of estimated values for hydraulic conductivity (K) and the constant of proportionality (A) determined from a program of slug testing at GEMS. Parameters estimated using the non oscillating nonlinear Hvorslev model described in section III.D.

F. PUMPING TEST OF BEDROCK WELL

Introduction

As part of our continuing effort to characterize the geohydrology of the GEMS site, we performed a pumping test on the 0-6 well (Table 1 of Section IV.A) which is drilled ten feet into bedrock. We decided to do this after earlier well development work at the site showed that the bedrock well was capable of producing 5-10 gallons per minute. Unfortunately, no other wells at the site are currently completed into the bedrock. Therefore, no observation well was available for taking data except the pumping well itself. We knew that typically a data set from a single pumping well was difficult to analyze due to complicating factors such as the presence of the pump and possible well bore storage effects. Also, a sensitivity analysis usually shows that a single pumping well is not very sensitive to some parameters. In particular, the storage coefficient is usually not very well determined for a single pumping well. We decided to perform the test anyway to see what estimates of bedrock parameters could be made and to take samples of the bedrock water over time to look at the geochemistry.

The Pumping Test

The bedrock pumping test was performed in late April of 1992. We monitored the background water levels in the bedrock well (0-6) and two nearby alluvial wells screened at 65 feet (Well 0-5) and at 55 feet (Well 0-7) for a few days before and after the pumping test to see if there was any significant trend that would need to be subtracted out of the collected pumping test data. Also, we monitored barometric pressure during the same time periods to see if any corrections should be made for changing barometric conditions. The largest deviation observed that could be attributed to either a trend or barometric fluctuation was .11 feet of water. No correction was applied to the data since pumping-induced drawdown was in the tens of feet.

During the pumping test we collected data from the three wells (0-6, 0-5, and 0-7) and from a flowmeter that was in the pump discharge line. All of this data set was collected automatically by a data logger and stored in computer readable format on floppy disks for later analysis. The pump was turned on and allowed to pump at 6.01 gpm (average value of flowmeter data) for one hour. At that point, the flow rate was increased to 8.04 gpm (average value of flowmeter data) for one hour. After two hours the pump was shut down and data were taken during recovery. Figure 1 shows a plot of the data collected in the pumping well versus time.

Data Analysis

Attempts to analyze the complete data set shown in Figure 1 with SUPRPUMP (see section II.B) in a consistent manner have met with some difficulty. Different segments of the data (first pumping period, second pumping period, and recovery period) seem to indicate different values of the aquifer parameters. Clearly, the real world situation is much more complex than the simple models in SUPRPUMP can handle. It appears that further numerical analysis with a more complex model is needed. The bedrock well extends ten feet into the bedrock from the base of the alluvium and is screened for the lower five feet. It would seem likely that the base of the alluvium is acting like a constant head boundary and producing a lot of leakage. This is borne out by the fact that during the pumping test the water levels in the alluvial wells changed by less than .2 ft. Also, partial penetration and well bore storage effects may be important. All of these things can be addressed with further analysis by a numerical model. However for this report, time has only permitted a preliminary analysis of the data with SUPRPUMP.

The first attempt to analyze the data used the Theis well function, which is the simplest well function. Figure 2 shows the data from the first pumping period (one hour) and the resulting Theis curve fit. Clearly, the Theis curve does not fit the data at later times. The actual data flattens out while the Theis curve continues to decline. The obvious thought is that the leakage from the overlying alluvium is causing the data to flatten out due to an approach to steady state. SUPRPUMP allows leakage in one of its well functions, so the leaky well function was used to fit the data as shown in Figure 3. The fit is now fairly good except for a region where the actual data falls a little below the leaky curve. The fitted parameters are:

$$T \text{ (transmissivity)} = 10.94 \text{ ft.}^2/\text{day}$$

$$K \text{ (hydraulic cond.)} = 2.19 \text{ ft./day}$$

$$S \text{ (storage)} = .245$$

$$L \text{ (leakage)} = 1.21 \text{ ft}^{-1}$$

Conclusions

The hydraulic conductivity (about 2 ft./day) determined here is considerably lower than that determined from slug tests in the overlying alluvium. Also, the storage coefficient of .245 is typical of an unconfined situation, not a semi-confined leaky aquifer. As mentioned earlier, later portions of the data give fitted parameters somewhat different from those given here. These difficulties are yet to be resolved. However, one thing seems clear from this data: there is a lot of leakage into the bedrock aquifer from the alluvial aquifer. This leakage shows up as a large leakage parameter (L) and a large

storage coefficient (S). This idea of leakage from the overlying alluvium is borne out by the geochemical analysis of the water (Section IV.C). The need for further analysis of this data with a numerical model seems to be indicated.

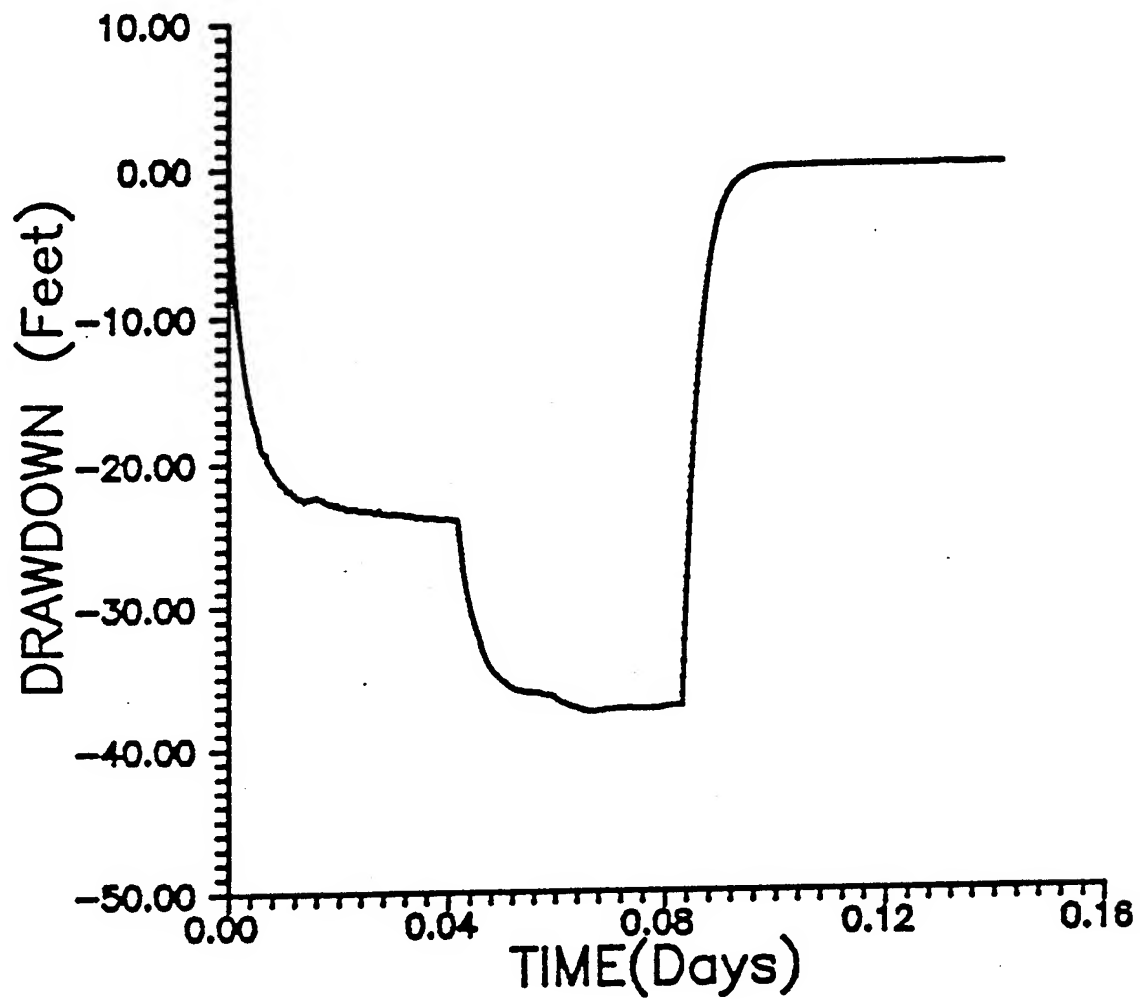


Figure 1. Drawdown data from all three periods (two pumping and one recovery).

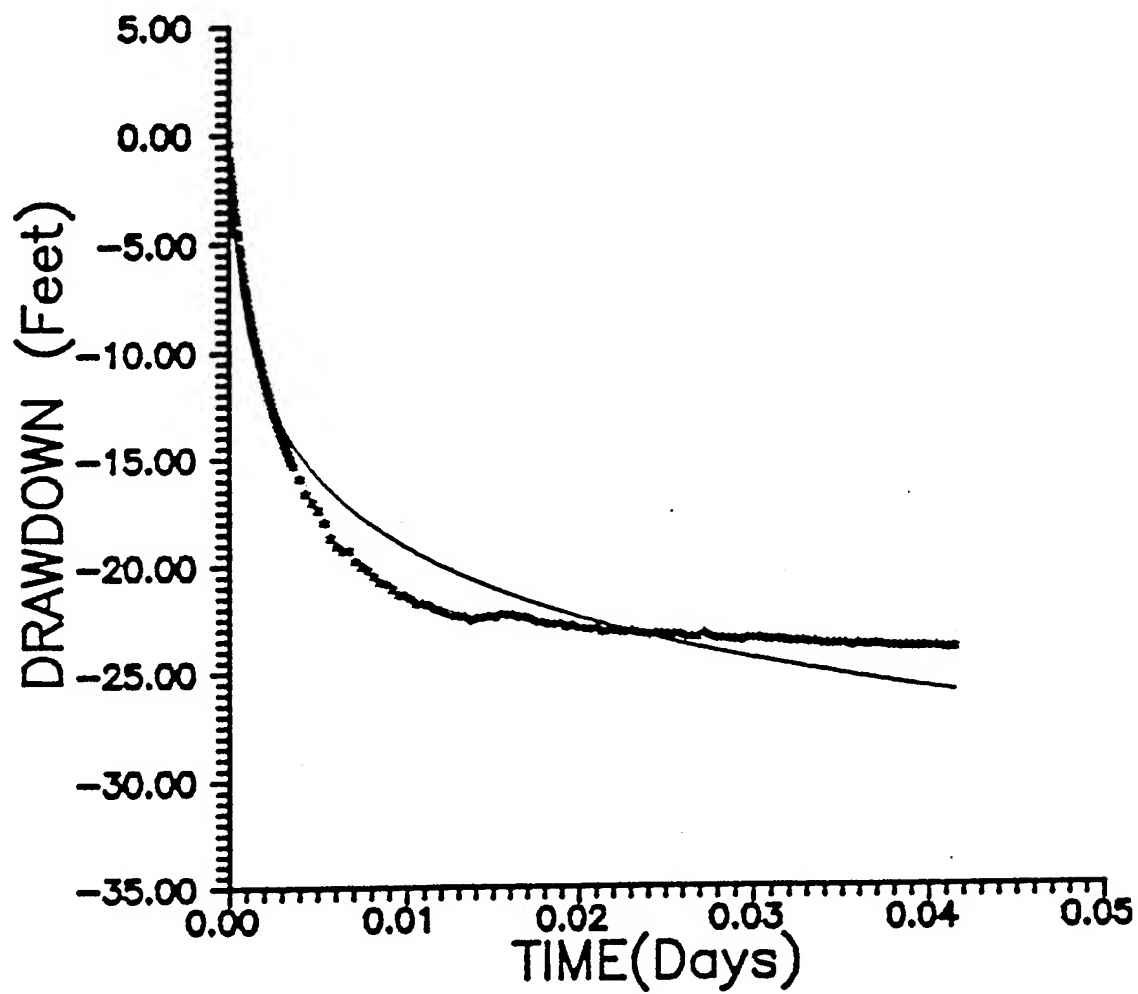


Figure 2. Fit of first period drawdown data to the Theis well function (solid curve).

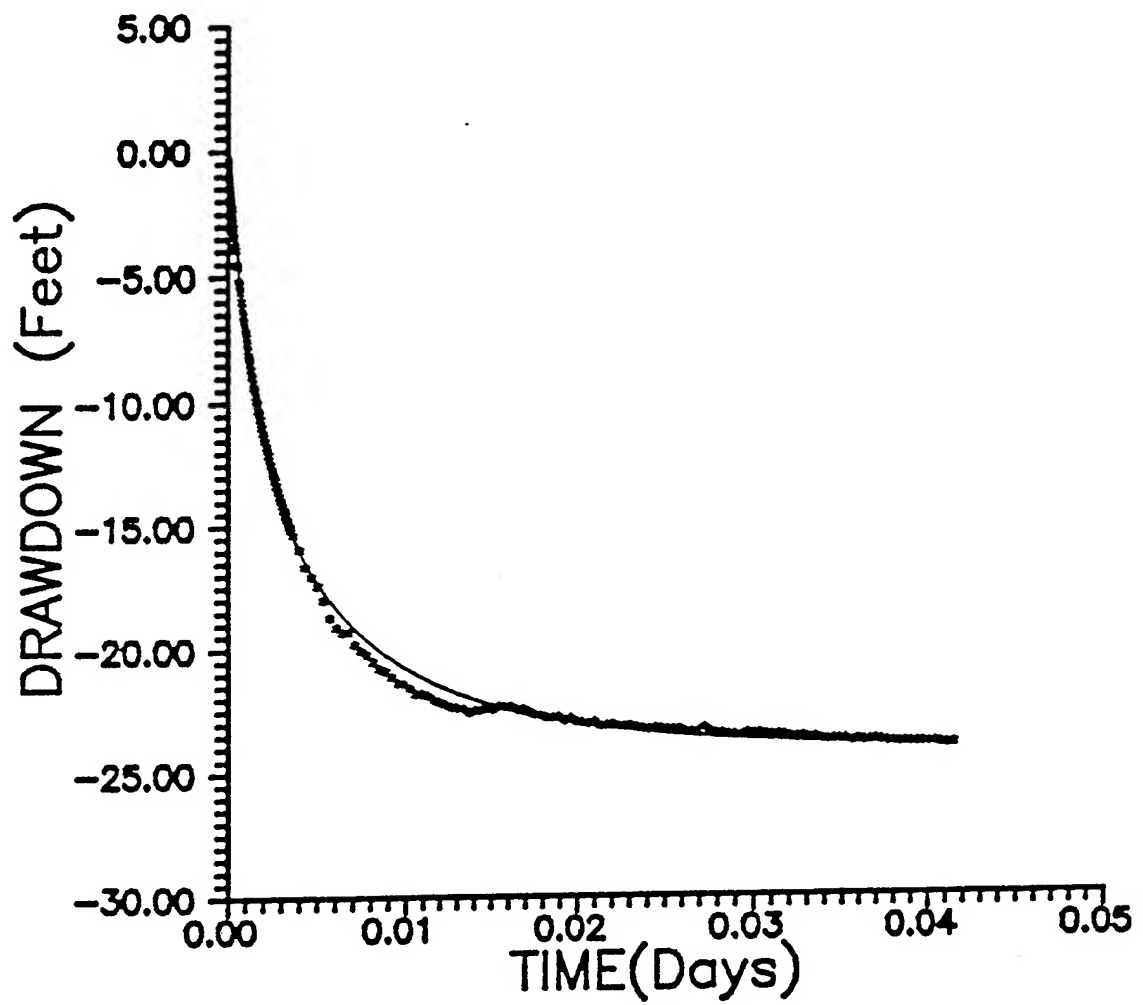


Figure 3. Fit of first period drawdown data to the leaky well function (solid curve).

G. WIRELINE LOGGING ACTIVITIES - GEMS NATURAL GAMMA AND INDUCTION LOG SURVEY

Introduction

As part of the effort to describe the spatial variations in lithologic properties in the subsurface at GEMS, natural gamma and induction log surveys were performed in strategically located wells penetrating the sand and gravel section and the overlying silt and clay section. The surveys were run using logging equipment recently purchased by the Kansas Geological Survey. The goals of the surveys were (1) to determine the lateral extent of distinct lithologies with the greatest resolution possible, (2) to establish a data base that would aid in the planning of future logging and groundwater investigations, and (3) to familiarize the research group with logging theory and the field equipment in preparation for future research and experimentation. A typical set of logs from GEMS well 1-7 are shown in Figure 1.

Formation Induction

Induction borehole tools contain a transmitter and a receiver coil, positioned vertically with a specified separation distance. A medium frequency alternating current is passed through the transmitter coil, producing a magnetic field about the coil. The vertical component of the magnetic field induces a current in a ring of formation material between the transmitter and receiver coils, but outside the borehole. The magnitude of the electric current is proportional to the electrical conductivity (or resistivity) of the formation. This current will also produce a magnetic field that will induce a current in the receiver coil. The voltage measured at the receiver coil is also proportional to the electrical properties of the formation and is converted to conductivity (right column in Figure 1) and resistivity (reciprocal of conductivity, middle column of Figure 1) by an automated calibration curve. These properties are measured periodically as the borehole tool is raised in the well and are plotted versus depth. The resulting curve is called an induction log.

The electrical conductivity and resistivity of a formation are a measure of the materials ability to carry or resist an electric current. Different lithologies have different electrical properties. Shale, for example, generally has a high electrical conductivity and a correspondingly low resistivity. On the other hand, clean sandstone generally has a low conductivity and a high resistivity. Identifying these relative differences on an induction log allows a geologist to identify changes in lithology in the subsurface.

In most geologic material, the porosity and pore fluid chemistry are more important controls on the electrical properties of the material than the mineral grains (Dobrin and Savit, 1988). This inherent property will allow the determination of aquifer hydraulic properties by observing the movement of a conductive groundwater tracer with a borehole induction tool. An application of this idea is presented in section IV.H.

The initial induction logs from GEMS are as expected. Repeat logs (from the same borehole) display no deviation due to changes in logging rate or lag time between repeat runs. The contact between the sand and gravel aquifer and the overlying silt and clay aquitard is obvious in all of the logs. The water table and smaller subunits (1 to 3 m thick) are also identifiable. The observed lithologic contacts were correlated between wells by hand and with an interactive computer program. The results of the correlation will be discussed below.

Natural Gamma Radiation

A natural gamma ray log is a plot of the amount of gamma radiation emitted from a segment of geologic material surrounding a borehole versus depth (left column in Figure 1). The source of the gamma rays is the decay of radioactive elements naturally occurring in the rock. Trace levels of radioactive isotopes of potassium, thorium, and uranium are concentrated in fine-grained sedimentary deposits. Chemical weathering of rocks containing feldspar minerals produces clay minerals that may contain up to 1% potassium and are the largest source of formation radioactivity (Ellis, 1987). Thorium is quite rare, but is associated with heavy minerals that are often resistive to chemical and physical erosion. As a result, they remain as erosional remnants of their parent rock and become concentrated during transportation due to their high relative density. Uranium-bearing minerals are also quite rare, but when present, they are commonly from the precipitation of uranium salts and are frequently found in organic-rich shales (Ellis, 1987).

The gamma rays produced from these sources are detected by a scintillator. This device contains a NaI crystal that is sensitive to radiation and emits a pulse of light when struck by a gamma ray. A photomultiplier detects the minute flashes of light and transforms them into an electrical pulse that is monitored and counted. Our natural gamma-ray counter is encased in the same tool that houses the induction devise. The two sensors act independently and record data simultaneously.

Natural gamma ray logs have been used by geologists for correlation of lithologies between wells, identification of subsurface lithologies, and for the estimation of the volume of clay in an observed stratigraphic unit. Traditionally, correlation of

natural gamma logs is attained with resolution measured in feet. Typical objectives are: the elevation of the base of a reservoir cap composed of shale overlying a porous limestone, or the thickness of an aquifer at a certain location. The magnitude of variation in natural gamma emissions across these boundaries of distinctly different lithologies is quite great and is easily identified on a log. However, if one is interested in identifying small (10 to 20 %) variations of clay content in thin beds within a sand aquifer, much greater resolution is needed. Procedures for collecting data to be analyzed at this scale (resolution of one foot or greater) are poorly outlined. As a result, a detailed investigation of the nature of radioactive decay and the methods used to measure it is necessary to collect the data correctly and accurately interpret the results.

The instantaneous rate of decay of radioactive elements in the earth is not constant. If the rate of decay is measured over a short time interval, the value obtained may over- or underestimate the true rate. However, if measured over a long period of time, random variations in the instantaneous rate of decay will cancel each other out and a reliable value for the rate can be obtained.

As the gamma ray counter is raised in a well, it continuously measures the rate of decay over a specified time interval (0.1 seconds for our counter). All of the rates measured as the tool (device containing the gamma ray counter) is raised in the well are averaged over a specified vertical interval. Therefore, each value on a log is the average of several samples of the rate of decay. To increase the accuracy of the result obtained per vertical interval, more 0.1 second samples of the rate must be averaged. This can be accomplished by increasing the length of the vertical interval of the borehole that the rate is averaged over, or by increasing the time the radiation sensor measures rates for each vertical interval (decreasing the rate the sensor is raised in the borehole).

The initial natural gamma ray logs collected display poor well-to-well correlation at the desired resolution. It is known from cores from GEMS that bedding exists in the sand and gravel aquifer at the scale of 0.02 to 0.3 m, yet natural gamma logs from wells separated by only 2.1 m, allow only the correlation of beds at the scale of 1 to 3 m. Considering that this material was deposited by point bar accretion, beds 0.1 m thick and greater should be laterally continuous over a distance of 2.1 m.

The lack of correlation at this scale with gamma ray logs suggests that variation in gamma radiation produced by changes in lithology are drowned by variability in the decay rates. It is possible that the contribution of gamma rays from the feldspar content in the sand is much greater than that from the clay. If the feldspar content in the sand is relatively consistent with depth, and the variations comprising the bedding are produced only by differences in grain-size and/or clay content, then it is possible that the

contribution of the lithologic variation is negligible compared to the statistical variability in the contribution of the feldspar.

An experiment was conducted in an attempt to better assess the importance of the variability in decay rates. The tool was held at the same vertical position in the borehole for approximately ten minutes, while continuously recording the natural gamma radiation. The variability observed during that period accounted for essentially all of the variation observed on the original logs from the sand and gravel aquifer. Clearly, most of the variation in gamma radiation due to the changes in lithology seen in the cores is completely obliterated by the variability in the decay rates.

At this same time, we learned from the manufacturer of the logging equipment that the zone of influence of the tool is a sphere with a radius of approximately 1 m. Because such a large segment of geologic material is sampled for each measurement interval, the contribution of gamma radiation from a thin bed in this sphere will be averaged with the radiation from the entire sphere and will be decreased if not entirely masked by the variability in the rate of gamma ray emission for the entire sphere.

These developments are discouraging, but we still hope to attain better vertical resolution. In order to decrease the uncertainty in the natural gamma values obtained, even slower logging rates can be used to allow more 0.1 second rates to be averaged. Repeat logs can also be run. The values from each repeat log can be added at every interval and averaged. This will also decrease the variability by essentially doubling the averaging time for each repeat log added. A statistical review of the data already collected is currently underway to determine a logging strategy that would minimize the uncertainty in the log values and the time spent in the field. An investigation of the expected contributions of gamma radiation from the feldspar grains and the changes in clay content seen in cores is also being conducted to determine the origin of the observed gamma ray signal.

Despite the high level of statistical noise in the natural gamma logs from the initial survey, some lithological correlations can be made between the eight wells logged. The boundary between the sand and gravel section and the overlying silt and clay section are definitively identifiable in each well. Subsections, ranging in thickness from 1 to 3 m, are identified in both sections and can be correlated across the site. Other subsections however, are distinctly apparent in one well and seemingly absent in adjacent wells. The signals from these units may be present on the logs, but are masked by the variability in the gamma emissions, or by the large averaging volume.

Computer Correlation

In addition to the hand correlation of the logs, a computer program, CORRELATOR (Olea, 1988), was also used to aid in the well-to-well correlation. The program uses two logs from each well. One log must be sensitive to the clay content in the lithologic sequence, and the second must measure a lithologic property that is laterally consistent on a regional scale. Natural gamma and formation induction logs were chosen for the correlation. The resulting correlation is statistically high across the site and appears reasonable considering the environment of deposition of the deposits. Although the correlation is statistically high, the resolution of laterally continuous lithologies is still less than what was anticipated.

Conclusion

An understanding of lateral continuity is vitally important for any investigation of the physical controls on groundwater flow. Clearly, a vertical resolution of a few tenths of a meter will be difficult to obtain. Further work is needed to assess the minimum resolution that can be obtained.

Typical Natural Gamma and Induction Log from GEMS Well 1-7

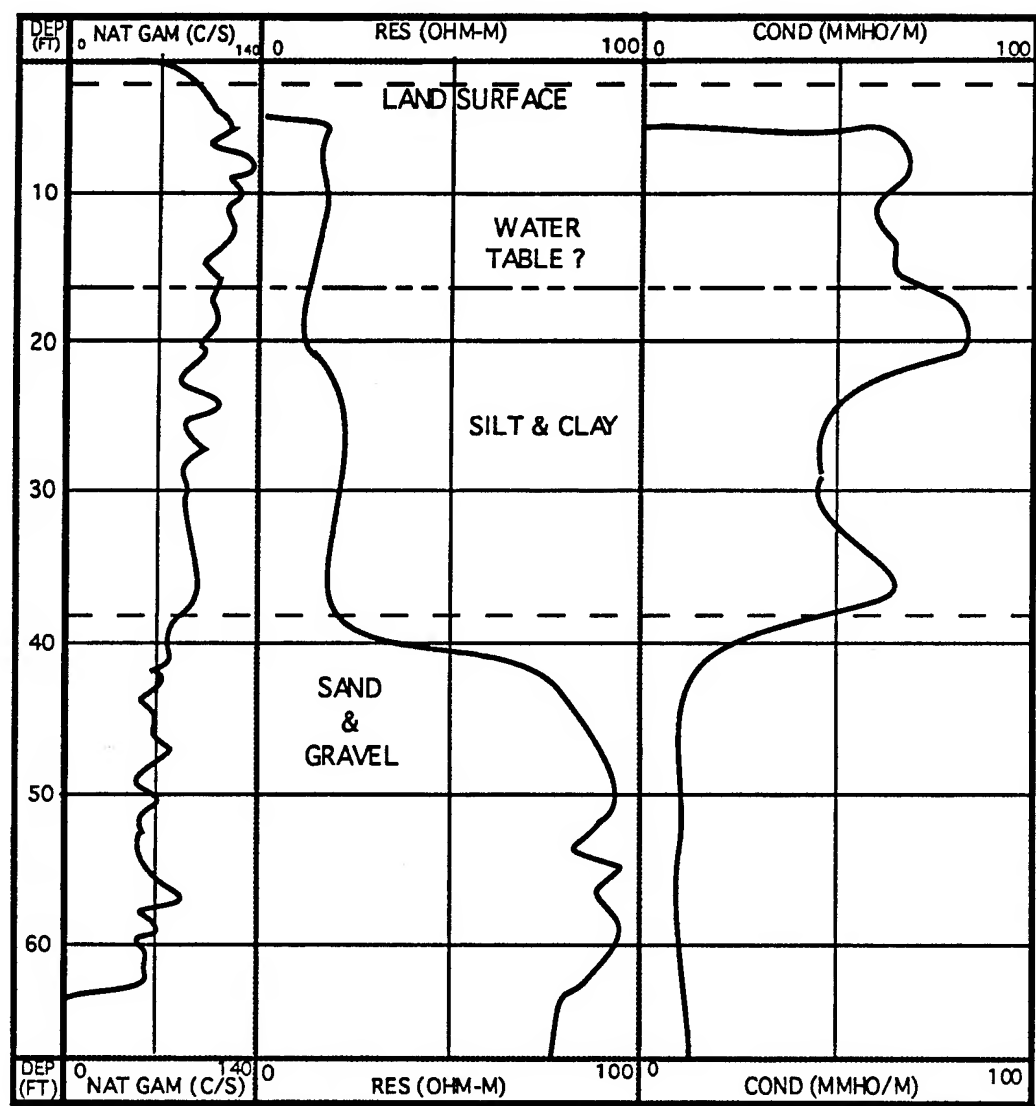


Figure 1.

H. AN EVALUATION OF A BOREHOLE INDUCTION SINGLE-WELL TRACER TEST TO CHARACTERIZE THE DISTRIBUTION OF HYDRAULIC PROPERTIES IN AN ALLUVIAL AQUIFER

Abstract

In order to assess the potential of a borehole induction single-well tracer test to characterize the vertical distribution of hydraulic properties, a series of tracer tests was performed at a field site in the Kansas River alluvium. The procedure involves the injection of a nonreactive, electrically conductive tracer into a well under artificially induced, steady-state flow conditions. Vertical variations in the rate of the horizontal invasion of the injected tracer solution are computed from repeated logs using a focussed induction borehole probe. These data are employed to construct vertical profiles of effective porosity and hydraulic conductivity at the injection well. Although modification of the procedure was necessary in order to ensure that model assumptions are valid, to reduce monitoring error, and to remove the effects of a near-well drilling-induced disturbed zone, the tracer test appears to have considerable potential for accurate characterization of alluvial aquifers.

Introduction

Background

In order to predict the movement of water and pollutants accurately in the subsurface, it is necessary to understand the factors controlling their transport. Spatial variability in aquifer hydraulic parameters may produce differential flow (contrasting flow rates), greatly influencing groundwater flow and transport (Freeze and Cherry, 1979). Therefore, accurate characterization of parameter spatial variability is critical if reliable predictions of contaminant transport are to be made.

Taylor *et al.* (1990) recently evaluated commonly employed methods for estimating spatially varying hydraulic properties in unconsolidated geologic formations. They conclude that due to near-hole drilling disturbances, inadequate sediment sampling techniques, and sampling bias, current methods have significant limitations. Clearly, refinement of current methods or the development of new methods is needed if hydrogeologists are to keep pace with increasing demands for reliable predictions of contaminant transport.

The borehole induction single-well tracer test is a new method of aquifer characterization apparently first reported in the groundwater literature by Taylor and Molz (1990). The method provides estimates of vertical variations in horizontal hydraulic properties at a scale that has been difficult to obtain in the past. Detailed information of this kind can greatly improve the understanding of the primary controls on subsurface flow and transport at a site.

To date, there have been no published evaluations of the borehole induction single-well tracer test method. Although the study of Taylor and Molz (1990) produced reasonable results, a more thorough evaluation of the method is needed. The following subsection summarizes the tracer test method, its application at a research site of the Kansas Geological Survey, and important refinements that are required in the originally proposed approach.

Field Site

Five tracer tests were conducted at the Geohydrologic Experimental and Monitoring Site (GEMS). The bedrock beneath GEMS is a silty sandstone of the Pennsylvanian Douglas Group (Davis and Carlson, 1952). The bedrock at the site is covered by approximately 22 m of unconsolidated Kansas River alluvium of the early Wisconsinan Newman terrace (Davis and Carlson, 1952). The alluvium is composed of approximately 11 m of sand and gravel overlain by 11 m of silt and clay. The sand and gravel unit, the focus of this study, is composed primarily of quartz, feldspar, and chert grains and contains an average of 2 to 3 weight percent silt and clay (McElwee *et al.*, 1993). Cores from this unit display cross-bedding, variable grain size and clay content, and clay drapes measuring approximately 1 to 3 cm in thickness. The average phi size and hydraulic conductivity determined from repacked core material are -0.02 and 58.26 m/day, respectively (McElwee *et al.*, 1993).

The underlying Pennsylvanian bedrock and the overlying silt and clay unit hydraulically restrict groundwater flow in the sand and gravel, forming a leaky confined aquifer. Water levels in the sand and gravel and the silt and clay intervals are approximately 7 m and 5 m from the land surface, respectively. The lateral hydraulic gradient in the confined aquifer ranges from approximately $2\text{E-}3$ to $4\text{E-}3$ throughout the year and is directed approximately S20°E. The four injection wells used for the five tests are constructed of 0.051 m diameter PVC pipe and are fully screened across the sand and gravel interval.

Tracer Test Methodology

Summary of Method

The Taylor and Molz (1990) tracer test method involves the injection of a nonreactive, electrically conductive tracer solution into a well under artificially induced, steady-state flow conditions (Figure 1). As the tracer solution enters the aquifer through the well screen, it moves radially outward, displacing the native pore fluid. Since the electrical conductivity of a formation is significantly controlled by porosity and pore fluid chemistry (Dobrin and Savit, 1988), a considerable increase in the formation conductivity occurs as the tracer advances radially outward from the well. The invasion of the tracer is monitored by repeated logs using a focussed induction borehole probe. The rate of invasion as a function of depth is determined from the induction logs. Detailed vertical profiles of the effective porosity and hydraulic conductivity are constructed using the tracer invasion rates, the induced hydraulic gradient, and the observed change in formation electrical conductivity as the tracer solution invades the aquifer.

Tracer Injection

Induced steady-state flow conditions were produced in the injection well prior to the introduction of the tracer solution. This was accomplished by pumping native GEMS groundwater using a 0.089 m diameter submersible pump (*Simer*, model 9BC) from a 0.102 m diameter PVC well (0-8, see section IV.A for a well map) screened in the sand and gravel aquifer, and directly discharging it into the injection well. The pumping well was located far enough from the injection well (> 20 m) that drawdown at the injection well due to pumping was negligible. A constant injection rate of 14 - 45 gal./min. (depending on the test) was used for input to the injection well. When the water level in the injection well stabilized, flow within the volume of the aquifer adjacent to the well was assumed to be at steady state.

Once steady-state flow conditions were achieved, a concentrated saline solution was pumped from a storage tank directly into the line between the pumping and injection wells. The tracer solution (water from pumping well and concentrated saline solution) discharged into the injection well at the land surface, cascaded down the well, and entered the aquifer through the well screen. The tracer replaced the native pore fluid as it was transported radially outward under the induced hydraulic gradient. As the tracer advanced, the conductivity of the formation increased. This change was monitored throughout the test with repeated surveys using a borehole induction tool.

Tracer injection continued until the tracer traveled a radial distance of roughly 2.5 m from the well (the approximate radial detection limit of the induction tool). During

this time, 21,600 - 38,000 L (5700 - 10,000 gal.) of tracer solution were injected into the aquifer. The exact volume depended on the porosity of the media and the length of the screened interval. Injection periods varied from 4 to 8 hours depending on the test.

Tracer Solution

A dilute NaCl solution was used for the tracer due to the high solubility, relative inertness, low cost, and low toxicity of NaCl. The specific conductivity of the tracer solution (115 - 200 mS/m) was roughly 2 to 3 times the specific conductivity of the native groundwater (64.5 mS/m). During each test, approximately 7 - 37 kg of NaCl was pumped into the aquifer.

The saline solution was prepared and stored in a 1988 L (525 gal.) polyolefin storage tank. GEMS native groundwater, used as the solvent, was pumped into the tank from the pumping well prior to injection. To ensure complete dissolution of the solute and thorough mixing throughout the test, a small submersible pump (*Little Giant*, model 2E) was used to continuously circulate the solution. A second submersible pump (*Grundfos*, model MP1) was used to pump the concentrated saline solution from the tank, into the main injection line.

Induction logging

The electrical conductivity of the formation adjacent to the injection well was logged before, during, and after tracer injection with a focussed induction borehole probe manufactured by *Century Geophysical Corporation* (model 9510). The borehole probe contains a pair of transmitter coils carrying an alternating electric current. This current produces an alternating magnetic field in the formation surrounding the tool. The magnetic field induces current loops in the formation outside the well. This current creates a magnetic field that induces an electric current in a pair of receiver coils inside the induction probe. The magnitude of the current in the receiver coils is a function of the initial current in the transmitter coils and the ability of the formation to conduct the current loops. As the electrically conductive tracer solution invades the formation, the ability of the formation to conduct an electric current increases. The borehole induction tool measures this change and enables the position of the tracer front with respect to the injection well to be estimated. During the tracer tests, the conductivity of the formation was measured at 0.030 m intervals as the induction tool was slowly raised in the injection well. The conductivity readings (units of mS/m) were transmitted in digital form to the land surface and stored in a computer.

The injection well was logged with the induction probe four times prior to the initiation of tracer injection. Pretest experiments showed that statistical variability in log values is reduced by computing average logs from repeated measurements. Four was chosen for the number of repeat logs as a compromise between logging time and variability reduction in log values. Following the initiation of tracer injection, the injection well was initially logged every 20-35 minutes to monitor the radial invasion of the tracer solution into the aquifer. Logging continued at increasing time intervals until the tracer solution approached the radial detection limit of the induction probe. This state was assumed to have been reached when conductivity logs showed little change with continued injection. At that time, the injection well was logged four more times and tracer injection was terminated.

Test Monitoring

During practice injection tests and the first tracer test, pressure transducers (*Instrumentation Northwest*) were placed in the pumping, injection, and observation wells to monitor water levels. These data were recorded by a data logger (analog - digital converter: *Iotech*, model ADC488/16; P.C.: *Zenith*, model ZW-241-82; software: *Scentech*, Turbolab 1.0) and used to determine the induced hydraulic gradient in the vicinity of the injection well. For the remaining tests, the water level in the injection well was monitored with an electric water level tape (*Solinst*) and sometimes with pressure transducers.

A flow meter (*Omega*, model FP-5800) attached to a 0.025 m inner diameter PVC flow-through pipe fitting monitored the tracer solution injection rate. The meter was inserted into the main injection line downstream of the point of introduction of the concentrated saline solution. The meter was monitored with a data logger or by visual inspection.

A fluid conductivity cell (*Hach*, model 44600) monitored the electrical conductivity of the tracer solution in the injection line. This meter also served as a check to ensure that the pumping well and tracer tank pumps were operating properly. A second conductivity cell (*Solomat*, Chemistry Module 4007) identified the appearance of the tracer solution at the bottom of the screened interval of the injection well in three of the initial four tests. During two tests, the tracer solution reached the bottom of the well within three minutes of the start of tracer injection. In the third test, the tracer solution reached the bottom of the well within 10 minutes.

Remediation

Following the completion of each test, the injection well was pumped to remove the tracer from the aquifer. The injection well was pumped using an air-lift system (air compressor: *Curtis*, model ES-20) at a rate approximately equal to or greater than the tracer injection rate. Pumping from the injection well continued until 1.5 - 3.1 pore volumes (one pore volume is defined here as a volume equivalent to the volume of tracer solution injected) were removed. During this time, the specific conductivity of the discharge returned to the pretest level. The water pumped out during remediation was transported off site (> 50 m) using irrigation pipe and discharged onto the land surface. Most of the discharge contained Cl^- levels well below EPA specified drinking water standards and offered no threat to the natural environment. The tracer was removed primarily because of potential interference with future tests at the site.

During tracer removal the specific conductivity of the discharge was periodically measured at the surface. An approximate mass balance (comparison of tracer injected to tracer removed) showed that between 20 and 60 percent of the tracer was removed. Repeated formation conductivity logs suggested that some of the tracer was still present near the injection well following remedial pumping. Further pumping, however, removed no additional detectable tracer. It is suspected that during tracer injection a significant volume of tracer solution moved preferentially in some intervals, traveling beyond the influence of remedial pumping.

Theory of Tracer Test Data Analysis

Porosity Estimation

It has been shown experimentally that a relationship exists between formation electrical conductivity, native pore water electrical conductivity, and porosity (Archie, 1942). This relation, Archie's Law, is described in most geophysical logging texts (e.g., Bateman, 1985; Dewan, 1983; Ellis, 1987; Schlumberger, 1989). The Taylor and Molz (1990) tracer test method employs this relation to construct a model of formation conductivity that is used to estimate the effective porosity of the formation from the induction logs.

This model defines the electrical conductivity of the formation (σ_{fm}) as a sum of a contribution from the matrix (σ_m) and that from the pore fluid (σ_{pf}):

$$\sigma_{fm} = \sigma_m + \sigma_{pf} \quad (\text{IV.H.1})$$

The contribution from the pore fluid can be represented by Archie's Law:

$$\sigma_{pf} = (\sigma_f \theta^m) / \alpha \quad (\text{IV.H.2})$$

where σ_f = electrical conductivity of the pore fluid, θ = porosity, m = cementation factor, and α = tortuosity.

Substituting Archie's Law into Equation (IV.H.1) yields:

$$\sigma_m = \sigma_m + (\sigma_f \theta^m) / \alpha \quad (\text{IV.H.3})$$

From the induction logs taken before tracer injection and those taken after the tracer moves beyond the radial detection of the tool (henceforth termed tracer saturation), the formation conductivity when the aquifer is saturated with pore fluid of two different electrical conductivities is known. Equation (IV.H.3) can therefore be written as 2 equations:

$$\sigma_{fm1} = \sigma_m + \frac{(\sigma_{f1} \theta^m)}{\alpha} \quad (\text{IV.H.4})$$

$$\sigma_{fm2} = \sigma_m + \frac{(\sigma_{f2} \theta^m)}{\alpha} \quad (\text{IV.H.5})$$

where σ_{fm1} and σ_{fm2} are the formation conductivity before and after tracer saturation, respectively, and σ_{f1} and σ_{f2} are the conductivity of the native pore water and the tracer solution, respectively. Subtracting Equation (IV.H.4) from (IV.H.5) and solving for porosity yields:

$$\theta = \left[\frac{(\sigma_{fm2} - \sigma_{fm1})}{(\sigma_{f2} - \sigma_{f1})} \alpha \right]^{1/m} \quad (\text{IV.H.6})$$

The cementation factor (m) and tortuosity (α) are empirical factors dependent on lithology and pore structure. It has been shown that for unconsolidated sands these variables are approximately 1.4 and 1.0, respectively (Jackson et al., 1978).

Radius of Tracer Invasion

The radius of tracer invasion is determined for each induction log using the radial dependence relationship for the induction probe response. The formation conductivity at a single interval is a weighted average of the conductivity adjacent to that interval. The relationship between the magnitude of contribution and the radial distance from the probe is called the response function. Figure 2 displays the normalized theoretical radial response function for the probe used for this work (*Century Geophysical Corporation*, unpublished). This curve displays how the probe weights the conductivity of specific portions of the formation around the probe to determine an average formation conductivity for each interval. The shape of this curve is a function of receiver and transmitter coil geometry and can be theoretically determined (Saito, 1982).

Figure 3 is a plot of the cumulative sum of the theoretical radial responses. This function, $Z(R)$, can be used to relate changes in formation conductivity during tracer injection to the depth of tracer invasion. This function is related to the formation conductivity measured during the injection tests in the following way:

$$Z(R) = \frac{(\sigma_a - \sigma_{fm1})}{(\sigma_{fm2} - \sigma_{fm1})} \quad (IV.H.7)$$

where σ_a is a formation electrical conductivity measured at a specific time during tracer injection. Given σ_a , σ_{fm1} , and σ_{fm2} , a value for $Z(R)$ is calculated, and Figure 3 is used to determine the position of the tracer solution front at the time of a particular induction log.

Hydraulic Conductivity Estimation

Knowing the radial position of the tracer solution front as a function of time and the effective porosity, Taylor and Molz (1990) estimate hydraulic conductivity by equating a simple geometric representation of radial plug flow and Darcy's Law. The volume of pore fluid within a vertical segment of an aquifer can be represented by a cylinder with the well at the center:

$$V = \pi R^2 b \theta \quad (IV.H.8)$$

where V = volume, R = radius of cylinder, b = height of cylinder, and θ = porosity. The discharge into this volume can be written as:

$$Q = \pi R^2 b \theta / t \quad (\text{IV.H.9})$$

where Q = discharge, and t = time since initiation of tracer injection.

Discharge into this segment can also be written using Darcy's Law:

$$Q = -2\pi r b K (dh / dr) \quad (\text{IV.H.10})$$

where r = arbitrary radius for head evaluation (not related to R), K = hydraulic conductivity, and h = hydraulic head.

Equation (IV.H.10) is a separable differential equation which can be integrated with respect to r and h :

$$\int_{h_e}^{h_w} dh = -\frac{Q}{2\pi b K} \int_{r_e}^{r_w} \frac{dr}{r} \quad (\text{IV.H.11})$$

where h_w is the induced hydraulic head (difference between static and steady-state water levels) at r_w , the radius of the injection well, and r_e is the minimum radius where the induced head is near zero (h_e). The solution for this equation is:

$$h_w - h_e = -\frac{Q}{2\pi b K} [\ln r_w - \ln r_e] \quad (\text{IV.H.12})$$

Equation (IV.D.12) reduces to:

$$Q = \frac{2\pi b K H}{\ln\left(\frac{r_e}{r_w}\right)} \quad (\text{IV.H.13})$$

where $H = h_w$.

Equating Equations (IV.H.9) and (IV.H.13), and solving for K yields:

$$K = \frac{R^2 \theta}{2Ht} \ln \frac{r_e}{r_w} \quad (\text{IV.H.14})$$

Given R (radius of tracer invasion at time t) and θ determined for each induction tool sample interval (0.03 m), and r_e/r_w and H , Equation (IV.H.14) can be used to estimate K for each log interval.

Application Problems

Data Interpretation

The results from the first four tracer tests (in injection wells 1-7, 5-1, 9-1, and 11-1, see section IV.A for a well map) did not agree with results from previous studies at the site. Figure 4 contains formation electrical conductivity logs obtained before, during, and after tracer injection in well 5-1. The interval from 16 - 17 m shows little change in formation conductivity during tracer injection. This observation suggests the permeability in this interval is very small. Permeameter and grain-size analyses of cores from this well, however, do not display the pronounced low permeability interval.

Figure 5 contains porosity profiles determined from the tracer test and the analysis of core sediment from well 5-1 (Butler and McElwee, 1994). Note the relative magnitude of the estimates determined from the two methods. The average tracer test effective porosity and core total porosity are 0.121 and 0.264, respectively. Mackay *et al.* (1986) report tracer test and core porosity estimates from an unconsolidated alluvial aquifer near Borden, Ontario. The estimates of effective and total porosity for this aquifer are 0.30 and 0.33, respectively. The ratio of effective to total porosity for GEMS and the Borden site is 0.46 and 0.90, respectively. The GEMS data suggests that less than half of the pores in the aquifer are continuous. This observation seemed unlikely, considering that the aquifer is composed of unconsolidated sand and gravel. It was expected that the effective to total porosity ratio would be closer to that observed at the Borden site.

Figure 6 contains hydraulic conductivity (K) profiles determined from the tracer test and the permeameter analysis of repacked core material from well 5-1 (Butler and McElwee, 1994). Again, note the relative magnitude of the estimates determined from the two methods. The average tracer test and permeameter K estimates are 2.04 and 48.2 m/day, respectively. The permeameter K represents disturbed samples because the original formation pore geometry was destroyed. The tracer test K represents groundwater movement in the principle flow direction and in the natural undisturbed environment. Therefore, the tracer test K should be greater than the permeameter K . The

fact that the average tracer test K is over an order of magnitude lower than the average permeameter K suggested that the tracer test data was in error.

All of the first four tracer tests produced similar questionable results. A simple sensitivity analysis of the tracer test model suggested that the primary controls on the parameter estimates were the induced hydraulic gradient, rate of tracer advance, and observations from the induction probe. These controls were studied to determine how they were contributing to the underestimation of the hydraulic parameters.

Tracer Solution Aeration

The tracer solution discharged into the injection well at land surface and cascaded down the well. It was hypothesized that during this descent, air bubbles entrapped in the turbulent column of water moved into the aquifer with the injected water. Once in the aquifer, the bubbles could clog pores, reducing the hydraulic conductivity of the near-well material and therefore increasing the induced hydraulic head in the injection well.

Field experiments were conducted to determine if air was introduced into the aquifer during tracer injection. In order to minimize air entrapment, a drop pipe (0.032 m ID) was placed inside the well (0.051 m ID). Water was pumped to the injection well, where it entered the drop pipe. The pipe housed the injected water during its descent in the well. The water discharged from the drop pipe approximately 2.4 m below the static water level in the well. The drop pipe was completely filled with tracer solution during injection, thereby minimizing contact between the injected water and the atmosphere.

Injection tests were performed with and without the drop pipe in order to assess if there was a difference in the induced head produced by the two approaches. Water was pumped from well 0-8 using a 0.089 m diameter submersible pump (*Simer*, model 9BC). The water entered injection well 1-7 at a constant rate of approximately 51 L/min. (13.6 gal./min.) for both tests. Pressure transducers, positioned 6.7 m below the static water level, were used to monitor the induced head. Figure 7 is a plot of the induced head versus time in injection well 1-7 for the two approaches. This plot displays greater induced head during the test without the drop pipe, suggesting air entered the aquifer and reduced the hydraulic conductivity of the near-well formation.

The possible presence of air in the formation presents serious problems for this tracer test method. Not only does the air clog pores, altering the hydraulic properties that are the subject of the investigation, but also the presence of air reduces the formation conductivity observed during tracer injection (air is less conductive than saline tracer solution). This decrease in formation conductivity alters the relationship between the induction readings and the hydraulic properties. As a result of these experiments, it was

concluded that a drop pipe must be used during tracer injection in order to eliminate aeration of the injection solution and subsequent introduction of air into the aquifer.

Aquifer and Well Head Losses

In addition to tracer aeration, head losses also contributed to the large induced heads observed during the first series of tracer tests. Head changes in an injection or pumping well result from phenomena in both the aquifer and well (Kruseman and de Ridder, 1990). Aquifer head losses result from gradient-induced laminar flow. They are time-dependent and linearly proportional to discharge. Well head losses consist of both linear and non-linear components. Linear well head losses result from well installation disturbances (skin) and friction in the well casing and screen. Non-linear well head losses result from turbulent flow in the well screen, casing, and aquifer near the screen.

Field experiments were performed to assess aquifer and well head losses during injection. Water was pumped from well 0-8 using a 0.089 m diameter submersible pump (*Franklin Electric*, model 2443050117). The water was discharged at 57 L/min. (15 gal./min.) into well 5-1 via the injection drop pipe. The discharge end of the drop pipe was 0.070 m above the static water level. Following the initiation of injection, the discharge end of the drop pipe was continuously below the water level in the well. Pressure transducers, placed at the bottom of the well and above the screen, monitored changes in water levels during injection. Once steady-state flow conditions were achieved, the lower pressure transducer was raised at 0.305 to 0.610 m (1.0 to 2.0 ft.) intervals in an attempt to observe vertical variations in the induced head. Pressure transducer observations from each interval were recorded with a data logger. Figure 8 is a plot of the induced head versus depth. The induced head at the top and bottom of the water column is 0.95 and 0.05 m, respectively. The plot displays rapid head loss in the top 10 m of the water column. The initial head loss, in the interval from 5 to 12 m, is slightly non-linear (concave downward) and is attributed to friction between the turbulent injection fluid and the well casing. The Reynolds number determined for this interval is 22,700 (well above the criteria for turbulent flow), providing support for this interpretation. The most significant head loss occurred in the interval from 12 to 15 m (just below the top of the well screen) and is attributed to linear aquifer and well losses and non-linear well losses in the screen. The induced head in the lower 6 m of the screen is small, but constant.

These observations have important implications for the tracer tests because the induced head measured during the tracer tests is likely to be inflated due to head losses above the screen. The results also imply that most of the injected tracer solution entered

the aquifer through the upper portion of the screened interval (12 to 15 m). Although the induction logs show that the tracer entered the lower portion of the aquifer during tracer injection, the tracer solution did not appear at the bottom of injection well 9-1 until 10 minutes after the initiation of tracer injection. Since the volume injected during the first 10 minutes represents several well volumes, this observation supports the hypothesis that most of the tracer entered the aquifer through the upper portion of the screened interval.

In an attempt to eliminate the observed vertical head variations in the injection well, the above injection test was repeated several times with a perforated drop pipe that extended to the bottom of the well. The drop pipe, perforated only in the screened interval, was constructed to distribute the injection solution throughout the entire interval. Several experiments were conducted with different perforation distributions and sizes to produce a vertical head profile that was sustainable, reproducible, and quantifiable. The final drop pipe design is illustrated in Figure 9. The pipe is perforated in the lower 4.6 m of the 9.1 m screened interval. The perforations increase in size and frequency with depth.

During the final drop pipe experiments, an injection rate of 106 l/min. (28 gal./min.) was used to induce an average head of 0.09 m in injection well 5-1. Figure 10 is a plot of the vertical distribution of induced head after 1.5 hr. of injection. Note that the head above and below the top of the screen is relatively constant. This implies the head losses observed in Figure 8 have been eliminated, and that a uniform distribution of injection solution exits with depth.

Tracer Solution Concentration

It is important that the change in formation electrical conductivity during tracer injection is large relative to the resolution of the borehole induction tool. If a weak saline solution is used, the increase in formation conductivity during tracer injection may be masked by noise in the readings from the induction tool. The accuracy of the induction tool used in this study, as defined by the manufacturer, is $\pm 5\%$ at 30 mS/m. Assuming an average value of 30 mS/m for formation conductivity during tracer injection, this error corresponds to a range of approximately ± 1.50 mS/m.

The total maximum change in formation conductivity during the injection of solutions of electrical conductivity two and three times that of the background pore fluid was 6 and 14 mS/m, respectively. Clearly, the measured changes during the test conducted using a tracer solution with a conductivity twice that of background contains considerable error. To reduce the impact of measurement error, the electrical conductivity of the tracer solution should be at least three times that of the background

pore fluid conductivity. Error in induction measurements can also be reduced if averaged values of formation conductivity from repeat logs are used rather than values obtained from a single log.

Note that increasing the salinity of the tracer solution in order to increase the signal to noise ratio may induce chemical reactions within the aquifer. Significant changes in the cation ratios may initiate cation exchange on clay particles. Dissolution or precipitation of minerals such as calcite and aragonite may occur due to the common ion effect (if a Ca salt is used) or to an increase in ionic strength. Some of these reactions are kinetically fast and may alter the hydraulic properties of the aquifer during injection.

Permeameter analyses of cores from GEMS were conducted in the Kansas Geological Survey Core Properties Laboratory to determine the extent of hydraulic property alteration due to tracer-induced chemical reactions (laboratory protocol for the permeameter analysis is described in McElwee and Butler 1993). Hydraulic conductivity was measured for seven cores saturated with GEMS native pore water. The measurements were repeated with a saline solution similar to that used during the tracer tests. The two sets of measurements showed no change in hydraulic conductivity that could be attributed to chemical reactions between the tracer solution and the aquifer material. As a result, it was concluded that no changes in hydraulic properties occurred during the tracer tests due to the introduction of the tracer solution into the aquifer.

Repeated Tracer Test

Introduction

Based on the results of the above-described investigations, a second tracer test was conducted in GEMS well 5-1 using the revised procedure. Refinements were also made to the Taylor and Molz (1990) method of data analysis in order to improve the reliability of the parameter estimates. The results obtained from this tracer test are reasonable considering the nature of the aquifer material and are consistent with laboratory permeameter results from the same well.

Tracer Test Methodology

With the exception of the use of the perforated drop pipe, the repeated test followed the procedure described earlier. The tracer solvent was pumped from well 0-8 using a 0.089 m diameter submersible pump (*Franklin Electric*, model 2443050117). The tracer injection rate (including water from the pumping well and the concentrated saline solution) was 112 L/min. (29.5 gal./min.). The head in the injection well was monitored with pressure transducers positioned at the bottom of the well and above the

top of the well screen. The induced head was determined from static and steady-state water levels observed each time the injection pumps were turned on and off. The average induced head at the bottom and top of the screened interval was 0.104 and 0.087 m, respectively. The slope from this vertical gradient was used to estimate the induced head for each 0.03 m section of the screened interval.

Prior to each induction logging period, tracer injection was terminated, and the drop pipe and pressure transducers were removed from the injection well. This procedure was necessary because there was not room in the injection well for all of the equipment at the same time. Termination of injection is assumed to have little influence on the movement of the tracer due to the low relative regional gradient, the short time required to log the well (approximately 15 min.), and the very short time necessary to achieve steady-state flow conditions following the initiation of injection (determined from pressure transducer data to be approximately 1.5 min.). The well was logged four times before and at the end of tracer injection and twice during six intervals during injection. Between logs, the induction probe was lowered in a nearby well in order to keep the probe in thermal equilibrium with the aquifer temperature. The specific conductivity of the background groundwater and injection solution was 60.8 and 193 mS/m, respectively. Tracer injection lasted for 5.70 hr. During this time, 38,240 L (10,100 gal.) of tracer solution, amounting to approximately 37 kg of NaCl, discharged into the well. Remedial pumping removed approximately 60 % of the NaCl.

Data Analysis

Tracer Injection:

Figure 11 displays average formation electrical conductivity logs obtained before, during, and after tracer injection (Huettl, 1994). As the tracer invaded the aquifer, the measured formation conductivity increased. Note that much of the variation existing prior to injection (log at 0.00 hr.) remains after the tracer solution approached the radial detection limit of the induction tool (log at 5.70 hr.). This implies that even when the aquifer is saturated with the saline tracer, the contribution of the matrix conductivity to the total formation conductivity dominates over the combined contribution from porosity and pore fluid.

The Taylor and Molz (1990) method of parameter estimation summarized earlier assumes that tracer injection continues until the invading solution moves beyond the radial detection limit of the induction tool. After that time, the formation conductivity will not change with continued injection. Figure 12 displays the change in formation conductivity during tracer injection at four arbitrarily chosen intervals in well 5-1. In all

four intervals, the formation conductivity appears to be asymptotically approaching an upper limit. This suggests that the tracer solution is close to the induction probe's radial detection limit at 5.70 hr. and the assumption of tracer saturation is reasonable.

Porosity Estimation:

As stated earlier, the Taylor and Molz (1990) method of porosity estimation adopts a model of the relationship that exists between formation conductivity, pore water conductivity, and porosity. Equation (IV.H.6) provides a means of estimating effective porosity using this model. Figure 13 contains calculated and measured porosity profiles for well 5-1. The solid curve is data determined by the tracer test assuming tracer solution saturation at 5.70 hr and empirical factors $m = 1.4$ and $\alpha = 1.0$. The dotted curves are confidence intervals determined by assuming 10 % error in the empirical factors. The dashed curve is data determined from grain-size analysis of sediment from cores from the same well (Butler and McElwee 1994). The average effective and total porosity estimates are 0.19 and 0.26, respectively. Note that the tracer test effective porosity is a minimum estimate because the tracer solution may not have entirely reached the radial detection limit of the induction probe. Figure 12 shows that the formation conductivity may have increased approximately 1 mS/m if injection had continued. This change would result in an increase of 0.010 in effective porosity.

Although the tracer test values are considerably lower than the permeameter values, the tracer test values are reasonable because they represent only the interconnected pores that were filled with tracer solution during injection.

Radius of Tracer Invasion:

The radial sensitivity of the induction probe (Figure 2) is determined theoretically from knowledge of magnetostatics and the induction probe coil geometry (Saito, 1982). The cumulative sum of these radial contributions (Figure 3) and Equation (IV.H.7) were used to estimate the radial position of the tracer solution front for each induction log displayed on Figure 11.

Figure 14 displays the estimated radius of tracer invasion at several times during injection using the theoretical cumulative radial response function. Empirical estimates of the average radius of tracer invasion for the entire screened interval were also made for each time that an induction log was taken during tracer injection. These estimates were made by determining the volume of aquifer invaded by the injected tracer solution assuming an average effective porosity of 0.193 and a constant tracer injection rate of 112 l/min. Figure 15 displays these estimates along with the average theoretical radius of

tracer invasion determined for each curve in Figure 14. These plots show that the radius of tracer invasion determined using the theoretical model is underestimated during early injection times and overestimated during later times. This observation suggests that the theoretical response function may be inappropriate in this field environment.

Assuming that the tracer reached the detection limit of the induction probe prior to the termination of injection during the repeated tracer test, an empirical cumulative radial response function can be generated. The average cumulative radial response, $Z(R)$ [Equation (IV.H.7)], was determined for each induction log obtained during tracer injection. This value represents the percent of the total injection-induced change in formation conductivity that occurred by the time that induction log was obtained. When these values are plotted against the empirically determined average radius of tracer invasion for that time, the resulting plot is an empirically derived cumulative radial response function. Figure 16 displays computed empirical cumulative radial response functions. The solid curve represents a function determined assuming the empirical estimates of tracer invasion shown in Figure 15. The dotted curves represent "confidence interval" functions. They were determined from empirical estimates of tracer invasion derived from the porosity confidence intervals in Figure 13. The theoretical function is provided for comparison.

Figure 17 displays the radius of tracer invasion determined with the empirical response function. These values directly correlate with the empirical estimates in Figure 15. Figure 17 shows that the tracer invaded the aquifer uniformly in the interval from 13 to 16 m. Differential flow is observed in the lower portion of the screened interval, represented by a zone of relative rapid invasion centered at 18 m.

Hydraulic Conductivity Estimation:

Equation (IV.H.14), which is used to estimate hydraulic conductivity (K), defines a linear relationship between R^2 and t (where R = radius of tracer invasion determined at 0.03 m intervals for each induction log from time t since initiation of tracer injection). Figure 18 is a plot of R^2 versus t determined at a depth of 17.98 m in well 5-1 using the theoretical and empirical response functions. The non-linearity observed in the theoretically determined values further demonstrates the previously discussed inappropriateness of the theoretical function.

According to equation (IV.H.14), all plots of R^2 versus t should be straight lines passing through the origin. A linear regression of R^2 (determined using the empirical response function) and t was performed to determine the slope and y-intercept for each 0.03 m interval of well 5-1. Figure 19 displays the y-intercept values. The intervals from

the upper 5/8 of the screened section have consistently negative intercepts, while the lower 3/8 have consistently positive intercepts.

The empirical radial response function (Figure 16) used to determine the radius of tracer invasion is a cumulative sum of the contributions of formation conductivity from all zones within the radial detection limit of the induction tool. Therefore, the contribution to formation conductivity from a drilling-induced disturbed zone (skin) adjacent to the borehole will influence every estimate of tracer radial invasion. As a result, all estimates of tracer invasion will be shifted by a constant factor that is a function of the hydraulic properties and size of the disturbed zone. This shift is represented by the non-zero y-intercepts shown in Figure 19. This constant factor is amplified by squaring R for the determination of K [Equation (IV.H.14)]. The non-zero y-intercept produces a changing slope and thus a time dependence in the K values determined from each R at a specific interval. Figure 20 displays the time dependence in K values produced by these effects using the data in Figure 18.

The positive and negative intercepts represent high and low permeability skins, respectively. These disturbances result from sediment churning, compaction, collapse, and smearing during drilling and development operations. The change from a low to a high permeability skin observed in Figure 19 is likely due to smearing of silt and clay from the upper alluvial unit on the inside of the borehole as the drilling flights penetrated the underlying sand and gravel.

These observations suggest that, contrary to the Taylor and Molz (1990) procedure, the application of Equation (IV.H.14) with individual values of R^2 and t for K estimation is not appropriate for wells with a drilling-induced disturbed zone. Individual values for R^2 and t in Equation (IV.H.14) must be replaced with the slope of R^2 versus t , which will eliminate the influence of a near-well disturbed zone on the estimated K values. Although this slope method produces only one value of K for each depth interval, it is clearly more accurate than averaging several values determined by the Taylor and Molz (1990) method.

Figure 21 displays hydraulic conductivity profiles for well 5-1. The solid and dotted curves are smoothed data (nine point running average) estimated with the R^2 and t slope method. The solid curve data was computed using values of R estimated with an empirical response function derived assuming the tracer-test-determined effective porosity (0.193). The dotted curve was computed using R values estimated with an empirical response function derived assuming the average laboratory-determined total core porosity (0.264). The dashed curve is data determined from permeameter tests performed on repacked core material from the same well (Butler and McElwee, 1994).

The average tracer test and permeameter K estimates are 137 and 48.2 m/day, respectively. As expected, the tracer test values are greater than those determined from repacked sediment samples. This is due to the orientation of the sediment particles and structures relative to the lateral radial flow of the tracer. The tracer test and permeameter data show good correlation of relative spatial trends in K. Both data sets display a relatively low permeability zone centered at approximately 16.0 - 16.5 m.

The average tracer test K estimates determined with different empirical response functions are very similar. The K values, assuming tracer-test-determined effective porosity and laboratory-determined core total porosity, are 137 and 134 m/day, respectively. K values were also determined (but not displayed) using values of R computed from the "confidence interval" response functions in Figure 16. The average porosity values used to construct these response functions are 0.148 and 0.238. The corresponding K estimates are 154 and 136 m/day, respectively. These average K estimates represent a wide range of porosity values (coefficient of variation = 24.2 %), but display little variation (coefficient of variation = 6.6 %). This observation suggests that the tracer test model for K estimation is not sensitive to variations in porosity.

It is important to note that the tracer test parameter estimates are not discrete observations. Figure 3 displays the manner in which conductivity contributions from zones at different radial distances are averaged by the induction tool. This averaging masks some natural variation. Permeameter tests performed on cores and repacked sediment samples produce parameter estimates for a much smaller volume. These parameter estimates show considerably more variation, but are biased because they either represent flow normal to bedding planes or flow through disturbed samples. In short, the tracer test parameters are averages from a larger aquifer volume than the permeameter parameters, but are more accurate because they represent *in situ* observations made under flow conditions similar to those that exist in nature.

A final check on the absolute magnitude of the tracer test K estimates can be conducted by comparing them to an average K determined for the whole screened interval by the Thiem Equation (Kruseman and de Ridder, 1990):

$$K = \frac{Q}{2\pi bH} \ln\left(\frac{r_e}{r_w}\right) \quad (\text{IV.H.15})$$

If Q (discharge) = 161 m³/day, b (aquifer thickness) = 9.14 m, H (induced head) = 0.096 m, r_e (effective radius) = 2.62 m (assumed to equal the average maximum extent of tracer invasion), and r_w (radius of well) = 0.025 m, then K = 136 m/day. This value compares

very well to the value of 137 m/day determined by averaging the K values determined for each vertical interval. The similarity in these estimates suggests that the magnitude of the tracer test K estimates is accurate.

Geologic Interpretation

The results of the final tracer test and data from cores retrieved during the installation of the injection well provide insight into the near-surface geology at GEMS. The formation induction and natural gamma logs obtained during a pre-tracer test survey reveal a fining-upward sequence composed of two distinct units of roughly equal thickness (approximately 11 m) for well 5-1.

X-rays of core display cross-bedded sand and gravel and clay drapes in the lower unit, indicating fluvial deposition (Blatt *et al.*, 1980). Sieve analyses of unconsolidated core sediment from this unit (McElwee and Butler, 1993) display a fining-upward trend, typical of fluvial channel deposits (Allen, 1965). The fining-upward trend, however, is not observed as a decreasing-upward trend in tracer test K. This may be the result of variations in particle sorting and packing during deposition. The mean K for the tracer test data is 137 m/day, typical of silty to clean sands (Freeze and Cherry, 1979). The mean tracer test effective porosity is 0.19. This value is low for unconsolidated sands (typically 0.25 - 0.50, Freeze and Cherry, 1979) and may be attributed to exceptionally poor particle sorting and tight particle packing. There appears to be no consistent correlation between effective porosity, K, and grain size.

Cores from the upper unit are composed of silt and clay. This interval appears homogenized by bioturbation, and contains rootlets and organic matter. These observations indicate subaerial exposure.

The basal sand and gravel alluvial unit is interpreted as laterally accreted river channel deposits. The overlying silt and clay alluvial unit is interpreted as vertically accreted floodplain deposits. It is likely that the two units represent a single lateral migration of the Kansas River.

Conclusion

The borehole induction single-well tracer test appears to be theoretically sound. It has considerable potential for accurate and detailed characterization of vertical variations in effective porosity and the radial component of hydraulic conductivity. Modifications of the originally proposed procedure have been made in order to ensure that the model assumptions are valid, to reduce monitoring error, and to remove the effects of a near-well, drilling-induced disturbed zone. These modifications include the use of a perforated

drop pipe to eliminate the introduction of air into the aquifer during tracer injection and to create a quantifiable head distribution in the injection well. Averaged induction logs were used for parameter estimation in order to increase accuracy by decreasing the impact of noise in the induction probe readings. The theoretically determined cumulative radial response function was replaced with an empirically derived function that preserved mathematical relationships defined by the theoretical analysis model. Finally, refinements have been made in the method of data analysis such that the technique can be used for wells with both high and low permeability skins.

The method has advantages over traditional aquifer characterization methods. It is superior to other *in situ* single-well methods, such as slug and pumping tests, in that it is relatively insensitive to drilling-induced disturbances and may have higher vertical resolution. The tracer test parameter estimates are superior to permeameter estimates because the parameters are determined for the principle flow direction and in the natural undisturbed environment. The only major drawback of the tracer test method is the high cost of the borehole induction probe.

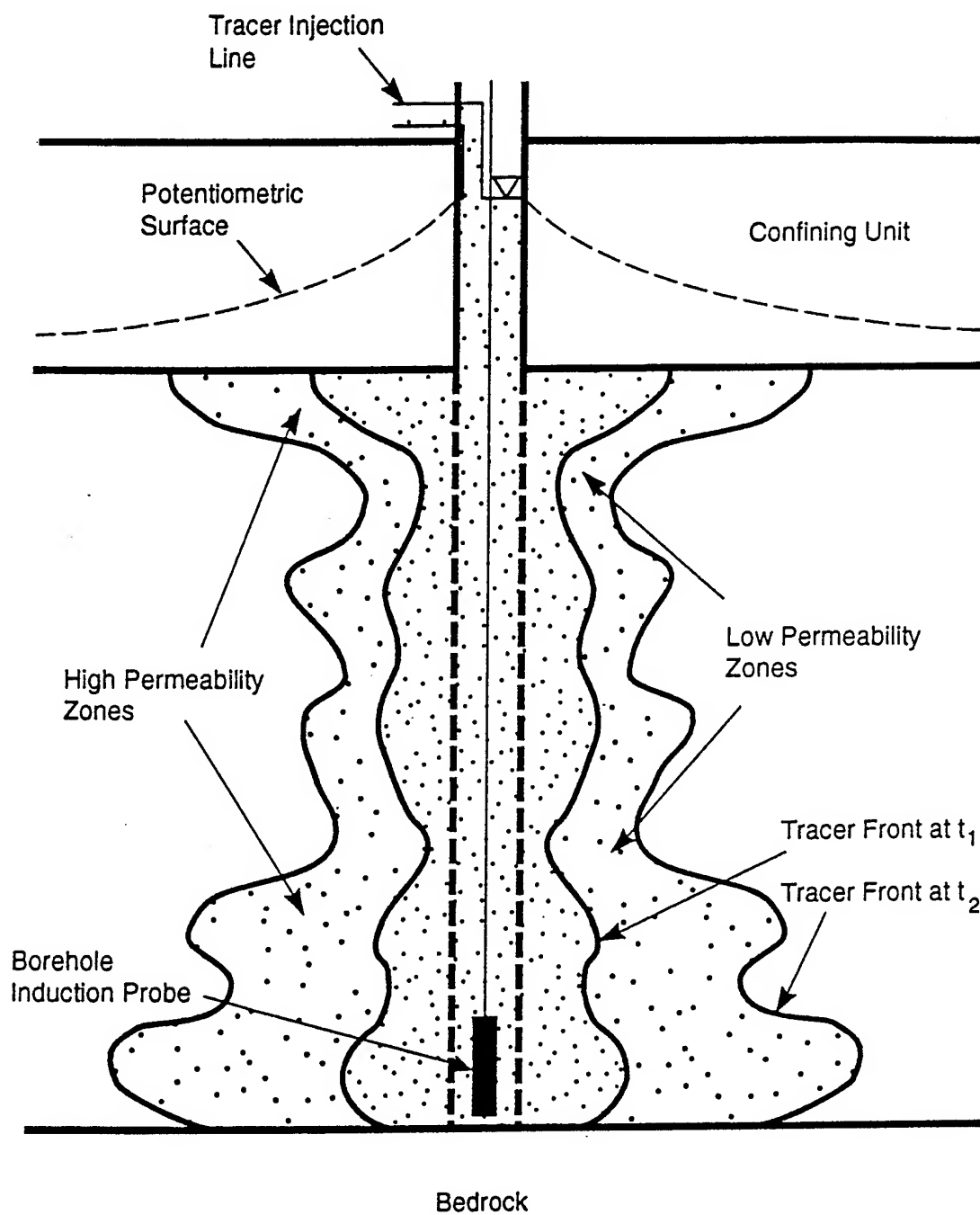


Figure 1. Illustration of single-well tracer test (modified from Huettl *et al.*, 1993).

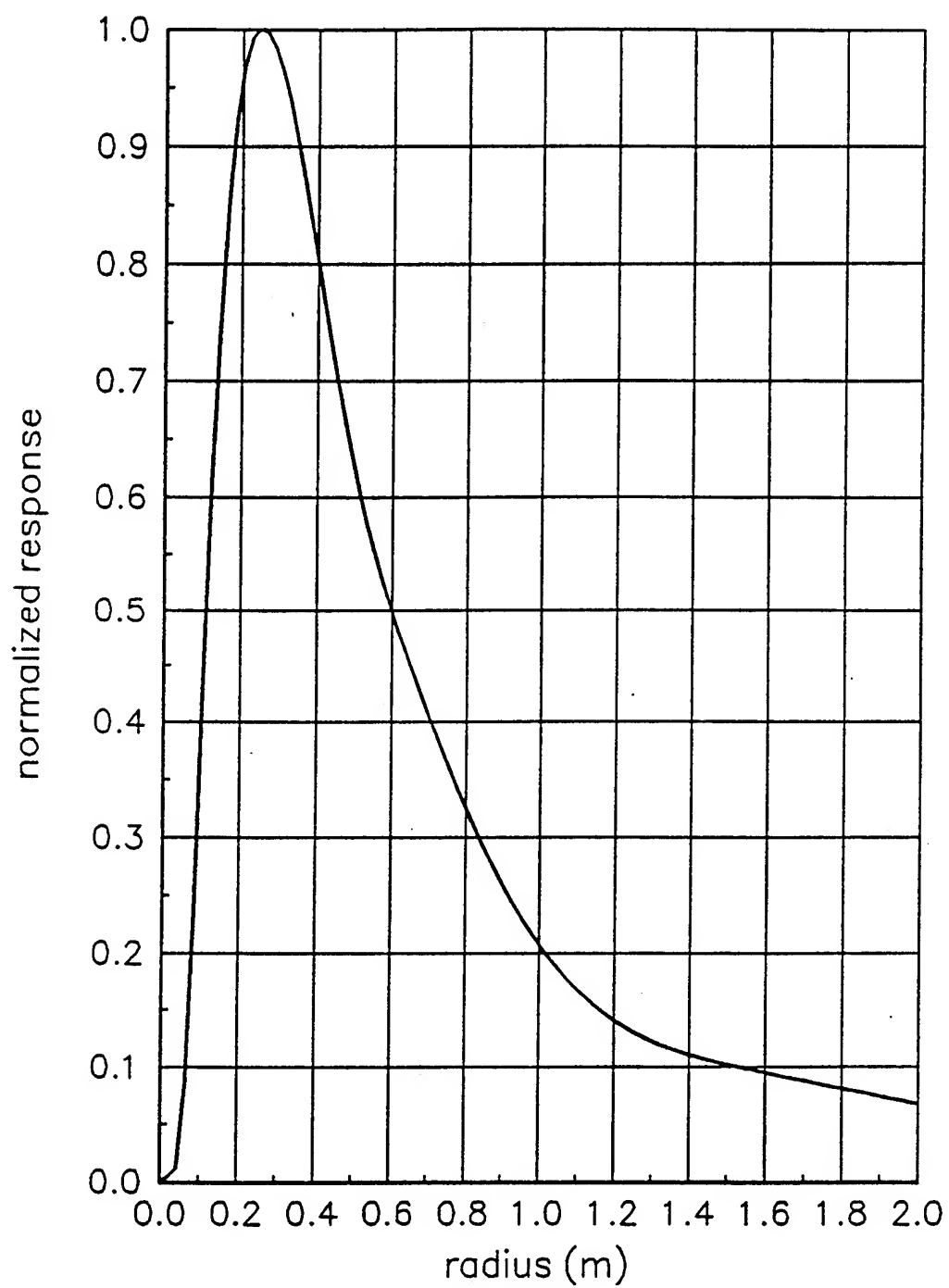


Figure 2. Induction probe theoretical radial response function (modified from *Century Geophysical Corporation*, unpublished).

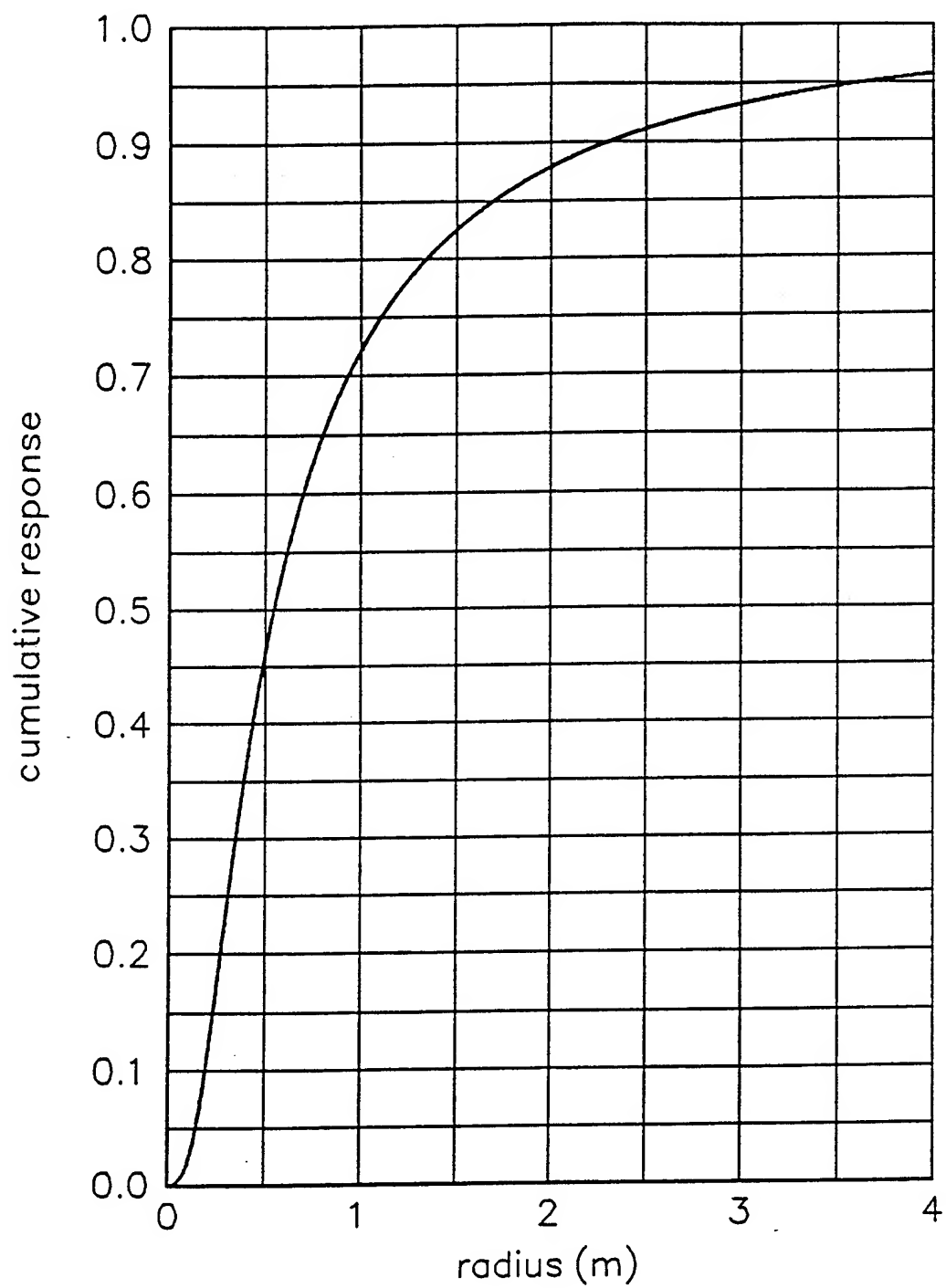


Figure 3. Induction probe theoretical cumulative radial response function (modified from *Century Geophysical Corporation*, unpublished).

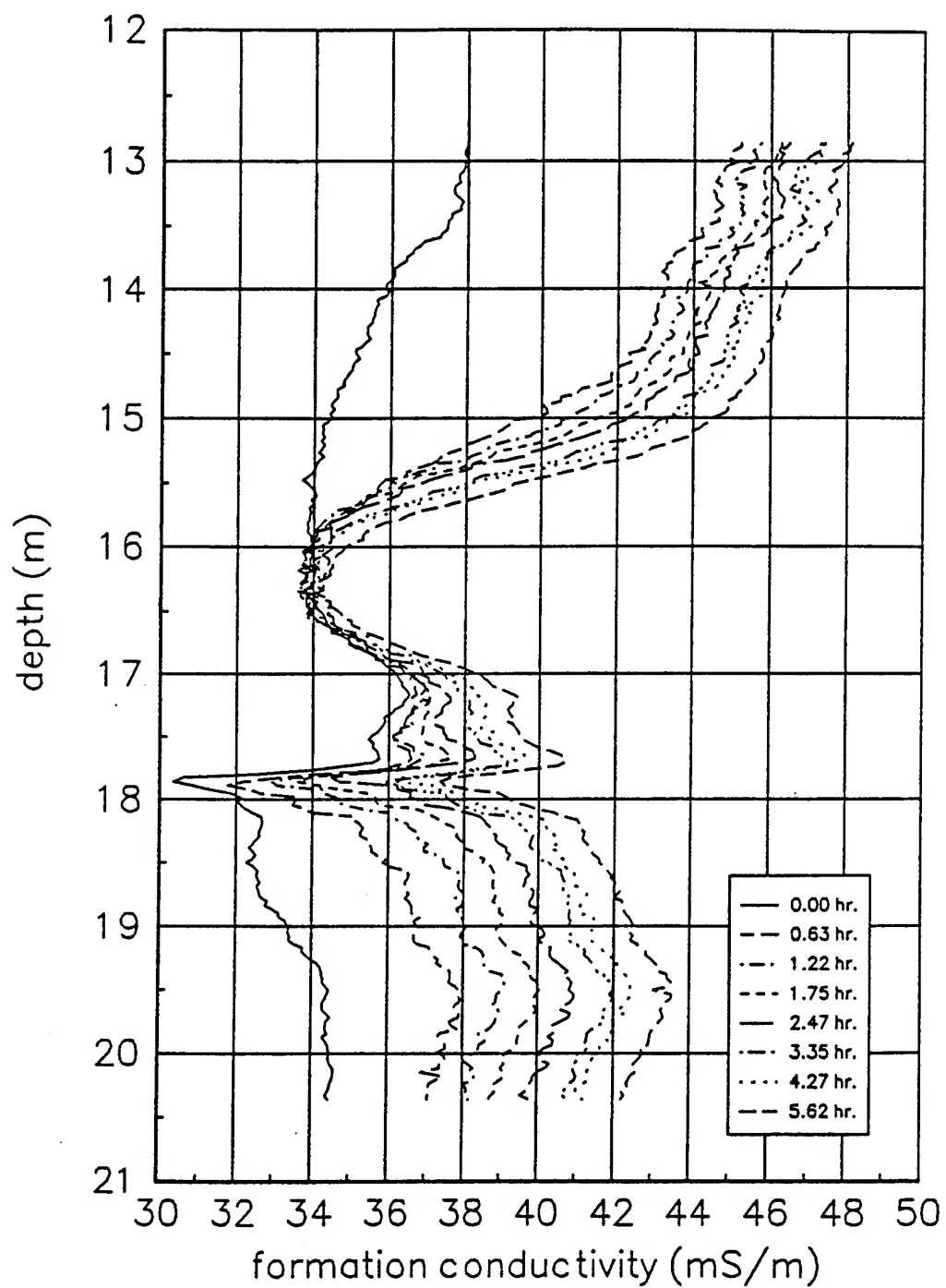


Figure 4. Formation conductivity before, during, and after tracer injection in well 5-1.

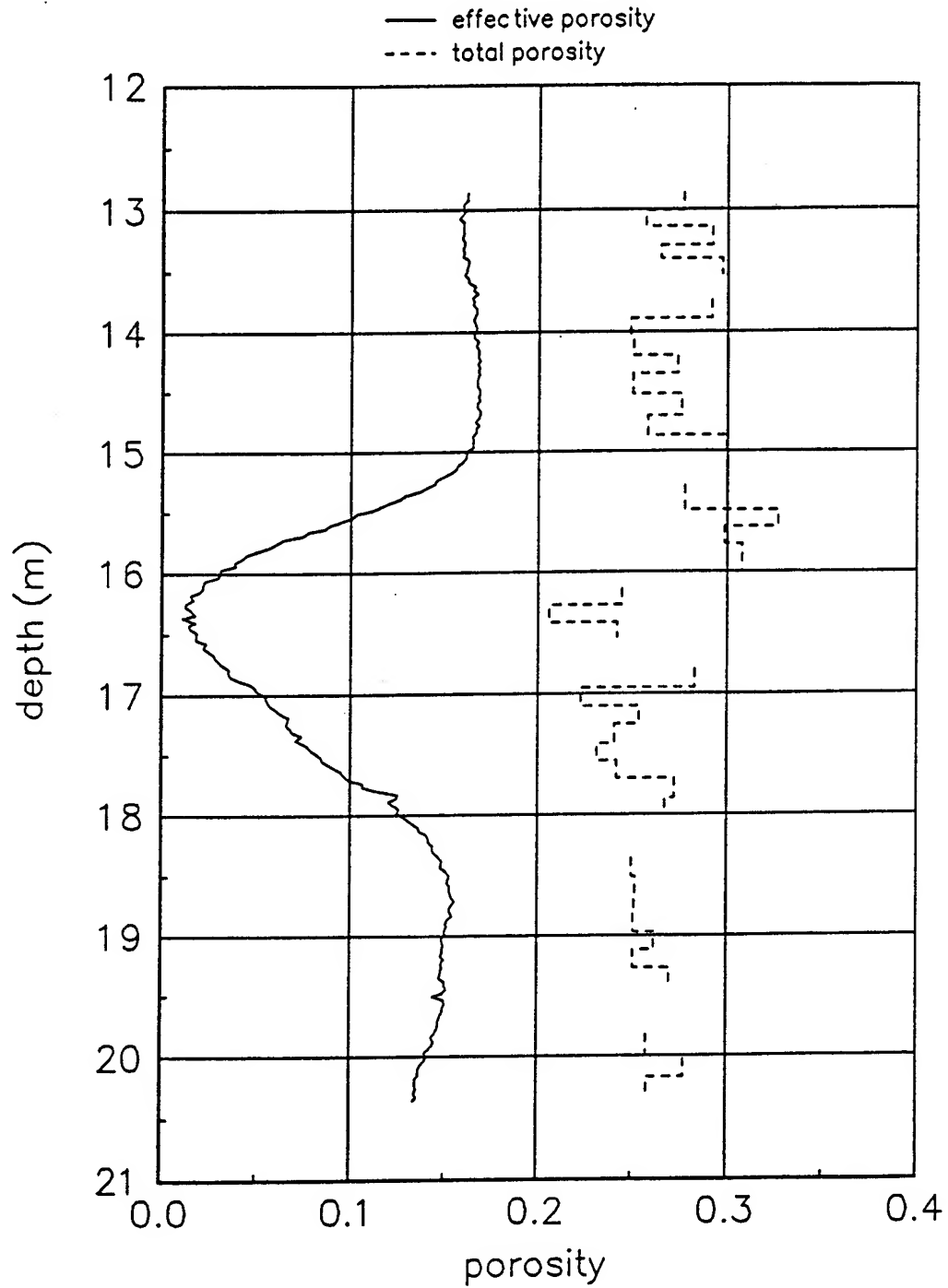


Figure 5. Porosity profiles from well 5-1. Total porosity from Butler and McElwee (1994).

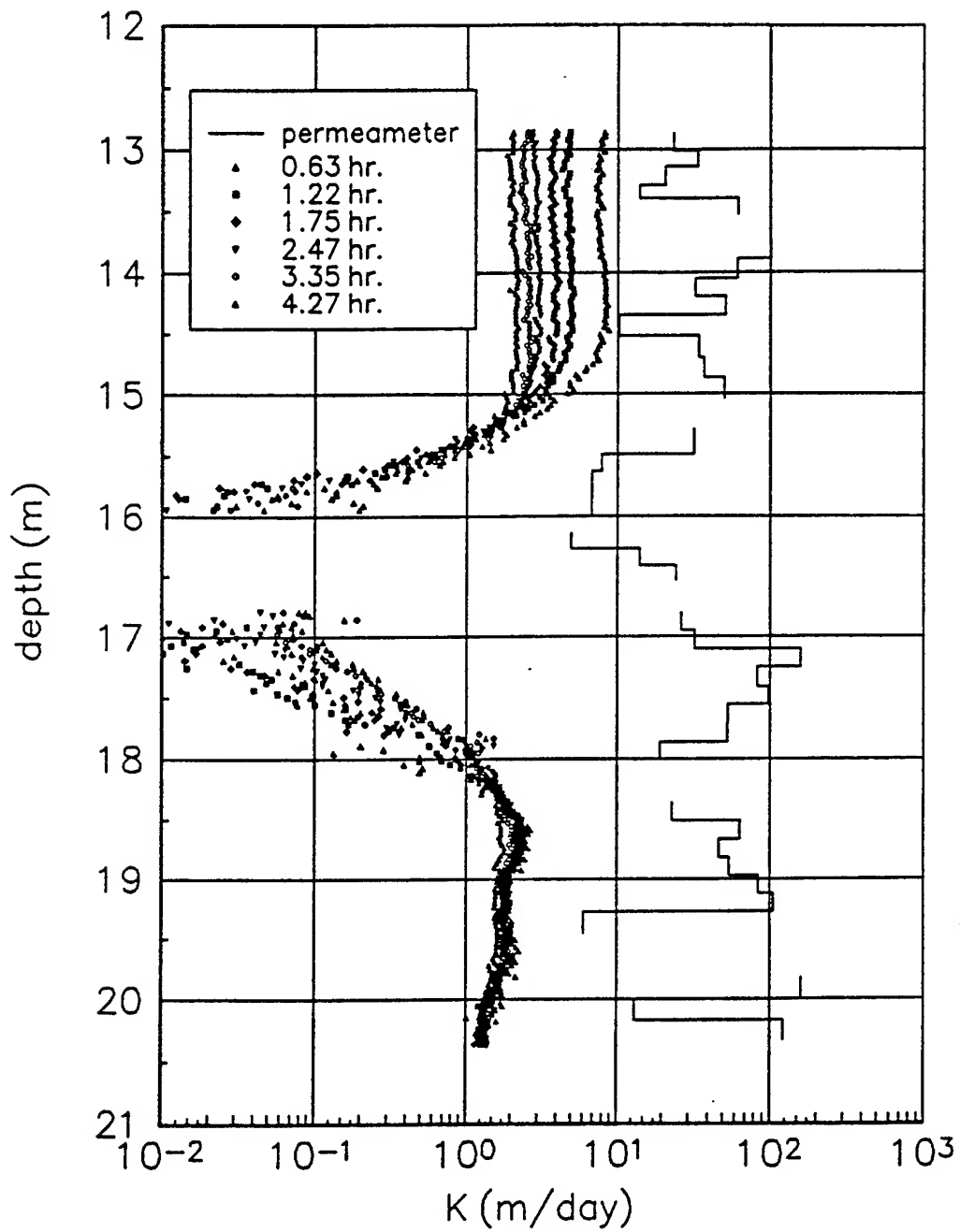


Figure 6. Hydraulic conductivity profiles from well 5-1. Permeameter data from Butler and McElwee (1994).

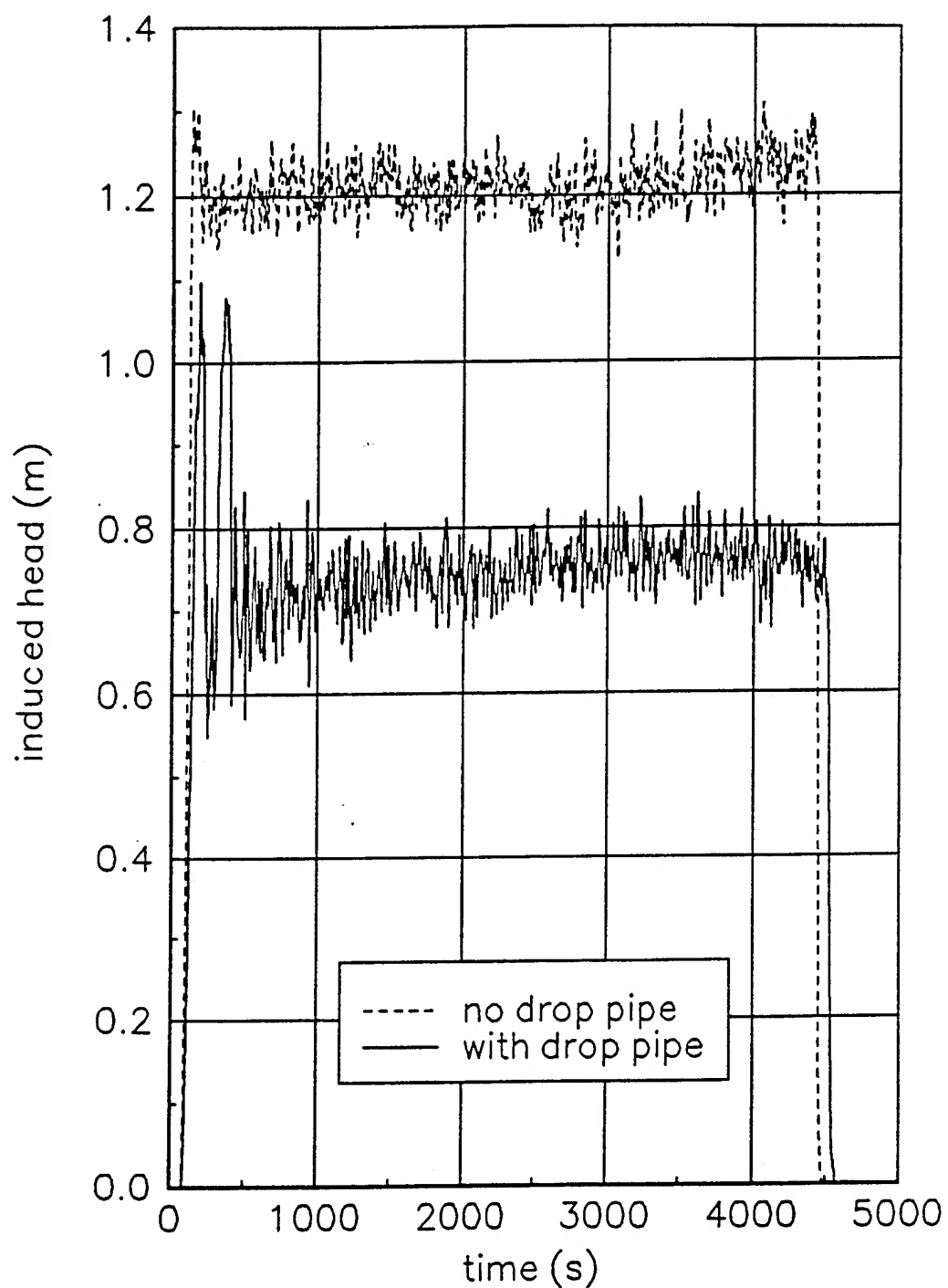


Figure 7. Induced head versus time in well 1-7 with and without injection drop pipe ($Q = 51 \text{ L/min}$).

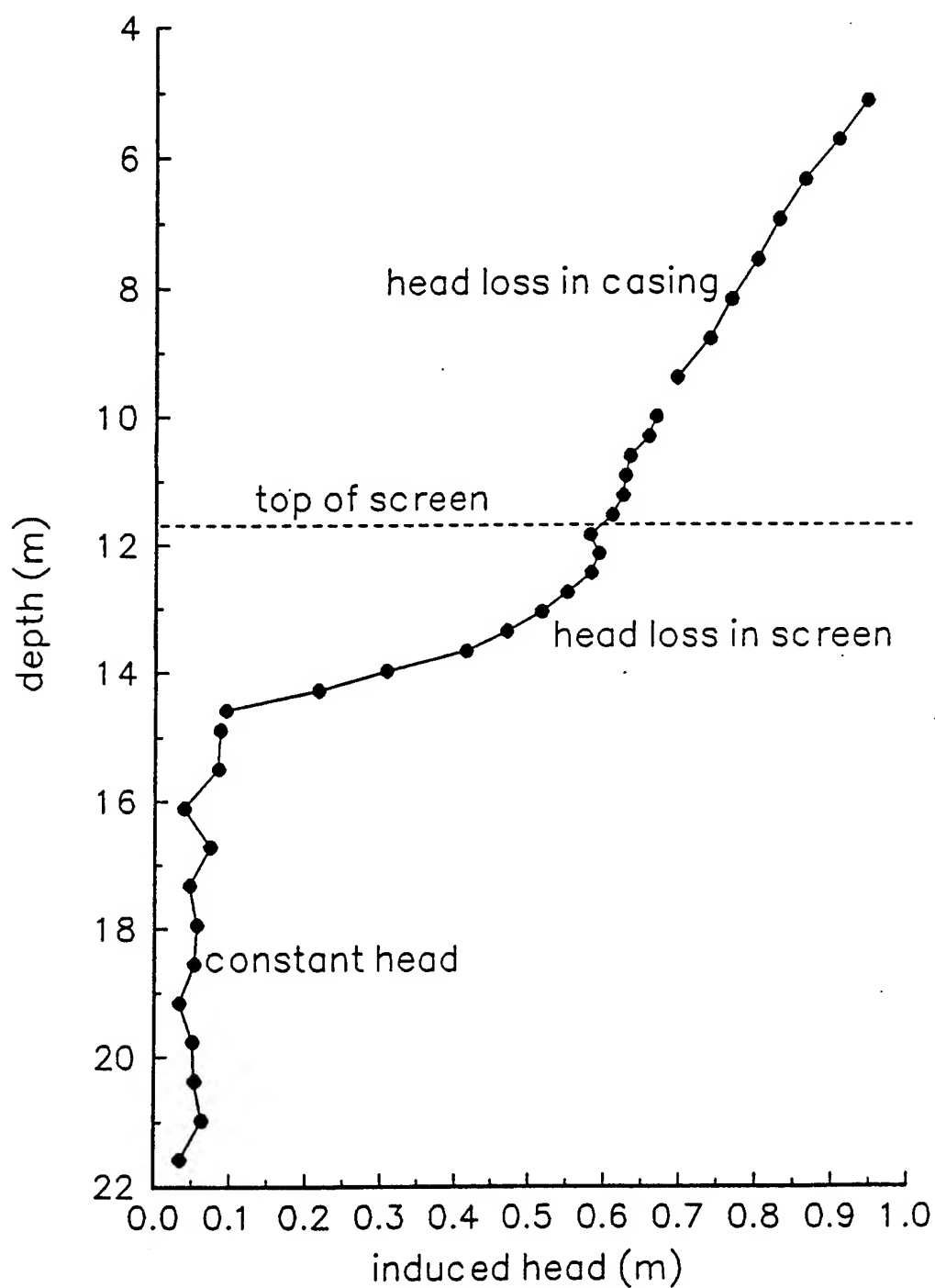


Figure 8. Head loss during injection in well 5-1 ($Q = 57 \text{ L/min.}$).

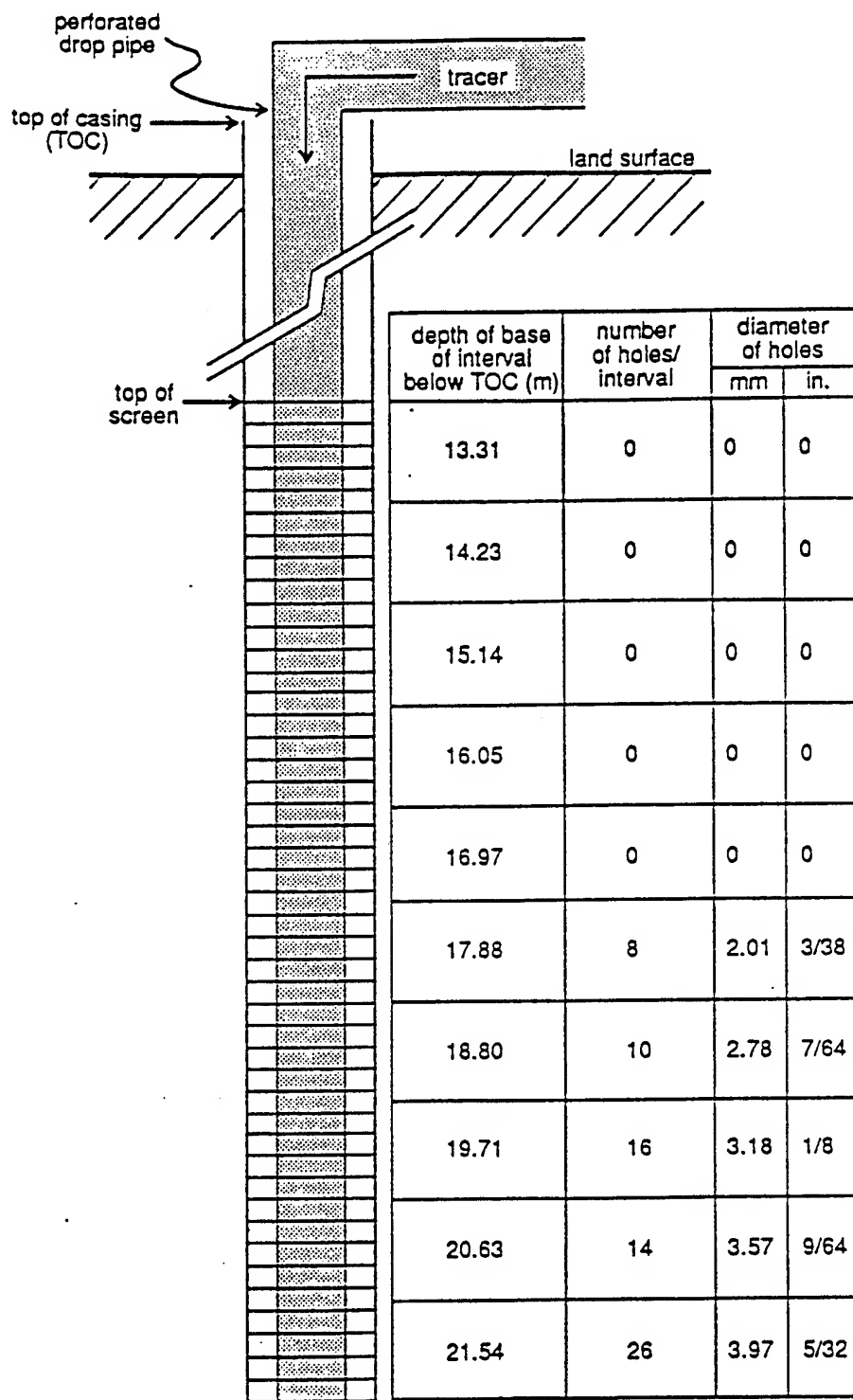


Figure 9. Illustration of the final drop pipe design, including the size and distribution of the perforations.

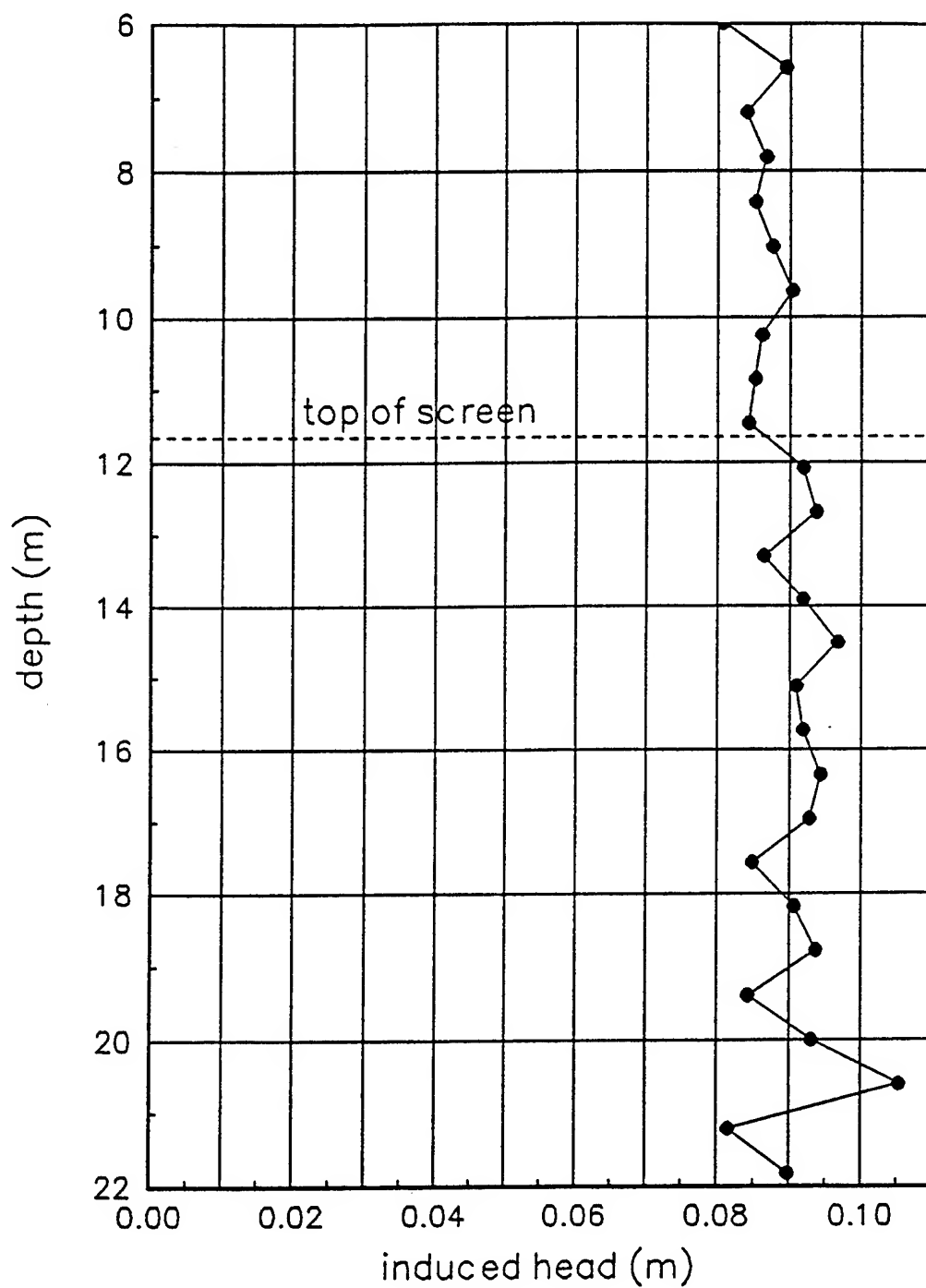


Figure 10. Vertical distribution of induced head in well 5-1 with final injection drop pipe design ($Q = 106 \text{ L/min.}$).

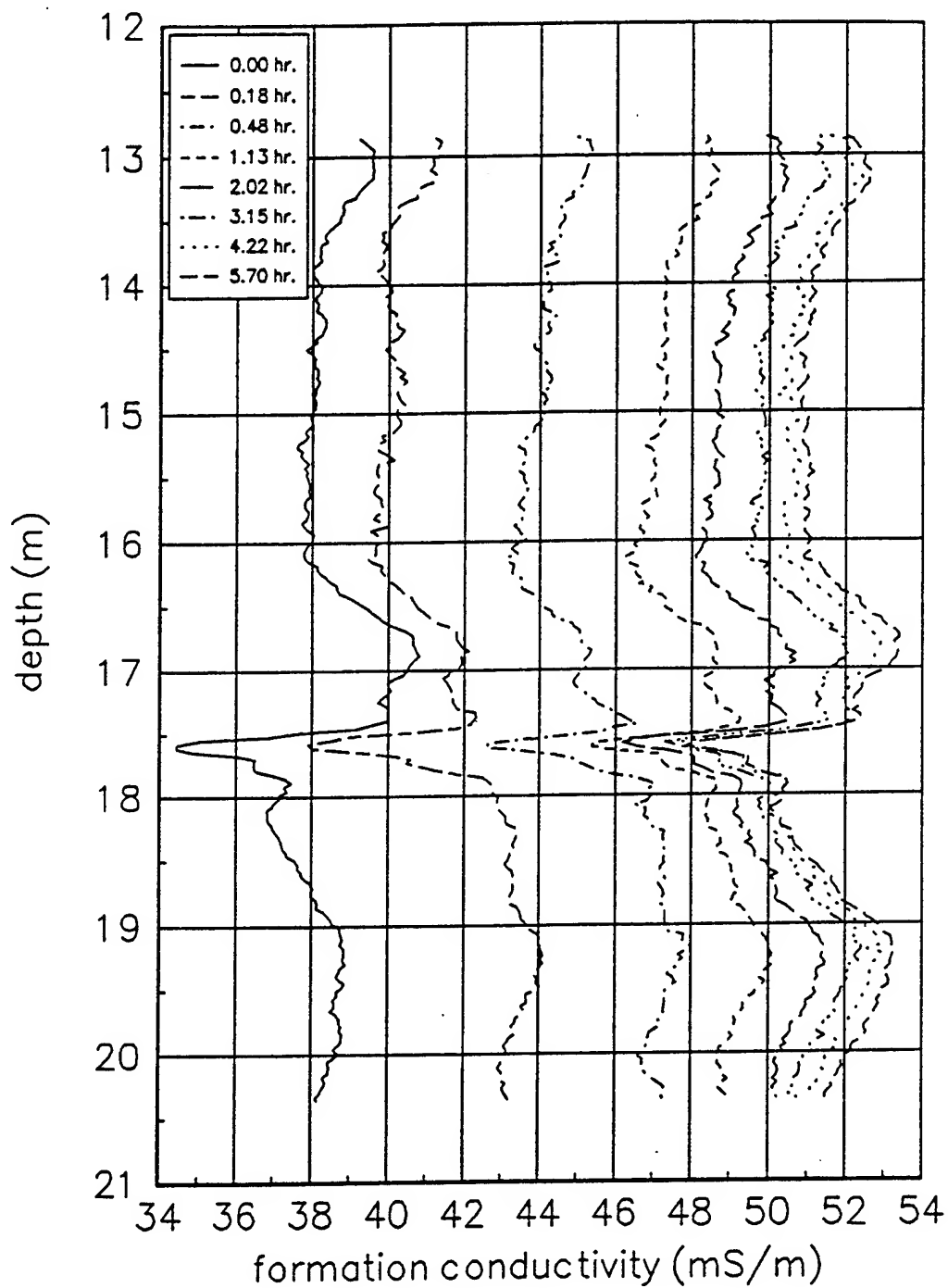


Figure 11. Average formation conductivity before, during, and after the second tracer test in well 5-1.

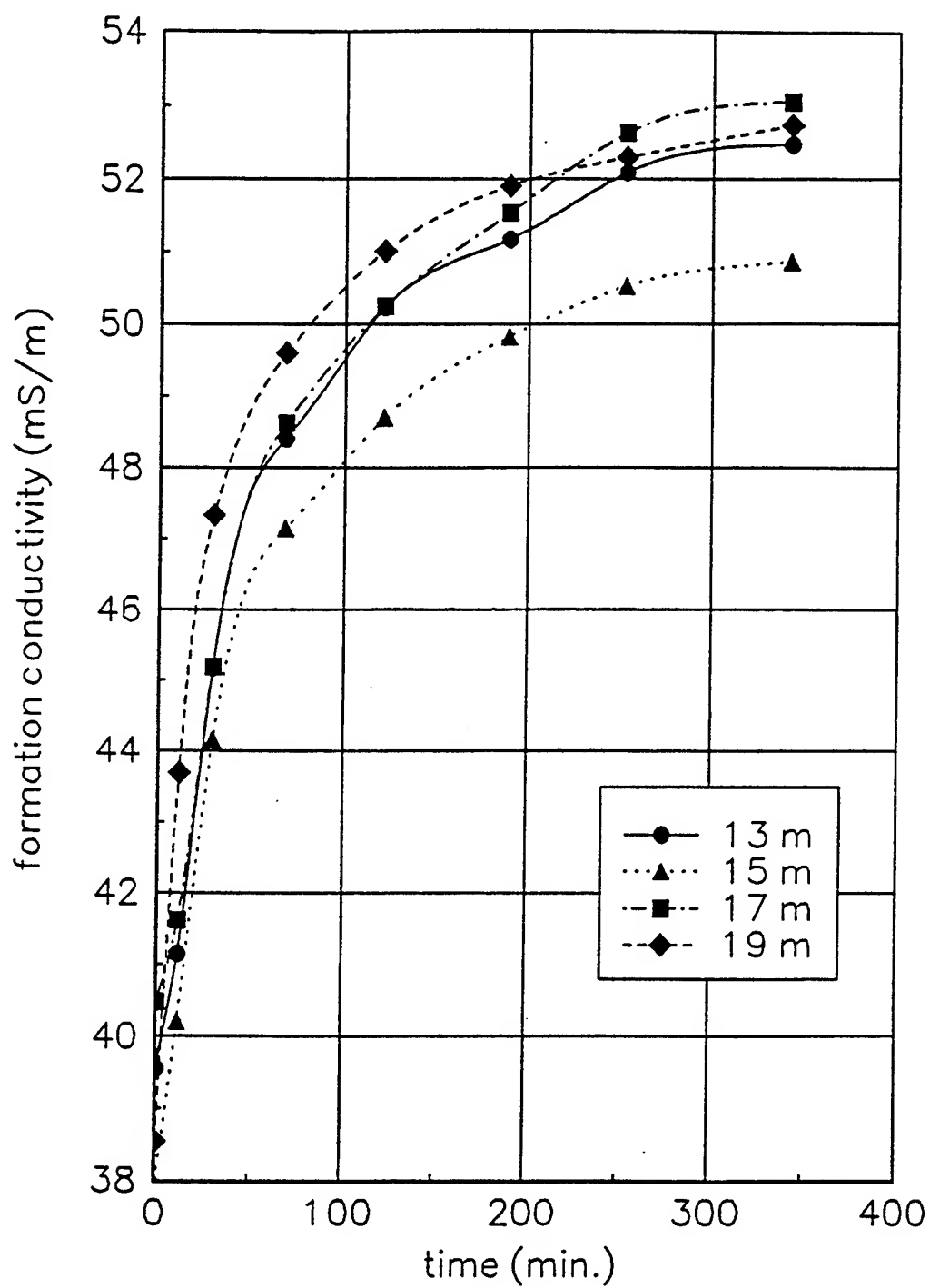


Figure 12. Formation conductivity during tracer injection in well 5-1 at arbitrarily chosen intervals.

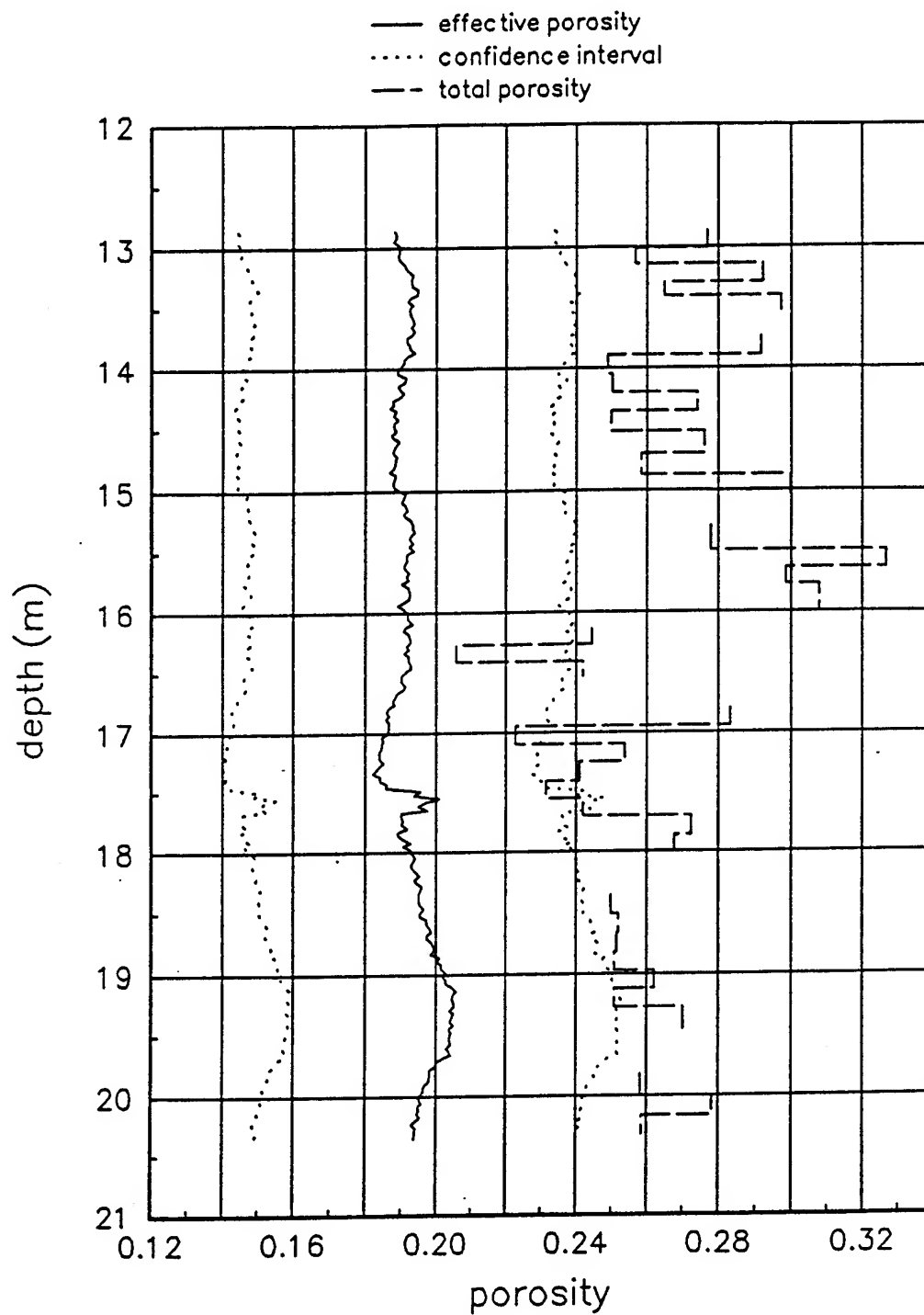


Figure 13. Porosity profiles for well 5-1. Total porosity from Butler and McElwee (1994).

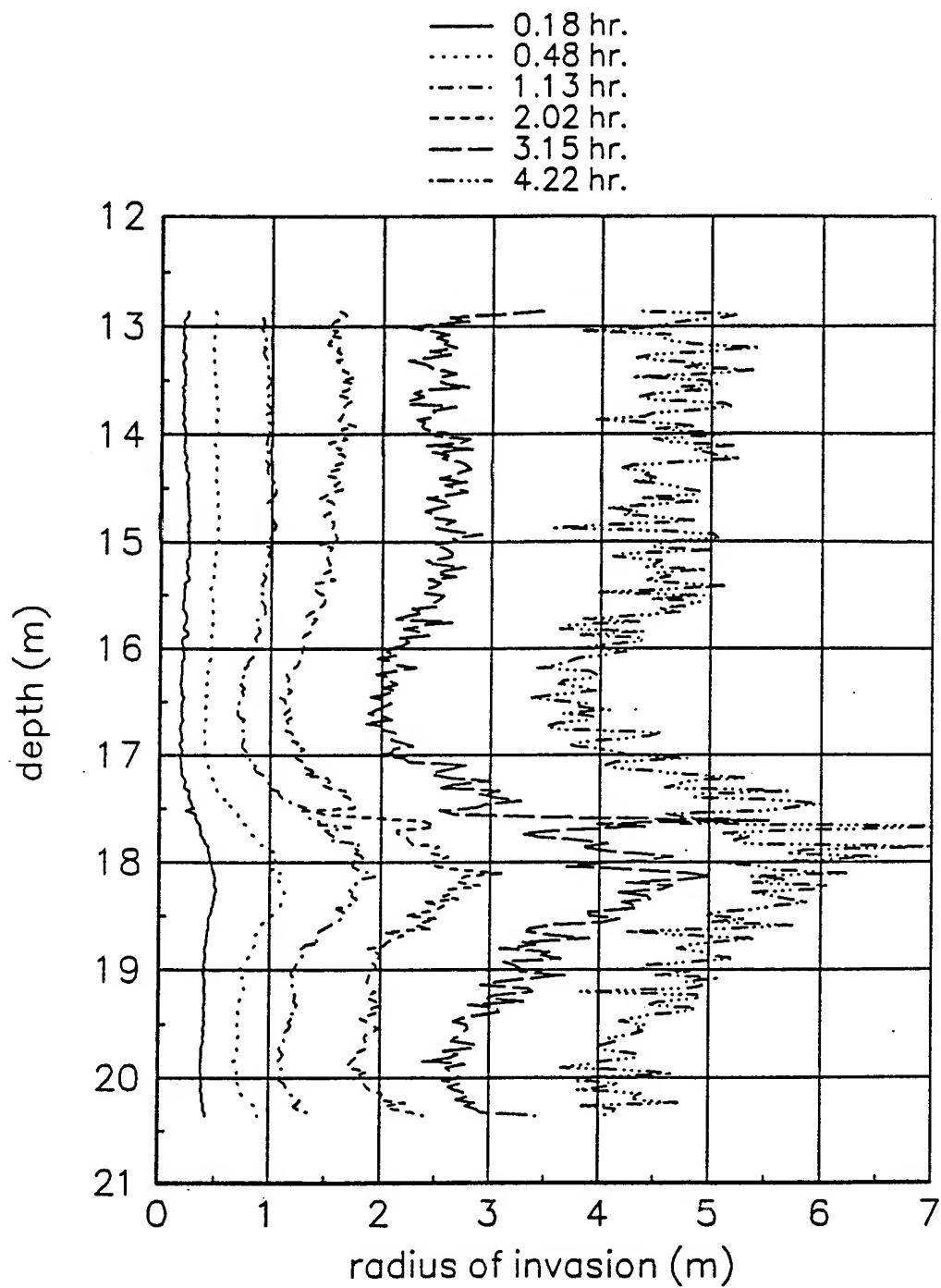


Figure 14. Radius of tracer invasion in well 5-1 determined with the theoretical cumulative radial response function.

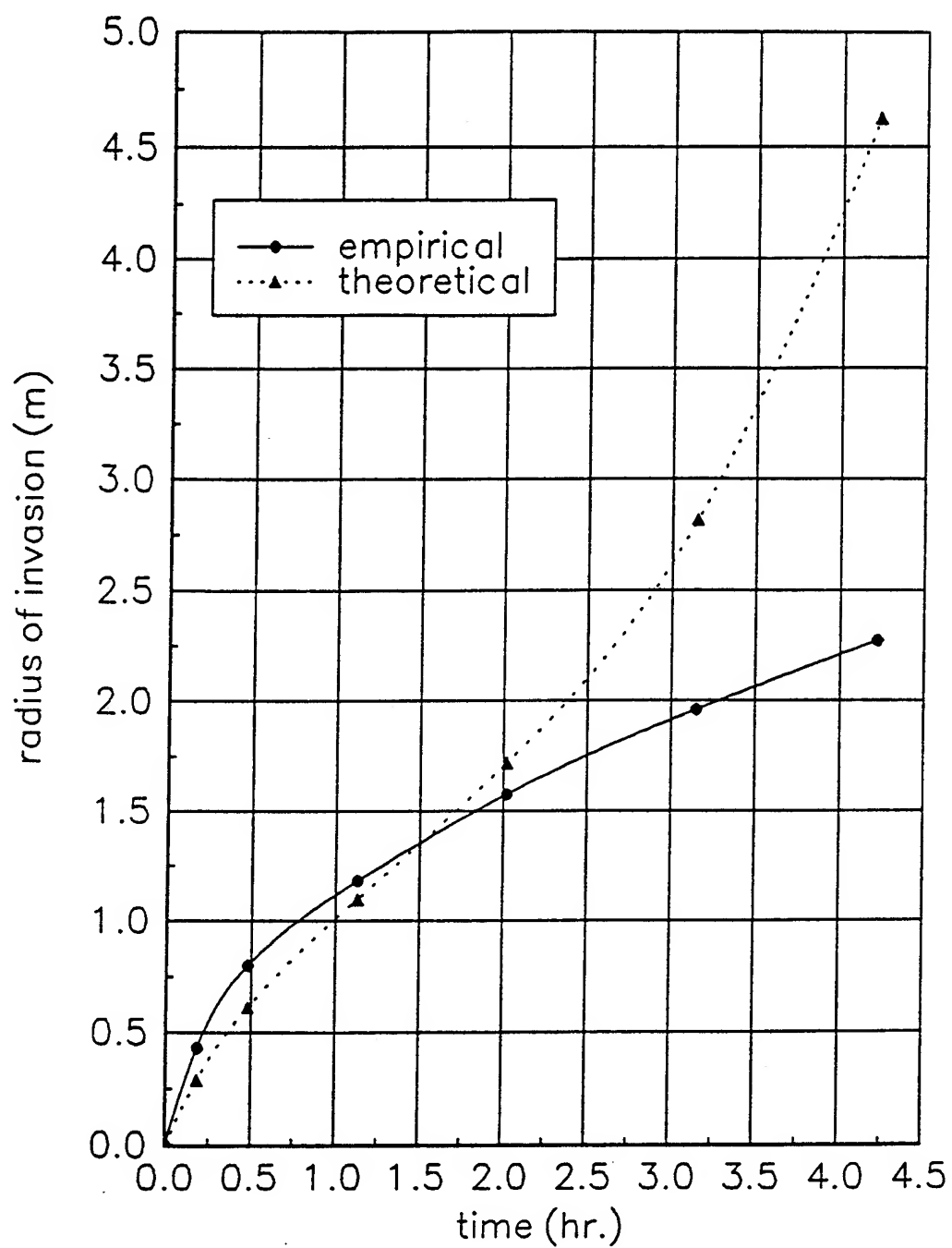


Figure 15. Theoretical and empirical estimates of the average radius of tracer invasion determined for the entire screened interval of well 5-1.

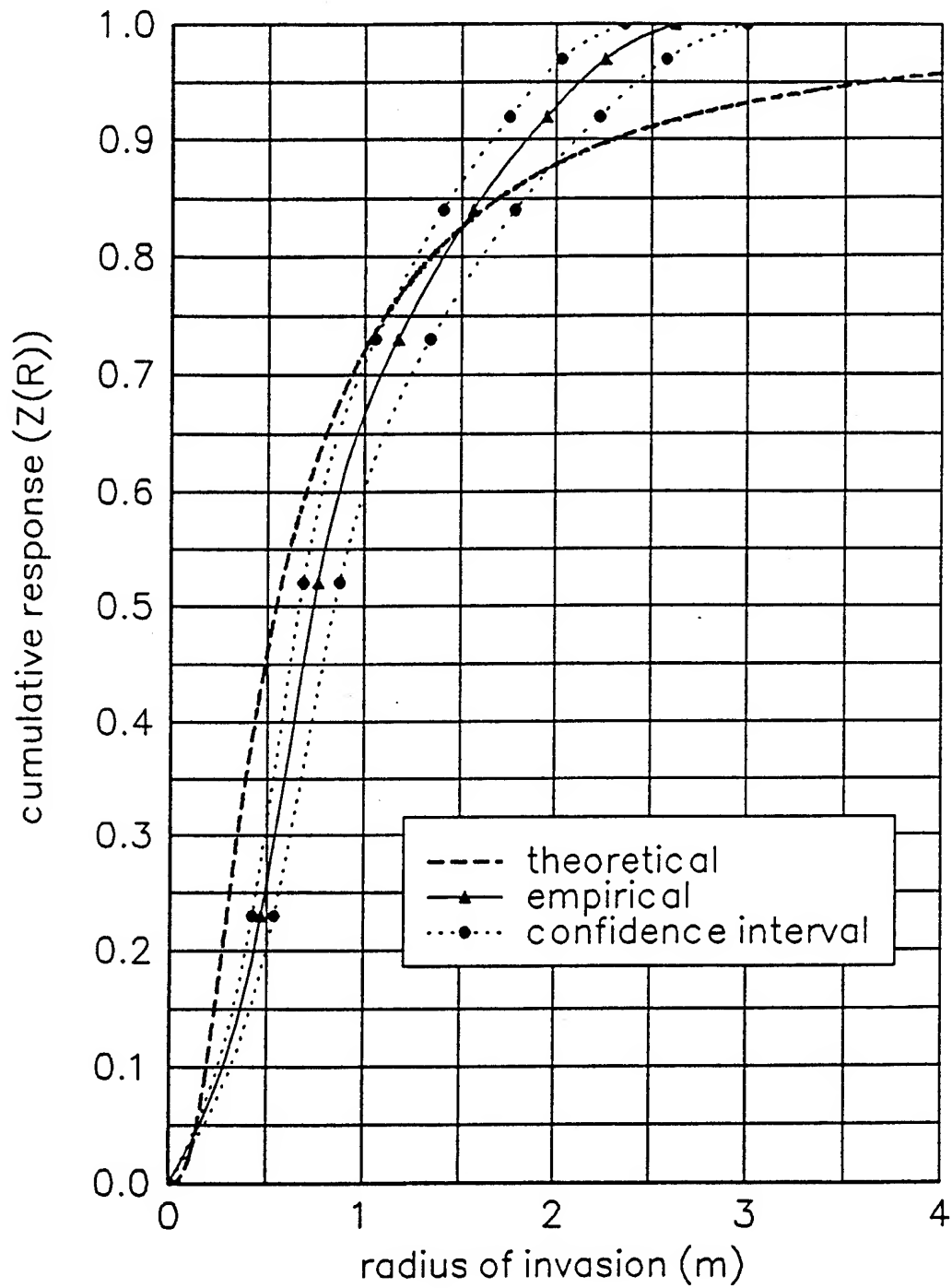


Figure 16. Induction tool empirical cumulative radial response functions.

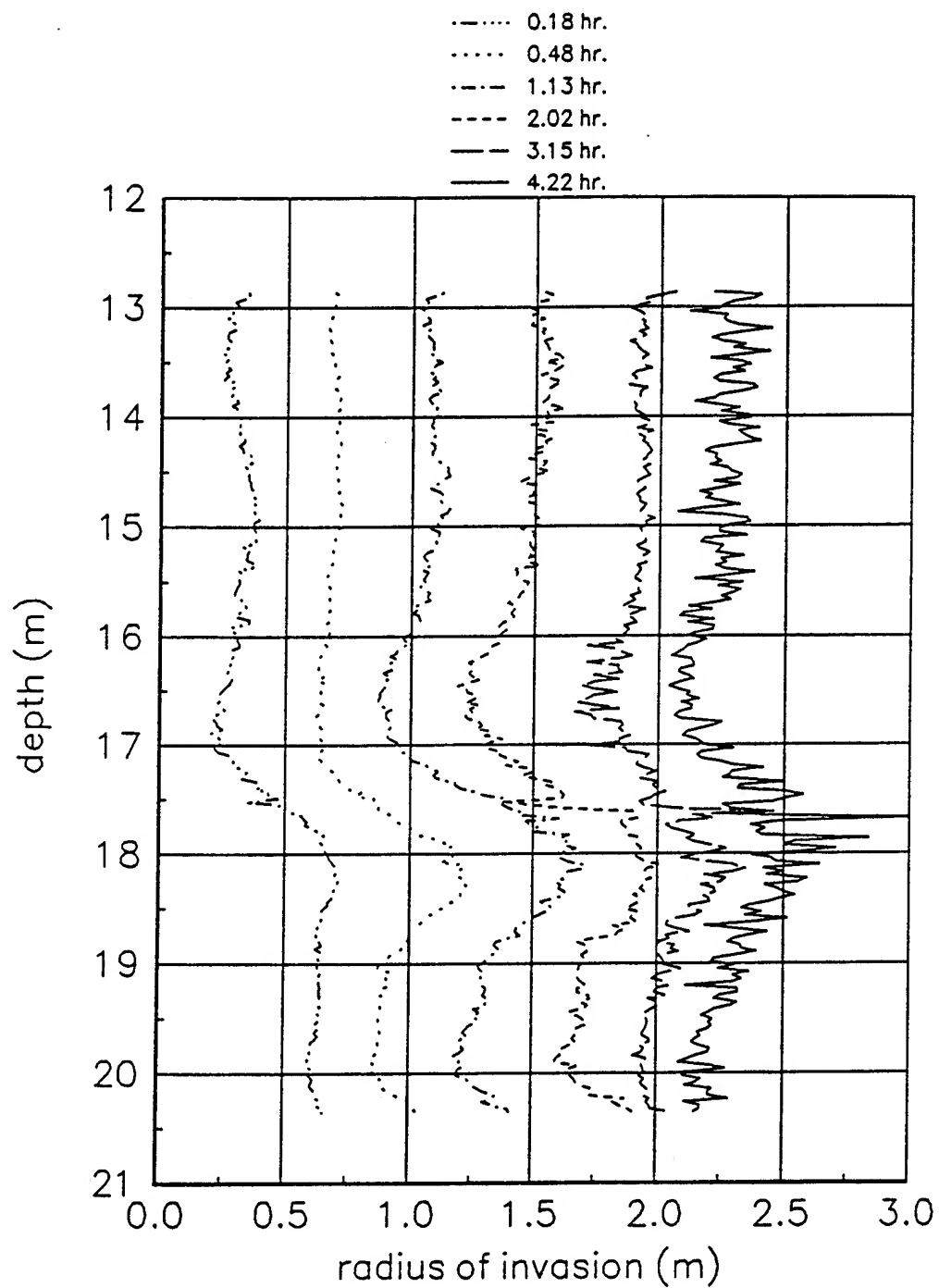


Figure 17. Radius of tracer invasion in well 5-1 determined with the empirical cumulative radial response function.

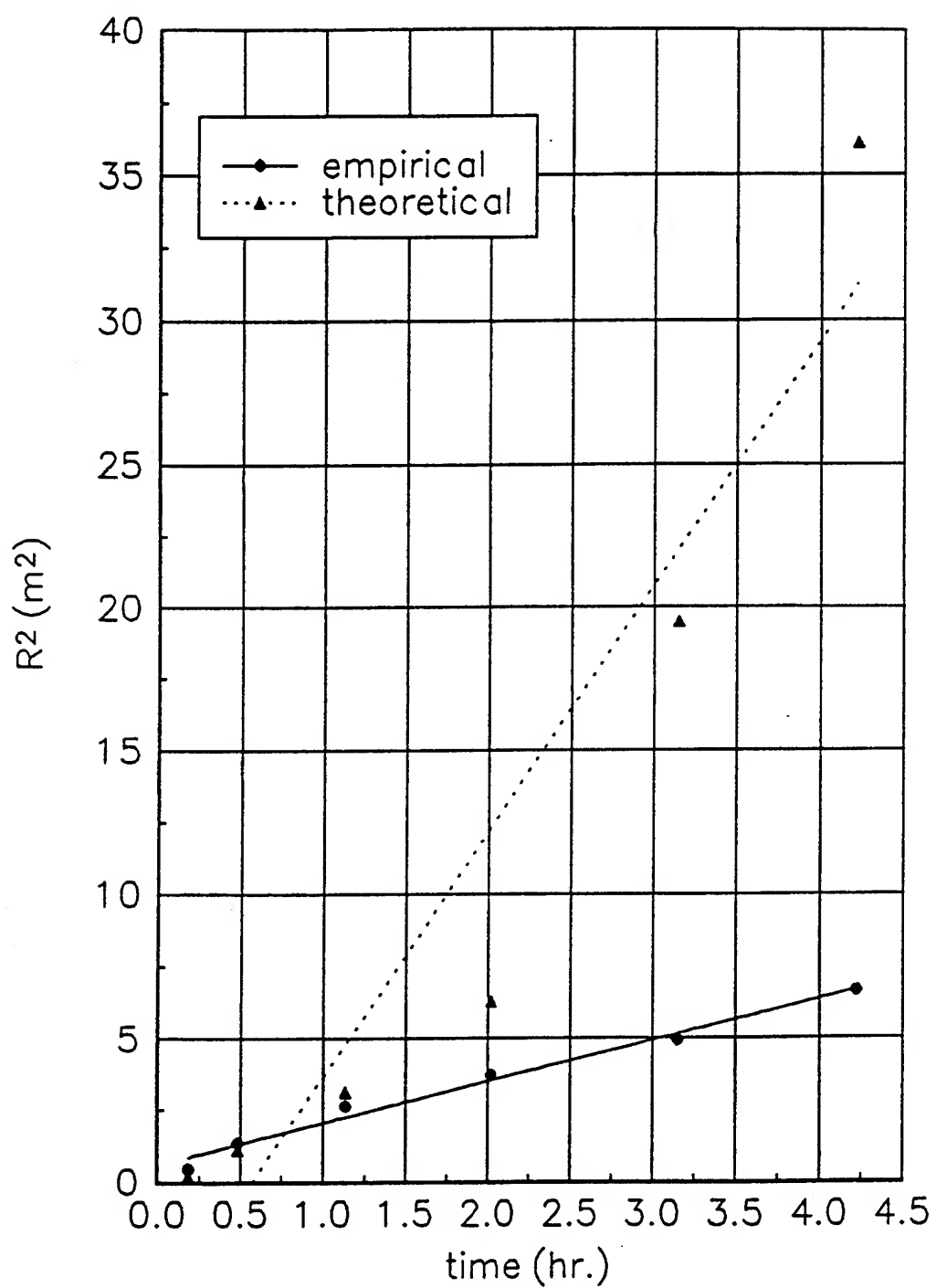


Figure 18. Radius of tracer invasion squared versus time determined at 17.98 m in well 5-1.

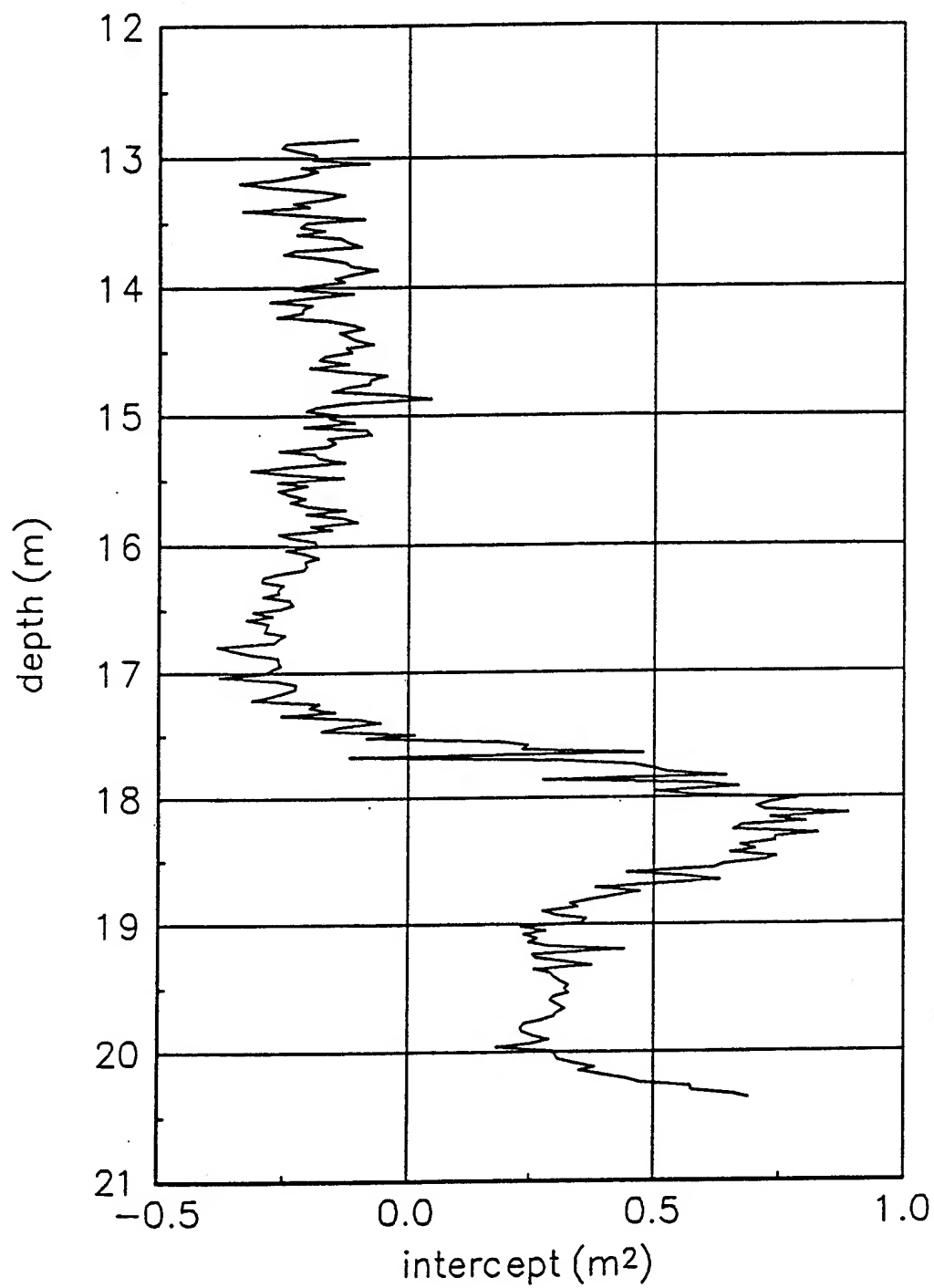


Figure 19. Y-intercept values from R^2 versus t plots determined for each 0.03 m interval of well 5-1.

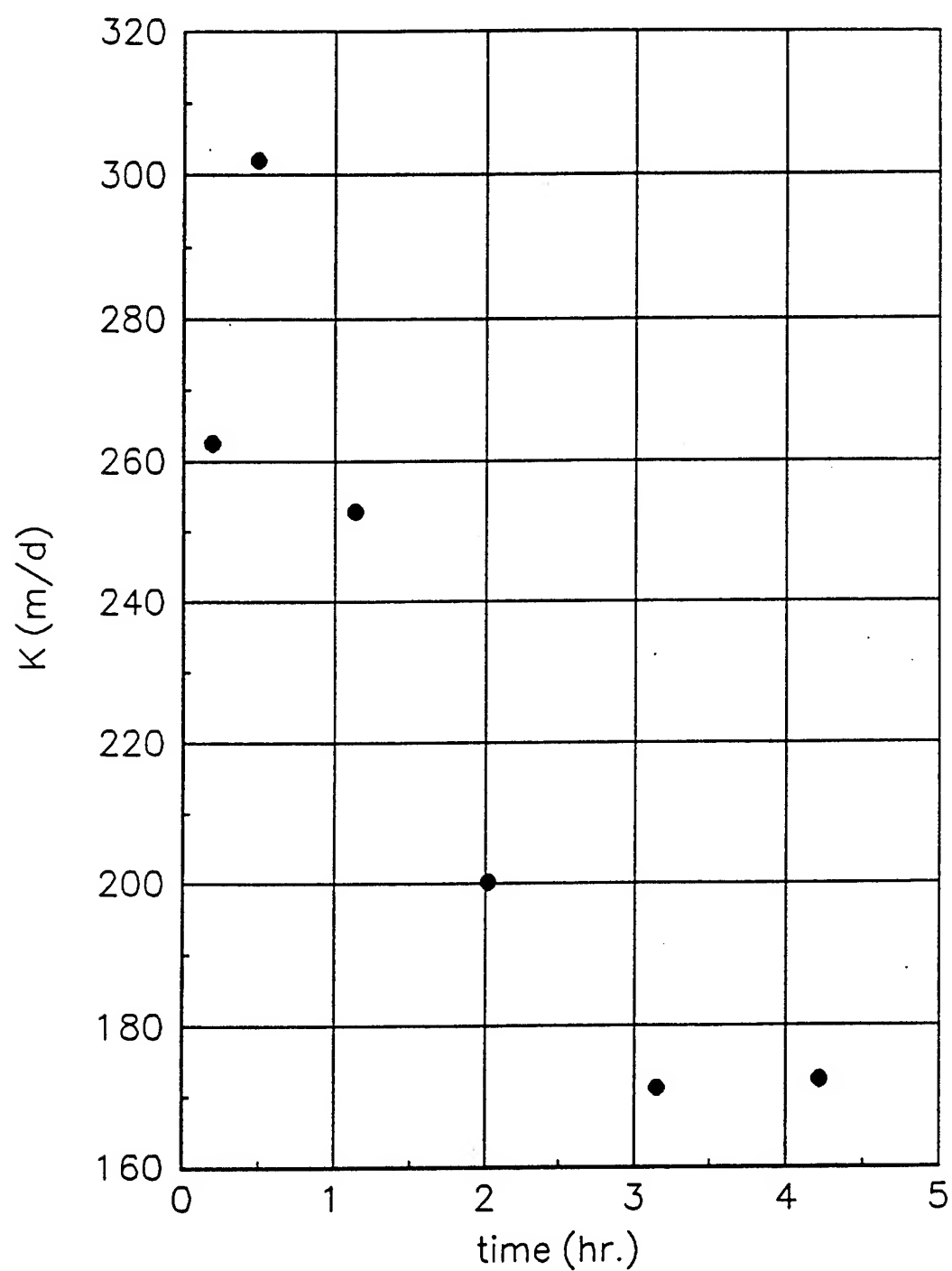


Figure 20. Time dependence in calculated hydraulic conductivity at 17.98 m in well 5-1 due to the presence of a skin.

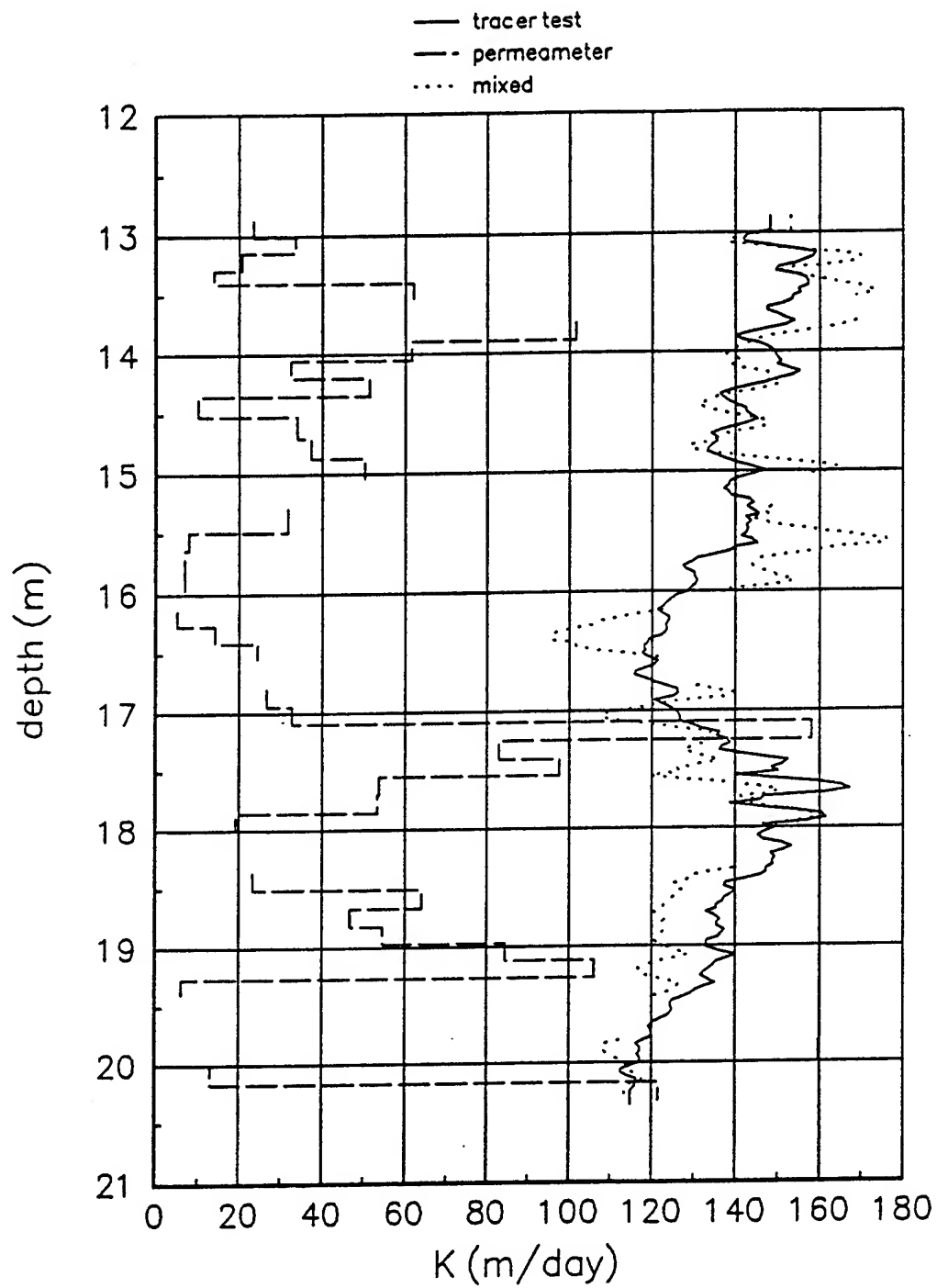


Figure 21. Hydraulic conductivity profiles for well 5-1. Permeameter data from Butler and McElwee (1994).

I. HIGH-RESOLUTION SEISMIC REFLECTION STUDY

Introduction

Seismic-reflection surveys have been extensively used for more than 60 years to image the subsurface for petroleum exploration. The successful use of the technique in shallow engineering applications, however, depends on several key conditions. First and foremost is the existence of acoustic velocity and/or density contrasts between geologic units in the subsurface. The second relates to the ability of the near-surface to propagate high-frequency seismic signal. Finally, the acquisition parameters and recording equipment must be compatible with the proposed target, resolution requirements, and environmental constraints of the survey. The application of shallow, high-resolution seismic reflection methods to specific geologic situations or problems requires a thorough understanding of the basic principles (See Appendix B from the first year report, McElwee and Butler, 1992).

Shallow high-resolution seismic-reflection profiles can be useful in characterizing shallow structures significant in a variety of hydrogeologic settings. High-resolution seismic reflection has only recently developed as a practical and effective method for identifying zones of low permeability (Birkelo et al., 1987; Merey et al., in press), unconsolidated layers above bedrock (Steeple and Miller, 1990, Grantham, 1990), and mapping shallow (<30 m) bedrock surfaces (Hunter et al., 1984; Miller et al., 1989; Miller et al., 1990). The shallow seismic-reflection technique is inexpensive (relative to drilling) and can often decrease the need for drilling by an order of magnitude. While the seismic-reflection method can identify variations in the bedrock surface and stratigraphic relationships, it can give only estimates of depth; explicit identification of lithologies requires confirmation drilling.

This report displays and interprets seismic-reflection data acquired and processed to determine the feasibility of delineating stratigraphic or structural features of potential hydrogeology significance between the 30-35 ft deep clay/sand interface and the top of a 70 ft deep bedrock surface. A series of walkaway noise tests and 650 ft of CDP seismic data on 4 lines were acquired in the Kansas River valley at the GEM site (Figure 1). The walkaway tests included five different sources and seven analog low cut filter settings with a total apparent spread length of approximately 96 ft. A 200 shot point CDP survey with 2 ft station spacing and a 250 shot point CDP survey with 1 ft station spacing were conducted using the downhole 30.06 rifle, 100 Hz geophones, 280 Hz and 400 Hz analog low cut filters, and a Geometrics 2401x 48 channel seismograph. The acquisition dates of the two CDP surveys were separated by one year. The near-surface conditions were

drastically different for the two surveys (moisture conditions) resulting in significant differences in overall data quality. The data were acquired and processed with the bedrock surface as the primary target. However, data acquired during the second survey focused primarily on discontinuous intra-alluvial features that lay between the clay/sand interface and bedrock.

Data Acquisition

All data for this study were acquired with an EG&G Geometric's 2401x seismograph. The Geometric's seismograph amplifies, filters (analog), digitizes the analog signal into a 15-bit word, and stores the digital information in a demultiplexed format. The 280 or 400 Hz low cut filters have an 18 dB/octave rolloff from indicated -3 dB points. The 1/5 ms sampling interval resulted in a 5000 Hz sampling frequency, recording 1024 samples for a record length of 204 ms. The 2401x is a 48 channel floating point seismograph.

A variety of field parameters and equipment were tested to insure optimization of recorded data. The sources for the testing included downhole 30.06 and 50 caliber rifles (Steeple et al., 1987), 12 and 8 gauge auger guns (Healey et al., 1991), and a 7.3 kg sledge hammer (Neitzel, 1958). The receivers for the entire study were single Mark Products L-40A 100 Hz geophones. When two receivers were used they were planted in an in-line array to attenuate source-generated air coupled wave.

The production seismic profiles were preceded by an extensive series of tests. Proper matching of high- and low-cut filters for acoustic characteristics and targets at this site allowed optimization of the seismograph's dynamic range. Source-to-receiver offsets on walkaways ranged from 1 to 96 ft with receivers spaced at 1 ft intervals. Reflections, direct wave, refractions, ground roll, and air-coupled wave can all be easily identified on walkaway data. Reflections can be interpreted on unprocessed data recorded with 140 Hz and higher lowcuts. All aspects of the testing were instrumental in fine-tuning the acquisition parameters and equipment for the CDP portion of this study and in determining the potential of several variations in the acquisition process.

Production data for this study were acquired using the 30.06 downhole rifle, 100 Hz geophones, 1 or 2 ft station spacings, 2 or 8 ft source to nearest receiver distance, 280 Hz or 400 Hz low cut and 1000 Hz high cut analog filters. The 280 Hz and 400 Hz analog low cut filters shaped the pre-amplified spectra, enhancing the higher frequency components of the recorded energy (Steeple, 1990). The near source-to-receiver offset would have allowed the recording of any intra-alluvial reflection with sufficient signal strength to set the seismograph's least significant bit. The quality of bedrock and intra-

alluvial reflections suggest the acquisition parameters and equipment were matched for this site and the associated geologic target. Parameters were selected to enhance the bedrock reflection recorded during the walkaway tests. The bedrock reflection can be easily interpreted on most field files across the lines.

Data Processing

Data processing was done on an Intel 80486-based microcomputer using *Eavesdropper*. The processing flow was similar to those used in petroleum exploration (Table 1). The main distinctions relate to the conservative use and application of correlation statics, precision required during velocity and spectral analysis, extra care during muting operations, and lack of deconvolution.

The air-coupled wave and the cyclic nature of the direct wave energy on the data collected the first year was not removable with spectral filtering and was not sufficiently attenuated during the 24-fold CDP stacking process to allow reflections shallower than bedrock to become apparent. The nearby trees, pumping well head, and monitor well clusters proved to provide a source of reflected air coupled wave that affected the entire data set. All attempts to remove the air-coupled wave proved futile. The reflections present on field files possessed statics problems and trace-to-trace amplitude irregularities which combined with the air-coupled wave problems to inhibit the effectiveness of established shallow reflection processing techniques. F-k filtering improved the coherency and signal-to-noise of reflecting events above the bedrock surface. F-k filtering improved slightly the signal-to-noise ratio on stacked data. Only coherent energy interpretable on raw field files were interpreted as reflections after the application of the f-k filter. F-k filtering was not effective enhancing the reflections interpretable on field files from the second year. The f-k filter was used to enhance, not expose, previously unidentifiable events.

For most basic shallow, high-resolution seismic reflection data processing, steps/operations are a scaled down version of established petroleum based processing techniques and methods. However, processes such as deconvolution have basic assumptions that are violated by most shallow data sets. Migration is another operation that due to non-conventional scaling (vertical and/or horizontal) many times may appear to be necessary when in actuality geometric distortion may be simple scale exaggeration. Processing/ processes used on data for this report have been carefully executed with no assumptions and with care not to create artifacts.

Seismic data from the first year were processed to enhance the bedrock reflection. The processing flow deviated from normal shallow reflection processing during the

muting and filtering aspects. The filtering was much narrower band and the muting was much more severe. The muting was necessary to reduce the contamination of the pre-bedrock reflection arrivals with noise that adversely effected many of the correlation statics routines and resulted in coherent events that were not the direct result of near-vertically incident reflections.

Walkaway Noise Tests

Preliminary experiments with various parameters and equipment included the 7.3 kg sledge hammer, downhole 30.06 rifle, downhole 50 caliber, 12 gauge auger gun, and 8 gauge auger gun as sources and 50, 100, 140, 200, 280, and 400 Hz analog low cut filters (See first year report McElwee and Butler, 1992, Appendix D). Figure 2 shows a typical walkaway noise test using the 30.06 rifle as an energy source. The direct wave has a strong presence from first arrival to the bottom of the record. The very repetitive nature of this arrival is a direct result of the relatively narrow bandwidth of the wavelet and the high acoustic impedance contrast between the near-surface material and the clay interface at several feet of depth. The high acoustic contrast between the near-surface material and the clay layer channels the energy, creating a standing wave that travels within the low velocity near-surface material. The narrow band nature of the energy makes both analog and digital filtering relatively ineffective. Ground roll is difficult to identify even with no analog low cut filter. This is probably a result of the attenuative nature of the 100 Hz geophones and the near-surface material. Reflection from interfaces deeper than the bedrock surface can be interpreted directly on walkaway displays with analog low cut filters greater than about 100 Hz.

The 96 channel walkaways were recorded by maintaining 48 receiver locations and occupying two different source location separated by 48 ft. This pseudo walkaway recording method resulted in an apparent discontinuity between receiver locations 48 and 49. This signal difference is actually a result of variability in the source locations.

Reflections from the bedrock surface can be identified on most walkaways when the analog low cut filter is in excess of 100 Hz. The dominant frequency and signal-to-noise ratio was significantly higher with the downhole 30.06 than with any other source tested. The air-coupled wave and ringy direct and refracted waves represent the most significant obstacles to the recording of high quality reflection events from interfaces shallower than the bedrock surface. The dominant frequency of the bedrock reflection is approximately 200 Hz.

The 70 msec event on most records between 75 and 96 ft offset is interpreted to be the bedrock reflection at this site. The apparent NMO velocity is approximately 3000

ft/sec. The walkaways from the auger gun have slightly more air wave and lower dominant frequency. The 50 cal data as well possess a lower dominant frequency, more air wave, and are sufficiently energetic to overdrive the near offset receivers. The sledge hammer proved an extremely noisy source with significantly more ground roll and air coupled wave. Considering signal quality, dominant frequency, relative source energy, and site preparation, the 30.06 represented the ideal source for the site and geologic target.

Results

Unequivocal identification of reflection energy on field files is essential for accurate interpretation of CDP stacked sections. Many of the field files acquired for the production portion of the survey have confidently identifiable reflection events at approximately 65 ms (Figure 3). The 65 ms reflection has a dominant frequency of approximately 140 Hz and an apparent NMO velocity of around 3000 ft/sec. This represents an approximate depth to the reflector of 70 ft and a vertical resolution potential of about 5 ft. The signal-to-noise ratio on the field file is sufficient to confidently identify bedrock reflections on many files at offsets longer than about 50 ft. The air coupled wave is the highest amplitude event on most files and increases the background noise of near-vertically incident reflection energy arriving later in time.

Analysis of processed field files improves confidence in interpretations of CDP-stacked sections (Figures 3 and 7). Digital filtering, first arrival muting, appropriate trace balancing, bad trace editing, f-k filtering (on the first year's CDP lines), and trace balancing were key processes in improving the pre-stack appearance of reflections interpretable on raw field files. The reflection event identifiable at approximately 65 ms is less evident and possesses almost a 40% drop in dominant frequency on files recorded during the production portion of the first year's study in comparison to walkaway files. Frequency content of the second year's data is consistent with that achieved during the walkaway portion of the first year's research. This drop in overall signal quality on the first year's data predicates care and a conservative approach to interpretations of coherent energy on stacked data. Both the first and second year's data possesses unique characteristics of potential significance to the detection and mapping of alluvial features.

The event interpretable at 8 ft of offset and 30 ms on line 1 from the first year is suggested to be the reflection from the clay/gravel interface at approximately 30 ft on line 1 (Figure 3). An uphole velocity check shot allows confident correlation between the time seismic section and depth of events present above the bedrock surface (Figure 4). The event is high amplitude and possess some apparent hyperbolic curvature, especially on

processed field files. However, the event has characteristics that make it difficult to confidently rule out an alternate interpretation that identifies it as a refracted arrival. Due to the hyperbolic nature of the event and the coherency at offsets at least as short as 8 ft, it will be interpreted as the clay/gravel reflector on CDP stacked data.

The bedrock reflection is coherent on field files at offset from 30 to 96 ft on line 1 from the first year's research (Figure 3). On all files the bedrock reflection is at least interpretable at offset in excess of 80 ft. At offsets longer than about 75 ft the pull-up and associated stretch necessary to correct for non-vertical incidence is sufficient to drop the dominant frequency by as much as 25% (Miller, 1992). To reduce the detrimental effects of the NMO stretch a stretch mute can be applied. However, if the stretch is reduced to less than 15%, information at offsets greater than 50 ft are muted leaving only the very close offset energy. Due to the minimal amount of reflected energy returning from the bedrock surface at offsets less than 50 ft, an excessive amount of stretch was necessary to produce an interpretable section. The reflection wavelets were allowed to stretch almost 50% before muting was permitted. The effects of this are evident on moved-out field files. The allowance of excess stretch was a necessary trade off on this data set to maintain sufficient coherency on the bedrock reflection.

Coherent events can be interpreted across the entire CDP stacked section of line 1 from the first year (Figure 5). The stacked section possesses nominal 24 CDP fold redundancy as a result of the 48 channel recording system and selected recording geometry. The dominant frequency of most CDP stacked reflection energy is between 100 and 175 Hz. The stacking velocity ranged from 1900 to 3500 ft/sec. Variation in the depth to the clay/gravel interface at approximately 30 ft is no greater than 2 ft across the 170 ft of CDP line acquired for this study. The bedrock reflection possesses the decrease in dominant frequency resulting from the over-stretching of reflection wavelets necessary to compensate for non-vertical incidence. Anomalies on the bedrock surface, such as the one interpreted at CDP location 270 could represent localized topographic relief on the bedrock surface of as much as 7 ft. Drill data from the area has encountered apparent relief of no greater than approximately two feet. Source-to-receiver offsets were not conducive to the recording of reflections from interfaces deeper than about 70 ft. Reflection events from within the Pennsylvanian sediments are interpretable on the stacked section at times greater than 80 ms but do not possess the coherency and wavelet consistency possible due to the focused nature of this survey.

Only subtle indications of reflection from within the gravel portion of the section can be interpreted on the line 1 data from the first year (Figure 5). Between CDP's 290 and 340 there is some indication of a reflection at a time of 42 ms. The event could be

interpreted as a lens type feature with erosional termination at CDP 310 and 330 resulting in a 'hole' in the center of the lens. This interpretation is speculative but is a possibility in an alluvial setting such as this. This lens feature is probably less than 5 ft thick with an areal extent of no greater than 50 ft. The gravel portion of the section (between 30 and 70 ft) is for the most part acoustically transparent.

The most significant feature interpretable on the bedrock surface of line 1 from the first year is present between CDP 260 and 300 (Figure 5). This feature appears to be a small bedrock mound with an associated low, possibly filled with bedrock rubble. The significance of this event can not be fully ascertained without drilling/coring. The maximum change in bedrock elevation across this feature is about 6-7 ft. A defocusing of seismic energy is evident in the 80 ms reflection as a result of the severity of the dip on the bedrock between CDP 260 and 300. Another feature between CDP 360 and 400 could represent another bedrock rubble zone with undulations in the bedrock surface and associated fill. Confident interpretations of reflections associated with intra-alluvial features initially requires detailed confirmation drilling to establish key criteria for evaluation.

Reflections are easily interpretable from interfaces beneath the bedrock surface on line 2 (Figure 6). Line 2 intersected line 1 (Figure 5) at approximately CDP 700. The near-surface along this line was very disturbed due to the high level of truck activity associated with the drilling of dense clusters of monitor wells. The static introduced by this activity are significant resulting in velocity anomalies that made reflection from the shallow portion of the section difficult to identify. The apparent dip on the bedrock surface is probably related to velocity variation across the line. Undulations similar to those interpreted on line 1 can be inferred on line 2. If the interpretation of the bedrock surface is accurate, when the static problem that produced the apparent dip on reflections from beneath the bedrock surface is corrected for, the bedrock surface dips slightly to the southeast. It is also possible that the interpreted bedrock surface is actually intra-alluvial features that are discontinuous across the line and when interpreted in a continuous manner appear to possess dip.

The events that appear to be coherent between 40 and 60 msec could represent acoustic boundaries within the alluvium. Some indication of the gravel/clay interface is suggested at about 35 to 40 msec. The interpreted reflection from the gravel interface possesses a narrow frequency bandwidth and is much more discontinuous than on the line 1 section. The dominant frequency of reflection on this line is approximately 200 Hz, which is about 30 % better than that observed on line 1. This would suggest a 30% increase in vertical resolution. The data has only limited potential for mapping the clay/

gravel interface, but does allow for more speculation than line 1 about intra-alluvial material between the basal contact of the clay and the bedrock surface.

Reflections on field files from lines 3 and 4 can be interpreted during all stages of pre-stack processing (Figure 7). The reflection from bedrock has classic hyperbolic curvature with an origin time of approximately 55 msec. Problems with the air coupled wave and the ringing direct/refracted wave are evident on raw files. The dead traces on shot gather 79 is a result of the large pumping well and associated well curb or platform. The inconsistency in reflection arrivals is evident on processed shot gathers. The dominant frequency on filtered field files is in excess of 300 Hz. Processing clearly enhances the coherency and resolution of the data and appears to generate a sufficient increase in signal-to-noise ratio to allow for a good CDP stacked section.

Line 3 (Figure 8) acquired in the second year of research did not seem to have as good a signal to noise ratio as line 4 (Figure 9). This was probably a result of the near-surface that had been significantly altered during the installation of three different well clusters and a large pumping well, which was avoided during the acquisition of line 4. The apparent diffraction centered on about CDP 180 is the result of the large pumping well and the associated well pad (8 ft square cement pad) and power pole. This apparent diffraction is air-wave echo that could not be removed during processing. Subtle indications of a coherent reflection can be interpreted on the extreme southwest end of the line. The diffraction looking event with air wave velocity on the extreme southwest end of line 3 is suspected to be from the road bank or trees that were at the edge of the study area. The data do possess some reflection energy. Only hints of reflections can be interpreted across most of line 3. Various processing techniques were tested to determine if the coherent reflections observed on field files from line 3 could be enhanced to form uniform reflections on CDP stacked records. All attempts to generate a stack section of the data with coherent reflections across the entire section were met with only limited success. Reflections are present in the data as evident on processed field files and in places on the CDP stacked section.

The shorter line acquired during the second year's research (line 4) does possess interpretable reflection information (Figure 9). A strong event at approximately 52 to 55 msec is interpreted to be the bedrock alluvial interface. The dominant frequency of this event is nearly double the reflection interpreted as bedrock on line 1. Subtle undulations on the bedrock surface could be indicative of either velocity variations between the surface and bedrock or structure on the bedrock surface. Both possible interpretations have been suggested at this site on previous data sets. The event interpreted at approximately 35 msec is most likely the basal contact of the clay. Slight changes in

arrival time of this event could represent variations in thickness of the clay unit. The extreme variability obviously present in this area is bore out by the close proximity of line 3 and 4. Line 4 was placed only 8 ft southeast of line 3. At approximately CDP 370 to 390 drill hole information suggests an anomaly within the otherwise consistent clay unit. This anomaly could be interpreted as a pull up on the bedrock surface or a slightly deeper basal reflection arrival (2 msec) from the clay in that area. The time window between the base of the clay and top of the bedrock surface appears to be relatively quiet with only a rare coherency over distances of more than a couple of traces. The increased frequency content and decreased receiver spacing improved the resolution of the data set and verified the lack of any interfaces with significant acoustic variability between the base of the clay and top of bedrock.

Conclusions

Shallow seismic reflection can be used to delineate structural features present between the clay/gravel interface at about 30 ft and the bedrock surface at slightly more than 70 ft. The close proximity and total number of boreholes on this site would suggest that any feature which could potentially alter the hydrologic characteristics at this site between the ground and bedrock surface should have been detected by direct contact. The subtle events interpreted just below the clay/gravel interface at several places on both lines 1 and 4 could represent localized stratigraphic changes that could alter the local hydrologic properties. The presence of the deeper reflection events allows confidence in the interpretations of relative topographic change on the bedrock surface on lines 1, 2, and 4 as actual elevation changes and not as caused by near-surface irregularities.

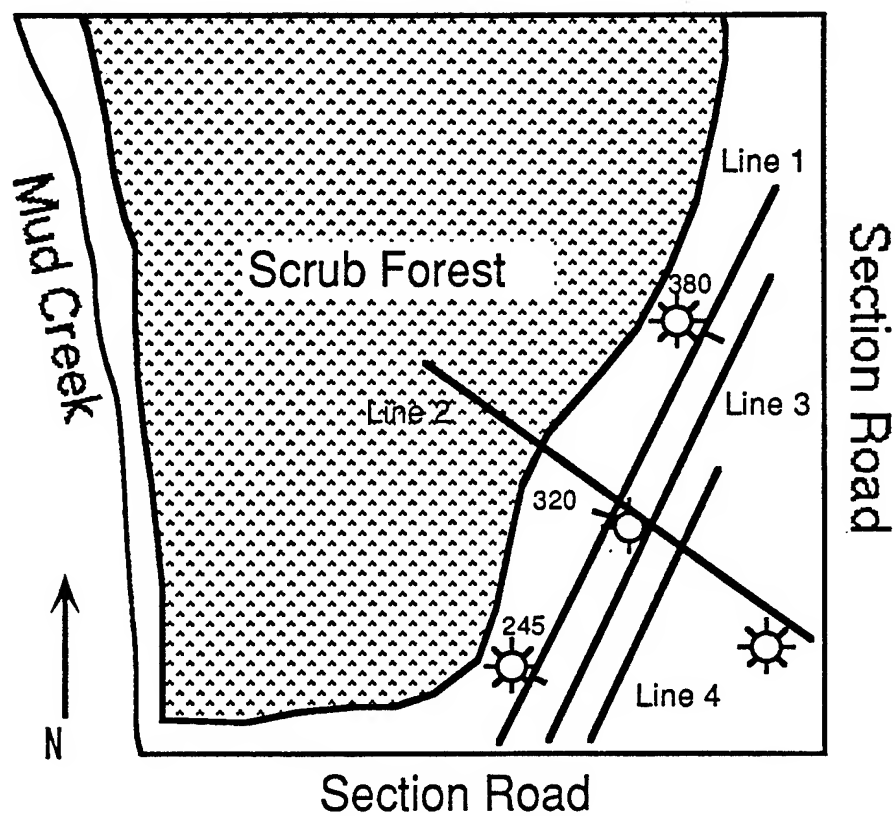
The data quality of the data set as a whole (lines 1, 2, 3, and 4) is extremely variable. This is due in part to the time between the acquisition of the various lines, changes in saturation, and inconsistencies in the near-surface as a result of vehicle and/or drilling activities. Due to the extremely close spacing of boreholes and borehole activities much of the ground surface has been non-uniformly altered. The high resolution seismic method is very sensitive to near-surface conditions. Improvement in signal-to-noise and dominant frequency would be possible in this area if data were acquired in relatively undisturbed locations.

Data collected during the second year suggest that the variable saturation present in the very near-surface causes sufficient static problems to be extremely detrimental to the stacking of reflections with dominant frequencies in excess of 350 Hz. Improvements in the processing of data with this much variability will be critical to allow vertical

resolution on the order of one-half foot at this site. The processed, unstacked data possess the potential to resolve beds as thin as 0.5 ft.

Recommendations

Continuous core holes will be necessary to completely analyze the effectiveness of shallow seismic reflection at this site to delineate inter-alluvial features. Borings will not be sufficient to definitely determine the cause of some of the reflections between the basal contact of the clay and the bedrock surface as interpreted on lines 1, 2, and 4. The reflection technique should be correlated with existing hydrologic data to extract any hidden significance associated with anomalies not interpreted as coherent reflection events on the CDP stacked sections.



- ⊗ High-capacity Pumping Well
- ⊛ Nest of 2" Piezometers
- └ 245 - Seismic line and associated CDP numbers.

Figure 1. Map of the GEMS site showing locations of seismic lines.

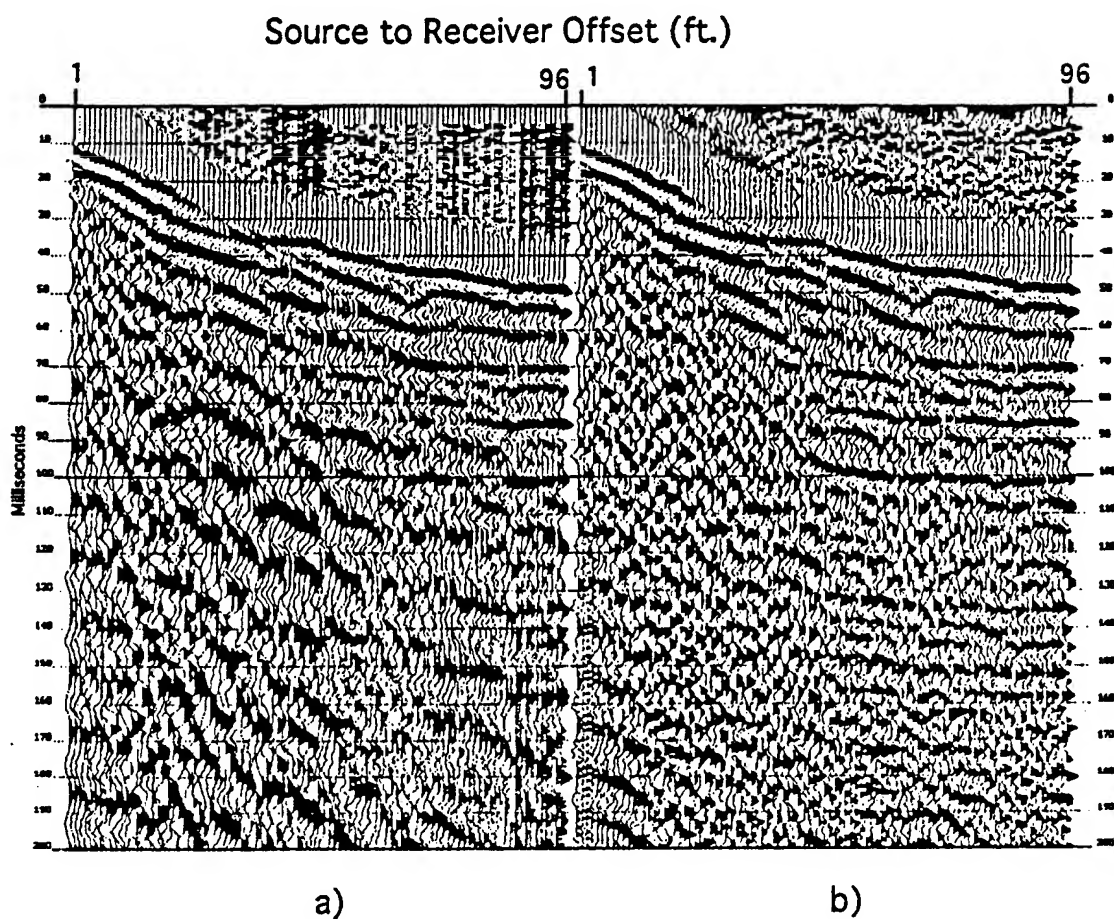


Figure 2. A typical walkaway noise test record with the downhole 30.06 rifle. a) represents the raw field file with a 25 ms AGC scale, b) represents a) with a 100 Hz digital low cut filter. These data were recorded with analog low cuts at 200 Hz.

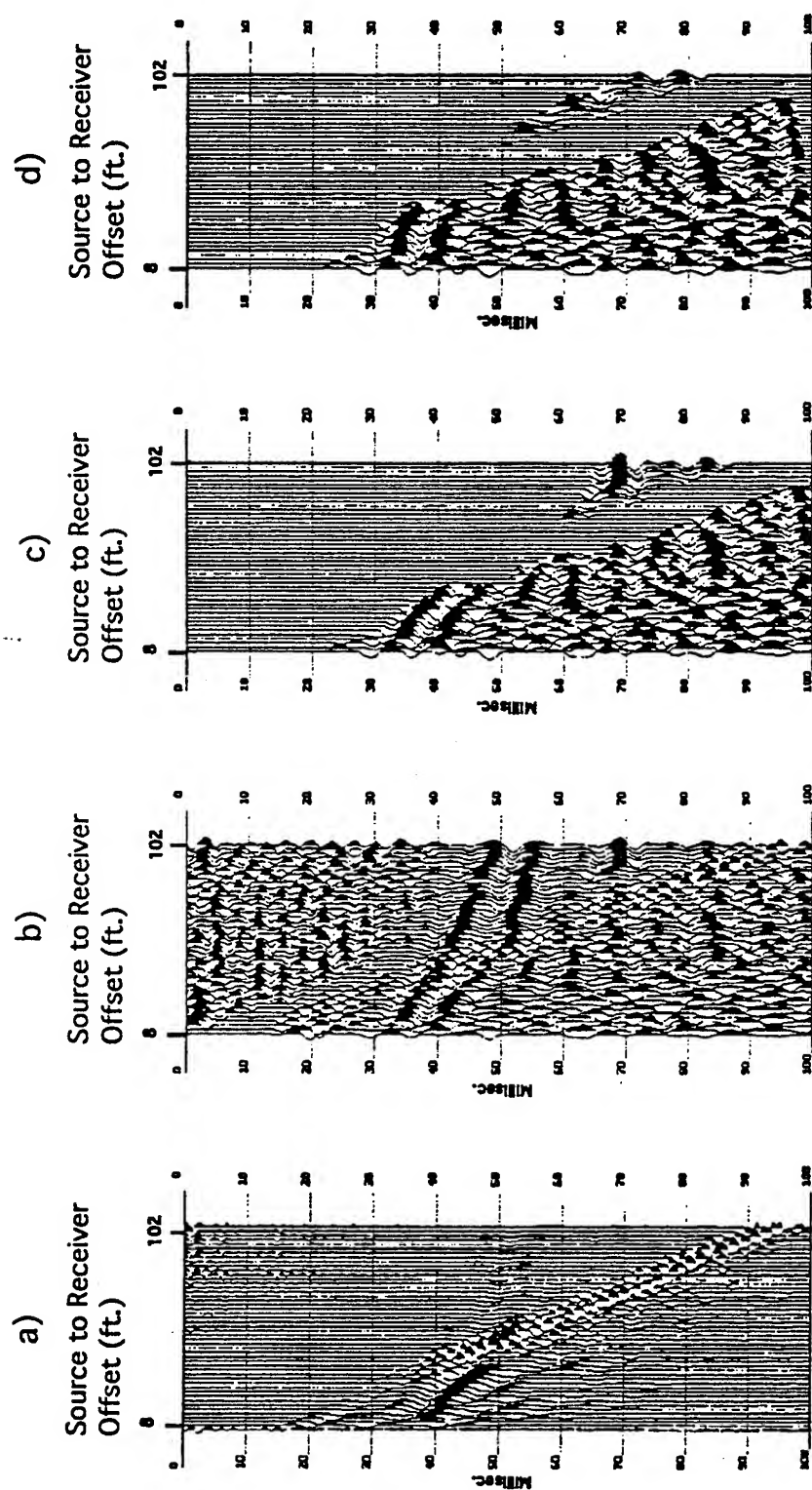


Figure 3. Selected field file displaying the processing sequence. a) raw field file normalized, b) f-k filtered, AGC scaled to 25 ms, and digital filtering 125 to 250 Hz, c) appropriate muting and trace balancing, d) moved out to adjust for non-vertical incidence.

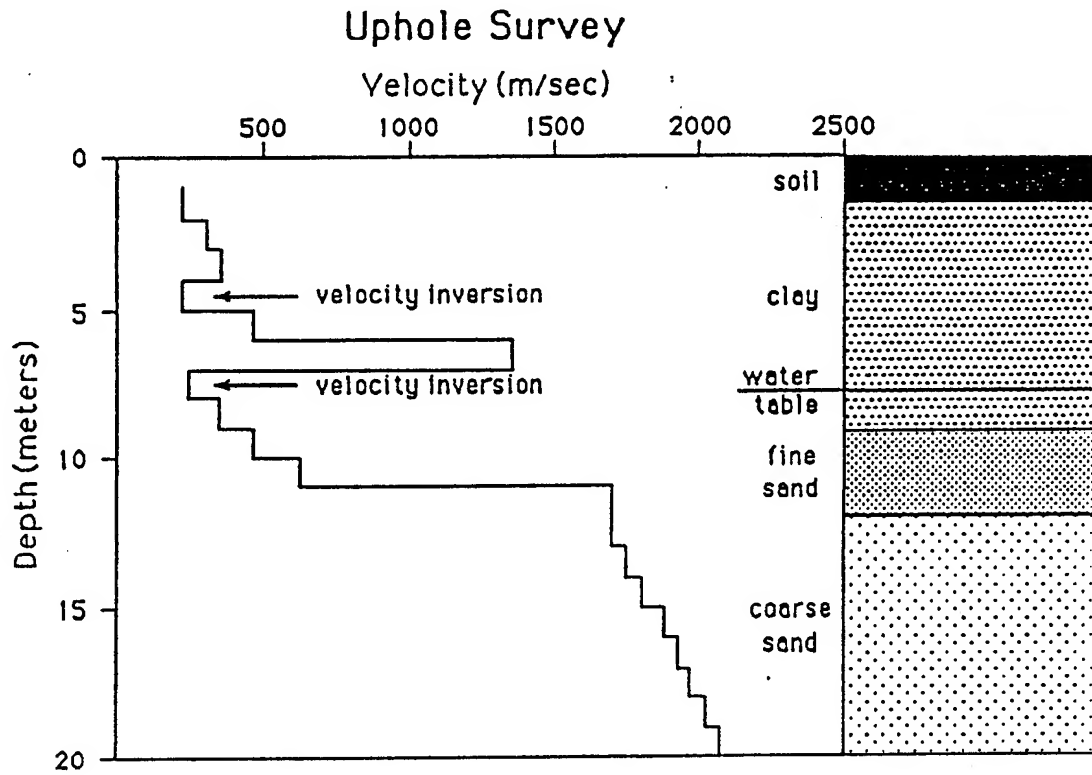


Figure 4. Uphole survey and associated geologic cross-section (from Grantham, 1990).

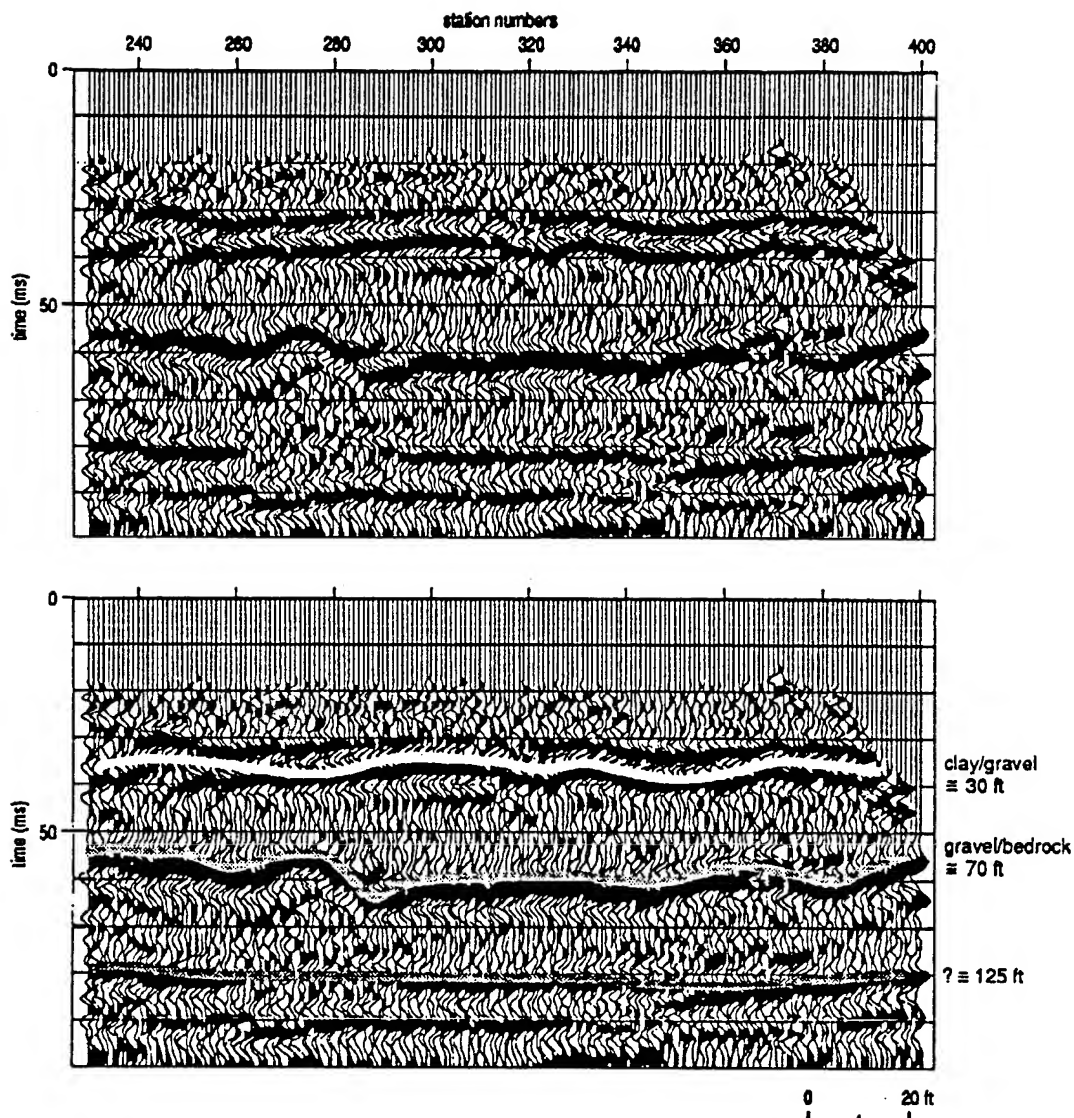
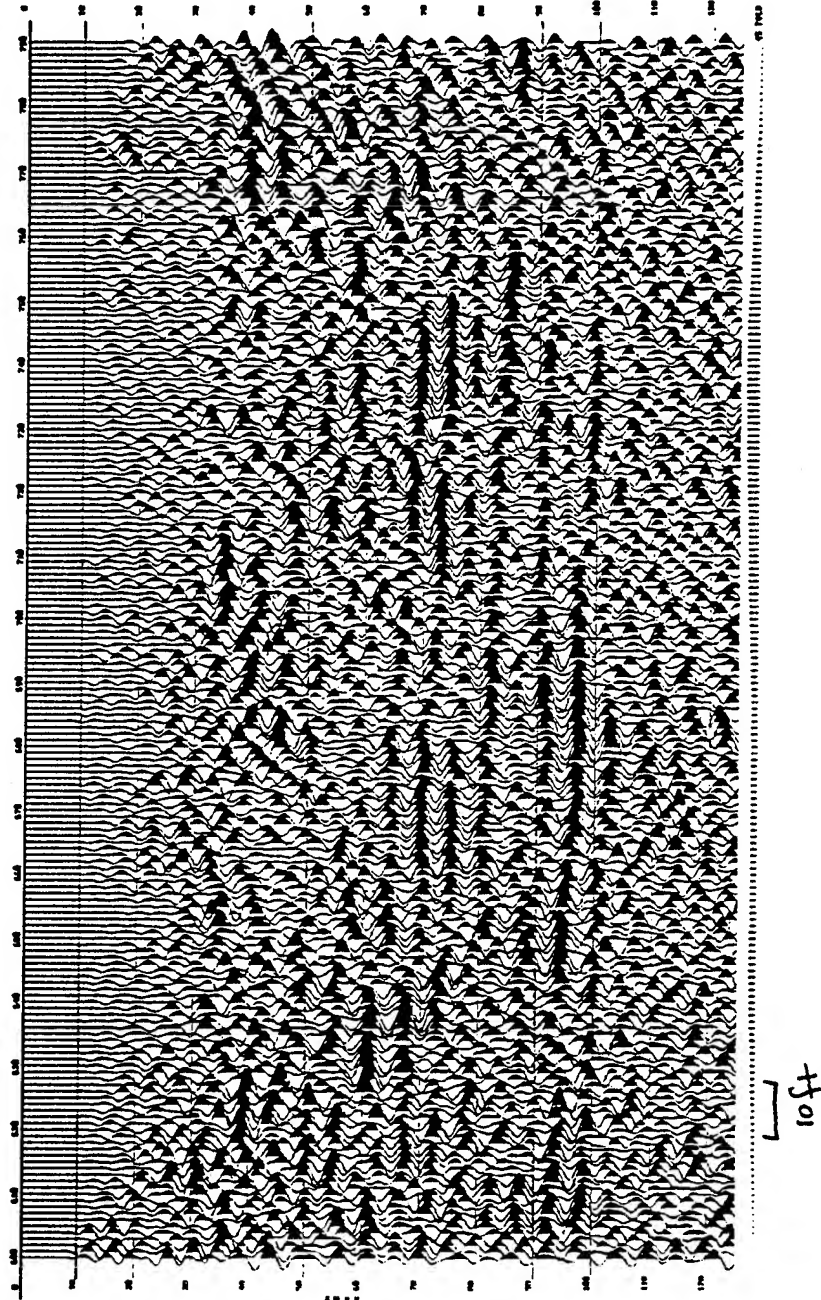


Figure 5. CDP stacked, 24 fold seismic reflection section from GEMS line 1. At least three reflection events are easily interpretable on the stacked section. The interpretation suggest several feature of acoustic significance that could influence the hydrologic setting.

Figure 6a.

LINE #2
CDP Numbers

NNN



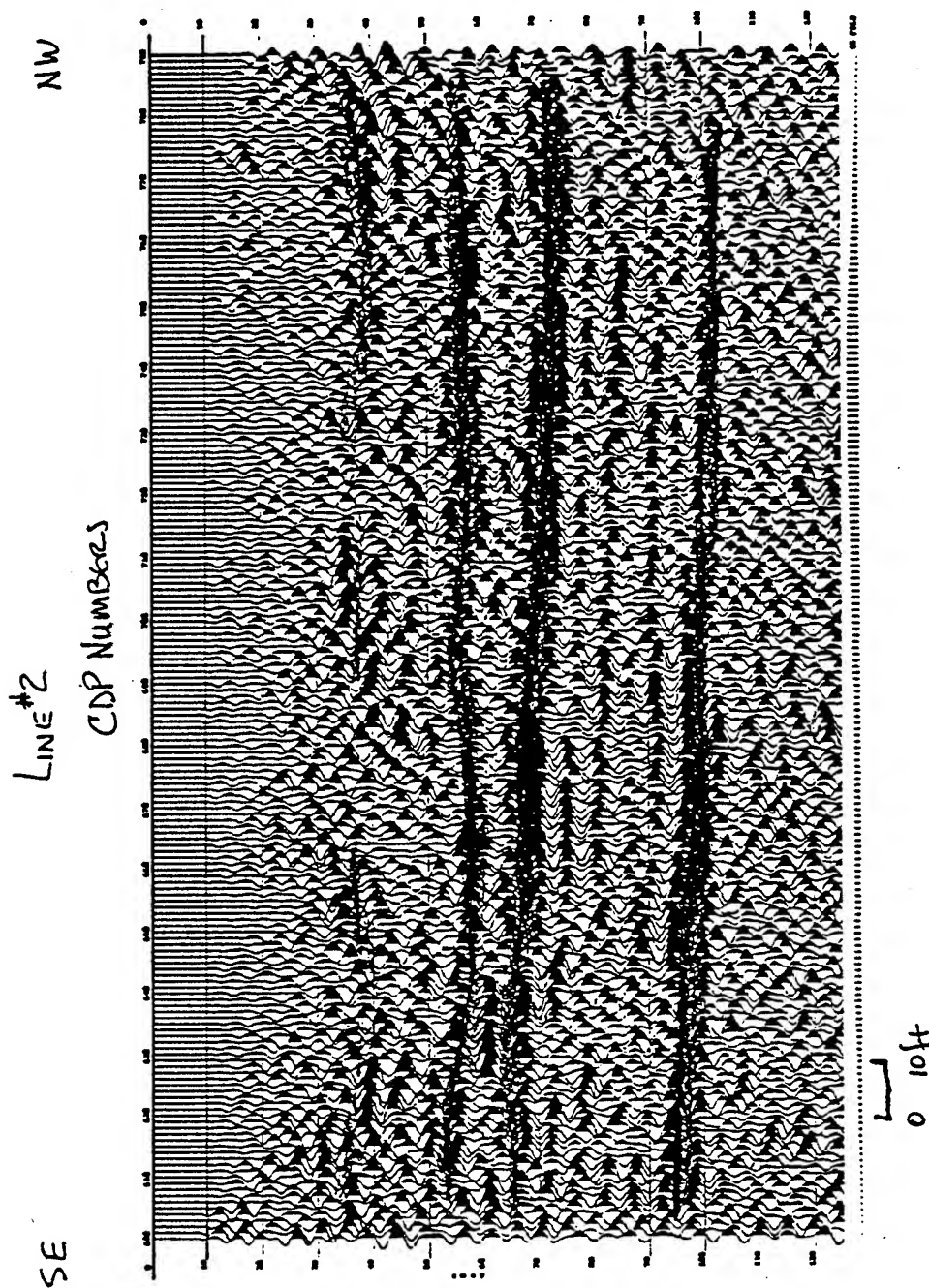


Figure 6b. CDP stacked, 24-fold seismic reflection from line 2. Good coherency can be observed on the uninterpreted data (a) across most of the line. The bedrock surface as well as two reflection events within the consolidated sedimentary section and the proposed clay/gravel interface are interpreted on the stacked section (b). The stacked data possess good coherency on arrivals beneath the bedrock surface and hints of potential reflections from the base of the clay unit.

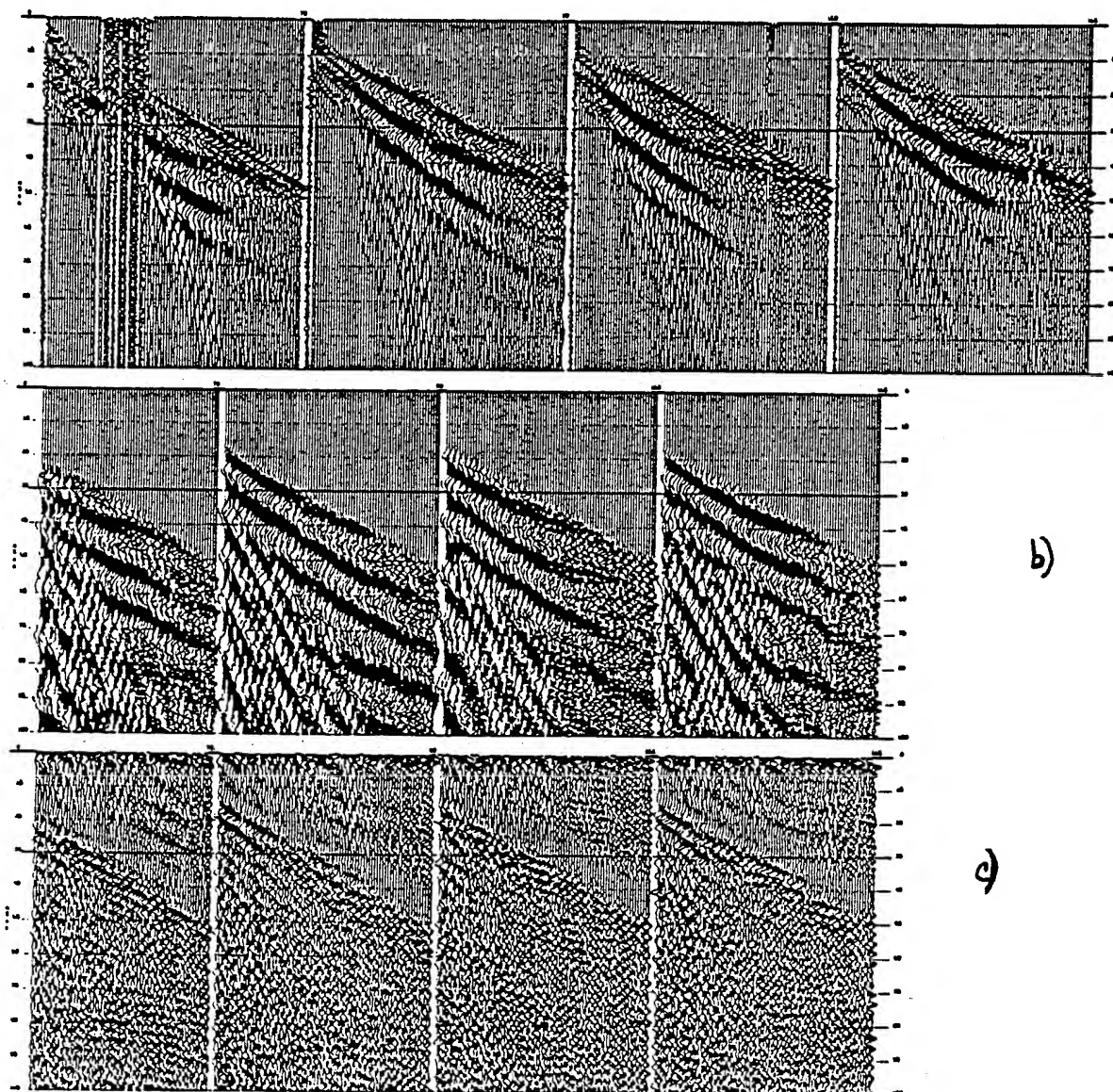


Figure 7. Shot gathers from various location on lines 3 and 4. (a) Unprocessed files, (b) first arrival muted files, and (c) filtered files.

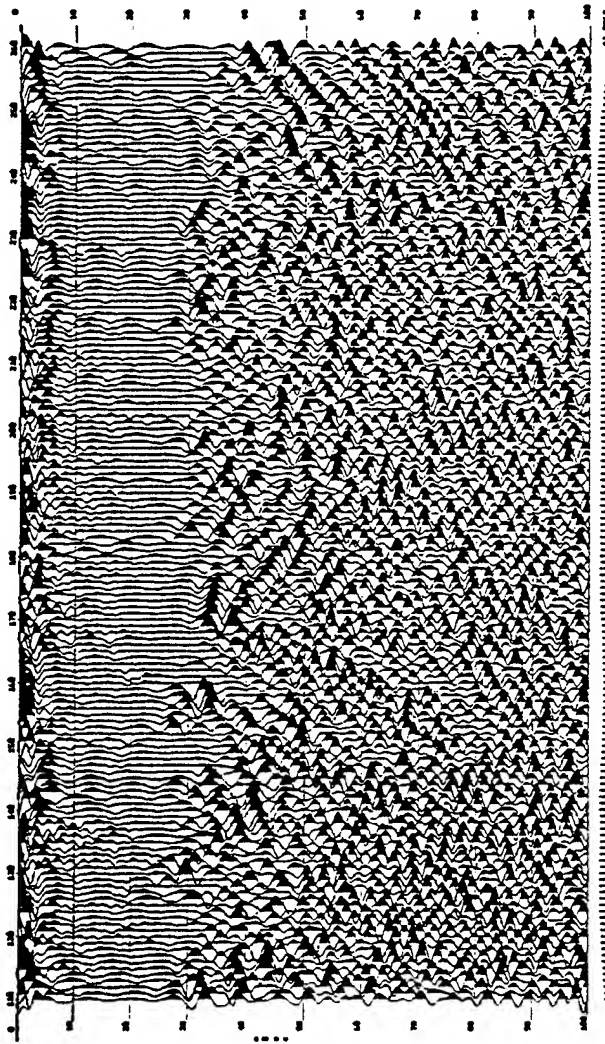


Figure 8. CDP stacked section from line 3. Some indication of reflection from 50 msec exist across the line. The effects of the large pumping well and road bank/trees are evident at CDP 170 and 260.

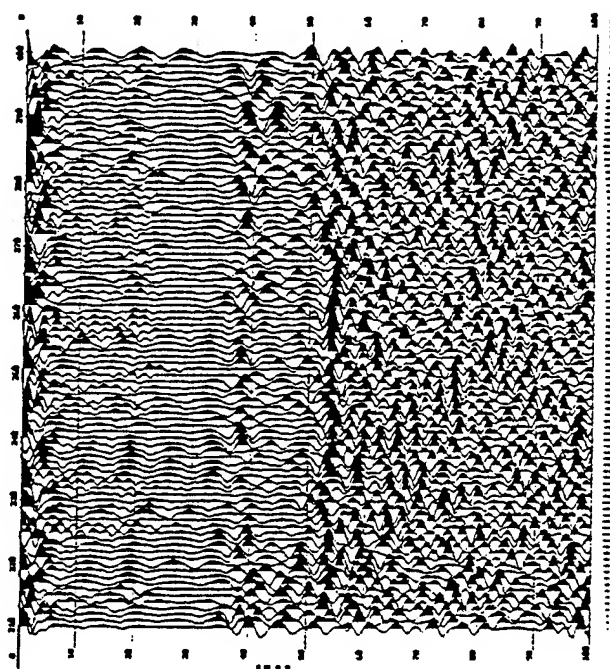


Figure 9. CDP stack of line 4. The effects of the road bank/trees evident on line 3 can be observed here at CDP 310. The signal-to-noise is much better on this line. The 50 msec bedrock reflection is easily interpretable with the base of the clay also visible across most of the line.

TABLE 1

format from SEG2 to KGSSEGY

preliminary editing

trace balancing

first arrival muting

surgical muting

assign geometries

sort into CDPs

velocity analysis

spectral analysis

surface consistent statics

residual statics

digital filtering

secondary editing

CDP stack

amplitude normalization

display

Table 1

Processing flow for CDP stacked data in Figure 5. Parameters were determined by analysis of each prior step as well as through iterative analysis of particular operations.

V. CONSTRUCTION PROJECTS AND EQUIPMENT PURCHASES

Field Equipment

Considerable construction and assembly of equipment has taken place during every year of this project. An additional complete bladder sampler was constructed the first year as a backup to the first. This would allow uninterrupted sampling in case the first one should sustain damage (which it did). We traveled to Otis Air Force Base on Cape Cod, Mass. to demonstrate our bladder sampler to the USGS, June 9-14, 1991. The sampler performed well there and has received a lot of attention nationally. The continued consistent performance of our bladder sampler is very significant in that we can reliably obtain the samples needed for the characterization of the hydraulic conductivity distribution in coarse sand and gravel formations.

A portable field trailer (commercial travel trailer) has been outfitted to handle our equipment for all standard field work. This will take the place of the field laboratory structure that was originally proposed. We felt this portable field unit would give us much more flexibility. The field trailer was invaluable during the bromide tracer test when sampling was done at all hours of the day and night.

A new highly accurate and flexible IEEE-488 bus-based data acquisition system (including hardware and software) has been obtained and an interface has been constructed for our pressure transducers. This system is much more interactive with the user through a personal computer and, makes our hydraulic data acquisition easier and more efficient.

Our research indicates that the air driven jackhammer is the preferred method of driving the sampler, so we obtained a used air compressor and jackhammer for all future sampling. The jackhammer has also proved to be an excellent method of installing the multilevel samplers for the bromide tracer test.

Pumping and developing two inch wells is a difficult operation without the correct equipment. Until recently, few methods were available for that purpose except air lifting, jet pumps (with their inherent difficulty in priming), hand bailers, and surge blocks. We have obtained two items that make this work much easier. The first is a PVC hand pump capable of yielding a few gallons per minute. It comes in five foot sections and can be screwed together for whatever depth is needed. The second item is a Grundfos submersible pump which will go down a two inch well and pump at up to nine gallons per minute at shallow depths. It is powered by a converter which runs on 220 AC volts. The converter produces variable frequency voltage to power the pump which means the

pump can be run at variable rates. We have found the pump to be very valuable at GEMS; it produces its full rated flow at maximum rpm and can be readily adjusted to lower rates.

Several additional pieces of field equipment have been constructed. One of these is a portable grout machine for making a water impermeable seal between the well casing and the wall of the hole. This grouting is necessary for two reasons. First, most state regulations require it to prevent surface contamination of the aquifer. Second, the hydraulic tests that we perform require a good seal if we hope to measure the true aquifer permeability and not some permeability of the bore hole. In past years, we have done this grouting with the full drill rig and that has prevented the timely grouting of some wells (they have stood open for up to four weeks). With this new portable system, the grouting can be done in less than an hour or two after drilling the hole. Another piece of equipment we have constructed allows slug testing directly through the center of hollow stem auger flights while drilling. We constructed this equipment because it seemed that sometimes a well skin was being developed around the well in the process of drilling and completing it. With this arrangement, a screened section of casing is driven ahead of the auger flights into virgin aquifer material and a slug test performed there. The only disturbance is due to driving the pointed two inch casing into place. This procedure gives us the best chance of testing relatively undisturbed aquifer material in situ. Another piece of constructed equipment was a tripod for lowering equipment down a well. The equipment to be lowered typically is a pump or packer on the end of pump rods or cable. The tripod is powered by an electric winch that runs off car batteries and is highly controllable. It was designed to easily raise and lower equipment weighting about three hundred pounds or less (in testing, it could lift around nine hundred pounds at its upper limit). At the GEMS site, where shallow depths are the rule, we do not need this much lifting power except when working with larger pumps in four inch or larger diameter holes, as we did in the bromide tracer test.

An additional piece of equipment we acquired is an ultrasonic level indicator for directly measuring the water level in a well. Traditionally, we use pressure transducers to infer what the water level is by measuring the pressure. However, when the water column is moving or accelerating the pressure may not give a correct indication of the water level due to inertial effects. In coarse sand and gravel aquifers, such as at GEMS, the water velocity in the well casings during slug tests can be high, so these effects can be pronounced. With this piece of equipment we have an independent check of the water level which is compared to the pressure transducers.

In year two of this project new larger diameter auger flights were purchased. Our previously owned auger equipment would only allow the installation of 2 inch wells. This is a great restriction in terms of the usefulness of the well. The smaller wells are generally fine for observation only situations. However, if the well needs to be pumped the small diameter puts severe restrictions on the capacity. We purchased 75 feet of 6 1/2 inch ID and 10 inch OD auger flights. This allows augering to bedrock at the GEMS site. Wells drilled with these new auger flights will accept 4 inch well casings. Larger pumps and more instrumentation can be put down these wells, as was needed for the bromide tracer test.

New survey equipment, including a transit, tripod, measuring tape, and tape stretcher has been acquired. Older KGS survey equipment, which we had been using, failed and needed to be replaced. The new equipment allows two axis angles to be measured in addition to elevations. With this equipment we have been able to produce a map to scale of the GEMS site showing the locations of wells. This map can be found in section IV.A.

Two field pressure transducers failed in year two and had to be replaced. Repair would have been near the replacement price, so new improved versions were obtained at a good price by trading in the old ones. The new transducers have desiccant chambers to remove moisture which may enter through the surface vent tube.

A portable digital borehole logging system for small-diameter boreholes (.05 m ID or larger) was purchased from Century Geophysics by the Kansas Geological Survey during grant year 92-93. Money from this grant was used as part of the payment for the logging system. The system consists of a surface unit, which is essentially a weatherized 386 IBM-compatible laptop computer; an electrical winch, steel cable, and tripod; and two downhole probes. The two probes are a focused induction probe (four coil focused conductivity) for electrical conductivity measurements and a probe for measuring the temperature and conductivity of the borehole fluid. Note that both probes also have a natural gamma detector (employing a Na(Tl) scintillation crystal) for measuring the natural radiation in the subsurface and each probe performs all digitizing downhole prior to signal transmission to surface unit. Also note that the induction probe is designed so that measurements are essentially unaffected by fluid or plastic casing in the well. Use of this unit at GEMS is discussed in Sections IV.G and H of this report.

The single well tracer test work described in section IV.H required a mechanism to pump 2 inch PVC wells at high volumes (30-45 gal/min). It was determined that an air lifting arrangement would perform satisfactorily. Therefore, a 3 HP 230 volt air compressor was purchased. This compressor performed well and was used for the

remediation phase of the single well tracer test work, as well as for development operations on the larger diameter holes drilled for the bromide tracer test.

The work of section III.D dealing with nonlinear slug tests reveals that the response of these nonlinear slug tests depends on the magnitude of the initial slug. The initial slug is usually placed on top of an inflated and closed packer. The packer is then opened and the response measured versus time. There is a continuing question of how important the packer is in all this. We wonder if some of the nonlinearity is due to frictional forces in the packer flow-through pipe. This pipe is the smallest diameter in the system and could be a significant agent of nonlinear head loss. To investigate this possibility we have built an alternate system of inducing slug tests using either pressurized gas (nitrogen) or a vacuum. Since the packer is absent, we can compare data from the same well with and without the packer to see if there is a significant difference. In building this apparatus it was necessary to buy a gas pressure transducer and a high accuracy gas pressure test gauge. Together, these allow the gas or vacuum pressures applied to the well to be measured very accurately. This system is operational and has been used to collect data twice in the field. However, the data analysis is very preliminary and additional field work needs to be done.

A major focus of the effort during project year three was to design and perform a tracer test at GEMS. This required numerous purchases and construction projects. The area at GEMS chosen for the tracer test is north of nest 00 and the array is oriented a little west of the north-south line (see section IV.A) approximately along the local groundwater gradient. This area was a bit lower than other areas and it tended to be wet for a considerable time after rains. We were concerned about our ability to develop the site for the tracer test in its original state. Therefore, we spent \$3000 on site preparation, bringing in fill dirt and large gravel. This expenditure was split between state and federal funding. The site is now accessible in almost all weather for light vehicles and can be accessed with heavy equipment soon after rains.

In performing the bromide tracer test, it was necessary to inject bromide tracer into the injection well under constant head conditions throughout the screened area. We injected the bromide spiked water from the surface, which allowed the water to free fall and build up velocity head. Earlier work had shown us that this led to higher head at the top of the screen which decayed rapidly with depth. To insure that this velocity did not build up, we built a velocity diffuser. The diffuser consisted of a 4 inch PVC casing 4-5 feet long filled with coarse gravel. Measurements in the well during injection showed that it was very effective in creating a constant head condition throughout the screened area.

We manufactured 24 MLS well casings to be used in the bromide tracer monitoring array. Over 25,000 feet of 1/4 inch polyethylene tubing was used in constructing the 24 samplers and about 1680 feet of 1 1/4 inch PVC casing. Each MLS well has 17 ports connected to the surface by 1/4 inch polyethylene tubing. All seventeen of these tubes must be threaded (a difficult task) through each section (10 foot standard length) of PVC casing. There are two kinds of MLS wells as detailed in Figure 1; one has two feet spacing between ports (regular) and one has one foot spacing between ports (detailed). The regular samplers contain 5 ports in each of the first three sections of casing and 2 ports in the fourth section. The detailed samplers have 9 ports in the first section and 8 in the second section. These section divisions are shown in Figure 1. Originally, the 1/4 inch tubing was cut 5 feet longer than shown in Figure 1, for the purposes of construction. The color sequence for the 1/4 inch tubing is a mirror image around port location 8; this was done to make the most efficient use of material from 500 foot reels.

The 1/4 inch tubes run through the center of the 1 1/4 inch casing and come out the side of the casing to form ports periodically (every 2 feet for regular samplers and every 1 foot for detailed samplers). These ports are formed by about 3 inches of the 1/4 inch tubing protruding from the larger casing and tied to it with two stainless steel wires. The tubing has been cut at approximately a 45 degree angle and the end covered with a screen material consisting of a piece of nylon hose. The screen material is held in place by the two stainless steel wires which also secure the port to the larger casing. Figure 2 shows the details of a typical port in a schematic way.

After the hole has been drilled, an MLS well casing is lowered into place. The regular MLS well casings were cut back to 38 feet above the top port. The detailed MLS well casings were cut back to 53 feet above the top port. Generally, this left about a foot or less of 1 1/4 inch PVC casing sticking out of the ground. The 1/4 tubing was cut back to a convenient length (about 14 inches above the top of casing) and permanently labeled three ways to avoid confusion: First, the tubes are uniformly color coded for depth (as shown in Figure 1); Second, they are marked with a sequential port number (also shown in Figure 1); and Third, they are labeled with the depth below top of casing (also shown in Figure 1). The marking are done with a permanent marker and covered with clear heat shrink tubing for durability. For completion, the well tops are covered with 2 inch PVC casing using a water tight neoprene connector between the 1 1/4 inch and 2 inch PVC casings. All 24 MLS well casings have been manufactured and installed at the GEMS site. The bromide tracer array is made up of 23 of these multilevel samplers.

We purchased two ten-channel peristaltic pumps for pumping each of the 17 ports of each MLS well. This means that all ports on a given well can be pumped simultaneously. After the ports have been developed properly and are yielding 150 ml/min or more (all except approximately 5 out of 408 have been successfully pumped), it should be possible to sample one well completely in approximately 10 minutes allowing for sample storage and changeover time to the next well. During the bromide tracer test it was necessary to sample all affected wells many times during the duration of the tracer test. This necessity made it imperative that we be able to complete sampling a given well in as little time as possible. This was the justification for buying two multichannel peristaltic pumps. To further improve our sampling efficiency we built a cart to hold the pumps, the associated tubing, and the sample bottles. This cart is on wheels and can easily be pushed from one well to the next. The full sample bottles can be unloaded quickly from the sample bottle shelf and it can be reloaded with empty sample bottles rapidly. This sampling arrangement was very successful during the tracer test, we were able to average 10-12 minutes per well for complete sampling. Almost 6000 samples were collected for analysis in an efficient manner.

Approximately 1800 sample vials (50 ml) were purchased to hold the water samples until the analyses could be made. Trays and boxes to hold these vials were also fabricated. Typically a box would hold either 100 or 150 samples. This made for easy storage and transport to and from the field.

Laboratory Equipment

The following additions to laboratory capability were added in the first year of this project. A laboratory pressure standard was constructed to calibrate all pressure transducers (both field and laboratory) and establish their accuracy. A laboratory grade power supply was obtained to supply voltage to pressure transducers and other laboratory equipment. Three new laboratory pressure transducers were acquired to replace some older ones that have or will fail. Miscellaneous small hand tools were also acquired so that tools were not shared between field and laboratory activities. A vacuum pump was obtained to help in sample resaturation (accurate determination of hydraulic conductivity requires that the samples be as free of air as possible). The laboratory apparatus for measuring hydraulic conductivity on cores was upgraded for greater accuracy by adding digital temperature measurement and a caliper for measuring water levels in the manometers.

During year two of the project the laboratory apparatus for measuring hydraulic conductivity on sand and gravel cores was upgraded for greater efficiency and the

number of stations was doubled to eight. We had a backlog of sand and gravel samples to be run in the laboratory. During this grant period it was decided that the number of sample stations should be doubled from four to eight. In the process of doing this several changes were made to allow greater efficiency. Several valves were added to make each sample station relatively independent of the others. That way each sample can be mounted or dismounted as needed. Ten new laboratory pressure transducers were acquired to replace some older ones that have or will fail and to expand the system by four stations.

Equipment to measure the hydraulic conductivity of low permeability samples, such as silt and clay, was acquired. This equipment allowed us to measure the hydraulic conductivity of silt and clay samples that were acquired in year two from the upper 35 foot portions of four cored wells. In addition we saved some samples from the lower 35 foot region of sand and gravel that had a significant percentage of fine material. These samples were obtained with the bladder sampler in the lower region, but would not flow significantly when mounted in our permeameter designed for sand and gravel samples. Therefore, these sample have been run on this apparatus. The flexible wall permeability cell handles sample sizes up to 4 inches in diameter. We obtained the necessary equipment to run samples of diameters 1.38 inches and 2.5 inches. The system also includes a triaxial permeability panel for accurate measurement of volume changes and flow rates with regulators and pipettes. In addition, the system has digital transducer readout with an RS-232 serial port for computer interface. It was set up and the appropriate supply lines such as air and water were run. During the last period of the grant it has been used extensively to measure hydraulic conductivity of low permeability samples and the results are shown in section IV.B.

An electronic function or signal generator and combination frequency counter was obtained to calibrate our flow meter. The flow meter is capable of being used in several different pipe sizes. However, it has to be calibrated for each one. For any of the hydraulic tests where accurate flow rate measurement is essential, the flow meter is an important piece of equipment. This purchase allows us to quickly and accurately calibrate the flow meter. Previously, we had borrowed calibration equipment from another group at KGS.

Near the end of the 92-93 grant year, a portable water quality monitoring system for use in the field (surface and .05 m and greater ID boreholes) and laboratory was purchased from SOLOMAT Neotronics with funds from this grant. This system consists of a data logger and five sensors for measuring various water quality parameters. The sensors purchased were a combination bromide ion selective electrode, a temperature-

compensated galvanic dissolved oxygen probe, a pH/temperature combination epoxy electrode, and two 1.0 K dip conductivity probes. Note that each sensor and attached cable can be placed down a well and completely submerged to water depths of up to 15 meters. This system was extensively utilized in the field and laboratory during the third year of this project.

Six pairs of ion specific electrodes (ISE) and reference electrodes have been purchased for rapid analysis of the water samples for the bromide tracer test. A device for holding 5 of the electrode pairs and efficiently inserting them simultaneously into 5 sample vials was built. The output from the electrodes was measured by a data logger. In this way, we were able to measure the bromide concentration of 5 samples simultaneously. Using this method we were able to keep up with the field sampling, generally having the analysis results within 24 hours of the collection time.

Computer Laboratory

A computationally intensive project like this one needs the benefit of state-of-the-art computers. A computer laboratory has been set up to give access to the computers for both research and teaching. We acquired various machines throughout the duration of this project to upgrade our computing capabilities. The laboratory currently contains six computers: two 486 machine running at 66 MHz (easily upgradable to Pentium technology), two 486 machines running at 33 MHz, and two 386 machines running at 25 MHz. Some of our older 286 and 386 machines have been removed from the computer lab and have been used in the field or permeability lab for data acquisition. In the computer lab a network for printer sharing has been set up so that every computer has access to a high quality laser printer. Two Hewlett Packard laser printers and a Hewlett Packard Scanjet IIC scanner are available in the computer laboratory. In addition, a Power Macintosh machine is available in the office of the PI and a 486 machine running at 33 MHz is used in the office of the CoPI. An Apple IICI is also available in another office. Each computer is connected to our mainframe computer (Data General machine) either by direct cable or through an Ethernet card. In this way, each computer can act as a terminal into the mainframe and information can be shared between all systems. The computers with Ethernet cards are attached to the University Ethernet Backbone network. This connection allows direct access to the Internet and many other computing networks across the US. Miscellaneous software has been purchased to allow the computers to function efficiently or perform specialized tasks.

The computer laboratory is used by our research group and other geohydrology graduate students. The computer laboratory allows hands-on computer training for

geohydrology graduate students through formal class work. We continue to teach two classes (Physics 727/Geology 771, Finite Element Methods, and Physics 727/Geology 771, Finite Difference Methods), which greatly utilize the laboratory. In addition, we have made the laboratory available for other computer oriented classes taught by other hydrogeology faculty members. We expect this computer laboratory to continue to be a valuable asset to our research and graduate education in geohydrology.

Figure 1.
Polyethylene Tubing Detail
Multilevel Sampler Construction

Regular MLS Depth Below Top of Casing	Port number and Color		Detailed MLS Depth Below Top of Casing	
70 feet	First Section	1. Natural	First Section	70 feet
68 "		2. Black		69 "
66 "		3. Blue		68 "
64 "		4. Green		67 "
62 "		5. Orange		66 "
60 "	Second Section	6. Red		65 "
58 "		7. Yellow		64 "
56 "		8. Natural		63 "
54 "		9. Yellow		62 "
52 "		10. Red	Second Section	60 "
50 "	Third Section	11. Orange		59 "
48 "		12. Green		58 "
46 "		13. Blue		57 "
44 "		14. Black		56 "
42 "		15. Natural		55 "
40 "	Fourth Section	16. Natural		54 "
38 "		17. Natural		53 "

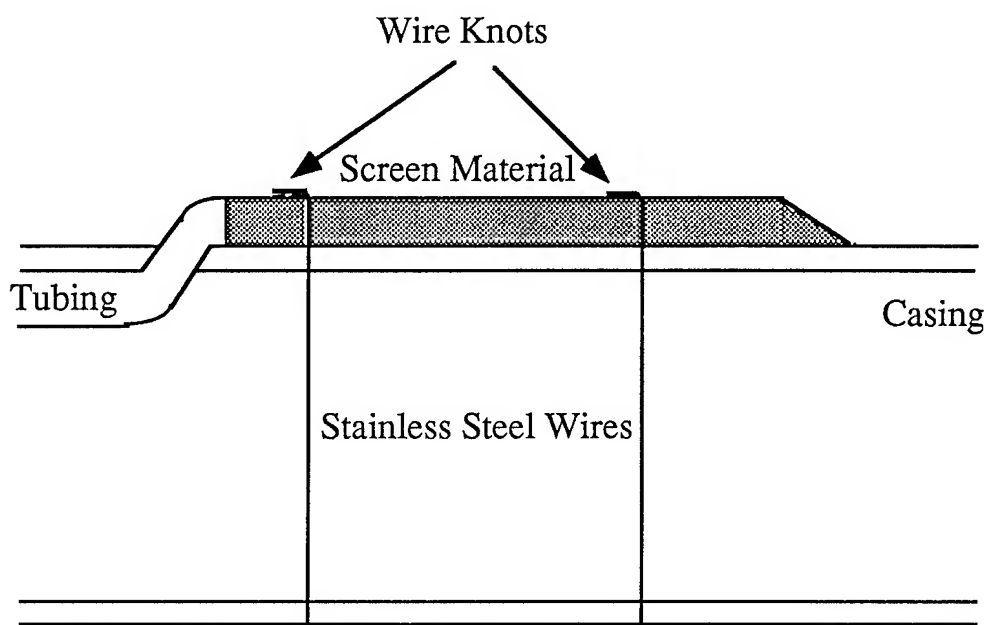


Figure 2. MLS Sampler port detail.

VI. PERSONNEL AND PRODUCTIVITY ISSUES

A. PUBLISHED AND PLANNED PAPERS

Published Papers

The following five papers were published or accepted for publication during the grant period by peer-reviewed journals and the complete text of each is contained in Appendices A-E.

- McElwee, C.D., Bohling, G.C., and Butler, J.J., Jr., 1995, Sensitivity analysis of slug tests: Part 1, the slugged well: *Journal of Hydrology*, v. 164, pp. 53-67.
- McElwee, C.D., Butler, J.J., Jr., Bohling, G.C., and Liu, W.Z., 1995, Sensitivity analysis of slug tests: Part 2, Observation wells: *Journal of Hydrology*, v. 164, pp. 69-87.
- Hyder, Z., Butler, J.J., Jr., McElwee, C.D., and Liu, W.Z., 1994, Slug tests in partially penetrating wells, *Water Resources Research*, v. 30, no. 11, pp. 2945-2957.
- Butler, J.J., Jr., Bohling, G.C., Hyder, Z., and McElwee, C.D., 1994, The use of slug tests to describe vertical variations in hydraulic conductivity: *Journal of Hydrology*, v. 156, pp. 137-162.
- Butler, J.J., Jr. and McElwee, C.D., and Liu, W.Z., 1995, Improving the reliability of parameter estimates obtained from slug tests: accepted for publication in *Ground Water*.

The following eight abstracts of papers given at professional meetings dealing with our DoD sponsored work were published during the grant period. The material also exists as KGS open file reports.

- Bohling, G.C., Hyder, Z., Liu, W.Z., Butler, J.J., Jr., and McElwee, C.D., 1991, A numerical model of slug tests in layered geologic systems: *Eos, Trans. Amer. Geophys. Union*, v. 72, no. 44, p. 146. Also KGS Open-File Report no. 91-62, 22 pp.
- McElwee, C.D., Butler, J.J., Jr., Bohling, G.C., and Liu, W.Z., 1991, The use of observation wells with slug tests: *Eos, Trans. Amer. Geophys. Union*, v. 72, no. 44, p. 220. Also KGS Open-File Report no. 91-63, 32 pp.
- McElwee, C.D. and Butler, J.J., Jr., 1992, Effective transmissivities from slug tests in wells with a skin: *Eos, Trans. Amer. Geophys. Union*, v. 73, no. 14, p. 126. also KGS Open-File Report no. 92-12, 21 pp.
- McElwee, C.D., Butler, J.J., and Bohling, G.C., 1992, Nonlinear analysis of slug tests in highly permeable aquifers using a Hvorslev-type approach: *Eos, Trans. Amer. Geophys. Union*, v. 73, no. 43, p. 164. also KGS Open-File Report no. 92-39, 22 pp.
- Bohling, G.C., 1993, Hydraulic tomography in two-dimensional, steady-state groundwater flow: *Eos, Trans. Amer. Geophys. Union*, v. 74, no. 16, p. 141. also KGS Open-File Report no. 93-17, 24 pp.

McElwee, C.D., Zenner, Z., Butler, J.J., Jr. and Bohling, G.C., 1993, Unified analysis of slug tests including nonlinearities, inertial effects and turbulence: *Eos, Trans. Amer. Geophys. Union*, v. 74, no. 43, p. 235. Also KGS Open-File Report no. 93-45, 23 pp..

Huettl, T.J., Butler, J.J., Jr., and McElwee, C.D., 1993, A borehole induction single-well tracer test to characterize spatial variations in aquifer flow properties: *Eos, Trans. Amer. Geophys. Union*, v. 74, no. 43, p. 319. Also KGS Open-File Report no. 93-48, 19 pp.

Butler, J.J., Jr. and McElwee, C.D., 1994, Improving the reliability of parameter estimates obtained from slug tests: *Eos, Trans. Amer. Geophys. Union*, v. 75, no. 16, p. 151. Also KGS Open-File Report no. 94-21, 29 pp.

Papers Submitted for Publication

The following papers have been or very soon will be submitted for publication in peer-reviewed journals.

Bohling, G.C. and McElwee, C.D., Hydraulic tomography in two-dimensional groundwater flow: has been submitted to *Water Resources Research*..

McElwee, C.D., Zenner, Z., Butler, J.J., Jr. and Bohling, G.C., Unified analysis of slug tests including nonlinearities, inertial effects and turbulence: to be submitted to *Water Resources Research*..

Papers Planned or in Preparation

The following papers are planned for future publication in professional journals. Currently they exist as informal Kansas Geological Survey Open File Reports.

Liu and Butler, A time-continuous numerical model for well tests in heterogeneous aquifers, *Journal of Hydrology*.

McElwee, C.D. and Butler, J.J., Jr., 1992, Effective transmissivities from slug tests in wells with a skin: KGS Open-File Report no. 92-12, 21 pp.

B. LIST OF PARTICIPATING PERSONNEL

McElwee, C.D.- PI, is a Senior Scientist at the Kansas Geological Survey (KGS) in the Mathematical Geology Section and is also an Adjunct Professor in the Geology and Physics Departments of the University of Kansas (KU).

Butler, J.J. Jr. - Co-PI, is an Associate Scientist at the KGS in the Geohydrology Section and is also an Adjunct Assistant Professor in the KU Geology Department.

Bohling, G.C. - Investigator, is a Research Assistant in the Mathematical Geology Section at KGS.

Macpherson, G.L. - Investigator, is an Assistant Professor in the KU Geology Department.

Miller, R.D. - Investigator, is an Assistant Scientist at the KGS and is the Chief of the Exploration Services Section of the KGS.

The following students have, at some time, been supported by this grant.

Mennicke, C.M. - was a student Research Assistant in the Mathematical Geology Section at KGS and is working on a Ph.D. degree in the KU Geology Department. She is currently employed by the Kansas Department of Health and Environment.

Huettl, T. - was a student Research Assistant in the Mathematical Geology Section at KGS and has finished (1995) a Master's degree in the KU Geology Department.

Hyder, Z. - was a student Research Assistant in the Mathematical Geology Section at KGS and has finished (1995) a Ph.D. degree in the KU Civil Engineering Department.

Beilfuss, M.L. - was a student hourly employee who was an undergraduate student in the KU Geology Department.

Orcutt, M. - is a student Research Assistant in the Geohydrology Section at KGS and is working on a Master's degree in the Architectural Engineering Department at KU.

Gonuguntla, S. - is a student Research Assistant in the Mathematical Geology Section at KGS and is working on a Master's degree in the Civil Engineering Department at KU.

The following students have contributed to this work in substantial ways, however they have not been primarily supported by this grant.

Liu, W. - is a student Research Assistant in the Geohydrology Section at KGS and is working on a Ph.D. degree in the KU Civil Engineering Department.

Zenner, M. - was a student Research Assistant in the Geohydrology Section at KGS and was working on a Ph.D. degree in the KU Civil Engineering Department.

C. INTERACTIONS WITH OTHER RESEARCH GROUPS

Professional Meetings Attended and Papers Presented

Carl McElwee and Geoff Bohling attended the Fall AGU (American Geophysical Union) meeting in San Francisco in December 91 and gave two papers.

James J. Butler, Jr. attended the 8th Annual Water and the Future of Kansas Conference and gave a paper on Hydrogeologic characterization of hazardous waste sites.

Carl McElwee attended the Spring AGU meeting in Baltimore in May 92 and gave one paper.

Carl McElwee attended the Fall AGU (American Geophysical Union) meeting in San Francisco in December 92 and gave a paper on the nonlinear analysis of slug test data.

Geoff Bohling attended the Spring AGU meeting in Baltimore in May 93 and gave a paper on hydraulic tomography.

James Butler attended the NGWA (National Ground Water Association) sponsored Outdoor Action Conference in Las Vegas in May 93.

Carl McElwee attended the National Convention of the National Ground Water Association, Kansas City, MO, Oct. 17-20, 1993.

Carl McElwee, Jim Butler, Terrance Huettl, and Zafar Hyder attended the Fall American Geophysical Union (AGU) meeting in San Francisco in December 1993 and gave three papers.

Jim Butler attended the Spring AGU meeting in Baltimore in May 1994 and gave one paper.

USGS trip to Otis Air Force Base

Carl McElwee traveled to Otis Air Force Base on Cape Cod, Mass. to demonstrate our bladder sampler to United States Geological Survey (USGS) researchers, June 9-14, 1991. There are a number of pollution problems at the base, our work was involved with a study of a sewage plume (LeBlanc, 1984; Hess and LeBlanc, 1987). Kathryn Hess of the New England District of the USGS Water Resources Division organized and supervised the field tests. Our sampler and the Waterloo sampler were compared in a variety of situations. Our sampler performed well there and has received a lot of attention nationally. At deeper depths, where heaving is a problem and recovery is

difficult, our sampler performed consistently. It seems that this bladder sampler can be very useful in a variety of situations where samples are needed to characterize the hydraulic conductivity distribution in coarse sand and gravel.

University of Nebraska

Dr. Vitaly Zlotnik is the leader of a research group working on well testing at the University of Nebraska at Lincoln. Jim Butler and Carl McElwee have had numerous discussions throughout the grant period with Dr. Zlotnik and his graduate students on various issues related to slug tests in alluvial aquifers. Jim Butler traveled to the University of Nebraska at Lincoln to give an invited talk and to meet with researchers in hydrogeology, Jan. 31 - Feb. 1, 1992. The talk, entitled "Well testing in heterogeneous formations", was part of the T. Mylan Stout Lecture Series in the Dept. of Geology. Carl McElwee gave an invited talk, as part of the same seminar series, on his recent work involving nonlinear slug test analysis on Feb. 18, 1994.

Sabbatical at the University of Birmingham, England

Carl McElwee worked at the University of Birmingham with Dr. K. R. Rushton and his Groundwater Research Group for four months, while keeping in close contact with the group and research here at the Kansas Geological Survey by e-mail. Dr. Rushton's book *Seepage and Groundwater Flow* published by John Wiley and Sons, Inc. in 1979 is a well respected treatment of groundwater modeling. He is known for his wide ranging applications of models to real world problems. Currently, there are eleven professionals in the Groundwater Research Group at the University of Birmingham. Dr. Rushton and this group continue to have an active research program that incorporates projects throughout the United Kingdom and the world. Dr. Rushton has done much work involving hydraulic testing for aquifer parameters and did some of the early work in looking at heterogeneities through hydraulic testing. It was a valuable experience allowing interaction with a number of groundwater professionals and graduate students having a variety of experience and interests on the issue of heterogeneity.

TNO Institute of Applied Geosciences, The Netherlands

Carl McElwee traveled to the TNO Institute of Applied Geosciences in The Netherlands Dec. 5-9, 1994 to demonstrate our bladder sampler and to consult on coring in unconsolidated aquifers. The bladder sampler worked very well in the tests and was loaned to investigators in the Geo-Hydrology Department of TNO for use in coring nine wells. They needed pristine samples at various depths to do a detailed characterization of the geochemistry. The Dutch have

used the sampler at greater depths (up to about 125 feet) than we have and it still seems to work well.

D. TEACHING ACTIVITIES

In conjunction with the tracer test work, we taught a graduate seminar course entitled Dispersivity and Tracer Tests at GEMS (Geol 791, Spring 1994) for 3 hours credit. We had 3 students sign up for credit. However, numerous students and permanent staff at KGS audited the course. The classroom portion of the course consisted of reviewing the groundwater literature on various aspects of tracer tests, while the field portion consisted of constructing and installing multilevel sampler well casings. Field Hydrogeology (Geol. 572) was also taught during the fall of 1992. Much of the teaching field work was done at the GEMS site.

The computer laboratory has been used by our research group and other hydrogeology graduate students throughout the grant period. The computer laboratory allows hands-on computer training to hydrogeology graduate students through formal class work. We have taught two numerical modeling classes, Finite Difference Methods (Fall semesters) and Finite Element Methods (Spring semesters), throughout the grant period. In addition, we have made the laboratory available for other computer oriented classes taught by other hydrogeology faculty members. We expect this computer laboratory to continue to be a valuable asset to our research and graduate education in hydrogeology.

VII. SUMMARY OF PROJECT RESEARCH AND OUTLOOK FOR FUTURE RESEARCH

A. SUMMARY OF PROJECT RESEARCH

A considerable amount of equipment was purchased, constructed and assembled each year of this project in order to support the research effort. The first year this equipment included an additional bladder sampler, a trailer mounted air compressor and jack hammer for driving the core sampler, a laboratory calibration system for pressure transducers, a portable field trailer, a tripod and winch system for moving equipment into and out of a well, and interfaces for data acquisition equipment. The purchased equipment for the second year included new pressure transducers for field and laboratory use, a permeameter for the measurement of the hydraulic conductivity of low permeability samples, a portable water quality monitoring system for use in the field and laboratory, new large diameter auger flights for drilling larger diameter monitoring wells, new surveying equipment, a portable digital borehole logging system for small-diameter boreholes, and additional computer equipment. A considerable number of lesser items for field and laboratory use was also constructed and assembled at the Kansas Geological Survey during the second year of this project. During the third year the purchased equipment included a high capacity portable air compressor for pumping small-diameter wells, two 10-channel peristaltic pumps for water-quality sampling, and three additional computers for data processing and analysis. Again, a considerable amount of equipment for field and laboratory use was also constructed and assembled during the third year of this project. The constructed equipment included a field cart to hold the peristaltic pumps and associated equipment during sampling, and a well-head apparatus for the performance of pressurized slug tests. In addition, as a result of the prolonged water logging of GEMS that occurred due to the heavy rains in the spring and summer of 1993, access to all portions of GEMS was significantly improved during this year. Fill dirt was added and the site was leveled and covered with gravel to provide an all-weather surface.

A major focus of each year of this project was on the use of well tests to describe spatial variations in hydraulic conductivity. This research on well tests in heterogeneous formations had both theoretical and field components.

The theoretical work was directed at developing a better understanding of the type of information that can be obtained from well tests in heterogeneous units. The technique of sensitivity analysis was used to give guidelines for designing effective slug tests and was employed to study the form of the effective parameters obtained from slug tests in

wells surrounded by a finite-radius zone of low permeability (well skin). These effective parameters are shown to be heavily influenced by the properties of the well skin. We have developed an empirical formula for the effective transmissivity obtained from a slug test in the presence of a skin that appears to be quite general. In particular, the formula seems to provide very good estimates of the parameters obtained from analyses employing the Hvorslev (1951) or Cooper et al. (1967) models. Clearly, however, analysis of slug tests in the presence of a skin is a very difficult problem and will require maximum effort to obtain good results. Finally, sensitivity analysis was used for the detailed analysis of slug tests with observation wells. This analysis showed that the use of observation wells in slug tests can significantly improve the reliability of the estimated parameters.

Since traditional modeling techniques are of limited effectiveness for the analysis of well-test data from wells in heterogeneous formations, a new numerical model, which is continuous in time and employs an approximate representation of flow in the well bore, was developed. This model incorporates the effects of partial penetration, anisotropy, finite-radius well skins, and upper and lower boundaries of either a constant-head or an impermeable form. Initially, this model was used in a detailed study of slug tests in layered aquifers. The results of this study help delineate the conditions under which multilevel slug tests can be used to provide accurate information concerning the vertical variations in hydraulic conductivity along the well bore. This model was also employed to develop a series of dimensionless plots that can be utilized by field practitioners to assess the amount of error introduced into parameter estimates through use of a particular method for data analysis. If it appears that conventional approaches will not provide acceptable parameter estimates for a test in a particular configuration, the semianalytical solution developed here can be used to analyze the response data.

Several theoretical investigations of pulse-test methods were carried out during the grant period. One investigation involved the application of the principles of tomography, which has proven to be a valuable technique for imaging heterogeneous material using various forms of wave energy, to the characterization of spatial variations in flow properties. Pressure pulses in a groundwater system are diffusive in nature and are generally exponentially attenuated with distance (sometimes called the slow wave), so the range of investigation will be smaller than for systems in which the pressure pulse travels as a propagating wave. Initial results of our work appear promising for some simple models. The basic configuration of the hydraulic conductivity distribution can be successfully estimated for simple models with low levels of noise. However, additional work is needed to fully assess the potential of this method. Another theoretical

investigation of pulse tests employed a sinusoidally varying signal to investigate a simple two-zone aquifer separated by a linear boundary. Five parameters are required to completely describe this system. Due to correlations between parameters, it is difficult to determine all five parameters simultaneously. However, one to three parameters can usually be determined when given appropriate response data at selected observation locations. Both analytical and numerical approaches were explored in an attempt to assess whether discrete zones in heterogeneous formations could be characterized with pulsing (in this case sinusoidally varying) signals. There were two major results of this work: 1) a sinusoidal signal generated at a central well can be transmitted quite large distances relative to the dimensions of most sites of groundwater contamination, and 2) the sinusoidal signal can be analyzed for amplitude and phase to yield some useful information about heterogeneities, in particular the location of fairly discrete boundaries. Although at this point the capabilities of hydraulic tomography and pulse testing are unknown, they clearly deserve further investigation.

The major field component in the early part of this study of well tests in heterogeneous formations mainly concentrated on an assessment of multilevel slug tests in highly permeable alluvium. A prototype multilevel slug-test system, built at the KGS, was tested at GEMS. The results of the multilevel tests indicated that slug tests in the sand and gravel section at GEMS are being affected by mechanisms not accounted for in the conventional theory on which the standard methods for slug-test data analysis are based. The existence of these mechanisms were reflected by a concave downward curvature on log head versus arithmetic time plots, a dependence of slug-test responses on the magnitude of the induced slug (H_0), and systematic deviations between plots of the test data and the best-fit conventional models. In addition, late-time oscillatory behavior is seen at certain wells. Because of these observed deviations from conventional theories, we have developed a general unified model incorporating the effects of nonlinearities, inertia, viscosity, changing casing radii, and velocity distributions to explain the anomalous behavior observed at GEMS. Although the effects of viscosity and changing casing radii are negligible in most cases, the effects of nonlinearities, inertia, and velocity distributions can be quite important. Application of this model to several sets of data from slug tests at GEMS produced very promising results. Additional work is needed to clearly understand some of the physical processes underlying the model parameters. A program of multiwell slug tests (slug tests with observation wells) was initiated at GEMS during the second year of the research. The results of this program of field testing and a complementary theoretical analysis demonstrated that the assumption of a fully screened well can introduce a very large amount of error into parameter estimates determined from

response data at observation wells. A new analytical model, which allows partial penetration at both the stressed and observation wells, was developed. Application of this model to data from GEMS yielded parameters that were in keeping with the values obtained from the laboratory analysis of cores.

Although the slug test has the potential to provide very useful information about the transmissive and storage properties of a formation, considerable care must be given to all phases of test design, performance, and analysis if the potential of the technique is to be fully realized. In an attempt to improve the reliability of parameter estimates obtained from a program of slug tests, a series of practical guidelines for slug tests were proposed on the basis of the field and theoretical investigations of this research. Two very important points arise from this series of guidelines: 1) it is critical that a series of slug tests at a given well be performed in order to assess whether conventional theory is applicable (i.e. is there a dependence on initial head or mechanism of test initiation, is there a well skin that is developing during the course of testing, etc.); and 2) the analysis of the response data must be done using the most appropriate model and with considerable care.

In addition to the research on well tests in heterogeneous formations, a significant amount of the work throughout the grant period was directed at increasing our knowledge of the subsurface at GEMS. This work included hydraulic testing of wells in the aquifer and underlying bedrock at GEMS; a detailed study of the aqueous geochemistry of the alluvium and underlying bedrock; continued drilling and sampling activities; further modifications of the bladder sampler developed at the KGS; continued laboratory analyses of the cores obtained with the bladder sampler; a detailed wireline log survey; experimentation with a new single-well tracer test method that involves using a wireline logging system and an electrically conductive tracer to delineate vertical variations in hydraulic conductivity and porosity; and a detailed seismic survey. These characterization efforts, which continued throughout this project, were directed towards the development of a detailed picture of the subsurface at GEMS, so that we can better assess the results of the hydraulic and tracer tests that have been and will be performed at the GEMS site.

A major thrust of the work for the latter portion of the grant period involved preparation and performance of an induced-gradient bromide tracer test at GEMS in late summer and fall of 1994. Twenty-four multilevel sampling wells (17 sampling ports per well) were constructed and installed during an intensive field effort in the spring and summer of 1994. Sampling well locations were based on a theoretical investigation of appropriate designs for the tracer-test monitoring well array. The final design was a

compromise between theoretical considerations and operational logistics (e.g., the minimum well spacing dictated by the size of the drilling rig, etc.). The bromide tracer test began October 7, 1994 and continued until November 10, 1994, during which time approximately 6000 samples were collected and analyzed. Preliminary analysis of the data has been completed and has given us the most detailed picture of subsurface hydraulic conductivity to date. Valuable extensions of this research would include further processing of the bromide concentration data and conducting additional tracer tests to investigate issues of reproducibility and the influence of test format (dipole versus single well, forward versus reverse flow, etc.) on parameter estimates. To our knowledge, these issues of reproducibility and influence of test format have not yet been adequately addressed in the research community.

B. OUTLOOK FOR FUTURE RESEARCH

The network of 23 multilevel sampling wells at GEMS is an extremely valuable resource. This array will undoubtedly be used in the future for a variety of experiments aimed at developing a better understanding of flow and transport in heterogeneous media. The first experiment planned for the future will be a repeat of the tracer test reported here. In this repeat test, we will employ a sampling strategy, based on the results of the test reported here, that will allow us to get complete breakthrough data at all ports of interest. It will be very interesting to assess how reproducible the results will be between the two experiments. Additional possible future tests with conservative tracers could include interchanging the injection and discharge wells, introducing the tracer at the center of the network (TMO-1), and introducing the tracer into select vertical intervals. The array could also be used in the dipole mode (as opposed to single discharge well induced gradient tests) to see if similar hydraulic conductivity distributions are inferred from the dipole analysis. Future research also is planned with tracers of different chemical mobility and biological susceptibility in order to assess how biochemical processes are affected by formation heterogeneity. Clearly, this network of multilevel sampling wells that has been established as a result of this project should prove to be an excellent resource for future research and teaching activities in hydrogeology at the University of Kansas.

A major field and theoretical emphasis of this research was on slug tests. As reported previously, results of considerable practical significance were obtained through this work. However, there are still several areas of additional work that need to be pursued before the full potential of this technique can be realized. Areas of future work will include the use of slug tests to characterize the vertical component of hydraulic

conductivity, further investigations of the use of slug tests in wells with low-permeability well skins, and the use of slug tests in wells screened across the water table. Although the theoretical work on the unified nonlinear slug-test model presented here appears very promising, further field work is clearly required to fully understand the physical basis of the model parameters. An extensive series of field tests should be done in order to thoroughly assess model performance and parameter variation under a wide range of conditions. The completion of the field verification of this model would allow the slug test method to be extended to high conductivity aquifers and would be a very valuable asset to most practicing hydrogeologists. Many contamination sites occur in coarse sand and gravel aquifers and methods are needed for characterization of the hydraulic conductivity using slug tests, which are logistically preferable to other kinds of hydraulic tests.

In this research, we also examined pulse testing methods (both single pulses and sinusoidally varying signals) for delineation of lateral variations in flow properties. The limited theoretical analysis presented here indicates that these methods do hold promise. An extensive program of field testing, however, is clearly required. Only very limited field work has been done (not reported here) to show that pulsing signals can be reliably produced and propagated over significant distances at GEMS. The distance that the signal can be propagated will vary from site to site and depends on the storage properties at that site. At GEMS we have observed significant changes in amplitude due to changes in propagation direction, even after correcting for normal decay with distance. This implies that we are measuring amplitude changes due to aquifer heterogeneity. Thus, further theoretical and experimental work is clearly required to thoroughly assess the potential of the approach.

An important theoretical finding of this research was that hydraulic tomography appears to have considerable potential for the characterization of spatial variations in flow properties. Although the work on this technique is still in its initial phases, it is clear that this approach is worthy of an aggressive program of theoretical and experimental research. The network of multilevel sampling wells should prove to be an excellent resource for the field verification of this method.

Finally, as part of the site characterization activities complementing this research, a large data set was collected describing the spatial variations of hydraulic conductivity, porosity, and various grain-size parameters on the scale of a small core. A detailed geostatistical analysis of these data is clearly required in order to better understand the nature of spatial variations in heterogeneous alluvium.

VIII. REFERENCES

- Allen, J.R.L., 1965, Fining-upward cycles in alluvial successions: *Geological Jour.*, v. 4, pp. 229-246.
- Amos, D. E., 1986, Algorithm 644, a portable package for Bessel functions of a complex argument and nonnegative order, *ACM Transactions of Mathematical Software*, v. 12, no. 3, pp. 265-273.
- Archie, G.E., 1942, Electrical resistivity log as an aid in determining some reservoir characteristics: *Trans.*, AIME 146.
- Baker, S.R. and Friedman, G.M., 1969, A non-destructive core analysis technique using x-rays: *Jour. Sed. Petrology*, v. 39, no. 4, pp. 1371-1383.
- Barker, J.A. and Herbert, R., 1992, A simple theory for estimating well losses: With application to test wells in Bangladesh: *Applied Hydrology*, pp. 20-31.
- Bateman, R.M., 1985, *Open-Hole Log Analysis and Formation Evaluation*: IHRDC, Boston, MA, 647 pp.
- Bear, J., 1972, *Dynamics of Fluids in Porous Media*: American Elsevier Publishing Co., Inc., New York, pp. 182-184.
- Birkelo, B.A., Steeples, D.W., Miller, R.D., and Sophocleous, M.A., 1987, Seismic reflection study of shallow aquifer during a pumping test: *Ground Water*, v. 25, pp. 703-709, Nov.-Dec.
- Blatt, H., Middleton, G., and Murrey, R., 1980, *Origin of Sedimentary Rocks*: Prentice-Hall, Englewood, NJ, 782 pp.
- Boggs, J. M., Young, S. C., Beard, L. M., Gelhar, L. W., Rehfeldt, K. R., and Adams, E. E., 1992, Field study of dispersion in a heterogeneous aquifer, 1. Overview and site description: *Water Resources Research*, v. 28, no. 12, pp. 2381-3291.
- Boggs, J.M., Young, S.C., Hemond, H.F., Richardson, L., and Schaefer, M.E., 1988, Evaluation of tracer sampling devices for the macrodispersion experiment: Electric Power Research Institute (EPRI), Research Project 2485-5, Interim Report.
- Bohling, G.C., McElwee, C.D., Butler, J.J., Jr., and Liu, W.Z., 1990, User's guide to well test design and analysis with SUPRPUMP version 1.0: KGS Computer Program Series no. 90-3, 95 pp.
- Bohling, G.C. and McElwee, C.D., 1992, SUPRPUMP: An interactive program for well test analysis and design: *Ground Water*, v. 30, no. 2, pp. 262-268.
- Bohling, G.C. and McElwee, C.D., 1992, SUPRPUMP: An interactive program for well test analysis and design: *Ground Water*, v. 30, no. 2, pp. 262-268.
- Butler, J.J., Jr., 1986, Pumping Tests in Nonuniform Aquifers: A deterministic and stochastic analysis (Ph.D. dissertation): Stanford Univ., Stanford, CA. 220 pp.

- Butler, J.J., Jr., and McElwee, C.D., 1990, Variable-rate pumping tests for nonuniform aquifers: *Water Resources Research*, v. 26, no. 2, pp. 291-306.
- Butler, J. J., Jr., McElwee, C. D., Bohling, G. C., and Healey, J. M., 1991, Hydrogeologic characterization of hazardous waste sites: Kansas Water Resources Research Inst. Contribution No. 289, 129 pp.
- Butler, J.J., Jr., and C.D. McElwee, 1994, Well-Testing Methodologies for Characterizing Heterogeneities in Alluvial-Aquifer Systems: Second Year Report, Project Report to United States Geological Survey Water Resources Research Program, U.S. Dept. of Interior, 171 pp.
- Butler, J.J., Jr., Bohling, G.C., Hyder, Z., and McElwee, C.D., 1994, The use of slug tests to describe vertical variations in hydraulic conductivity: *Jour. of Hydrology*, v. 156, pp. 137-162.
- Century Geophysical Corp., unpublished, Report describing the design and test of a prototype four coil slim induction tool, Century Geophysical Corp., Tulsa, OK, 12 pp.
- Chen, H.T., and Chen, C.K., 1988, Hybrid Laplace transform/finite element method for two-dimensional heat conduction: *J. Thermophys.*, v. 2, no. 1, pp. 31-36.
- Chirlin, G.R., 1989, A critique of the Hvorslev method for slug test analysis: the fully penetrating well: *Ground Water Monitoring Review*, v. 9, no. 2, pp. 130-138.
- Cooper, H.H., Bredehoeft, J.D., and Papadopoulos, I.S., 1967, Response of a finite-diameter well to an instantaneous charge of water: *Water Resour. Res.*, v. 3, no.1, pp. 263-269.
- Crump, K.S., 1976, Numerical inversion of Laplace transforms using a Fourier series approximation: *J. Assoc. Comput. Mach.*, v. 23, no. 1, pp. 89-96.
- Davis, S.N., and Carlson, W.A., 1952, Geology and ground-water resources of the Kansas River valley between Lawrence and Topeka, Kansas: Kansas Geological Survey Bull. 96, pp. 201-276.
- De Hoog, F.R., Knight, J.H., and Stokes, A.N., 1982, An improved method for numerical inversion of Laplace transforms: *SIAM J. Sci. Stat. Comput.*, v. 3, no. 3, pp. 357-366.
- Desbarats, A. J., 1993, Geostatistical analysis of interwell transmissivity in heterogeneous aquifers: *Water Resour. Res.*, v. 29, no: 4, pp. 1239-1246.
- Dewan, J.T., 1983, *Essentials of Modern Open-Hole Log Interpretation*: Pennwell Books, Tulsa, OK, 361 pp.
- Dobrin, M.B., and Savit, C.H., 1988, *Introduction to Geophysical Prospecting*: McGraw-Hill, Inc., N.Y., NY, 842 pp.

- Dubner, H., and Abate, J., 1968, Numerical inversion of Laplace transforms by relating them to the finite Fourier cosine transform: *J. Assoc. Comp. Mach.*, v. 15, no. 1, pp. 115-123.
- Ellis, D.V., 1987, *Well Logging For Earth Scientists*: Elsevier Science Publishing Company, Inc., N.Y., NY, 519 pp.
- Environmental Protection Agency, 1984, Test Method--The determination of inorganic anions in water by ion chromatography--Method 300.0: U.S. Environmental Protection Agency, EPA-600/4-84-017, 5 pp.
- Fishman, M.J. and Friedman, L. C., eds., 1989, Methods for determination of inorganic substances in water and fluvial sediments: U. S. Geological Survey, *Techniques of Water-Resources Investigations*, Book 5, Chapter A1, 545 pp.
- Freeze, R.A., and Cherry, J.A., 1979, *Groundwater*, Prentice-Hall, Inc., Englewood Cliffs, NJ, 604 pp.
- Frind, E. O, and Matanga, G. B., 1985, The dual formulation of flow for contaminant transport modeling, 1, Review of theory and accuracy aspects: *Water Resour. Res.*, v. 21, no. 2, pp. 159-169.
- Garabedian, S. P., 1987, Large-scale dispersive transport in aquifers--Field experiments and reactive transport theory: Ph.D. dissertation, Massachusetts Institute of Technology, 290 pp.
- Garabedian, S. P., Gelhar, L. W., and Celia, M. A., 1988, Large-scale dispersive transport in aquifers: Field experiments and reactive transport theory: MIT Ralph M. Parsons Laboratory Report Number 315, 280 pp.
- Geer, F.C. van, 1982, An equation based theoretical approach to network design for groundwater levels using Kalman filters: IAHS Publ., no. 136, pp. 241-250, pp. 25-36.
- Geer, F.C. van, 1984, Kalman filter calibration of error covariance matrix of a groundwater model: In *Symposium proceedings on Stochastic Hydraulics*, IAHA, Urbana, Illinois, U.S.A., pp. 26-36.
- Gelb, A., 1974, *Applied optimal estimation*, The M.I.T. Press, 374 pp.
- Gelhar, L. W., Welty, C., and Rehfeldt, K. R., 1992, A critical review of data on field-scale dispersion: *Water Resources Research*, v. 28, no. 7, pp.1955-1974.
- Grantham, R.L., 1990, Feasibility of using seismic reflection to detect gas trapped in alluvial materials: Masters thesis, University of Kansas Department of Geology.
- Guppy, K.H., Cinco-Ley, H., Ramey, H.J., Jr., and Samaniego-V., F., 1982, Non-Darcy flow in wells with finite-conductivity vertical fractures: *Soc. of Pet. Eng. Jour.*, Oct., pp. 681-698.
- Gurtin, M.E., 1965, Variational principles for initial value problems: *Q. App. Math.*, v. 22, pp. 252-256.

- Hackett, G., 1987, Drilling and constructing monitoring wells with hollow-stem augers Part 1: Drilling considerations: *Ground Water Monitoring Review*, v. VII, no. 4, pp. 51-62.
- Hansen, A.G., 1967, *Fluid Mechanics* : John Wiley and Sons, Inc., New York, pp. 134-137.
- Hayashi, K., Ito, T., and Abe, H., 1987, A new method for the determination of in situ hydraulic properties by pressure pulse tests and application to the Higashi Hachimantai geothermal field: *J. Geophys. Res.*, v. 92, no. B9, pp. 9168-9174.
- Healey, J., Anderson, J., Miller, R.D., Keiswetter, D., Steeples, D.W., and Bennett, B., 1991, Improved shallow seismic-reflection source: building a better Buffalo : *Soc. Explor. Geophys. Exp. Abs.*, v. 1, p. 588-591.
- Huettl, T.J., 1994, An evaluation of a borehole induction single-well tracer test to characterize the distribution of hydraulic properties in an alluvial aquifer: Master's Thesis, Dept. of Geol., Univ. of Kansas, Lawrence, Ks.
- Huettl, T.J., Butler, J.J., Jr., McElwee, C.D., 1993, A borehole induction single-well tracer test to characterize spatial variations in aquifer flow properties: Kansas Geological Survey Open-File Report 93-48, 19 pp.
- Hunter, J.A., Pullan, S.E., Burns, R.A., Gagne, R.M., and Good, R.L., 1984, Shallow seismic-reflection mapping of the overburden-bedrock interface with the engineering seismograph--Some simple techniques: *Geophysics*, v. 49, p. 1381-1385.
- Hvorslev, M.J., 1951, Time lag and soil permeability in ground-water observations, Bull no. 36, Waterways Exper. Sta., Corps of Engrs., U.S. Army, 50 pp.
- Ingersoll, L.R., Zobel, O.J., and Ingersoll, A.C., 1948, Heat conduction with engineering and geological conditions, McGraw-Hill.
- Jackson, P.D., Taylor-Smith, D., and Stanford, P.N., 1978, Resistivity-porosity-particle shape for marine sands: *Geophysics*, v. 43, no. 6, pp. 1250-1268.
- Javandel, I., Doughty, C., and Tsang, C. F., 1984, Groundwater Transport: Handbook of Mathematical Models, American Geophysical Union Water Resources Monograph 10, 228 pp.
- Javandel, M.S., and Witherspoon, P.A. ,1968, Application of the finite element method to transient flow in porous media: *Soc. Pet. Eng. J.* , v. 8, pp. 241-252.
- Jiang, X., 1991, A field and laboratory study of scale dependence of hydraulic conductivity: M.S. thesis, Univ. of Kansas, Lawrence, Ks., 149 pp.
- Johnson, C.R., Greenkorn, R.A., and Woods, E.G., 1966, Pulse-testing: A new method for describing reservoir flow properties between wells: *J. of Pet. Tech.*, pp. 1599-1604.

- Kabala, Z.J., Pinder, G.F., and Milly, P.C.D., 1985, Analysis of well-aquifer response to a slug test: *Water Resour. Res.*, v. 21, no.9, pp. 1433-1436.
- Kalman, R.E., 1960, A New Approach to Linear Filtering and Prediction Problems: *Journal of Basic Engineering*, pp. 35-45.
- Kalman, R.E. and Bucy, R.S., 1961, New Results in Linear Filtering and Prediction Theory: *Journal of Basic Engineering*, pp. 95-108.
- Keely, J.F., and Boateng K., 1987, Monitoring well installation, purging and sampling techniques, Part 1: Conceptualizations: *Ground Water*, v. 25, no. 3, pp. 300-313.
- Kipp, K.L., Jr., 1985, Type curve analysis of inertial effects in the response of a well to a slug test: *Water Resour. Res.*, v. 21, no.9, pp. 1397-1408.
- Kreyszig, E., 1983, *Advanced Engineering Mathematics*: John Wiley and Sons, New York, pp. 75-81.
- Kruseman, G.P., and de Ridder, N.A., 1990, *Analysis and Evaluation of Pumping Test Data*, International Institute for Land Reclamation and Improvement, Wageningen, The Netherlands, 287 pp.
- Li, L., Barry, D. A., Culligan-Hensley, P. J., and Bajracharya, K., 1994, Mass transfer in soils with local stratification of hydraulic conductivity: *Water Resources Research*, v. 30, no. 11, pp.2891-2900.
- Lim, H.C. and Lee, K.S., 1992, Process Control and Optimization: in *Ponds, M.-N., Bioprocess Monitoring and Control*, Hanser Publisher.
- Liu, W.Z., and Butler, J.J., Jr., 1991, A time-continuous finite difference approach for flow and transport simulations: Kansas Geol. Survey, Open File Report 91-20, 19 pp.
- Mackay, D.M., Freyberg, D.L., McCarthy, P.L., Roberts, P.V., and Cherry, J.A., 1986, A natural gradient experiment on solute transport in a sand aquifer, 1, Approach and overview of plume movement: *Water Resour. Res.*, v. 22, no. 13, pp. 2017-2029.
- Macpherson, G. L., 1993, Preliminary assessment of nitrate at two sites in Kansas--comparison of alluvial aquifer and fractured limestone: Kansas Water Resources Research Institute Report, Contribution No. 305, 39 p.
- Macpherson, G. L., and M. K. Schulmeister, 1994, Source(s), fate and residence time of nitrate in ground water at two sites in Kansas--A comparison of carbonate and alluvial aquifers: Kansas Water Resources Research Institute Report No. C2020-08, Contribution No. 312, 81 p.
- McElwee, C.D., 1987, Sensitivity analysis of ground-water models, in Jacob Bear and M. Yavuz Corapcioglu: *Proceedings of the 1985 NATO Advanced Study Institute on Fundamentals of Transport Phenomena in Porous Media*: Martinus Nijhoff Publishers, Dordrecht, The Netherlands, pp. 751-817.

- McElwee, C.D., and Butler, J.J., Jr., 1989, Slug testing in highly permeable aquifers (abstract): GSA 1989 Annual Mtg. Abstract with Program, p. A193.
- McElwee, C.D., Butler, J.J., Jr., Liu, W.Z., and Bohling, G.C., 1990, Effects of partial penetration, anisotropy, boundaries and well skin on slug tests: *Eos, Trans. Amer. Geophys. Union*, v. 71, no. 17, p. 505.
- McElwee, C.D., Butler, J.J., Jr., and Healey, J.M., 1991, A new sampling system for obtaining relatively undisturbed samples of unconsolidated coarse sand and gravel: *Ground Water Monitoring Review*, v. 11, no. 3, pp. 182-191.
- McElwee, C.D. and Butler, J.J., Jr., 1992, Characterization of heterogeneities controlling transport and fate of pollutants in unconsolidated sand and gravel aquifers: First year report: Project Report to Air Force Office of Scientific Research, University Research Initiative, Research Initiation Program, U.S. Dept. of Defense, Kansas Geological Survey Open-File Report 92-20, 209 pp.
- McElwee, C.D. and Butler, J.J., Jr., 1993, Characterization of heterogeneities controlling transport and fate of pollutants in unconsolidated sand and gravel aquifers: Second year report: Project Report to Air Force Office of Scientific Research, University Research Initiative, Research Initiation Program, U.S. Dept. of Defense, Kansas Geological Survey Open-File Report 93-21, 221 pp.
- McElwee, C.D. and Butler, J.J., Jr., 1994, Characterization of heterogeneities controlling transport and fate of pollutants in unconsolidated sand and gravel aquifers: Third year report: Project Report to Air Force Office of Scientific Research, University Research Initiative, Research Initiation Program, U.S. Dept. of Defense, Kansas Geological Survey Open-File Report 94-32, 237 pp.
- McElwee, C.D., Butler, J.J., Jr. and Bohling, G.C., 1995, Sensitivity analysis of slug tests II: Observation wells: *Journal of Hydrology*, v. 164, pp. 69-87..
- Merey, C., Miller, R.D., Ticken, E.J., and Lewis, J.S., in press, Hydrogeological characterization using a shallow seismic reflection survey at Fort Ord, California: *Soc. Expl. Geophys. Exp. Abs.*
- Miller, R.D., 1992, Normal moveout stretch mute on shallow-reflection data: *Geophysics*, v. 57, pp. 1502-1507.
- Miller, R.D., Steeples, D.W., and Brannan, M., 1989, Mapping a bedrock surface under dry alluvium with shallow seismic reflections: *Geophysics*, v. 54, pp. 1528-1534.
- Miller, R.D., Steeples, D.W., Hill, R., and Gaddis, B., 1990, Identifying intra-alluvial and bedrock structures shallower than 30 meters using seismic-reflection techniques: Soc. Explor. Geophys. volumes on Geotechnical and Environmental Geophysics, Stan Ward, ed., *Volume 3: Geotechnical*, pp. 89-97.
- Minning, R.C., 1982, Monitoring well design and installation: Proceedings of the Second National Symposium on Aquifer Restoration and Ground Water Monitoring, Columbus, Ohio, pp. 194-197.

- Moench, A. F., 1989, Convergent radial dispersion: A Laplace transform solution for aquifer tracer testing: *Water Resources Research*, v. 25, no. 3, pp. 439-447.
- Moench, A. F., 1991, Convergent radial dispersion: A note on evaluation of the Laplace transform solution: *Water Resources Research*, v. 27, no. 12, pp. 3261-3264.
- Moench, A.F., and Hsieh, P.A., 1985, Analysis of slug test data in a well with finite-thickness skin: in *Memoirs of the 17th Intern. Cong. on the Hydrogeology of Rocks of Low Permeability*, v. 17, pp. 17-29.
- Molz, F.J., Guven, O., and Melville, J.G., 1989, Characterization of the hydrogeologic properties of aquifers: The next step: in: *Proc. of the Conf. on New Field Techniques for Quantifying the Physical and Chemical Properties of Heterogeneous Aquifers*, National Water Well Association, pp. 407-418.
- Moridis, G.J., and Reddell, D.L., 1991, The Laplace transform finite difference method for simulation of flow through porous media: *Water Resour. Res.*, v. 27, no. 8, pp. 1873-1884.
- Morin, R.H., LeBlanc, D.R., and Teasdale, W.E., 1988, A statistical evaluation of formation disturbance produced by well-casing installation methods: *Ground Water*, v. 26, no. 2, pp. 207-217.
- National Research Council, 1990, Ground Water Models--Scientific and Regulatory Applications: National Academy Press, 303 p.
- Neitzel, E.B., 1958, Seismic reflection records obtained by dropping a weight: *Geophysics*, v. 34, p. 58-80.
- Nelson, R. W., 1960, In-place measurement of permeability in heterogeneous media, 1, Theory of a proposed method: *J. Geophys. Res.*, v. 65, no. 6, pp. 1753-1758.
- Nelson, R. W., 1961, In-place measurement of permeability in heterogeneous media, 2, Experimental and computational considerations: *J. Geophys. Res.*, v. 66, no. 8, pp. 2469-2478.
- Nelson, R. W., 1968, In-place determination of permeability distribution for heterogeneous porous media through analysis of energy dissipation: *Soc. Pet. Eng. J.*, v. 8, no. 1, pp. 33-42.
- Neuman, S. P., 1973, Calibration of distributed parameter groundwater flow models viewed as a multiple-objective decision process under uncertainty: *Water Resour. Res.*, v. 9, no. 4, pp. 1006-1021.
- Novakowski, K.S., 1989, Analysis of pulse interference tests: *Water Resources Research*, v. 25, no. 11, pp. 2377-2387.
- Olea, R.A., 1988, Correlator--an interactive computer system for lithostratigraphic correlation of wireline logs: *Petrophysical Series*, no. 4, Kansas Geological Survey, Lawrence, KS, 85 pp.

- Orion Research, 1991, Model 94-35 and 94-53 halide electrodes instruction manual: Orion Research Incorporated, Form IM9435,3, 29 pp.
- Palmer and Johnson, 1989, Chapter 2, Physical processes controlling the transport of contaminants in the aqueous phase: *in Environmental Protection Agency, Transport and Fate of Contaminants in the Subsurface*, EPA/625/4-89/019, pp. 5-22.
- Papadopoulos, I.S., 1966, Nonsteady flow to multiaquifer wells: *J. Geophys. Research*, v. 71, no. 20, pp. 4791-4797.
- Papadopoulos, I.S., and Cooper, H.H., Jr., 1967, Drawdown in a well of large diameter: *Water Resour. Res.*, v. 3, no. 1, pp. 241-244.
- Parker, J. C., and van Genuchten, M. Th., 1984, Flux-averaged and volume-averaged concentrations in continuum approaches to solute transport: *Water Resources Research*, v. 20, no. 7, pp. 866-872.
- Parkhurst, D. L., Thorstenson, D. C., and Plummer, L. N., 1980, PHREEQE--A computer program for geochemical calculations: U. S. Geological Survey, *Water-Resources Investigations*, 80-96, 195 pp.
- Parmakian, J., 1963, *Waterhammer Analysis*: Dover Pub., New York, 161pp.
- Perry, C.A. and Hart, R.J., 1985, Installation of observation wells on hazardous waste sites in Kansas using a hollow-stem auger: *Ground Water Monitoring Review*, v. V, no. 4, pp. 70-73.
- Peterson, J. E., Paulsson, B. N. P., and McEvilly, T. V., 1985, Application of algebraic reconstruction techniques to crosshole seismic data: *Geophysics*, v. 50, no. 10, pp. 1566-1580.
- Pickens, J.F., Cherry, J.A, Grisak, G.E., Merritt, W.F., and Risto, B.A., 1978, A multilevel device for ground-water sampling and piezometric monitoring: *Ground Water*, v. 16, no. 5, pp. 322-327.
- Pollock, D. W., 1988, Semianalytical computation of path lines for finite-difference models: *Ground Water*, v. 26, no. 6, pp. 743-750.
- Press, W.H., Teukolsky, S.A., Vetterling, W.T., and Flannery, B.P., *Numerical Recipes in FORTRAN*, Cambridge Univ. Press, Cambridge, UK, 963 pp.
- Prijambodo, R., Raghavan, R., and Reynolds, A.C., 1985. Well test analysis for wells producing layered reservoirs with crossflow: *Soc. Pet. Eng. J.*, pp. 380-396.
- Raghavan, R., 1989, Behavior of wells completed in multiple producing zones: *SPE Formation Evaluation*, v. 4, no. 2, pp. 219-230.

- Rushton, K.R., and Chan, Y.K., 1977, Numerical pumping test analysis in unconfined aquifers: *J. Irrigation and Drainage Div.*, v. 103(IR1), pp. 1-12.
- Russell, D.G., and Prats, M., 1962, Performance of layered reservoirs with crossflow-single-compressible-fluid case: *Soc. of Petr. Eng. J.* (Dec., 1962), pp. 53-67.
- Sacher, H., 1983, Beruecksichtigung von Unsicherheiten bei der Parameterschaetzung fuer mathematisch-numerische Grundwasser-modelle: Dissertation, RWTH Aachen.
- Saito, A., 1982, Theory and application of induction logging for civil engineering: unpublished Masters Thesis, Colorado School of Mines, Golden, CO, 69 pp.
- Schlumberger, 1989, *Log Interpretation/Applications*, Schlumberger Educational Services, Houston, TX, 227 pp.
- Schwarz, H.R., 1986, Numerische Mathematik: Teubner Stuttgart.
- Scott, D. M., 1992, Evaluation of flow net analysis for aquifer identification: *Ground Water*, v. 30, no. 5, pp. 755-764.
- Sen, Z., 1984, Adaptive Pumping Test Analysis: *J. of Hydrology*, v. 74, pp. 259-270.
- Settari, A., and Aziz, K., 1974, A computer model for two-phase coning simulation: *Society of Petroleum Eng.*, v. 14, no. 3, pp. 221-236.
- Singh, S.R. and Shakya, S.K., 1989, A nonlinear equation for groundwater entry into well screens: *Jour. of Hydrology*, v. 109, pp. 95-114.
- Statistical Sciences, 1993, *S-PLUS User's Manual, Version 3.2*, Seattle: StatSci, a division of MathSoft, Inc.
- Steeple, D.W., 1990, Early spectral shaping boosts data quality: *Oil and Gas Journal*, v. 88, no. 38, pp. 49-55.
- Steeple, D.W., Miller, R.D., and Knapp, R.W., 1987, Downhole .50-caliber rifle—an advance in high-resolution seismic sources: *Soc. Explor. Geophys., Exp. Abs.*, 57th Ann. Mtg., pp. 76-78.
- Steeple, D.W., and Miller, R.D., 1990, Seismic-reflection methods applied to engineering, environmental, and ground-water problems: Soc. Explor. Geophys. volumes on Geotechnical and Environmental Geophysics, Stan Ward, ed., *Volume 1: Review and Tutorial*, pp. 1-30.
- Stehfest, H., 1970, Numerical inversion of Laplace transforms: *Commun. ACM.*, v. 13, no. 1, pp. 47-49.
- Stites, W., and Chambers, L., 1991, A method for installing miniature multilevel sampling wells: *Ground Water*, v. 29, no. 3, pp. 430-432.

- Stone, D.B. and Clarke, G.K.C., in press, Estimation of subglacial hydraulic properties from induced changes in basal water pressure: a theoretical framework for borehole response tests: *J. of Glaciology*.
- Streltsova, T.D., 1988, *Well Testing in Heterogeneous Formations*: John Wiley & Sons, Inc., New York, 413 pp.
- Sudicky, E.A., 1989, The Laplace transform Galerkin technique: A time-continuous finite element theory and application to mass transport in groundwater: *Water Resour. Res.*, v. 25, no. 8, pp. 1833-1846.
- Sudicky, E.A., and McLaren, R.G., 1992, The Laplace transform Galerkin technique for large-scale simulation of mass transport in discretely fractured porous media: *Water Resour. Res.*, v. 28, no. 2, pp. 499-514.
- Talbot, A., 1979, The accurate numerical inversion of Laplace transforms: *J. Inst. Math. Appl.*, v. 23, pp. 97-120.
- Taylor, K., and Molz, F., 1990, Determination of hydraulic conductivity and porosity logs in wells with a disturbed annulus: *Jour. of Contaminant Hydrology*, no. 5, pp. 317-332.
- Taylor, K., Wheatcraft, S., Hess, J., and Molz, F., 1990, Evaluation of methods for determining the vertical distributions of hydraulic conductivity: *Ground Water*, v. 28, no. 1, pp. 88-98.
- Thorbjarnarson, K. W., and Mackay, D. M., 1994, A forced-gradient experiment on solute transport in the Borden aquifer, 2. Transport and dispersion of the conservative tracer: *Water Resources Research*, v. 30, no. 2, pp. 385-399.
- Valocchi, A. J., 1986, Effect of radial flow on deviations from local equilibrium during sorbing solute transport through homogeneous soils: *Water Resources Research*, v. 22, no. 12, pp. 1693-1701.
- van der Kamp, G., 1976, Determining aquifer transmissivity by means of well response tests: The underdamped case: *Water Resources Research*, v. 12, no. 1, pp. 71-77.
- van Dyke, N.V.R., Rhodes, J.R., Richardson, D.W., and McTigue, W.H., 1993, Evaluating confined aquifer properties using the pneumatic displacement method and the repeated pressure pulse technique: in *Proc. of the Seventh National Outdoor Action Conf.*, Ground Water Management Series, v. 15, pp. 405-419.
- Vela, S. and McKinley, R.M., 1970, How real heterogeneities affect pulse-test results: *Soc. Pet. Eng. J.*, v. 10, pp. 181-191.
- Vennard, J.K., and Street, R.L., 1975, *Elementary Fluid Mechanics*: Wiley and Sons, New York, 740pp.
- Voss, C.I., 1984, A Finite-Element Simulation Model for Saturated-Unsaturated, Fluid-Density-Dependent Ground-Water Flow with Energy Transport or Chemically-Reactive Single-Species Solute Transport: U.S. Geological Survey, National

Center, Reston, Virginia. Prepared in Cooperation with U.S. Air Force Engineering And Service Center, Tyndall A.F.B., Florida.

Weast, R. C., ed., 1985, CRC Handbook of Chemistry and Physics: CRC Press, Inc., Boca Raton, Florida.

Welty, C., and Gelhar, L.W., 1994, Evaluation of longitudinal dispersivity from nonuniform flow tracer tests: *Journal of Hydrology*: v. 153, pp. 71-102.

Zapico, M.M., 1987, Aquifer evaluation procedures-core acquisition and an assessment of slug tests: M.Sc. Thesis, University of Waterloo.

Zapico, M.M., Vales, S. and Cherry, J.A., 1987, A wireline piston core barrel for sampling cohesionless sand and gravel below the water table: *Ground Water Monitoring Review*, v. VII, no. 3, pp. 74-82.

IX. APPENDICES

**Appendix A. Sensitivity Analysis of Slug Tests. Part 1. The Slugged Well,
Published in the *Journal of Hydrology*,
Volume 164, pages 53-67, 1995.**

[2]

Sensitivity analysis of slug tests. Part 1. The slugged well

C.D. McElwee*, G.C. Bohling, J.J. Butler, Jr.

Kansas Geological Survey, 1930 Constant Ave., Lawrence, KS 66047, USA

Received 30 September 1993; revision accepted 25 June 1994

Abstract

In this paper, we apply the techniques of sensitivity analysis to the Cooper et al. model for slug tests in confined aquifers. A sensitivity analysis of slug-test responses can provide valuable information concerning optimal test design (within the limitations of the chosen model). The sensitivity analysis enables a family of generic sensitivity coefficients for transmissivity (T) and storage coefficient (S) to be defined by two parameters α (related to S) and β (related to time and T). Two facts stand out from this family of curves. First, the sensitivity to S is much lower than that to T ; second, the sensitivity curves for T and S are very similar in shape (i.e. the correlation is high) making it difficult to reliably estimate both T and S . Sensitivity analysis shows that the estimated standard errors of the parameters are inversely proportional to the initial head (H_0), so large initial heads should be used when possible. Generally, an increased number of measurements improves parameter estimation, if properly placed in time. Early time measurements are important for defining H_0 accurately. The best estimates for T and S are obtained by minimizing the correlation between the sensitivity coefficients for T and S and sampling at points of maximum sensitivity.

1. Introduction

The use of slug tests for site characterization is a common practice in hydrogeology owing to the logistical and financial advantage of the procedure. Tests can be performed quickly and inexpensively with a minimum of equipment. One of the earliest investigations was by Hvorslev (1951) using a formulation which assumed local steady state conditions in the aquifer but a finite size well casing and screen. Some of the earliest time varying work was done by Ferris and coworkers (Ferris and

* Corresponding author.

Knowles, 1954; Ferris et al., 1962); however, they assumed an infinitely small well bore. Cooper et al. (1967, henceforth designated the CBP solution) were the first to consider a well of finite diameter in a quantitative way. It is their solution that this paper will be based upon, since it gives the temporal and spatial response to a slug test in a homogeneous, isotropic, infinite aquifer fully penetrated by the slugged well. Later authors have considered many aspects of slug tests and their application to more complicated situations; the literature is extensive. Papadopoulos et al. (1973) extended the original CBP work to aquifers with very low storage coefficients. Others have considered various aspects of field procedures (Black, 1978; Patterson and Devlin, 1985; Priddle, 1989). The extension of slug tests to very tight formations has been considered by Bredehoeft and Papadopoulos (1980) and Neuzil (1982). Pandit and Miner (1986) consider better interpretation methods and Marschall and Barczewski (1989) extend the analysis to the frequency domain. This is only a small sampling of the slug test literature and was chosen only because it relates more closely to the present paper. A good review of auger hole, piezometer, and slug tests is given by Boak (1991). A review of slug test modeling is given by Chirlin (1990).

Even though slug tests are commonly used and relatively easy to perform, the tests should be planned carefully in order to insure that the maximum amount of information is obtained. At the Kansas Geological Survey, we have instituted a program to study heterogeneity in alluvial aquifers. Slug tests are an integral part of that program, so we have undertaken a detailed study of the information provided by slug tests in a variety of situations. This paper is the first of a planned series presenting our results. In this paper we will employ the CBP model for slug tests to demonstrate the use of sensitivity analysis (McElwee, 1987) for designing more effective slug tests. A sensitivity analysis of slug-test responses can provide valuable information concerning optimal test design. Such an analysis allows issues regarding the quantity and timing of measurements, and the magnitude of the initial displacement to be addressed. This allows aquifer parameters to be determined to the desired accuracy within the limitations of the chosen model. It should be stressed that in many complex geologic environments the CBP model may not be adequate. However, this study should give valuable general insights that are applicable to more complex situations.

2. Analytical solution

The CBP analytical solution for the head inside a slugged well with finite radius is

$$H(\alpha, \beta, H_0) = \frac{8H_0\alpha}{\pi^2} \int_0^\infty \frac{\exp(-\beta x^2/\alpha)}{x\Delta(x)} dx \quad (1)$$

where

$$\Delta(x) = [xJ_0(x) - 2\alpha J_1(x)]^2 + [xY_0(x) - 2\alpha Y_1(x)]^2 \quad (2)$$

$$\beta = \frac{Tt}{r_c^2} \quad (3)$$

and

$$\alpha = \frac{r_s^2}{r_c^2} S. \quad (4)$$

where x is an integration variable, J and Y are Bessel functions and r_s and r_c are the screen and casing radii, respectively.

This analytical solution shows that slug-test response can be expressed as a function of three parameters: H_0 , the initial head displacement; α , a dimensionless parameter related to screen and casing radii and the storage coefficient; and β , a dimensionless time scale involving transmissivity and the casing radius. Often it is convenient to define the relative (normalized) head response

$$h = \frac{H}{H_0} \quad (5)$$

A plot of h vs. β is shown in Fig. 1 for $\alpha = 10^{-3}$. When h is plotted versus β , it forms a generic type curve that is valid for any transmissivity, as long as α is unchanged (when the casing and screen radii are equal α is just the storage coefficient). If α is allowed to vary, a family of type curves is generated. Graphical curve matching to this family of curves has been the traditional method of obtaining aquifer parameters from slug test data. It is well known that it is difficult to obtain a unique match for α (and therefore S) since the curves are very similar in shape (Cooper et al., 1967).

3. Sensitivity analysis

Sensitivity analysis (McElwee, 1987; Knopman and Voss, 1987; Sun and Yeh,

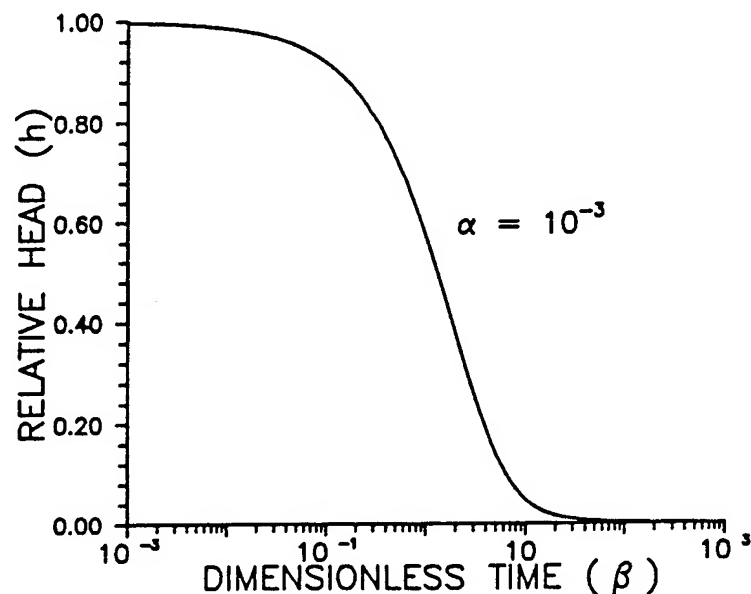


Fig. 1. A plot of relative head (H/H_0) vs. dimensionless time (Tt/r_c^2) for the CBP solution.

1990a,b) can be used to look at the effect of changing various parameters on the head. A first order Taylor series expansion can be performed and used to define sensitivity coefficients for the parameters (in this case T , S , and H_0).

$$H^{m+1} = H^m + U_T^m \Delta T^{m+1} + U_S^m \Delta S^{m+1} + U_{H_0}^m \Delta H_0^{m+1} \quad (6)$$

In Eq. (6), H^{m+1} is the estimated experimental head after the $m + 1$ st perturbation in the parameters and H^m is the head evaluated from the analytical solution with the m th estimates of the parameters. The Δ values are simply perturbations in the parameters, usually chosen to minimize error between the model values and field data values in the process of identifying the aquifer parameters. The sensitivity coefficients

$$U_T = \frac{\partial H}{\partial T}, \quad U_S = \frac{\partial H}{\partial S}, \quad U_{H_0} = \frac{\partial H}{\partial H_0} \quad (7)$$

are simply derivatives of the head with respect to the parameters and may be evaluated analytically or numerically. The sensitivity coefficients are a measure of how much the head changes when a parameter is changed by a small amount, and therefore, are very useful to examine in some detail. However, it is very difficult to compare the relative effects of certain parameters using these sensitivities coefficients because the numerical values of the parameters vary widely. A more diagnostic sensitivity coefficient, the normalized sensitivity coefficient (denoted here by a prime), is obtained by multiplying by the parameter.

$$U'_T = T \frac{\partial H}{\partial T}, \quad U'_S = S \frac{\partial H}{\partial S}, \quad U'_{H_0} = H_0 \frac{\partial H}{\partial H_0} \quad (8)$$

These normalized sensitivity coefficients can be plotted on the same graph and will give a good indication of the relative importance of various parameters. The unit of the normalized sensitivity coefficient is the same as the length unit used for H . Parameter variations are now defined as a decimal fraction of the original parameter.

$$\Delta T' = \frac{\Delta T}{T}, \quad \Delta S' = \frac{\Delta S}{S}, \quad \Delta H_0' = \frac{\Delta H_0}{H_0} \quad (9)$$

Using Eqs. (8) and (9) one can write Eq. (6) alternatively with prime quantities.

One other type of sensitivity coefficient will also be useful. Each of the previously defined normalized sensitivity coefficients can be written explicitly showing how H_0 the initial displacement, and h , the relative head enter.

$$U'_T = T \frac{\partial H}{\partial T} = H_0 T \frac{\partial h}{\partial T} = H_0 u'_T \quad (10a)$$

$$u'_T = T \frac{\partial h}{\partial T} = \beta \frac{\partial h}{\partial \beta} \quad (10b)$$

$$U'_S = S \frac{\partial H}{\partial S} = H_0 S \frac{\partial h}{\partial S} = H_0 u'_S \quad (11a)$$

$$u'_S = S \frac{\partial h}{\partial S} = \alpha \frac{\partial h}{\partial \alpha} \quad (11b)$$

$$U'_{H_0} = H_0 \frac{\partial H}{\partial H_0} = H_0 h = H = H_0 u'_{H_0} \quad (12a)$$

$$u'_{H_0} = h \quad (12b)$$

Eqs. (10)–(12) clearly show that the normalized sensitivity coefficients are directly proportional to H_0 . Thus, the height of the initial slug displacement should be as large as possible to achieve greater sensitivity. (Note that there may be other factors that limit the maximum height of the initial slug displacement for practical applications.) If H_0 is factored out of each expression we are left with the normalized sensitivities of relative head (dimensionless and denoted by u' in Eqs. (10)–(12)). These sensitivity coefficients are only functions of α and β . For a given value of α , a generic curve can be plotted versus β that is valid for any value of transmissivity. Eqs. (10)–(12) may be evaluated analytically or numerically from Eqs. (1) and (5).

Fig. 2 shows curves for u'_T and u'_S for α equal 10^{-3} . All possible values of T are represented by these two curves as long as α remains constant. Note that this figure clearly shows that the system is much more sensitive to T than S , since the maximum amplitude of u'_T is about ten times larger than that of u'_S . The sensitivities to T and S peak near $\beta = 2.0$ when $\alpha = 10^{-3}$, and have a certain characteristic width along the β (dimensionless time) axis (Fig. 2). In general, a large number of measurements should be taken near the maximum sensitivity so that the shape of the sensitivity curve through time is well represented.

The use of derivative type curves to help resolve non-uniqueness in type curve matching for slug tests has been explored by some authors (Karasaki et al., 1988).

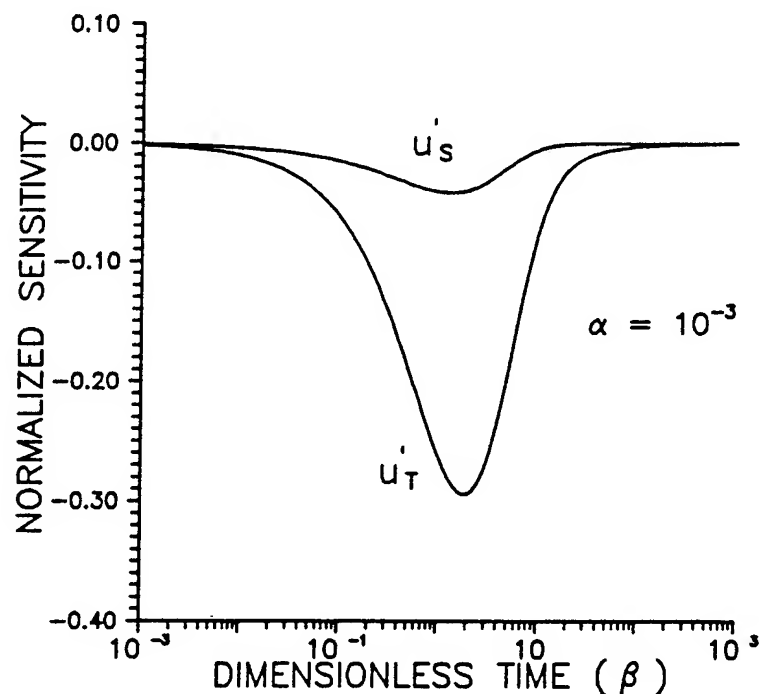


Fig. 2. A plot of generic normalized sensitivities (dimensionless) vs. dimensionless time (Tt/r_c^2) for a given α (Sr_s^2/r_c^2).

It can be easily shown that the derivative curves of h versus natural log β (dimensionless time) are in fact just the sensitivity curves u'_T . This comes from a simple extension of Eq. (10b)

$$u'_T = T \frac{\partial h}{\partial T} = \beta \frac{\partial h}{\partial \beta} = \frac{\partial h}{\partial (\ln \beta)}$$

Therefore peaks in derivative curves correspond to points of maximum sensitivity to T . The point of maximum sensitivity to T can be found as follows

$$\frac{\partial u'_T}{\partial (\ln \beta)} = \frac{\partial^2 h}{\partial (\ln \beta)^2} = 0$$

It is clear that this equation defines the inflection point on curves such as that shown in Fig. 1. This is an alternate way of defining the point of maximum sensitivity and could be used in the field by plotting recently acquired data.

Plotting sensitivity coefficients versus time allows the quantity and timing of measurements to be appropriately selected. Fig. 3 shows sensitivity curves for three different values of α . The sensitivity to T increases and that to S decreases with decreasing α . Therefore, as the casing radius increases relative to the screen radius or S decreases, slug-test responses are less sensitive to S . Also, it can be seen that the maximum sensitivities generally occur when β is in the range of 0.1–10.

In some slug tests we have performed in very permeable aquifers, an offset is observed between the measured and fitted initial displacement H_0 . There may be some early time effects making H_0 imprecise that are not accounted for in the CBP model. These effects could be more important if one is using a weighted slug on a rope. Therefore, it may be useful to use H_0 as a fitted parameter. From Eq. (12b), it

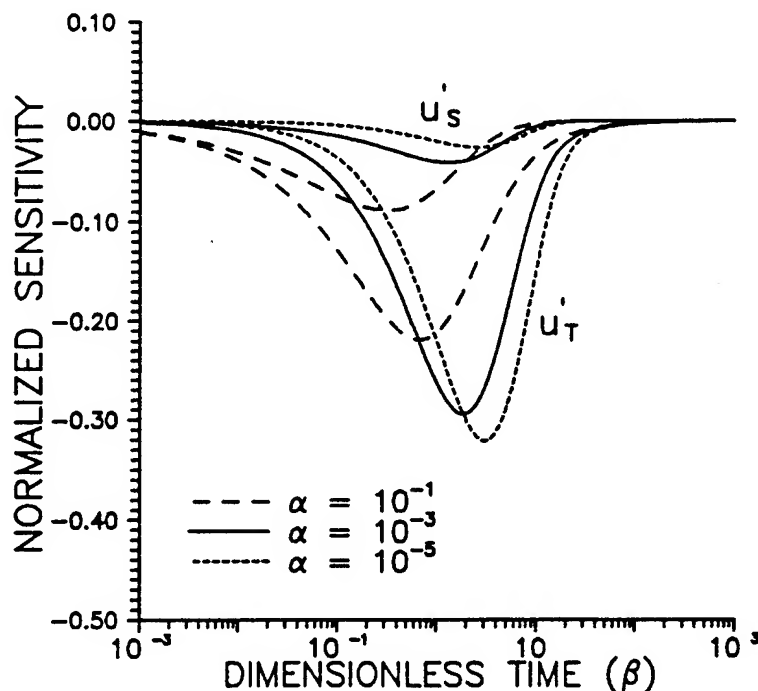


Fig. 3. The family of generic normalized sensitivity (dimensionless) curves for selected values of α .

should be clear that Fig. 1 can also be viewed as a plot of the normalized sensitivity of relative head to H_0 .

4. Parameter estimation and error analysis

A common method for performing parameter estimation involves minimizing a squared error functional such as

$$E = \sum_i (H_i^e - H_i^{m+1})^2 \quad (13)$$

where H_i^e is the observed experimental head and H_i^{m+1} is the $m + 1$ st head calculation at index point i . Index point i can represent any measurement in space or time; although, here we will only be using measurements from the slugged well over time. An attempt is made to minimize the error between the observed head and the calculated head by changing the parameters a small amount Δ , as shown in Eq. (6). Eq. (13) represents the $m + 1$ st such attempt or iteration. Substitution of Eq. (6) into Eq. (13) leads to

$$E = \sum_i (H_i^e - H_i^m - U_T^m \Delta T^{m+1} - U_S^m \Delta S^{m+1} - U_{H_0}^m \Delta H_0^{m+1})^2 \quad (14)$$

which is the error functional to be minimized by solving for the Δ values of the parameters. This procedure allows the parameters to be updated after each iteration and the search continued until the parameter values converge. A computer program for automated least squares analysis using sensitivity analysis, SUPRPUMP (Bohling and McElwee, 1992), has been used in this work to calculate the parameter changes and iterate until convergence is achieved.

The sensitivity design matrix $[A]$ arises naturally out of the process of minimizing the error functional (McElwee, 1987; Butler and McElwee, 1990) in Eq. (14) and a particular element is defined by

$$a_{i,j} = [A]_{i,j} = \sum_{k=1}^n U_i(k) U_j(k) \quad (15)$$

$i, j = H_0, T, \text{ or } S$

as a sum over time (and also space if multiple measurement points are used) of products for any two sensitivity coefficients. If we are fitting all three parameters (H_0 , T , and S) then the sensitivity design matrix is 3×3 . The least squares solution for the delta parameter changes can be expressed in terms of the inverse of $[A]$ (McElwee, 1987). In general, the solution is well behaved if the diagonal elements are large and nearly equal and the off-diagonal elements are small. This will be the case if the sensitivity coefficients are large and do not have similar shapes over the chosen measurement times (and measurement locations for multiple observation wells). One way to measure the similarity of the sensitivity coefficients is to define

the sensitivity correlation matrix $[C]$ (Butler and McElwee, 1990) as

$$c_{i,j} = [C]_{i,j} = \frac{a_{i,j}}{\sqrt{a_{i,i}a_{j,j}}} \quad (16)$$

$[C]$ will have ones on the diagonal and the off-diagonal terms will vary between plus or minus one. If any of the off-diagonal terms are exactly one, the inverse of $[A]$ does not exist and the inverse problem can not be solved for aquifer parameters. From a practical standpoint, any time the magnitudes of the off-diagonal elements get considerably above 0.9 the $[A]$ matrix becomes ill-conditioned rather rapidly and the inverse solution becomes more unreliable. For a more mathematical discussion of this problem, which is related to rank deficiency (see Gill et al., 1981).

In situations when an inverse of $[A]$ can be found, the reliability of the parameter estimates can be assessed by looking at the parameter covariance matrix defined as

$$\text{cov}(P) = [B] = [A]^{-1} \sigma^2 \quad (17)$$

where σ^2 is the head variance. The form shown here results from some simplifying assumptions about the errors in head such as additive, zero mean, uncorrelated and constant variance (Beck and Arnold, 1977). With these assumptions, the estimated standard errors (ESE) of the parameters are given by the square roots of the diagonal elements of the parameter covariance matrix.

$$\text{ESE}(P_i) = \sqrt{b_{i,i}} \quad (18)$$

These ideas can be illustrated by application to the generic sensitivity coefficients, u'_T

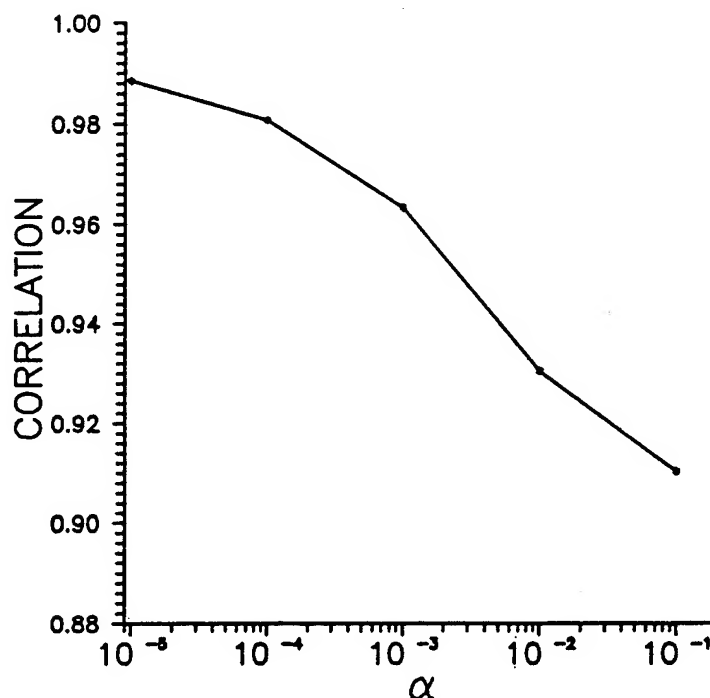


Fig. 4. Correlation between the normalized sensitivities for T and S as a function of α for the given sampling scheme.

and u'_S , of Fig. 3, which are functions only of α and β . Fig. 4 shows the correlation between u'_T and u'_S as a function of α . The sensitivity coefficients have been sampled 20 times per log cycle for β (normalized time) ranging from 10^{-3} to 10^{+5} and summed according to Eq. (16) in order to produce Fig. 4. Notice that the correlation between S and T increases as α decreases and goes to about 0.99 when α is 10^{-5} . However, even if α is four orders of magnitude greater at 10^{-1} the correlation is still about 0.91. This high correlation is the reason why it is usually difficult to determine both S and T reliably from a slug test. Fig. 5 shows the estimated standard error (ESE) for S and T (calculated from Eq. (18) and normalized by the actual parameter value) as a function of α for the same sampling in β (normalized time) as used for Fig. 4 and assuming the standard error in head (σ) is about 1% of H_0 . Notice that the error in T remains below 6% while the error in S climbs to about 66% when α is 10^{-5} . This reflects the fact shown earlier that the sensitivity coefficient maximum for T is much greater than that for S .

5. Typical application

The Kansas Geological Survey is currently carrying out research on subsurface characterization methodology at a site in the Kansas River alluvium. Parameters typical of slug tests at that site will be used to generate sensitivity coefficients and illustrate some of the points made earlier. The normalized sensitivity coefficients for H_0 , T and S are shown in Fig. 6, when the hydraulic conductivity is $8.8 \times 10^{-5} \text{ m s}^{-1}$ (25 ft day $^{-1}$), the storage coefficient is 10^{-4} , and the radii r_s and r_c are both 0.025 m

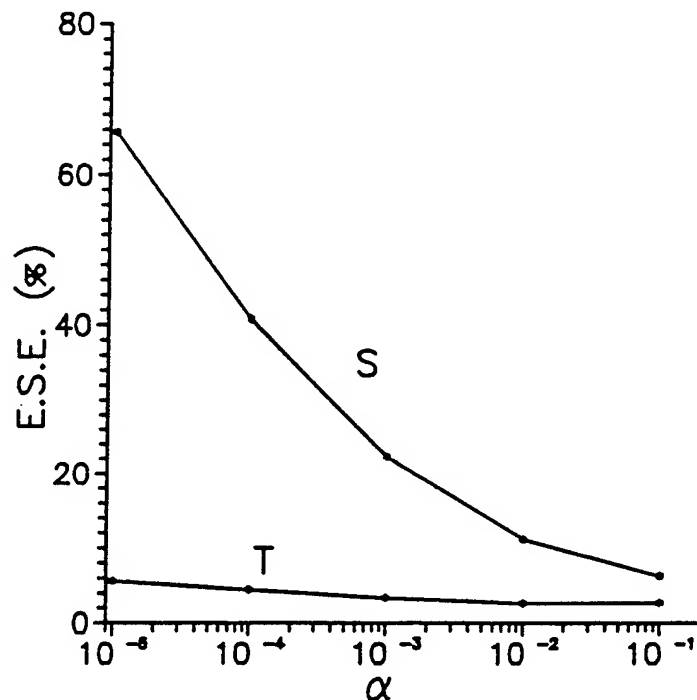


Fig. 5. Estimated standard error for T and S as a function of α for the given sampling scheme ($\sigma = 0.01 H_0$).

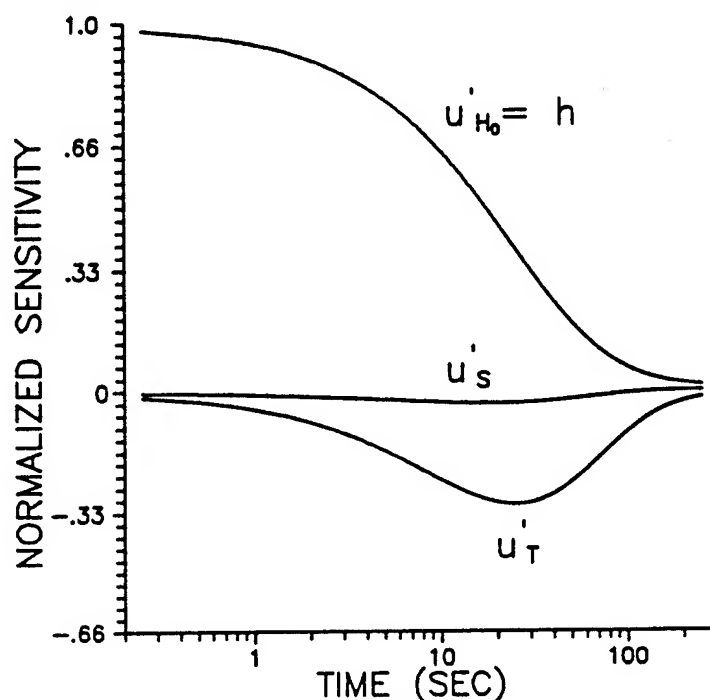


Fig. 6. Normalized sensitivity coefficients (dimensionless) for a typical slug test in the Kansas River alluvium.

(1 in). In this case α and S are equivalent. The initial displacement of water H_0 is 7.61 m (300 in or 25 ft) and the screened interval on the well is 0.76 m (30 in). These physical parameters are used for all the remaining figures (Figs. 6–9). The maximum normalized sensitivity to H_0 occurs at small times and is about 1. However, the maximum values for the normalized sensitivity to T and S occur at about 25 s and are about -0.33 for u'_T and about -0.033 for u'_S . Fig. 6 clearly shows that the head responses are least sensitive to S . Notice that if data had only been taken during the first 20 s, the very similar shape of all three curves would produce a very large correlation between the three parameters. Clearly, the majority of information about this slug test will be obtained in the first 100 s of data; after that, all sensitivities are low and decreasing. Slug tests in porous material such as illustrated here are completed in very short times; therefore, it is necessary to use high quality pressure transducers and high speed computer recording together with a positive method for introducing the slug in a near-instantaneous fashion (such as a packer with a valve which can be opened quickly from the surface). For good definition of H_0 , a number of measurements at early time are needed. For the best definition of T and S however, a good sampling of measurements should occur near the sensitivity maximum around 25 s.

The effect of the initial displacement (H_0) on the estimated standard error of all three parameters is shown in Fig. 7 (note that Figs. 7–9 all assume a standard error in head of 0.0063 m (0.25 in)). Eqs. (10)–(12) show that the normalized sensitivity coefficients are directly proportional to H_0 , so the estimated standard error should be inversely proportional to H_0 . Fig. 7 shows that as the initial head is varied from 1.27 to 7.61 m (50–300 in) the estimated standard error of all parameters decreases by

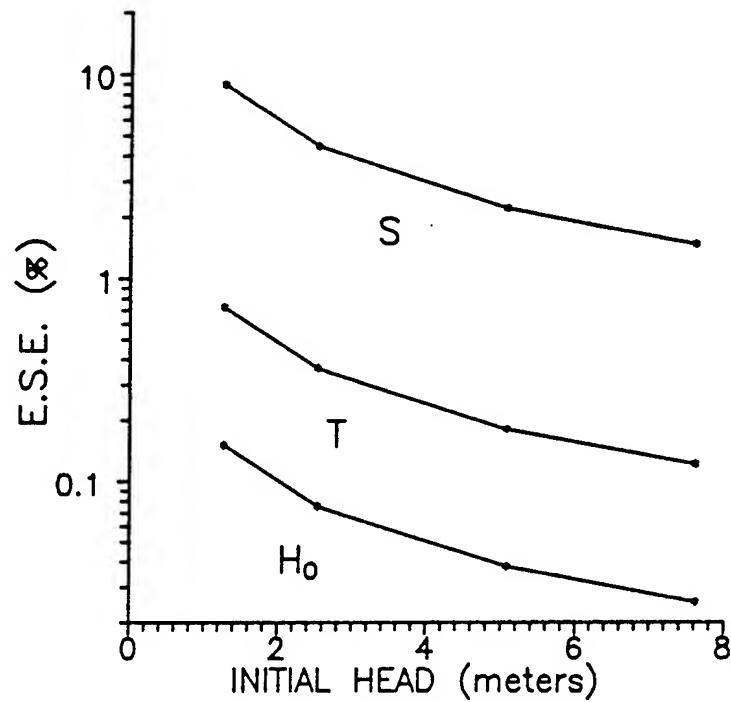


Fig. 7. Estimated standard error of the parameters as a function of the initial head for a typical slug test in the Kansas River alluvium.

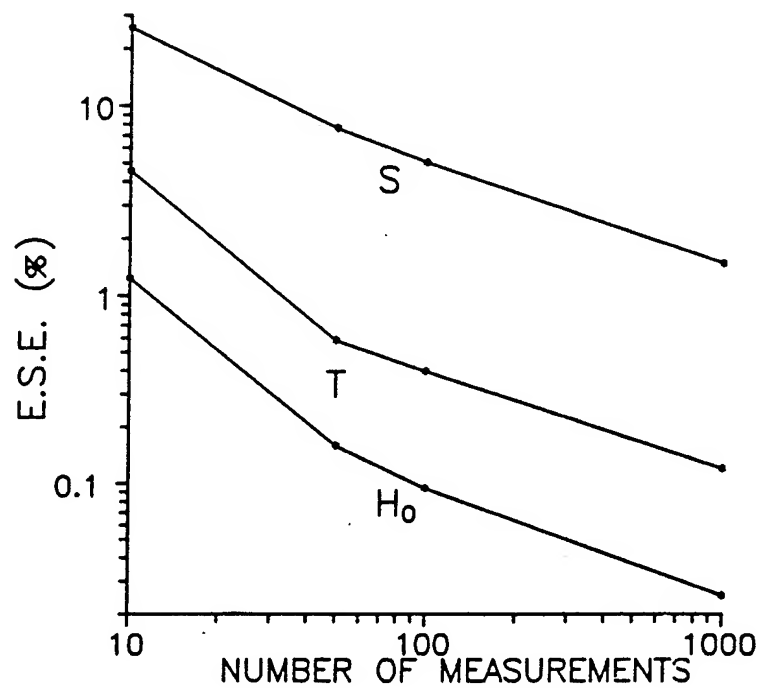


Fig. 8. Estimated standard error of the parameters as a function of the number of measurements for a typical slug test in the Kansas River alluvium.

nearly an order of magnitude. Fig. 7 was produced by assuming a thousand equally spaced measurements over 250 s (4 Hz sample rate, which is quite achievable with electronic data acquisition equipment).

Fig. 8 is a plot for our specific example which shows the effect of changing the number of equally spaced measurements over the first 250 s. Results have been plotted for 10, 50, 100 and 1000 time measurement points, assuming as before that the standard error in head is 0.0063 m (0.25 in). The lowest sample rate is about the most one could achieve with a mechanical tape arrangement. There is a significant decrease (an order of magnitude or more) in the estimated standard error for all parameters as the number of measurements is increased. Note that the slug tests are always the least sensitive to the storage coefficient (S), as expected from earlier sensitivity analysis. Generating the kind of data shown in Fig. 8, for a range of anticipated aquifer parameters, allows one to plan the number of measurements necessary to obtain the desired experimental accuracy in a given situation. Uniform sampling in time is not necessary and is not the optimum way to sample; however, it was chosen here because that is the standard option on many data acquisition systems.

Placement of measurements in time is also important as we have noted earlier, because sampling at maximum sensitivity and minimizing correlation are both critical. Suppose that one concluded from Fig. 8 that about 50 time measurements were adequate. Fig. 9 shows the predicted estimated standard error for the three parameters when 50 measurements, 1 s apart, are used in different time sections of the slug test. The moving center point of this measurement interval is plotted versus estimated standard error in Fig. 9. The lowest estimated standard errors occur when

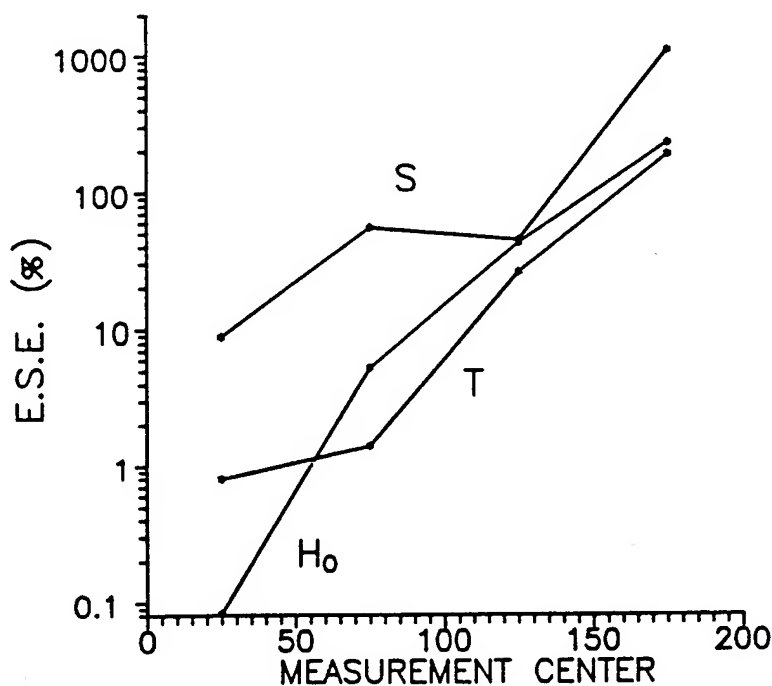


Fig. 9. Estimated standard error of the parameters as a function of the placement of the measurement interval for a typical slug test in the Kansas River alluvium.

measurements are made over the first 50 s which includes sampling of all the sensitivity maxima. In general, as the 50 measurements are moved to larger times the estimated standard error increases owing to decreasing sensitivity at larger times. However, the curve for S shows a kink when the measurement center is at 125 s, which is caused by changing correlation with T . In general, the estimated standard error depends both on the magnitudes of the sensitivities sampled and the correlation that exists between any two sensitivities with that particular sampling scheme.

6. Summary and conclusions

In conclusion, sensitivity analysis is useful for designing better slug tests. Generic sensitivity coefficients for T and S can be defined using a dimensionless time parameter (β) that incorporates the transmissivity. Each value of α (related to storage coefficient) gives a different sensitivity curve, so a family of curves is generated. Two facts stand out from this family of curves. First, the sensitivity to S is much lower than that to T . Second, the sensitivity curves for T and S are very similar in shape, therefore the correlation is high. As a result of these two facts, T and S usually can not both be reliably estimated unless very high quality data with appropriate sampling are available. Usually, the estimate for transmissivity is much better than that for the storage coefficient. This difference in the quality of the two estimates increases with smaller values of α .

Sensitivity analysis shows that the estimated standard errors of the parameters are inversely proportional to H_0 . Therefore, large initial heads should be used whenever possible. This will not always be possible due to other conflicting considerations. We have observed non-linear effects associated with large initial heads in some high conductivity aquifers, and the present paper does not consider such effects. Non-linear effects can be tested for by measuring the slug test response with different initial heads. All responses should fit on a single curve similar to Fig. 1, with no head dependence if non-linear effects are negligible.

Generally, an increased number of measurements improves parameter estimation, if they are properly placed in time. Early time measurements are important for defining H_0 accurately, however, they do little for determining T and S . In order to obtain the best estimates for T and S , measurement times should be selected to minimize the correlation between the sensitivity coefficients for T and S and to sample at points of maximum sensitivity. High density data sampling is best done with high quality pressure transducers and high speed data sampling using computers or data loggers. If a large amount of high quality data is taken during the test, it is always possible to take subsamples of the data set to achieve various goals later.

Acknowledgments

The research for this paper was sponsored in part by the Kansas Water Resources Research Institute through grants from the US Geological Survey (USGS). This

research was also sponsored to a lesser degree by two other agencies: the Air Force Office of Scientific Research, Air Force Systems Command, USAF, under grant or cooperative agreement number, AFOSR 91-0298 and the US Geological Survey (USGS), Department of the Interior, under USGS award number 14-08-0001-G2093. The views and conclusions contained in this document are those of the authors and should not be interpreted as necessarily representing the official policies, either expressed or implied, of the Air Force Office of Scientific Research, of the US Geological Survey, or of the US Government. The US Government is authorized to reproduce and distribute reprints for Governmental purposes notwithstanding any copyright notation thereon.

References

- Beck, J.V. and Arnold, K.J., 1977. *Parameter Estimation in Engineering and Science*. John Wiley, New York.
- Black, J.H., 1978. The use of slug tests in groundwater investigations. *Water Serv.*, March: 174–178.
- Boak, R.A., 1991. Auger hole, piezometer, and slug tests: A literature review. MSc. Thesis, Groundwater Engineering, Department of Civil Engineering, University of Newcastle upon Tyne.
- Bohling, G.C. and McElwee, C.D., 1992. SUPRPUMP: An interactive program for well test analysis and design. *Ground Water*, 30: 262–268.
- Bredehoeft, J.D. and Papadopoulos, I.S., 1980. A method for determining the hydraulic properties of tight formations. *Water Resour. Res.*, 16: 233–238.
- Butler, Jr., J.J. and McElwee, C.D., 1990. Variable-rate pumping tests for nonuniform aquifers. *Water Resour. Res.*, 26: 291–306.
- Chirlin, G.R., 1990. The slug test: The first four decades. In: *Proc. NWWA 1990 Cluster of Conferences, 20–21 February 1990, Groundwater Management and Wellhead Protection*. NWWA, Dublin, OH, pp. 365–381.
- Cooper, H.H., Bredehoeft, J.D. and Papadopoulos, I.S., 1967. Response of a finite-diameter well to an instantaneous charge of water. *Water Resour. Res.*, 3: 263–269.
- Ferris, J.G. and Knowles, D.B., 1954. The slug test for estimating transmissibility. *U. S., Geol. Surv., Ground Water Note* 26.
- Ferris, J.G., Knowles, D.B., Brown, R.H. and Stallman, R.W., 1962. *Theory of aquifer tests*. U. S., Geol. Surv., Water-Supply Pap. 1536-E.
- Gill, P.E., Murray, W. and Wright, M.H., 1981. *Practical Optimization*. Academic, London.
- Hvorslev, M.J., 1951. Time lag and soil permeability in ground-water observations. *U. S. Army, Corps of Eng., Waterways Exp. Stn, Bull. No.* 36.
- Karasaki, K., Long, J.C.S. and Witherspoon, P.A., 1988. Analytical models of slug tests. *Water Resour. Res.*, 24: 115–126.
- Knopman, D.S. and Voss, C.I., 1987. Behavior of sensitivities in the one-dimensional advection–dispersion equation: Implications for parameter estimation and sampling design. *Water Resour. Res.*, 23: 253–272.
- Marschall, P. and Barczewski, B., 1989. The analysis of slug tests in the frequency domain. *Water Resour. Res.*, 25: 2388–2396.
- McElwee, C.D., 1987. Sensitivity analysis of ground-water models. In: J. Bear and M. Yavuz Corapcioglu (Editors), *Proc. 1985 NATO Advanced Study Institute on Fundamentals of Transport Phenomena in Porous Media*. Martinus Nijhoff, Dordrecht, pp. 751–817.
- Neuzil, C.E., 1982. On conducting the modified slug test in tight formations. *Water Resour. Res.*, 18: 439–441.
- Pandit, N.S. and Miner, R.F., 1986. Interpretation of slug test data. *Ground Water*, 24: 743–749.
- Papadopoulos, I.S., Bredehoeft, J.D. and Cooper, H.H., 1973. On the analysis of slug test data. *Water Resour. Res.*, 9: 1087–1089.

- Patterson, R.J. and Devlin, J.F., 1985. An improved method for slug tests in small-diameter piezometers. *Ground Water*, 23: 804–805.
- Priddle, M., 1989. A slug test packer for five-centimeter (two-inch) wells. *Ground Water*, 27: 713–714.
- Sun, N.-Z. and Yeh, W.W.-G., 1990a. Coupled inverse problems in groundwater modeling 1. Sensitivity analysis and parameter identification. *Water Resour. Res.*, 26: 2507–2525.
- Sun, N.-Z. and Yeh, W.W.-G., 1990b. Coupled inverse problems in groundwater modeling 2. Identifiability and experimental design. *Water Resour. Res.*, 26: 2525–2540.

**Appendix B. Sensitivity Analysis of Slug Tests. Part 2. Observation Wells,
Published in the *Journal of Hydrology*,
Volume 164, pages 53-67, 1995.**

[2]

Sensitivity analysis of slug tests Part 2. Observation wells

C.D. McElwee*, J.J. Butler, Jr., G.C. Bohling, W. Liu
Kansas Geological Survey, 1930 Constant Ave., Lawrence, KS 66047, USA

Received 30 September 1993; revision accepted 25 June 1994

Abstract

An earlier paper (Part 1, this issue) dealt with the use of sensitivity analysis for the design of a slug test that would give reasonably accurate estimates of the aquifer parameters by an informed choice of the number and times of measurements. An investigation of the radial dependence of the Cooper et al. analytical solution for a slug test in a confined aquifer shows that the use of one or more observation wells can vastly improve the parameter estimates, particularly the estimate of the storage parameter. Generally, the observation well must be fairly close (about 10 m or less) to the slugged well to be effective. The storage coefficient must be small in order to see the effect of the slug at greater distances from the stressed well. Since the temporal and spatial dependence of the sensitivities for transmissivity and storage are considerably different, the addition of one or more observation wells will substantially reduce the correlation between these two parameters, which will result in much better estimates than are usually obtained in slug tests. These ideas are illustrated using typical data representative of our research sites.

1. Introduction

Slug tests are commonly used for site characterization because they are relatively easy and inexpensive to perform. Although a great deal of information about the aquifer hydraulic parameters in the vicinity of the stressed well is contained in slug test data, it is unclear if current practices are actually yielding accurate estimates of those parameters. At the Kansas Geological Survey (KGS), we have been studying the capabilities and limitations of the slug test as a tool for site characterization. This is the second paper in a series detailing our findings. An earlier paper (McElwee et al., 1995) dealt with the use of sensitivity analysis to design a slug test that would give

* Corresponding author.

reasonable estimates of homogeneous aquifer parameters by an informed choice of the number and times of measurements.

Most practitioners know that slug tests are not very sensitive to the storage coefficient; the reasons for this are explained in the earlier paper (McElwee et al., 1995). The complete analytical solution of Cooper et al. (1967, henceforth designated the CBP solution) includes the time-varying radial dependence of head away from the slugged well. Most researchers use the form restricted to the slugged well itself and simply measure head data in the slugged well. In this paper we investigate the use of observation wells with slug tests. Since slug tests are often used as a rapid, inexpensive, and sometimes first attempt at characterizing a site, many times observation wells are not available. However, we also know from experience that sometimes other wells, which were installed for other purposes, are available nearby. It is probably not economically feasible most times to install observation wells specifically for use with slug tests. On the other hand, if nearby wells are available we advocate that the field investigator consider using them as observation wells. The objective of this paper is to show that the use of one or more observation wells can vastly improve the parameter estimates, particularly the estimate for storage. The tools we use for this study are sensitivity analysis (McElwee, 1987) and an automated well test analysis package, SUPRPUMP (Bohling and McElwee, 1992), developed at the KGS.

A number of other researchers have considered the radial dependence of slug tests and/or the use of observation wells with slug tests, although, not in the quantitative manner presented here. Ramey et al. (1975) were perhaps the first to investigate the radius of influence of a slug test. They showed that a measurable response in an observation well could be observed at a distance of 100 well radii or more from the stressed well under favorable conditions. However, they did not advocate the routine use of observation wells. They simply wanted to refute arguments that slug tests were affecting only a small volume of the aquifer. Walter and Thompson (1982) advocated using repeated slug test pulses with observation wells in tight formations. However, they used the Ferris and Knowles (1954) solution with its assumption of vanishing stressed well radius (i.e. no well bore storage). The advantages of using observation wells with slug tests that Walter and Thompson saw were that a larger volume was tested, that storativity can be determined from the observation well response, and that anisotropy may be determined. Barker and Black (1983) and Black (1985) also considered the concept of the radius of influence of a slug test, which they defined as the radius where a given fraction of the initial slug input (H_0) can be measured in an observation well. Sageev (1986) presented a good discussion of radius of influence and showed some detailed curves for head in observation wells. He pointed out that wellbore storage in observation wells can dramatically reduce the response there, and suggested that packers be used in observation wells to reduce the effect of observation wellbore storage. Karasaki et al. (1988) presented slug-test solutions for various geometries that may be encountered in heterogeneous systems, including head (interference) responses at observation wells for slug tests. They graphed head response at some radial distances and came to the conclusions that: (1) fairly large responses can be observed at wells a considerable distance away under the right conditions; (2) curves characterizing different storativities are uniquely different at

the observation well; and (3) transmissivity and storativity can be estimated independently. Novakowski (1989) also considered pulse interference tests (observing slug test responses at observation wells). He developed solutions including wellbore storage effects at the observation well, thus extending the earlier work of Sageev (1986). (He also recommended isolating the observation interval with packers to minimize observation wellbore storage effects.) Novakowski gave his solutions in Laplace space and used the Talbot algorithm for inversion. He presented the radial response of a slug test for some cases and defined a graphical analysis procedure to overcome borehole storage effects at the observation well. Chirlin (1989) realized that the head distribution as a function of radius around a slugged well was different for the Hvorslev (1951) and CBP solutions, but he did not suggest the use of observation wells to determine the storage coefficient. He did show some contours of head versus radius for the CBP model. Chirlin (1990) later commented on the radius of influence of a slug test and noted that “it would not be unusual to have a radius of investigation equal to hundreds of well radii”. However, the use of observation wells for parameter estimation was not addressed. Recently, Guyonnet et al. (1993) have analyzed the volume of investigation for a slug test. They considered the effect of various boundaries on the slugged well response, but they did not explicitly consider the use of measurements from an observation well.

In this paper we attempt to quantify the use of observation well data along with slugged well data to determine aquifer parameters. Generic plots of relative head show the radius of influence of a slug test as a function of α (storage coefficient and well radii), β (transmissivity and time), and r (observation radius). Plots of sensitivity coefficients versus α , β , and r are used to illustrate the regions where time and space measurements give the greatest sensitivity to the aquifer parameters. The issue of correlation between parameters, in particular T and S , is addressed. Graphically, the sensitivity coefficients show why measurements in the slugged well are relatively insensitive to S and why the addition of an observation well reduces the correlation and provides better estimates of S . The paper concludes with applications to data typical of our research sites.

2. Analytical solution for slug tests

The complete CBP analytical solution for the radial dependence of head around a slugged well having a finite radius is given by

$$H\left(\alpha, \beta, H_0, \frac{r}{r_s}\right) = \frac{2H_0}{\pi} \int_0^{\infty} \frac{\exp(-\beta x^2/\alpha)}{\Delta(x)} F\left(x, \alpha, \frac{r}{r_s}\right) dx \quad (1)$$

where

$$F\left(x, \alpha, \frac{r}{r_s}\right) = \left\{ J_0\left(x \frac{r}{r_s}\right) [xY_0(x) - 2\alpha Y_1(x)] - Y_0\left(x \frac{r}{r_s}\right) [xJ_0(x) - 2\alpha J_1(x)] \right\} \quad (2)$$

and

$$\Delta(x) = [xJ_0(x) - 2\alpha J_1(x)]^2 + [xY_0(x) - 2\alpha Y_1(x)]^2 \quad (3)$$

x is the variable of integration, J and Y are Bessel functions, and r_s and r_c are the screen and casing radii, respectively. The variables α and β are defined as

$$\beta = \frac{Tt}{r_c^2} \quad (4)$$

$$\alpha = \frac{r_s^2}{r_c^2} S \quad (5)$$

This analytical solution shows that slug-test responses can be expressed as a function of four parameters: α , a parameter related to screen and casing radii and the storage coefficient; β , a dimensionless time involving transmissivity and the casing radius; H_0 , the initial head displacement; and r/r_s , the distance to an observation well divided by the screen radius. It is often convenient to use relative head (h), which is defined as

$$h = \frac{H}{H_0} \quad (6)$$

It should be stressed that in many complex geologic environments the CBP model may not be adequate. However, this study should give valuable specific insight when the CBP model is applicable and perhaps general insight to more complex situations. It should be emphasized at this point that these analytically predicted responses, Eq. (1), are assuming no observation wellbore storage. If indeed open boreholes of substantial radii are used as observation wells, the response obtained will be much smaller owing to wellbore storage effects. For this reason, we will assume from here on that a packer has been placed in the observation well to minimize wellbore storage effects. The effectiveness of the packer will depend on the elastic properties of the gland material under the given inflation pressures. If packers in good condition of nearly the same diameter as the hole are used with inflation pressures of 50 psi or more, they should be adequate in shallow wells.

3. Sensitivity analysis

Sensitivity analysis (McElwee, 1987) can be used to look at the effect of a small parameter change on the head. Background material is presented in some detail in the first paper (McElwee et al., 1994) and will only be briefly summarized here for completeness. A first-order Taylor series expansion can be performed and used to define normalized sensitivity coefficients of relative head to the parameters, in this case T , S , and H_0 . These sensitivity coefficients

$$u'_T = T \frac{\partial h}{\partial T} = \beta \frac{\partial h}{\partial \beta} \quad (7)$$

$$u'_S = S \frac{\partial h}{\partial S} = \alpha \frac{\partial h}{\partial \alpha} \quad (8)$$

$$u'_{H_0} = \frac{\partial H}{\partial H_0} = h \quad (9)$$

are simply derivatives of the head with respect to the parameter and may be evaluated analytically or numerically. Sensitivity coefficients are a measure of how much the head changes when a parameter is changed by a small amount; therefore, they are very useful to examine in some detail. The sensitivity coefficients defined by Eqs. (7)–(9) are normalized sensitivities to relative head (dimensionless) and may be compared on a single plot to infer the relative sensitivity of the three parameters. Sensitivity coefficients may be positive or negative, the sign merely indicating the direction of change in head caused by a change in the parameter. These sensitivity functions are only functions of α , β and r/r_s . For given values of α and r/r_s , a generic sensitivity curve can be plotted versus β , which is valid for any value of transmissivity; differing transmissivity values simply scale the time differently. In a similar manner, given values for α and β , a plot can be made showing the radial dependence of the sensitivity coefficient. The fact that may vary over a wide range gives rise to a family of curves in each of these plots. All normalized sensitivity plots in the following sections are of Eqs. (7)–(9) and are dimensionless.

4. Relative head or sensitivity to H_0

Figs. 1–4 display the dependence of the relative head (h), or the sensitivity to H_0 (u'_{H_0} , Eq. (9)), on the parameters α , β , and the normalized radius (r/r_s). Fig. 1 shows the response that would be expected at several observation well distances, each response in time being a bell-shaped curve whose maximum amplitude decays with distance from the slugged well. At about $175r_s$, the response has fallen to about $0.01 H_0$ at a dimensionless time of 10 for $\alpha = 10^{-3}$. Fig. 2 shows the radial dependence for various dimensionless times. From Figs. 1 and 2 it is clear that responses from the stressed (slugged) well can propagate significant distances (50 – $100 r_s$) in the radial direction. Fig. 2 shows that the area of influence spreads with time, but that the response decays and becomes diffuse at later times. Figs. 3 and 4 are designed to show the effect of α (related to storage coefficient and the ratio of screen radius to casing radius squared) on the response in time and space. Clearly, smaller α 's result in larger responses in space and time. For $\alpha = 10^{-5}$ it is clear that significant responses can be propagated to distances of over 200 screen radii. It would clearly be beneficial to construct a well with a casing radius several times the screen radius if that did not create an economical or logistic problem. A factor of just over 3 increase in the ratio of casing radius to screen radius will decrease α by an order of magnitude, thereby increasing the response at observation wells, whatever the naturally occurring storage coefficient.

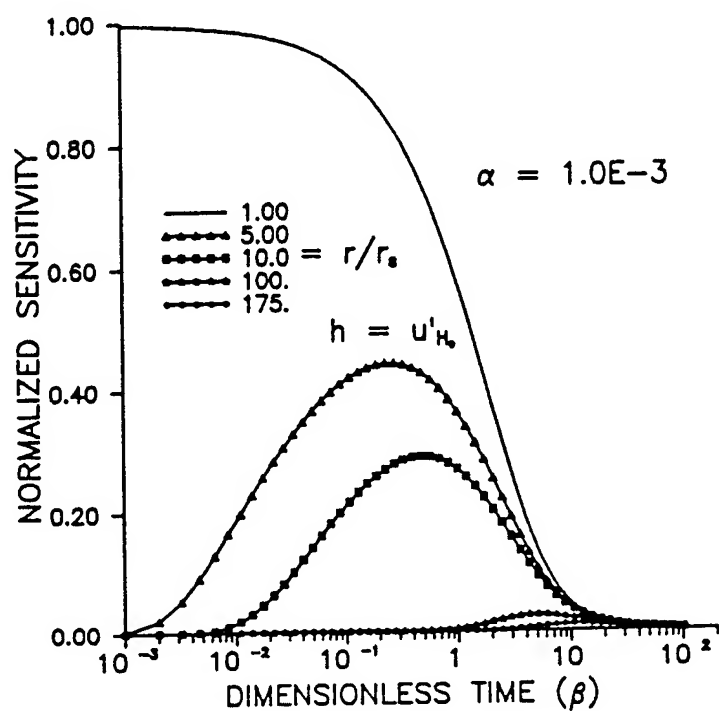


Fig. 1. Variation of u'_{H_0} with time for various r/r_s .

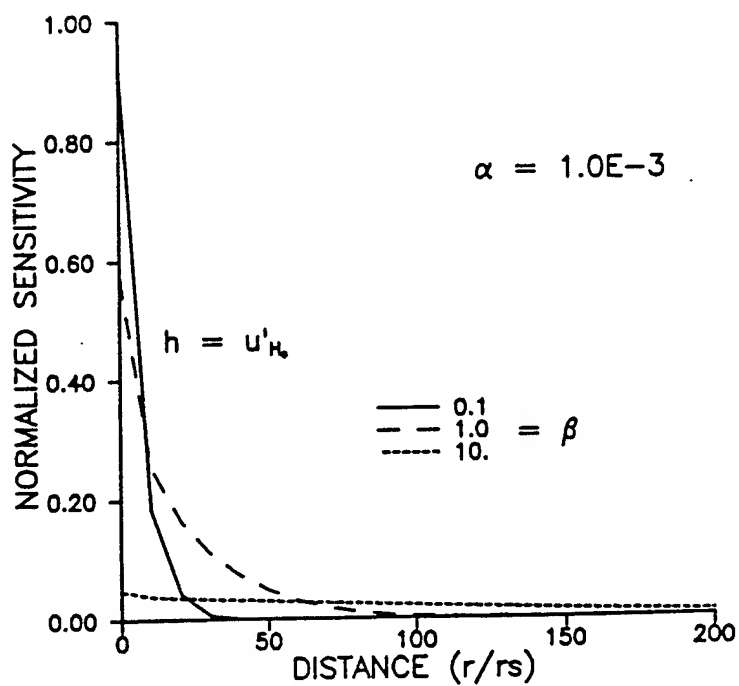
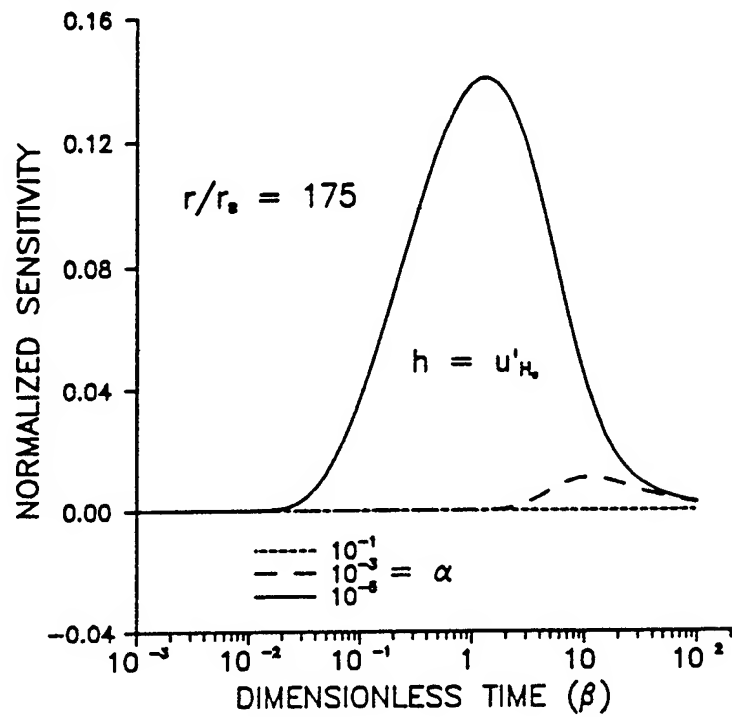
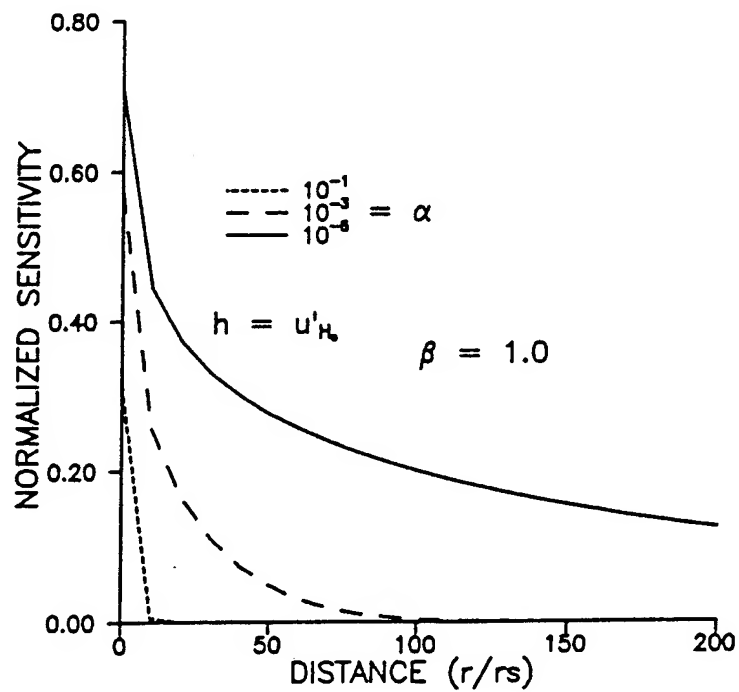


Fig. 2. Variation of u'_{H_0} with distance for various times.

Fig. 3. Variation of u'_{H_0} with time for various α .Fig. 4. Variation of u'_{H_0} with distance for various α .

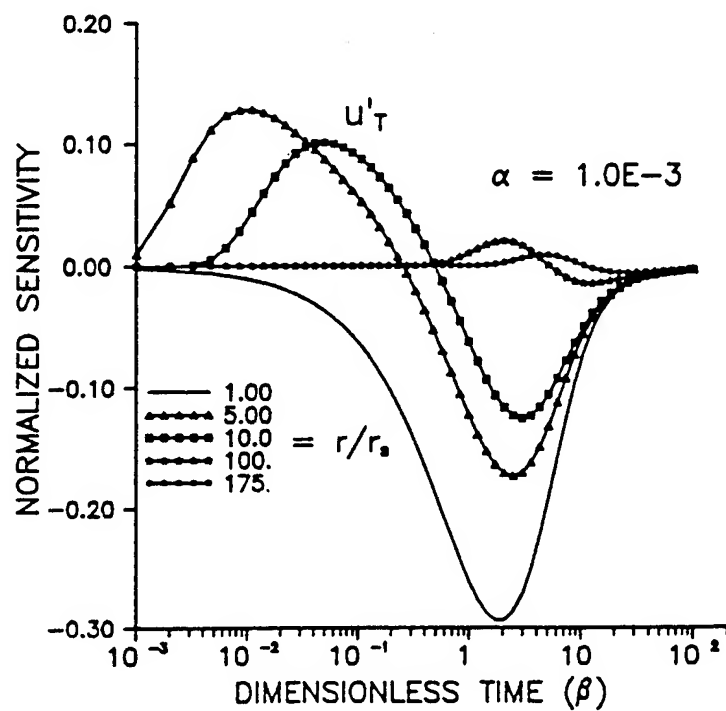


Fig. 5. Variation of u'_T with time for various r/r_s .

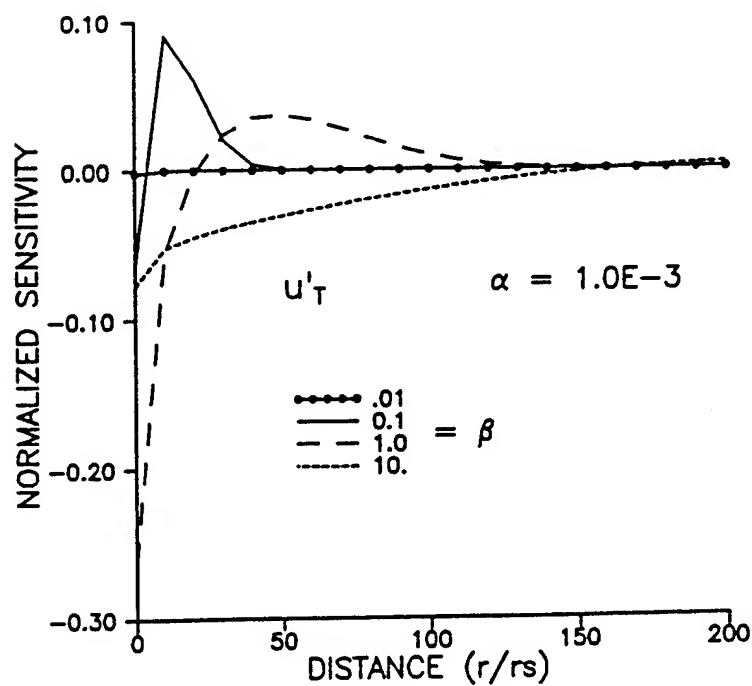
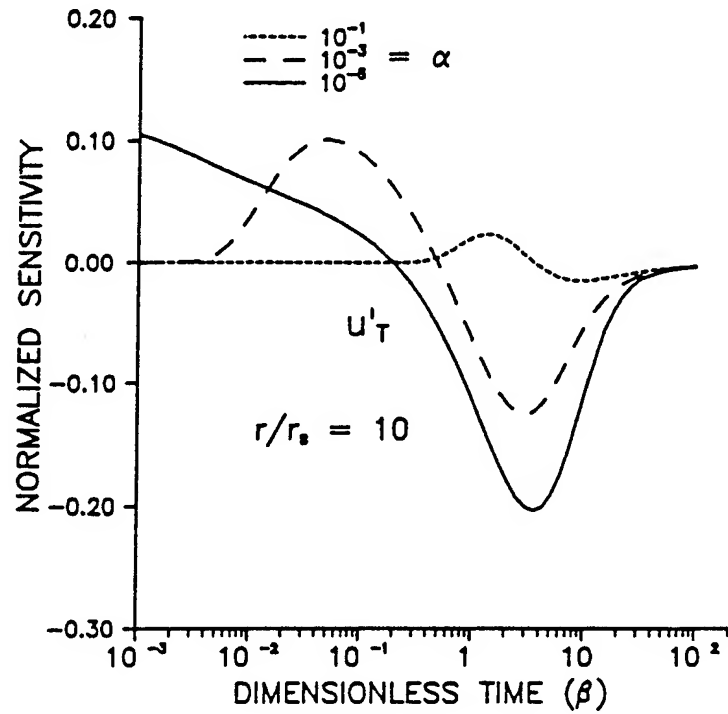
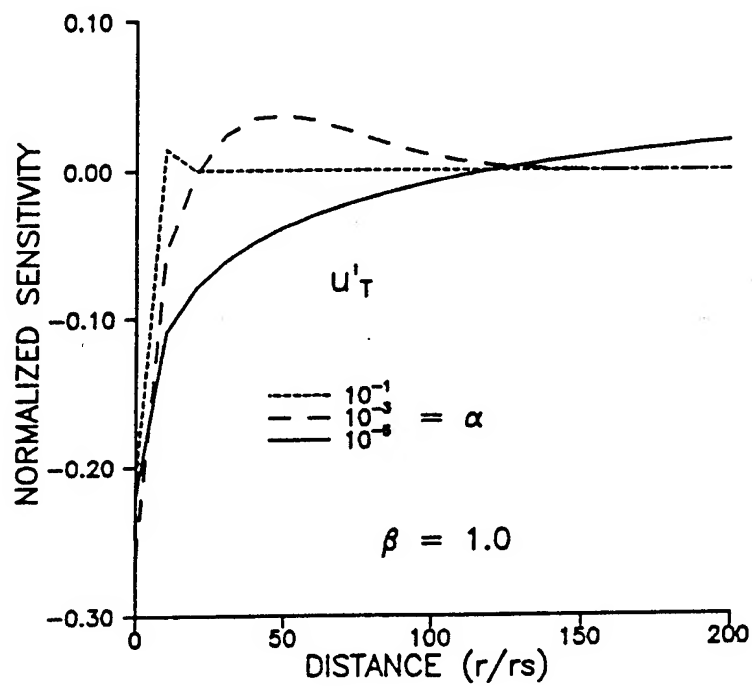


Fig. 6. Variation of u'_T with distance for various times.

Fig. 7. Variation of u'_T with time for various α .Fig. 8. Variation of u'_T with distance for various α .

5. Sensitivity to transmissivity

Figs. 5–8 illustrate the dependence of the sensitivity to transmissivity (u'_T) on time, distance, and α . As shown on Figs. 5 and 6, the sensitivity to transmissivity has positive and negative lobes in time and space except for $r = r_s$. These figures (5 and 6) indicate that the maximum sensitivity to transmissivity occurs near the slugged well. Somewhat surprising is the fact that for early times the maximum sensitivity to transmissivity is near but not at r_s . A given observation well will be sensitive to the transmissivity over a definite time interval (Fig. 5), with the magnitude of the sensitivity decaying rapidly with increasing r . Figs. 7 and 8 illustrate the dependence of the sensitivity to transmissivity on α . The maximum amplitude of the sensitivity seems to vary inversely with α (Fig. 7), while the amplitude at $r = r_s$ does not seem to have a strong dependence on α (Fig. 8). As noted previously, a small α is required for sensitivities to propagate a considerable distance from the slugged well (Fig. 8).

6. Sensitivity to storage

Figs. 9–12 illustrate the dependence of the sensitivity to storage (u'_S) on α , β , and r . Figs. 9 and 10 indicate that the maximum sensitivity does not occur at $r = r_s$, but rather at a distance which increases with time. Fig. 10 shows that the pulse of sensitivity to storage moves out to larger distances while widening and decaying with increasing time. Fig. 11 shows that, for a chosen r , the maximum amplitude

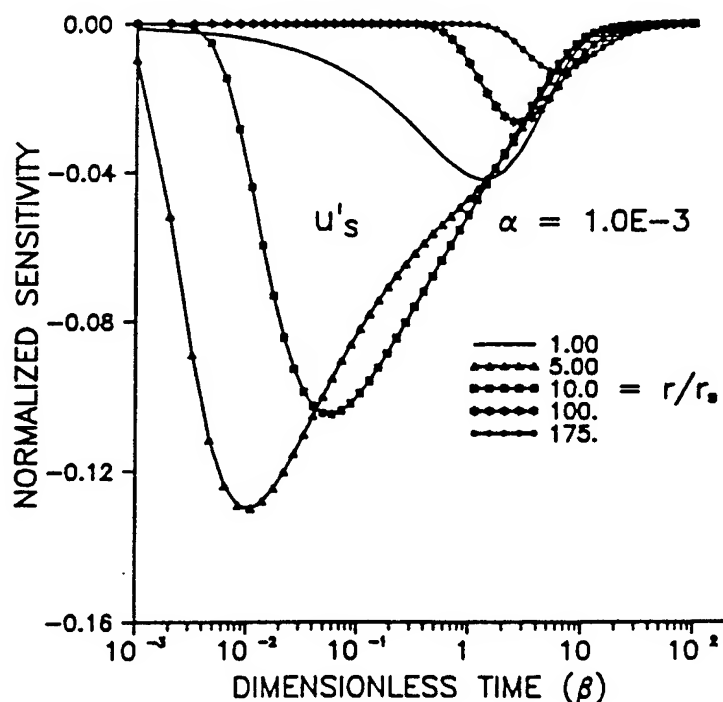
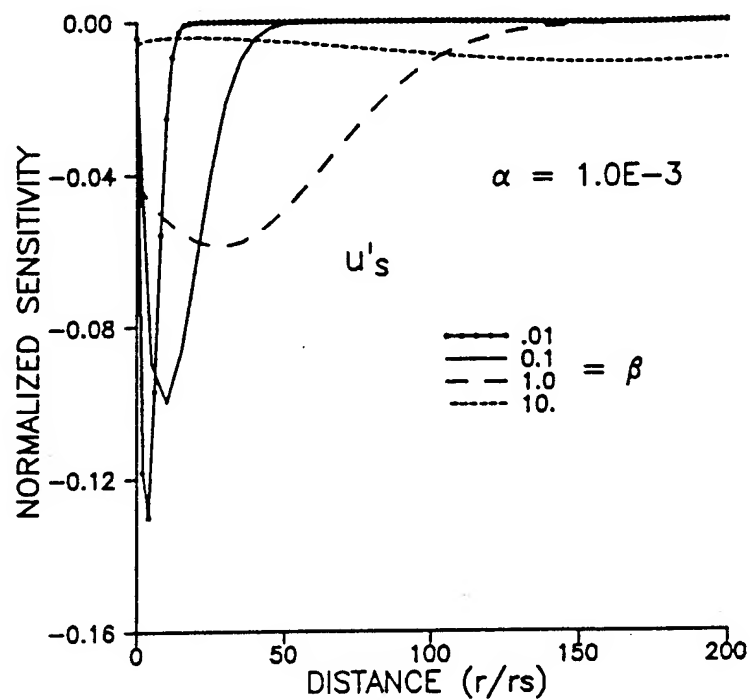
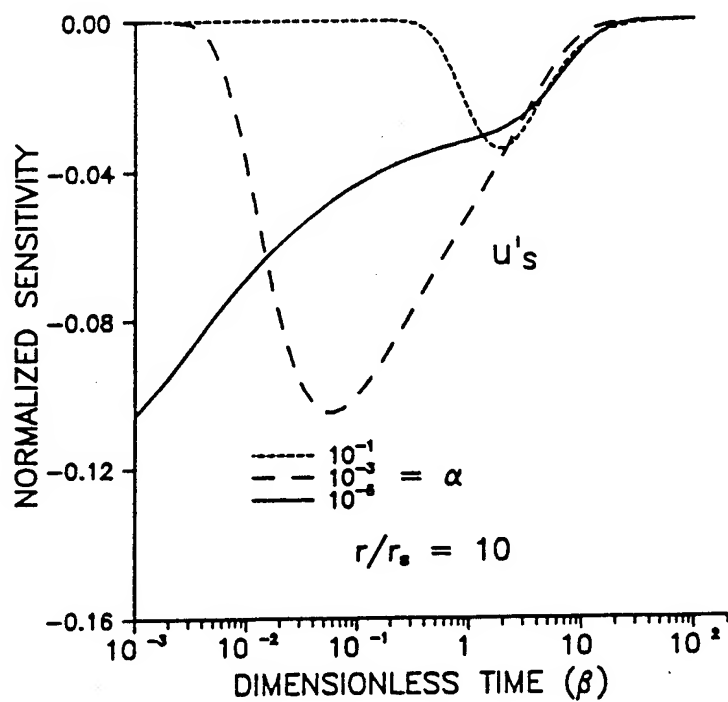


Fig. 9. Variation of u'_S with time for various r/r_s .

Fig. 10. Variation of u'_s with distance for various times.Fig. 11. Variation of u'_s with time for various α .

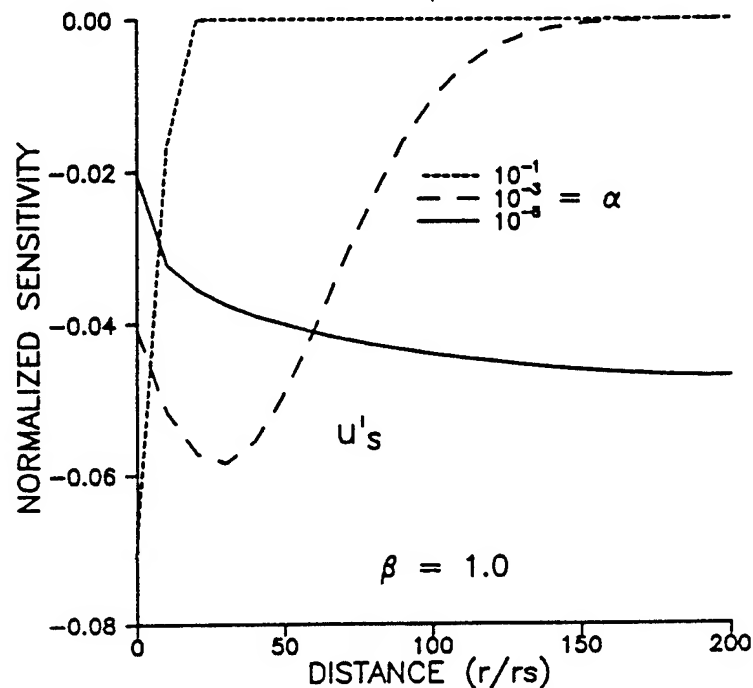


Fig. 12. Variation of u'_s with distance for various α .

of the sensitivity is inversely proportional to α and occurs at earlier times for smaller α 's. The dependence on α shown in Fig. 12 reveals that the signal for the sensitivity with respect to storage propagates much farther from the well for smaller values of α .

7. Parameter estimation and error analysis

The first paper of this series (Part 1, McElwee et al., 1995) and other papers (McElwee, 1987; Butler and McElwee, 1990) present a detailed discussion of the relationship of parameter estimation and error analysis to sensitivity coefficients, so that material will only be briefly summarized here. A common method of performing parameter estimation involves minimizing a squared error functional which can be written in terms of sensitivity coefficients (Eq. (14), Part 1). The sensitivity design matrix $[A]$ (Eq. (15), Part 1) arises naturally out of the process of minimizing the error functional. In general, the solution is well behaved if the diagonal elements are large and nearly equal and the off-diagonal elements are small. This will be the case if the sensitivity coefficients are large and do not have similar shapes over the chosen measurement times and locations. One way to measure the similarity of the sensitivity coefficients is to define the sensitivity correlation matrix (Eq. (16), Part 1). The reliability of the parameter estimates can be assessed by looking at the parameter covariance matrix (Eq. (17), Part 1). Usually some simplifying assumptions about the errors in head such as additive, zero mean, uncorrelated and constant variance (Beck and Arnold, 1977) are made. With these assumptions, the estimated standard errors

(ESE) of the parameters and confidence intervals can be related to the square root of the diagonal elements of the parameter covariance matrix (Eq. (18), Part 1). A computer program for automated least squares analysis of well-test data using sensitivity analysis, SUPRPUMP (Bohling and McElwee, 1992), has been used in this work to do the parameter estimation and to compute sensitivity correlations and confidence intervals.

8. Correlation of u'_T and u'_S

Fig. 13 is from our earlier paper (Part 1, McElwee et al., 1995) showing that the shape of the sensitivities with respect to transmissivity and storage at $r = r_s$ are extremely similar except for amplitude. This means that responses in a slugged well are much more sensitive to T than S and that there will be high correlation between these two parameters. Consequently, rarely can one determine both T and S with only data from the slugged well (Part 1, McElwee et al., 1995). On the other hand, Fig. 14 shows the same two sensitivities for an observation well at $r = 10r_s$. The sensitivity coefficient plots have considerably different shapes and nearly the same maximum amplitude. This means that the observation well is much more sensitive to storage than the slugged well and that the correlation between T and S will be dramatically reduced by the use of an observation well. In the next two sections these ideas of using one or more observation well with a slug test are illustrated for some cases of practical interest.

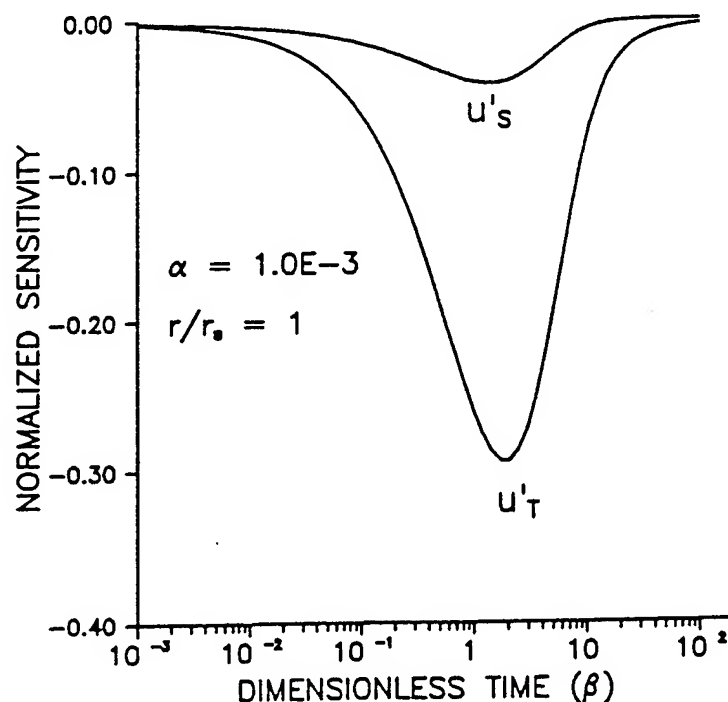


Fig. 13. A comparison of sensitivities (u'_T and u'_S) at the screen radius.

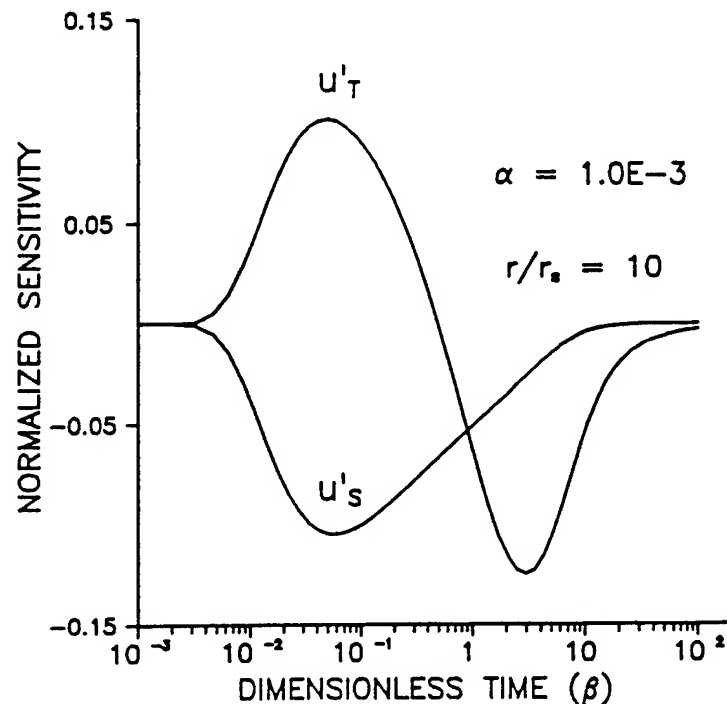


Fig. 14. A comparison of sensitivities (u'_T and u'_S) at a distance of 10 screen radii from the slugged well.

9. Simulation for a field site in an alluvial aquifer

At the KGS, we have developed a field site in the Kansas River alluvium for carrying out research on hydraulic testing. The shallow subsurface at this site consists of about 10.7 m (35 ft) of coarse sand and gravel overlain by about 10.7 m (35 ft) of silt and clay. The following is a simulation of expected results at this site in the very conductive lower sand and gravel zone. From earlier laboratory work and aquifer tests we know some average values for K , T and S . $K \approx 91.3 \text{ m day}^{-1}$ (300 ft day $^{-1}$ or 0.208 ft min $^{-1}$); $T \approx 91.3 \text{ m day}^{-1} \times 10.7 \text{ m} = 974 \text{ m}^2 \text{ day}^{-1}$ (7.28 ft 2 min $^{-1}$); $S \approx 0.00063$.

We simulate the results for a slugged well and two observation wells at 1.5 m (5 ft) and 3.0 m (10 ft) away, taking data with a high sample rate over a 3 min interval (slug tests have a very short duration in this media). The initial slug height is taken as 3 m (10 ft). It is assumed the slugged well is 0.10 m (4 in) in diameter and all wells are fully screened. The simulated data are rounded to the nearest 0.03 m (0.1 ft) and then analyzed with the SUPRPUMP program (Bohling and McElwee, 1992). The results are shown in Table 1 for three different data sets: (1) data from the slugged well only; (2) data from the slugged well and one observation well; and (3) data from the slugged well and both observation wells.

The ranges of T and S shown in Table 1 are the approximate 95% confidence limits calculated by SUPRPUMP. The correlation between the two parameters (Corr.) is also shown. The root mean squared deviation (rms Dev.) is an indication of the average level of noise present or the degree of lack of fit to the theoretical model.

Table 1
Simulated alluvial results

	Slugged well only	Slugged well + obs. well	Slugged well + 2 obs. wells
Range of T ($\text{m}^2 \text{day}^{-1}$)	951–1070	966–986	969–987
Range of S ($\times 10^{-3}$)	0.178–0.722	0.616–0.666	0.609–0.648
Corr.	0.98	0.54	0.44
rms Dev. (m)	0.0079	0.0079	0.0076
Remarks	Trouble converging	Converging rapidly	

The rms deviation of near 0.0076 m (0.025 ft) is consistent with data rounded to the nearest 0.03 m (0.1 ft). Table 1 shows that when only slugged well data are analyzed, the calculated ranges for T and S are relatively broad and there is an extremely high correlation of 0.98 between T and S . As a result, the SUPRPUMP program sometimes has trouble converging to a unique solution, depending on the starting values. Note that although the addition of one or two observation wells does not greatly improve the model fit (rms deviation), the width of the parameter ranges and the magnitude of the correlation are significantly decreased. As a result, the SUPRPUMP program converges rapidly to a unique solution in most cases, being much less sensitive to starting values. The reason for this can be seen by plotting contours of

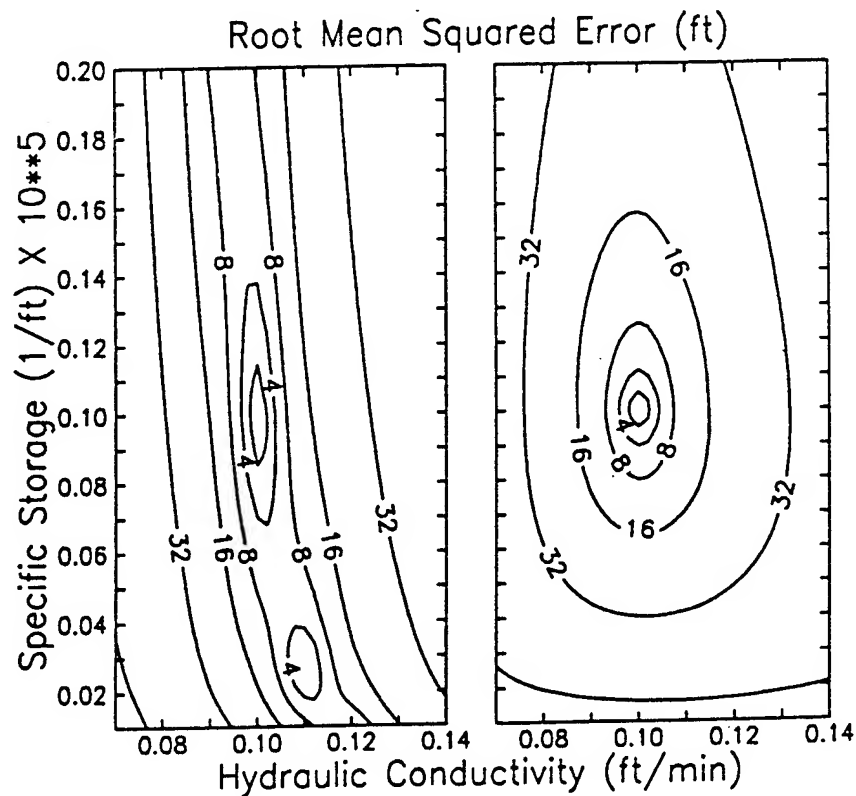


Fig. 15. Error functional contours plotted vs. specific storage and hydraulic conductivity when only the slugged well data are used (left side) and when both slugged well and observation well data are used (right side).

the error functional (Eq. (13), Part 1, McElwee et al., 1995) versus trial parameter values (T and S) for two cases: (1) for slugged well data alone, and (2) for data from both the slugged well and the observation well. Fig. 15 illustrates this point for a slightly different aquifer configuration but similar to that used in this section. In the case of Fig. 15 we are plotting the error functional versus two parameters, specific storage and hydraulic conductivity. The plot on the left in Fig. 15 displays the error functional when only data from the slugged well are used. It is easy to see that the minimum is elongated along the y -axis and that a potential false local minimum exists at smaller values of specific storage. In contrast, the plot on the right in Fig. 15 includes data from the slugged well and an observation well. Including observation well data makes the error functional contours more nearly circular and the minimum much more clearly defined. There is no indication of a possible false local minimum. Therefore, it is easier to arrive at good fitted values with a fitting program.

Actually, we have had trouble observing the expected level of response at the alluvial field site described; a number of things may be contributing to that problem. Until recently only 2 in wells were available for testing; we expect that larger diameter wells will increase the magnitude of the signal at observation wells. Other possible problems include partial penetration in some wells and the effect of leakage by the overlying aquitard. Additional work at this site indicates that partial penetration of some wells may be our main problem in observing the expected level of response. McElwee and Butler (1993) show that partial penetration effects can reduce the expected response from the CBP model by an order of magnitude. However, for a nearly ideal confined system with a fairly small storage coefficient and a long screen, the use of observation wells with slug tests should produce good results as seen in the next section.

10. Results from Dakota aquifer, Lincoln County, Kansas

A program of well testing is being carried out by the KGS as part of a regional study of the Dakota aquifer (a sandstone aquifer of Cretaceous age) in Kansas. At one site in Lincoln County, Kansas, two wells (0.102 m (4 in) and 0.051 m (2 in) in diameter and about 30 m (100 ft) deep), screened over similar intervals (24–30 m (80–100 ft)), are located 6.46 m (21.2 ft) apart. A number of slug tests were carried out at this site and they illustrate some of the concepts discussed in this paper. These tests consisted of introducing a slug at the larger of the two wells and measuring the responses both at the stressed well and at the observation well. Measurements from the observation well were taken using a transducer placed below a packer located just above the top of the screen. The packer enabled effects associated with wellbore storage at the observation well to be kept very small. Three different data sets were used in the analysis of the test responses: (1) data from the stressed well only; (2) data from the observation well only; and (3) data from both the stressed well and the observation well. The results of these three analyses are shown in Table 2.

Fig. 16 shows the field measurements and fitted model results for the analysis using the third data set. The model seems to fit the field data extremely well. Although the

Table 2
Dakota aquifer results

	Slugged well	Obs. well	Slugged well + obs. well
T ($\text{m}^2 \text{day}^{-1}$)	7.20	8.03	8.26
S ($\times 10^{-4}$)	2.0	0.51	0.52
Corr.	0.99	0.27	0.49
rms Dev (m)	0.0067	0.0084	0.0112

actual parameter values for this site are not known, the results of the sensitivity analysis and the previous theoretical example indicate that the parameters in Table 2 from the second and third data sets are probably more representative of conditions at the site than the parameters from the first data set. Note that the dramatic decrease in correlation is seen when data from an observation well are employed making the $[A]$ matrix (Eq. (15), Part 1) much better conditioned. Additional work on the analysis of this data has shown that it is important to make a critical analysis of the best effective screen radius to use in the definition of α (Eq. 5). This choice will usually lie somewhere between the actual screen radius and the radius of the gravel pack. The choice of best effective screen radius is much more important if only data from the slugged well are used in the analysis. The analysis of observation well data is much less sensitive to effective screen radius. In the case of Table 2, it is possible to make the estimate for S obtained by analyzing only slugged well data agree with the other two analyses by the appropriate choice of effective screen radius. However, if one does not have observation well data, it is not possible to go through this procedure to obtain consistency of all the analyses.

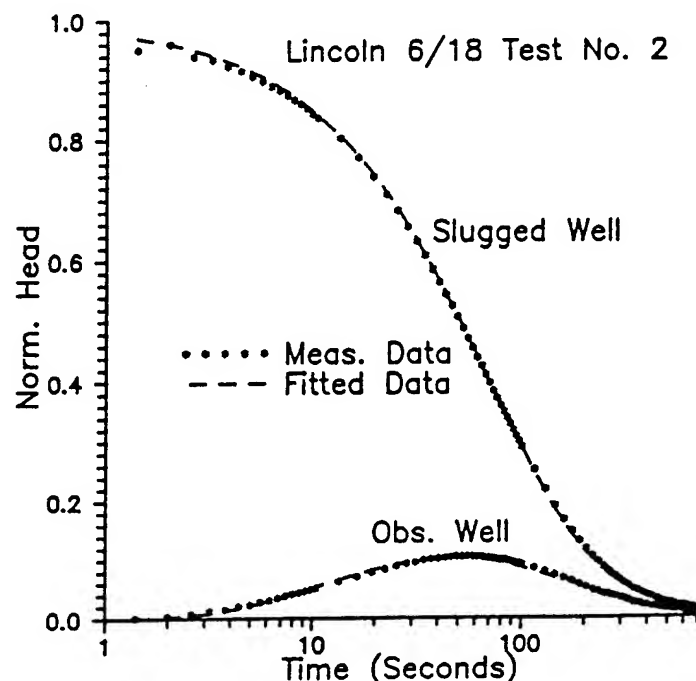


Fig. 16. Experimental and fitted results for the Dakota aquifer test, Lincoln County Kansas.

11. Conclusion

An investigation of the radial dependence of the Cooper et al. (1967) analytical solution for a slug test in a confined aquifer has shown that the use of one or more observation wells can vastly improve fitted parameter estimates, particularly the estimate of the storage parameter. It is usually not practical to install an observation well solely for use in a slug test, however, many times nearby wells are available. Generally, the observation well must be fairly close (about 10 m or less) to the slugged well to be effective. Other mitigating factors such as leakage and partial penetration should be minimal for optimum results. The storage coefficient and the ratio of screen radius to casing radius must be small in order to see the effect of the slug at greater distances from the slugged well. The observation well should be packed off in order to remove or minimize the lagging and damping effect on the signal that occurs due to wellbore storage at the observation well. Since the temporal and spatial dependence of the sensitivities to transmissivity and storage are considerably different, the addition of one or more observation wells will substantially reduce the correlation between these two parameters, which will result in estimates of greater reliability than normally obtained from slug tests.

These ideas have been illustrated using typical data from our research sites. Theoretically, both field examples could benefit from using observation wells with the slug test. However, in practice it has been difficult to see a significant response in observation wells in the leaky alluvial case; several potential problems have been identified. However, observation wells should be most useful in nearly ideal confined systems with a low storage coefficient or α . From a practical standpoint, α can be lowered by about an order of magnitude when using a casing radius a little over three times the screen radius. The other example, from a consolidated sandstone aquifer, bears out this conclusion and shows good agreement with the theory presented here. In this case, the use of an observation well has greatly aided in the determination of the storage coefficient. In conclusion, the use of observation wells with slug tests can significantly improve the reliability of the aquifer parameter estimates where suitable conditions exist.

Acknowledgment

This research was sponsored in part by the Air Force Office of Scientific Research, Air Force Systems Command, USAF, under grant or cooperative agreement number, AFOSR 91-0298. This research was also supported in part by the US Geological Survey (USGS), Department of the Interior, under USGS award number 14-08-0001-G2093. The views and conclusions contained in this document are those of the authors and should not be interpreted as necessarily representing the official policies, either expressed or implied, of the Air Force Office of Scientific Research, of the US Geological Survey, or of the US Government. The US Government is authorized to reproduce and distribute reprints for Governmental purposes notwithstanding any copyright notation thereon.

References

- Barker, J.A. and Black, J.H., 1983. Slug tests in fissured aquifers. *Water Resour. Res.*, 19: 1558–1564.
- Beck, J.V. and Arnold, K.J., 1977. *Parameter Estimation in Engineering and Science*. John Wiley, New York.
- Black, J.H., 1985. The interpretation of slug tests in fissured rocks. *Q. J. Eng. Geol.*, 18: 161–171.
- Bohling, G.C. and McElwee, C.D., 1992. SUPRPUMP: An interactive program for well test analysis and design. *Ground Water*, 30: 262–268.
- Butler, Jr. and McElwee, C.D., 1990. Variable-rate pumping tests for nonuniform aquifers. *Water Resour. Res.*, 26: 291–306.
- Chirlin, G.R., 1989. A critique of the Hvorslev method for slug test analysis: The fully penetrating well. *Ground Water Mon. Rev.*, 9: 130–138.
- Chirlin, G.R., 1990. The slug test: The first four decades. In: *Proc. NWWA 1990 Cluster of Conferences, 20–21 February 1990, Groundwater Management and Wellhead Protection, NWWA*. pp. 365–381.
- Cooper, H.H., Bredehoeft, J.D. and Papadopoulos, I.S., 1967. Response of a finite-diameter well to an instantaneous charge of water. *Water Resour. Res.*, 3: 263–269.
- Ferris, J.G. and Knowles, D.B., 1954. The slug test for estimating transmissibility. U.S., Geol. Surv., *Ground Water Note* 26.
- Guyonnet, D., Mishra, S. and McCord, J., 1993. Evaluating the volume of porous medium investigated during slug tests. *Ground Water*, 31: 627–633.
- Hvorslev, M.J., 1951. Time lag and soil permeability in ground-water observations. U.S. Army, Corps Eng., *Waterways Exp. Stn. Bull.* No. 36.
- Karasaki, K., Long, J.C.S. and Witherspoon, P.A., 1988. Analytical models of slug tests. *Water Resour. Res.*, 24: 115–126.
- McElwee, C.D., 1987. Sensitivity analysis of ground-water models. In: J. Bear and M. Yavuz Corapcioglu (Editors), *Proc. 1985 NATO Advanced Study Institute on Fundamentals of Transport Phenomena in Porous Media*. Martinus Nijhoff, Dordrecht, pp. 751–817.
- McElwee, C.D. and Butler, Jr., J.J., 1993. Characterization of heterogeneities controlling transport and fate of pollutants in unconsolidated sand and gravel aquifers: Second year report. *Open File Rep. 93-21*, Kansas Geological Survey.
- McElwee, C.D., Bohling, G.C. and Butler, Jr., J.J., 1995. Sensitivity analysis of slug tests. Part 1. The slugged well. *J. Hydrol.*, 164: 53–67.
- Novakowski, K.S., 1989. Analysis of pulse interference tests. *Water Resour. Res.*, 25: 2377–2387.
- Ramey, Jr., H.J., Agarwal, R.G. and Martin, I., 1975. Analysis of 'slug test' or DST flow period data. *J. Can. Pet. Technol.*, 14: 37–47.
- Sageev, A., 1986. Slug test analysis. *Water Resour. Res.*, 22: 1323–1333.
- Walter, G.R. and Thompson, G.M., 1982. A repeated pulse technique for determining the hydraulic properties of tight formations. *Ground Water*, 20: 186–193.

**Appendix C. Slug Tests in Partially Penetrating Wells,
Published in *Water Resources Research*,
Volume 30, number 11, pages 2945-2957, 1994.**

Slug tests in partially penetrating wells

Zafar Hyder, James J. Butler, Jr., Carl D. McElwee, and Wenzhi Liu

Kansas Geological Survey, University of Kansas, Lawrence

Abstract. A semianalytical solution is presented to a mathematical model describing the flow of groundwater in response to a slug test in a confined or unconfined porous formation. The model incorporates the effects of partial penetration, anisotropy, finite-radius well skins, and upper and lower boundaries of either a constant-head or an impermeable form. This model is employed to investigate the error that is introduced into hydraulic conductivity estimates through use of currently accepted practices (i.e., Hvorslev, 1951; Cooper et al., 1967) for the analysis of slug-test response data. The magnitude of the error arising in a variety of commonly faced field configurations is the basis for practical guidelines for the analysis of slug-test data that can be utilized by field practitioners.

Introduction

The slug test is one of the most commonly used techniques by hydrogeologists for estimating hydraulic conductivity in the field [Kruseman and de Ridder, 1989]. This technique, which is quite simple in practice, consists of measuring the recovery of head in a well after a near instantaneous change in water level at that well. Approaches for the analysis of the recovery data collected during a slug test are based on analytical solutions to mathematical models describing the flow of groundwater to/from the test well. Over the last 30 years, solutions have been developed for a number of test configurations commonly found in the field. Chirlin [1990] summarizes much of this past work.

In terms of slug tests in confined aquifers, one of the earliest proposed solutions was that of Hvorslev [1951], which is based on a series of simplifying assumptions concerning the slug-induced flow system (e.g., negligible specific storage, finite effective radius). Much of the work following Hvorslev has been directed at removing one or more of these simplifying assumptions. Cooper et al. [1967] developed a fully transient solution for the case of a slug test in a well fully screened across a confined aquifer. Moench and Hsieh [1985] extended the solution of Cooper et al. to the case of a fully penetrating well with a finite radius well skin. A number of workers [e.g., Dougherty and Babu, 1984; Hayashi et al., 1987] have developed solutions for slug tests in wells partially penetrating isotropic, confined aquifers. Butler and McElwee [1990] presented a solution for slug tests in wells partially penetrating confined aquifers that incorporates the effects of anisotropy and a finite-radius skin at the test well. In most field applications, the methods of Hvorslev [1951] or Cooper et al. [1967] are used. The error that is introduced into hydraulic conductivity estimates by employing these models in conditions where their assumptions are inappropriate has not yet been fully evaluated. Note that Nguyen and Pinder [1984] proposed a method for the analysis of data from slug tests in wells partially penetrating confined aquifers that has received a fair amount of use. Recently, however, Butler and Hyder [1993] have shown

that the parameter estimates obtained using this approach must be viewed with considerable skepticism owing to an error in the analytical solution upon which the model is based.

In terms of slug tests in unconfined aquifers, solutions to the mathematical model describing flow in response to the induced disturbance are difficult to obtain because of the nonlinear nature of the model in its most general form. Currently, most field practitioners use the technique of Bouwer and Rice [1976; Bouwer, 1989], which employs empirical relationships developed from steady state simulations using an electrical analog model, for the analysis of slug tests in unconfined flow systems. Dagan [1978] presents an analytical solution based on assumptions similar to those of Bouwer and Rice [1976]. Amoozegar and Warrick [1986] summarize related methods employed by agricultural engineers. All of these techniques result from the application of several simplifying assumptions to the mathematical description of flow to a well in an unconfined aquifer (e.g., negligible specific storage, finite effective radius, representation of the water table as a constant-head boundary). As with the confined case, the ramifications of these assumptions have not yet been fully evaluated.

In this paper a semianalytical solution is presented to a mathematical model describing the flow of groundwater in response to an instantaneous change in water level at a well screened in a porous formation. The model incorporates the effects of partial penetration, anisotropy, finite-radius well skins of either higher or lower permeability than the formation as a whole, and upper and lower boundaries of either a constant-head or an impermeable form. This model can be employed for the analysis of data from slug tests in a wide variety of commonly met field configurations in both confined and unconfined formations. Although packers are not explicitly included in the formulation, earlier numerical work has shown that such a model can also be used for the analysis of multilevel slug-test data when packers of moderate length (0.75 m or longer) are employed [e.g., Bliss and Rushton, 1984; Butler et al., 1994a].

The major purpose of this paper is to use this solution to quantify the error that is introduced into parameter estimates as a result of using currently accepted practices for the analysis of response data from slug tests. The magnitude of

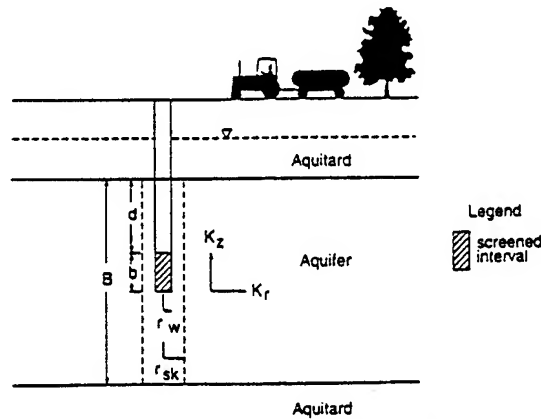


Figure 1. Cross-sectional view of a hypothetical confined aquifer (notation explained in text).

the error arising in a variety of commonly met field configurations serves as the basis for practical guidelines that can be utilized by field practitioners. Although such an investigation of parameter error could be carried out using either a numerical or analytical model, the analytical model described in the previous paragraph is employed here in order to provide a convenient alternative for data analysis when the error introduced by conventional approaches is deemed too large for a particular application.

Statement of Problem

The problem of interest here is that of the head response, as a function of r , z , and t , produced by the instantaneous introduction of a pressure disturbance into the screened or open section of a well. For the purposes of this initial development, the well will be assumed to be located in the confined aquifer shown in Figure 1. Note that, as shown on Figure 1, there is a well skin of radius r_{sk} that extends through the full thickness of the aquifer. The skin has transmissive and storage properties that may differ from the formation as a whole. Flow properties are assumed uniform within both the skin and formation, although the vertical (K_z) and radial (K_r) components of hydraulic conductivity may differ.

The partial differential equation representing the flow of groundwater in response to an instantaneous change in water level at a central well screened in a porous formation is the same for both the skin and the aquifer and can be written as

$$\frac{\partial^2 h_i}{\partial r^2} + \frac{1}{r} \frac{\partial h_i}{\partial r} + \left(\frac{K_{zi}}{K_{ri}} \right) \frac{\partial^2 h_i}{\partial z^2} = \left(\frac{S_{zi}}{K_{ri}} \right) \frac{\partial h_i}{\partial t} \quad (1)$$

where h_i is the head in zone i [L]; S_{zi} is the specific storage of zone i [1/L]; K_{zi} , K_{ri} are the vertical and radial components, respectively, of the hydraulic conductivity of zone i [L/T]; t is time [T]; r is radial direction [L]; z is vertical direction, $z = 0$ at the top of the aquifer and increases downward [L]; i is the zone designator, for $r \leq r_{sk}$, $i = 1$, and for $r_{sk} \leq r$, $i = 2$; and r_{sk} is the outer radius of skin [L].

The initial conditions can be written as

$$h_1(r, z, 0) = h_2(r, z, 0) = 0 \quad r_w < r < \infty \quad 0 < z < B \quad (2)$$

$$H(0) = H_0 \quad (3)$$

where r_w is the screen radius [L], B is aquifer thickness [L], H is level of water in well [L], and H_0 is height of initial slug, equal to level of water in well at $t = 0$ ($H(0)$), [L].

The boundary conditions are the following:

$$h_2(\infty, z, t) = 0 \quad t > 0 \quad 0 \leq z \leq B \quad (4)$$

$$\frac{\partial h_1(r, 0, t)}{\partial z} = \frac{\partial h_1(r, B, t)}{\partial z} = 0 \quad r_w < r < \infty \quad t > 0 \quad (5)$$

$$\frac{1}{b} \int_d^{d+b} h_1(r_w, z, t) dz = H(t) \quad t > 0 \quad (6)$$

$$2\pi r_w K_{r1} \frac{\partial h_1(r_w, z, t)}{\partial r} = \frac{\pi r_c^2}{b} \frac{dH(t)}{dt} \square(z) \quad t > 0 \quad (7)$$

where d is distance from the top of the aquifer to the top of the screen [L]; b is screen length [L]; r_c is radius of well casing (casing and screen do not have to be of equal radius) [L]; and $\square(z)$ is the boxcar function, equal to zero at $z < d$, $z > b + d$, and equal to 1 otherwise.

In order to ensure continuity of flow between the skin and the formation, auxiliary conditions at the skin-formation boundary ($r = r_{sk}$) must also be met:

$$h_1(r_{sk}, z, t) = h_2(r_{sk}, z, t) \quad 0 \leq z \leq B \quad t > 0 \quad (8)$$

$$K_{r1} \frac{\partial h_1(r_{sk}, z, t)}{\partial r} = K_{r2} \frac{\partial h_2(r_{sk}, z, t)}{\partial r} \quad (9)$$

$$0 \leq z \leq B \quad t > 0$$

Equations (1)–(9) approximate the flow conditions of interest here. Appendix A provides the details of the solution derivation. In summary, the approach employs a series of integral transforms (a Laplace transform in time and a finite Fourier cosine transform in the z direction) to obtain functions in transform space that satisfy the transform-space analogs of (1)–(9). The transform-space function that is obtained for the head in a partially penetrating well with a finite-radius well skin in an anisotropic confined aquifer can be written in a nondimensional form as

$$\Phi(p) = \frac{(\gamma/2)\Omega}{[1 + (\gamma/2)p\Omega]} \quad (10)$$

where $\Phi(p)$ is the Laplace transform of $H(t)/H_0$, p is the Laplace-transform variable, $\alpha = (2r_w^2 S_{z2} b)/r_c^2$, $\gamma = K_{r2}/K_{r1}$, and

$$\Omega = \int_0^{t+1} \{F_c^{-1}[F_c(\omega)f_1]\} d\eta$$

where ω is the Fourier-transform variable, $F_c(\omega)$ is the finite Fourier cosine transform of $\square(z)$, F_c^{-1} is the inverse finite Fourier cosine transform,

$$f_1 = \frac{[\Delta_2 K_0(\nu_1) - \Delta_1 I_0(\nu_1)]}{\nu_1 [\Delta_2 K_1(\nu_1) + \Delta_1 I_1(\nu_1)]}$$

$$\eta = z/b; \zeta = d/b; \nu_i = (\psi_i^2 \omega^2 + R_i \rho)^{0.5}; \psi_i = (A_i/a^2)^{0.5}; \\ A_i = K_{zi}/K_{ri}; a = b/r_w; R_1 = \gamma \alpha / 2\lambda; R_2 = \alpha / 2; \lambda = S_{z2}/S_{z1};$$

$$\Delta_1 = K_0(\nu_1 \xi_{sk}) K_1(\nu_2 \xi_{sk}) - \left(\frac{N}{\gamma}\right) K_0(\nu_2 \xi_{sk}) K_1(\nu_1 \xi_{sk});$$

$$\Delta_2 = I_0(\nu_1 \xi_{sk}) K_1(\nu_2 \xi_{sk}) + \left(\frac{N}{\gamma}\right) K_0(\nu_2 \xi_{sk}) I_1(\nu_1 \xi_{sk});$$

$$N = \nu_1/\nu_2 \quad \xi_{sk} = r_{sk}/r_w.$$

For the unconfined case the upper no-flow boundary condition in (5) is changed into a constant-head boundary condition, so the upper and lower boundary conditions are rewritten as

$$h_i(r, 0, t) = 0 \quad r_w < r < \infty \quad t > 0 \quad (11)$$

$$\frac{\partial h_i(r, B, t)}{\partial z} = 0 \quad r_w < r < \infty \quad t > 0 \quad (12)$$

Appendix A also provides the details of the solution derivation for the unconfined case. The transform-space function that is obtained for the head in a partially penetrating well with a finite-radius well skin in an anisotropic unconfined aquifer can be written in a nondimensional form as

$$\Phi_{uc}(p) = \frac{(\gamma/2)\Omega^*}{[1 + (\gamma/2)\rho\Omega^*]} \quad (13)$$

where $\Phi_{uc}(p)$ is the Laplace transform of $H(t)/H_0$ for the unconfined case;

$$\Omega^* = \int_{\zeta}^{\zeta+1} \{F_{\tau}^{-1}[F_{\tau}(\omega^*) f_1]\} d\eta;$$

$F_{\tau}(\omega^*)$ is the modified finite Fourier sine transform of $\square(z)$; and ω^* is the Fourier transform variable for the modified sine transform.

For expressions of the complexity of (10) and (13), the analytical back transformation from transform space to real space is only readily performed under quite limited conditions. In the general case the transformation is best performed numerically. Numerical evaluation of the Fourier transforms and their inversions was done here using discrete Fourier transforms [Brigham, 1974], thereby allowing computationally efficient fast Fourier transform techniques [Cooley and Tukey, 1965] to be utilized. This approach, which is briefly outlined in Appendix B, did not introduce significant error into the inversion procedure. An algorithm developed by Stehfest [1970], which has been found to be of great use in hydrologic applications [Moench and Ogata, 1984], was employed to perform the numerical Laplace inversion.

Several checks were performed in order to verify that (10) and (13) are solutions to the mathematical model outlined here. Substitution of (10) and (13) into the respective transform-space analogs of (1)–(9) and (11)–(12) demonstrated that the proposed solutions honor the governing equation and auxiliary conditions in all cases. In addition, if the test well is assumed to be fully screened across an isotropic, confined aquifer, (10) reduces to the Laplace-space form of the solutions of Moench and Hsieh [1985] and Cooper et al.

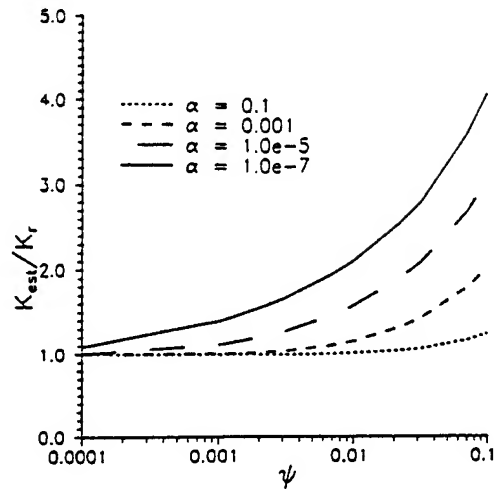


Figure 2. Plot of conductivity ratio (Cooper et al. estimate (K_{est}) over actual conductivity (K_r)) versus $\psi((K_z/K_r)^{1/2}/(b/r_w))$ as a function of $\alpha((2r_w^2 S_z b)/r_c^2)$ for the case of a well screened near the center of a very thick aquifer ($\beta \approx 64$, $\zeta \approx 32$).

[1967] for the skin and no-skin cases, respectively. Similarly, if the test well is assumed to be partially screened across an isotropic, confined aquifer, (10) reduces to the Laplace-space form of the solution of Dougherty and Babu [1984, equation (62)]. Butler et al. [1993b] describe additional checks performed with a numerical model to verify the solutions proposed here.

Ramifications for Data Analysis

As discussed in the introduction, the primary purpose of this paper is to evaluate the error that is introduced into parameter estimates through use of currently accepted practices to analyze response data from slug tests performed in conditions commonly faced in the field. This evaluation is carried out by using (10) and (13) to simulate a series of slug tests. The simulated response data are analyzed using conventional approaches. The parameter estimates are then compared with the parameters employed in the original simulations to assess the magnitude of the error introduced into the estimates through use of a particular approach for the data analysis. The simulation and analysis of slug tests were performed in this work using SUPRPUMP, an automated well-test analysis package developed at the Kansas Geological Survey [Bohling and McElwee, 1992].

Partial Penetration Effects

The first factor examined here was the effect of partial penetration on parameter estimates in a homogeneous aquifer (no-skin case). Figure 2 displays a plot of the hydraulic conductivity ratio (K_{est}/K_r) versus ψ , where ψ is the square root of the anisotropy ratio (K_z/K_r)^{1/2} over the aspect ratio (b/r_w), for a configuration in which the upper and lower boundaries are at such a large distance from the screened interval that they have no effect ($\beta = B/b \approx 64$, $\zeta = d/b \approx 32$). In this case the hydraulic conductivity estimates are obtained using the solution of Cooper et al. [1967], which assumes that the well is fully screened across the aquifer (i.e., flow is purely radial). Figure 2 shows that the error

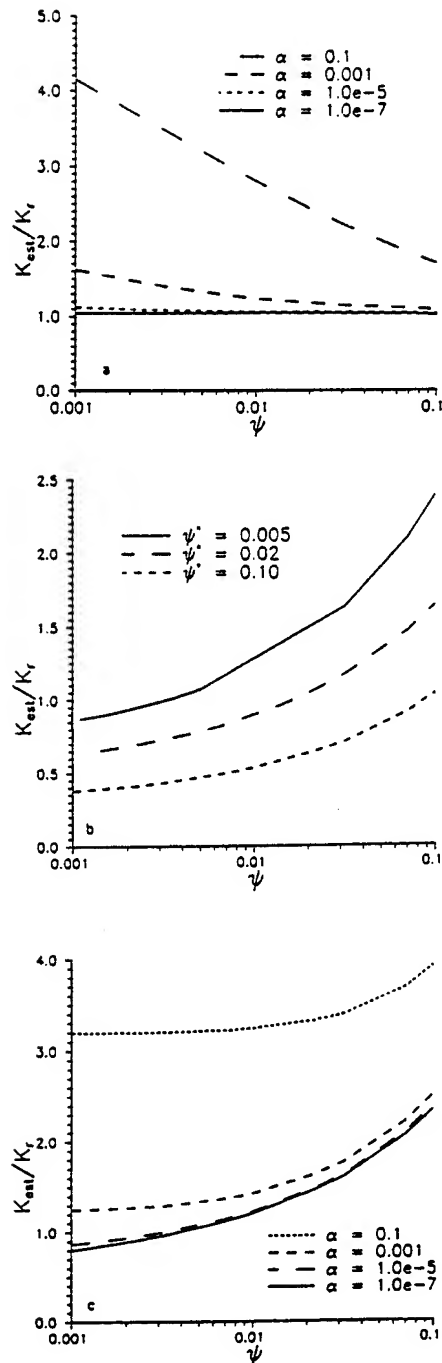


Figure 3. Plot of conductivity ratio (Hvorslev estimate (K_{est}) over actual conductivity (K_r)) versus $\psi((K_z/K_r)^{1/2}/(b/r_w))$ for the case of a well screened near the center of a very thick aquifer ($\beta = 64$, $\zeta = 32$). (a) Hvorslev estimates obtained with (14) (anisotropy ratio known) as a function of $\alpha((2r_w^2 S_z b)/r_c^2)$. (b) Hvorslev estimates obtained with (14) (anisotropy ratio unknown) as a function of ψ^* (ψ term with an assumed anisotropy ratio) for $\alpha = 1.0 \times 10^{-5}$. (c) Hvorslev estimates obtained with the fully penetrating well variant of the Hvorslev model (assuming an effective radius of $200r_w$) as a function of $\alpha((2r_w^2 S_z b)/r_c^2)$.

arising from the radial flow assumption diminishes with decreases in ψ . This is as expected, since ψ reflects the proportion of vertical to radial flow in the slug-induced flow system. Decreases in ψ correspond to decreases in the anisotropy ratio or increases in the aspect ratio, the effect of both of which is to constrain the slug-induced flow to the interval bounded by the top and bottom of the well screen (i.e., the proportion of radial flow increases). In addition, Figure 2 shows that the error in the conductivity estimates decreases greatly with increases in α , the dimensionless storage parameter. This is in keeping with the results of Hayashi *et al.* [1987], who noted that, for a constant aspect ratio, vertical flow decreases with increases in the storage parameter. Based on Figure 2, it is evident that application of the Cooper *et al.* solution to data from slug tests performed in conditions where ψ is less than about 0.003 should introduce little error into the conductivity estimates. For isotropic to slightly anisotropic systems, this ψ range corresponds to aspect ratios greater than about 250. Only in the case of a very low dimensionless storage parameter will significant error (>25%) be introduced into the estimates. Note that Figure 2 should be considered an extension of the findings of Hayashi *et al.* [1987] to the case of slug tests in open wells, a more common configuration for groundwater applications than the shut-in pressurized slug test configuration that they examined.

Currently, the most common method for analysis of slug tests in partially penetrating wells in confined aquifers is that proposed by Hvorslev [1951]. Hvorslev developed a model that can be used for the analysis of slug tests performed in a screened interval of finite length in a uniform, anisotropic, vertically unbounded medium. Figure 3a displays a plot analogous to Figure 2 for the case of the Hvorslev model being used to obtain the conductivity estimates. Note that the Hvorslev model requires the use of a "shape factor," which is related to the geometry of the well intake region. The shape factor used in Figure 3a is that for case 8 described by Hvorslev [1951] and results in the following expression for the radial component of hydraulic conductivity:

$$K_{HV} = \frac{r_c^2 \ln \{1/(2\psi) + [1 + (1/(2\psi))^2]^{1/2}\}}{2bT_0} \quad (14)$$

where K_{HV} is the estimate for the radial component of hydraulic conductivity obtained using the Hvorslev model and T_0 is the basic time lag, the time at which a normalized head of 0.37 is reached. As the aspect ratio gets large ($1/2\psi$ gets large), (14) will reduce to Hvorslev's expression for a fully penetrating well (case 9) if the effective radius (distance beyond which the slug-induced disturbance has no effect on heads) is set equal to the screen length in case 9. Note that the anisotropy ratio, which appears in the ψ term, and K_{HV} are perfectly correlated in (14), so these parameters cannot be estimated independently.

In Figure 3a, all analyses were performed using (14) while assuming that the anisotropy ratio was known. Given the difficulty of reliably estimating the degree of anisotropy in natural systems, this assumption must be considered rather unrealistic. Therefore, the analyses were repeated assuming that the degree of anisotropy was not known. However, since the anisotropy ratio and K_{HV} cannot be estimated independently, some value for the anisotropy ratio must be

assumed for the analysis. This assumption of an arbitrary anisotropy ratio will give rise to an apparent ψ (ψ^*) value, which is the square root of the assumed anisotropy ratio over the aspect ratio. Figure 3b displays results obtained for slug tests analyzed using different ψ^* values. When considered in order of decreasing magnitude, the ψ^* curves correspond to aspect ratios of 10, 50, and 200, respectively, for the case of an assumed anisotropy ratio of 1 (a common assumption in field applications). These curves will apply to different aspect ratios when an anisotropy ratio other than 1 is assumed.

Often, field analyses are performed using the fully penetrating well model of Hvorslev (case 9). For this approach, some assumption must be made concerning the effective radius of the slug test. In a frequently cited publication, the U.S. Department of the Navy [1961] recommends that an effective radius of 200 times the well radius be employed. Figure 3c displays the error that is introduced into conductivity estimates when that recommendation is adopted.

Figure 3a indicates that the estimates provided by (14) will be reasonable for moderate to small values of dimensionless storage if the anisotropy ratio is known. At larger α , however, the error introduced into the parameter estimates increases beyond the limit of what is considered reasonable for this investigation ($\pm 25\%$). Note that in Figure 3a, as in the remaining figures of this paper, the smallest ψ value plotted is 0.001. This is a result of the relationships shown in Figure 2, which indicate that, except in the case of very small values of dimensionless storage, the Cooper et al. model is the appropriate tool for analysis for ψ values less than 0.001.

Figure 3b indicates that the quality of the estimates provided by (14) will be dependent on the assumed apparent ψ (ψ^*) value for the case of an unknown anisotropy ratio. This figure demonstrates that for each ψ^* value there is a range of actual ψ for which the Hvorslev method will provide reasonable estimates. Although it is difficult to summarize the results of Figure 3b succinctly, it is clear that, if the assumed anisotropy is moderately close to the actual anisotropy (within a factor of 2–3), the Hvorslev estimate will meet the criterion of reasonability employed here ($\pm 25\%$). It can be readily shown that the ψ^* curves of Figure 3b are related to one another by a simple multiplicative factor. This relationship enables curves for ψ^* values other than those considered here to be generated by multiplying the K_{est}/K_r ratio for one of the curves given in Figure 3b by a factor consisting of the ratio of the natural logarithm term from (14) for the curve to be generated over the same term for the curve in Figure 3b. Although several standard references

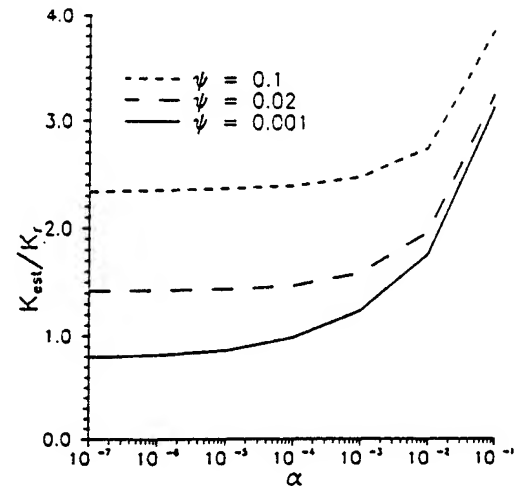


Figure 4. Plot of conductivity ratio (Hvorslev estimate (K_{est}) over actual conductivity (K_r)) versus $\alpha((2r_w^2 S_b)/r_c^2)$ as a function of $\psi((K_r/K_r)^{1/2}/(b/r_w))$ for the case of a well screened near the center of a very thick aquifer ($\beta = 64$; $\zeta = 32$; $\psi^* = 0.005$).

[e.g., Freeze and Cherry, 1979] recommend use of the isotropic form of (14), these results indicate that such an approach is only appropriate in isotropic to slightly anisotropic systems. This recommendation will result in a consistent underprediction of hydraulic conductivity in moderately to strongly anisotropic systems.

Figure 3c indicates that the fully penetrating well model of Hvorslev (using an effective radius of 200 times the well radius) is appropriate in conditions where ψ is less than about 0.01 for moderate to small values of dimensionless storage. This ψ range corresponds to an aspect ratio greater than 100 for isotropic systems. For strongly anisotropic systems (K_r/K_r , considerably less than 1), the aspect ratios at which the fully penetrating well model becomes appropriate are much smaller. Given the form of the fully penetrating well model of Hvorslev employed here and the earlier discussed relationship between the fully and partially penetrating variants of the Hvorslev model, it should be clear that the curves on Figure 3c correspond to a ψ^* value of 0.005. Using the relationships discussed in the previous paragraph, the curves plotted in Figure 3c can be employed to generate all needed ψ^* curves for common values of the dimensionless storage parameter. Table 1 presents the results from Figure 3c in a tabular form, so that the reader can generate the curve needed for a particular application. Since the ψ^* curves can be readily related to one another, the results presented in the remainder of this paper will be for one particular ψ^* value ($\psi^* = 0.005$), which as stated above, also corresponds to the fully penetrating well model of Hvorslev. The tabulated values for all the curves presented here are given by Hyder [1994].

Figures 3a–3c show that the quality of the Hvorslev estimates deteriorates rapidly as dimensionless storage increases above 0.001. Figure 4 graphically displays the large errors that are introduced into parameter estimates as α approaches 1 for the same conditions as shown in Figure 3c. Clearly, the Hvorslev model must be used with extreme caution at large values of the dimensionless storage param-

Table 1. Tabulated Values of the Conductivity Ratio for the Plots of Figure 3c

ψ	$\alpha = 0.1$	$\alpha = 0.001$	$\alpha = 1.0 \times 10^{-5}$	$\alpha = 1.0 \times 10^{-7}$
1.00×10^{-3}	3.196	1.249	0.867	0.803
2.23×10^{-3}	3.198	1.275	0.950	0.909
3.16×10^{-3}	3.203	1.293	1.001	0.964
7.07×10^{-3}	3.221	1.374	1.150	1.125
1.00×10^{-2}	3.244	1.429	1.233	1.210
2.22×10^{-2}	3.330	1.641	1.491	1.470
3.20×10^{-2}	3.399	1.774	1.638	1.615
7.10×10^{-2}	3.693	2.225	2.108	2.076
1.00×10^{-1}	3.920	2.508	2.388	2.347

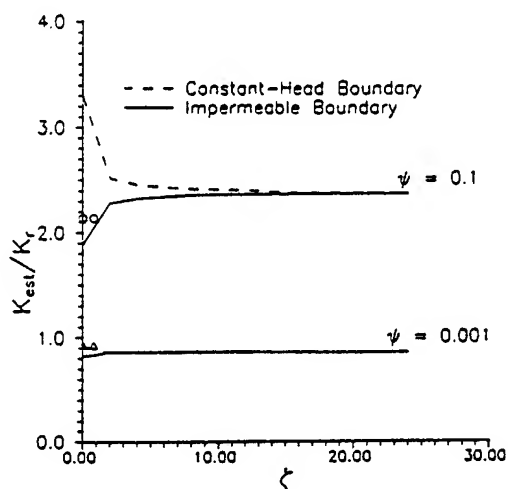


Figure 5. Plot of conductivity ratio (Hvorslev estimate (K_{est}) over actual conductivity (K_r)) versus $\zeta(d/b)$ as a function of $\psi((K_r/K_r)^{1/2}/(b/r_w))$. Solid lines designate impermeable upper boundary; dashed lines designate constant-head upper boundary; circles and triangles designate estimates obtained using the semi-infinite variant of the Hvorslev model for ψ values of 0.1 and 0.001, respectively; $\beta \approx 64$; $\alpha = 1.0 \times 10^{-5}$; $\psi^* = 0.005$.

eter. Since Figure 2 indicates that the Cooper et al. model provides excellent conductivity estimates at large values of dimensionless storage, the Cooper et al. model should always be employed when such dimensionless storage values are expected. As shown by Chirlin [1989], large values of dimensionless storage will often be reflected in a distinct concave upward curvature in a log head versus time plot. Note that the ψ curves on Figure 4 become nearly horizontal as α decreases. Therefore the results that are discussed in this paper concerning the viability of the Hvorslev model at α values of 10^{-5} – 10^{-7} should be very good approximations for conditions where α values are smaller than 10^{-7} .

An important goal of this paper is to define guidelines for the field practitioner. Since in actual field applications the aspect ratio should be a known quantity, guidelines based on the magnitude of the aspect ratio would be preferred. Although the general lack of information concerning anisotropy and specific storage introduces uncertainty, the results of this section can be used to roughly define aspect ratio guidelines for the analysis of response data from slug tests in partially penetrating wells. Clearly, at large aspect ratios (greater than 250), the Cooper et al. [1967] model is the most appropriate tool for data analysis. In strongly anisotropic systems (K_r/K_r , considerably less than 1), the Cooper et al. model will be applicable at much smaller aspect ratios. Although it is difficult to accurately estimate the degree of anisotropy from slug-test response data, Butler et al. [1993a] present a simple approach that can be used to assess if significant anisotropy is present. In the general case, the fully penetrating well model of Hvorslev [1951] would be the best approach for analyzing response data from wells of aspect ratios between 100 and 250. At smaller aspect ratios the partially penetrating model of Hvorslev is best in the most general case. However, the most appropriate model for any particular application will depend on the anisotropy ratio

and specific storage. If some reasonable estimates can be made about these parameters, Figures 2–4 and Table 1 can be used to assess which method is most appropriate for that specific application. Note that the model of Cooper et al. should be employed at all aspect ratios when the dimensionless storage parameter is large.

Boundary Effects

The previous discussion has focused on the effects of partial penetration in a vertically infinite system. Although one might suspect that most natural systems can be considered as vertically infinite for the purposes of the analysis of response data from slug tests, there may be situations in which the upper and/or lower boundaries of the system influence the response data. Thus the next factor examined here was the effect of impermeable and constant-head boundaries in the vertical plane on parameter estimates. Figure 5 displays a plot of the hydraulic conductivity ratio versus the normalized distance to a boundary ($\zeta = d/b$). Results are shown for both impermeable and constant-head boundaries. In all cases, an apparent ψ (ψ^*) value of 0.005 is used to obtain the conductivity estimates. It is clear from Figure 5 that a boundary will only have a significant effect (>25%) on parameter estimates when the screen is very close to the boundary (i.e., $\zeta < 1-2$) and ψ is relatively large. If there is any degree of anisotropy in hydraulic conductivity, the influence of the boundary will be considerably lessened. Note that Hvorslev [1951] also proposed a semi-infinite, partially penetrating well model (single impermeable boundary with screen extending to boundary) for slug tests. The equation for estimation of hydraulic conductivity in this case is the same as (14) except ψ is used instead of 2ψ in the logarithmic term. The circles and triangles in Figure 5 show the estimates that would be obtained using this model for the confined case. Clearly, the semi-infinite variant of the Hvorslev model is only necessary at large ψ values (wells of small aspect ratios in isotropic aquifers). As the proportion of vertical flow decreases (ψ gets small), the semi-infinite model becomes slightly inferior to the vertically infinite form of the Hvorslev model. Although all of the parameter estimates in Figure 5 were obtained using the Hvorslev model, the method of Bouwer and Rice [1976] would normally be employed if an unconfined boundary is suspected. Hyder and Butler [1994] provide a detailed discussion of the error introduced into parameter estimates using the Bouwer and Rice model.

The above discussion focuses on results when only a single boundary is influencing the response data. In thin formations, one may face conditions when both the upper and lower boundaries are close enough to the screen to be affecting the slug-test responses. Figure 6 displays a plot of the hydraulic conductivity ratio versus normalized aquifer thickness ($\beta = B/b$) for the case of a well screen located at the center of the unit. Clearly, in thin confined systems, the pair of impermeable boundaries will have a significant effect on Hvorslev estimates for relatively large values of ψ . In thin unconfined systems, the lower impermeable boundary acts in an opposite manner to the upper constant-head boundary, so that the estimates are more reasonable than in the single-boundary case.

The results of this section indicate that, except in cases of very thin formations ($\beta < 10$), screens located very close to a boundary ($\zeta < 5$), and large values of ψ (>0.05), the

assumption of a vertically infinite system introduces a very small amount of error into the parameter estimates obtained using the Hvorslev model. Thus the relationships presented in Figures 3 and 4 can be considered appropriate for the vast majority of field applications. Note that no analyses were performed in this section using the Cooper et al. [1967] model. In the previous section, a range of aspect ratios (>250) was defined for which the Cooper et al. model would provide reasonable estimates. Since boundaries in the vertical plane will only introduce sizable errors into parameter estimates when there is a considerable component of vertical flow, the effects of boundaries will be very small if the Cooper et al. model is only applied over the previously defined range.

Well-Skin Effects

The results of the previous sections pertain to the case of slug tests performed in homogeneous formations. Often, however, as illustrated in Figure 1, well drilling and development create a disturbed, near-well zone (well skin) that may differ in hydraulic conductivity from the formation in which the well is screened. It is important to understand the effect of well skins on conductivity estimates in order to avoid using estimates representative of skin properties to characterize the formation as a whole.

Figure 7a illustrates the effect of a well skin on conductivity estimates obtained using the Hvorslev model ($\psi^* = 0.005$) for a broad range of contrasts between the conductivity of the skin and that of the formation. Clearly, the existence of a well skin can have a dramatic effect on the Hvorslev estimates. In the case of a skin less permeable than the formation, a conductivity estimate differing from the actual formation value by over an order of magnitude can easily be obtained. Figure 7a displays results for the case of a skin whose outer radius is twice that of the well screen ($\xi_{sk} = r_{sk}/r_w = 2$). Figure 7b shows how the results depend on the thickness of the skin for the case of a skin 1 order of magnitude less conductive than the formation ($\gamma = 10.0$).

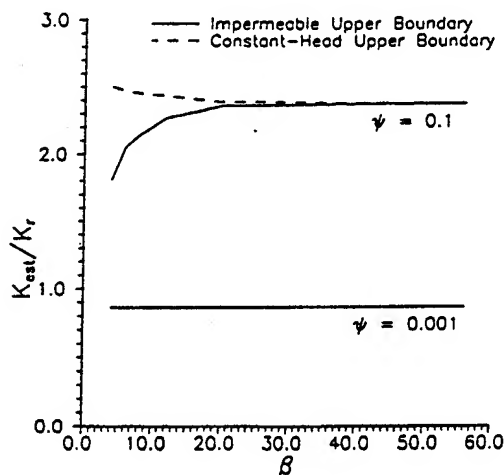


Figure 6. Plot of conductivity ratio (Hvorslev estimate (K_{est}) over actual conductivity (K_r)) versus $\beta(B/b)$ as a function of $\psi((K_r/K_{r1})^{1/2}/(b/r_w))$. Solid lines designate impermeable upper boundary; dashed lines designate constant-head upper boundary; $\alpha = 1.0 \times 10^{-5}$; $\psi^* = 0.005$.

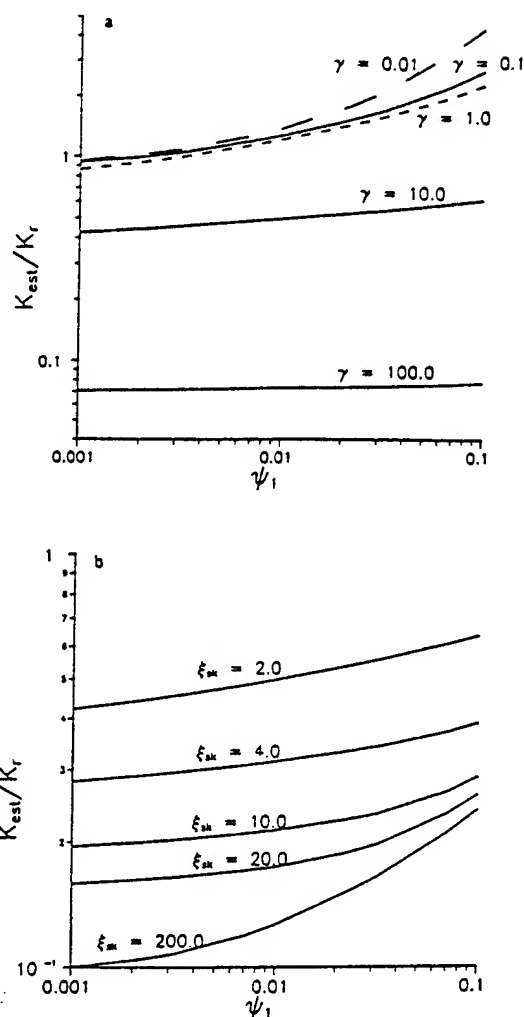


Figure 7. Plot of conductivity ratio (Hvorslev estimate (K_{est}) over actual formation conductivity (K_r)) versus $\psi_1((K_{r1}/K_r)^{1/2}/(b/r_w))$ for the case of high and low conductivity well skins ($\beta = 64$, $\zeta = 32$, $\alpha = 1.0 \times 10^{-5}$, $\psi^* = 0.005$, $\psi_1 = \psi_2$, $\lambda = 1$). (a) Hvorslev estimates as a function of $\gamma(K_{r2}/K_{r1})$ for $\xi_{sk} = 2$. (b) Hvorslev estimates as a function of $\xi_{sk}(r_{sk}/r_w)$ for $\gamma = 10.0$.

Note that when the skin radius equals the effective radius assumed in the Hvorslev fully penetrating well model ($\xi_{sk} = 200$), the estimated conductivity will approach that of the skin for small values of ψ .

Figure 8 displays a plot of a simulated slug test and the best fit Hvorslev model, which is representative of all the low-conductivity skin cases shown in Figures 7a and 7b. As can be seen from Figure 8, the Hvorslev model matches the simulated data extremely well. In fact, a large number of additional simulations have shown that the Hvorslev fit for the low-conductivity skin case is almost always better than that for the homogeneous case. This is especially true at small ψ values (moderate to large aspect ratios), where the response data for the homogeneous case generally will display a distinct concave upward curvature [e.g., Chirilin, 1989].

At moderate to small ψ values, an underlying assumption of the Hvorslev model is that there is an effective radius

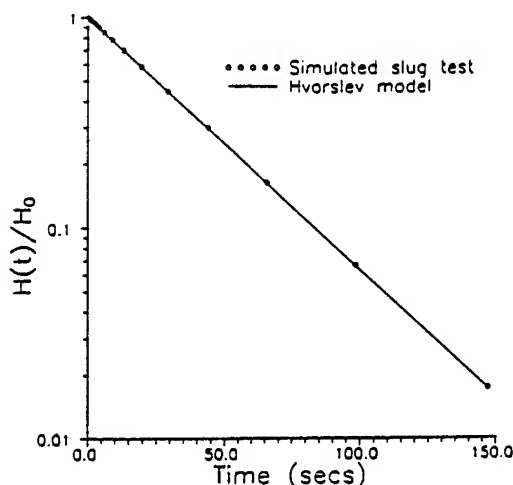


Figure 8. Normalized head versus time plot of simulated slug test and the best fit Hvorslev model for the case of a skin 2 orders in magnitude less conductive than the formation ($b/r_w = 50$; $r_{sk} = 0.10$ m, $r_w = r_c = 0.05$ m, $S_{r1} = S_{r2} = 1.0 \times 10^{-5}$ m $^{-1}$, $K_{r2} = K_{c2} = 0.001$ m/s, $K_{r1} = K_{c1} = 0.00001$ m/s).

beyond which the slug-induced disturbance has no effect on aquifer heads. In the low-conductivity skin case, this assumption is a very close approximation of reality, for almost all of the head drop occurs across the skin; heads in the formation are essentially unaffected by the slug test [e.g., Faust and Mercer, 1984]. Another major assumption of this model is that the specific storage has no influence on the response data. In most cases the thickness of the skin is relatively small, so the influence of the specific storage of the skin on slug-test responses is essentially negligible. Thus the assumptions of the Hvorslev model actually appear to be more reasonable in the low-conductivity skin case than in the homogeneous case. So, if one assumes an effective radius equal to the skin radius (e.g., $\xi_{sk} = 200$ in Figure 7b), the estimated conductivity will be a reasonable approximation of the conductivity of the skin at moderate to small ψ values. Hyder and Butler [1994] show that a low-conductivity skin has a similar effect on parameter estimates obtained using the Bouwer and Rice [1976] method.

Figure 9 illustrates the effect of a well skin on conductivity estimates obtained using the Cooper et al. model. In general, the effect of a skin on the Cooper et al. model estimates is similar to that seen with the Hvorslev model. Again, the effect of a low-conductivity skin is quite pronounced. If the specific storage is assumed known or constrained to physically realistic values, application of the Cooper et al. model to data from a well with a low-conductivity skin will produce an estimate that is heavily weighted toward the conductivity of the skin. In addition, there will always be a considerable deviation between the best fit Cooper et al. model and the response data in a manner similar to that shown in Figure 10. At small ψ values (moderate to large aspect ratios), the combination of an excellent Hvorslev fit and a systematic deviation between the Cooper et al. model and the test data appears to be a very good indication of a low-conductivity skin. At larger ψ values (lower aspect ratios), however, such a combination is also an indication of a strong component of vertical flow. Note that McElwee and Butler [1992] have

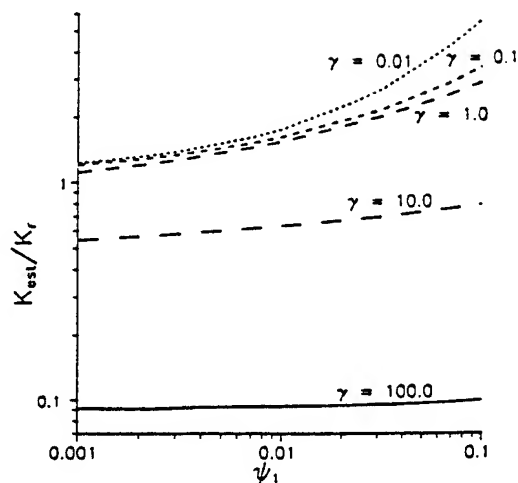


Figure 9. Plot of conductivity ratio (Cooper et al. estimate (K_{est}) over actual formation conductivity (K_r)) versus $\psi_1 ((K_{c1}/K_{r1})^{1/2}/(b/r_w))$ as a function of $\gamma (K_{r2}/K_{r1})$ for $\xi_{sk} = 2$ ($\beta \approx 64$, $\zeta \approx 32$, $\alpha = 1.0 \times 10^{-5}$, $\psi_1 = \psi_2$, $\lambda = 1$).

proposed an empirical equation that relates the Cooper et al. conductivity estimate to skin and formation properties. The practical use of this equation is limited, however, since estimation of formation conductivity from the Cooper et al. estimate requires knowledge of skin conductivity and thickness.

In the high-conductivity skin case, as shown in Figures 7a and 9, conductivity estimates will be greater than the formation conductivity as a result of a considerable amount of vertical flow along the more conductive skin. The difference will be greatest at large ψ values because of the larger proportion of vertical flow under those conditions. Note that the difference between the two high-conductivity skin cases ($\gamma = 0.01$ and 0.1) decreases at small ψ values because of the lessening importance of vertical flow. If the radius of the well

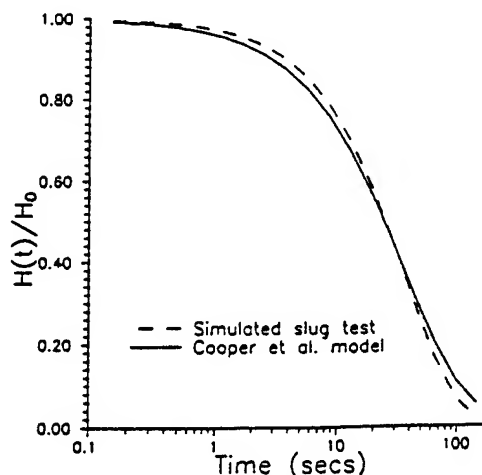


Figure 10. Normalized head versus time plot of simulated slug test and the best fit Cooper et al. model for the case of a skin 2 orders in magnitude less conductive than the formation (parameters as in Figure 8).

screen is set to the nominal screen radius in the analysis, there will always be an offset between the high-conductivity skin cases and the homogeneous case at small ψ values, as shown in Figures 7a and 9.

Since there is a very small head drop in the radial direction across a high-conductivity skin, one might expect that parameter estimates for the high-conductivity skin case could be considerably improved by assuming the radius of the well screen equals the radius of the high-conductivity skin. Although such an approach will decrease the offset at small ψ values displayed in Figures 7a and 9, additional simulations have shown that the gains obtained through this approach are quite modest (less than 10%). The reason for these smaller than might have been expected gains is that an increase in the well radius only influences α and ψ . As has been shown in plots in the previous sections, hydraulic conductivity estimates are not strongly affected by moderate changes in these dimensionless variables. The major cause of the differences between the high-conductivity skin and homogeneous cases shown in Figures 7a and 9 is the uncertainty concerning the screen length. Since screen length is a term in the dimensionless time variable ($\tau = (bK_{r2})/r_c^2$), an error in the screen length estimate of a certain magnitude directly translates into an error in the estimated hydraulic conductivity of the same magnitude. Thus uncertainty about the value to use for the screen length can introduce considerable error into the conductivity estimates. In the case of a partially penetrating well, the high-conductivity skin (e.g., the gravel pack) will normally be of greater length than the well screen. In this situation, the length of the high-conductivity skin, and not the nominal length of the well screen, is the quantity of interest. This larger-than-the-nominal screen length can be termed the "effective screen length" for the purposes of this discussion. In Figures 7a and 9 the high-conductivity skin cases were analyzed assuming that the nominal screen length was the appropriate screen length for the analysis. At large ψ values, such an approach is clearly incorrect. A more appropriate approach would have been to attempt to estimate the actual effective screen length. If there is an adequate seal in the annulus, the effective screen length should be the length of the gravel pack up to that seal. However, in cases where the length of the high-conductivity skin is considerably longer than the nominal screen length, such as in Figures 7a and 9, where the skin extends to the upper boundary of the formation, the effective screen length will be dependent on the conductivity contrast between the formation and the skin. Further work is required to develop approaches for estimation of the effective screen length in such situations.

Summary and Conclusions

A semianalytical solution to a model describing the flow of groundwater in response to a slug test in a porous formation has been presented. The primary purpose for the development of this model was to assess the viability of conventional methods for the analysis of response data from slug tests. The results of this assessment can be summarized as follows.

1. In a homogeneous formation the Cooper et al. model will provide reasonable estimates (within 25%) of the radial component of hydraulic conductivity for ψ values less than about 0.003. For isotropic to slightly anisotropic systems, this ψ range corresponds to aspect ratios greater than about

250 (much smaller aspect ratios for strongly anisotropic formations). In systems with a large dimensionless storage ($\alpha > 0.01$) the Cooper et al. model should provide reasonable estimates at virtually all commonly used aspect ratios. The viability of this model at $\psi < 0.003$ is only in question for configurations with very small values of dimensionless storage ($\alpha < 10^{-6}$).

2. In a homogeneous formation the Hvorslev model (case 8) will provide reasonable estimates of the radial component of hydraulic conductivity at moderate to small values of dimensionless storage ($\alpha < 10^{-4}$) for a broad range of ψ values if the magnitude of the anisotropy ratio is known. If the anisotropy ratio is not known, which is the situation commonly faced in the field, the Hvorslev model will provide reasonable estimates if the assumed anisotropy ratio is within a factor of 2-3 of the actual ratio. Table 1 allows the error introduced by the anisotropy ratio assumption to be readily assessed for any value of the assumed anisotropy. If the effective radius is assigned a value 200 times the well radius, the fully penetrating variant of the Hvorslev model (case 9) will provide reasonable conductivity estimates for ψ values less than 0.01.

3. Except in cases of large values of ψ (> 0.05), and very thin formations ($\beta < 10$) or well screens located very close to a boundary ($\zeta < 5$), upper or lower boundaries will have little influence on parameter estimates obtained using conventional approaches. If the formation has any degree of anisotropy in hydraulic conductivity, the range of conditions over which boundary effects are significant will be quite limited. In general, the assumption of a vertically infinite system introduces a very small amount of error into parameter estimates. Relationships developed for vertically infinite systems should thus be appropriate for most field applications.

4. In the case of a low-conductivity skin, neither the Hvorslev nor the Cooper et al. model provides reasonable estimates of hydraulic conductivity of the formation. Both approaches will yield estimates that are heavily weighted toward the conductivity of the skin. The underlying assumptions of the Hvorslev model actually appear to be more reasonable in the low-conductivity skin case than in the homogeneous case. At small ψ values (moderate to large aspect ratios) the combination of an excellent fit of the Hvorslev model to the test data and a systematic deviation between the test data and the best fit Cooper et al. model appears to be a very good indication of a low-conductivity skin.

5. In the case of a high-conductivity skin the Cooper et al. model will provide reasonable estimates of formation conductivity at small ψ values. The fully penetrating well variant of the Hvorslev model (effective radius 200 times the well radius) will provide viable estimates at ψ values less than about 0.01. The quality of the estimates for both models can be slightly improved if the radius of the screen is set equal to an approximate skin radius. At $\psi > 0.01$ the viability of Hvorslev conductivity estimates will strongly depend on the quality of estimates for the effective screen length. In such conditions the length and radius of the gravel pack should be used in place of the nominal screen length and radius, respectively, for the analysis of the response data.

The results of this assessment indicate that there are many commonly faced field conditions in which the conventional methodology for the analysis of response data from slug tests

appears viable. Since the definition of what constitutes a reasonable parameter estimate will be application dependent, the user can consult the figures of this paper to assess if the introduced error is acceptable for a specific application. If it appears that conventional approaches will not provide acceptable parameter estimates for a test in a particular configuration, the model developed here can be used to analyze the response data. *Butler et al.* [1993a] describe a series of slug tests in both consolidated and unconsolidated formations in which the model described in this article is employed for the data analysis. Considerable experience is required, however, for successful application in configurations with low-conductivity skins or a moderate degree of anisotropy owing to uncertainties introduced by a high degree of parameter correlation.

Note that the results of this study must be considered in light of the three major assumptions used in the mathematical definition of the slug-test model employed in this work. First, in (7) we adopted the commonly employed assumption of a uniform radial hydraulic gradient along the well screen as a mathematical convenience. In actuality, one would suspect that the gradient would be larger at either end of the screen, producing a U-shaped profile in the vertical plane. *Butler et al.* [1993b], however, have performed detailed simulations with a numerical model to show that the use of this mathematical convenience introduces a negligible degree of error to the results reported here and virtually all practical applications.

Second, in (8) and (9) we assumed that the skin fully penetrates the formation being tested. Although this assumption is appropriate for the case of multilevel slug tests performed in a well fully screened across the formation, it is clearly not representative of reality in the general case. For tests in wells with a low-conductivity skin, however, this assumption is of little significance, since a low-conductivity skin will not serve as a vertical conduit. In this situation, flow in response to a slug-induced disturbance will be primarily constrained to an interval bounded by the top and bottom of the well screen. In the case of a high-conductivity skin, this assumption will produce considerably more vertical flow in the skin than would actually occur. *Butler et al.* [1993b], however, have shown through numerical simulation that a slug test performed in a partially penetrating well with a high-conductivity skin that extends to the bottom of the screen is indistinguishable from a slug test performed in a similar configuration in which the well screen terminates against a lower impermeable layer. Thus for the high conductivity skin cases examined here, the slug tests were simulated assuming that the screen abutted against a lower impermeable layer. Note that this approach is only appropriate for a skin considerably more conductive (i.e., larger by a factor of 2-3) than the formation and considerably longer than the nominal screen length. Thus the high-conductivity skin results presented here should be considered representative of bounding, worst case conditions.

Third, in (11) we assumed that the water table could be represented as a constant-head boundary. Given the small amount of water that is introduced to/removed from a well during a slug test, this assumption is considered reasonable under most conditions. The cases in which this assumption may be suspect are that of a well that is screened across the water table or a well screened over a deeper interval with a

gravel pack that extends above the water table. Ongoing numerical and field investigations are currently being undertaken to assess the error that is introduced through this assumption and to suggest approaches for data analysis when that error is deemed unacceptably large [*Butler et al.*, 1994b].

Appendix A

In this section the mathematical derivations of the solutions discussed in the main body of the text are presented. For the sake of generality, the solutions are obtained in a dimensionless form. The solutions will be presented here as transform-space expressions. Details concerning the scheme used to numerically invert these expressions to real space are given in Appendix B. Note that the expressions given here are only for the head within the stressed well. Solutions for heads outside the stressed well are available from the authors upon request.

Confined Aquifer Solution

Equations (1)–(9) describe the flow conditions of interest here. To work with the most general form of the solution, this derivation is performed using dimensionless forms of (1)–(9). The dimensionless analogs of (1)–(9) are as follows:

$$\frac{\partial^2 \phi_i}{\partial \xi^2} + \frac{1}{\xi} \frac{\partial \phi_i}{\partial \xi} + \psi_i^2 \frac{\partial^2 \phi_i}{\partial \eta^2} = R_i \frac{\partial \phi_i}{\partial \tau} \quad (A1)$$

$$\phi_i(\xi, \eta, 0) = 0 \quad \xi > 1 \quad 0 < \eta < \beta \quad (A2)$$

$$\Phi(0) = 1 \quad (A3)$$

$$\phi_2(\infty, \eta, \tau) = 0 \quad \tau > 0 \quad 0 \leq \eta \leq \beta \quad (A4)$$

$$\frac{\partial \phi_i(\xi, 0, \tau)}{\partial \eta} = \frac{\partial \phi_i(\xi, \beta, \tau)}{\partial \eta} = 0 \quad \xi > 1 \quad \tau > 0 \quad (A5)$$

$$\int_{\xi}^{\xi+1} \phi_1(1, \eta, \tau) d\eta = \Phi(\tau) \quad \tau > 0 \quad (A6)$$

$$\frac{\partial \phi_1(1, \eta, \tau)}{\partial \xi} = \frac{\gamma}{2} \frac{d\Phi(\tau)}{d\tau} \square(\eta) \quad \tau > 0 \quad (A7)$$

$$\phi_1(\xi_{sk}, \eta, \tau) = \phi_2(\xi_{sk}, \eta, \tau) \quad 0 \leq \eta \leq \beta \quad \tau > 0 \quad (A8)$$

$$\frac{\partial \phi_1(\xi_{sk}, \eta, \tau)}{\partial \xi} = \gamma \frac{\partial \phi_2(\xi_{sk}, \eta, \tau)}{\partial \xi} \quad 0 \leq \eta \leq \beta \quad \tau > 0 \quad (A9)$$

where

$$\phi_i = h_i/H_0 \quad \xi = r/r_w \quad \eta = z/b$$

$$\tau = (tbK_{r2})/(r_c^2) \quad \psi_i = (A_i/a^2)^{0.5}$$

$$A_i = K_{zi}/K_{ri} \quad a = b/r_w$$

$$R_1 = \gamma\alpha/2\lambda \quad R_2 = \alpha/2$$

$$\lambda = S_{z2}/S_{z1} \quad \beta = B/b$$

$$\Phi = H/H_0 \quad \gamma = K_{r2}/K_{r1} \quad \alpha = (2r_w^2 b S_{s2})/r_c^2$$

$$\square(\eta) = 0 \quad \eta < \zeta \quad \eta > \zeta + 1$$

$$\square(\eta) = 1 \quad \text{elsewhere}$$

$$\zeta = d/b \quad \xi_{sk} = r_{sk}/r_w$$

A solution can be obtained for (A1)–(A9) through the use of integral transforms [Churchill, 1972]. A Laplace transform in time followed by a finite Fourier cosine transform in the η direction produces a Fourier-Laplace space analog to (A1) of the following form:

$$\frac{\partial^2 \bar{\phi}_i}{\partial \xi^2} + \frac{1}{\xi} \frac{\partial \bar{\phi}_i}{\partial \xi} - (\psi_i^2 \omega^2 + R_i p) \bar{\phi}_i = 0 \quad (\text{A10})$$

where $\bar{\phi}_i$ is the Fourier-Laplace transform of ϕ_i , $f(\xi, \omega, p)$; ω is the Fourier-transform variable, equal to $(n\pi)/\beta$, $n = 0, 1, 2, \dots$; and p is the Laplace-transform variable.

The Fourier-Laplace space solution to (A10) is quite straightforward, as (A10) is simply a form of the modified Bessel equation [Haberman, 1987]. A solution can therefore be proposed in the form

$$\bar{\phi}_i = C_i K_0(\nu_i \xi) + D_i I_0(\nu_i \xi) \quad (\text{A11})$$

where $\nu_i = (\psi_i^2 \omega^2 + R_i p)^{0.5}$; C_i, D_i are constants; K_i is a modified Bessel function of the second kind of order i ; and I_i is a modified Bessel function of the first kind of order i .

Using the transform-space analogs of auxiliary conditions (A4) and (A6)–(A9), the constants in (A11) can be evaluated. Since the focus of interest in most slug tests is responses in the stressed well, only the transform-space expression for head at a radial distance of $\xi = 1$ is given here:

$$\bar{\phi}_1(1, \omega, p) = \frac{\gamma}{2} [1 - p\Phi(p)] F_c(\omega) f_1 \quad (\text{A12})$$

where $\Phi(p)$ is the Laplace transform of $\Phi(t)$, the nondimensional form of $H(t)$; $F_c(\omega)$ is the finite Fourier cosine transform of $\square(z)$, equal to

$$\frac{2}{\omega} \sin\left(\frac{\omega}{2}\right) \cos\left(\frac{\omega(1+2\xi)}{2}\right) \quad \omega = n\pi/\beta$$

$$n = 1, 2, 3, \dots$$

and equal to 1, $\omega = 0$;

$$f_1 = \frac{[\Delta_2 K_0(\nu_1) - \Delta_1 I_0(\nu_1)]}{\nu_1 [\Delta_2 K_1(\nu_1) + \Delta_1 I_1(\nu_1)]};$$

$$\Delta_1 = K_0(\nu_1 \xi_{sk}) K_1(\nu_2 \xi_{sk}) - \left(\frac{N}{\gamma}\right) K_0(\nu_2 \xi_{sk}) K_1(\nu_1 \xi_{sk});$$

$$\Delta_2 = I_0(\nu_1 \xi_{sk}) K_1(\nu_2 \xi_{sk}) + \left(\frac{N}{\gamma}\right) K_0(\nu_2 \xi_{sk}) I_1(\nu_1 \xi_{sk});$$

$$N = \nu_1/\nu_2$$

The application of an inverse finite Fourier cosine transform to (A12) for η within the screen and utilization of the Laplace-space analog of (A6) produces the following expression for head in the stressed well:

$$\Phi(p) = \frac{\gamma}{2} [1 - p\Phi(p)] \Omega \quad (\text{A13})$$

where

$$\Omega = \int_{\zeta}^{\zeta+1} \{F_c^{-1}[F_c(\omega) f_1]\} d\eta;$$

F_c^{-1} is the inverse finite Fourier cosine transform.

Solving for $\Phi(p)$ yields

$$\Phi(p) = \frac{(\gamma/2)\Omega}{[1 + (\gamma/2)p\Omega]} \quad (\text{A14})$$

Appendix B provides details of the fast Fourier transform scheme used to invert the expression in the Ω term. The algorithm of Stehfest [1970] was used to perform the numerical Laplace inversion of (A14).

Unconfined Aquifer Solution

For the unconfined case, (A5) is replaced by the dimensionless analogs of (11) and (12):

$$\phi_i(\xi, 0, \tau) = 0 \quad \xi > 1 \quad \tau > 0 \quad (\text{A15})$$

$$\frac{\partial \phi_i(\xi, \beta, \tau)}{\partial \eta} = 0 \quad \xi > 1 \quad \tau > 0 \quad (\text{A16})$$

A solution for (A1)–(A4), (A6)–(A9), and (A15)–(A16) is obtained using the same approach as in the confined case. The Fourier-Laplace expression for head at a radial distance of $\xi = 1$ in the unconfined case can be written as

$$\bar{\phi}_{1u}(1, \omega^*, p) = \frac{\gamma}{2} [1 - p\Phi_{uc}(p)] F_s(\omega^*) f_1 \quad (\text{A17})$$

where $\bar{\phi}_{1u}$ is the Fourier-Laplace transform of ϕ_{1u} , the nondimensional form of h_1 for the unconfined case; $\Phi_{uc}(p)$ is the Laplace transform of the nondimensional form of $H(t)$ for the unconfined case; $F_s(\omega^*)$ is the modified finite Fourier sine transform of $\square(z)$, equal to

$$\frac{2}{\omega^*} \sin\left(\frac{\omega^*(2\xi+1)}{2}\right) \sin\left(\frac{\omega^*}{2}\right);$$

and ω^* is the Fourier transform variable for the modified sine transform, equal to $(n\pi)/2\beta$, $n = 1, 3, 5, \dots$.

The application of an inverse modified finite Fourier sine transform to (A17) for η within the screen and rewriting in terms of $\Phi_{uc}(p)$ produces the following expression:

$$\Phi_{uc}(p) = \frac{(\gamma/2)\Omega^*}{[1 + (\gamma/2)p\Omega^*]} \quad (\text{A18})$$

where

$$\Omega^* = \int_{\zeta}^{\zeta+1} \{F_s^{-1}[F_s(\omega^*) f_1]\} d\eta.$$

The modified finite Fourier sine transform employed in the unconfined case requires a bit of discussion. The standard finite Fourier sine transform is quite useful when a constant head is maintained at both boundaries. In the unconfined case the upper boundary ($\eta = 0$) is defined as a constant-

head condition, while the lower boundary ($\eta = \beta$) is defined as a no-flow condition. Churchill [1972] presents the modified finite Fourier sine transform

$$F_s(n) = \int_0^\beta f(\eta) \sin\left(\frac{n\pi\eta}{2\beta}\right) d\eta \quad n = 1, 3, 5, \dots \quad (\text{A19})$$

as an example of a Sturm-Liouville transformation. When this modified sine transform is applied to the second-order derivative with respect to η , integration by parts yields

$$\int_0^\beta \frac{\partial^2 \phi_i}{\partial \eta^2} \sin\left(\frac{n\pi\eta}{2\beta}\right) d\eta = -\omega^{*2} \phi_i + \omega^* \phi_i(0) - (-1)^n \frac{\partial \phi_i(\beta)}{\partial \eta} \quad (\text{A20})$$

where

$$\omega^* = (n\pi)/2\beta \quad n = 1, 3, 5, \dots$$

For the boundary conditions employed here, (A20) reduces to

$$-\omega^{*2} \phi_i \quad (\text{A21})$$

Appendix B

In this section, details are presented of the procedures employed to numerically invert the transform-space expressions derived in Appendix A. As discussed in the main text, the fast Fourier transform (FFT) procedure was employed to perform the required Fourier transforms/inversions in this work. In order to demonstrate that the discrete Fourier transforms introduced negligible error into the numerically inverted solution, a comparison between the discrete solution and the continuous form is discussed.

For the confined case (cf. (A14)), a finite Fourier cosine transform was employed. The continuous form of this transform can be written as

$$F_c(n) = \int_0^\beta f(\eta) \cos\left(\frac{n\pi\eta}{\beta}\right) d\eta \quad (\text{B1})$$

where F_c is the finite Fourier cosine transform and $f(\eta) = F_c(\omega)f_1$.

In order to utilize the FFT procedure, (B1) is approximated using a discrete Fourier transform:

$$F_c(n) \approx \Delta \sum_{k=0}^{N-1} f(\Delta k) \cos\left(\frac{n\pi k}{N}\right) \quad (\text{B2})$$

$$n = 0, 1, 2, \dots, N-1$$

where N , the number of equally spaced points between 0 and β , must be an integer power of 2; and Δ is the interval between equally spaced points, equal to β/N .

For the unconfined case (cf. (A18)) a modified finite Fourier sine transform was employed. The continuous form of this transform can be written as

$$F_s(n) = \int_0^\beta f_{uc}(\eta) \sin\left(\frac{n\pi\eta}{2\beta}\right) d\eta \quad n = 1, 3, 5, \dots \quad (\text{B3})$$

where F_s is the modified finite Fourier sine transform and $f_{uc}(\eta) = F_s(\omega^*)f_1$. Equation (B3) is only defined for odd-numbered n . For ready implementation with standard FFT algorithms, (B3) is rewritten in terms of a continuous sequence of n :

$$F_s(n) = \frac{[1 + (-1)^{n+1}]}{2} \int_0^\beta f_{uc}(\eta) \sin\left(\frac{n\pi\eta}{2\beta}\right) d\eta \quad (\text{B4})$$

$$n = 1, 2, 3, \dots$$

Equation (B4) is now approximated using a discrete Fourier transform:

$$F_s(n) \approx \frac{[1 + (-1)^{n+1}]}{2} \Delta \sum_{k=1}^{N-1} f_{uc}(\Delta k) \sin\left(\frac{n\pi k}{2N}\right) \quad (\text{B5})$$

$$n = 1, 2, \dots, N-1$$

Equations (B2) and (B5) can be directly implemented in standard FFT algorithms. In this work an FFT algorithm given by Press *et al.* [1992] was employed. The total number of sampling points (N) in η was constrained, such that there would always be at least 10 points within the screened interval.

In order to check on the approach outlined above, an additional series of simulations was performed in which the continuous forms of the finite Fourier transforms were employed for the required transforms/inversions. The Ω term that is employed in (A14) can be written in the continuous form as

$$\Omega = \frac{f_1(n=0)}{\beta} + \frac{8\beta}{\pi^2} \sum_{n=1}^{\infty} \frac{f_1(n)}{n^2} \sin^2 \frac{n\pi}{2\beta} \cos^2 \left(\frac{n\pi(1+2\zeta)}{2\beta} \right) \quad (\text{B6})$$

The Ω^* that is employed in (A18) can be written in continuous form as

$$\Omega^* = \frac{16\beta}{\pi^2} \sum_{n=1}^{\infty} \frac{f_1(n)}{n^2} \sin^2 \frac{n\pi}{4\beta} \sin^2 \left(\frac{n\pi(1+2\zeta)}{4\beta} \right) \quad (\text{B7})$$

In all cases the inversion of (B6) and (B7) produced results that were virtually indistinguishable from those found using an FFT algorithm with (B2) and (B5). The computational time, however, was significantly greater.

The inverse Laplace transform, the final step of the numerical inversion procedure, was performed here using the algorithm of Stehfest [1970]. Sixteen terms were used in the summation of the Stehfest algorithm for all the cases examined in this work. Note that the procedures discussed here are implemented in a series of Fortran programs found in the work by Hyder *et al.* [1993].

Acknowledgments. This research was sponsored in part by the Air Force Office of Scientific Research, Air Force Systems Command, USAF, under grant or cooperative agreement number AFOSR 91-0298. This research was also supported in part by the Department of the Interior, U.S. Geological Survey, through the Kansas Water Resources Research Institute. The views and conclusions contained in this document are those of the authors and should not be interpreted as necessarily representing the official policies, either expressed or implied, of the U.S. government.

References

- Amoozegar, A., and A. W. Warrick, Hydraulic conductivity of saturated soils: Field methods, in *Methods of Soil Analysis, Part 1, Physical and Mineralogical Methods*, Agron. Monogr. Ser. 9, edited by A. Klute, pp. 735-770, American Society of Agronomy, Madison, Wisc., 1986.
- Bliss, J. C., and K. R. Rushton, The reliability of packer tests for estimating the hydraulic conductivity of aquifers, *Q. J. Eng. Geol.*, 17, 81-91, 1984.
- Bohling, G. C., and C. D. McElwee, SUPRPUMP: An interactive program for well test analysis and design, *Ground Water*, 30(2), 262-268, 1992.
- Bouwer, H., The Bouwer and Rice slug test—An update, *Ground Water*, 27(3), 304-309, 1989.
- Bouwer, H., and R. C. Rice, A slug test for determining hydraulic conductivity of unconfined aquifers with completely or partially penetrating wells, *Water Resour. Res.*, 12(3), 423-428, 1976.
- Brigham, E. O., *The Fast Fourier Transform*, 252 pp., Prentice-Hall, Englewood Cliffs, N. J., 1974.
- Butler, J. J., Jr., and Z. Hyder, An assessment of the Nguyen and Pinder method for slug test analysis, *KGS Open File Rep. 93-46*, 25 pp., Kansas Geol. Surv., Lawrence, 1993.
- Butler, J. J., Jr., and C. D. McElwee, Hydrogeologic characterization of hazardous waste sites, *Contrib. Kans. Water Resour. Res. Inst.*, 283, 114 pp., 1990.
- Butler, J. J., Jr., W. Z. Liu, and D. P. Young, Analysis of October 1993 slug tests in Stafford, Pratt, and Reno Counties, south-central Kansas, *KGS Open File Rep. 93-52*, 70 pp., Kans. Geol. Surv., Lawrence, 1993a.
- Butler, J. J., Jr., C. D. McElwee, and Z. Hyder, Slug tests in unconfined aquifers, *Contrib. Kans. Water Resour. Res. Inst.*, 303, 67 pp., 1993b.
- Butler, J. J., Jr., G. C. Bohling, Z. Hyder, and C. D. McElwee, The use of slug tests to describe vertical variations in hydraulic conductivity, *J. Hydrol.*, 156, 137-162, 1994a.
- Butler, J. J., Jr., C. D. McElwee, and Z. Hyder, Slug tests in unconfined aquifers—Year two, *Contrib. Kans. Water Resour. Res. Inst.*, 310, 1994b.
- Chirlin, G. R., A critique of the Hvorslev method for slug test analysis: The fully penetrating well, *Ground Water Monit. Rev.*, 9(2), 130-138, 1989.
- Chirlin, G. R., The slug test: The first four decades, *Ground Water Manage.*, 1, 365-381, 1990.
- Churchill, R. V., *Operational Mathematics*, 481 pp., McGraw-Hill, New York, 1972.
- Cooley, J. W., and J. W. Tukey, An algorithm for machine calculations of complex Fourier series, *Math. Comput.*, 19, 297-301, 1965.
- Cooper, H. H., Jr., J. D. Bredehoeft, and I. S. Papadopoulos, Response of a finite-diameter well to an instantaneous charge of water, *Water Resour. Res.*, 3(1), 263-269, 1967.
- Dagan, G., A note on packer, slug, and recovery tests in unconfined aquifers, *Water Resour. Res.*, 14(5), 929-934, 1978.
- Dougherty, D. E., and D. K. Babu, Flow to a partially penetrating well in a double-porosity reservoir, *Water Resour. Res.*, 20(8), 1116-1122, 1984.
- Faust, C. R., and J. W. Mercer, Evaluation of slug tests in wells containing a finite-thickness skin, *Water Resour. Res.*, 20(4), 504-506, 1984.
- Freeze, R. A., and J. A. Cherry, *Groundwater*, 604 pp., Prentice-Hall, Englewood Cliffs, N. J., 1979.
- Haberman, R., *Elementary Applied Partial Differential Equations*, 547 pp., Prentice-Hall, Englewood Cliffs, N. J., 1987.
- Hayashi, K., T. Ito, and H. Abe, A new method for the determination of in situ hydraulic properties by pressure pulse tests and application to the Higashi Hachimantai geothermal field, *J. Geophys. Res.*, 92(B9), 9168-9174, 1987.
- Hvorslev, M. J., Time lag and soil permeability in ground-water observations, *Bull. 36*, 50 pp., Waterw. Exp. Sta., U.S. Army Corps of Eng., Vicksburg, Miss., 1951.
- Hyder, Z., Analysis of slug tests in partially penetrating wells, Ph.D. thesis, Univ. of Kans., Lawrence, 1994.
- Hyder, Z., and J. J. Butler Jr., Slug tests in unconfined formations: An assessment of the Bouwer and Rice technique, *Ground Water*, in press, 1994.
- Hyder, Z., W. Z. Liu, and J. J. Butler Jr., Software for the evaluation of semianalytical solutions for slug tests in partially penetrating wells, *KGS Comput. Program Ser. 93-1*, 42 pp., Kans. Geol. Surv., Lawrence, 1993.
- Kruseman, G. P., and N. A. de Ridder, Analysis and evaluation of pumping test data, *ILRI Publ. 47*, 377 pp., Int. Inst. for Land Reclamation and Improvement, The Netherlands, 1989.
- McElwee, C. D., and J. J. Butler Jr., Effective transmissivities from slug tests in wells with a skin, *KGS Open File Rep. 92-12*, 31 pp., Kans. Geol. Surv., Lawrence, 1992.
- Moench, A. F., and P. A. Hsieh, Analysis of slug test data in a well with finite-thickness skin, *Mem. IAH Int. Congr. Hydrogeol. Rocks Low Permeability*, 17(2), 17-29, 1985.
- Moench, A., and A. Ogata, Analysis of constant discharge wells by numerical inversion of Laplace transform solutions, in *Groundwater Hydraulics*, *Water Resour. Monogr.*, vol. 9, edited by J. Rosenzhein and G. D. Bennett, pp. 146-170, AGU, Washington, D. C., 1984.
- Nguyen, V., and G. F. Pinder, Direct calculation of aquifer parameters in slug test analysis, in *Groundwater Hydraulics*, *Water Resour. Monogr.*, vol. 9, edited by J. Rosenzhein and G. D. Bennett, pp. 222-239, AGU, Washington, D. C., 1984.
- Press, W. H., S. A. Teukolsky, W. T. Vetterling, and B. P. Flannery, *Numerical Recipes in FORTRAN*, 963 pp., Cambridge University Press, New York, 1992.
- Stehfest, H., Numerical inversion of Laplace transforms, *Commun. ACM*, 13(1), 47-49, 1970.
- U.S. Department of the Navy, Bureau of Yards and Docks, *Design Manual: Soil Mechanics, Foundations, and Earth Structures*, vol. DM-7, chap. 4, Alexandria, Va., 1961.
- J. J. Butler Jr., Z. Hyder, W. Liu, and C. D. McElwee, Kansas Geological Survey, University of Kansas, 1930 Constant Avenue, Lawrence, KS 66047.

(Received July 6, 1993; revised June 13, 1994; accepted June 23, 1994.)

Appendix D. The Use of Slug Tests to Describe Vertical Variations in Hydraulic Conductivity,
Published in the *Journal of Hydrology*,
Volume 156, pages 137-162, 1994.

[2]

The use of slug tests to describe vertical variations in hydraulic conductivity

James J. Butler, Jr.*, Geoffrey C. Bohling, Zafar Hyder, Carl D. McElwee
Kansas Geological Survey, 1930 Constant Avenue, Campus West, Lawrence, KS 66046-2598, USA

(Received 17 April 1993; revision accepted 28 September 1993)

Abstract

Multilevel slug tests provide one means of obtaining estimates of hydraulic conductivity on a scale of relevance for contaminant transport investigations. A numerical model is employed here to assess the potential of multilevel slug tests to provide information about vertical variations in hydraulic conductivity under conditions commonly faced in field settings. The results of the numerical simulations raise several important issues concerning the effectiveness of this technique. If the length of the test interval is of the order of the average layer thickness, considerable error may be introduced into the conductivity estimates owing to the effects of adjoining layers. The influence of adjoining layers is dependent on the aspect ratio (length of test interval/well radius) of the test interval and the flow properties of the individual layers. If a low-permeability skin is present at the well, the measured vertical variations will be much less than the actual variations, owing to the influence of the skin conductivity on the parameter estimates. A high-permeability skin can also produce apparent vertical variations that are much less than the actual, owing to water flowing vertically along the conductive skin. In cases where the test interval spans a number of layers, a slug test will yield an approximate thickness-weighted average of the hydraulic conductivities of the intersected layers. In most cases, packer circumvention should not be a major concern when packers of 0.75 m or longer are employed. Results of this study are substantiated by recently reported field tests that demonstrate the importance of well emplacement and development activities for obtaining meaningful estimates from a program of multilevel slug tests.

1. Introduction

Over the last decade, a considerable amount of theoretical, laboratory, and field research on the mechanisms of large-scale solute transport has identified the spatial

* Corresponding author.

distribution of hydraulic conductivity as a significant factor in determining how a plume of a conservative tracer will move in the subsurface (e.g. Dagan, 1986; Freyberg, 1986; Gelhar, 1986; Moltyaner and Killey, 1988; Hess et al., 1992). The measurement of hydraulic conductivity in the subsurface on a scale of relevance for contaminant transport investigations, however, has proven to be a rather difficult task. Conventional pumping tests will provide large-scale volumetric averages of hydraulic conductivity, which may be of rather limited use in transport investigations (e.g. Butler and Liu, 1993). Multi-well tracer tests, which can provide information on the average inter-well conductivity, are expensive in terms of time, money and effort. Other techniques are needed if information on conductivity variations is to be used by practicing hydrogeologists outside the research community.

Techniques that have been reported in the literature include multilevel (straddle-packer) slug tests, borehole flowmeter surveys, laboratory core analyses, correlation with geophysical logs, and a variety of single-well tracer tests. Melville et al. (1991) described a program of multilevel slug tests at a research site, and showed that the results compare favorably with the information obtained from a large-scale multi-well tracer test. A number of workers in both the petroleum and groundwater fields (e.g. Hufschmied, 1986; Ehlig-Economides and Joseph, 1987; Morin et al., 1988; Molz et al., 1989; Rehfeldt et al., 1989; Hess et al., 1992) have shown that borehole flowmeters have the potential to provide detailed information about the vertical variations in hydraulic conductivity at a well. Laboratory analysis of sampled cores is undoubtedly the most common method of assessing vertical variations in hydraulic conductivity. However, the collection of reasonably intact cores in permeable unconsolidated materials, the geologic media in many contaminant transport investigations, can be difficult (e.g. Zapico et al., 1987; McElwee et al., 1991). In addition, the time and expense of performing permeameter analyses on a complete set of cores can be considerable. Taylor et al. (1990) described several recently developed techniques for characterizing vertical variations in hydraulic conductivity. One particularly interesting approach is the single-well electrical tracer test (Taylor and Molz, 1990), which involves using a focused induction downhole probe to measure changes in electrical conductivity as an electrically conductive tracer moves away from the borehole.

The focus of this paper is the evaluation of multilevel slug tests as a source of information on vertical variations in the radial component of hydraulic conductivity. Slug tests have both economic and logistical advantages over the other techniques described above. A logistical advantage that cannot be overemphasized for waste-site investigations is that a slug test can be configured so that water is neither added nor removed from the test well. Such a slug test can be initiated by introducing (or removing) an object of known volume to (or from) the water column, or by pneumatic means (e.g. Orient et al., 1987; McLane et al., 1990). Problems arising as a result of the injection of waters of different compositions or the disposal of potentially contaminated waters can thus be avoided.

A number of workers have examined multilevel slug tests or the related multilevel constant-head injection test, using both analytical and numerical approaches. In terms of analytical approaches, Dagan (1978) employed Green's functions and a steady-state approximation to simulate tests in partially penetrating wells in uncon-

finned flow systems. Dougherty and Babu (1984) presented a fully transient analytical solution for slug tests performed in partially penetrating wells in isotropic confined systems. Hayashi et al. (1987) developed an analytical solution for multilevel slug tests in vertically unbounded, isotropic confined systems that explicitly includes the effects of packers above and below the test zone. Butler et al. (1990; see also McElwee et al., 1990) presented a solution for slug tests in partially penetrating wells in vertically bounded, anisotropic confined units that includes the effect of a finite-radius well skin. None of the above contributions, however, considered the effects of formation layering, owing to the difficulty of incorporating a general representation of formation layering into an analytical solution. Karasaki (1986) looked at the effect of layering on a slug test performed in a well that is fully screened across a layered aquifer, in which flow is only in the radial direction. An extension to the general case of unrestricted flow in the vertical direction has apparently not been attempted.

In terms of numerical approaches, Braester and Thunvik (1984) presented the results of a series of transient numerical simulations of multilevel constant-head injection tests. In a somewhat similar study, Bliss and Rushton (1984) used a steady-state model to simulate constant-head injection tests in a fractured aquifer. More recently, Widdowson et al. (1990) used a steady-state numerical model to develop an approach for analyzing multilevel slug tests based on a method similar to that of Dagan (1978). Melville et al. (1991) employed this approach to analyze multilevel slug tests from an experimental field site.

Although several of the studies cited above have touched upon important aspects of the issue of the viability of multilevel slug tests, there are still many unanswered questions about the usefulness of the information provided from such tests under conditions commonly faced in the field, where anisotropy, layering, and well skins of either higher or lower permeability than the undamaged formation may influence the measured response data. The purpose of this paper is to address many of these questions in the context of a theoretical assessment of the potential of multilevel slug tests to provide information about vertical variations in hydraulic conductivity in the vicinity of the well bore. As no general analytical solution has been developed for the case of slug tests in layered aquifers, this assessment will be performed through numerical simulation. The major objectives of this work are: (1) to assess possible techniques for the analysis of slug tests in layered systems; (2) to evaluate the effects of various geologic features (e.g. density of layering, anisotropy within layers, distance from boundaries, etc.) and well-construction features (e.g. well skins, length of the test interval, etc.) on the parameters estimated from slug-test data; (3) to explore the nature of vertical averaging in slug tests in layered aquifers; (4) to assess the effects of packer length and determine under what conditions packer circumvention may be an important mechanism; (5) to make recommendations on the performance of multilevel slug tests in layered systems that can be utilized by the field practitioner.

2. Problem statement

The problem of interest here is that of the head response, as a function of r , z , and t ,

produced by the instantaneous introduction of a slug of water into a portion of the screened interval of a well. As shown in Fig. 1, the portion of the screened interval into which the slug is introduced is isolated from adjacent screened sections of the well by a pair of inflatable packers (straddle packer). Different intervals of the screen can be tested by moving the string of packers and pipes up and down in the well. A third packer is set above the top of the screen, isolating the well casing from the screened sections of the well outside the test interval. It should be noted that this configuration is in keeping with that commonly used in the field for multilevel slug tests (e.g. Melville et al., 1991; Butler and McElwee, 1992). In this analysis, flow properties are assumed to be invariant in the angular direction, and radial variations are limited to changes between a well skin created during drilling and development and the adjacent formation. Variations in flow properties of any magnitude are allowed between layers in the vertical direction.

The partial differential equation representing the flow of groundwater in response to the instantaneous introduction of a slug of water at a central well is:

$$\frac{\partial}{\partial r} \left(K_r \frac{\partial h}{\partial r} \right) + \frac{K_r}{r} \frac{\partial h}{\partial r} + \frac{\partial}{\partial z} \left(K_z \frac{\partial h}{\partial z} \right) = S_s \frac{\partial h}{\partial t} \quad (1)$$

where h is the hydraulic head (L), K_r is the component of hydraulic conductivity in the radial direction (L/T), K_z is the component of hydraulic conductivity in the vertical direction (L/T), S_s is the specific storage (1/L), t is the time (T), r is the radial direction (L), and z is the vertical direction (L).

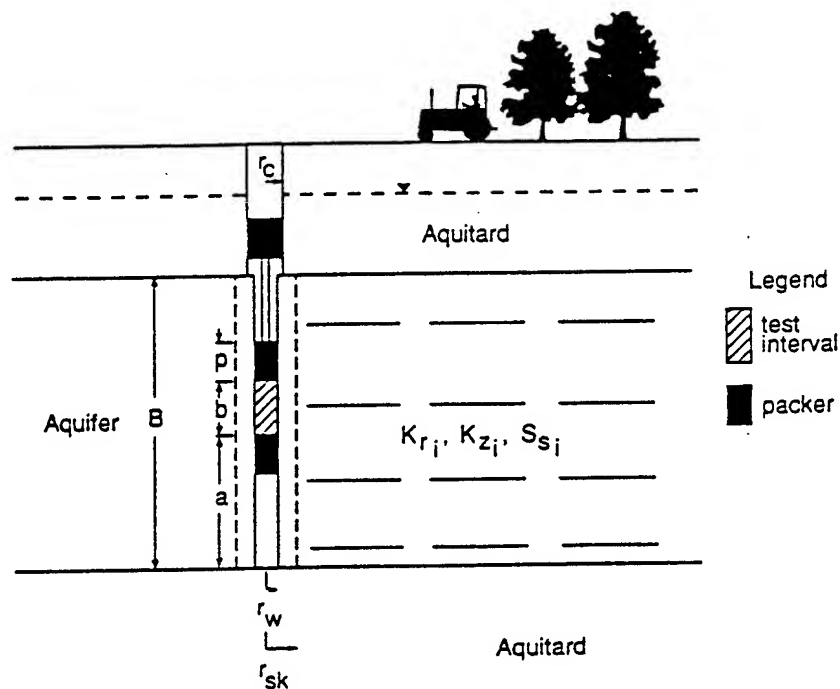


Fig. 1. Cross-sectional view of multilevel slug-test configuration (r_w , radius of test interval; r_c , radius of well casing above screen; r_{sk} , radius of skin; B , thickness of aquifer; a , distance of the bottom of the test interval above the base of the aquifer; b , width of the test interval; p , packer length; K_{r_i} , K_{z_i} , S_{s_i} , radial component of conductivity, vertical component of conductivity, and specific storage, respectively, of layer i). Layering is assumed to extend throughout the cross-section.

The initial conditions can be written as

$$h(r, z, 0) = 0, \quad r_w < r < \infty, \quad 0 \leq z \leq B \quad (2)$$

$$h(r_w, z, 0) = \begin{cases} H_0, & a \leq z \leq a + b \\ 0, & \text{elsewhere} \end{cases} \quad (3)$$

where r_w is the radius of the screen in the test interval (L), B is the thickness of the aquifer (L), H_0 is the height of the initial slug (L), a is the distance of the bottom of the test interval above the base of the aquifer (L), and b is the width of the test interval (L).

The boundary conditions are as follows:

$$h(\infty, z, t) = 0, \quad t > 0, \quad 0 \leq z \leq B \quad (4)$$

$$\frac{\partial h(r, 0, t)}{\partial z} = \frac{\partial h(r, B, t)}{\partial z} = 0, \quad r_w < r < \infty, \quad t > 0 \quad (5)$$

$$h(r_w, z, t) = H(t), \quad t > 0, \quad a \leq z \leq a + b \quad (6)$$

$$2\pi r_w \int_a^{a+b} K_r \frac{\partial h(r_w, z, t)}{\partial r} dz = \pi r_c^2 \frac{dH(t)}{dt}, \quad t > 0 \quad (7)$$

$$\frac{\partial h(r_w, z, t)}{\partial r} = 0, \quad t > 0, \quad a - p \leq z < a, \quad a + b < z \leq a + b + p \quad (8)$$

$$\frac{\partial h(0, z, t)}{\partial r} = 0, \quad t > 0, \quad 0 \leq z < a - p \quad (9)$$

$$\frac{\partial h(r_p, z, t)}{\partial r} = 0, \quad t > 0, \quad a + b + p < z \leq B \quad (10)$$

where $H(t)$ is the head within the well in the test interval (L), r_c is the radius of the cased portion of the well above the upper packer (L), r_p is the radius of the pipe through which the slug has been introduced to the test interval (L), and p is the length of the straddle packer (L). It should be noted that the conditions (8), (9), and (10) are a no-flow condition for the portion of the screen sealed by the packers, a symmetry boundary below the packers, and a no-flow condition along the pipe connecting the straddle packers to the upper packer, respectively.

Eqs. (1)–(10) describe the flow conditions of interest here. Given the generality of the property variations allowed in the vertical direction, analytical approaches are not feasible. Thus, for this work, a numerical model was employed to obtain approximate solutions to the mathematical model represented by the above equations.

3. Numerical model

In this work, a cylindrical-coordinate, three-dimensional, finite-difference model

(3DFDTC), developed at the Kansas Geological Survey (Butler and McElwee, 1992), was employed to simulate multilevel slug tests. The model was centered on the well in which the slug tests were being performed. The influence of well bore storage is taken into consideration using an approach based on earlier work of Settari and Aziz (1974), Rushton and Chan (1977), and Butler (1986). As described by Butler (1986), the approach is based on rewriting the classical pipe flow equation (Vennard and Street, 1975) in a formulation similar to Darcy's Law and defining a term (involving the friction factor, the cross-sectional area of the well bore, and distance along the well bore) analogous to hydraulic conductivity. This approach allows flow

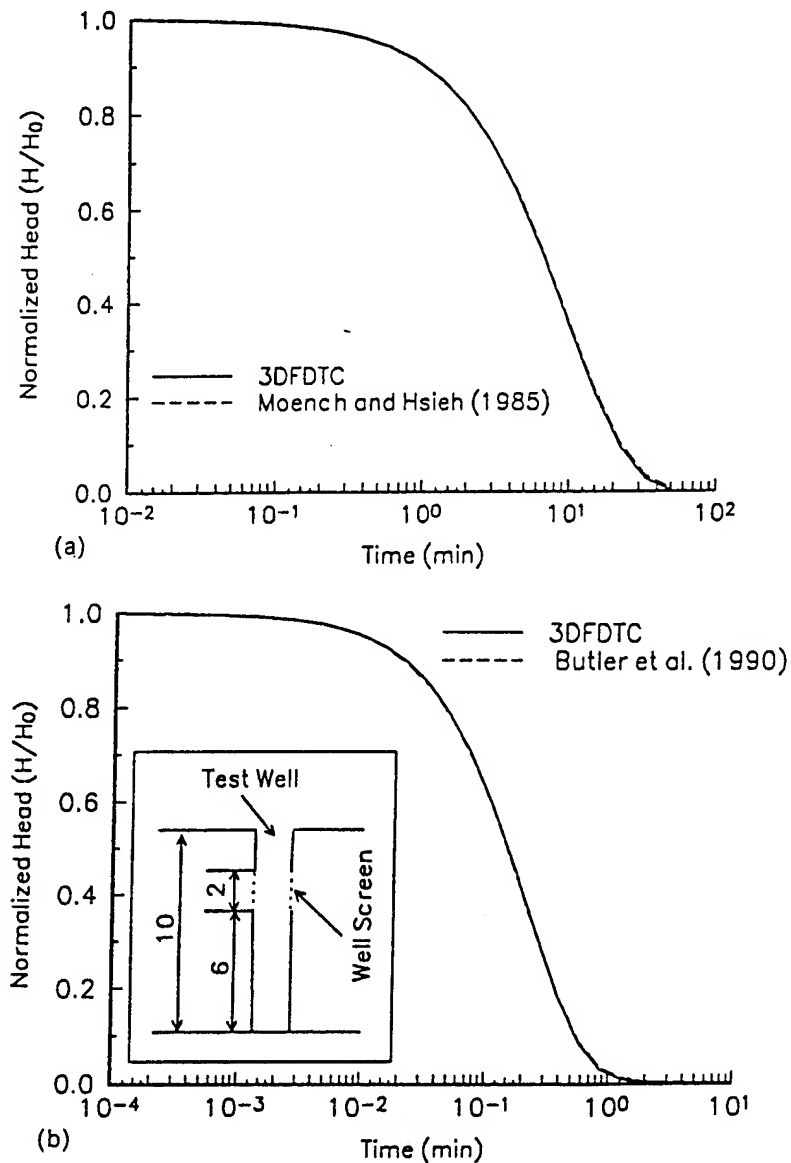


Fig. 2. Plots of normalized head ($H(t)/H_0$) vs. time comparing analytical solutions with 3DFDTC results. (a) Comparison of Moench and Hsieh (1985) solution with 3DFDTC results ($r_w = 0.167$ m, $r_{sk} = 0.33$ m, $T_{sk} = 0.001$ m² min⁻¹, $S_{sk} = 0.001$, $T_{aq} = 1$ m² min⁻¹, $S_{aq} = 0.00001$). (b) Comparison of Butler et al. (1990; see also McElwee et al., 1990) solution with 3DFDTC results ($r_w = 0.167$ m, $K = 0.1$ m min⁻¹, $S_s = 0.000001$ m⁻¹).

inside the well bore to be governed by the porous media flow equation (Eq. (1)). It should be noted that the implementation of this approach for this study produces an approximation of well-bore behavior that is equivalent to the hydrostatic head assumption employed in most analytical representations of the well bore (e.g. Papadopoulos and Cooper, 1967; Cooper et al., 1967).

To demonstrate the validity of the well-bore approximation, the model has been checked against many analytical solutions for both pumping and slug tests. Two examples of such comparisons are presented here. The first example illustrates model performance when the hydraulic conductivity of adjacent grid cells differs by several orders of magnitude. A slug test in a well surrounded by a low-permeability well skin of finite radius was simulated. The well was assumed to be screened throughout the aquifer. Fig. 2(a) illustrates a comparison of the heads simulated by 3DFDTC with the results from the analytical solution of Moench and Hsieh (1985) for a slug test in a well with a skin of finite radius. The plots of the results are essentially the same. The small differences that do exist are attributed mainly to the error caused by the spatial discretization scheme employed in 3DFDTC (20 nodes in the radial direction from 0.1 to 37 364 m using equal log spacing). Further simulations have shown that, on increasing the number of nodes in the radial direction, the difference between the analytical solution and 3DFDTC results will gradually disappear.

The second example is selected to illustrate model performance when there is a strong component of vertical flow, such as might occur in multilevel slug tests. A slug test is simulated in a well that is screened for only a portion of the aquifer thickness. The aquifer is assumed to be homogeneous and isotropic with respect to flow properties. Fig. 2(b) displays a comparison of the heads simulated by 3DFDTC with the results of the analytical solution of Butler et al. (1990; see also McElwee et al., 1990) for a slug test in a well partially penetrating a confined aquifer. As with the previous example, 3DFDTC yields results that are essentially indistinguishable from those of the analytical solution. It should be noted that the error introduced by the radial discretization scheme employed in these examples was considered acceptable for the purposes of this work. Further issues concerning the vertical discretization scheme are discussed in a later section.

4. Techniques for analysis of slug tests in layered systems

The approach employed in this research was to simulate a series of multilevel slug tests using the 3DFDTC model, and then estimate the hydraulic conductivity of the portion of the formation opposite the screened interval from the simulated results. Several methods were considered for the analysis of the simulated slug-test responses. The most commonly used methods for the analysis of slug-test data in confined aquifers are the approaches of Cooper et al. (1967), henceforth designated as the CBP model, and Hvorslev (1951). As the CBP model was developed for slug tests performed in wells fully screened across an aquifer, the method of Hvorslev was the major focus of this work.

Hvorslev (1951) developed a series of models for the analysis of slug tests

performed in confined aquifers. A major assumption of the Hvorslev approach is that the specific storage of the aquifer can be neglected. As the head response at the test well is relatively insensitive to specific storage (Cooper et al., 1967), this assumption may be acceptable in many cases. Each of the well–aquifer configurations that Hvorslev considered requires the use of a ‘shape factor’, which is related to the geometry of the well intake region. The shape factor used here is that of Case 8 described by Hvorslev (1951), which is for a configuration consisting of a well with a screened interval of finite length located in a uniform, vertically unbounded, aquifer with a horizontal to vertical anisotropy in hydraulic conductivity. The Hvorslev model for this case is in the form of a two-parameter (K_r and anisotropy ratio) function:

$$h(t) = H_0 \exp(-t/T_0) \quad (11)$$

where

$$T_0 = (\pi r_c^2)/FK_r$$

$$F = (2\pi b)/(\ln \{mb/2r_w + [1 + (mb/2r_w)^2]^{1/2}\})$$

$$m = (K_r/K_z)^{1/2}$$

Unfortunately, the two parameters in (11) are perfectly correlated, so they cannot be estimated independently. Eq. (11) can be rearranged to produce the following expression for the estimated hydraulic conductivity:

$$K_{HV} = \frac{r_c^2 \ln \{mb/2r_w + [1 + (mb/2r_w)^2]^{1/2}\}}{2bt_0} \quad (12)$$

where K_{HV} is the hydraulic conductivity estimated using the Hvorslev model and t_0 is the time at which a normalized head of 0.37 is reached. Clearly, an anisotropy ratio must be assumed to estimate K_{HV} .

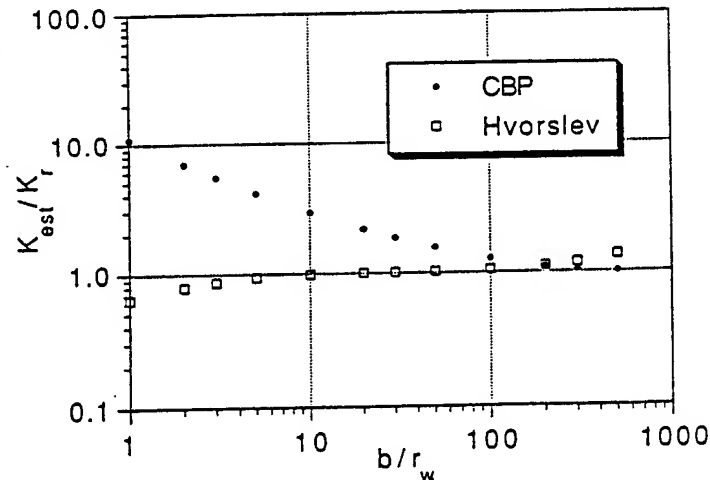


Fig. 3. Plot of aspect ratio (b/r_w) vs. conductivity ratio (K_{est}/K_r) for the case of boundaries at a large distance from the test interval.

An initial series of simulations was performed using 3DFDTC to assess the viability of the Hvorslev model for the estimation of hydraulic conductivity from multilevel slug-test data. Fig. 3 presents the results of a set of simulations in which the effects of the magnitude of the aspect ratio (b/r_w) on conductivity estimates, obtained from slug tests in a uniform aquifer, are investigated. Aspect ratios extending over two orders of magnitude were employed to evaluate parameter estimates over the range of conditions expected in multilevel slug tests. It should be noted that conductivity estimates obtained using both the Hvorslev and CBP models are included on this plot to illustrate the dependence of both models on aspect ratio. Fig. 3 indicates that the Hvorslev model should provide acceptable parameter estimates (within 20% of the actual conductivity) for aspect ratios between 3 and 300. The CBP model provides better estimates than the Hvorslev model at large aspect ratios (200 or higher) as a result of the slug-test responses becoming increasingly similar to those from a fully screened well at large aspect ratios.

The results presented in Fig. 3 are for the case of the test interval being at a large distance from a formation boundary (infinite aquifer case). Fig. 4 depicts the results of a further set of simulations in which the effects of an impermeable boundary on parameter estimates are examined. In these simulations, the test interval, which has an aspect ratio of five, is progressively moved from the center of the aquifer to the upper impermeable boundary. A test interval with a small aspect ratio and an isotropic aquifer were employed to emphasize the effects of vertical flow. The boundary effects are straightforward. As the test interval approaches the boundary, the vertical flow out of the interval is constrained, resulting in a decrease in the K_{HV} estimate. It should be noted that the effect of an impermeable horizontal boundary is less dramatic with larger aspect ratios and/or the presence of a pronounced anisotropy ($K_r > K_z$). Thus, Figs. 3 and 4 indicate that for the aspect ratios commonly employed in programs of

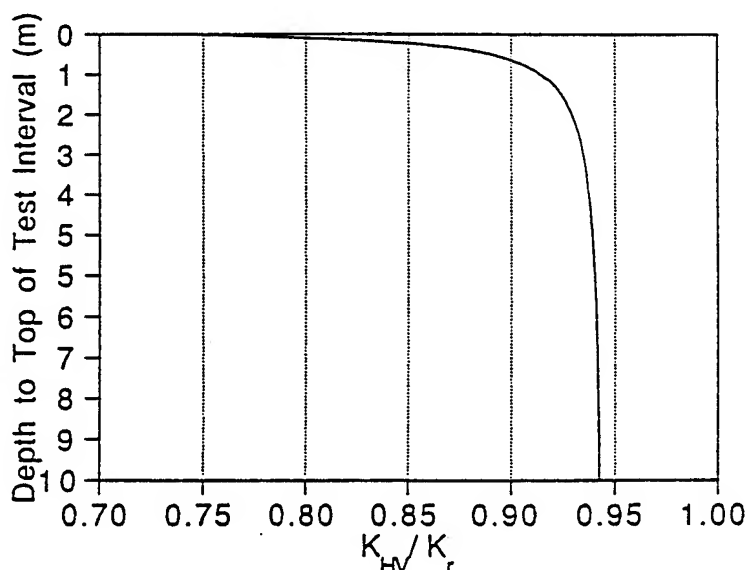


Fig. 4. Plot of conductivity ratio (K_{HV}/K_r) vs. depth to top of test interval (aspect ratio (b/r_w) = 5, impermeable boundary assumed at zero). (Note that in Fig. 3 (infinite aquifer case) K_{HV}/K_r = 0.94 for this aspect ratio.)

multilevel slug tests, the Hvorslev model should provide acceptable estimates as long as the test interval is several meters below an impermeable boundary.

Although the focus of this discussion has been on the Hvorslev model, several additional models were considered for the analysis of the simulated slug tests. As discussed in the Introduction, Butler et al. (1990; see also McElwee et al., 1990) have developed an analytical solution for slug tests in partially penetrating wells with skins, which can be readily configured to analyze data from multilevel slug tests in homogeneous, anisotropic aquifers. Although this solution avoids the simplifying approximations of the Hvorslev approach, the calculated parameters are not significantly different from those of Hvorslev for the range of aspect ratios commonly employed in multilevel slug tests. A major drawback of this model is that it is computationally intensive as a result of the use of both Fourier and Laplace integral transforms to obtain the solution.

Dagan (1978) and Widdowson et al. (1990) have developed techniques for the analysis of multilevel slug tests that are based on a series of graphs or charts developed from simulation of slug tests under conditions similar to those considered by Hvorslev (1951). A major drawback of these techniques is that new simulations are required for each well-aquifer configuration that is examined.

The Hvorslev model was considered the most appropriate model for use here, given the results of the simulations presented in Figs. 3 and 4 and its advantages in terms of computational efficiency. Thus, in the remainder of this paper, the Hvorslev model is employed for the analysis of simulated slug-test responses. The analyses were performed using the implementation of the Hvorslev model found in the SUPRPUMP automated well-test analysis package of the Kansas Geological Survey (Bohling and McElwee, 1992). This use of the Hvorslev model, however, should not be considered a blanket endorsement of the approach, as the model must be used with caution when analyzing actual field data, owing to its neglect of storage effects on slug-test responses (Chirlin, 1989), its poor performance in the presence of a well skin (Butler et al., 1990), and its increasing error in wells with very small aspect ratios (Hvorslev, 1951).

5. Dependence of multilevel slug-test results on density of layering

The simulations discussed in the previous section illustrate the performance of multilevel slug tests in ideal homogeneous systems. Many aquifers in nature, however, consist of layers of differing flow properties. To address the effects of layering on multilevel slug tests, a hypothetical aquifer, made up of alternating layers of constant thickness consisting of two distinct materials (denoted here as A and B), was constructed. Although layering in natural systems is clearly more complex than this configuration, the use of an alternating two-component system will allow the major effects of layering on a program of multilevel slug tests to be assessed.

The base set of parameters for this layered aquifer model are given in Table 1. A grid of 20 nodes in the radial direction (the same discretization scheme as used in simulations of Fig. 2) and 48–96 nodes in the vertical direction was employed. The

Table 1
Parameters for layered aquifer model

$H_0 = 1.0$ m
$r_w = 0.05$ m
$K_A = 2.0 \times 10^{-5}$ m s ⁻¹
$K_B = 2.0 \times 10^{-4}$ m s ⁻¹
$S_{SA} = S_{SB} = 1.0 \times 10^{-5}$ m ⁻¹
$B =$ aquifer thickness = 30 m
$r_{bnd} =$ radial distance to outer boundary = 37 364 m

number of nodes in the vertical varied depending on the layering and test interval length used in a particular scenario. To assess the error introduced by the various vertical discretization schemes, a number of additional simulations were performed using increasingly finer vertical discretization. In all cases, the discretization schemes used here were found to introduce an error of less than 2% to the calculated parameters. These errors were considered acceptable for the purposes of this work. It should be noted that in simulations using very small test intervals (0.156 m), the thickness of the aquifer (B) was decreased from the base case of 30 m to 15 m. In all cases, however, the results reported here were for test intervals far enough away from a boundary for boundary effects to be negligible.

The results of the simulations of slug tests in layered aquifers are presented using the range of conductivities estimated from a series of slug tests performed as the

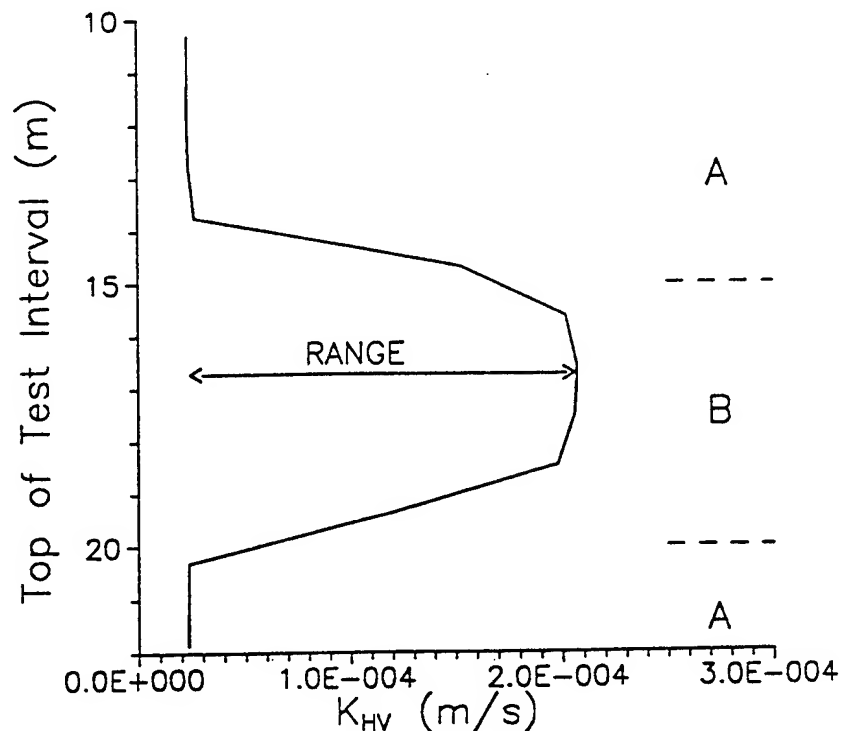


Fig. 5. Plot of estimated conductivity vs. depth to top of test interval for multilevel slug tests simulated in a layered aquifer consisting of alternating layers of material A and B (see Table 1; L (layer thickness) is 5 m, and b (length of test interval) is 1.25 m). Range is defined as distance between the maximum and minimum estimated conductivity.

packer string was moved in small increments up the well bore. Fig. 5 displays a plot of hydraulic conductivity values estimated from such a series of multilevel slug-test simulations in which the packer string is moved in 0.94 m increments up the well bore. The results are shown for only a portion of the series of alternating high- and low-conductivity layers to clarify the definition of the range as the distance between the peak and trough of the conductivity vs. depth plot. The range of estimated conductivities was considered a succinct way to display the manner in which the actual conductivity variations are being distorted in the results of a program of multilevel slug tests. In addition to the range, however, the estimated maximum and minimum conductivity values are also considered, so that the degree of over- or underestimation of layer conductivities is clear. It should be noted that the slight overestimation of K_A and K_B shown in Fig. 5 is in keeping with the results displayed in Fig. 3 for a test interval of the same aspect ratio ($b/r_w = 25$).

The first set of layered-aquifer simulations was designed to investigate the effect of layering density on multilevel slug tests. For these simulations, the test interval length was constrained to be less than or equal to the layer thickness, which was assumed to be constant for any particular simulation. In a later section, simulations using test intervals of lengths greater than the layer thickness are described. Fig. 6 displays the results of a series of simulations in which the test interval length was assumed to equal layer thickness. In these simulations, the test interval length (and thus the layer

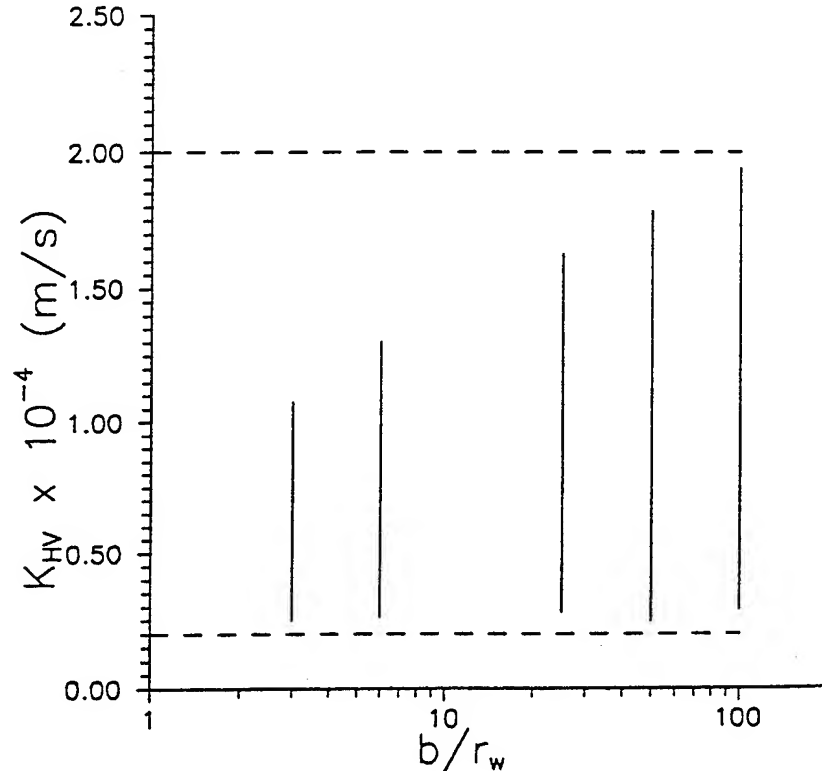


Fig. 6. Plot of range of estimated conductivities vs. aspect ratio (b/r_w). (Note that layer thickness changes in the same manner as b .) Lower and upper dashed lines indicate the conductivities of Layers A and B, respectively.

thickness) was gradually decreased from 5 m (aspect ratio of 100) to 0.156 m (aspect ratio approximately three). The results are displayed in the form of a plot of the range of the estimated conductivities vs. aspect ratio. Clearly, the range of estimated conductivities decreases significantly with decreases in aspect ratio. It should be noted that most of this decrease is a result of the conductivity estimated for layer B becoming increasingly smaller than the actual conductivity owing to suppression of vertical flow by the adjoining layers of material A. Hayashi et al. (1987) described how a decrease in aspect ratio promotes partial penetration effects, i.e. vertical flow from either end of the test interval. Thus, adjoining lower-conductivity layers will have a greater impact on slug-test responses as the aspect ratio decreases and the importance of vertical flow increases.

The general result of these simulations is that the effect of adjoining layers on multilevel slug tests becomes increasingly important as the layers decrease in thickness. Fig. 6, however, should only be considered as an example of these effects. The exact nature of the influence of adjoining layers will depend on a number of additional factors, including the specific storage of the layers and the degree of anisotropy in layer conductivity. The above simulations were performed assuming a specific storage of $1 \times 10^{-5} \text{ m}^{-1}$. Additional simulations have shown that use of a lower specific storage value results in the pressure disturbance induced by the slug test spreading out more rapidly in all directions, causing the effect of adjoining lower-conductivity layers to be accentuated. The increased influence of adjoining lower-conductivity layers produces considerably lower values for the estimated layer B conductivities. Likewise, a specific storage greater than that used in Fig. 6 lessens the influence of adjoining layers on conductivity estimates. Thus, the specific storage can have a considerable influence on the estimated conductivity in layered systems. This is in contrast to slug tests in homogeneous systems, where specific storage has relatively little influence on conductivity estimates obtained from heads at the test well (Cooper et al., 1967).

The addition of anisotropy ($K_r > K_z$) into the configuration does not produce results significantly different from those shown in Fig. 6. The influence of adjoining layers is clearly diminished by the addition of anisotropy as a result of the suppression of vertical flow. The suppression of vertical flow itself, however, causes a decrease in the estimated conductivities. The net result is a decrease in the conductivities estimated for both layers and estimated conductivity ranges slightly narrower than those displayed in Fig. 6. It should be noted that the analyses described in this section were performed with the Hvorslev model, assuming an isotropic aquifer. This is a reasonable assumption, because one will not normally know what degree of anisotropy is appropriate. As discussed above, the anisotropy ratio and the horizontal conductivity are perfectly correlated in the Hvorslev model. Thus, some error will always be introduced into the parameter estimates as a result of the uncertainty concerning anisotropy.

The results displayed in Fig. 6 were obtained assuming that the test interval length was equal to layer thickness. If the test interval length is less than the layer thickness, adjoining layers will have less of an impact on the estimated conductivity. Fig. 7 shows the results of a series of simulations in which the layer thickness was

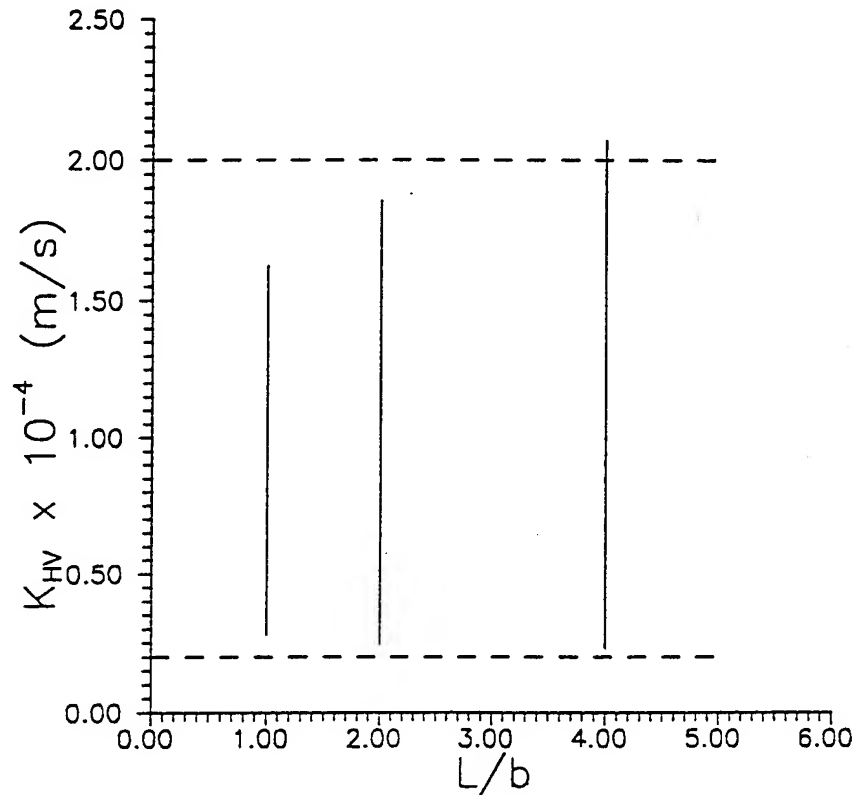


Fig. 7. Plot of range of estimated conductivities vs. L/b . (Note that b remains constant (1.25 m) for the cases displayed in this plot.) Lower and upper dashed lines indicate the conductivities of Layers A and B, respectively.

progressively increased, while the test interval, which was centered within the layer, was not changed (constant aspect ratio of 25). As expected, increases in the ratio of layer thickness to test interval length decrease the impact of adjoining layers. In Fig. 7, the effects of adjoining layers are essentially negligible for ratios of four or greater (overestimation of K_r seen at $L/b = 4$ is in keeping with Fig. 3). It should be noted that the exact nature of the decrease in the effects of adjacent layers will depend on the aspect ratio (the larger the aspect ratio, the more rapid the decrease). Clearly, however, the use of a test interval length considerably smaller than the average layer thickness will greatly improve the information obtained from a program of multi-level slug tests. When the results of Figs. 6 and 7 are considered together, it is also clear that r_w should be kept as small as practically possible to decrease the impact of the effects of small aspect ratios.

6. Dependence on well skins

The results depicted in Figs. 6 and 7 were determined for the ideal case, in which formation layering extends to the well screen. Often, however, as illustrated in Fig. 1, well drilling and development creates a near-well zone (well skin) of properties differing from those of the formation in which the well is screened. An additional

series of simulations was performed here to assess the effects of well skins on multi-level slug-test results.

Fig. 8 shows the results from a set of simulations in which a low-permeability well skin was employed. The results are displayed in the form of a plot of the range of estimated conductivities vs. simulation case. These results show that the addition of a low-permeability skin produces a near-complete suppression of the vertical variations in conductivity (calculated conductivity ranges are 2.9% and 1.7% of actual for Cases A and B, respectively). In addition to the suppression of the conductivity variations, the estimated conductivities are much lower than in the case with no skin, as a result of the heavy weighting of the low-permeability skin in the parameter estimates. Butler et al. (1990; see also McElwee et al., 1990) discussed the nature of the weighting of a low-permeability well skin in conductivity estimates obtained using the Hvorslev model. It should be noted that the estimated conductivities are lower in Case B as a result of the greater importance of vertical flow with smaller aspect ratios. In this case, the vertical flow is being suppressed by the low-permeability well skin, resulting in lower calculated conductivities.

A well skin may be of higher permeability than the formation as a result of voids forming along the well screen during well emplacement activities or a high-permeability sand pack. A high-conductivity skin can serve as a conduit for additional

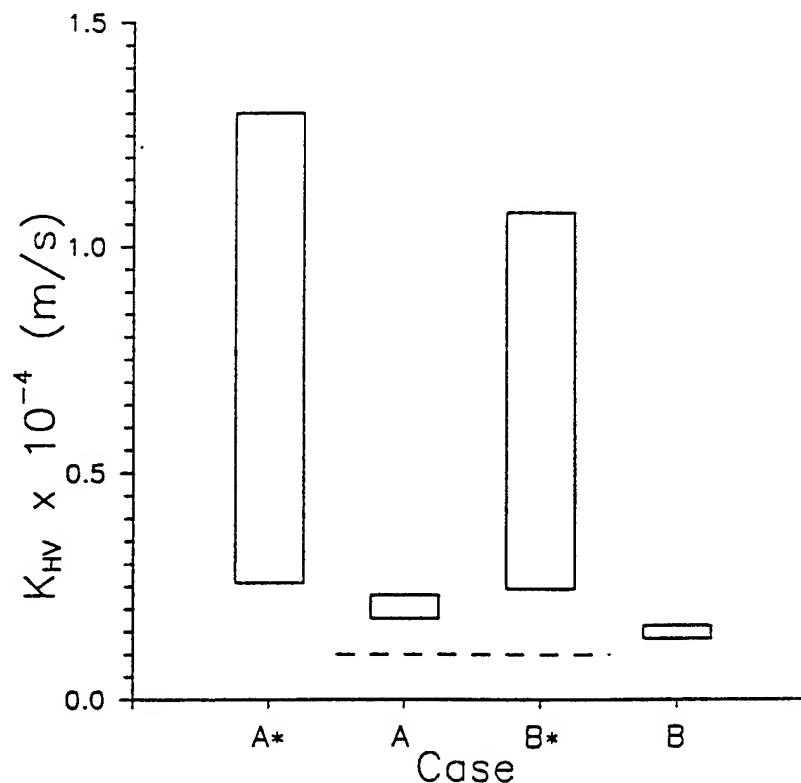


Fig. 8. Plot of range of estimated conductivities vs. simulation case for the low-permeability ($K_{sk} = 0.00001 \text{ m s}^{-1}$) skin scenario (Case A*, case with no skin, $L = b = 0.312 \text{ m}$; Case A, $L = b = 0.312 \text{ m}$, $r_{sk} = 0.11 \text{ m}$; Case B*, case with no skin, $L = b = 0.156 \text{ m}$; Case B, $L = b = 0.156 \text{ m}$, $r_{sk} = 0.11 \text{ m}$). Dashed line indicates the skin conductivity.

vertical flow. Fig. 9 shows the results of a series of simulations in which a high-permeability skin of 0.11 m in radius was employed for most cases. Once again, the results are given in the form of a plot of the range of estimated conductivities vs. simulation case. It should be noted that, in relatively thick layers, the width of the calculated conductivity range does not change greatly from that in the case with no skin (compare Cases C* and C), although the estimated conductivities themselves increase significantly. As the thickness of the layers decreases, the layers become thin enough that, when the test interval is opposite a layer of material A, substantial amounts of water flow vertically along the well skin and into the layers of material B. This results in a great increase in the conductivity estimated for layers of material A and a dramatic decrease in the calculated conductivity range. As shown by Case G, this effect increases with the thickness of the skin. Clearly, a highly conductive skin in an aquifer consisting of thin layers can cause multilevel slug tests to be of rather limited effectiveness for describing vertical variations in hydraulic conductivity.

Given that a highly conductive skin can greatly limit the effectiveness of multilevel slug tests, a series of additional simulations was performed to assess whether measures could be taken during well construction to reduce the effect of a conductive skin. One possibility suitable for wells where the sand pack is the high-conductivity

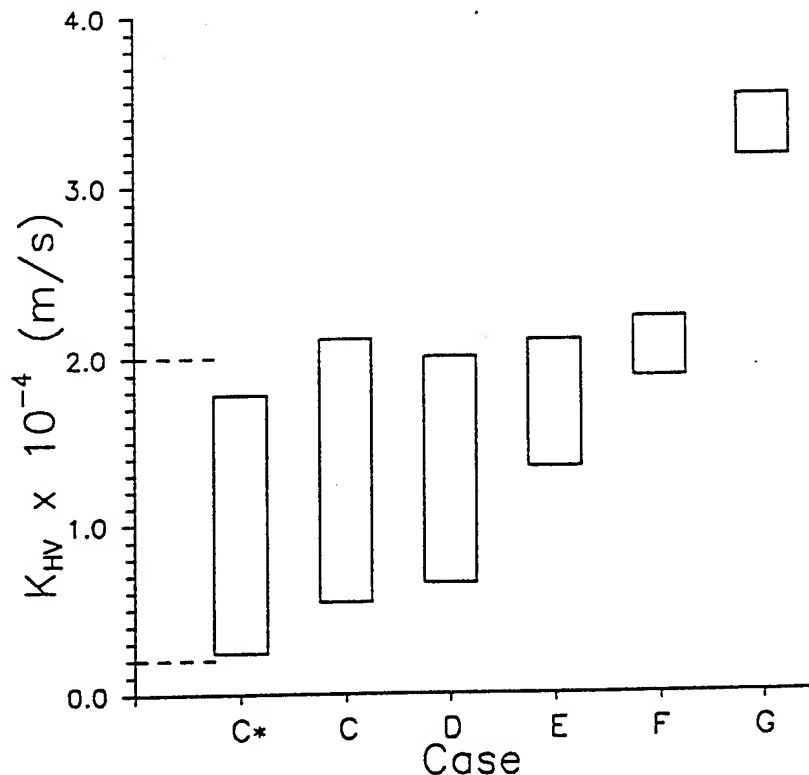


Fig. 9. Plot of range of estimated conductivities vs. simulation case for the high-permeability ($K_{sk} = 0.001 \text{ m s}^{-1}$) skin scenario (Case C*, case with no skin, $L = b = 2.5 \text{ m}$; Case C, $L = b = 2.5 \text{ m}$, $r_{sk} = 0.11 \text{ m}$; Case D, $L = b = 1.25 \text{ m}$, $r_{sk} = 0.11 \text{ m}$; Case E, $L = b = 0.312 \text{ m}$, $r_{sk} = 0.11 \text{ m}$; Case F, $L = b = 0.156 \text{ m}$, $r_{sk} = 0.11 \text{ m}$; Case G, $L = b = 0.312 \text{ m}$, $r_{sk} = 0.22 \text{ m}$). Lower and upper dashed lines indicate the conductivities of Layers A and B, respectively.

skin would be to place very thin layers (1–2 cm) of low-conductivity material (e.g. bentonite pellets) in the sand pack at an interval similar to the length of the planned test interval. These layers would serve to decrease the vertical movement of water in the sand pack, but would have very little impact on horizontal flow. This scheme was evaluated here by simulating slug tests in wells with high-conductivity skins in which an anisotropy in conductivity was assumed for the skin. Fig. 10 presents the results of a series of simulations in which anisotropy ratios (K_r/K_z) of one, two, and 10 were employed (K_r remaining constant and K_z decreased). As shown in the figure, increases in the anisotropy ratio cause the calculated conductivity range to increase and the estimated conductivities to decrease towards the value for the case with no skin. These results indicate that if a well is to be used for multilevel slug tests, the emplacement of periodic thin layers of low-conductivity material in the sand pack would be useful in partially mitigating the effect of a high-conductivity skin. Unfortunately, in cases where the high-conductivity skin is not the sand pack (e.g. uncased wells in consolidated rock), such an approach would not be possible, thereby making it difficult to remove the effect of a high-conductivity skin in those situations. It should be noted that the successful emplacement of periodic layers of bentonite in the sandpack should produce much greater anisotropy ratios (more than 1000) than those employed here. However, practically speaking, it will be difficult to insure that unbroken layers of bentonite have been placed at the desired locations. Lower

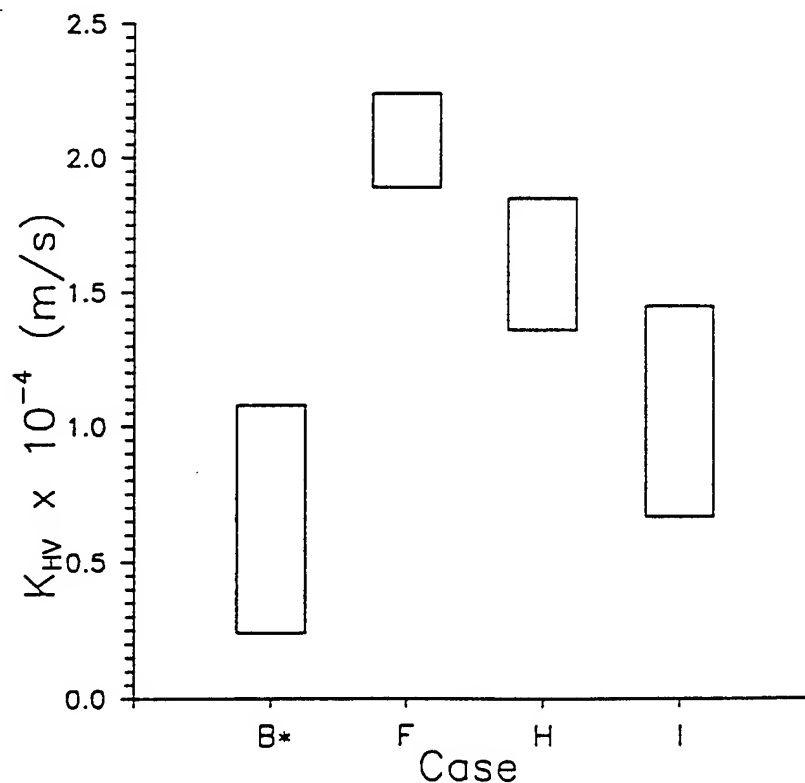


Fig. 10. Plot of range of estimated conductivities vs. simulation case for the high-permeability skin with anisotropy scenario (Case B*, case with no skin, $L = b = 0.156$ m; Case F, same as in Fig. 9; Case H, same as Case F except $K_{r(\text{skin})}/K_{z(\text{skin})} = 2$; Case I, same as Case F except $K_{r(\text{skin})}/K_{z(\text{skin})} = 10$).

anisotropy ratios were therefore employed here to yield conservative estimates of the expected behavior.

7. Vertical averaging in slug tests in layered aquifers

One issue of considerable interest to hydrogeologists is the way in which flow properties are averaged in various types of hydraulic tests in heterogeneous systems (e.g. Desbarats, 1992; Harvey, 1992). As a number of layers may be spanned by the test interval in a multilevel slug test, the issue of the manner in which the properties of those layers are averaged to form the effective parameter estimated from the response data is of some importance. In this work, the nature of this vertical averaging was explored empirically through numerical simulation.

The initial step of this investigation was to assess the manner in which hydraulic

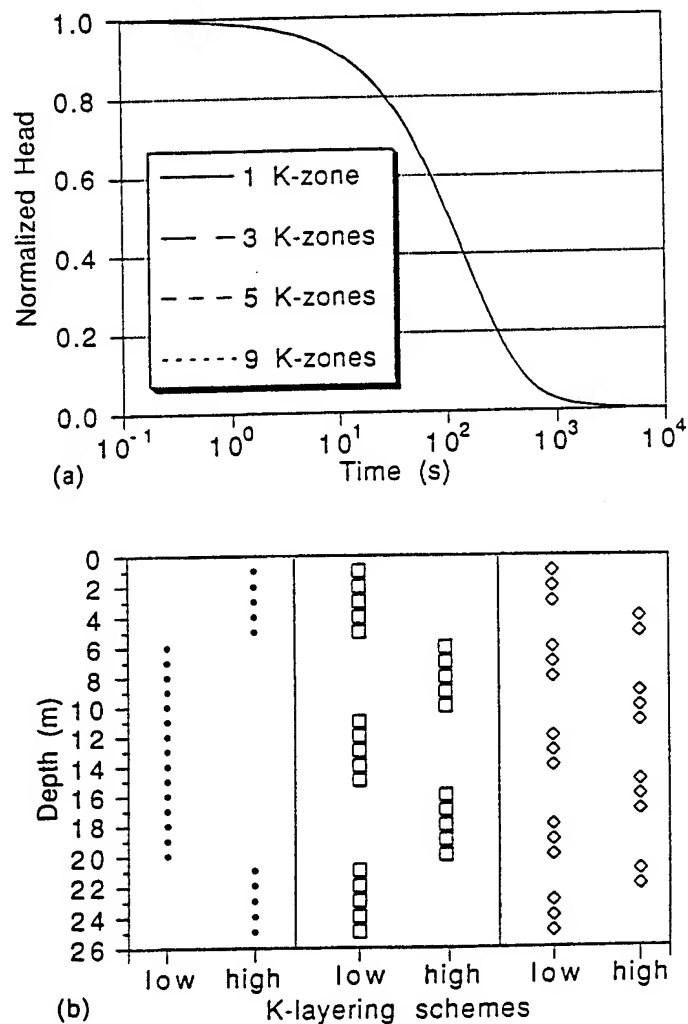


Fig. 11. Effects of variable layering on fully penetrating slug-test results. (a) Plot of normalized head ($H(t)/H_0$) at the test well vs. time. (b) Layering schemes employed in the simulations shown in (a) (low and high conductivities defined in Table 2).

conductivity values that vary in the vertical direction are averaged in a slug test performed over the entire screened interval of a well fully penetrating the aquifer (fully penetrating slug test). A set of four simulations were performed. These simulations consisted of a uniform, anisotropic aquifer case, and three layered-aquifer cases with alternating layers of high and low conductivity. The layering schemes are shown in Fig. 11(b) and the parameter values used in each case are given in Table 2. It should be noted that all three layering schemes have a thickness-weighted average K_r of 9.2×10^{-5} , which is the same value for K_r as used in the uniform aquifer case.

Fig. 11(a) shows the results of the simulations for the case of head in the test well. As shown in this figure, the simulated heads at the test well are essentially identical in the uniform and all three layered cases. Clearly, slug tests over the entire screened interval in fully penetrating wells can provide little information about vertical variations in conductivity when the test well is the measurement location. In all cases, the estimated conductivity will be a thickness-weighted arithmetic average of the horizontal conductivities of the individual layers. It should be noted that this result is an extension of the work of Karasaki (1986), who found the same result using an analytical solution for slug tests in layered aquifers in which there is no vertical flow between layers. Thus, the vertical averaging in fully penetrating slug tests appears to be independent of the degree of vertical flow between layers. It is important to stress that there is vertical flow in the layered simulations of Fig. 11. These and additional simulations have shown that there will be considerable differences in head in the vertical direction outside of the test well ($r > r_w$) during a fully penetrating slug test in a layered aquifer (Butler and McElwee, 1992). Apparently, the flow between layers is in some sort of hydraulic balance dependent on the thickness of layers, the density of layering, layer flow properties, etc., such that the response at the central test well is independent of the degree of vertical flow.

As Fig. 11(a) shows that no indication of layering will be evident from the head response at the test well in a fully penetrating slug test, an obvious question of importance for multilevel slug tests is how much will layering be suppressed as the test interval becomes larger than the average layer thickness. Additional simulations have shown that the degree of suppression will depend on vertical variations in the arithmetic average of the conductivities of the test interval and the aspect ratio. In all cases, when the aspect ratio is much greater than 200, the estimated conductivity can be assumed to be a thickness-weighted average of the conductivities of the layers intersected by the test interval. It should be noted that this statement is based on

Table 2
Parameters for analysis of vertical averaging

Uniform, anisotropic case

$K_r = 9.2 \times 10^{-5} \text{ m s}^{-1}$, $K_z = 9.2 \times 10^{-6} \text{ m s}^{-1}$

Layered cases

Low-conductivity layer: $K_r = 2.0 \times 10^{-5} \text{ m s}^{-1}$, $K_z = 2.0 \times 10^{-6} \text{ m s}^{-1}$

High-conductivity layer: $K_r = 2.0 \times 10^{-4} \text{ m s}^{-1}$, $K_z = 2.0 \times 10^{-5} \text{ m s}^{-1}$

the assumption that the slug-test responses will be analyzed with the model of Cooper et al. (1967) for aspect ratios greater than 200, in keeping with the results displayed in Fig. 3.

8. Effect of packer length

All the multilevel slug-test simulations described above were performed assuming that the well was cased everywhere in the aquifer except at the test interval (infinite packer) in order to remove any effects related to the circumvention of the packers from the results. In field applications, however, packer circumvention is a very real concern. Increased vertical flow owing to packer circumvention can result in an overestimation of layer conductivities and an underestimation of the degree of vertical variations.

A series of additional simulations was performed to assess the effect of packer length on parameters estimated from multilevel slug tests. In the 3DFDTC model, packers are simulated as no-flow boundaries in the well bore, so there is no restriction on the length of the modelled packers. Four configurations were employed in this analysis to allow the effects of packer length to be evaluated in homogeneous and layered situations, both with and without a high-conductivity skin (see Table 3 for the

Table 3
Parameter sets for packer simulations

Case 1

$$K_A = K_B = 2 \times 10^{-5} \text{ m s}^{-1}$$

$$S_{SA} = S_{SB} = 1 \times 10^{-5} \text{ m}^{-1}$$

$$b = 0.15 \text{ m}$$

Case 2

$$K_A = 2 \times 10^{-5} \text{ m s}^{-1}$$

$$K_B = 2 \times 10^{-4} \text{ m s}^{-1}$$

$$S_{SA} = S_{SB} = 1 \times 10^{-5} \text{ m}^{-1}$$

$$b = 0.15 \text{ m}$$

$$L = 0.15 \text{ m}$$

Case 3

$$K_A = K_B = 2 \times 10^{-5} \text{ m s}^{-1}$$

$$S_{SA} = S_{SB} = 1 \times 10^{-5} \text{ m}^{-1}$$

$$K_{sk} = 0.001 \text{ m s}^{-1}$$

$$b = 0.15 \text{ m}$$

$$r_{sk} = 0.11 \text{ m}$$

Case 4

$$K_A = 2 \times 10^{-5} \text{ m s}^{-1}$$

$$K_B = 2 \times 10^{-4} \text{ m s}^{-1}$$

$$S_{SA} = S_{SB} = 1 \times 10^{-5} \text{ m}^{-1}$$

$$K_{sk} = 0.001 \text{ m s}^{-1}$$

$$b = 0.15 \text{ m}$$

$$L = 0.15 \text{ m}$$

$$r_{sk} = 0.11 \text{ m}$$

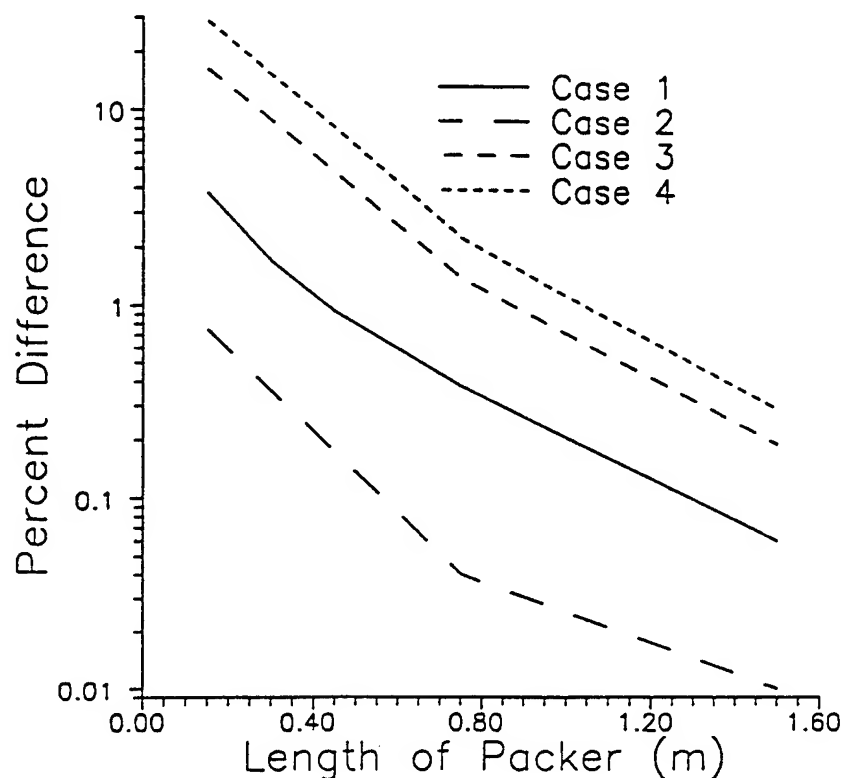


Fig. 12. Plot of packer length vs. normalized difference $((K_{\text{packer}} - K_{\infty \text{ packer}})/K_{\infty \text{ packer}} \times 100)$ for Cases 1–4 of Table 3. Plotted results are for case of test interval opposite layer A.

parameters used in each configuration). Cases 1 and 2 were designed to assess behavior in homogeneous and layered situations, respectively, in the absence of a high-conductivity skin, and Cases 3 and 4 were designed to assess behavior in the same systems in the presence of a high-conductivity skin.

Fig. 12 presents the results of these simulations in the form of a plot of packer length against the difference between the estimated conductivity using a packer of that length (K_{packer}) and the estimated conductivity using an infinite packer ($K_{\infty \text{ packer}}$) normalized by the infinite packer estimate. It should be noted that a dramatic decrease in this difference is seen in all cases with an increase in packer length. This plot clearly indicates that a highly conductive skin will exacerbate packer circumvention problems. In all cases, however, these results demonstrate that the relationships derived in this work are essentially the same as would be obtained using packers of 0.75–1.5 m in length, which is the length range of many commercially available packers. Given that the skin is 50 times more permeable than layer A, these results should be considered conservative, worst-case estimates. Thus, packers greater than 0.75 m in length should prevent packer circumvention in the vast majority of field applications. Bliss and Rushton (1984) found similar results for the effect of packer length on constant-head injection tests. It should be noted that the results reported here are dependent on the thickness of the high-conductivity skin. In cases where very thick skins are suspected, longer packers or a number of packers in series should be employed. However, as demonstrated in an earlier section, a thick high-conductivity

skin will hinder the effectiveness of multilevel slug tests even without packer circumvention.

9. Recent field experiences

Recently reported field experiences with multilevel slug tests in unconsolidated aquifers support some of the findings of this study. Melville et al. (1991) reported on a program of multilevel slug tests for which the results compared favorably with information obtained from tracer tests. Butler and McElwee (1992), on the other hand, described a program of multilevel slug tests for which the results indicated essentially no vertical variations in flow properties, a finding that was not in agreement with existing core data. Although the test procedures followed in both studies were similar, the well drilling and emplacement procedures were not. Melville et al. (1991) described a procedure of well emplacement using mud rotary drilling followed by forcing a slotted pipe of slightly smaller diameter into the drilled hole. The small annular space between the slotted pipe and the drilled hole was filled by collapsing material from the borehole wall. The wells were then extensively developed to remove as much of the drilling mud as possible from the formation. Butler and McElwee (1992) described a procedure of well emplacement using hollow-stem auger drilling followed by placing a slotted pipe down the center of the augers and withdrawing the auger flights from about the pipe. In this case, a much larger annular space was formed, which was then filled by a natural sand pack consisting of material collapsing inward from the borehole wall. Permeameter analyses of cores from this same formation (Jiang, 1991; Butler and McElwee, 1992) have shown that repacked cores have considerably higher conductivities than the original sampled cores, indicating that the collapsed zone would probably form a skin of higher conductivity than the formation as a whole. The poor results of the tests reported by Butler and McElwee (1992) may well be due to preferential water movement along this thick high-conductivity skin. The success of the Melville et al. (1991) program appears to be largely due to the thin well skin coupled with unremoved drilling muds that are apparently preferentially impeding vertical flow. Although their approach seems to have met with success, the results of Melville and coworkers could have suffered from the same effects as illustrated in Fig. 8 without a very extensive program of well development. Thus, it is clear that well drilling and development procedures cannot be overemphasized in the planning of multilevel slug tests.

An approach for multilevel slug testing in unconsolidated formations that appears to minimize many of the problems arising as a result of well emplacement was described by Hinsby et al. (1992). This approach is based on progressively driving a well point and short screen into the formation. At any level desired, well driving can be stopped and a slug test performed. Although the results of the slug tests will still be a function of layering density, etc., as outlined here, this approach appears to have less potential for producing a thick high-conductivity skin along the driven pipe. Work currently under way at the Kansas Geological Survey and elsewhere is evaluating this approach in more detail.

10. Summary and conclusions

This paper reports the results of a series of numerical experiments designed to assess the potential of slug tests for the purpose of describing vertical variations in the radial component of hydraulic conductivity. Although most natural systems will not consist of the ideal two-component system of repetitive layers considered here, such a conceptual model allows considerable insight to be gained concerning behavior in more complex systems. Five general conclusions, which are independent of the particular parameter values employed here, can be drawn from this work:

(1) when the length of the test interval is of the order of the average layer thickness, considerable error can be introduced into the description of vertical variations in hydraulic conductivity as a result of the influence of layers adjoining the test interval. The magnitude of the influence of the adjoining layers will strongly depend on the aspect ratio (test interval length/ r_w). The specific storage of the tested interval will also be an important factor.

(2) Regardless of layering density, a low-conductivity skin will make it difficult to describe vertical variations in hydraulic conductivity because the estimated conductivity will be strongly influenced by the conductivity of the skin.

(3) A high-conductivity skin will make it difficult to describe vertical variations in hydraulic conductivity when the test interval and the average layer thickness are both small. In this case, a large amount of vertical flow can occur along the skin, making it difficult to detect the existence of layers of low conductivity. Periodic emplacement of thin, low-conductivity layers in the sand pack can help decrease vertical flow and allow a more accurate description of the conductivity variations to be obtained.

(4) When the aspect ratio is large (more than 200), a slug test will yield an approximate thickness-weighted average of the hydraulic conductivities of the layers intersecting the test interval if the data are analyzed with the model of Cooper et al. (1967) (exact average in the case of a fully penetrating slug test). As the aspect ratio decreases, the properties of layers outside of the test interval will influence the calculated conductivity owing to the increased vertical flow.

(5) Packer circumvention should not be a major problem in most field applications when packers of 0.75 m or longer are employed. Packer circumvention is of greatest concern in the case of a thick, high-conductivity skin.

In summary, multilevel slug tests can provide considerable information about vertical variations in hydraulic conductivity under the right conditions. The best conditions would be thick layers, with test intervals considerably smaller than the average layer thickness. Even under these conditions, however, well skins can dramatically decrease the effectiveness of the approach. Considerable attention must therefore be given to well construction and development, to minimize the impact of a well skin on test results. Results from recently reported field tests demonstrate the importance of well construction and development procedures.

It should be noted that the findings of this study must be considered in the light of two major assumptions employed here. First, the simulated responses from each slug

test were analyzed using a homogeneous-aquifer model, an approach in keeping with standard field practices. Analysis of each test in isolation from the others in the same series of multilevel tests, however, led to the strong dependence of test results on layering density and, in many cases, to a significant underestimation of the actual conductivity variations. A more rigorous approach would be to analyze all the test results together using a numerical model coupled to an optimization routine. An initial attempt at such an approach for a series of drill-stem tests has been given by Yu and Lloyd (1992). Even if such a technique was used, however, it would not remove the effects of well skins or vertical averaging from test results. Given the nature of current field practices, the approach employed here was considered appropriate.

Second, the findings discussed in this paper were based on a series of simulations performed in perfectly stratified aquifers, i.e. layering is continuous throughout the entire model domain. Although many natural systems consist of a series of discontinuous layers, the rate of variation in flow properties in the direction perpendicular to the plane of layering would be expected to be considerably larger than that in the direction parallel to layering (Butler, 1986; Hess et al., 1992). Thus, the results presented here should be applicable to most field situations. Further work, however, is required to assess fully the effect of layer discontinuity on slug tests.

Acknowledgments

This research was sponsored in part by the Air Force Office of Scientific Research, Air Force Systems Command, USAF, under grant or cooperative agreement AFOSR 91-0298, and by the US Geological Survey (USGS), Department of the Interior, under USGS award 14-08-0001-G2093. The views and conclusions contained in this document are those of the authors and should not be interpreted as necessarily representing the official policies, either expressed or implied, of the US Government.

References

- Bliss, J.C. and Rushton, K.R., 1984. The reliability of packer tests for estimating the hydraulic conductivity of aquifers. *Q. J. Eng. Geol.*, 17: 81–91.
- Bohling, G.C. and McElwee, C.D., 1992. SUPRPUMP: an interactive program for well test analysis and design. *Ground Water*, 30(2): 262–268.
- Braester, C. and Thunvik, R., 1984. Determination of formation permeability by double-packer tests. *J. Hydrol.*, 72: 375–389.
- Butler, Jr., J.J., 1986. Pumping tests in nonuniform aquifers: a deterministic and stochastic analysis. Ph.D. dissertation, Stanford University, Stanford, CA, 220 pp.
- Butler, Jr., J.J. and Liu, W.Z., 1993. Pumping tests in nonuniform aquifers: the radially asymmetric case. *Water Resour. Res.*, 29(2): 259–269.
- Butler, Jr., J.J. and McElwee, C.D., 1992. Well-testing methodologies for characterizing heterogeneities in alluvial-aquifer systems: first year report. *Kans. Geol. Surv. Open-File Rep.*, 92-53, 152 pp.
- Butler, Jr., J.J., McElwee, C.D., Bohling, G.C. and Healey, J.M., 1990. Hydrogeologic characterization of hazardous waste sites. *Kansas Water Resources Research Inst., Manhattan, KS, Contrib.* 283, 114 pp.

- Chirlin, G.R., 1989. A critique of the Hvorslev method for slug test analysis: the fully penetrating well. *Ground Water Monit. Rev.*, 9(2): 130–138.
- Cooper, Jr., H.H., Bredehoeft, J.D. and Papadopoulos, I.S., 1967. Response of a finite-diameter well to an instantaneous charge of water. *Water Resour. Res.*, 3(1): 263–269.
- Dagan, G., 1978. A note on packer, slug, and recovery tests in unconfined aquifers. *Water Resour. Res.*, 14(5): 929–934.
- Dagan, G., 1986. Statistical theory of groundwater flow and transport: pore to laboratory, laboratory to formation, and formation to regional scale. *Water Resour. Res.*, 22(9): 120S–134S.
- Desbarats, A.J., 1992. Spatial averaging of transmissivity in heterogeneous fields with flow toward a well. *Water Resour. Res.*, 28(3): 757–767.
- Dougherty, D.E. and Babu, D.K., 1984. Flow to a partially penetrating well in a double-porosity reservoir. *Water Resour. Res.*, 20(8): 1116–1122.
- Ehlig-Economides, C.A. and Joseph, J.A., 1987. A new test for determination of individual layer properties in a multilayered reservoir. *SPE Formation Eval.*, 2(3): 261–283.
- Freyberg, D.L., 1986. A natural gradient experiment on solute transport in a sand aquifer, 2. Spatial moments and the advection and dispersion of nonreactive tracers. *Water Resour. Res.*, 22(13): 2031–2046.
- Gelhar, L.W., 1986. Stochastic subsurface hydrology from theory to applications. *Water Resour. Res.*, 22(9): 135S–145S.
- Harvey, C.F., 1992. Interpreting parameter estimates obtained from slug tests in heterogeneous aquifers. M.S. Thesis, Stanford University, Stanford, CA, 99 pp.
- Hayashi, K., Ito, T. and Abe, H., 1987. A new method for the determination of in situ hydraulic properties by pressure pulse tests and application to the Higashi Hachimantai geothermal field. *J. Geophys. Res.*, 92(B9): 9168–9174.
- Hess, K.M., Wolf, S.H. and Celia, M.A., 1992. Large-scale natural gradient tracer test in sand and gravel, Cape Cod, Massachusetts, 3. Hydraulic conductivity variability and calculated macrodispersivities. *Water Resour. Res.*, 28(8): 2011–2027.
- Hinsby, K., Bjerg, P.L., Andersen, L.J., Skov, B. and Clausen, E.V., 1992. A mini slug test method for determination of a local hydraulic conductivity of an unconfined sandy aquifer. *J. Hydrol.*, 136: 87–106.
- Hufschmied, P., 1986. Estimation of three-dimensional anisotropic hydraulic conductivity field by means of single well pumping tests combined with flowmeter measurements. *Hydrogeologie*, 2: 163–174.
- Hvorslev, M.J., 1951. Time lag and soil permeability in ground-water observations. *US Army Corps Eng. Waterways Exp. Sta. Bull.* 36, 50 pp.
- Jiang, X., 1991. A field and laboratory study of scale dependence of hydraulic conductivity. M.S. Thesis, University of Kansas, Lawrence, 149 pp.
- Karasaki, K., 1986. Well test analysis in fractured media. Ph.D. Dissertation, University of California, Berkeley, 239 pp.
- McElwee, C.D., Butler, Jr., J.J., Liu, W.Z. and Bohling, G.C., 1990. Effects of partial penetration, anisotropy, boundaries and well skin on slug tests (abstract). *EOS*, 71(17): 505.
- McElwee, C.D., Butler, Jr., J.J., and Healey, J.M., 1991. A new sampling system for obtaining relatively undisturbed samples of unconsolidated coarse sand and gravel. *Ground Water Monit. Rev.*, 11(3): 182–191.
- McLane, G.A., Harrity, D.A. and Thomsen, K.O., 1990. A pneumatic method for conducting rising and falling head tests in highly permeable aquifers. *Proc. 1990 NWWA Outdoor Action Conf.*
- Melville, J.G., Molz, F.J., Guven, O. and Widdowson, M.A., 1991. Multilevel slug tests with comparisons to tracer data. *Ground Water*, 29(6): 897–907.
- Moench, A.F. and Hsieh, P.A., 1985. Analysis of slug test data in a well with finite-thickness skin. In: *Mem. 17th Int. Congr. on Hydrogeology of Rocks of Low Permeability*, Int. Assoc. Hydrogeo. pp. 17–29.
- Moltzan, G.L. and Killey, R.W.D., 1988. Twin Lake tracer tests: longitudinal dispersion. *Water Resour. Res.*, 24(10): 1613–1627.
- Molz, F.J., Morin, R.H., Hess, A.E., Melville, J.G. and Guven, O., 1989. The impeller meter for measuring aquifer permeability variations: evaluation and comparison with other tests. *Water Resour. Res.*, 25(7): 1677–1686.

- Morin, R.H., Hess, A.E. and Paillet, F.L., 1988. Determining the distribution of hydraulic conductivity in a fractured limestone aquifer by simultaneous injection and geophysical logging. *Ground Water*, 26(5): 587–595.
- Orient, J.P., Nazar, A. and Rice, R.C., 1987. Vacuum and pressure test methods for estimating hydraulic conductivity. *Ground Water Monit. Rev.*, 7(1): 49–50.
- Papadopoulos, I.S. and Cooper, Jr., H.H., 1967. Drawdown in a well of large diameter. *Water Resour. Res.*, 3(1): 241–244.
- Rehfeldt, K.R., Hufschmied, P., Gelhar, L.W. and Schaefer, M.E., 1989. Measuring hydraulic conductivity with the borehole flowmeter. Rep. EN-6511, Electric Power Res. Inst., Palo Alto, CA.
- Rushion, K.R. and Chan, Y.K., 1977. Numerical pumping test analysis in unconfined aquifers. *J. Irrig. Drainage Div.*, 103(IR1): 1–12.
- Settari, A. and Aziz, K., 1974. A computer model for two-phase coning simulation. *Soc. Pet. Eng. J.*, 14(3): 221–236.
- Taylor, K. and Molz, F., 1990. Determination of hydraulic conductivity and porosity logs in wells with a disturbed annulus. *J. Contaminant Hydrol.*, 5: 317–332.
- Taylor, K., Wheatcraft, S., Hess, J., Hayworth, J. and Molz, F., 1990. Evaluation of methods for determining the vertical distribution of hydraulic conductivity. *Ground Water*, 28(1): 88–98.
- Vennard, J.K. and Street, R.L., 1975. *Elementary Fluid Mechanics*. Wiley, New York, 740 pp.
- Widdowson, M.A., Molz, F.J. and Melville, J.G., 1990. An analysis technique for multilevel and partially penetrating slug test data. *Ground Water*, 28(6): 937–945.
- Yu, Y.H. and Lloyd, J.W., 1992. A multi-layered radial flow model interpretation of drill stem test data. *J. Hydrol.*, 136: 73–86.
- Zapico, M., Vales, S. and Cherry, J., 1987. A wireline piston core barrel for sampling cohesionless sand and gravel below the water table. *Ground Water Monit. Rev.*, 7(3): 74–82.

Appendix E. Improving the Reliability of Parameter Estimates Obtained From Slug Tests,
Accepted for publication in *Ground Water*, 1995.

**IMPROVING THE RELIABILITY OF PARAMETER ESTIMATES OBTAINED FROM
SLUG TESTS**

James J. Butler, Jr., Carl D. McElwee, and Wenzhi Liu
Kansas Geological Survey
1930 Constant Ave.
Lawrence, KS 66047

August 1994

Prepared for submission to
Ground Water

ABSTRACT

The slug test is one of the most commonly used field methods for obtaining in-situ estimates of hydraulic conductivity. Despite its prevalence, this method has received criticism from many quarters in the groundwater community. This criticism emphasizes the poor reliability of the estimated parameters, a condition that is primarily a product of the somewhat casual approach that is often employed in slug tests. Recently, the Kansas Geological Survey (KGS) has pursued research directed at improving methods for the performance and analysis of slug tests. Based on extensive theoretical and field research, a series of guidelines have been proposed that should enable the reliability of parameter estimates to be improved. The most significant of these guidelines are: 1) three or more slug tests should be performed at each well during a given test period; 2) two or more different initial displacements (H_0) should be used at each well during a test period; 3) the method used to initiate a test should enable the slug to be introduced in a near-instantaneous manner and should allow a good estimate of H_0 to be obtained; 4) data-acquisition equipment that enables a large quantity of high quality data to be collected should be employed; 5) if an estimate of the storage parameter is needed, an observation well other than the test well should be employed; 6) the method chosen for analysis of the slug-test data should be appropriate for site conditions; 7) use of pre- and post-analysis plots should be an integral component of the analysis procedure, and 8) appropriate well-construction parameters should be employed. Data from slug tests performed at a number of KGS field sites demonstrate the importance of these guidelines.

INTRODUCTION

The slug test is a widely used technique for the in-situ estimation of hydraulic conductivity at sites of suspected groundwater contamination (Kruseman and de Ridder, 1989; Chirlin, 1990). Parameter estimates obtained from slug tests can be used for a variety of purposes including prediction of contaminant transport, design of large-scale pumping tests, and design of remediation schemes. Recently, however, this technique has received a considerable amount of criticism in the groundwater literature (e.g., Osborne, 1993). A primary cause of this criticism is the discrepancy that is often observed between estimates obtained from slug tests and those obtained from other information collected as part of the site investigation (e.g., geologic and geophysical logs, core samples, pumping tests, etc.). Although spatial variability and the different scales at which the various information was obtained can explain a portion of the observed discrepancy (e.g., Butler, 1990), a significant component of this difference undoubtedly arises as a result of the somewhat casual attitude that is often directed at the performance and analysis of slug tests. Since slug tests have considerable logistical and economic advantages over alternative approaches, it is imperative that these tests be done in such a manner so as to yield parameter estimates of as high a reliability as possible. The purpose of this paper is to propose practices for the performance and analysis of slug tests that should increase the reliability of the resulting parameter estimates.

Since 1989, the Kansas Geological Survey (KGS) has pursued extensive theoretical and experimental research on slug tests in porous formations. A major component of this effort has been a thorough examination of currently accepted practices. This work has resulted in the definition of a series of guidelines for the design, performance and analysis of slug tests. We have found that adherence to these guidelines can greatly improve the reliability of parameter estimates obtained from a program of slug testing. The major purpose of this paper is to describe the most significant of these guidelines. In the following sections, each of the proposed guidelines is explained in detail. Tests from a variety of KGS field sites are used as examples to demonstrate the importance of the proposed guidelines.

PROPOSED SLUG-TEST GUIDELINES

1. THREE OR MORE SLUG TESTS SHOULD BE PERFORMED AT A GIVEN WELL

According to conventional theory (e.g., Cooper et al., 1967), data from repeat slug tests at the same well should coincide when graphed in a normalized format (measured deviations from static normalized by the magnitude of the initial displacement, i.e. the size of the slug (H_0)). Figure 1 is a plot of a series of slug tests from a well in Lincoln County, Kansas, in which the response data conform to conventional theory, despite a variation of almost a factor of four in the magnitude of the initial displacement (H_0). Unfortunately,

however, data from repeat slug tests at the same well will often not plot in this ideal manner. Figure 2 displays data from a series of slug tests from another well at the same site in Lincoln County in which there was considerable variation in test responses. Since the pattern of responses shown on Figure 2 does not indicate a reproducible dependence on H_0 (test 3 on 5/21 and test 11 on 6/26 have similar H_0 but yield Cooper et al. parameter estimates that differ by close to a factor of two), this behavior is most likely an indication that the gravel pack or a portion of the formation in the vicinity of the well is being altered during the course of testing to form a low-permeability well skin. One possible explanation is that some fine material is being mobilized by the introduction of the slug and is moving in a manner that produces progressive decreases in formation permeability during the course of testing. Without doing a series of tests at a given well, this behavior would not be identified and thus properties reflective of the skin could inadvertently be assigned to the formation. A minimum of three tests is suggested in order that the effects of an evolving skin can be separated from a dependence on H_0 (discussed in the next section). Clearly, considerable attention must be given to well construction and development in order to minimize the possibility of skin development during the course of testing. Note that Dax (1987) describes results from a series of slug tests in which the wells are gradually clogged through time as a result of accumulation of material in the well and incrustation of the well

screen. The test responses displayed on Figure 2 are not thought to be a result of such a process of gradual clogging. The large differences in response time that are seen between tests performed on the same day are strong evidence in support of the hypothesis of mobilization of fine material leading to a decrease in near-well permeability.

2. TWO OR MORE DIFFERENT INITIAL DISPLACEMENTS SHOULD BE USED DURING TESTING AT A GIVEN WELL

As stated in the preceding section, conventional theory maintains that slug-test responses should be independent of the magnitude of the initial displacement (H_0). In confined formations of moderate to low permeability ($Kb < 15-20 \text{ m}^2/\text{d}$, where K is hydraulic conductivity and b is screen length), this assumption appears quite sound (e.g., Figure 1 of this paper and Herzog (1994)). In very permeable systems, however, a dependence on H_0 is often seen. Figure 3 is a plot from a series of tests in the semiconfined alluvial aquifer underlying the Geohydrologic Experimental and Monitoring Site (GEMS) in Douglas County, Kansas. A very strong dependence on H_0 is seen in these data, producing an inverse relationship between H_0 and hydraulic conductivity estimates obtained using conventional methods (i.e. Hvorslev (1951) and Cooper et al. (1967)). The tests displayed on Figure 3 were performed in a series of cycles from low to high H_0 . As shown in the figure, repeat tests with the same

approximate H_0 from different cycles coincided, verifying that the observed behavior is a reproducible function of H_0 and not a result of an evolving skin. In order to identify a dependence on H_0 , a series of tests in which H_0 varies between tests should be performed. A variation in H_0 of a factor of two or greater is recommended. In addition, the first and last tests should use the same H_0 so that the effects of an evolving skin can be separated from the H_0 dependence. Figures 4A and 4B display response data from such a test series in the alluvial aquifer underlying the Great Bend Prairie region of south-central Kansas. The coincidence of the normalized plots on Figure 4B indicates that the test responses are independent of H_0 , the formation is not being altered during testing, and that the responses are independent of whether the slug was induced by raising or lowering the water level in the well. It is strongly recommended that such a series of tests always be performed. Failure to do so can potentially introduce considerable error into the hydraulic conductivity estimates obtained from a program of slug tests.

The first and last tests in the series shown in Figure 4 employed initial displacements of similar magnitude but differing signs. According to conventional theory, responses should be independent of whether the test was initiated by an injection (slug in) or withdrawal (slug out) mechanism. The results of the tests shown in Figure 4 (and all other slug tests performed by

the authors in wells screened in formations of moderate to low permeability) indicate that, as long as the water level in the well is not driven below the top of the screen during the test, the responses will be essentially independent of the mechanism used for test initiation (i.e. injection versus withdrawal). In wells screened in very permeable formations, however, it is possible that test responses are dependent on the mechanism used for test initiation. Current ongoing work is attempting to clarify this issue.

The above discussion of the dependence of test responses on the magnitude of H_0 is appropriate for wells in confined formations and those in unconfined formations screened at least a certain minimum distance below the water table. In wells screened close to or across the water table, one may observe a dependence on H_0 as a result of differences in the effective length of the screen through which water flows into/out of the well. In such wells, one may also observe a dependence of test responses on the mechanism of test initiation (i.e. injection versus withdrawal). Dahl and Jones (1993) report a series of tests in which there is a clear dependence on H_0 and the mechanism of test initiation. Figure 5 reproduces one set of tests reported by Dahl and Jones (1993). These tests were performed at the same well using different initial displacements and different mechanisms of test initiation. Hyder et al. (1993) have recently proposed an approximate analytical solution that can model the dependence both on H_0 and on the mechanism of test

initiation for such situations. Butler et al. (1994) provide estimates of the necessary minimum distance below the water table for test responses to be independent of H_0 .

3. THE SLUG SHOULD BE INTRODUCED IN A NEAR-INSTANTANEOUS FASHION AND A GOOD ESTIMATE OF THE INITIAL DISPLACEMENT SHOULD BE OBTAINED

Conventional methodology for the analysis of slug-test data requires that the slug-induced disturbance be introduced in an instantaneous fashion and that the magnitude of the initial displacement (H_0) be known. Thus, the method used to initiate a slug test must satisfy both of these requirements. In systems of moderate to low permeability, most common methods of test initiation will enable the slug to be introduced in a manner that can be considered instantaneous relative to the timing of the resulting head responses. In addition, measurements taken immediately after test initiation should yield a good estimate of H_0 . In very rapidly responding systems, however, satisfying these requirements may prove difficult.

Figure 6 displays data from a series of tests performed in the same permeable alluvial aquifer as in Figure 3. In this case, the slug was introduced by pneumatic means (i.e. pressurizing the air column in the well casing (producing a depression of the water level) followed by a very rapid depressurization (e.g., McLane et al., 1990; Levy and Pannell, 1991)). The "actual H_0 " values shown in Figure 6 (1.03 m and

4.20 m for tests 1 and 4, respectively) are based on measurement of the air pressure in the well casing using a high-accuracy gas pressure transducer, while the head readings were taken using a submersible pressure transducer. The difference between the H_0 readings taken with the gas pressure transducer and the submersible pressure transducer (0.20 m and 1.03 m for tests 1 and 4, respectively) is a result of the time for depressurization (on the order of several tenths of a second) being too slow for such a rapidly responding system. The use of the H_0 from the submersible pressure transducer, in conjunction with the lower-than-expected radial hydraulic gradient arising from the non-instantaneous slug introduction, will lead to an estimate of hydraulic conductivity that is lower than the actual conductivity of the formation. A comparison between the apparent H_0 (in this case the reading from the submersible pressure transducer) and the expected H_0 (in this case the reading from the gas pressure transducer) is a simple way to assess if the instantaneous-introduction assumption is being upheld. Note that further testing at the same site showed that there was no difference between the H_0 readings in wells screened in material of moderate to low permeability.

Although the example displayed in Figure 6 was from a pneumatic slug test, more severe problems would actually be expected in tests initiated by the addition or removal of a solid slug because of the longer time needed for introduction of the slug. Packer-based systems, in which the slug is introduced by

opening the central pipe upon which the packer is mounted (e.g., Figure 4a of this paper and McElwee and Butler (1989)), provide one means of introducing the slug-induced disturbance in a near-instantaneous fashion in very permeable systems. This approach also enables a very good estimate of H_0 to be obtained. Note that Orient et al. (1987) and McLane et al. (1990), among others, suggest use of electric water-level indicators (electric tapes) to estimate H_0 for pneumatic slug tests. Although this approach can provide an approximate value of H_0 , a high-accuracy gas pressure transducer will provide a better estimate. Since high-accuracy gas pressure transducers are inexpensive, can be readily added to the standard pneumatic slug-test well head assembly, and can be readily connected to standard data-acquisition equipment, their use is strongly recommended for pneumatic slug tests.

4. APPROPRIATE DATA-ACQUISITION EQUIPMENT SHOULD BE EMPLOYED

Responses to a slug-induced disturbance can be measured either manually (electric tape, plopper, etc.) or electronically (pressure transducers connected to a data logger). For tests in wells screened in formations of moderate to low permeability, such as shown in Figure 1, manual methods can provide measurements of sufficient quality as long as a good estimate of H_0 is available. However, for tests in more permeable systems ($Kb > 15\text{-}20 \text{ m}^2/\text{d}$), such as shown in Figures 3-6, electronic methods must be employed, as manual methods will not provide measurements of sufficient density or accuracy. Earlier

theoretical work (McElwee et al., 1989) has shown that the reliability of parameter estimates is closely tied to the density and accuracy of measurements. In very rapidly responding wells (e.g., Figures 3 and 6), data-acquisition rates of at least several hertz are needed in order to clearly define the nature of the responses. Note that the need for rapid acquisition rates is of special concern in oscillating systems where slow collection rates will produce aliasing and other effects that may make data interpretation and analysis difficult. Given the capabilities of currently available data-acquisition equipment, data collection rates of several hertz are easily obtainable and, therefore, should always be used when rapid responses are expected.

5. AN OBSERVATION WELL SHOULD BE EMPLOYED FOR ESTIMATION OF THE STORAGE PARAMETER

It has frequently been observed that slug-induced responses at the test well are relatively insensitive to the value of the storage parameter (e.g., Cooper et al., 1967). McElwee et al. (1989) have used sensitivity analysis to demonstrate that reliable estimates of the storage parameter will be difficult to obtain using the density and quality of data that are normally collected during a single-well slug test. A primary reason for this condition is that the measured responses at the test well are much more sensitive to transmissivity (K_b) than to the storage parameter (S_b , where S_s is the specific storage). The limited sensitivity to the storage parameter that does exist is

highly correlated with the sensitivity to transmissivity. In addition, any uncertainties about the effective screen radius (nominal screen radius or radius of gravel pack or radius of developed zone) will have a much larger effect on estimates of the storage parameter than on estimates of transmissivity. Use of an observation well during a slug test can greatly improve this situation because the insensitivity and correlation effects are dramatically lessened (McElwee et al., 1991). Uncertainties about the effective screen radius also have much less of an effect when data from an observation well are used (Butler, 1994).

Figure 7 displays data from a multi-well slug test at the same site as in Figure 1. The two wells, which are screened over similar intervals, are 6.45 m apart. Owing primarily to uncertainty about the effective screen radius, the estimate of specific storage obtained using data from well Ln-2 alone is too large by a factor of between 3 and 4 (estimated $S_s = 2.98 \times 10^{-5} \text{ m}^{-1}$). When the analysis is performed using data from both wells (results shown in Figure 7), a specific storage estimate compatible with other information is obtained (estimated $K = 1.06 \text{ m/d}$; estimated $S_s = 8.49 \times 10^{-6} \text{ m}^{-1}$). Note that measurements from the observation well were taken using a transducer placed below a packer located just above the screen. The observation well was packed off in order to remove the lagging and damping of responses that occurs due to wellbore storage at the observation well (Novakowski, 1989).

Although it may not be practical to install observation wells solely for use in slug tests, the density of pre-existing monitoring wells is often such that this technique can be readily employed. Generally, the observation well must be fairly close (within ≈ 10 m) to the test well and screened over a similar vertical interval in order that the responses to the slug-induced disturbance can be discerned from background noise. The storage parameter must be quite small in order to employ wells at greater distances from the test well (Sageev, 1986; Karasaki et al., 1988; Novakowski, 1989; Guyonnet et al., 1993).

6. METHOD CHOSEN FOR DATA ANALYSIS SHOULD BE APPROPRIATE FOR SITE CONDITIONS

Most analyses of slug-test data are performed using one of four techniques: 1) the method of Hvorslev (1951) for fully and partially penetrating wells in confined aquifers; 2) the method of Bouwer and Rice (1976) for wells in unconfined aquifers screened below the water table; 3) the method of Cooper et al. (1967) for fully penetrating wells in confined aquifers; and 4) the method of Nguyen and Pinder (1984) for partially penetrating wells in confined aquifers. Recent theoretical work at the KGS has focused on the quality of the estimates provided by these techniques.

Figure 8 displays the results of a theoretical analysis of the error introduced into hydraulic conductivity estimates when applying the Cooper et al. model to data from a partially

penetrating well. The ψ quantity plotted on the x axis is the square root of the anisotropy ratio ($\sqrt{K_z/K_r}$) divided by the aspect ratio (b/r_w , where b is the screen length and r_w is the screen radius). The quantity plotted on the y axis is the hydraulic conductivity estimate provided by the Cooper et al. model (K_{est}) divided by the actual conductivity value (K_r). A series of curves are shown for different values of the dimensionless storage parameter ($\alpha = (2r_w^2 S_b)/r_c^2$, where r_c is the casing radius). Note that the α parameter used here is twice that defined by Cooper et al. (1967). Although the Cooper et al. estimates improve as ψ decreases (i.e. the proportion of vertical flow in response to the slug-induced disturbance decreases), Figure 8 shows that the Cooper et al. model will always provide an upper bound for the conductivity estimate. The quality of this bounding estimate will depend on the ψ and α values. For tests in wells of moderate to low aspect ratios sited in isotropic formations (i.e. the upper end of the plotted ψ range), Figure 8 indicates that the Cooper et al. model will provide estimates that are significantly greater than the actual formation conductivity for moderate to low α values.

Figure 9 displays results of a similar analysis for the partially penetrating well form of the Hvorslev method. In this variant of the Hvorslev method, an anisotropy ratio must be assumed, producing a ψ^* value (square root of assumed anisotropy

ratio divided by the aspect ratio) that is used in the analysis. This assumed ψ^* value may be quite different from the actual unknown ψ value of the well-formation configuration. Most standard references (e.g., Freeze and Cherry, 1979) recommend that the Hvorslev analysis be performed assuming an isotropic formation (i.e. $\psi^* = r_w/b$). The results displayed in Figure 9 indicate that this approach will produce a significant underestimation of hydraulic conductivity in moderately to highly anisotropic ($K_r > K_z$) formations, where the assumed ψ^* will be much greater than the actual ψ .

Figure 10 displays results for a similar analysis of the Bouwer and Rice method. In this case, two plots are given so that the effect of aspect ratio and anisotropy can be evaluated separately. Again, anisotropy ($K_r > K_z$) will produce a considerable underestimation of hydraulic conductivity in wells of moderate to small aspect ratio. Hyder et al. (in press) and Hyder and Butler (in press) provide further details of the theoretical analyses of the Cooper et al., Hvorslev, and Bouwer and Rice techniques. Use of plots such as Figures 8-10 for the selection of the appropriate method to employ for the analysis of slug-test data is strongly recommended. Use of these plots should considerably improve the reliability of the estimated parameters.

The fourth method for data analysis listed above, the Nguyen and Pinder method, is not recommended for the analysis of slug-test data. Butler and Hyder (1994) have recently shown that parameter estimates obtained using the Nguyen and Pinder method

must be viewed with skepticism owing to an error in the analytical solution upon which that model is based. For slug tests performed in partially penetrating wells under conditions where Figures 8-10 indicate that the standard methods do not appear capable of providing acceptable parameter estimates, the recently introduced KGS model for slug tests in partially penetrating wells (Hyder et al., in press; Hyder and Butler, in press) can be employed for the analysis of the response data.

The above discussion pertains to conditions where conventional slug-test theory is applicable. However, in cases where test responses are dependent on H_0 and the mechanism of test initiation (e.g., Figures 3 and 5), conventional theory is no longer viable. McElwee and Butler (1994) propose a model for the analysis of slug tests in highly permeable confined systems where a dependence on H_0 is observed. The model proposed by Hyder et al. (1993) can be used for the analysis of data from slug tests performed in wells screened near or across the water table if a dependence on H_0 and/or the mechanism of test initiation is observed. As emphasized earlier, it is critical that the series of slug tests performed at a well be designed so as to assess whether conventional theory is applicable.

7. USE OF PRE- AND POST-ANALYSIS PLOTS SHOULD BE AN INTEGRAL COMPONENT OF THE ANALYSIS

Currently, the vast majority of analyses of slug-test data are performed using automated fitting programs or procedures

involving manual fitting of straight lines to test data. Unfortunately, all too often, the analysis is performed by rote, with little attention paid to the form of the plots and the nature of the fit of the theoretical model to the test data. If the reliability of parameter estimates from slug tests is to be improved, more attention must be paid to all aspects of the analysis. Three examples are briefly given here to demonstrate the importance of these issues. Further details about the tests used for these examples can be found in Butler et al. (1993) and Butler and Liu (1994).

Figure 11 displays data and the best-fit Cooper et al. model from a test at the Lincoln County site (screen radius (r_w) = 0.071 m, casing radius (r_c) = 0.025 m, screen length (b) = 3.96 m; estimated $K=5.79 \times 10^{-4}$ m/d assuming $S_s=3.28 \times 10^{-6}$ m⁻¹). Note that specific storage was assumed known for the analysis based on an estimate obtained from a test at a higher interval at this site (Figure 7). The model fit in this case must be considered quite poor. The systematic deviation between the theoretical model and test data can be readily explained by an assumed specific storage that is too low. Justification for a higher specific storage can be found in Figure 12, which is a plot of the data in a semilog Hvorslev format. The distinct concave upward curvature seen on this plot is strong evidence (for a well of this aspect ratio) that the specific storage for the test interval is quite large (e.g., Chirlin, 1989). Therefore, the analysis was repeated without constraining the value of specific storage. Figure 13

displays the very good fit that was then obtained (estimated $K=2.68 \times 10^{-4}$ m/d; estimated $S_s=0.00041$ m¹ corresponding to an α value of 0.025). Note that the hydraulic conductivity estimate decreased by over a factor of two between the analyses of Figures 11 and 13, a further indication of the attention that must be paid to deviations between the fitted theoretical model and the test data. Also note that the good agreement shown in Figure 13 between the Cooper et al. model and the test data would be predicted from Figure 8 for a well of this aspect ratio ($b/r_w=55$), given the large α value. Because this well is of a moderate aspect ratio, the test data were also analyzed using the isotropic form of the earlier described KGS model for slug tests in partially penetrating wells (note that the isotropic form of the KGS model is equivalent to the model of Dougherty and Babu (1984)). As would be predicted from Figure 8, the conductivity estimate was the same as that obtained from the Cooper et al. model. This result is also in keeping with earlier theoretical work of Hayashi et al. (1987) who found that vertical flow due to a slug-induced disturbance decreases with increases in the storage parameter (i.e. at large values of the storage parameter, responses from fully penetrating well models and partially penetrating well models will coincide).

Figure 14 displays data and the best-fit Cooper et al. model from a test at a site in Pratt County, Kansas ($r_w=0.125$ m, $r_c=0.064$ m, $b=1.52$ m; estimated $K=42.04$ m/d assuming $S_s=3.28 \times 10^{-6}$ m¹). Again, a systematic deviation between the measured data and

the Cooper et al. model is shown. This type of deviation is often seen when applying a fully penetrating well model to data from a test in a partially penetrating well. The near-linear Hvorslev plot of the data shown in Figure 15 can be considered further support for the hypothesis of a deviation produced by a significant component of vertical flow. Hyder et al. (in press) state that a near-linear Hvorslev plot can be an indication of a significant component of vertical flow in response to a slug test in a partially penetrating well or a low-permeability well skin. Given the small aspect ratio ($b/r_w \approx 12$) and the coincidence of plots of normalized responses from five repeat tests at this well, the partially penetrating well explanation was considered the most likely. The data were therefore reanalyzed using the KGS model for slug tests in partially penetrating wells. Figure 16 displays the fit resulting from an analysis with the isotropic form of the KGS model (estimated $K=17.65$ m/d assuming $S_s=3.28 \times 10^{-6}$ m⁻¹). It is important to emphasize that the dramatic improvement in model fit between Figures 14 and 16 was not accompanied by an increase in the number of estimated parameters. The hydraulic conductivity estimate provided by the Cooper et al. model is 2.4 times larger than the KGS model conductivity estimate, an overprediction by the Cooper et al. model very close to what would be theoretically predicted from Figure 8 for a well of this aspect ratio in an isotropic formation, given the assumed α of 3.80×10^{-5} . Note that this assumed value of the dimensionless storage parameter (α) is much smaller than the estimate obtained

in the previous example. Also note that in Figure 16 and a number of the other figures in this article, the normalized head data show a good deal of fluctuation at very early times. These fluctuations are related to test initiation and should be ignored when considering the quality of the match between the best-fit model and the test data.

A final example illustrates the effect of an evolving low-permeability well skin. Figure 17 displays data in a semilog Hvorslev format from two tests in the series shown on Figure 2. Note that the degree of curvature of the plotted data is significantly smaller in test 11 than in test 3. Figure 18 is a plot of the test data and the best-fit Cooper et al. models ($r_w=0.071$ m, $r_c=0.025$ m, $b=3.66$ m; estimated $K_{5/21 \#3}=1.34$ m/d and $K_{6/11 \#11}=0.62$ m/d assuming $S_s=6.56 \times 10^{-6}$ m⁻¹). As shown in the figure, the nature of the deviation between the test data and the best-fit model changes between the two tests. The greater duration of the later test, the decrease in the degree of curvature shown on Figure 17, and the change in the nature of the deviation seen on Figure 18 are very strong evidence of a developing low-permeability skin. In the case of an evolving skin, the best option is to analyze data from tests before the skin becomes too pronounced. Test 3 of 5/21 was the first slug test performed at this well, so it should be the best test for analysis. The most likely explanation for the deviation between the theoretical model and test 3 data is that the assumed storage parameter is too low. The curvature of test 3 data displayed in Figure 17 is

strong support for this explanation. The results of a reanalysis of test 3 allowing the storage parameter to vary are shown in Figure 19 (estimated $K=1.01$ m/day; estimated $S_s=5.35 \times 10^{-5}$ m⁻¹).

The agreement between the fitted model and the test data is significantly better in this case. Note that the conductivity estimate obtained from this analysis is within 5% of the value obtained from the analysis of a multiwell slug test over the same vertical interval (see Figure 7). The estimated specific storage ($S_s=5.36 \times 10^{-5}$ m⁻¹), however, appears too large by a factor of six when compared to the value obtained from the multiwell test. This larger specific storage estimate is thought to be a result of the earlier-discussed lack of sensitivity of test responses to the storage parameter and uncertainty concerning the effective screen radius.

Although the analysis of test 3 appears to have been somewhat successful, analysis of tests in wells that display an evolving skin will, in general, be very difficult, as all available test data may be affected by the skin. Clearly, proper well construction and well development are essential in order to minimize the potential for the development of a well skin during a program of slug tests.

8. APPROPRIATE WELL-CONSTRUCTION PARAMETERS SHOULD BE EMPLOYED

The well-construction parameters are one of the more significant sources of uncertainty in the analysis of slug-test data. Specifically, the selection of values to use for the

effective screen length and radius can introduce considerable error into the analysis. Although the effective screen length has a much larger impact on parameter estimates, both quantities will influence estimates from slug tests through the dimensionless storage parameter (α) and, in partially penetrating wells, the aspect ratio (effective screen length/effective screen radius). In formations of moderate to low permeability ($Kb < 15\text{--}20 \text{ m}^2/\text{d}$), the gravel pack will usually be considerably more permeable than the formation itself. Therefore, as recommended by Palmer and Paul (1987) among others, the effective screen length should be the length of the gravel pack and the effective screen radius should be the radius of the gravel pack. In very permeable systems, however, the nominal screen radius and length will be more appropriate. There may be some uncertainty concerning the appropriate quantities to employ in wells screened in material of moderately high permeability. Appropriate sizing of the gravel pack, however, can largely remove this uncertainty from the analysis. In the examples of the preceding section, the radius of the gravel pack and the length of the gravel pack were used for r_w and b , respectively, in the analyses because the gravel pack was considerably more permeable than the formation in all cases. Butler (1994) provides further details concerning the effect of well-construction parameters on slug tests.

CONCLUSIONS

The slug test has the potential to provide very useful

information about the transmissive and storage properties of a formation. In order for the potential of this technique to be fully realized, however, considerable care must be given to all phases of test design, performance, and analysis. A series of guidelines has been outlined here that should allow the reliability of parameter estimates obtained from a program of slug testing to be improved. Two very important points arising from these guidelines cannot be overemphasized: 1) it is critical that a series of slug tests at a given well be designed so as to assess whether conventional theory is applicable (i.e. is there a dependence on initial head or mechanism of test initiation, is there a well skin that is developing during the course of testing, etc.); and 2) the analysis of the response data must be done using the most appropriate model and with considerable care. Unfortunately, the authors have found through repeated experience that inattention to the issues discussed in this article will produce parameter estimates that may differ considerably from reality. Finally, two additional points need to be emphasized. First, these guidelines developed out of research performed in flow systems for which a porous media representation is valid. The complexities of tests in fractured systems may give rise to additional guidelines of equal or greater importance to those outlined here. Second, although these guidelines developed from work done in formations of a wide range of hydraulic conductivity, this work did not involve tests in formations of extremely low hydraulic conductivity. Clearly, a number of

additional issues need to be considered for slug tests in very low conductivity media (e.g., Neuzil, 1981; Palmer and Paul, 1987; Beauheim, 1994).

ACKNOWLEDGMENT

This research was sponsored in part by the Air Force Office of Scientific Research, Air Force Systems Command, USAF, under grant or cooperative agreement number, AFOSR 91-0298. This research was also supported in part by the U.S. Geological Survey (USGS), Department of the Interior, under USGS award number 14-08-0001-G2093. The views and conclusions contained in this document are those of the authors and should not be interpreted as necessarily representing the official policies, either expressed or implied, of the U.S. Government.

REFERENCES

- Beauheim, R.L. 1994. Practical considerations in well testing of low-permeability media (abstract). EOS. v. 75, no. 16, pp. 151-152.
- Bouwer, H. and R.C. Rice. 1976. A slug test for determining hydraulic conductivity of unconfined aquifers with completely or partially penetrating wells. Water Resour. Res. v. 12, no. 3, pp. 423-428.
- Butler, J.J., Jr. 1990. The role of pumping tests in site characterization: Some theoretical considerations. Ground Water. v. 28, no. 3, pp. 394-402.
- Butler, J.J., Jr. 1994. The effect of well-construction parameters on slug tests. Kansas Geological Survey Open-File Rept. 94-27.
- Butler, J.J., Jr., and Z. Hyder. 1994. An assessment of the Nguyen and Pinder method for slug test analysis. Ground Water Monitoring and Remediation. v. 14, no. 4.
- Butler, J.J., Jr., and W.Z. Liu. 1994. Analysis of 1991-1992 slug tests in the Dakota aquifer of central and western Kansas. Kansas Geological Survey Open-File Rept. 93-1C.
- Butler, J.J., Jr., W.Z. Liu, and D.P. Young. 1993. Analysis of October 1993, slug tests in Stafford, Pratt, and Reno counties, south-central Kansas. Kansas Geological Survey Open-File Rept. 93-52, 70 pp.
- Butler, J.J., Jr., C.D. McElwee, and Z. Hyder. 1994. Slug tests in unconfined aquifers - Phase two. Kansas Water Resources

- Research Inst. Contribution No. 310, Manhattan, Ks.
- Chirlin, G.R. 1989. A critique of the Hvorslev method for slug test analysis: The fully penetrating well. Ground Water Monitoring Review. v. 9, no. 2, pp. 130-138.
- Chirlin, G.R. 1990. The slug test: the first four decades. Ground Water Management. v. 1, pp. 365-381.
- Cooper, H.H., J.D. Bredehoeft, and I. S. Papadopoulos. 1967. Response of a finite-diameter well to an instantaneous charge of water. Water Resour. Res. v. 3, no. 1, pp. 263-269.
- Dahl, S. and J. Jones. 1993. Evaluation of slug test data under unconfined conditions with exposed screens, and low permeability filter pack. Proc. of the 7th National Outdoor Action Conf. NGWA. pp. 609-623.
- Dax, A. 1987. A note on the analysis of slug tests. Jour. of Hydrology. v. 91, pp. 153-177.
- Dougherty, D.E. and D.K. Babu. 1984. Flow to a partially penetrating well in a double-porosity reservoir. Water Resour. Res. v. 20, no. 8, pp. 1116-1122.
- Freeze, R.A., and J.A. Cherry. 1979. Groundwater. Prentice-Hall, Inc., Englewood Cliffs, N.J. 604 pp.
- Guyonnet, D., S. Mishra, and J. McCord. 1993. Evaluating the volume of porous medium investigated during a slug test. Ground Water. v. 31, no. 4, pp. 627-633.
- Hayashi, K., T. Ito, and H. Abe. 1987. A new method for the determination of in situ hydraulic properties by pressure pulse tests and application to the Higashi

Hachimantai geothermal field. J. Geophys. Res. v. 92,
no. B9, pp. 9168-9174.

Herzog, B.L. 1994. Slug tests for determining hydraulic
conductivity of natural geologic deposits. In: D.E. Daniel,
and S.J. Trautwein (Editors), Hydraulic Conductivity and Waste
Contaminant Transport in Soils. ASTM STP 1142. American
Society for Testing and Materials.

Hvorslev, M.J. 1951. Time lag and soil permeability in ground-water
observations. Bull no. 36. Waterways Exper. Sta., Corps of
Engrs., U.S. Army, 50 pp.

Hyder, Z. and J.J. Butler, Jr. in press. Slug tests in unconfined
formations: An assessment of the Bouwer and Rice technique.
Ground Water.

Hyder, Z., Butler, J.J., Jr., and C.D. McElwee. 1993. An
approximate technique for analysis of slug tests in wells
screened across the water table (abstract). EOS. v. 74,
no. 43, p. 235.

Hyder, Z., J.J. Butler, Jr., C.D. McElwee, and W.Z. Liu. in press.
Slug tests in partially penetrating wells. Water Resour. Res.

Karasaki, K., J.C.S. Long, and P.A. Witherspoon. 1988. Analytical
models of slug tests. Water Resour. Res. v., 24, no. 1,
pp. 115-126.

Kruseman, G.P. and N.A. de Ridder. 1989. Analysis and Evaluation of
Pumping Test Data - ILRI publication 47. ILRI, The
Netherlands. 377 pp.

Levy, B.S. and L. Pannell. 1991. Evaluation of a pressure system

- for estimating in-situ hydraulic conductivity. Proc. of the 5th National Outdoor Action Conf. NWWA. pp. 131-146.
- McElwee, C. D. and J. J. Butler, Jr. 1989. Slug testing in highly permeable aquifers (abstract). GSA 1989 Annual Meeting Abstracts with Program. p. A193.
- McElwee, C.D. and J.J. Butler, Jr. 1994. Characterization of Heterogeneities Controlling Transport and Fate of Pollutants in Unconsolidated Sand and Gravel Aquifers: Third Year Report. Project Report to Air Force Office of Scientific Research, University Research Initiative, Research Initiation Program, U.S. Dept. of Defense.
- McElwee, C. D., Bohling, G. C., and J. J. Butler, Jr. 1989. Sensitivity analysis of slug tests. Kansas Geological Survey Open-File Rept. 89-33, 29 pp. (also in press at The Journal of Hydrology).
- McElwee, C.D., J.J. Butler, Jr., G.C. Bohling, and W.Z. Liu. 1991. The use of observation wells with slug tests: Kansas Geological Survey Open-File Rept. 91-63, 32 pp. (also in press at The Journal of Hydrology).
- McLane, G.A., Harritty, D.A., and Thomsen, K.O. 1990. A pneumatic method for conducting rising and falling head tests in highly permeable aquifers. Proc. of 4th Annual NWWA Outdoor Action Conf. pp. 1219-1231.
- Neuzil, C.E. 1981. On conducting the modified "slug" test in tight formations. Water Resour. Res. v. 18, no. 2, pp.439-441.
- Nguyen, V., and G.F. Pinder. 1984. Direct calculation of aquifer

- parameters in slug test analysis. In: J. Rosenshein and G.D. Bennett (Editors), Groundwater Hydraulics. AGU Water Resour. Monogr. No. 9, pp. 222-239.
- Novakowski, K.S. 1989. Analysis of pulse interference tests. Water Resour. Res. v. 25, no. 11, pp. 2377-2387.
- Orient, J.P., Nazar, A., and R.C. Rice. 1987. Vacuum and pressure test methods for estimating hydraulic conductivity. Ground Water Monitoring Review. v. 7, no. 1, pp. 49-50.
- Osborne, P.S. 1993. Suggested operating procedures for aquifer pumping tests. EPA/540/S-93/503. U.S. EPA, Office of Research and Development, 23 pp.
- Palmer, C.D., and D.G. Paul. 1987. Problems in the interpretation of slug test data from fine-grained tills. Proc. of the NWWA FOCUS Conf. on Northwestern Ground Water Issues. NWWA. pp. 99-123.
- Sageev, A. 1986. Slug test analysis. Water Resour. Res. v. 22, no. 8, pp. 1323-1333.

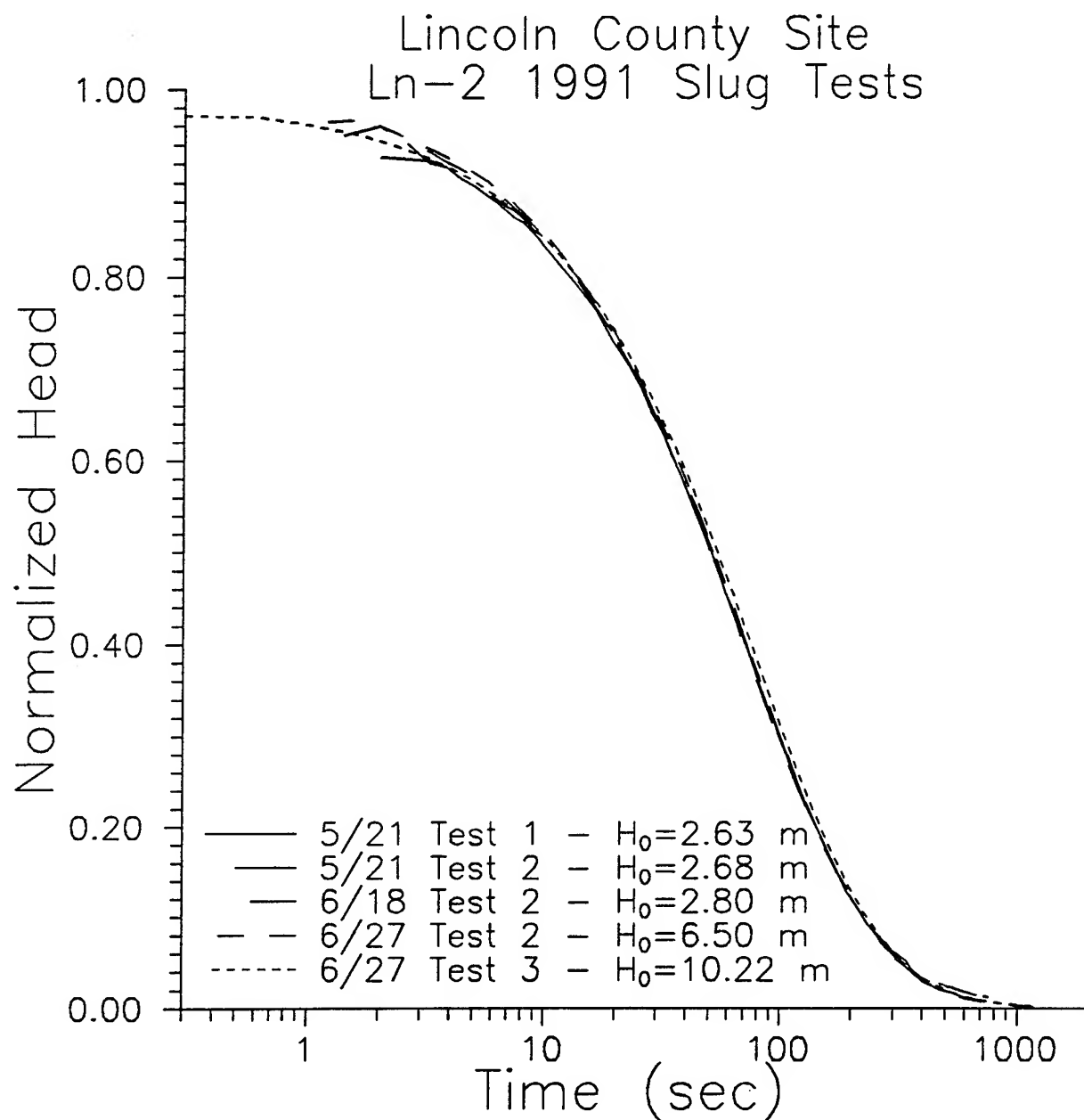


Figure 1

Lincoln County Site
Ln-3 1991 Slug Tests

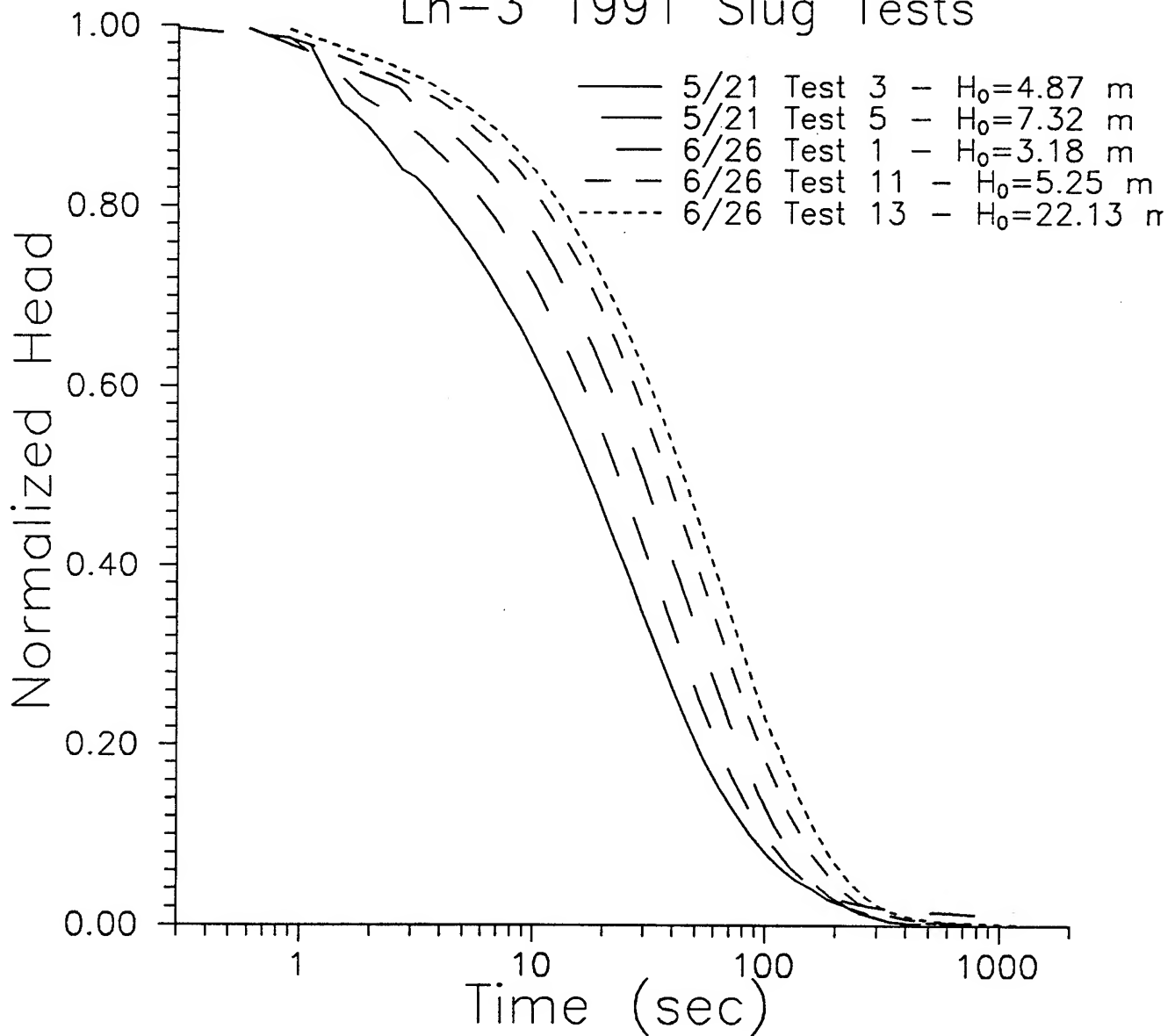


Figure 2

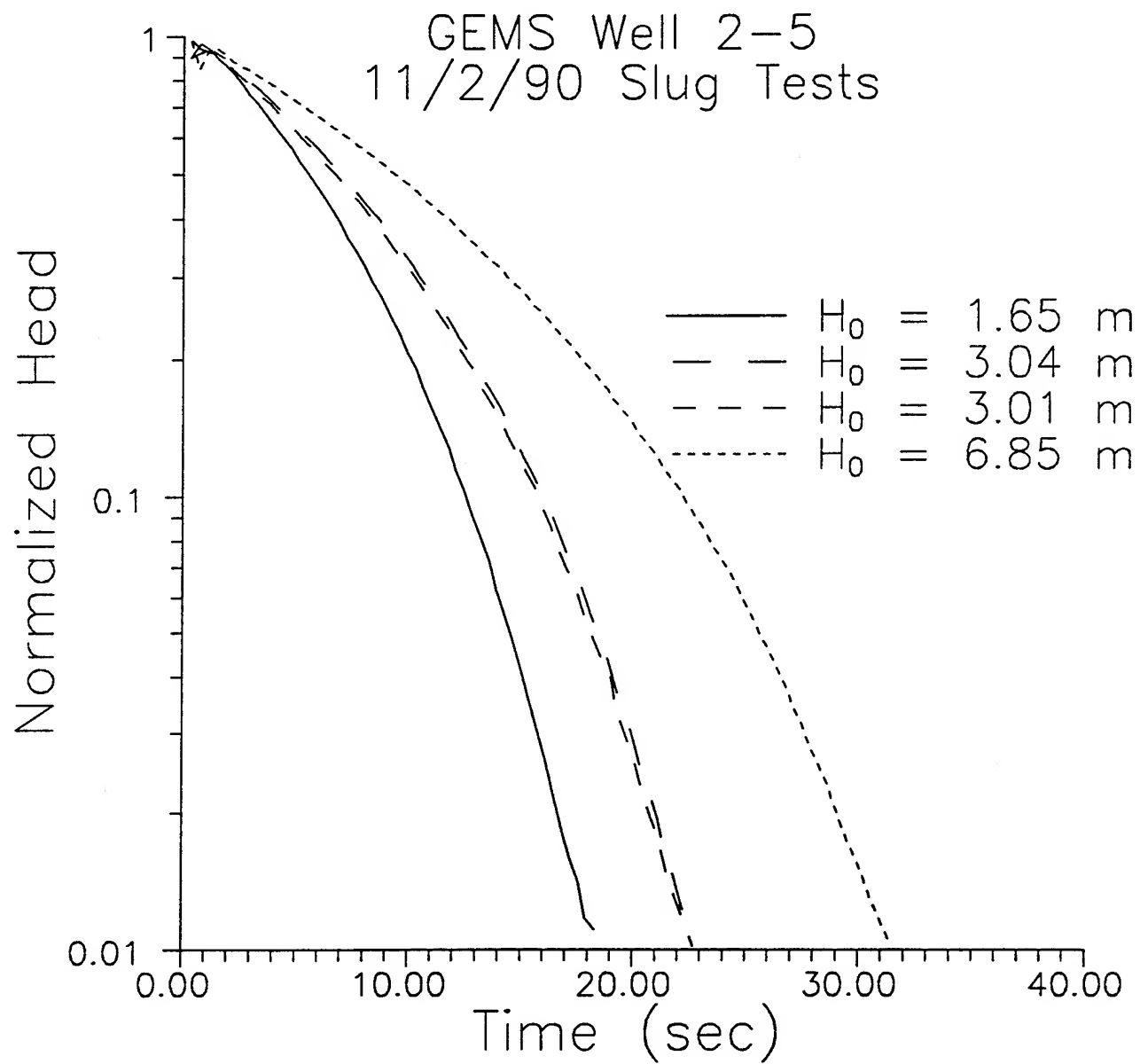


Figure 3

Stafford County Site 16, Well #3
10/15/93 Slug Tests

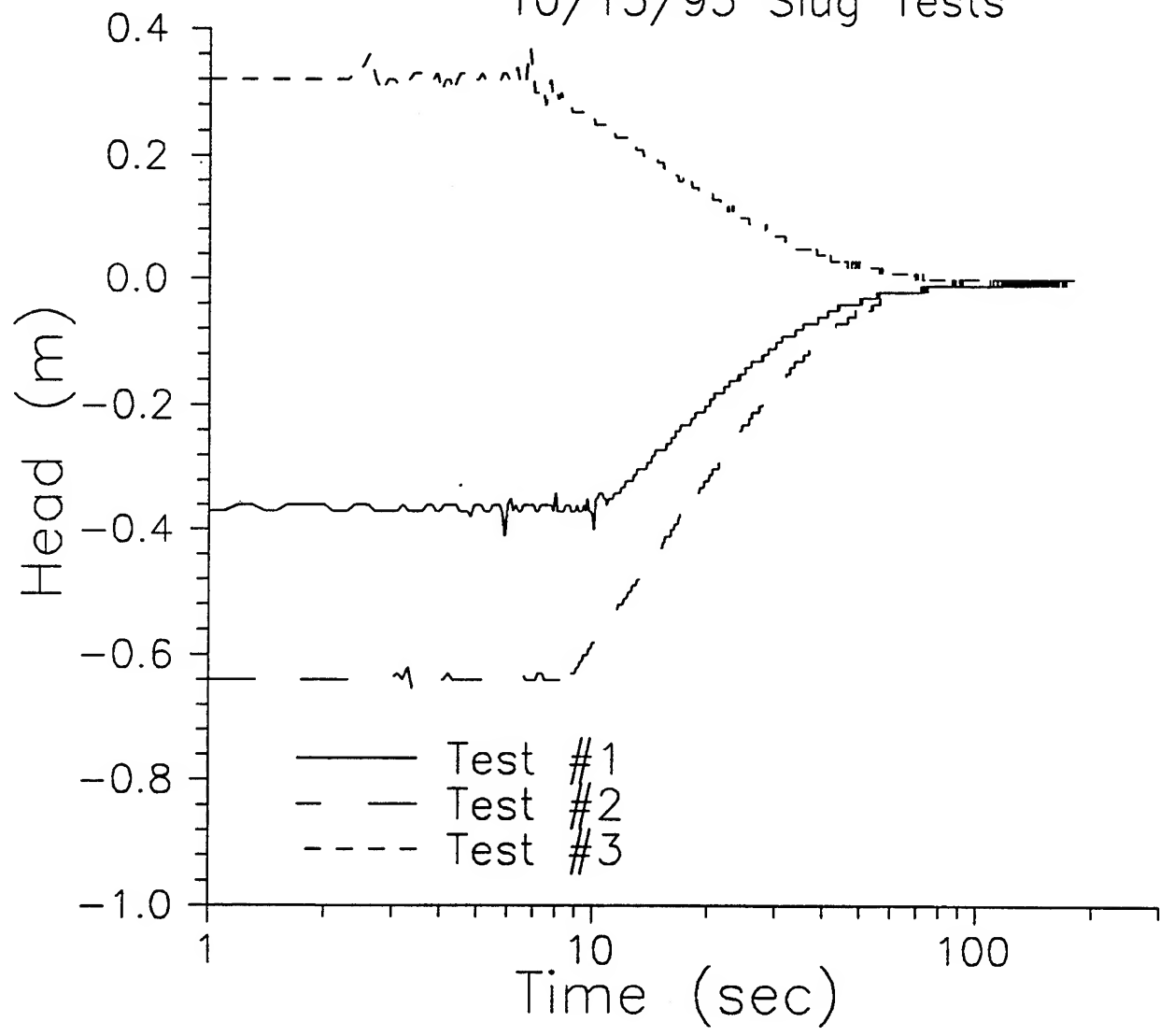


Figure 4a

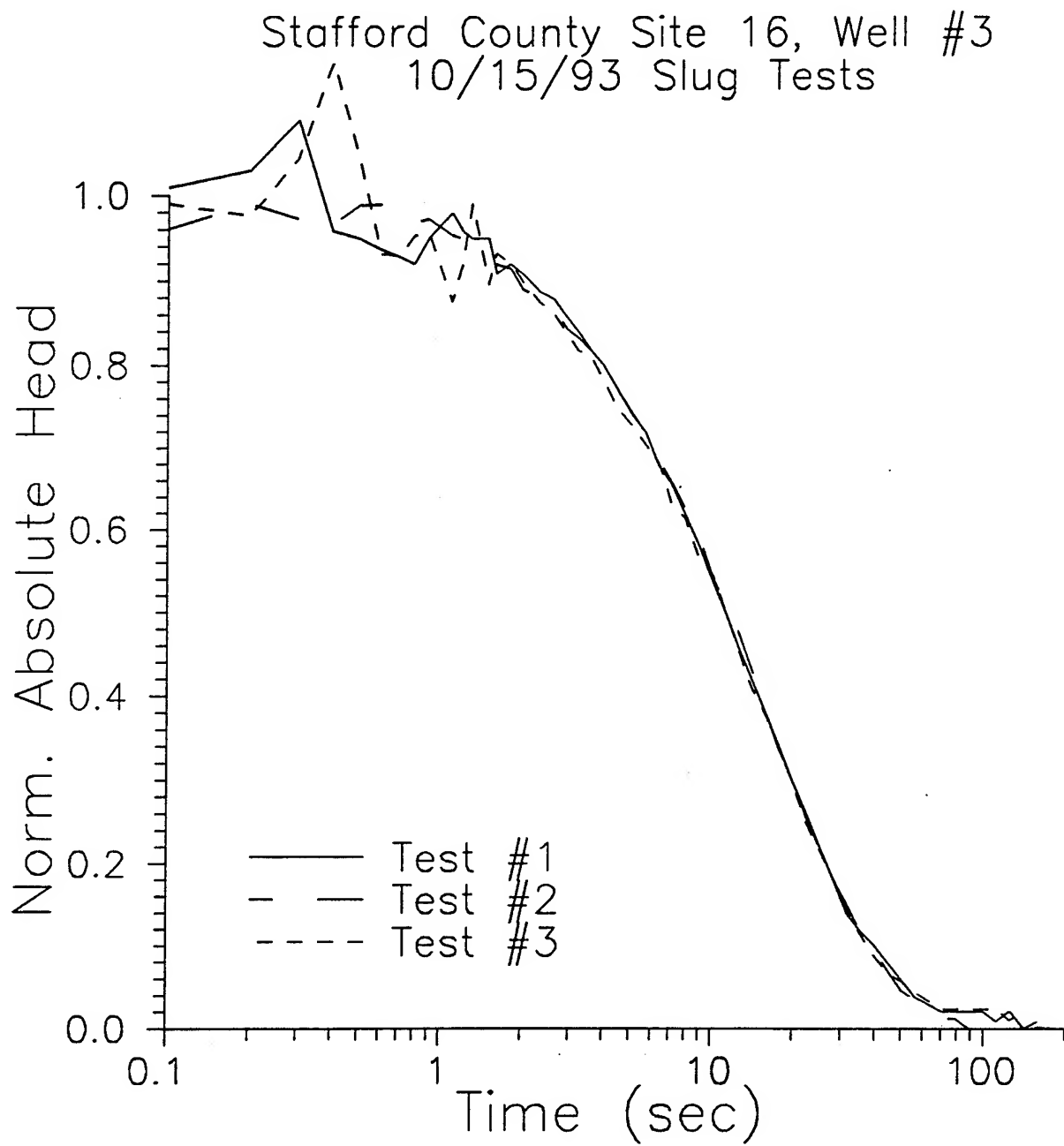


Figure 4b

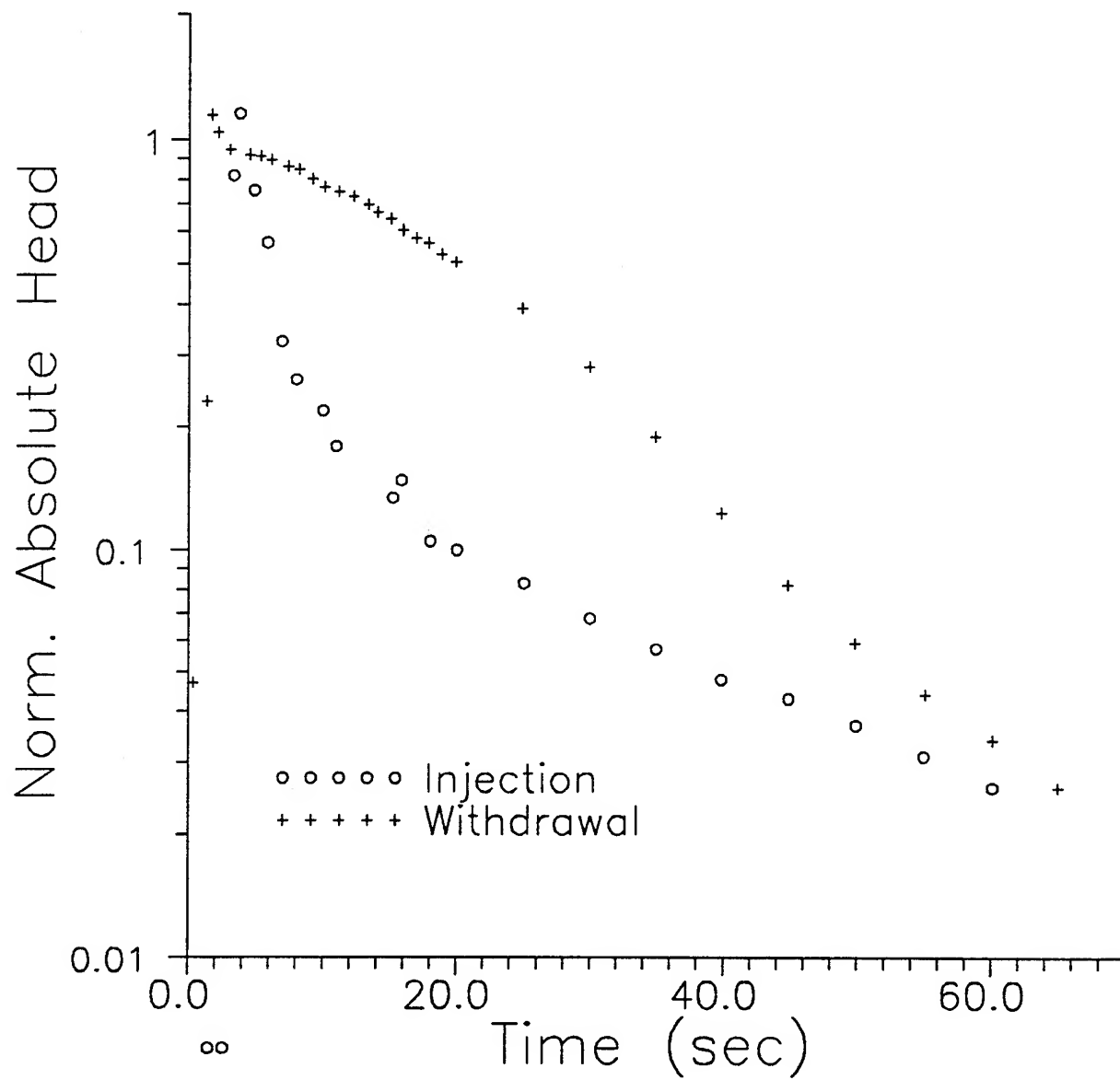


Figure 5a

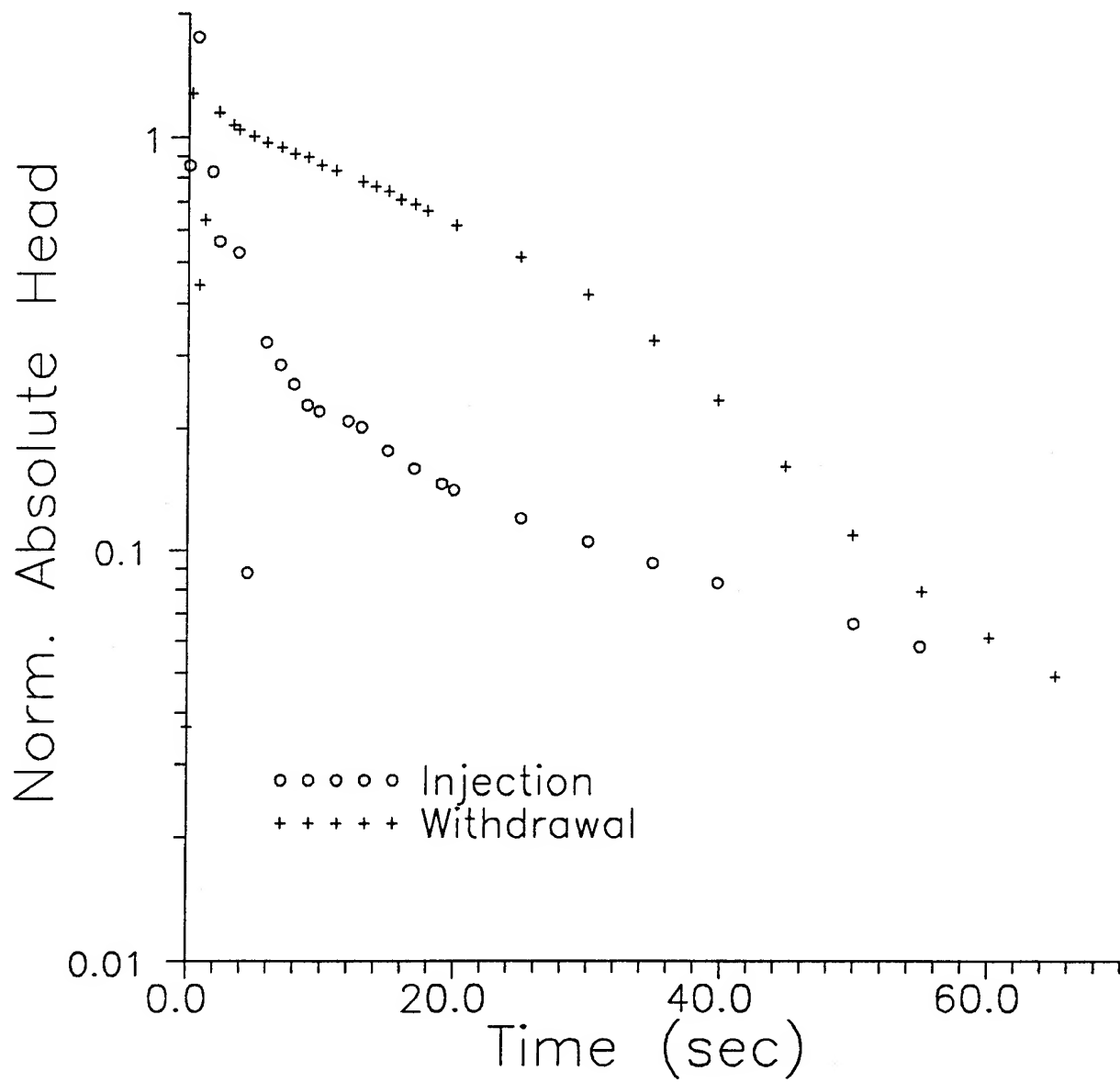


Figure 5b

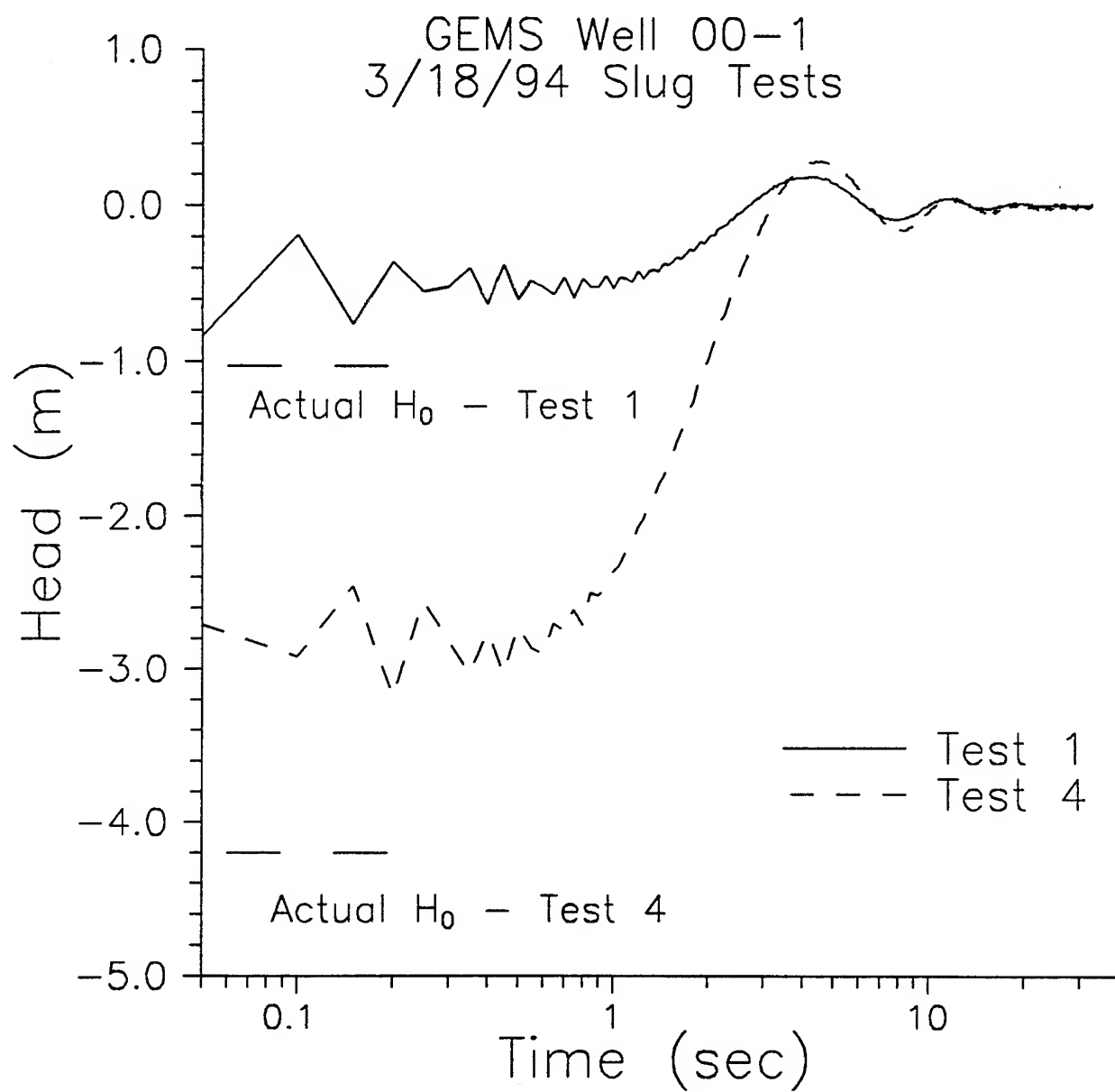


Figure 6

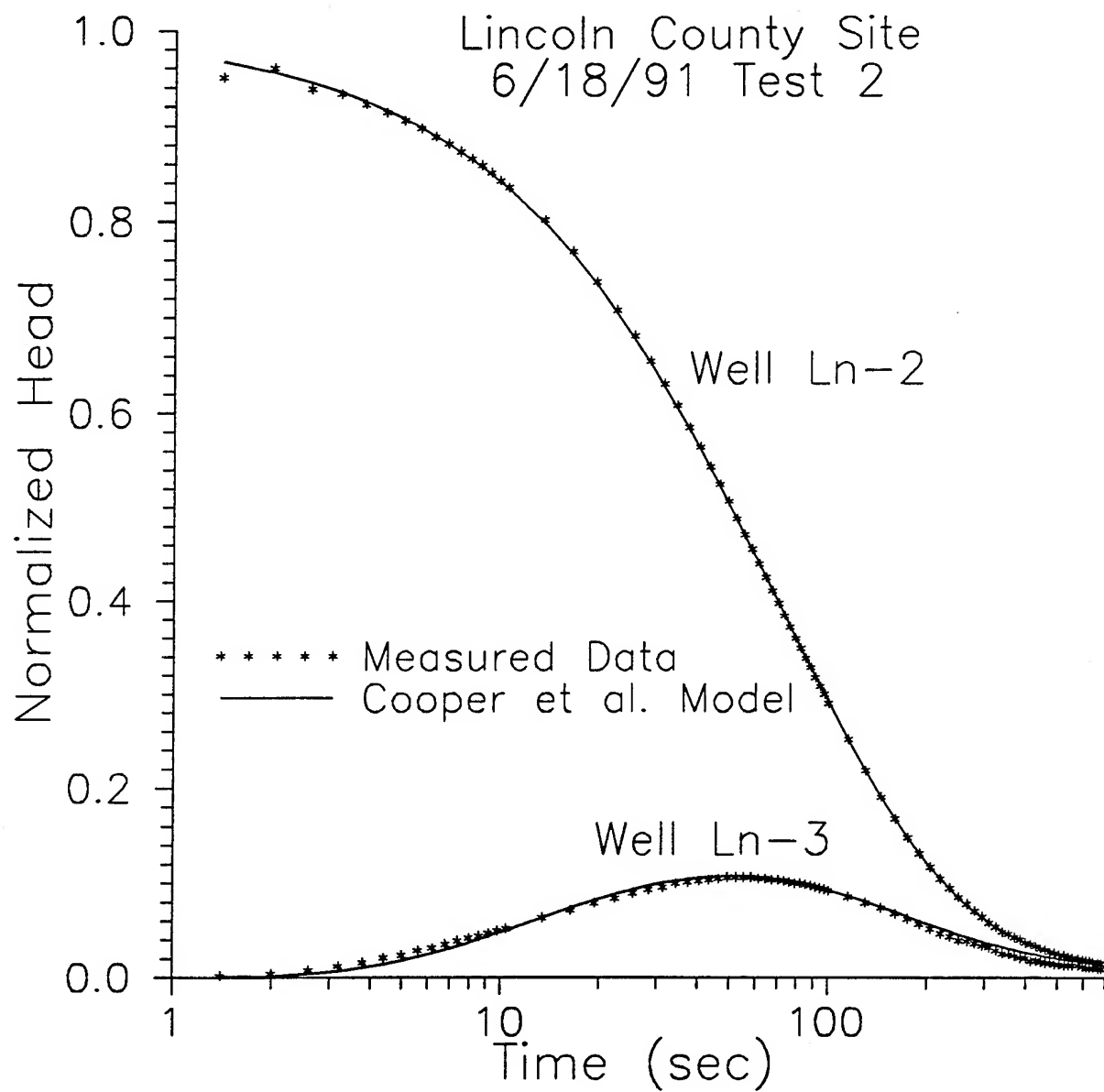


Figure 7

Error Introduced by Cooper et al. Model
When Applied to Case of Partially
Penetrating Well

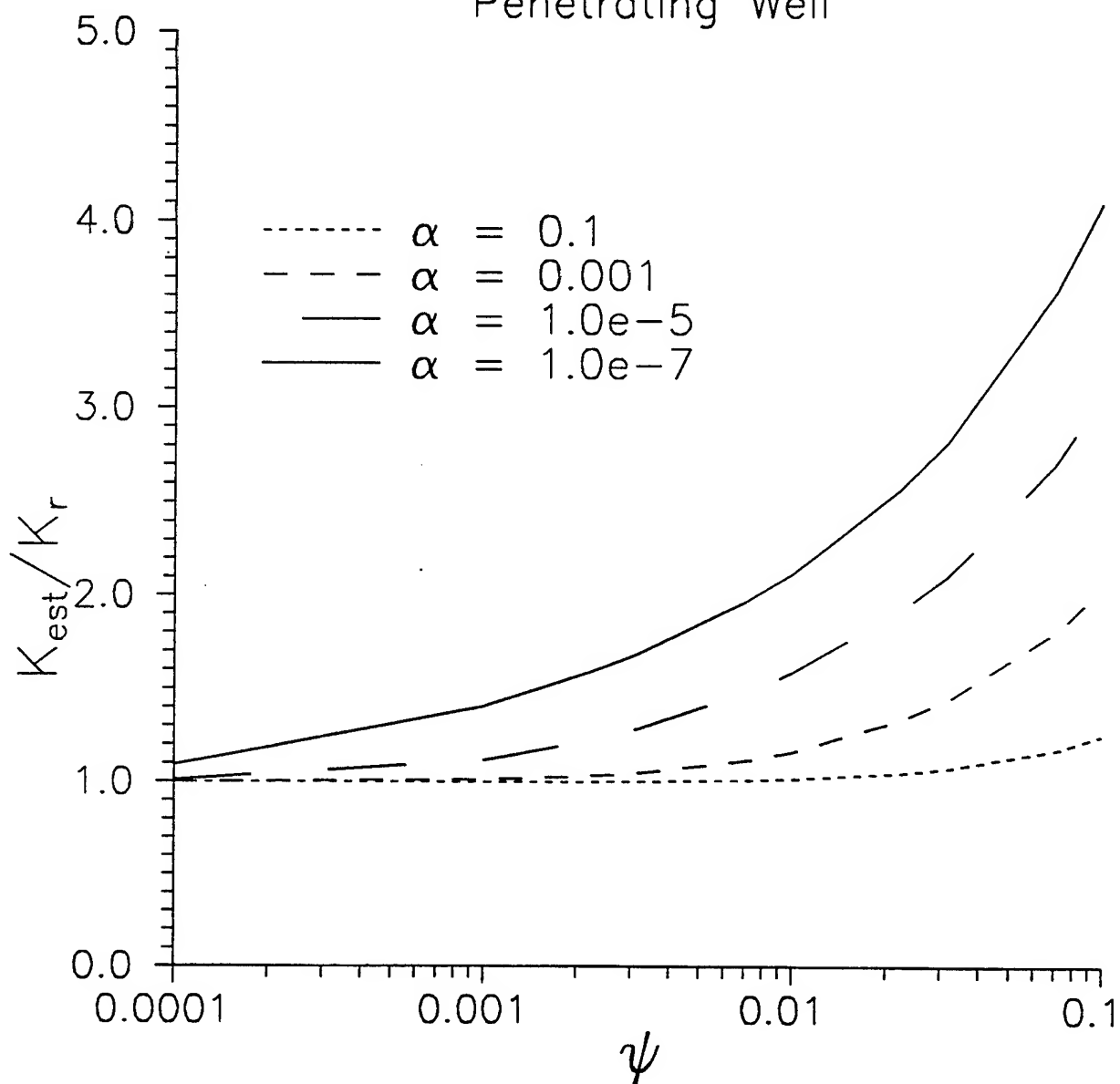


Figure 8

Error Introduced by Partially Penetrating
Hvorslev Model in Case of Unknown
Anisotropy

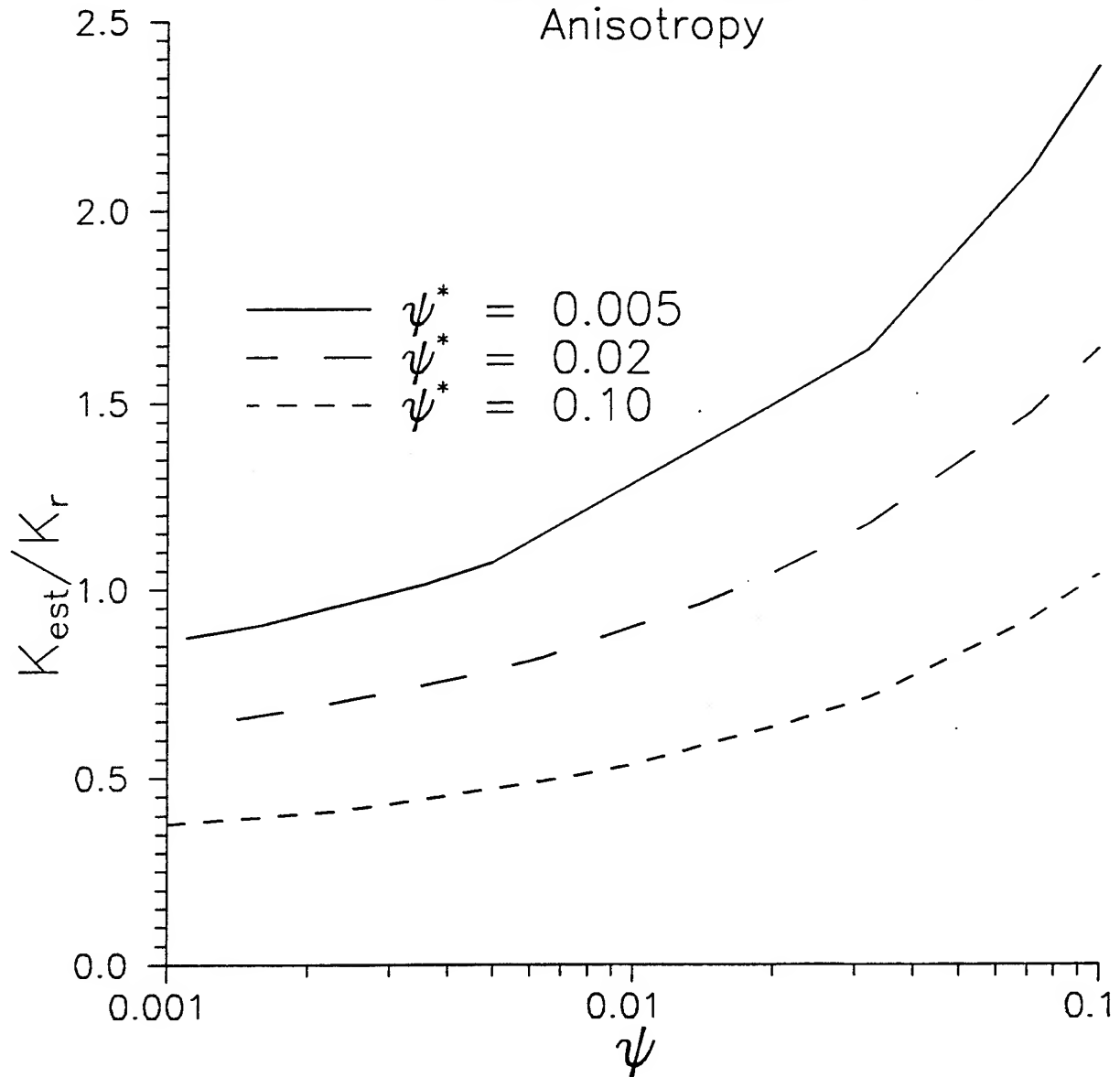


Figure 9

Error Introduced by Bouwer and Rice Model as a Function of Aspect Ratio

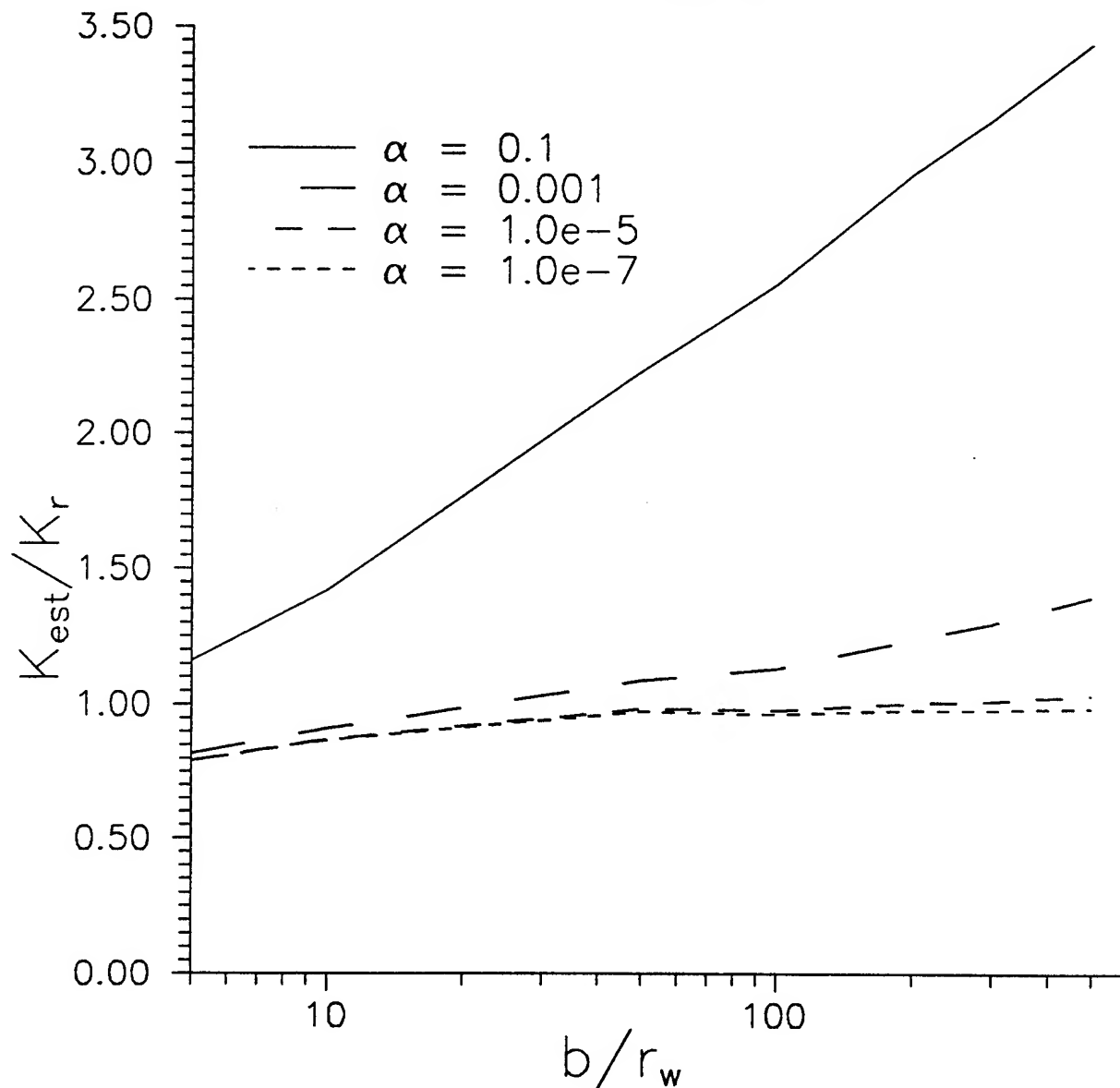


Figure 10a

Error Introduced by Bouwer and Rice Model as a Function of Anisotropy

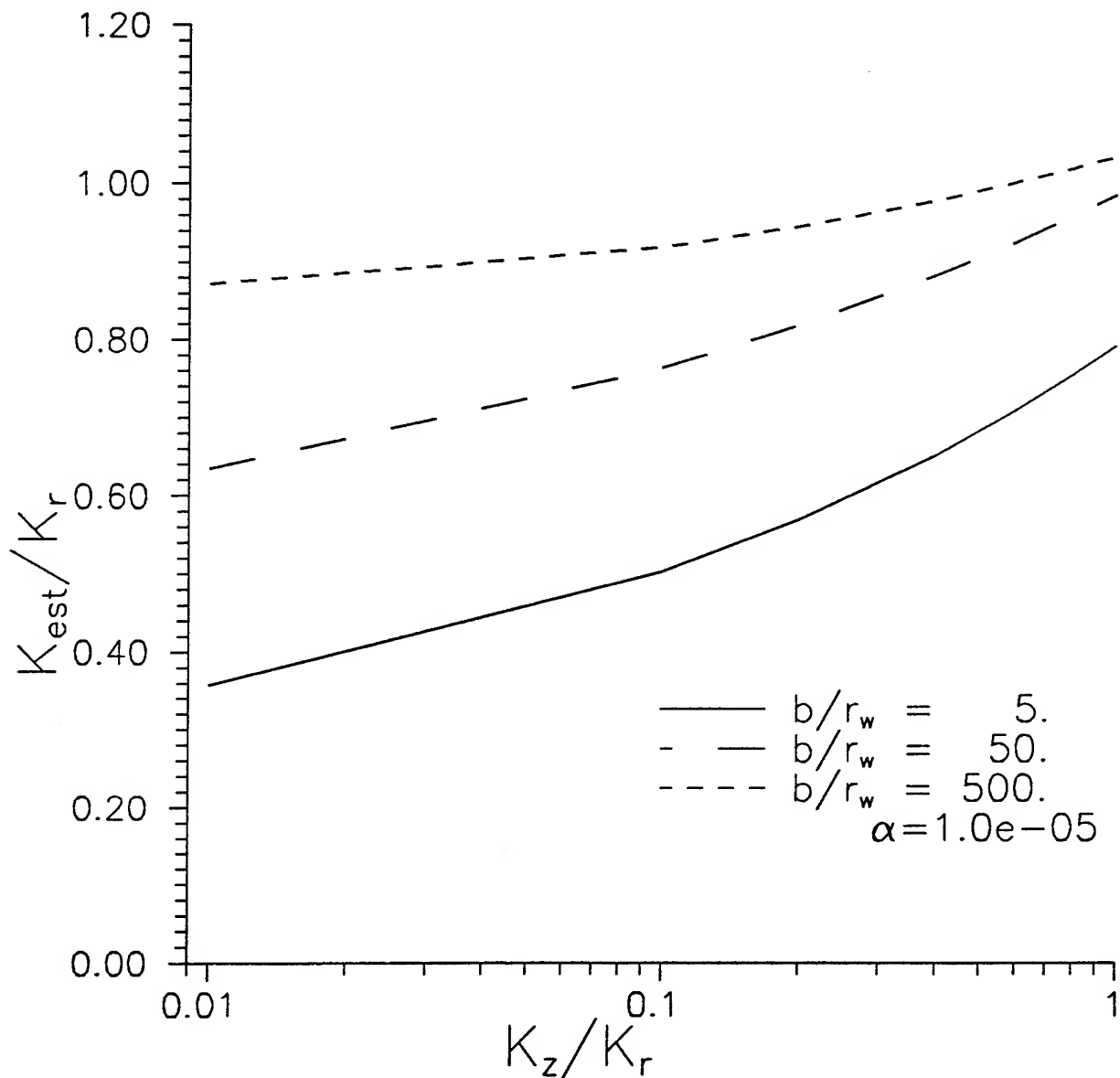


Figure 10b

Lincoln County Site
Ln-1 Slug Test - 6/91

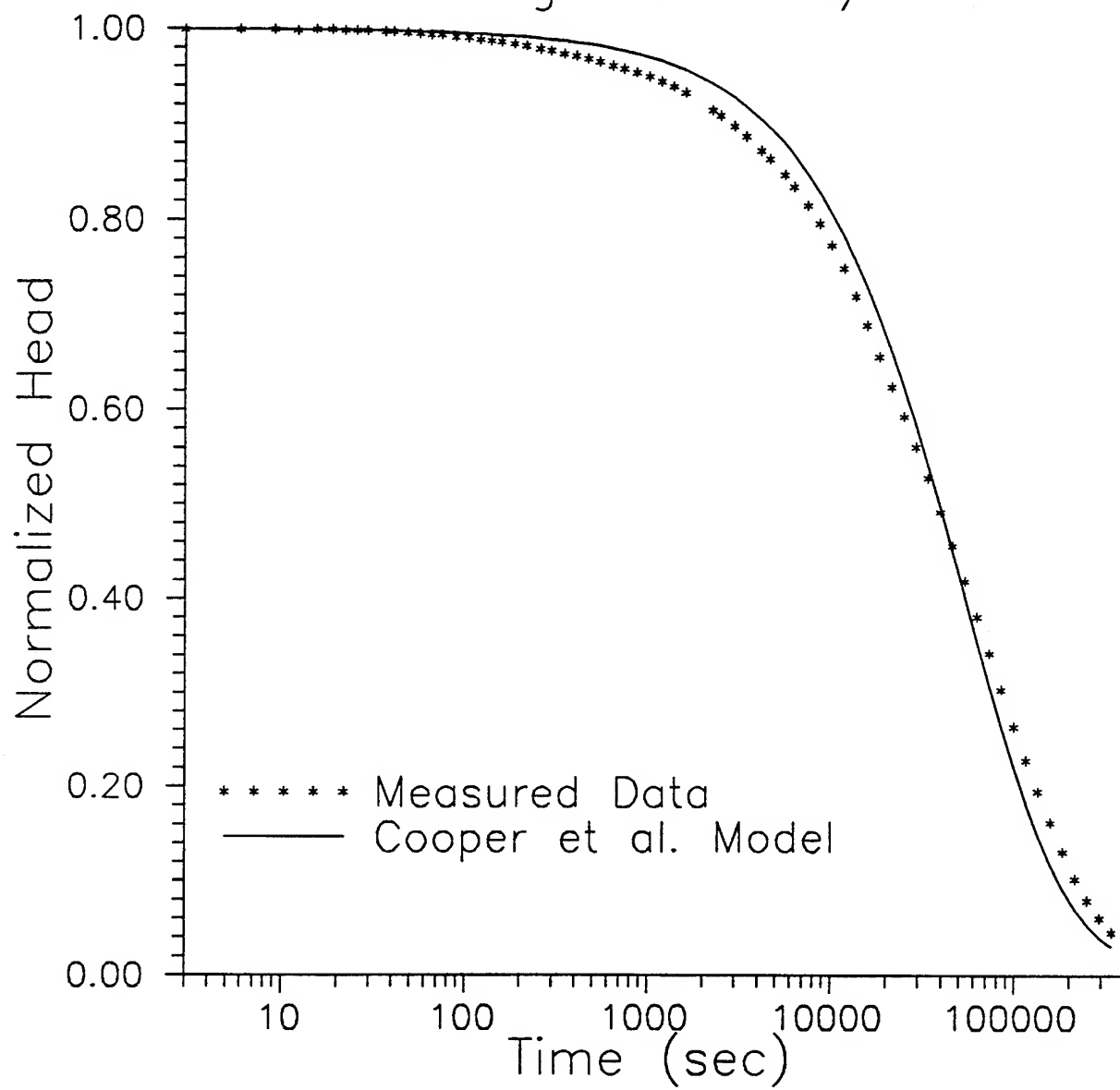


Figure 11

Lincoln County Site
Ln-1 Slug Test - 6/91

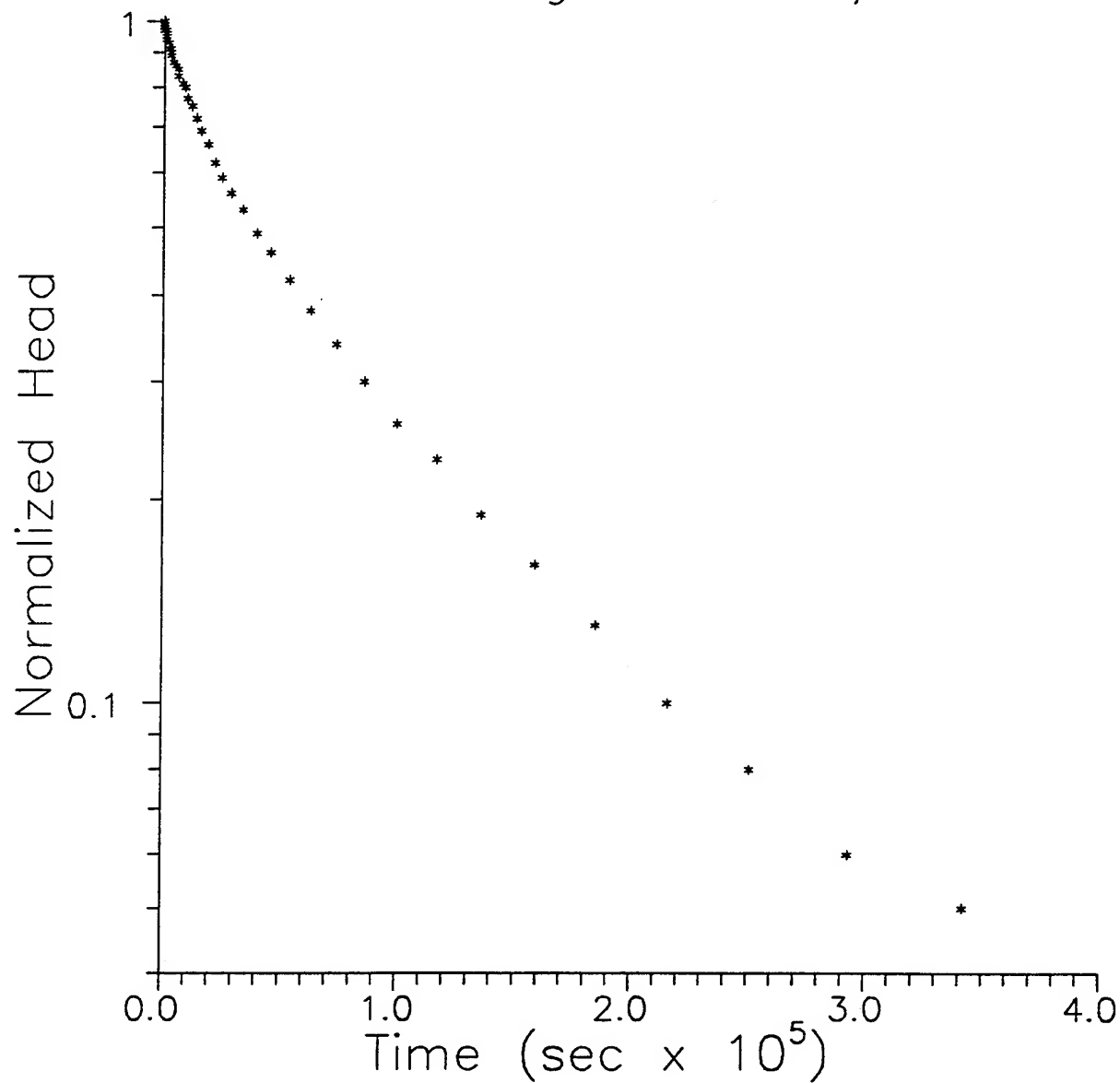


Figure 12

Lincoln County Site
Ln-1 Slug Test - 6/91

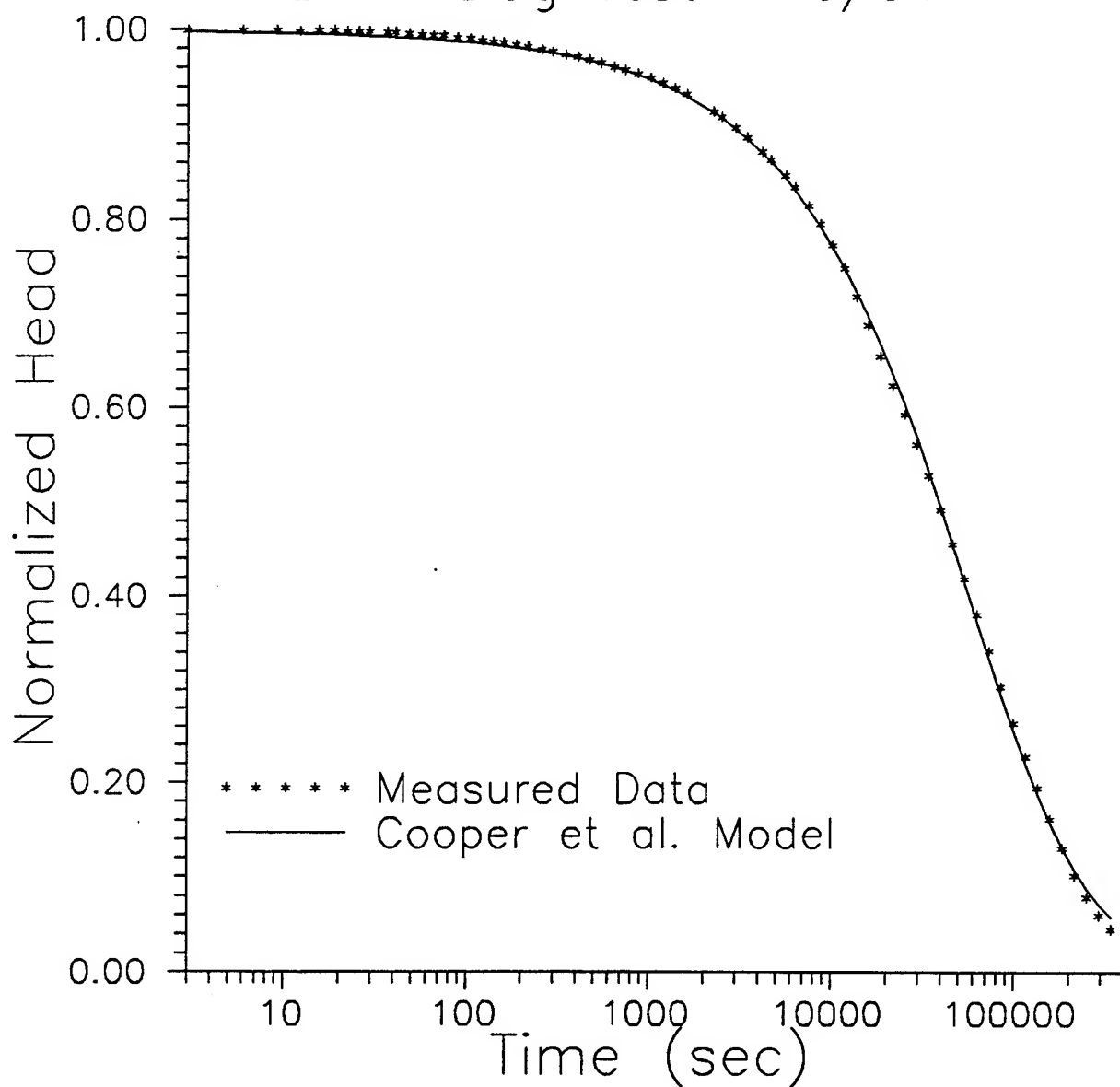


Figure 13

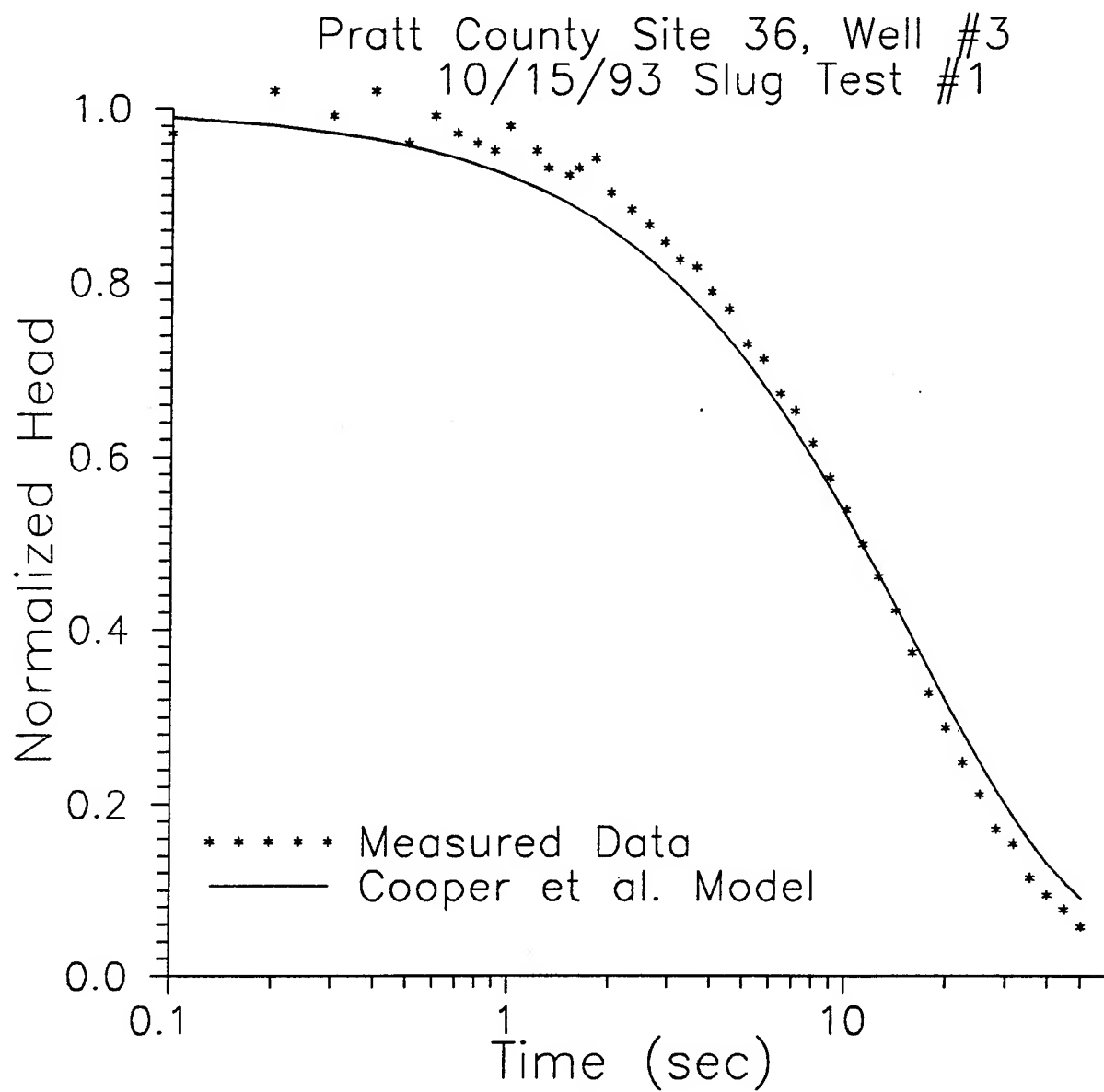


Figure 14

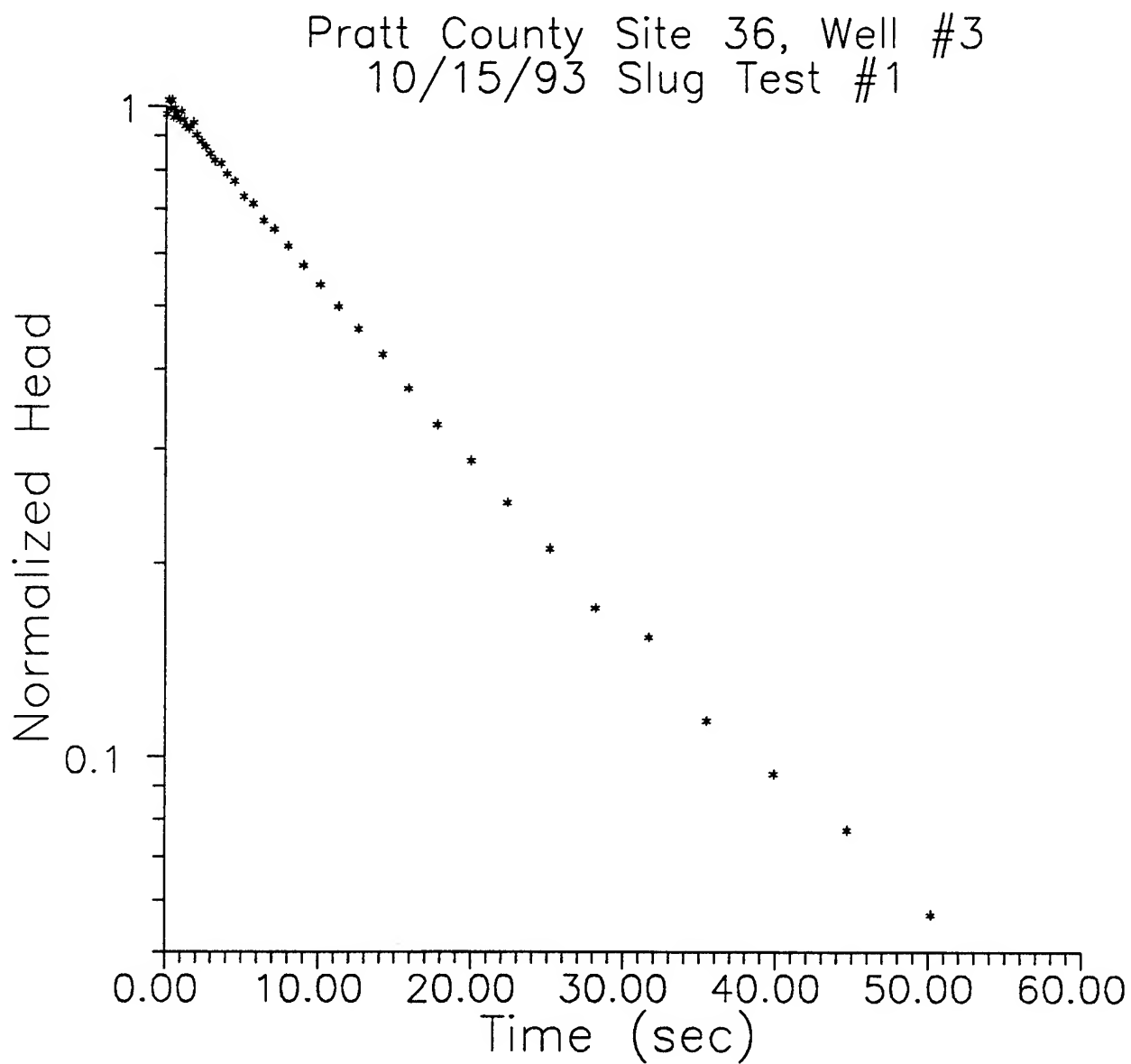


Figure 15

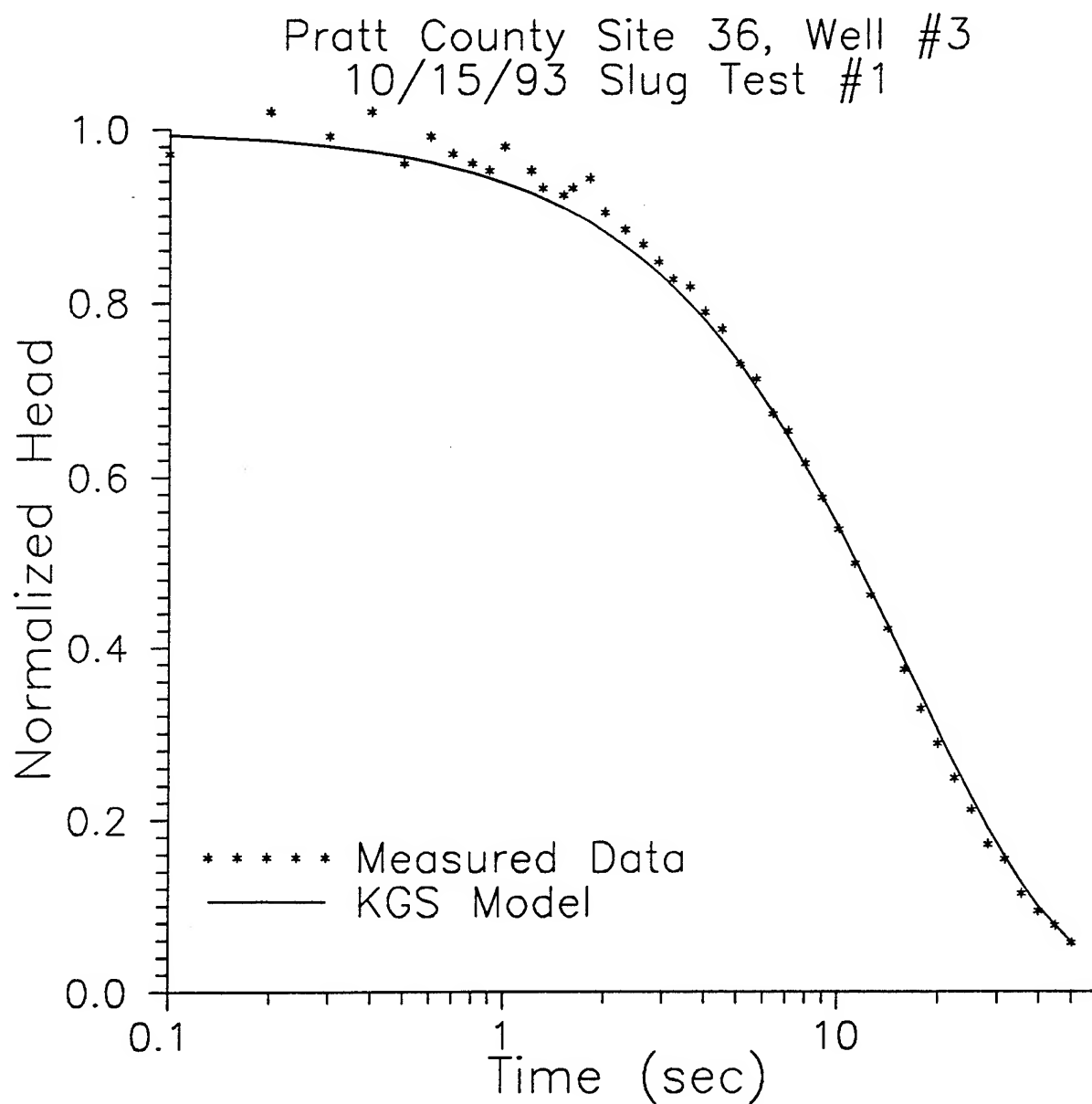


Figure 16

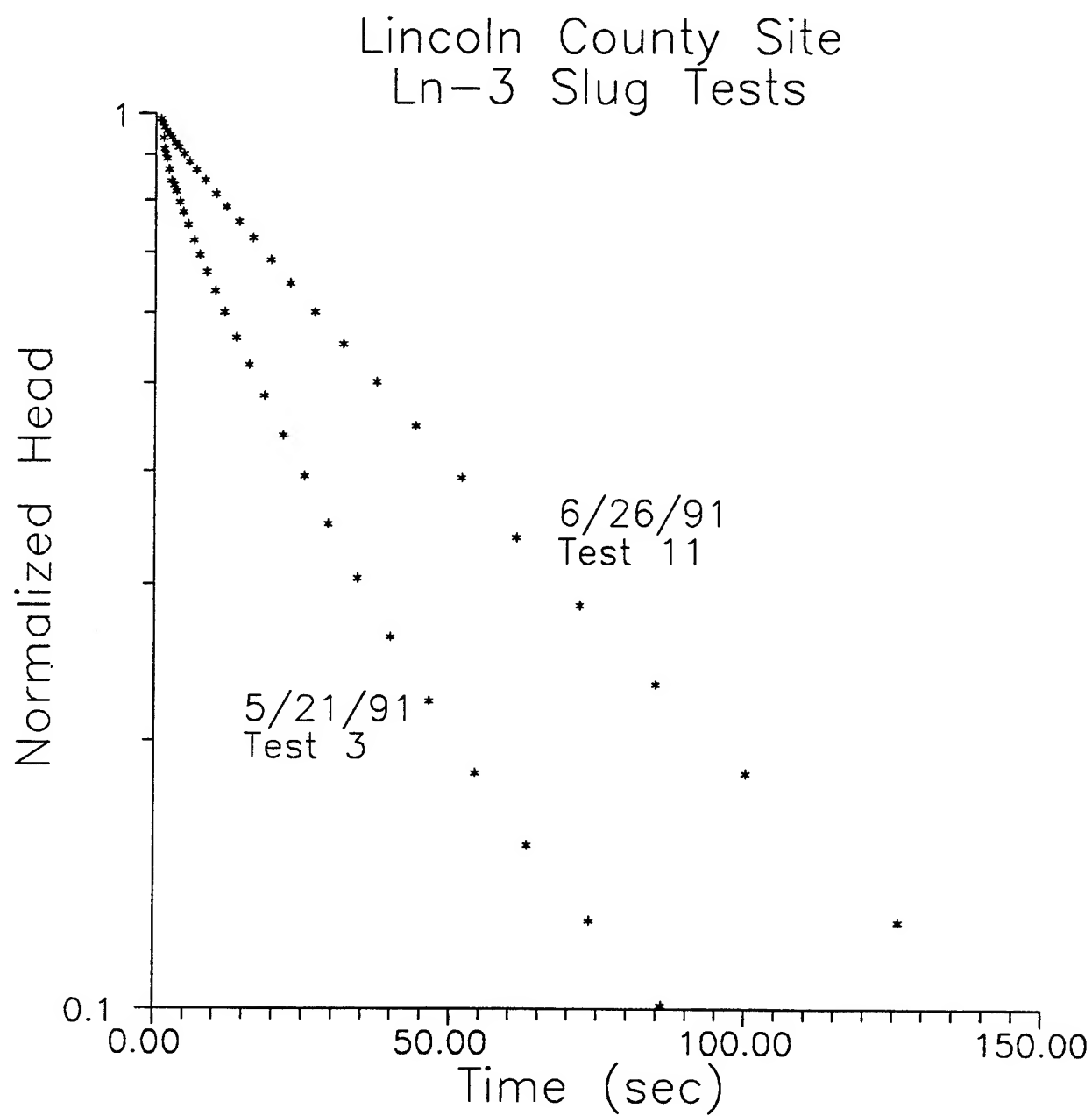


Figure 17

Lincoln County Site
Ln-3 1991 Slug Tests

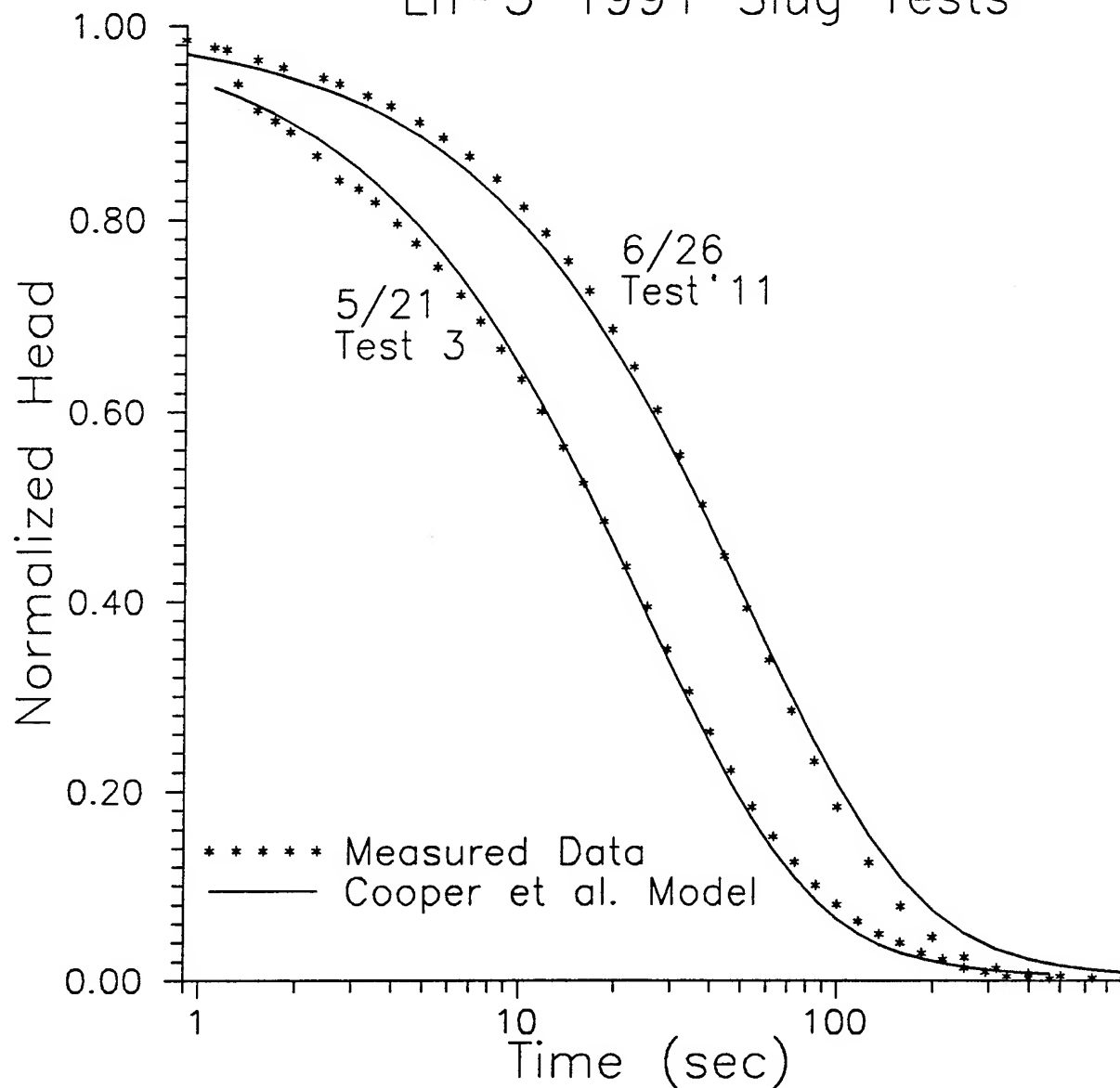


Figure 18

Lincoln County Site
5/21 Test 3
Well Ln-3

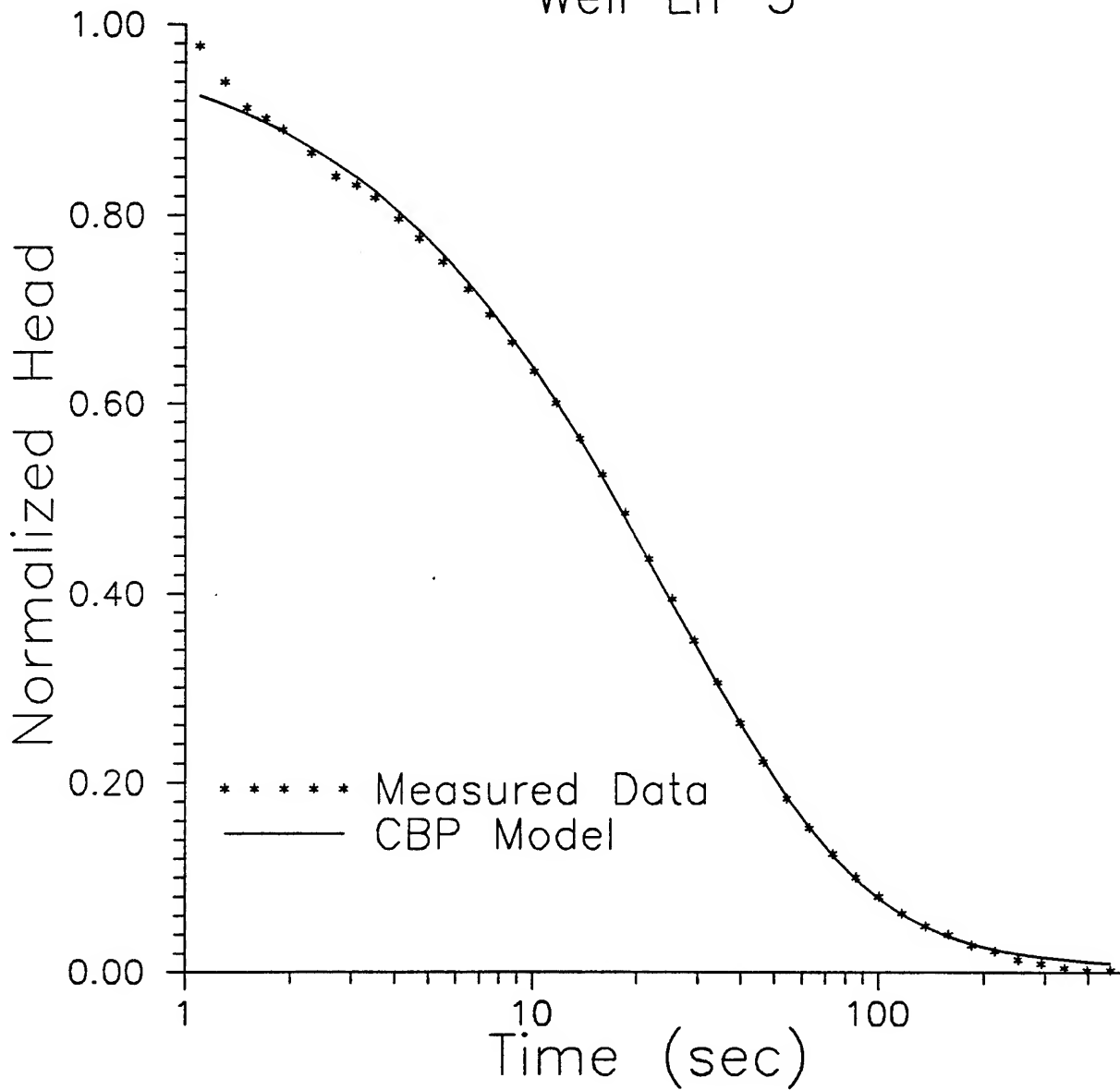


Figure 19